A very high-resolution analysis of the influence of bank roughness on the rate of river bank erosion processes

Rebecca Collins

A thesis presented for the degree of

Doctor of Philosophy

School of Science and the Environment

University of Worcester

19th December 2023

Abstract

River bank erosion is a significant contributor of sediment to our rivers and a changing climate poses new challenges for our understanding of these erosion processes. This study made use of very-high resolution terrestrial laser scanning and meteorological and flow observation data to attempt to identify the relative contributions of different erosion processes on a stretch of the River Arrow in Warwickshire, UK. Over 24 months, five sections of river bank were scanned seven times each, creating 6 time periods of change for the analysis. It was possible to identify subaerial erosion as the dominant erosion processes across all five of the study banks, contributing up to 98% of the erosion recorded. Through a series of linear regression models it was possible to identify maximum discharge, mean stage, maximum stage and peaks above the Q10 stage as statistically significant contributors to erosion, explaining 36.7% of the volume of erosion per m^2 per year across the whole bank face. The most interesting feature of these models was the direction of the model coefficients, with most of the flow variables exhibiting negative coefficients, suggesting that as flow increases erosion decreases. High flows were not generating erosion and were inhibiting other erosional processes, in particular that of subaerial erosion which was the most significant contributor to bank change during the study period. Meteorological variables were also modelled via linear regression and maximum temperature, total rainfall and

average rainfall were identified as significant contributors to erosion, but those models still only explained 19.7% of the subaerial erosion above the Q10 level and 23.7% of the total erosion volume. In addition to linear models, a principal components analysis was also carried out to try to explain more of the erosion. The PCA model explained an additional 7% of the erosion above the Q10 level using two components spanning the full range of meteorological variables calculated, with component one comprising positive contributions from cold hours, frost days, freeze thaw cycles, total rainfall, wetting and drying cycles, wet days and rain hours and negative contributions from mean and minimum temperature. Component two comprised positive contributions from maximum temperature and hot hours but negative contributions from average rainfall. The final part of this study sought to identify whether roughness had a significant effect on fluvial erosion. Roughness was calculated at three different scales - 0.5m, 0.25m, and 0.03m - and the effect of roughness on erosion was modelled using a series of further linear regression models. These models explained between 3.2% and 89.3% of the erosion value, when local erosion and local roughness were controlled for. Again, the coefficient values in these models were interesting, with greater roughness leading to greater erosion in the majority of cases for all three roughness scales. Interaction models, that measure the effect of multiple levels of independent variables on the relationship between another independent variable and the dependent variable, were undertaken to try to understand the combined effect of roughness at different scales. Fewer of these models were statistically significant - only 16 out of 30 - but the significant models frequently demonstrated that an increase in the roughness at the 0.5m scale resulted in a weakening of the relationship between roughness at the 0.03m scale and erosion. However, there still remain some inconsisten-

cies across the interaction models that require further analysis. Overall, the research was deemed successful, shedding new light on the process of bank erosion and identifying numerous opportunities for further research. In particular, more temporally dense measurements of erosion are needed to better understand the relationship between flow events and erosion, as well as attempting to respond more directly to high flow events by scanning before and after high flows to more directly attribute erosion directly to specific flow events.

Dedication

This thesis is dedicated to the wonderful family and friends that have been by my side through this near decade long process! To my beautiful children, Laura and Arthur, you give me strength, love and joy every day and I could not be prouder of you.

To my wonderful husband, Michael. Your love and support have kept me going when I wanted to quit and helped me believe in myself when I feared I would fail. Thank you. For everything. I love you.

To my parents, Terrie and Steve. I did it!

Declaration

I declare that the work herein is entirely my own, except where otherwise directly acknowledged.

Any reproduced figures have been done so with copyright permissions from the various copyright holders via RightsLink, with the exception of those that are available via creative commons licences or where specific copyright text has been requested by the publisher. All reproduced figures are fully acknowledged and attributed in the document. All unattributed figures are the author's own. A full list of copyright approvals for figures is available upon request.

Acknowledgements

This thesis represents almost a decade of part-time work alongside my career and family commitments and has been source of joy, fascination, agony, and every emotion in between. I want to thank anyone who has had to listen to me brainstorm, moan or complain throughout this whole process!

But there are, of course, a few people who deserve a special mention. My family - Mum, Dad, Laura, Arthur, Bethany and Stewart - who have supported me through this with encouraging words and cuddles on bad days and with tolerant patience when things are going well and I spend hours at a time animatedly talking about a cloud of dots.

My darling husband, Michael, who supported me throughout this process despite the fact that it dragged on for far longer than either of us ever imagined it would. Thank you for the hundreds of cups of tea, chocolate bars and occasional figurative kicks in the backside.

To Sophie Pearce, my PhD sister, who has helped me maintain my sanity with laughter, tears and Robert Downey Jr GIFs. Thank you for being a sounding board and a wonderful friend.

To James Atkins, for advice on equipment, field work and for listening to my occasional breakdowns over hours of processing lost due to unstoppable IT updates.

To Fleur Visser for always pushing me to do better and think about new ideas, even when I may not want to!

And finally to Professor Ian Maddock. I would never have been able to do this without your support. There are no words for how much your guidance has meant to me. From our first meeting when I was a mature undergraduate in 2009, you have been a source of inspiration and I am so very grateful for all the time you have spent helping and guiding both this thesis and my early lecturing career. From the bottom of my heart, thank you.

Contents

Abstract **ii**

Contents **ix**

List of Figures **xiv**

List of Tables **xxvi**

1 Introduction **1**

1.1 Sediment in Rivers 2

1.1.1 The importance of sediment in river catchments . . 2

1.1.2 Riverbank erosion as a management issue 5

1.1.3 The dynamic river system 10

1.2 River Bank Erosion Processes 17

1.2.1 Subaerial Erosion 18

1.2.2 Mass Wasting Erosion 20

1.2.3 Fluvial Erosion 22

1.3 Measuring River Bank Erosion 24

1.3.1 Erosion measurement techniques - A brief history . 24

1.3.2 Remote Sensing in the Fluvial Environment 30

1.3.3 Terrestrial laser scanning in River Science 36

1.4 Motivation, Aims and Objectives 39

1.4.1 Motivation 39

1.4.2 Research Aims and Objectives 40

1.5 Thesis Structure 42
1.6 Chapter Summary 44

2 Methods **45**
2.1 Terrestrial Laser Scanning of River Banks 45
2.2 Site Details - River Arrow 50
2.3 Terrestrial Laser Scan Data Acquisition 55
2.3.1 Leica ScanStation C10 55
2.3.2 Scanning protocol design 57
2.3.3 Site setup 60
2.3.4 Target based scan registration and cloud generation 64
2.4 Point Cloud Classification 66
2.5 Change Detection 70
2.6 Chapter Summary 74

3 Relative contributions of subaerial erosion, fluvial erosion and mass wasting processes on river bank change **76**
3.1 Introduction 77
3.1.1 Bank erosion in a Changing World 77
3.1.2 Bank Erosion - Processes and interactions 79
3.1.3 Bank erosion rates 81
3.2 Aims and Objectives 83
3.3 Methods 85
3.4 Results 90
3.4.1 Data Summary 90
3.4.2 Change Detection Results 97
3.4.3 Relative Contributions of Erosion Processes 109
3.5 Discussion 112
3.5.1 Patterns of erosion and deposition 112

3.5.2 Relative Contributions of Erosion Processes 118
3.5.3 Limitations 122
3.6 Chapter Summary 125

4 The influence of flow and meteorological conditions on erosion processes 127

4.1 Introduction 127
4.1.1 Controls on Bank Erosion 128
4.1.2 Fluvial Erosion 128
4.1.3 Subaerial Erosion 130
4.1.4 Mass Wasting Erosion 133
4.1.5 Summary 135
4.2 Aims and Objectives 136
4.3 Methods 136
4.3.1 Flow Data and fluvial erosion 137
4.3.2 Meteorological data and subaerial erosion 137
4.3.3 Data Analysis 141
4.4 Results 142
4.4.1 Influence of Flow Variables on Erosion 142
4.4.2 Influence of meteorological variables on erosion . . 149
4.4.3 Combination of Flow and Subaerial variables to predict erosion 162
4.4.4 Influence of meteorological variables on deposition . 163
4.5 Discussion 166
4.5.1 Flow and Meteorological controls on Erosion 166
4.5.2 Meteorological Conditions and deposition 170
4.5.3 Limitations 173
4.6 Chapter Summary 176

5 The influence of form roughness on riverbank erosion processes 178

5.1 Introduction 178

5.1.1 Roughness and Total Shear Stress 180

5.1.2 Self-limiting Bank Erosion? 186

5.1.3 Gaps in our knowledge 189

5.2 Aims and Research Question 190

5.3 Methods 190

5.3.1 Statistical analysis and the problem of spatial autocorrelation 192

5.3.2 Data analysis methods 197

5.4 Results 197

5.4.1 Patterns of bank roughness 197

5.4.2 Influence of roughness on erosion values 215

5.4.3 Roughness interactions 230

5.5 Discussion 244

5.5.1 Patterns of bank roughness 244

5.5.2 Bank roughness and erosion 247

5.5.3 Limitations 254

5.5.4 Model definition and handling of spatial data 255

5.6 Chapter Summary 256

6 Discussion and Conclusions 258

6.1 Aims and Objectives of this research 258

6.1.1 Research Aim and Objectives 258

6.2 Summary of Key findings 259

6.2.1 Dominance of erosion processes 259

6.2.2 Conditions generating most significant erosion . . . 261

6.2.3 Impact of roughness on fluvial erosion 263

6.2.4 Summary of study outcomes 265
6.3 Effectiveness of TLS data collection and analysis 266
6.3.1 TLS data collection and preparation 266
6.3.2 Data analysis 267
6.4 Limitations of research 269
6.4.1 Continuous and discontinuous data and the problems of temporal scales 269
6.4.2 Spatial autocorrelation and dense spatial data . . . 271
6.5 Opportunities for future research 272
6.6 Final conclusions 276

7 References 279

8 Appendices 306

A Pilot study of change detection techniques 307

B Volume change results 319

C Time Series Graphs of Erosion Values against Flow Variables 332

D Results of Correlation of Meteorological Variables 339

E Results of Variogram Analysis 341

F Linear regression of erosion against roughness and controls 347

List of Figures

1.1 Benefits and impacts on rivers 2
1.2 Theoretical habitat/sediment relationship 8
1.3 Schematic of equilibrium states 11
1.4 Equilibrium states over time 13
1.5 Erosion processes on a river bank 18
1.6 Riverbank mass failure mechanisms 21
1.7 Example of repeat cross profiling from Leopold and Wolman (1957) 25
1.8 Example of repeat cross profiling from Wolman (1959) . 26
1.9 Scematic diagram of the Photo-Electronic Erosion Pin . 29
1.10 Data types and resolutions 32
1.11 Example of early terrestrial photogrammetry experimental setup 33
1.12 Channel change along the Tana River, Kenya, measured using Landsat data 34
1.13 Overview of terrestrial laser scanning process 37
1.14 Number of publications containing the keywords "Terrestrial Laser Scanning" and "Rivers" according to a Web of Science database search 38
1.15 Overview of thesis structure 42

2.1 Benefits of multi angle scanning 46
2.2 Visual representation of precision and accuracy 48

2.3 River Arrow Catchment 51
2.4 Study banks on the River Arrow 52
2.5 Site photographs 53
2.6 River Arrow flow duration curve, 1981-2019 55
2.7 ScanStation C10 and 6-inch target 56
2.8 Survey data collection method 60
2.9 Site set up 62
2.10 Point cloud classification 67
2.11 Classifier results on training dataset 70
2.12 Principals of the M3C2 technique 71
2.13 Calculation of change volume using voxels 73

3.1 Downstream changes in sediment sources and the effect of sediment size (Abbas et al., 2023) 79
3.2 Workflow of data collection and processing for analysis . 86
3.3 Example of manual mass wasting segmentation 87
3.4 Linear regression for river level at Studley gauge vs water height on bank at time of each TLS scan 88
3.5 Bank height duration curves for each study bank, May 2017 - May 2019 based on the bank height data calculated in figure 3.5 89
3.6 Histograms of the spread of change data recorded on bank 1 91
3.7 Histograms of the spread of change data recorded on bank 2 92
3.8 Histograms of the spread of change data recorded on bank 3 93
3.9 Histograms of the spread of change data recorded on the upstream reach of bank 3 94

3.10 Histograms of the spread of change data recorded on the midstream reach of bank 3 95
3.11 Histograms of the spread of change data recorded on the downstream reach of bank 3 96
3.12 Comparison of the rate of change per metre squared per year across all of the the study banks 99
3.13 Bank 1 - Results of M3C2 change 100
3.14 Bank 2 - Results of M3C2 change 102
3.15 Bank 3 Upstream - Results of M3C2 change 104
3.16 Bank 3 Midstream - Results of M3C2 change 105
3.17 Bank 3 Downstream - Results of M3C2 change 107
3.18 All banks - Relative contributions of erosion processes . 111
3.19 Zoomed Ternary plots showing the data for each bank . 113
3.20 Figure from Leyland et al. (2015) showing erosion and deposition areas along the studied bank with histograms of the spread of erosion and deposition points. 115
3.21 Figures from Longoni et al. (2016) showing areas of erosion and deposition up to 0.4m along the studies banks with histograms of the spread of erosion and deposition points. 116
3.22 Figure from Foerst and Rüther (2018) showing erosion and deposition areas along one of the studied banks. . . 117
3.23 Model of erosion dominance 121
3.24 Model of erosion dominance with River Arrow erosion points 123

4.2 Discharge of the River Arrow as recorded at the Studley Gauge 138
4.1 Meteorological Gauge locations 139

4.3 Linear regression results for air temperature 140
4.4 boxplots of the different erosion variables per bank . . . 145
4.5 Correlation plot of flow variables for multivariate regression using all bank data 146
4.6 Daily air temperature data for the study period. The blue vertical lines represent the scan dates for banks 1 and 2, while the red-dashed vertical line represents the scan dates for bank 3. 149
4.7 Daily rainfall data for the study period. The blue vertical lines represent the scan dates for banks 1 and 2, while the red-dashed vertical line represents the scan dates for bank 3. 150
4.8 Correlation plot of meteorological variables for multivariate regression using all bank data 156
4.9 Plot of the percentage variance explained by each principal component 160
4.10 Comparison of the erosion rates between this study and that of Couper and Maddock (2001) 169
4.11 Results of soil volume changes following a) freeze-thaw cycles and b) wetting and drying cycles (Couper et al., 2002) 172

5.1 River bank roughness 180
5.2 Effect of form roughness on flow 182
5.3 Surface roughness by sand-clay content 186
5.4 Self-limiting bank erosion model 187
5.5 Diagram of roughness calculation technique 191
5.6 Bank 1 roughness at the large 0.5m scale 199
5.7 Bank 1 roughness at the medium 0.25m scale 200

5.8 Bank 1 roughness at the small 0.03m scale 201
5.9 Bank 2 roughness at the large 0.5m scale 202
5.10 Bank 2 roughness at the medium 0.25m scale 203
5.11 Bank 2 roughness at the small 0.03m scale 204
5.12 Bank 3 - Upstream roughness at the large 0.5m scale . 205
5.13 Bank 3 - Upstream roughness at the medium 0.25m scale 206
5.14 Bank 3 - Upstream roughness at the small 0.03m scale 207
5.15 Bank 3 - Midstream roughness at the large 0.5m scale . 208
5.16 Bank 3 - Midstream roughness at the medium 0.25m scale 209
5.17 Bank 3 - Midstream roughness at the small 0.03m scale 210
5.18 Bank 3 - Downstream roughness at the large 0.5m scale 211
5.19 Bank 3 - Downstream roughness at the medium 0.25m scale 212
5.20 Bank 3 - Downstream roughness at the small 0.03m scale 213
5.21 Comparison of coefficient values for the effect of roughness at the different roughness scales 221
5.22 Comparison of coefficient values for the effect of the lag roughness at different roughness scales with zoomed image inset 223
5.23 Roughness at the a) 0.5m scale, b) 0.25m scale and c) 0.03m scale against erosion for all time periods at Bank 1 224
5.24 Roughness at the a) 0.5m scale, b) 0.25m scale and c) 0.03m scale against erosion for all time periods at Bank 2 225
5.25 Roughness at the a) 0.5m scale, b) 0.25m scale and c) 0.03m scale against erosion for all time periods at the upstream reach of Bank 3 226

5.26 Roughness at the a) 0.5m scale, b) 0.25m scale and c) 0.03m scale against erosion for all time periods at the midstream reach of Bank 3 227

5.27 Roughness at the a) 0.5m scale, b) 0.25m scale and c) 0.03m scale against erosion for all time periods at the downstream reach of Bank 3 228

5.28 Interaction plot of the effect of roughness at each scale on erosion for the all Bank 1 data 232

5.29 Interaction plot of the effect of roughness at each scale on erosion for the all Bank 2 data 233

5.30 Interaction plot of the effect of roughness at each scale on erosion for the upstream reach of Bank 3. 234

5.31 Interaction plot of the effect of roughness at each scale on erosion for the downstream reach of Bank 3. 235

5.32 Roughness at the a) 0.5m scale, b) 0.25m scale and c) 0.03m scale against erosion for all time periods at Bank 1 238

5.33 Roughness at the a) 0.5m scale, b) 0.25m scale and c) 0.03m scale against erosion for all time periods at Bank 2 239

5.34 Roughness at the a) 0.5m scale, b) 0.25m scale and c) 0.03m scale against erosion for all time periods at the upstream reach of Bank 3 240

5.35 Roughness at the a) 0.5m scale, b) 0.25m scale and c) 0.03m scale against erosion for all time periods at the midstream reach of Bank 3 241

5.36 Roughness at the a) 0.5m scale, b) 0.25m scale and c) 0.03m scale against erosion for all time periods at the downstream reach of Bank 3 242

5.37 Zoomed figure of the roughness values at the 0.03m roughness scale for the upstream reach of Bank 3 during time periods E4 and E5 246

5.38 Structure of the upstream reach of Bank 3 taken during initial site investigation on 23rd May 2016 247

5.39 Zoomed view of a section of the Upstream reach of Bank 3 in a) true colour RGB values and b) roughness at the 0.03m scale values to demonstrate the contiguity between areas of lower roughness and areas of larger sediment and less steep bank. 248

5.40 Conceptual diagram of effect of high large scale roughness on flow separation 253

5.41 Conceptual diagram of effect of low large scale roughness on flow separation 253

6.1 Erosion dominance model (a) and model with points representing River Arrow data (b) 260

6.2 Deposition values at the Harrested Stream, Denmark from Veihe et al. (2011) 271

A.1 Mock river bank setup used for pilot study 308

A.2 Mock bank after soil removal 309

A.3 Pilot study point clouds pre and post cropping 310

A.4 Pilot study change detection workflow 310

A.5 Raster calculation settings 312

A.6 Results of the raster calculation 312

A.7 Results of the GCD calculation with a minimum level of detection of 1cm 313

A.8 Results of the GCD calculation with a minimum level of detection of 2cm 314
A.9 Results of the Cloud-to-Cloud comparison technique . . 315
A.10 Results of the Multiscale Model to Model Cloud comparison technique 316

C.1 Time series of Bank 1 erosion variables and river level . 333
C.2 Time series of Bank 2 erosion variables and river level . 334
C.3 Time series of total Bank 3 erosion variables and river level 335
C.4 Time series of Bank 3 Upstream reach erosion variables and river level 336
C.5 Time series of Bank 3 Midstream reach erosion variables and river level 337
C.6 Time series of Bank 3 Downstream reach erosion variables and river level 338

E.1 Variogram models for each time period on Bank1 342
E.2 Variogram models for each time period on Bank 2 343
E.3 Variogram models for each time period on the upstream reach of Bank 3 344
E.4 Variogram models for each time period on the midstream reach of Bank 3 345
E.5 Variogram models for each time period on the downstream reach of Bank 3 346

F.1 Linear regression plots of change due to fluvial erosion below the Q10 level against roughness at the 0.5m scale for each survey period on Bank 1 348

F.2 Linear regression plots of change due to fluvial erosion below the Q10 level against roughness at the 0.5m scale for each survey period on Bank 2 349

F.3 Linear regression plots of change due to fluvial erosion below the Q10 level against roughness at the 0.5m scale for each survey period on the upstream reach of Bank 3 350

F.4 Linear regression plots of change due to fluvial erosion below the Q10 level against roughness at the 0.5m scale for each survey period on the midstream reach of Bank 3 351

F.5 Linear regression plots of change due to fluvial erosion below the Q10 level against roughness at the 0.5m scale for each survey period on the downstream reach of Bank 3 352

F.6 Linear regression plots of change due to fluvial erosion below the Q10 level against roughness at the 0.25m scale for each survey period on Bank 1 353

F.7 Linear regression plots of change due to fluvial erosion below the Q10 level against roughness at the 0.25m scale for each survey period on Bank 2 354

F.8 Linear regression plots of change due to fluvial erosion below the Q10 level against roughness at the 0.25m scale for each survey period on the upstream reach of Bank 3 355

F.9 Linear regression plots of change due to fluvial erosion below the Q10 level against roughness at the 0.25m scale for each survey period on the midstream reach of Bank 3 356

F.10 Linear regression plots of change due to fluvial erosion below the Q10 level against roughness at the 0.25m scale for each survey period on the downstream reach of Bank 3 357

F.11 Linear regression plots of change due to fluvial erosion below the Q10 level against roughness at the 0.03m scale for each survey period on Bank 1 358

F.12 Linear regression plots of change due to fluvial erosion below the Q10 level against roughness at the 0.03m scale for each survey period on Bank 2 359

F.13 Linear regression plots of change due to fluvial erosion below the Q10 level against roughness at the 0.03m scale for each survey period on the upstream reach of Bank 3 360

F.14 Linear regression plots of change due to fluvial erosion below the Q10 level against roughness at the 0.03m scale for each survey period on the midstream reach of Bank 3 361

F.15 Linear regression plots of change due to fluvial erosion below the Q10 level against roughness at the 0.03m scale for each survey period on the downstream reach of Bank 3 362

F.16 Interaction plot of the effect of roughness at each scale on erosion for time period E1 on Bank 1 367

F.17 Interaction plot of the effect of roughness at each scale on erosion for time period E2 on Bank 1 368

F.18 Interaction plot of the effect of roughness at each scale on erosion for time period E3 on Bank 1 369

F.19 Interaction plot of the effect of roughness at each scale on erosion for time period E4 on Bank 1 370

F.20 Interaction plot of the effect of roughness at each scale on erosion for time period E5 on Bank 1 371

F.21 Interaction plot of the effect of roughness at each scale on erosion for time period E6 on Bank 1 372

F.22 Interaction plot of the effect of roughness at each scale on erosion for time period E5 on Bank 2 373

F.23 Interaction plot of the effect of roughness at each scale on erosion for time period E1 on the upstream reach of Bank 3 374

F.24 Interaction plot of the effect of roughness at each scale on erosion for time period E2 on the upstream reach of Bank 3 375

F.25 Interaction plot of the effect of roughness at each scale on erosion for time period E5 on the upstream reach of Bank 3 376

F.26 Interaction plot of the effect of roughness at each scale on erosion for time period E1 on the midstream reach of Bank 3 377

F.27 Interaction plot of the effect of roughness at each scale on erosion for time period E4 on the midstream reach of Bank 3 378

F.28 Interaction plot of the effect of roughness at each scale on erosion for time period E6 on the midstream reach of Bank 3 379
F.29 Interaction plot of the effect of roughness at each scale on erosion for time period E2 on the downstream reach of Bank 3 380
F.30 Interaction plot of the effect of roughness at each scale on erosion for time period E6 on the downstream reach of Bank 3 381

List of Tables

1.1 Summary of sediment source results for Wharfe and Ouse catchments (Walling et al., 1999) 4

2.1 A sample of river morphology studies using Terrestrial Laser Scanning techniques 49
2.2 River Arrow catchment characteristics 54
2.3 Site setup guidance and field notes 58
2.4 Scan data collection dates 63
2.5 Mean absolute error values for registered point clouds . 65
2.6 Classification Data 68

3.1 A sample of studies of bank erosion 84
3.2 Data collection dates 85
3.3 Bank heights at Q10 and Q50 Flows from calculate bank height data 89
3.4 Bank 1 Cloud Summaries 91
3.5 Bank 2 cloud summaries 92
3.6 Bank 3 complete cloud summaries 93
3.7 Bank 3 Upstream cloud summaries 94
3.8 Bank 3 Midstream cloud summaries 95
3.9 Bank 3 Downstream cloud summaries 96
3.10 Summary of calculated erosion values for all banks . . . 98
3.11 Mean erosion above and below Q10 level 109

3.12 Summary of erosion contributions for each bank and each time period 110
3.13 Erosion dominance model section descriptions 122

4.1 Summary of Flow characteristics at each bank for the study period 142
4.2 Correlation values for Flow Variables against Erosion Variables 144
4.3 Multivariate regression model of Flow Variables against Net Change summary 148
4.4 Multivariate regression models of selected independent variables against erosion variables summary 149
4.5 Summary of temperature variables for banks 1 and 2 . . 150
4.6 Summary of temperature variables for bank 3 151
4.7 Summary of rainfall variables for banks 1 and 2 151
4.8 Summary of rainfall variables or bank 3 151
4.9 Correlation values for meteorological variables against all bank erosion variables 152
4.10 Correlation values for meteorological variables against erosion variables above the Q10 level 153
4.11 Correlation values for meteorological variables against mass wasting erosion 154
4.12 Multivariate regression model of meteorological variables summary 157
4.13 Multivariate regression models of meteorological variables summary 158
4.14 Multivariate regression models of meteorological variables summary 159

4.15 List of variables contributing to the components of the PCA 161
4.16 Multivariate regression models of meteorological variables summary 162
4.17 Correlation values for meteorological variables against apparent deposition values 163
4.18 Multivariate regression models of total deposition volume against meteorological variables 165

5.1 Summary of Variogram data 195
5.2 Summary of bank roughness 214
5.3 Results of OLS regression between erosion and roughness at the 0.5m scale 216
5.4 Results of OLS regression between erosion and roughness at the 0.25m scale 218
5.5 Results of OLS regression between erosion and roughness at the 0.03m scale 219
5.6 Summary of OLS coefficients by roughness scale 221
5.7 Results of OLS regression between erosion and roughness compiled across each bank at all scales 229
5.8 Summary of slope coefficients for all bank interaction models 236
5.9 Summary of slope coefficients for the effect of local roughness on the relationship between point roughness and erosion. 243
5.10 Comparison of regression results between each of the roughness scales 249

6.1 Erosion dominance model section descriptions 260

6.2 Summary of variables contributing to the components of the PCA 262

A.1 Comparison of change detected by each tested change detection technique 317

B.1 Bank 1 - fluvial erosion contribution 323
B.2 Bank 1 - mass wasting contribution 324
B.3 Bank 1 - subaerial erosion contribution 324
B.4 Bank 2 Fluvial erosion 325
B.5 Bank 2 - sub-aerial erosion contribution 325
B.6 Bank 3 - fluvial erosion contribution 326
B.7 Bank 3 - mass wasting contribution 326
B.8 Bank 3 - subaerial erosion contribution 327
B.9 Bank 3 Upstream - fluvial erosion contribution 327
B.10 Bank 3 Upstream - mass wasting contribution 328
B.11 Bank 3 Upstream- subaerial erosion contribution 328
B.12 Bank 3 Midstream - fluvial erosion contribution 329
B.13 Bank 3 Midstream - mass wasting contribution 329
B.14 Bank 3 Midstream- subaerial erosion contribution . . . 330
B.15 Bank 3 Downstream - fluvial erosion contribution 330
B.16 Bank 3 Downstream - mass wasting contribution 331
B.17 Bank 3 Downstream- subaerial erosion contribution . . 331

D.1 Simple linear regression values for Meteorological Variables 340

F.1 Summary of slope coefficients for bank 1 interaction models 364

F.2 Summary of slope coefficients for Bank 2 and the upstream reach of Bank 3 interaction models 365
F.3 Summary of slope coefficients for midstream and downstream reaches Bank 3 interaction models 366

Chapter 1

Introduction

This introductory chapter aims to set the context within which this thesis is based and to provide the background for why research into riverbank erosion processes continues to be relevant and vital to our understanding of river systems. The research presented in this thesis seeks to identify and describe patterns of erosion and deposition on a riverbank (Chapter 4), the influence of different flow and meteorological conditions on the rates at which erosion processes occur (Chapter 5), and the influence of bank roughness on the rate of fluvial erosion processes (Chapter 6). This chapter seeks to provide background on the issue of bank erosion as a whole, as well as how emerging and advancing remote sensing technologies such as Terrestrial Laser Scanning can help to improve our understanding of bank erosion processes at the very fine scale. It will also identify some of the gaps in our current knowledge and provide the aims and objectives for this thesis. Finally, the chapter will conclude with a detailed description of the organisation of the thesis and the concepts that will be addressed in each chapter.

1.1 Sediment in Rivers

1.1.1 The importance of sediment in river catchments

Rivers are complex and diverse environments, ones that influence human activities in a number of different ways. Likewise, human activities have significant impacts upon the river systems around us, and historically, many of these impacts have been negative ones (figure 1.1). How we interact with our rivers and their floodplains is of vital importance for the future of our freshwater ecosystems, particularly under the increasing challenges that climate change and continued population growth will bring (Poff et al., 1997; Nilsson et al., 2007; Collins et al., 2011)

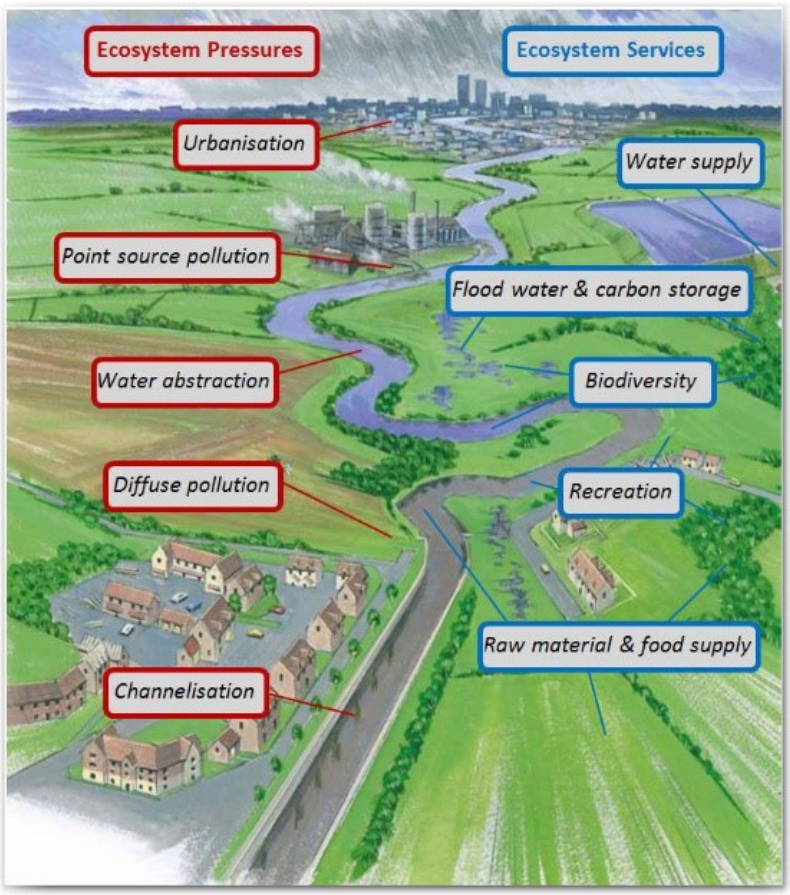

Figure 1.1: Visual representation of the societal benefits provided by rivers and some of the negative impacts human activity can have on rivers (RESTORE Partnership, 2013)

Sediment dynamics have been a topic of study for many decades, with Meade (1982) and Trimble (1983) conducting some of the most significant early studies of the sources, sinks and storage of sediment within river systems.

The sources of river sediment are varied and influenced by complex combinations of conditions and circumstances. River sediment sources can be divided into two very simple categories of surface erosion and channel erosion (Walling and Collins, 2005). The channel erosion category can be further divided into bed erosion and bank erosion, while the surface category is more complex and can be broken down in a number of different ways. Some researchers prefer to separate by erosion pathway (e.g. sheet wash, rill erosion, gully erosion as in Trimble (1983)) or by the land use type from which the material is being removed (e.g. woodland, pasture/-moorland, cultivation as in Walling and Collins (2005)). However they all represent sediment material which originated on the land and has been moved into the river via either drainage of the catchment, mass movement or wind erosion.

The proportions of fluvial sediment that can be attributed to surface erosion and channel erosion varies significantly between different catchments. Research conducted by Walling et al. (1999) found an average of 23% of the suspended sediment yield in the River Wharfe and 37% of the suspended sediment yield in the River Ouse, (both in Yorkshire, UK) could be attributed to erosion of the channel banks (bed erosion was not considered by these authors) over a five year monitoring period (1994-1999). They observed that these proportions increased following high flow events, where material was likely to have been entrained more readily thanks to the increased flow compared with periods of time when the channel was at lower flow. The remaining sediment came from surface sources, with

the dominant source being uncultivated topsoil in the Wharfe catchment (70%) and cultivated topsoil in the Ouse catchment (38%) (Table 1.1)

However, more recently, Cashman et al. (2018) identified significantly higher proportions of sediment in rivers were sourced from the channel. Their study of the Chesapeake Bay watershed (Fairfax County, Virginia, USA) found that 98% of river bed sediment and 91% of suspended sediment sampled following storm events had originated from the channel banks. Although they identified that this material would not all have come from erosion induced by that specific event, the likelihood is that material is being remobilised from in channel storage during storm events that has previously been eroded from the channel banks.

Table 1.1: Summary of sediment source results for Wharfe and Ouse catchments (Walling et al., 1999)

Catchment	Channel (%)	Uncultivated Topsoil (%)	Cultivated Topsoil (%)	Woodland (%)
River Wharfe	23	70	4	3
River Ouse	37	25	38	0

It is difficult to overstate the importance of riverbank erosion in terms of its effect on riparian land, fluvial habitats, flood risk and morphology, some of which will be elaborated in the next section. As a result, it is important to fully understand the processes by which erosion occurs, the conditions that affect the rate of erosion and the consequences that erosion events of different levels of frequency and magnitude will have on downstream habitat and morphology (Darby et al., 2007). The ability to observe the processes that generate erosion and deposition of bank materials is vital to allow river scientists, engineers, and those charged with the restoration of our fluvial environments, to understand the sources of sediment and erosional processes that deliver sediment and predict their impacts and protect against degradation (O'Neal and Pizzuto, 2011).

1.1.2 Riverbank erosion as a management issue

Many of the key physical, ecological and management issues within the fluvial environment are strongly influenced by the rate and frequency of riverbank erosion. Even small amounts of bank retreat can have wide reaching effects on infrastructure, agriculture and the ability to navigate the watercourse, posing hazards to those who depend on it for abstraction, drainage and recreation (Grove et al., 2013; Frankl et al., 2015). In addition, riverbank erosion provides significant quantities of the sediment found in watercourses, influencing the morphology and potential habitats that a river can support (Walling et al., 1999; Darby et al., 2010; Nardi et al., 2013; Cashman et al., 2018).

In England the responsibility for the management of rivers is divided amongst a number of organisations. The Environment Agency have responsibility for 'main rivers'; larger channels or streams that meet the main river criteria (including, but not limited to, whether they pose a flood risk to a significant number of properties or people, whether they drain or provide drainage opportunity for a reservoir or sewage treatment works, or where the channel can provide significant flood risk to a larger catchment). Other channels are considered as 'ordinary watercourses' and are the responsibility of local authority or local drainage boards. In Wales, river management is under the purview of Natural Resources Wales (NRW) and in Scotland river management is the responsibility of the Scottish Environmental Protection Agency (SEPA).

Each of these different organisations has responsibilities under the Water Framework Directive (WFD) to work to return watercourses to 'good ecological status' (European Union, 2000). Although the WFD does not directly tackle sediment, it recognises the links between sediment and

many of the issues that it does seek to address, e.g. habitat diversity, nutrient pollution and storage, heavy metal pollution etc (Brils, 2008). Since Brexit (the withdrawal of Great Britain from the European Union) in 2018, the WFD has been replaced with a series of regulations updated into existing UK law for each nation; the Water Environment (Water Framework Directive) (England and Wales) Regulations 2017, the Water Environment (Water Framework Directive) Regulations (Northern Ireland) 2017 and the Water Environment and Water Services (Scotland) Act 2003 .

These regulations are derived from the core principles of the EU WFD, the drive to achieve good ecological status, and retain these goals in UK law. Following Brexit the Office for Environmental Protection (OEP) was created as a new public body, under the umbrella of the Department for Environment, Food and Rural Affairs (Defra), to 'protect and improve the environment by holding government and other public bodies to account' (Office for Environmental Protection, 2022).

The morphology of a river system is heavily impacted by the quantity and size of the sediment within it. Both the sediment being carried by the water and the materials that make up the rivers banks and beds are significant factors influencing channel morphology (Hassan and Zimmermann, 2012). Where suspended sediment concentrations within the river are low, the erosive capability of that water is higher, resulting in bed incision. This bed incision also gives rise to reductions in lateral movement, preventing the natural evolution of the channel and reducing its connection to its riparian landscape (Rollet et al., 2014).

Where there is an excess of sediment, large scale deposition may occur, in many cases resulting in a shallowing of the channel and a loss of bed form variation. This can affect the navigability of the stream as well as

its morphological heterogeneity and channel geometry (Lane et al., 2007). This large-scale deposition can also result in an increase in flood risk within a location. The excess sediment reduces the hydraulic capacity of the channel, reducing the capability of the stream to take high flows (Pinter and Heine, 2005; Environment Agency, 2011)

As well as affecting the morphology and flow regime of rivers, sediment load also influences the structure, availability and heterogeneity of river habitats. Where sediment supplies are very low, there is very little habitat diversity, as there is very little sediment available to create a variety of habitats. Similarly, when there is a large quantity of sediment there is also very little habitat diversity as the sediment settles out over the bed to create a homogeneous benthic layer with little variability (Yarnell et al., 2006). Figure 1.2 shows the theoretical relationship between sediment supply and habitat heterogeneity, and although the actual relationship between these two characteristics is significantly more complex, it is clear that a deeper knowledge of the mechanisms that cause erosion, and their frequency, are a vital step in fully understanding and protecting our vulnerable river habitats.

Increased inputs of fine sediments, such as those eroded from stream banks, represents a globally recognised threat to benthic ecosystems and significant work has been done to understand both the spatial and temporal effects of such homogenisation (e.g. Collins et al. (2011), Jones et al. (2012), Mathers et al. (2017), McKenzie et al. (2020), Mathers et al. (2022)). Milner et al. (2021) found that the addition of a fine sediment pulse to a series of mesocosms containing either coarse or fine substrates generated a significant change in the makeup of macroinvertebrate communities within the stream. In particular, there was a significant change in the taxa identified in the drift assemblages downstream of the sedi-

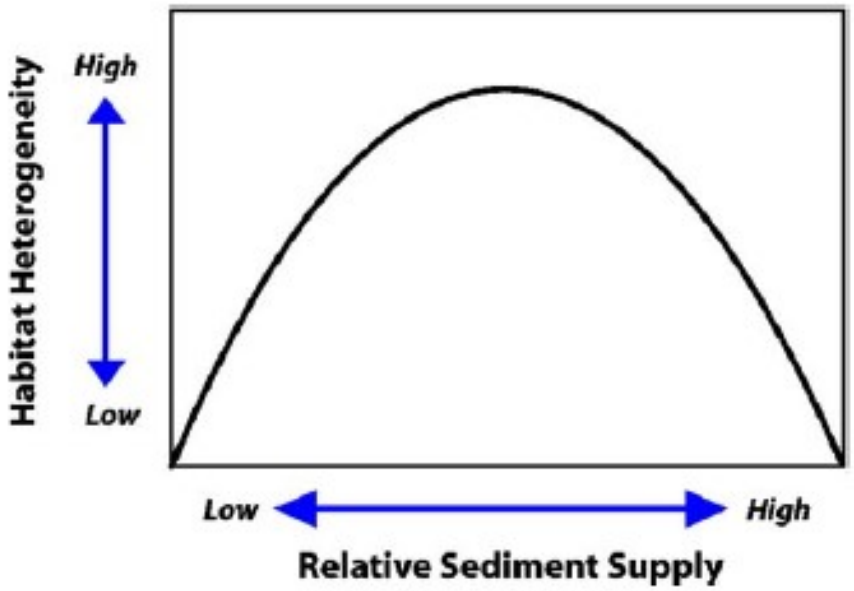

Figure 1.2: Theoretical relationship between habitat heterogeneity and sediment supply (Yarnell et al., 2006)

ment inputs, indicating that the input of sediment resulted in taxa being displaced from their prior habitat. The pulse also resulted in greater drift densities, indicating large numbers of macroinvertebrates, regardless of taxonomic differences, were being displaced during the initial sediment pulse. An improved understanding of the conditions that result in erosion of river banks, particularly those composed of fine sediments, serves to generate a catchment wide understanding of lotic environments, and thus support issues of management from both a geomorphological and ecological perspective.

Sediment can also provide an important supply of nutrients to an aquatic ecosystem. Nutrients such as nitrates (N) and Phosphates (P), metals such as Cadmium (Cd) and Lead (Pb), and organic compounds such as pesticides can all be stored in or on sediments (Taylor and Owens, 2009). When large quantities of these contaminated sediments are eroded or washed into our rivers, the water quality can be seriously impacted, posing a significant threat to the fluvial and riparian environment (Collins et al.,

2011).

In recent years anthropogenic activity has resulted in a marked increase in the amounts of fine sediment in rivers, however that has not necessarily led to an increase in that sediment arriving in the lower reaches of rivers (Owens et al., 2005). Instead, sediment storage in the upper and mid reaches of catchments is on the increase, particularly where impoundments, such as dams forming reservoirs, have prevented the continued downstream movement of sediment (Vörösmarty et al., 2003).

The impact of a reduction or restriction to sediment as a result of river regulation has been studied for many years, with authors such as Petts (1979) and Carling (1988) carrying out early work to understand the downstream influences of a lack of sediment. Immediate degradation downstream of the dam, where the released water has the lowest sediment load, has been observed to impact the downstream channel for as much as 69 times channel width (Petts, 1979; Brandt, 2000). In many locations a narrowing of the downstream channel occurs due to the reduced quantity of water flowing in the channel (Grant et al., 2003). However, Hupp et al. (2009) saw significant channel widening downstream of the Roanoak Rapids Dam in the Roanoak River, North Carolina, USA. This widening is due to increased erosion on the lower and mid bank, which often triggered mass wasting events.

The response of a river to a change in its upstream reaches can be difficult to predict, so an understanding of erosion and deposition processes, across multiple spatial and temporal scales will be an important part of ensuring that we can manage the sediment in our rivers effectively.

1.1.3 The dynamic river system

The dynamics of river systems have been a significant area of discussion within geomorphology for decades and the concept of equilibrium is one that has been used as a method for understanding river system dynamics, often by identifying forcing events that result in a shift from equilibrium, and then observing the processes that occur as a channel returns to equilibrium. Unfortunately, the importance of the equilibrium concept lacks clear and consistent agreement.

Equilibrium is the concept that a variety of forces working on a system are balanced, and the state of the system remains unchanged, until a change occurs in one (or many) of the controlling forces (Thorn and Welford, 1994). However, there are a number of types of equilibrium in geomorphology and each one attempts to explain variation in the observable form of our environment with a focus on different spatial and temporal scales.

Static equilibrium is where a system is 'at rest' (Thorn and Welford, 1994), and is not one that can be applied to real world geomorphological systems because it implies the presence of potential energy, but no kinetic energy.

Dynamic equilibrium is the concept that a system has forces acting upon it, but that those forces are balanced. In the case of geomorphology this would be the erosive force of the flowing water in balance with the resisting force of the material being eroded.

Equilibrium can also be neutral, stable or unstable. In a neutral state, a small change in the balance of forces results in no change to the system. Stable equilibrium is one where a change in the balance of forces, known as a displacement, results in a "restoring force" (Thorn and Welford, 1994: p667) that acts in opposition to the displacement and returns the system

to the same state (or position) as it was before the change. In unstable equilibrium, however, the displacement is larger and results in a force working in the same direction as the displacement, thus creating a positive feedback effect.

Metastable equilibrium represents a state whereby a small displacement will generate a restoring force and maintain equilibrium in the same state, but where a larger displacement will result in a positive feedback until the displacement ends, and thus a new stable equilibrium is formed. These different types of equilibrium are represented in figure 1.3.

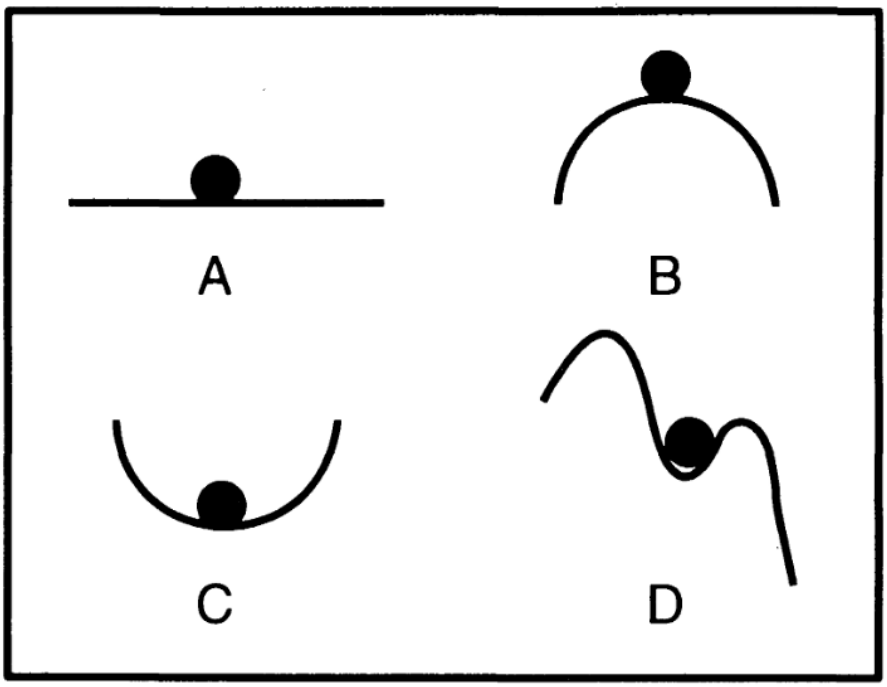

Figure 1.3: Schematic diagram of different equilibrium states. A) Neutral equilibrium, B) Unstable Equilibrium, C) Stable Equilibrium and D) Metastable Equilibrium (Thorn and Welford, 1994, © by American Association of Geographers, reprinted by permission of Informa UK Limited, trading as Taylor & Francis Group, www.tandfonline.com on behalf of by American Association of Geographers.)

Equilibrium is not a stationary property and systems can move through the different types of equilibrium states during their life based on the timing and scale of disruptions to the inputs and outputs of the system

(figure 1.4).

Steady state equilibrium is very similar to dynamic equilibrium, but is usually used to refer to whole systems, whereas dynamic equilibrium is used to describe smaller spatial and temporal scales. When a system is in steady-state, the inputs and outputs of sediment are in balance, resulting in very little change to the amount of sediment being stored within the system (Trimble, 1975; Meade, 1982). However, at the smaller scale within the system there may be a dominance of either the erosive or resisting forces.

Steady-state systems are very rare in the natural environment because when inputs of sediment start to increase, there is rarely a corresponding increase in the carrying capacity of the river to remove the sediment, and so the amount of sediment in storage begins to increase (Phillips and Slattery, 2006). This results in morphological changes as the sediment is deposited into storage areas throughout the catchment (Meade, 1982), as well as changes to habitat variability, flood risk and recreation.

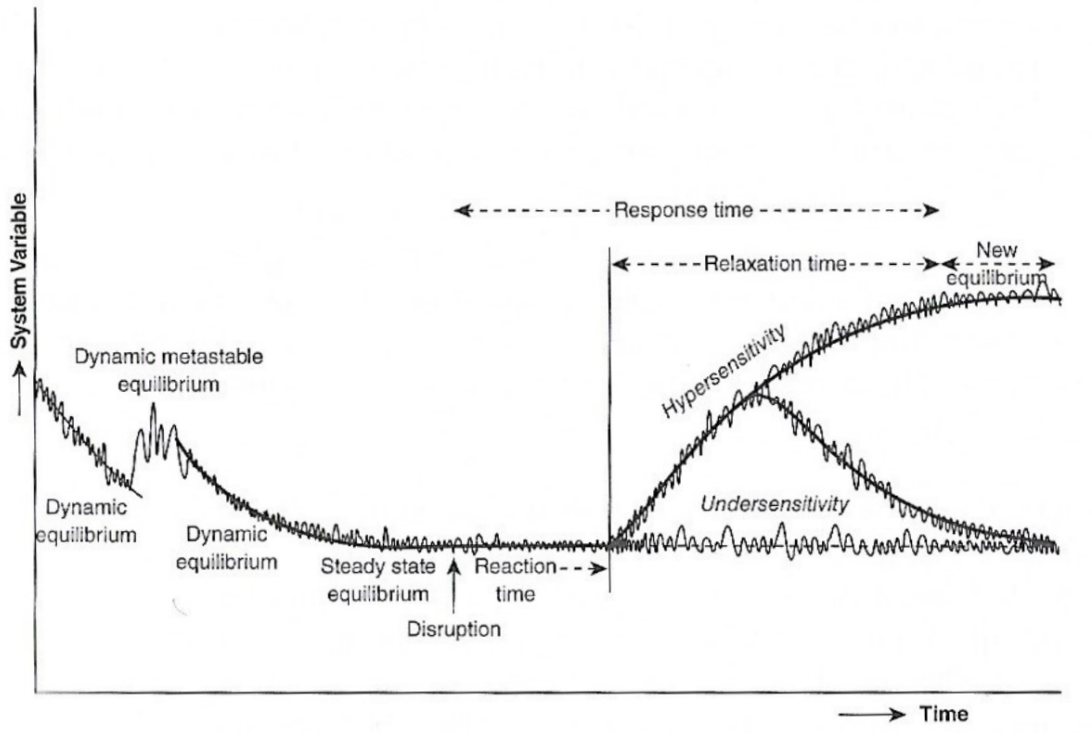

Figure 1.4: Diagrammatic representation of the types of equilibrium a system may experience over time (Gregory and Lewin, 2014)

Lane (1955) observed that equilibrium in fluvial geomorphology was usually associated with a channel reaching a state where the channel velocity is such that the stream can carry the sediment supplied by the catchment - no more, no less.

Lane's Stability Concept presents the expression in equation 1.1.

$$Q_s \, d \, \alpha \, Q_w \, S \tag{1.1}$$

Where Q_s is the sediment quantity, d is the size of the sediment (particle diameter), Q_w is the discharge of the stream and S is the slope of the stream. If these things remain in balance the stream will remain 'stable', i.e. neither erosion nor deposition process will dominate.

However, the challenge of equilibrium in fluvial geomorphology is that true

equilibrium will only be present for moments at a time, because variations in the supply of both water and sediment to the stream change with environmental, meteorological and human induced conditions.

In part as a result of the belief that a healthy river is one in equilibrium, riverbank erosion has historically been considered as an undesirable process, threatening riparian land, channel stability, river structures and increasing flood risk (Piégay et al., 2005). However bank erosion processes are of vital importance to the health and succession of riparian vegetation and create dynamic habitats for in-stream and riparian biota (Florsheim et al., 2008).

Erosion and deposition are part of a dynamic riverscape that is constantly migrating, creating in-channel and floodplain heterogeneity in morphology, habitat and flow characteristics. A number of different conceptual models discuss and analyse the connectivity of a river channel with its banks and riparian environment (Allen et al., 2020), but all highlight the complexity of the relationships between rivers and their surrounding environment.

The 'River Continuum Concept' (RCC) of Vannote et al. (1980) attempts to describe the interactions between communities throughout the river system. The longitudinal relationships between communities see downstream assemblages making use of surplus or waste products from upstream activities. In this framework the geomorphic processes working at a channel scale provide the energy required by these functional feeding relationships. These assemblages and communities tend towards an energy equilibrium over time, with different species dominating at different times to maximise consumption of energy. Although this model focuses on the longitudinal dynamics of a stream network, the same relationships

exist in the lateral dimension - with riparian communities developing to best utilise the kinetic energy of lateral processes and to reach equilibrium with the physical environment.

Unlike the RCC, the 'Flood Pulse Concept' of Junk et al. (1989) highlights the importance of the lateral relationship between the channel and its floodplain as a result of the predictable, long-duration or the unpredictable, short-duration flood pulse. Junk et al. (1989) argues that exchange between the riparian and floodplain environment during and after flood events dominates the provision of biomass to the stream, and thus that connection between a river and it's wider landscape is a greater determiner of the productivity of a watercourse than the longitudinal delivery of material from the upstream reaches.

The "Four dimensional nature of lotic ecosystems" model defined by Ward (1989) married the RCC and flood-pulse concepts together and proposed a more complex set of interactions along four dimensions. The longitudinal dimension of the RCC, the lateral dimension of the flood-pulse concept, a vertical dimension that accounts for surface water-groundwater interactions and a final time dimension that identifies and acknowledges the complexity of these interactions over different temporal scales.

The four dimensions concept recognises that spatial and temporal heterogeneity of river ecosystems exists in all four dimensions, and thus an holistic approach must be taken towards their analysis. In particular the framework considers disturbances in any of these dimensions as forces that disrupt interaction pathways which may respond in a variety of ways to restore the system's equilibrium over short and long-term temporal scales.

In 'River Restoration in Five Dimensions', Boon (1998) highlights the im-

portance of a different set of dimensions that must be considered for the conservation and restoration of rivers. These dimensions are the conceptual, the spatial, the temporal, the technological and the presentational.

These dimensions built on earlier work by Boon et al. (1992) which, like the conceptual models mentioned earlier, incorporated the longitudinal, lateral, vertical and temporal dimensions, as well as adding the new 'conceptual' dimension. When referring to river restoration the conceptual dimension embodies the motivations and drivers for restoration - or perhaps more accurately rehabilitation, as true restoration to a natural state is unlikely to be achievable in many cases.

As the five dimension model developed, the longitudinal, lateral and vertical dimensions were incorporated into the new spatial dimension. The spatial dimension of river restoration stresses the importance of restoring and maintaining connectivity between a river and it's lateral, longitudinal and vertical environment, ensuring the exchange of material, water and biomass. The model highlights the importance of the catchment as part of planning restoration. Not to attempt to carry out restoration at a catchment scale, which is rarely possible, but instead to consider the dynamics of the wider catchment morphology when planning even reach scale restorations.

The temporal dimension stresses the importance not only of the historical perspective of previous channel position but also the importance of the geomorphological history of a channel reach. Knowledge of the morphological drivers of previous channel position and how the channel responded to such drivers is key in ensuring a channel that is stable following it's restoration.

The Boon (1998) model also proposed the 'technological' dimension and

encouraged the use of emerging technologies, such as GIS and remote sensing techniques, to help support decision making and implementation of restoration projects. Arguably, this thesis applies itself to the technological dimension by using technology to try to provide a deeper understanding of controls on river bank erosion and deposition. However, Boon's recommendations also included the comment that technology be a tool in river restoration, but that it not dominate or drive the restoration process.

Each of these conceptual models highlights the importance of the connection between a river and its surrounding landscape and clearly show the importance of a greater understanding of the physical processes that form our rivers.

1.2 River Bank Erosion Processes

The processes that result in channel change through erosion can be split into three main categories; subaerial weathering and erosion, fluvial entrainment, and mass wasting (Lawler et al., 1999; Couper and Maddock, 2001; Grove et al., 2013). These three mechanisms are intrinsically linked together, with subaerial processes working continuously above the water level, fluvial erosion removing bank material through scour below the water surface, resulting in undercutting of the bank, which triggers mass failure (Rinaldi and Darby, 2007), however the area of bank on which each process can work is dictated by fluctuating water levels and exposure to meteorological forces, making bank erosion extremely difficult to predict and model (Midgley et al., 2012) (figure 1.5).

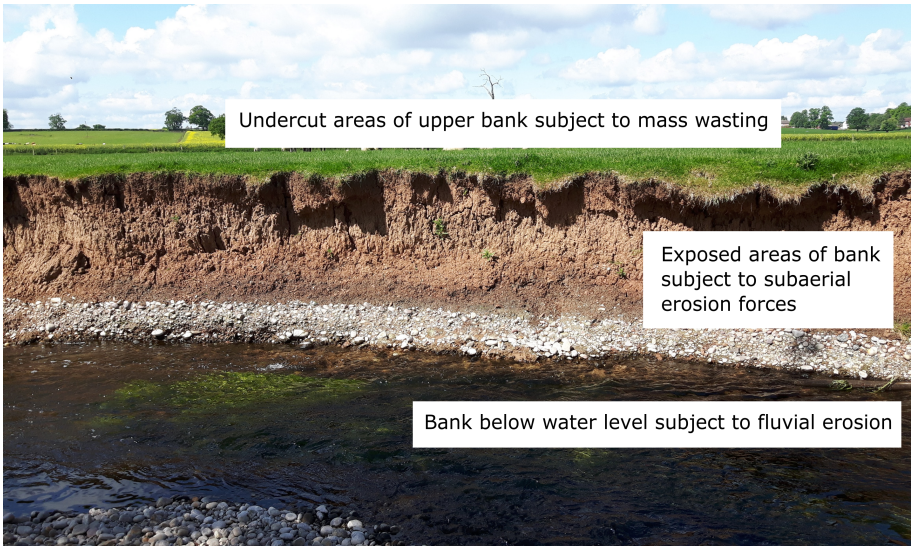

Figure 1.5: Representation of the different erosion processes at work on different sections on a river bank

1.2.1 Subaerial Erosion

Subaerial processes are described as those that act above the wetted perimeter of the channel, where the exposure to fluvial forces is limited to those times when the river is at high flow. Until recently, it has been a challenge to research the effect of subaerial processes in themselves, as partitioning them from the other two processes (fluvial erosion and mass wasting) was difficult due to the lack of precision of available measurement techniques for very small amounts of erosion.

Lawler et al. (1997) divided subaerial processes into three different categories to describe and explain the interactions between the water content of the soil and the effect on its subsequent erosion. These categories are pre-wetting, desiccation and freeze-thaw.

Pre-wetting is simply any process or action that increases the moisture content of the stream bank. This can include moisture delivered via precipitation, prolonged high flows, increased groundwater levels or ice/snow melt. As the moisture content in bank material increases, the forces that

act to maintain bank cohesion are weakened, and so the material is more susceptible to mass wasting events or entrainment through fluvial forces (Fox et al., 2007; Abidin et al., 2017). The diffuse flow of water out of riparian land via the bank face can result in seepage erosion, which can remove particles via a reduction in cohesion between individual particles and the greater soil matrix or via direct entrainment of soil particles in the ex-filtrating water (Fox and Wilson, 2010). This subsurface flow can also result in piping erosion, where preferential subsurface flow pathways are eroded into macro-pipes, which can become gullies if the roof of the pipes collapse at the surface (Faulkner, 2004). Direct erosion via raindrop impact can also occur, detaching individual particles of sediment from the surface via the transfer of energy from a raindrop landing on a surface (Kinnell, 2005).

Bank weathering and weakening can also occur through low moisture conditions, resulting in desiccation. When soil masses dry, desiccation cracks appear, breaking up the soil into a connected set of ped lumps which can be eroded when stream flow acts to break the peds off the bank through these desiccation cracks (Thorne and Tovey, 1981) or when the desiccation cracking reaches a critical point allowing for mass wasting to occur. Desiccation can also cause the erosion of individual soil particles as the cohesion between particles is lost and those at the surface can be eroded through aeolian processes or simply fall due to the effect of gravity (Grove et al., 2013).

The state in which moisture exists in the bank is also a factor in subaerial erosion. Freeze-thaw erosion has been identified as the third largest soil erosion process globally, behind water erosion and wind erosion (Zhang et al., 2007). Freeze-thaw cycles enlarge tension cracks between soil blocks making them more susceptible to mass wasting (Couper and Maddock,

2001). Needle-ice increases the pore spaces between soil particles, and thus reduces their cohesion, making them susceptible to fluvial erosion or to mass wasting. The action of thawing again reduces the cohesion between soil particles by increasing pore pressure, before freezing again and further expanding lines of weakness (Wolman, 1959).

The combined influence of these different factors can increase the rate at which mass wasting and fluvial erosion processes occur by weakening material and making it more readily available for removal by flow. However, they also result in the continuous loss of small quantities of material throughout the exposed bank area between high flow or mass wasting events and therefore can and should be considered as significant erosion processes in their own right.

1.2.2 Mass Wasting Erosion

Mass failure, or mass wasting, is caused when cohesion between bank materials is weakened or when supporting materials are removed, allowing for a mass of material to detach from the bank and move in one single event (Parker et al., 2008). Riverbank material can collapse via a number of different mechanisms and at different speeds depending on the size of the material, the moisture content and the angle of collapse. Examples of these can be seen in figure 1.6 taken from Nardi et al. (2012).

The most frequently observed type of mass failure on riverbanks is that of cantilever failure (Samadi et al., 2011). Cantilever failure can occur in three ways; 1) shear failure is the vertical failure of a block of material down a vertical surface along a lateral line of descent, 2) tensile failure is the failure of a block of material through detachment from its upper horizontal face under tensile stress, 3) beam failure is the toppling of the failing material, detached by either shear or tensile stress (figure 1.6 B1,

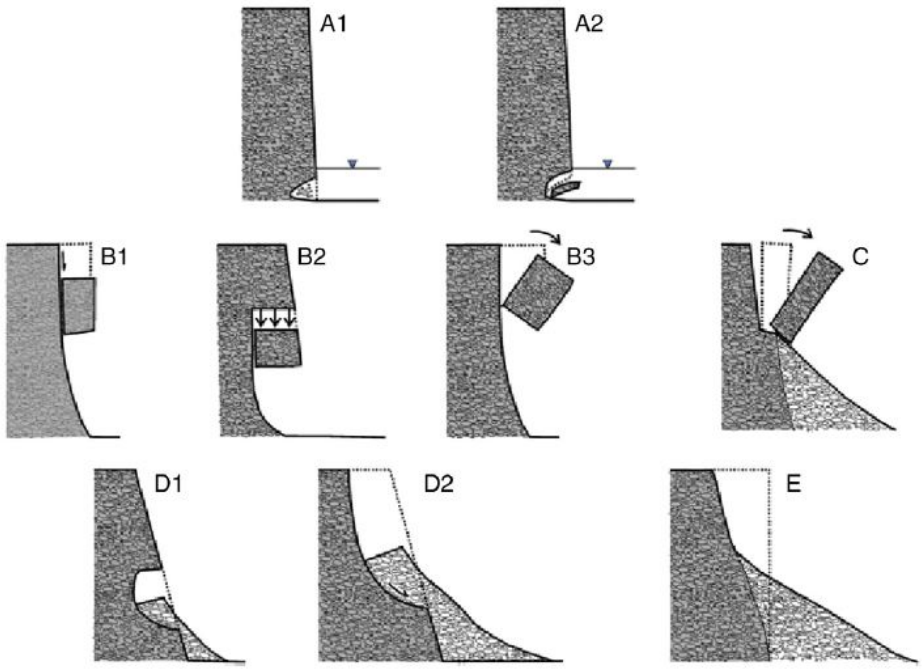

Figure 1.6: Riverbank mass failure mechanisms. A1 and 2 represent the loss of material through a loss of particle cohesion due to saturation of soil pore spaces. B1-3 represent the three different cantilever failures, shear, tensile and beam respectively. C is slab failure. D1 and 2 depict small scale (D1) and larger scale (D2) slide failures and E represents flow failures (Nardi et al., 2012)

B2 and B3 respectively).

Cantilever failure occurs in four stages (Patsinghasanee et al., 2017). First is fluvial erosion and the removal of material at the bottom of bank. Second is the formation and subsequent development of tension cracks between the unsupported block and the stable bank. Third is the failure of the block from the stable bank. The fourth and final stage is the subsequent removal of the failed material from the lower bank. The timescales for these different stages of the process can be highly variable depending on factors such as the soil moisture conditions, bank vegetation and the flow conditions (Arnez Ferrel et al., 2018).

Slab failures (figure 1.6 C) can be difficult to partition out from cantilever beam failures as they exhibit a similar topple style collapse, however they are identified by failure brought on not by undercutting but through a re-

duction of the cohesion between the block of material and its corresponding face due to cracks or fissures in the soil material (Patsinghasanee et al., 2017). These cracks are usually caused by freeze-thaw or desiccation processes within the soil of the upper portions of the bank.

Slides occur where material fails along a clearly defined shear surface (figure 1.6 D1 and D2). The material then moves as a cohesive mass and settles at the base of the bank, leaving behind a defined shear face, and a semi-mobile mass of material at the failure toe. Flow failures occur where material movement occurs without a clearly defined shear plane (figure 1.6 E). This is usually in material that has a very high moisture content.

1.2.3 Fluvial Erosion

Fluvial erosion is the process of in stream flow removing bank material. Entrainment begins when the force of the water on the bank material exceeds the forces holding the material in place. The lower the cohesion of the bank material or the higher the rate of flow, the more likely the material will be eroded by the streamflow (Julian and Torres, 2006). The mechanisms by which sediment can be entrained into rivers are well understood and can be broken down into three categories; lift, surface drag and form drag.

Lift is generated by differences in pressure below and above the particle causing it to be sucked into the flow. Surface drag, or skin drag, is essentially its shear stress (or the stress applied to a surface parallel to its position) while form drag is the pressure difference between upstream and downstream sides of the particle as a result of the shape of its stream-wise cross-section (Van Rijn et al., 1993). The stream must be flowing at a critical erosion velocity in order to generate the appropriate forces to entrain

particles. Once a sediment particle has been entrained into the stream it can move in a number of different ways until it is redeposited elsewhere.

The rate of bank erosion at the toe of the bank is widely accepted to be the dominant factor affecting the rate of long term bank retreat, creating the instabilities that allow for gravitationally activated mass wasting events by removing the underlying, supportive material (Thorne and Tovey, 1981).

The rate of hydraulic bank erosion has most commonly been calculated using an excess shear stress formulae, such as Partheniades (1965);

$$\epsilon = k(\tau_{sf} - \tau_c)^{\alpha}$$

where ϵ is the rate of erosion per area per unit time (e.g. m/y), k is the erosion coefficient, τ_{sf} is the skin drag component of boundary shear stress (Pa), τ_c is the critical shear stress and α is usually equal to 1 in bank erosion studies.

Excess shear stress models such as this have been used frequently and in multiple different geomorphological applications since their conception (e.g. Zhang et al. (1998), Simon et al. (2003), Rinaldi and Darby (2007), and Arnez Ferrel et al. (2018). However, their relative mathematical simplicity is undone by the difficulties that arise when trying to accurately estimate the parameters controlling the erosion, e.g. the skin drag. This is largely due to the high variability that exists in natural rivers and their bank materials.

This difficulty could be overcome if a reliable measurement of surface roughness can be used to partition out the skin drag components of shear stress (Darby et al., 2010). Through numerical models created by Kean and Smith (2006a) and Kean and Smith (2006b) it is possible to ascertain

the skin drag component of shear stress by using topographic modelling of the surface of interest. This topographic model, a representation of form roughness, can then be measured against subsequent change to help to ascertain the localised effect on erosion.

1.3 Measuring River Bank Erosion

1.3.1 Erosion measurement techniques - A brief history

Observing and recording change on the Earth's surface is a crucial part of the science of Geomorphology. The wide variety of different techniques that have been developed to measure channel change is reflective of the wide variety of different river environments that exist, and the complexity of the challenges facing geomorphologists to measure change in such environments. The tools and techniques used to measure such change have taken huge strides forward in the last 30 years thanks to the increasing development of remote sensing techniques (Brandt, 2000; Lu et al., 2004; Bangen et al., 2014; Duró et al., 2020b).

The choice of what techniques to use is based on a number of factors, including, but not limited to, the spatial scale of the study, available computing power and cost. Many of the existing manual measurement techniques have been in use for decades, their longevity down to their suitability for a variety of environments and study types.

Planimetric resurveying is the process of establishing the horizontal positions of different features within a study area. This technique was being employed as early as 1895 to observe the change in river position within a landscape. Allen (1895) recorded erosion rates upwards of 6.0m per year along the chosen study reaches in Iowa, USA. However, while this technique allows for the identification of channel movement within its land-

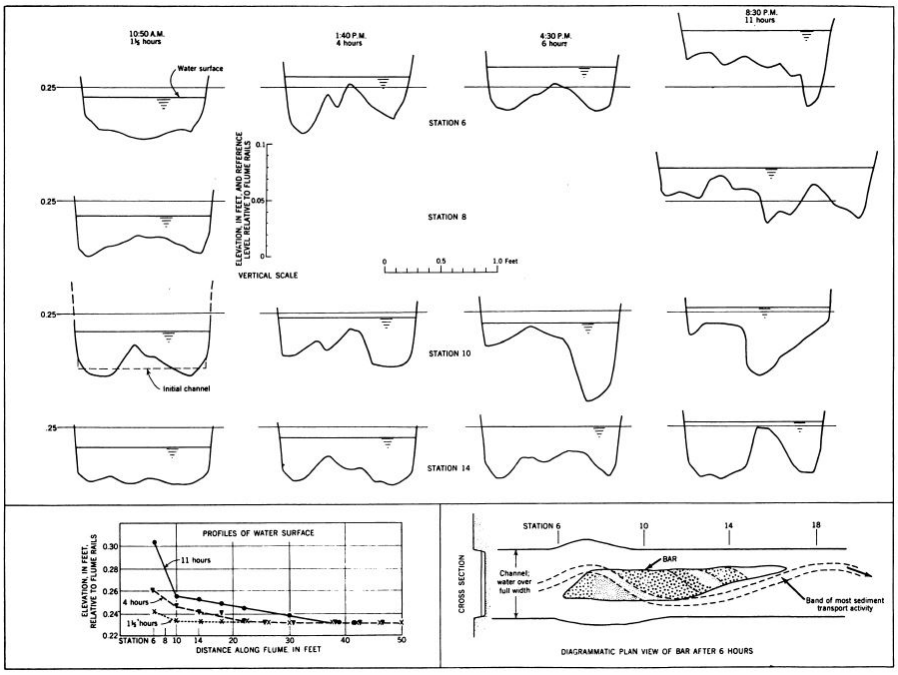

Figure 1.7: An example of the repeat cross profiling conducted by Leopold and Wolman (1957) to understand the evolution of channel pattern

scape over time scales of months - years, it provides very little information on the processes of erosion that are driving such change.

Repeated cross-profiling, the process of generating detailed cross-sections of the river channel using survey levels, was adopted significantly for the first time by Leopold and Wolman (1957). They made use of repeat cross-sections to understand the features and evolution of meandering, braided and straight river channels by cross-profiling a flume-channel at a number of different time periods. They combined their flume data with planimetric surveying of field sites to better understand the development of channels from braided to straight forms. An example of the profiles generate by Leopold and Wolman can be seen in figure 1.7.

Although this technique developed in flumes, Wolman (1959) went on to use repeat cross profiling on the Watts Branch, Maryland USA. These profiles allowed not only the retreat of the top of bank to be measured, but also the positions of the full bank profile and in channel features such as bars.

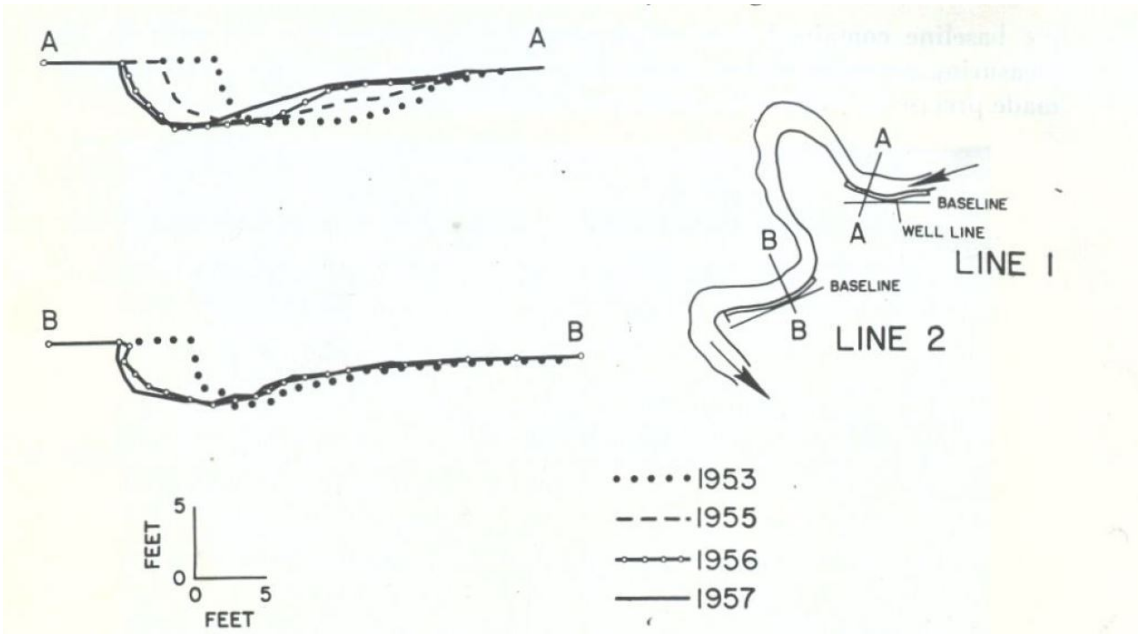

Figure 1.8: An example of the repeat cross profiling conducted by Wolman (1959) to understand the change in bank form along the Watts Branch, Maryland, USA

Cross profiling in wadeable streams also allowed for the bed position to be established, allowing changes to the location of the thalweg to be recorded for the first time. An example of Wolman (1959) cross-profile results can be seen in figure 1.8. Despite the advances that repeat cross-profiling allowed, there are limitations to the method. Linear cross-sections take account of the bank at specific positions, but do not record the spaces in between thus creating a spatially discontinuous dataset that does not represent the full picture of the changes that are occurring. Cross-profiling is also very challenging to apply on steep or vertical banks and areas of undercutting, meaning that banks exhibiting these structures cannot be accurately measured or represented.

Wolman (1959) was also a pioneer in the use of erosion pins, choosing to supersede the use of repeat cross profiling when difficulties relating to overhanging vegetation and recording changes at smaller timescales promoted a rethink of the experimental approach. Erosion pins are long, thin lengths of metal that are inserted horizontally into the bank face,

usually as part of a network of pins. Once inserted into the bank the exposed length of the pin is measured, usually using calipers for high accuracy. The pins are then left in the bank for a period of time before the exposed length is measured again. If there is an increase in the exposed length then erosion has occurred. If there is a decrease then deposition is deemed to have occurred.

Wolman's work on the Watts Branch was among the first to use erosion pins to measure river bank erosion. This work drew on the approach of Ireland et al. (1939) who used wooden stakes hammered into the ground to measure the upslope advancement of cutting heads of gullies on farmland to understand the effect of land use on the rate of gully erosion and to quantify the loss of soil through this gullying. Wolman (1959) refined the Ireland et al. (1939) approach by using thin metal rods in place of Ireland's wooden stakes. The use of erosion pins allowed for the spatial spread of erosion across a bank face to be recorded for the first time, providing some of the earliest insights into the spatial and temporal variation in bank erosion.

Erosion pins became one of the primary techniques for measuring bank erosion for the following decades, with numerous studies still making use of erosion pins today (Vietz et al., 2018; Myers et al., 2019; Kuznetsova et al., 2019; Kiosses et al., 2020). The collection of erosion pin data involves very little financial cost and they are suitable for a variety of different river bank environments. They are also simple to maintain, recording data requires little specialist knowledge and the data itself requires little post processing (Myers et al., 2019).

However, accounting for spatial variability across the bank is very difficult and they can themselves exacerbate local erosion through destabilisation

of the bank directly around the pin (Lawler, 1993) or by creating cracks in the bank face that result in greater erosion. If placed too closely together they can also act to bind the bank material, particularly in banks that are heavy in clay sediments, thus decreasing the susceptibility of the bank to erosion and artificially altering the rate of change on such surfaces. There is also some discussion around the occurrence of negative erosion pin values and whether they can truly be deemed to represent deposition or are endemic of pin disturbance, bank swelling around the pin or possible other factors (Couper et al., 2002).

An advance on the erosion pin technique was proposed by Lawler (1991) with the Photo-Electronic Erosion Pin or PEEP (figure 1.9). The PEEP system uses a clear plastic cylinder filled with photovoltaic cells connected in series. This cylinder is inserted into the bank like an erosion pin, but must be connected to a data logger to record the output of the cells. As the PEEP is exposed to more sunlight (through erosion of the bank material covering it), the energy output will be increased. Any deposition will result in a decrease in energy output. A control pin positioned somewhere above the bank surface can be used to measure the incident illumination conditions and this account for changes in the light reaching the cells due to diurnal cycles, cloud cover and temporary shading, thus creating a quasi-continuous measure of erosion.

Issues related to diurnal cycles and submersion reducing the amount of light reaching the sensor were largely overcome by the PEEP-3T system (Lawler, 2008) which makes use of a thermistor to aid in understanding the thermal regime of the soil and, in combination with the photo-voltaic cells, to provide better accounting of erosion during periods of low illumination.

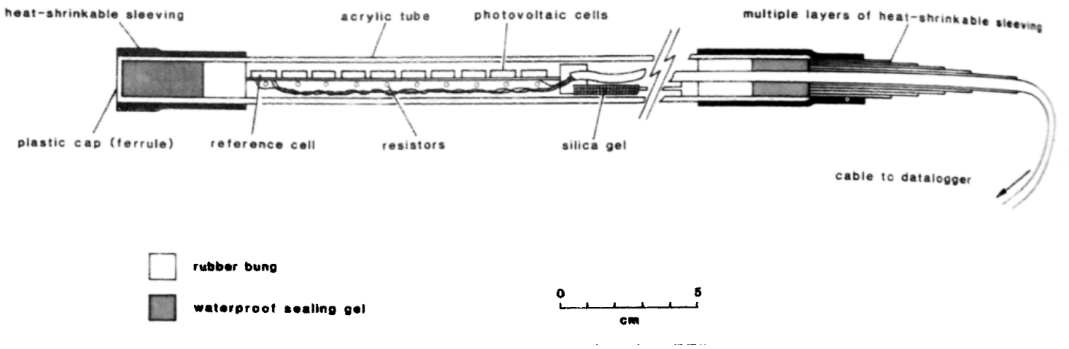

Figure 1.9: Schematic diagram of the Photo-Electronic Erosion Pin (PEEP) (Lawler, 1991)

The PEEP system is one of the few techniques that provides a near continuous record of erosion, however is it subject to all of the limitations of traditional erosion pins. There are also additional limitations, such as the need for the sensor to be attached to a data-logger. This makes the installation of such pins more complex and limiting the potential locations the technique can be applied at due to concerns such as interference with the logger or complications due to inundation. This can also mean that only a limited number of PEEP sensors can be installed in a bank, relying on additional measures to observe a greater spatial area. The PEEPs are also larger than a traditional erosion pin, which can simply be inserted into the bank by pushing or using a hammer. The PEEP systems requires a small hole to be bored in order to fit the pin in without damaging it, which in and of itself can cause weakening of the river bank and impact on the rate of erosion.

As a result of the limitations associated with historic techniques for measuring erosion, recent years have seen the proliferation of remote sensing techniques over survey or pin based measurements and some of these techniques will be reviewed in the next section.

1.3.2 Remote Sensing in the Fluvial Environment

Remote sensing is the science of obtaining information about a surface of interest from a distance (National Oceanic and Atmosperic Association, 2019). That surface can be a single tree or river unit or it can be the entire surface of the planet. The distance can be centimeters up to many hundreds of kilometers. Even simple photography is a form of remote sensing, capturing information about a surface without the need to interact with it.

There are many different types of remote sensing techniques, from ground based terrestrial laser scanning (TLS) to airborne techniques such as airborne photogrammetry (UAV photogrammetry), airborne laser scanning (ALS) and up to satellite sensors such as Landsat and Sentinel. The temporal, spatial, spectral and radiometric resolutions of these different techniques vary considerably, as does their cost and the ease with which data can be analysed. There is no 'one size fits all' technique for measuring river systems, so the technique must be chosen following consideration of both the needs and logistical limitations of the research.

Mapping of the land using photographs has been undertaken since the invention of the camera, and it's military advantages have been understood since the First World War (Avery, 1962). The use of aerial photographs to measure or describe the landscape flourished throughout numerous fields. The 1960s and 1970s saw the emergence of multi spectral data that could be collected across large scales through airborne platforms, and these techniques opened up the ability to conduct analysis of numerous different features of the hydrological environment, e.g. updates of navigation charts to identify shallowing waters (Polcyn and Rollin, 1969), mapping of landscape features (Lausch, 1970), and urbanisation (Tsouch-

laraki and Achilleos, 1970).

Satellite, airborne and terrestrial remote sensing platforms are now capable of providing suitable data for creating 3D models of target environments that can be manipulated and measured to a very high degree of accuracy. These technologies are also increasingly being used to identify and measure features of the fluvial environment such as catchment land cover (Weng, 2002), run-off calculations (Immerzeel et al., 2009), habitat characterisation (Tamminga et al., 2015), and edge erosion of wetland features such as marshes (Huff et al., 2019). There has also been recent surge in the use of remote sensing to identify hydrological features of rivers, such as fluvial topography (Woodget et al., 2015) and surface flow velocity (Lewis et al. 2018).

Remote sensing of the fluvial environment has a number of key benefits over more traditional techniques; such as repeat surveying (Leopold and Wolman, 1957), erosion pins (e.g. Hooke (1979), Couper and Maddock (2001), Couper et al. (2002), Couper (2003), and Kuznetsova et al. (2019)) and PEEP techniques (e.g. Lawler (1991), Lawler (2008), Zaimes et al. (2019), and Sutarto et al. (2020)). One of these key benefits is that of data coverage. For example, erosion pins became widely used following Wolman's (1959) research into erosion rates of the Watts Branch River in Maryland (USA). This study used pins set at 1m above the channel bed at 1.5m intervals laterally down the channel. Subsequent papers have used a much denser network of pins, such as Kuznetsova et al. (2019), who placed a network of pins across 6 different sites with distances between pins of between 0.20-0.60m depending on the bank material. The nature of erosion pins require large spaces between them to reduce the likelihood of destabilising large blocks of the bank material, and thus their spatial resolution is very low, with a maximum of 36 points per square

meter (based on a grid spacing of 20cm). Now consider current trends in TLS and Photogrammetry techniques, where data can be collected with 10,000 points per square meter (Heritage and Milan, 2009) or more, and the advantages of remote sensing technologies for high resolution change detection become ever clearer.

The technique chosen for any research of the fluvial environment should be decided with care, focused on the spatial and temporal scale over which the study is interested. The suitability of different techniques and platforms for data collection has been discussed through numerous reviews in recent years (e.g. Lu et al. (2004) and Tomsett and Leyland (2019); and has been summed up to good effect in figure 1.10, taken from Tomsett and Leyland, 2019.

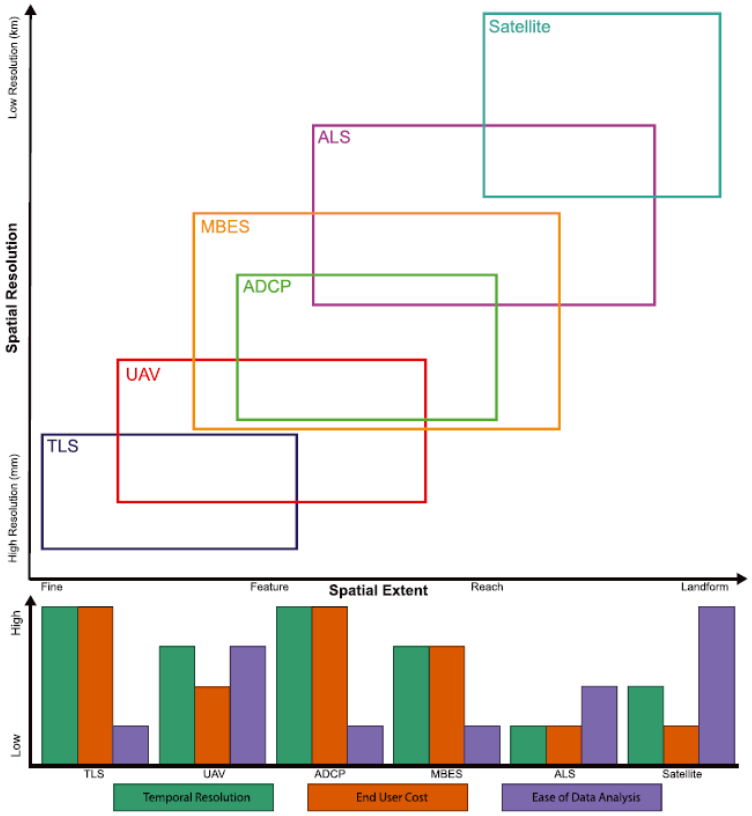

Figure 1.10: Resolution of different platforms for remotes sensing (Tomsett and Leyland, 2019)

The first use of a remote sensing technique for the detection of river bank erosion was that of terrestrial photogrammetry, or the use of cameras positioned in known locations taking images of a bank containing targets for alignment purposes. The earliest studies of this type were carried out by Painter et al. (1974), who used terrestrial photogrammetry to establish river bank erosion to better understand sediment loads in afforested catchments within the UK. Although the Painter paper does not provide details of the experimental setup, Lawler (1993) provided a summary diagram of the setup required for quality data acquisition, which can be seen in figure 1.11. Since then satellite data, photogrammetry, airborne LiDAR and Terrestrial Laser Scanning have all become prevalent in the field of bank erosion monitoring (Bangen et al., 2014; Lague, 2020).

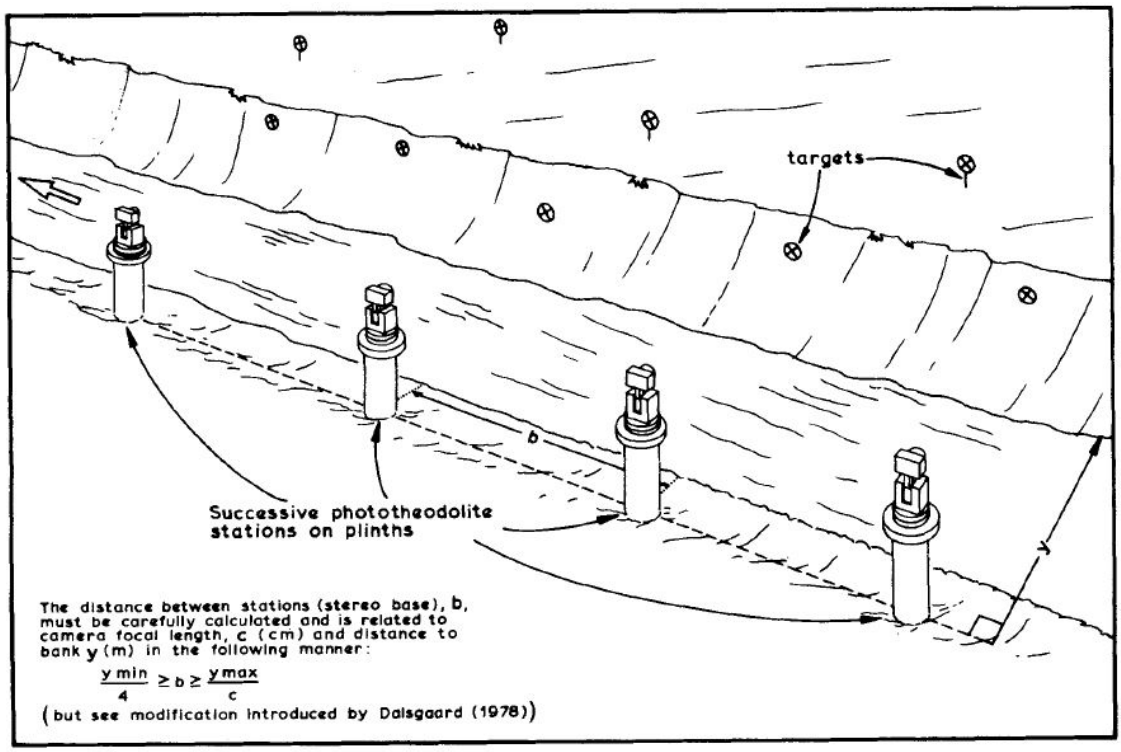

Figure 1.11: An example of the set up required to generate terrestrial photogrammetry data during the early days of the technique being adopted from Lawler (1993)

Satellite data has become a valuable tool for measuring river erosion due

to its ability to provide detailed and accurate information on a large scale. Remote sensing techniques, such as Synthetic Aperture Radar (SAR), Interferometric SAR (InSAR), and Optical imagery (Landsat and Sentinel), can be used to detect and monitor changes in river channels and banks over time.

Langat et al. (2019) used a combination of Landsat data and Aerial Photography to measure channel change on the Tana River, Kenya from 1975 to 2017. They were able to successfully identify catchment scale changes in the channel morphology. River channels were digitised using GIS and then compared across the years to measure the accretion, degradation and meandering of the river as shown in figure 1.12.

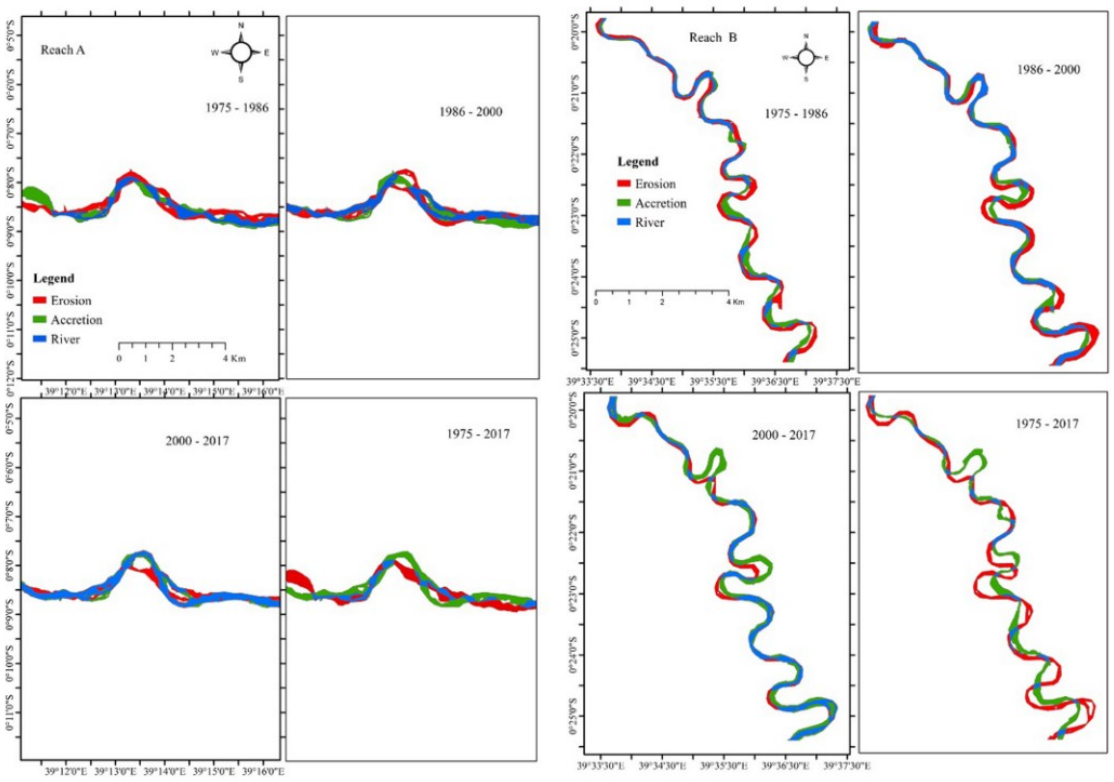

Figure 1.12: Results of Langat et al. (2019) channel change along the Tana River, Kenya, measured using Landsat data

Langat et al. (2019) found that the use of Landsat data allowed for an analysis of channel pattern changes over temporal and spatial scales that

would have been impossible to do with field data for reasons of time and spatial coverage. However, they did identify issues with identifying change below half a pixel, which for Landsat images acquired since the 1980s has meant that change below 15m is difficult to identify. However, such limitations are counterbalanced by the ease with which the data can be accessed and processed.

SAR data was used by Devrani et al. (2022) to identify flood inundation along the Ganga-Brahmaputra, in the Assam region of India. Again, the large scale of the study and the potential risks of carrying out field surveying during flood conditions meant that satellite data was the most suitable option for this study. The authors acquired Sentinel SAR 1 GRD data for 2018 - 2020 and used a combination of additional datasets, including Shuttle Radar Topography Mission (SRTM) drived DEMs of the study area, to identify the locations that would be inundated during a flood event. Identifying inundation areas and potential flow pathways through a landscape helps hydrologists and geomorphologists identify potential risks to infrastructure, agricultural land and the populations that may live in at risk regions, and satellite data allows large areas to be assessed in a timely manner to support policy making and management strategies.

Overall, satellite data provides a powerful tool for observing and measuring many attributes of rivers at the catchment and even the national scale, however there are limitations around its utility when looking at small or medium sized rivers, where changes are likely to be smaller than the minimum levels of detection for these low resolution datasets.

To help combat some of the scale issues when working with satellite data, airborne data collection methods have become prevalent in the study of reach to feature scale analyses. Airborne LiDAR data has been used to

evaluate rivers in many different contexts including mapping channel bed forms using green wavelength Airborne Lidar Bathymetry (ALB) (Saylam et al., 2020), monitoring erosion along large reaches of rivers in different environments (Rhoades et al., 2009; De Rose and Basher, 2011; Kessler et al., 2012; Kessler et al., 2013) and the identification of erosion hazards in rivers (Gutierrez et al., 2001; Joyce et al., 2014; Wang et al., 2016), to name but a few.

Thanks to the high resolution ($\sim$1m) of these datasets compared to their satellite counterparts, LiDAR techniques can be successfully applied anywhere from the catchment to the reach scale. The ability to filter the Digital Surface Models (DSM), which include vegetation, buildings and other surface features, to create bare earth Digital Terrain Models (DTM) means that it is possible to determine the topography of the flood plain at high levels of accuracy.

However, there are some limitations to the use of airborne LiDAR data. The low scanning angle and the potential shadowing effect of overhanging banks can cause underestimation of channel depth and bank height (Cavalli and Tarolli, 2011). This problem can be overcome with the use of Terrestrial Laser Scanning.

1.3.3 Terrestrial laser scanning in River Science

Like airborne LiDAR, Terrestrial Laser Scanners use pulses of laser light and time of flight calculations to determine the location of a surface (figure 1.13) and record that measurement as a point within a virtual 3-dimensional space, as an xyz coordinate known as a point cloud (Otepka et al., 2013; Koehl et al., 2020; Alexiou et al., 2021).

TLS has some significant advantages over airborne LiDAR, including its greater point densities, greater mobility and faster implementation (i.e.

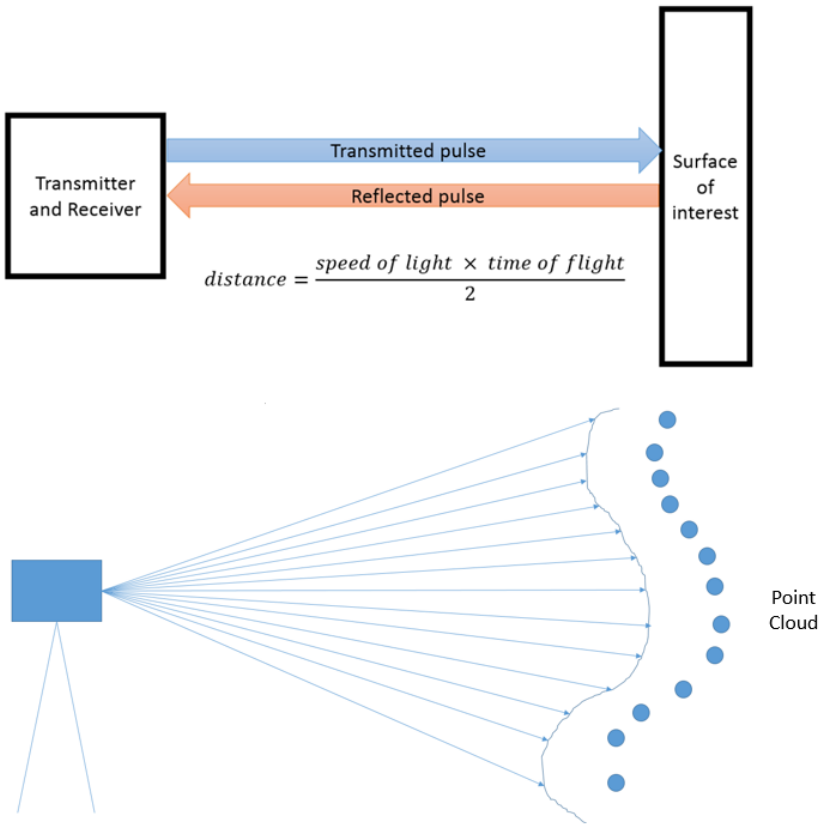

Figure 1.13: Overview of the data collection mechanism for terrestrial laser scannning

can react to a specific event almost immediately without the need to charter a flight, arrange flight paths or obtain flight approvals). Where TLS truly comes into it's own is in the observation of vertical or over-vertical surfaces (such as cliff faces, river banks etc) which would not be observed using airborne LiDAR (Young et al., 2010).

Chandler et al. (2002) stated that emerging TLS techniques "offer(s) potential, but the technology is currently prohibitively expensive and is not ideally suited to the rigours of fieldwork" (p632). However, since that time the technology has become more affordable and more rugged so that it can be effectively utilised in a variety of field environments. The wider availability of TLS equipment and the spatial resolution advantages have

resulted in an increasing number of researchers utilising TLS in studies of rivers and bank erosion.

A search of the Web of Science database for the terms "Terrestrial Laser Scanning" and "Rivers" generated almost 300 results between 2005 and 2022, with a clear increase in the number of studies utilising these methods over the last 17 years (figure 1.14). The increased prevalence of TLS studies prompted Heritage and Hetherington (2007) to develop a protocol for gathering laser scanning data which has been adopted by many authors working in the fluvial environment (e.g. Heritage and Milan (2009), Wheaton et al. (2010), Darby et al. (2010), Eitel et al. (2011), and Woodget et al. (2014)).

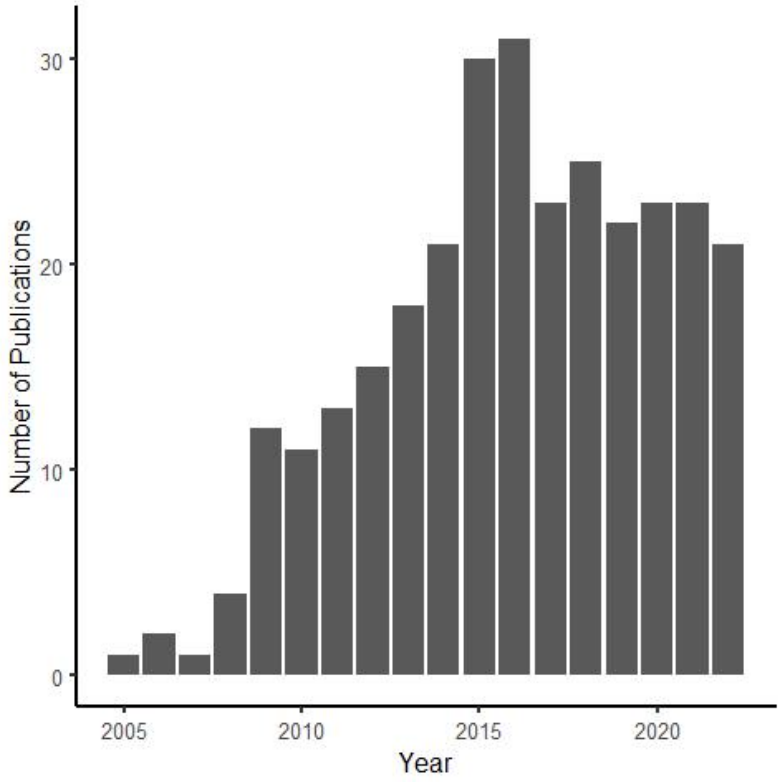

Figure 1.14: Number of publications containing the keywords "Terrestrial Laser Scanning" and "Rivers" according to a Web of Science database search

1.4 Motivation, Aims and Objectives

1.4.1 Motivation

As highlighted earlier in the chapter, understanding riverbank erosion is critical for the management of our rivers and to ensure the long-term health of our fluvial environments. It is important to understand rates of erosion, dominant erosion processes and the temporal and spatial variations impacting erosion, as erosion of channel bed and banks delivers significant quantities of sediment to our rivers. This sediment is a threat to our habitats, flood risk management capability and our infrastructure, so it is ever more vital be able to quantify, model and predict bank erosion, particularly under the increasing pressure caused by climate change.

Sub-aerial erosion can be treated as a preparatory process, weakening the bank material and lowering the critical threshold needed for fluvial erosion processes to work (Prosser et al., 2000; Julian and Torres, 2006). The action of those sub-aerial processes not only weakens the bank material, but also changes the roughness of the remaining surface, influencing the amount of skin drag that surface will exert on the flow. This has been identified as a possible controlling factor on the rate of fluvial erosion. However, sub-aerial erosion is also responsible for the removal of significant quantities of material in its own right.

The ability to partition out the significance of the different erosion processes – sub-aerial, fluvial and mass wasting – and to determine the influence of the different conditions responsible for the most significant change to surface roughness due to sub-aerial conditions such as freeze-thaw and wetting and drying has been limited by the spatial and temporal resolution at which morphological data could be collected.

Remote sensing is concerned with the obtaining of information about an object or area without direct physical interaction (Campbell and Wynne, 2011; National Oceanic and Atmosperic Association, 2019). Many remote sensing techniques allow for the collection of data on surface change at extremely high spatial resolutions ($\pm$5mm) and to collect those data rapidly and repeatedly. This is a significant improvement on the most widely used methods of previous decades, where erosion pins and PEEP techniques provided a much lower spatial resolution ($\pm$10cm) and could only provide details on comparatively large volumes of change due to the potential for error in the measurements (Lawler et al., 1999; Couper and Maddock, 2001; Couper et al., 2002). These much higher spatial resolutions also allow for data to be collected more regularly, as even small changes can be detected with a relatively high degree of accuracy. This provides the ability to monitor change not only at high spatial resolutions, but also at high temporal resolutions.

The advances that have been made in remote sensing techniques in recent years mean we are now in a position to analyse the specific influences of different meteorological and hydrological conditions, and determine their short and medium term effects on erosion rates. This research will make use of very high-resolution spatial data over a relatively short time scale to develop a deeper understanding of the processes that result in bank change, with focus on identifying the processes at work and the scales at which those processes are working.

1.4.2 Research Aims and Objectives

The overall aim of this research is;

To use very-high-resolution remote sensing and change detection analysis to increase our understanding of the evolution of riverbank erosion

processes and what role bank roughness plays in those processes.

This will be achieved through three main objectives;

1. To assess the relative importance of the three main erosion processes (sub-aerial, fluvial and mass-wasting) on the evolution of river bank surfaces (Chapter Three)
2. To identify what conditions are responsible for the most significant amounts of bank change related to each of the three erosion processes (Chapter Four)
3. To identify to what extent bank roughness influences the rate of fluvial erosion (Chapter Five)

These objectives can be achieved through the application of the methods listed below, each of which will be expanded upon within Chapter Two – Methods;

1. To collect repeated, very-high resolution topographic data of river-bank surfaces using a Terrestrial Laser Scanner.
2. To perform change detection showing the areas of the bank that are subject to most significant change and identify the dominant erosional process by which that change occurred.
3. To collect continuous river level, rainfall and surface temperature data from the study site and to use these data to identify the conditions responsible for the most significant quantities of different erosion processes between different surveys.
4. To quantify the roughness of different areas of the river bank surface.
5. To identify whether bank roughness has an influence on the rate of subsequent erosion via fluvial erosion processes.

1.5 Thesis Structure

This thesis has a 'non-conventional' structure due to the progressive nature of the work being carried out. Each successive results chapter builds on the outcomes of the previous chapter thus defining the direction of the work and therefore of the questions posed. As a result of this approach, this thesis does not contain a standalone literature review chapter. Instead, the literature review has been incorporated into this slightly longer than standard introduction chapter and into the introductions of the three results chapters to provide background and context to each of the three main aims of the study as they build upon one another. The outcome of this decision is a thesis structured into six chapters as shown in Figure 1.15.

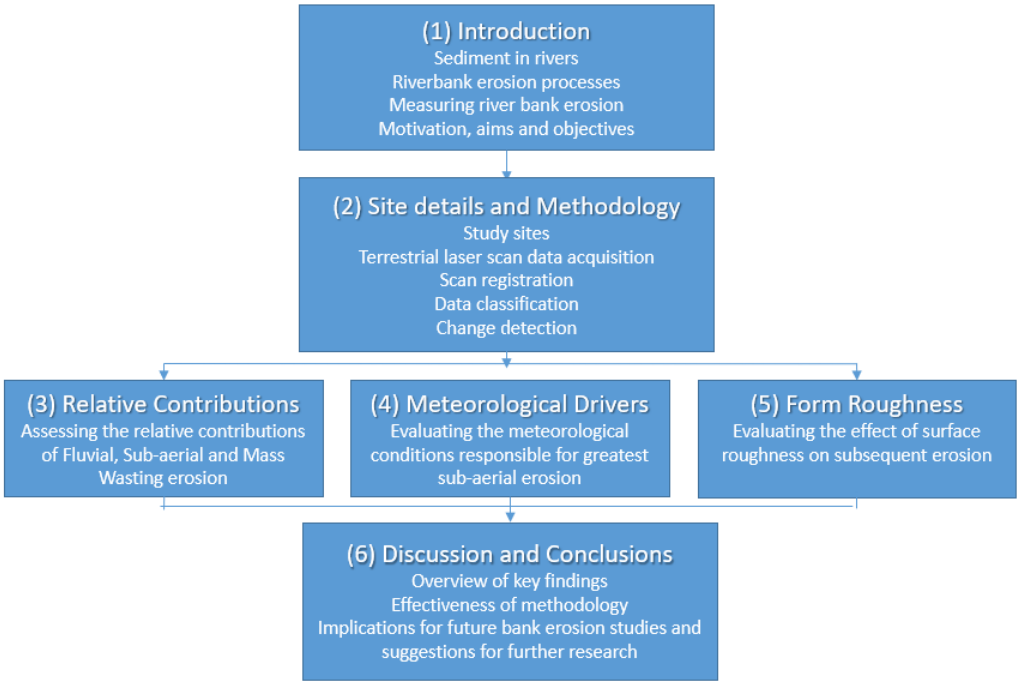

Figure 1.15: Overview of thesis structure

This introductory chapter has provided the background and wider context for the research, as well as information for why work of this kind is important, not only to fluvial scientists, but also to the wider populations that rely on rivers, directly or indirectly, in their daily lives. It has also introduced the key bank erosion processes acting on river banks. The introductory chapter has also provided some information on the methods by which bank erosion has been studied in the past and how contemporary technologies and techniques are poised to progress research in this field.

As this thesis does not contain a separate literature review chapter this introductory chapter is longer than might normally be expected in order to provide the background needed to understand the wider study. The individual results chapters contain a literature review section to provide the important literature that underpins the analysis and results presented in those chapters. This structure was chosen to allow for a targeted literature review for each chapter that more directly addresses the specific aims of each results chapter.

Chapter Two - Methods - provides some background of the use of TLS in the study of bank erosion before detailing the chosen field site and its suitability for this specific study. The investigative processes undertaken to create a reliable and repeatable set of methods are then discussed and summarised. The specific methods used for each of the three results chapters will be provided within those chapters.

Chapters three to five each cover one of the three objectives used to address our final aim. They provide a more detailed review of the existing academic literature relating to that area of the research before detailing the supplementary methods unique to each individual chapter. They then provide a detailed description of the results before moving into a brief dis-

cussion and critique of those results.

These chapters will be: -

Chapter Three – An assessment of the relative contributions of fluvial, subaerial and mass wasting erosion processes on bank retreat

Chapter Four – Evaluating the influence of flow and meteorological conditions on erosion processes

Chapter Five – Evaluating the effect of bank roughness on the rate of fluvial erosion

As each results chapter builds on the one before, Chapter Six - Discussion and Conclusions - is focused on bringing together the findings of each individual results chapter and critically evaluating the methods, results and conclusions drawn during each phase of the research. It will then conclude by suggesting possible paths for future research,

1.6 Chapter Summary

This chapter has provided an introduction to the importance of riverbank erosion and the processes by which it occurs. It has also provided an overview of the techniques by which previous research has been undertaken and so gives some context for the approach undertaken in this research. This chapter also provides detail of the aims and objectives of the research, as well as a detailed overview of the structure of this thesis and the questions being addressed within each chapter.

As defined earlier, a more detailed and specific literature review will be provided within each results chapter. Thus Chapter 2 provides details of the methods used to collect the very high-resolution TLS data that underpins all of the analysis throughout the results chapters.

Chapter 2

Methods

This chapter begins with an overview of Terrestrial Laser Scanning as a technique for monitoring river banks before introducing the primary study area and its catchment characteristics. It then details the individual river bank sites on which the research was conducted. It then moves on to discuss the six methods that were introduced in chapter 1 and that are common to all three of the results chapters, including the initial collection of Terrestrial Laser Scan (TLS) data, repeat survey methods, data registration and export, data classification and change detection.

2.1 Terrestrial Laser Scanning of River Banks

As introduced in the first chapter, TLS has become a valuable tool in the generation of high to very high resolution models of river banks for the purposes of mapping bank erosion and channel change. Alongside the developments in scanner capability, improvements in the technologies and techniques used for processing of TLS data have allowed us to interpret, compare and measure such data, to ensure that the techniques are reliable, accurate and repeatable. Collection of high-resolution point clouds using the TLS is relatively simple, with the biggest challenges coming from

the need for highly accurate surveying of scanner and target positions.

Light from the scanner travels in a straight line and so locations where the surface has a complex shape could be subject to occlusion. This is where the laser pulse cannot see through something that is blocking its view to other areas of the surface of interest. In any instance where the surface of interest has some complexity (almost always the case when surveying the natural environment), it is advisable to scan the surface of interest from multiple angles. This allows for data to be collected from multiple viewpoints and so limits the effects of occlusion in the overall survey, once all scan clouds have been combined (figure 2.1).

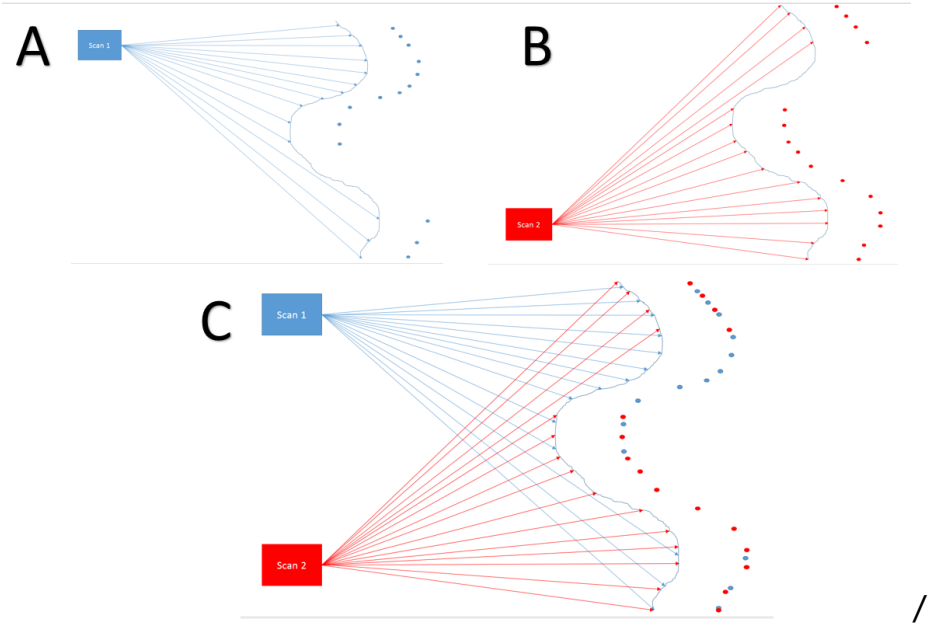

Figure 2.1: Scan occlusion and the benefit of multi angle scanning

When scanning from multiple locations it is important to put in control measures that allow the separate scans to be combined together into one coherent survey. This is usually done through the use of targets. These are often highly reflective circles or spheres that are mounted in the area surrounding the surface of interest. These targets are scanned from each scan position and given the same naming convention across all scans.

They then serve as tie-points to align different scans together to create a single detailed survey point cloud of the surface of interest (e.g. fig 2.1C)

Finally, for the purposes of most research, the point clouds will need to be georeferenced to move them from a virtual xyz coordinate system into an appropriate coordinate system for the location in which your site exists, e.g. British National Grid for UK sites, Gauss-Boaga for Italian sites, State Plane for US sites. This is usually carried out by surveying in the positions of scans and targets using either a total station or survey grade GPS. Those coordinates can then be applied to the scans while registering and provide the geospatial control that links them to the physical location where they were collected. Once the point cloud has been collected, registered and georeferenced it is possible to use it in a variety of ways to answer questions about the surface of interest, whether that be as a point cloud or converted into digital elevation models of the site.

Significant advances in the collection and post-processing of high-resolution remotely sensed data have meant that researchers are able to collect vast quantities of raw data quickly and with relative ease (Heritage and Hetherington, 2007; O'Neal and Pizzuto, 2011; Brasington et al., 2012; Leyland et al., 2015; Myers et al., 2019). However, this data's true value is in its very high spatial resolution, particularly where observations of individual channel features or grain size analyses are being undertaken.

Spatial resolution is the size of the smallest object that can be defined from an image or piece of data (Liang and Wang, 2019). Where resolution is high, small areas on the ground are covered by large areas in the data. However where resolutions are low, large areas on the ground are covered by small areas in the data. Remotely sensed data also works to a much higher degree of spatial precision and accuracy than many tra-

ditional techniques (Congalton and Green, 2019). When data points are collected, their recorded position relative to the point of interest is known as their accuracy. An accurate piece of data will very closely represent the spatial position of a feature. A data point's precision is a measure of the repeatability of the data collection. Where data points are clustered around the true value, then your data has precision. The wider the spread of data points the lower the precision (Figure 2.2).

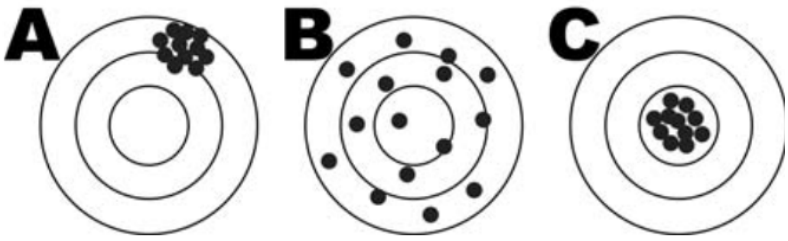

Figure 2.2: Visual representation of precision and accuracy. A) represents low accuracy but high precision, B) represents low precision but high accuracy and C) represents high accuracy and high precision (Yoshimura and Hasegawa, 2003) copyright © The Japanese Forest Society reprinted by permission of Informa UK Limited, trading as Taylor & Francis Group, www.tandfonline.com on behalf of The Japanese Forest Society

However there are now a number of different techniques available for the post processing and comparison of these data (table 2.1). DEM of Difference (DoD) has been frequently used to detect change across numerous research studies using TLS data, however emerging techniques such as Cloud to Cloud (C2C) comparison (e.g. Lane et al. (2003)), Multiscale Model to Model Cloud Comparison (M3C2) (Lague et al., 2013) and Geomorphic Change Detection (GCD) (Wheaton et al., 2010) are providing alternative methods for the comparison of dense point cloud data.

Table 2.1: A sample of river morphology studies using Terrestrial Laser Scanning techniques

Author (Year)	Study site	Site type	Coverage	Point Density	Scanner positions	Targets	Change detection method
Morche et al. (2008)	Reintal Valley, Germany	SC	900m^2	c.6700 per m^2	4	4	DEM of Difference
Heritage and Hetherington (2007)	River Wharfe, UK	SC	150m	c.7500 per m^2	21	60	None - Establishing scanning protocol
O'Neal and Pizzuto (2011)	South River, USA	SC	20m-30m reaches	point spacing of 2mm before classification and cleaning	2	3	5cm x 5cm gridded models created and subtracted from one another (similar to DEM of Difference technique)
Brasington et al. (2012)	River Feshie, Scotland	BR	1km reach	1765 per m^2 on average	18	43	ToPCAT
Brodu and Lague (2012)	Otira River gorge, New Zealand plus other non-river sites	SC	approx 80m	point spacing between 5 - 24mm	1	0	None - Establishing automated classification technique for complex environments
Picco et al. (2013)	Tagliamento River, Italy	BR	23.3ha	74 - 221 per m^2	21-38	not specified	Geomorphic Change Detection
Lague et al. (2013)	Rangitikei River, New Zealand	SC	500m	191 to 650 points per m^2	4-5	min of 3 up to 5 targets common between scan positions	M3C2
Leyland et al. (2015)	Cecina River, Italy	SC	60m	250k to 444k per m^2	3	4	DEM of Difference
Longoni et al. (2016)	Tartano Valley, Italy	SC	heights between 1.5m and 2.9m and lengths between 18m and 93m	1 point per cm^2	1	0	DEM of Difference
Hamshaw et al. (2017)	Lake Champlain Basin, Vermont, U.S.A.	SC	50 - 300m	typically 1 per cm^2	not specified	not specified	Plotting of cross sectional data for comparison of data collection techniques.
Foerst and Rüther (2018)	Breivikelva, Norway	SC	1100m	not specified	3	4	DEM of Difference

2.2 Site Details - River Arrow

The River Arrow, a tributary of the River Avon, is a small, lowland river flowing through North Worcestershire and Warwickshire, draining a catchment area of approximately 319km^2 (Figure 2.3). The river rises in the Lickey Hills in north Worcestershire (SO 996 753) and flows south-east through Warwickshire before discharging into the River Avon near the Village of Salford Priors (SP 082 507). The river's lowland catchment is underlain largely with Triassic sandstone, and it exhibits a meandering, pool-riffle morphology through its largely rural landscape. The catchment is dominated by grassland (39.96%) and arable/horticultural land (33.49%), with small patches of woodland (15.59%) sitting mostly in the upper areas of the catchment. Redditch, Studley and Alcester are the three main urban centres making up 10.23% of the catchment (National River Flow Archive (2023) as at April 2023).

The banks of interest are all located within a 1km reach of the river located near the town of Studley, Warwickshire (GR SP08130 63450) as shown in figure 2.4. This area has a long history of being used for bank erosion research, including Lawler (1994), Couper and Maddock (2001), Couper et al. (2002) and Couper (2003). The previous data acquired in these studies provides some historic data against which to compare the data recorded within this study. The soils along this stretch of river have a silt-clay content of between 36.7% and 43.2% (Couper and Maddock, 2001).

In the study reach there are a number of areas with deeply incised, steep banks positioned most prominently on the outside of actively eroding meander bends. There are several well vegetated point bars on the opposing channel sides, comprised of gravels and cobbles and colonised by grasses and nettles.

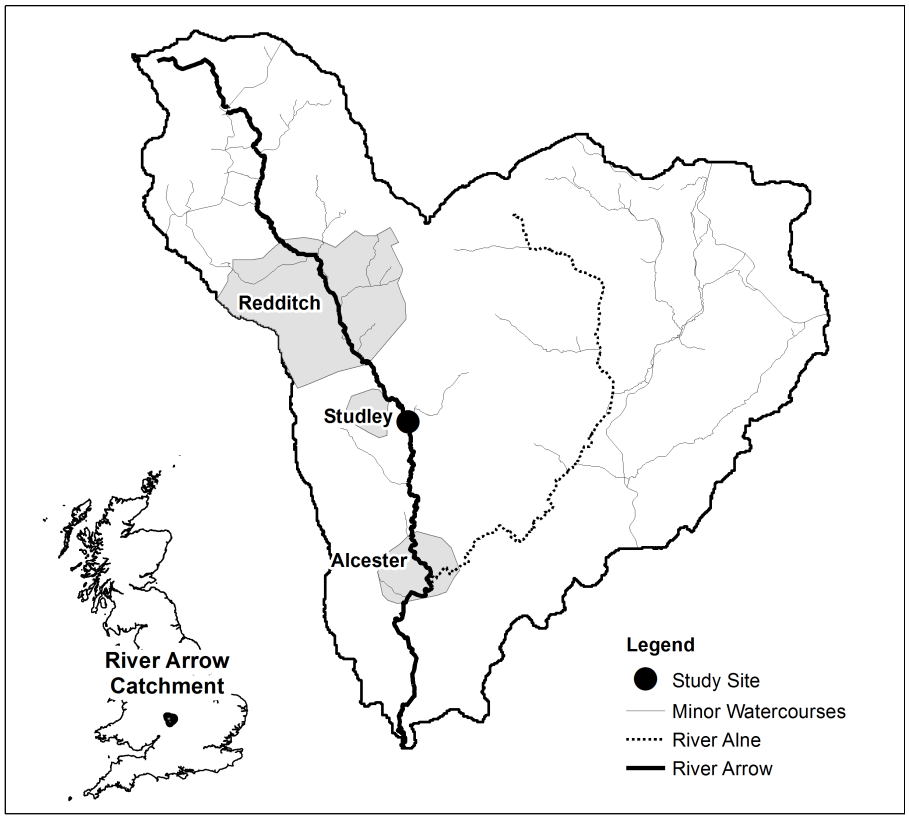

Figure 2.3: River Arrow Catchment

There are a number of locations within the study area where vegetation roots are responsible for maintaining small peds of bank material from collapsing. These areas were deemed likely to collapse at some point during the length of this research, which would allow the opportunity to witness small-scale mass wasting effects in action, and were part of the rationale for selecting the specific banks of interest within the study area.

For this research, three separate areas of bank were chosen for study. Each one exhibits different characteristics in terms of the degree and direction of curvature, however they are all of a similar height from average water level to top of bank, and they are positioned closely enough together that only one thermistor was required be representative of temperatures across the whole study area.

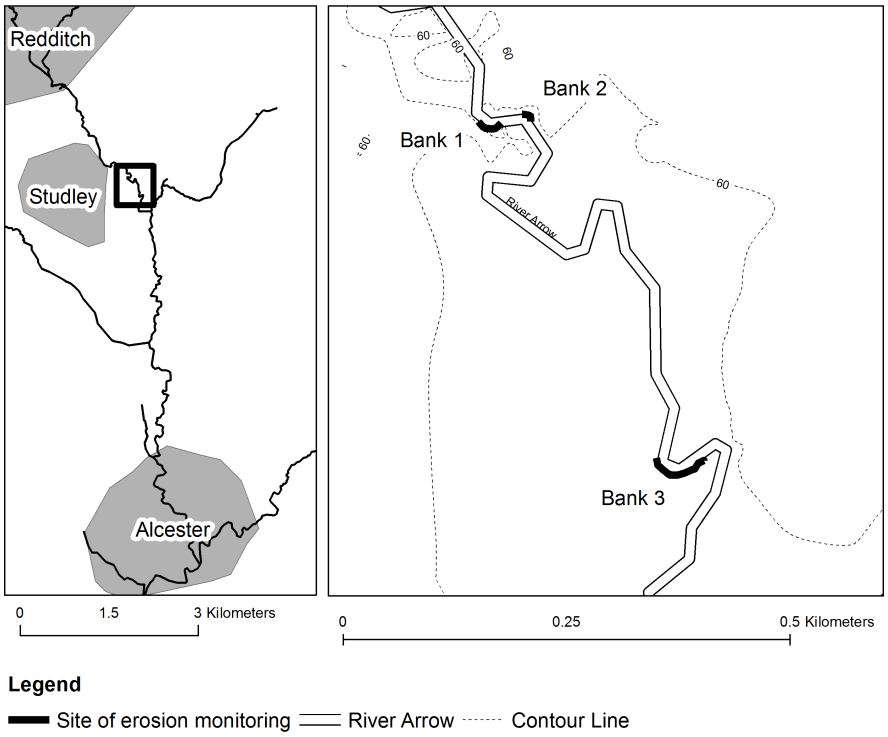

Figure 2.4: Study banks on the River Arrow

Bank 1 is a curved bank at the furthest upstream end of the site, of approximately 25m in length and 2.4m in height from channel bed (Figure 2.5). Bank 2 is roughly 25m downstream, with a similar bank height of roughly 2.4m from channel bed. It exhibits a tighter curvature and is roughly 18m in length.

Bank 3 is roughly 650m downstream (∼500m in a straight line) and is the longest of the three banks at approximately 80m. It is also the tallest at roughly 2.8m in height from channel bed. Bank 3 exhibits a much more obviously layered bank structure, with a clearly defined layer of cobble and gravel material in the lower bank, and much finer sands, clays and silts as you move up the bank profile (Figure 2.5). The top of the bank is well vegetated, with several areas of overhanging clasts of material that have had their supporting bank material eroded away and were deemed likely to fail during the period of study. The study sites are located within a large

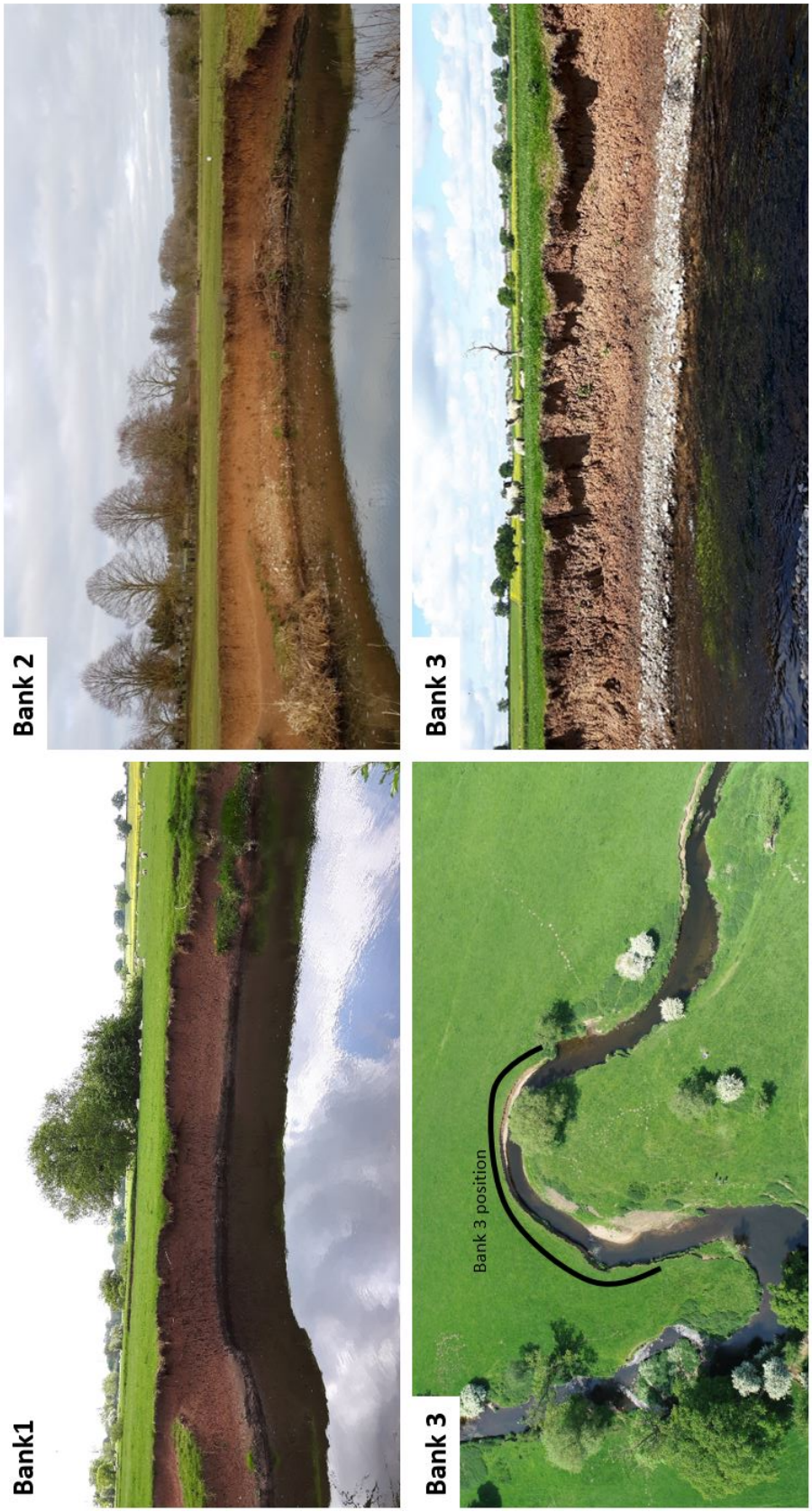

Figure 2.5: Site photographs

floodplain area used for the grazing of livestock, with unhindered access to the top of bank and numerous channel crossings within the overall study area. The top of bank is well vegetated with grasses and parts of the lower bank exhibit areas of vegetation during spring and summer, with strong dieback through the autumn and winter.

This site was chosen for this research due to its accessibility, the presence of numerous actively eroding banks, and an existing positive relationship with the landowner following numerous other studies which have been conducted at this site (Lawler, 1994; Couper and Maddock, 2001; Couper et al., 2002; Couper, 2003; Woodget et al., 2014; Woodget et al., 2016).

The Environment Agency have been monitoring flow on the River Arrow at Studley, (SP 07631 63978) approximately 850m upstream from Site 1, since 1981. Flow data shows that the site is sensitive to rainfall. The low flow discharge rate (Q95) is recorded as 0.18 cumecs and the high flow discharge is 1.670 cumecs. The maximum recorded discharge of 45.7m^3s^{-1} was recorded on 20th July 2007, which resulted in widespread flooding. The site's flow characteristics and flow duration curve can be seen in 2.2 and figure 2.6, respectively.

Table 2.2: River Arrow catchment characteristics

Characteristic	Value
Catchment Area (km^2)[a]	319
Mean Altitude (m asl)[a]	100
Base Flow Index [a]	0.53
Q10 (m^3s^-1)[b]	1.670
Q50 (m^3s^-1)[b]	0.459
Q95 (m^3s^-1)[b]	0.180
Index of flow variability (Q10/Q95)	9.278

[a] - Data from the National River Flow Archive, station 54007 Arrow at Broom
[b] - Long term duration data for River Arrow at Studley covering 1981 - 2019 provided by the Environment Agency via correspondence on 1st April 2019

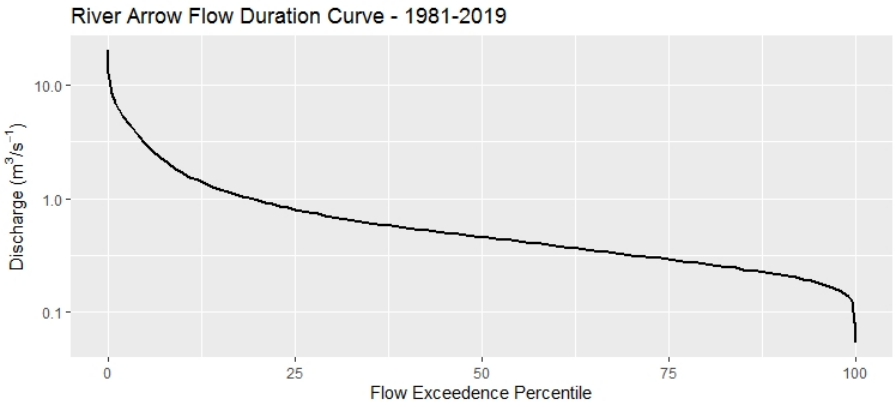

Figure 2.6: River Arrow flow duration curve, 1981-2019

2.3 Terrestrial Laser Scan Data Acquisition

2.3.1 Leica ScanStation C10

The very high resolution survey data collected for this research was obtained using the Leica ScanStation C10 (figure 2.7). The C10 is a survey grade, very high-speed laser scanner, containing an integrated camera, laser plummet and dual-axis compensator. It has a positional accuracy of ±6mm and a distance accuracy of ±4mm at 1m-50m from scanner. This provides a modelled surface precision of 2mm against any 'noise' (returns from atmospheric particulates, atmospheric moisture or vegetation movement) within the target environment (Leica Geosystems, 2012b).

The C10 uses a green light laser with a wavelength of 532nm, allowing for penetration through water, although the penetration depth varies with turbidity and turbulence (Pratomo et al., 2019). It also has a range of 300m with a scanning rate of 50,000 points per second through a full 360° horizontal view and 270° vertical view.

Unlike airborne LiDAR, the C10 is a tripod mounted system that can collect data in any light levels, so is not limited by cloud cover or by issues with low light that can be found in passive sensors. Being a terrestrial

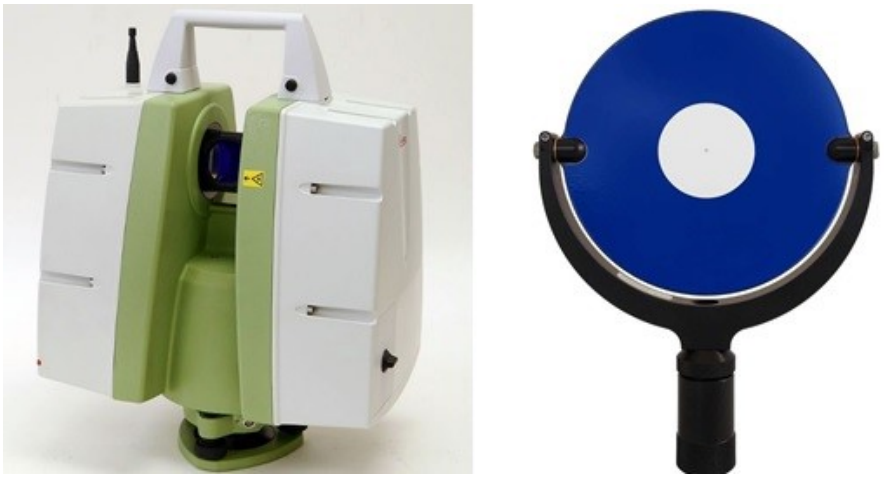

Figure 2.7: ScanStation C10 and 6-inch target

based system also makes it very effective for scanning low lying vertical surfaces, such as river banks. Moisture in the atmosphere at ground level (i.e. rain, mist and fog) can create considerable noise as individual droplets of water are capable of generating a laser return, making the scanner inappropriate for data collection in these conditions. It cannot be operated in high winds due to the potential for scanner movement.

Control of the scanner is achieved through the integrated touchscreen, which allows for selection of scan parameters including, but not limited to, horizontal range, vertical range, point resolution, image capture resolution and definition of target locations.

In order to combine multiple scans into one coherent point cloud, targets are required to provide reference points, known as 'tiepoints' for the registration process. The models provided with the C10 were six-inch circular, blue and white, tilt and turn targets (figure 2.7). These were mounted onto magnetic bases, providing optimal positioning accuracy and security against movement due to wind or interference.

Scan data was stored on the scanner's 80GB internal memory before being transferred to an external USB memory device for processing. Once

scanning was complete, data was uploaded into the Leica proprietary software Cyclone for registration, georeferencing, cleaning and then export to the chosen post processing software. Export files were produced in .pts format, for use in GIS and 3D rendering software.

2.3.2 Scanning protocol design

When collecting very-high resolution scan data it is vital that an appropriate scanning protocol and site setup is followed to allow for the greatest accuracy and precision for the collected data (Milan et al., 2007; Wheaton et al., 2010; Brasington et al., 2012). The main purpose of such a scanning protocol is to maximise the point coverage, minimise areas of occluded/missing data, maximise point density and minimise potential registration/meshing errors between scans.

The intended method for this study has been influenced to a large extent by the work of Heritage and Hetherington (2007) who were among the first to try and develop a consistent and effective scanning protocol for the fluvial environment. Their research involved the collection of over 17 million points across a 150m x 15m stretch of the River Wharfe, Deepdale, North Yorkshire, UK. They collected 21 overlapping scans of the area, varying their data collection points through the in-channel, upstream and downstream section of the site. These scans were then tied together through the use of 4 – 13 tiepoints depending on the location and scanner view. The tiepoints were identified manually using the visualised scan data in the field, and later georeferenced using surveyed points collected using a total station. The protocol they devised has been adopted widely throughout the literature (Heritage and Milan, 2009; Hodge et al., 2009; Brasington et al., 2012).

Table 2.3: The 11 step guidance developed by Heritage and Hetherington (2007) and the field notes used to design site setup

Guidance	Notes
Minimise scan distance to ensure greater scan point density	Scan locations chosen as close to surface of interest as possible within safe working practices and to allow for erosion of the banks without loss of target and scan sites. The resulting average scan distance was 5m, with a maximum scan distance of 35m.
Tilt the scanner towards the river channel to maximise the amount of data collected locally	Scanner capable of collecting data at 45 degrees below its direct line of sight so can 'see' into channel.
Select scan locations to minimise scan shadow effects caused by large obstructions	All scan locations avoid obstructed views to the surface of interest.
Where possible, optimise the scan angle by setting the instrument well above the scanned surface	Scanner set at maximum height at which it can be safely operate. Typically this was between 1.5m and 1.7m.
Collect independent tiepoint/error check data to minimise systematic bias introduced during scan cloud merging	All target/tiepoint locations surveyed using dGPS.
Use manually selected tiepoints for more accurate scan merging due to the ability to select their location in the scan data with high precision	Scanner and software accuracy has improved since this protocol was published, therefore is it deemed that targets/tiepoints can be reflector based for speed of site setup and data processing.
Where centimetre-scale accuracy is not required utilize a reflector system to exploit reflector auto detection algorithms in the software and reduce post processing time	See comment above.
Ensure that some targets/tiepoints are placed at the edges of the scanned error to minimise propagation of meshing errors	Targets/tiepoints set on bank top and well outside of the area of interest.
Ensure a good variation in x, y, and z dimensions when selecting target/tiepoint locations	Targets/tiepoints set on ground based markers chosen for a variety of x, y and z positions.
Repeat scans from the same location to densify the data collected and potentially reduce extreme errors	High-resolution scans from multiple positions provides high density of data and minimises the field time, post processing time, data storage requirements and potential for registering/meshing errors.
Avoid low angle scans across water surfaces	No low angle scans will be conducted.

The 11 steps they recommended for consideration when designing a scanning protocol, became the initial guidance for the site setup of the field sites used in this study (Table 2.3). Further guidance related to the use of reflector based targets was also taken from more contemporary studies (Leyland et al., 2015; Longoni et al., 2016; Hamshaw et al., 2017) to ensure the most robust scanning protocol possible.

Work conducted by Brasington et al. (2012) followed a similar data collection method, with a minimum of four targets visible from each scan

location while surveying the braided River Feshie in the Cairngorm Mountains, Scotland. Their study site extended over 1km longitudinally, and 100m laterally and contained a total of 43 target locations and was covered by 18 independent scan sites (i.e. different locations to those used for targets). Their set-up, while considerably larger than the site used in this research, highlighted the importance of overlapping scans where micro-scale topography was being observed. Where areas of data are missing, interpolation is used to fill in the gaps, however these interpolation tools do not plot a rough surface, merely a planar surface at a mathematically interpolated height to align with its neighbours. Over large study sites, small areas of interpolation in this manner will have a limited effect on the overall characterisation of roughness, however when observing micro-scale topography within a meso-scale site, those interpolation areas can have significant influences on the measurement of surface roughness (Brasington et al., 2012).

In more recent studies, TLS data has been compared to numerous other data collection techniques, including the use of rtkGPS, Total Stations and Structure-from-Motion Photogrammetry (SfM) (e.g. Hohenthal et al. (2011), Bangen et al. (2014), Cook (2017), Hamshaw et al. (2017), and Visser et al. (2019)). While SfM techniques can produce data of similar resolution and accuracy, it is less well suited to collecting data on vertical faces. The TLS is ideal for these situations as it can be positioned to allow for an orthogonal view, as opposed to the oblique view that could be achieved from the air. The suitability of TLS to bare earth sites has been demonstrated repeatedly in these studies, particularly when evaluating changes in surface roughness and feature topography (Eitel et al., 2011; O'Neal and Pizzuto, 2011; Picco et al., 2013; Lague et al., 2013; Leyland et al., 2015). After gathering information on the considerations that need

to be made when setting up a scanning protocol, site reconnaissance visits were carried out to assess the site for suitability and to develop the site setup and scanning methodology that would be adopted. The final workflow that was used to develop the site setup can be seen in figure 2.8.

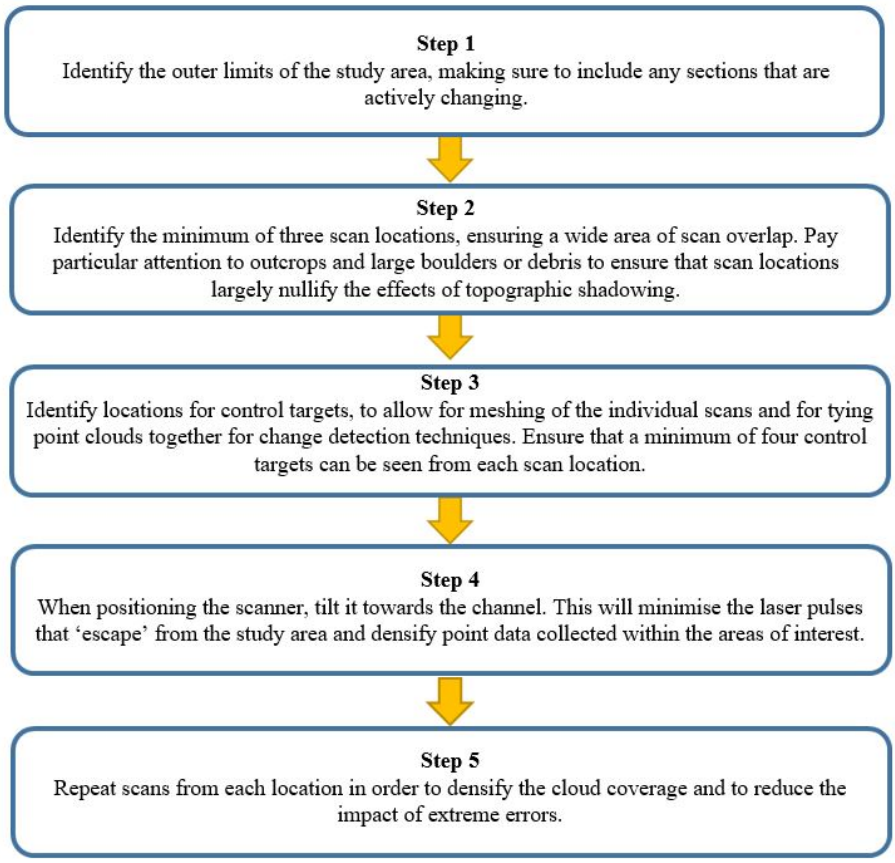

Figure 2.8: Method for survey data collection taking into account site specific conditions based on scanning protocols obtained from literature.

2.3.3 Site setup

The three banks of interest in this study were covered by two survey sites. Both Site 1 and Site 2 were set up with six 100 x 100mm permanent survey markers, secured into the ground using 500mm steel spikes. These markers provided the locations for all targets and surveys, with three at each site being solely target locations and three acting as both a scan

and target locations. The targets are placed directly on top of the permanent markers using a magnetic base, aligned with the marker surround to ensure stability and consistency across each survey. These permanent markers were surveyed using a Trimble R8 survey grade dGPS capable of accuracies of 0.005m horizontally and 0.020m vertically. The GPS coordinates provided the control and georeferencing for each subsequent scan (Eitel et al., 2011).

Each scan position was chosen to allow views to a minimum of four target positions, and all scans had a large degree of overlap to maximise point density and minimise obstructions and occluded data. The set-up of these sites can be seen in figure 2.9.

The scanner was set up above the relevant permanent marker, at a height at which the control screen can be safely viewed and operated but that still allowed the scanner to view the bottom of bank. The scan resolution was set to produce a point spacing of 0.05m at 100m from the scanner. The image capture parameters were left at their defaults, however the scan area had to be defined each time, as it was relative to the scanner position. The scan areas were made larger than the study areas to ensure that no data was lost from the outer edges of the sites.

Once the scan was completed, the targets were identified and scanned. Each individual target was picked out from a video view on the scanner touch screen and given its identifier, before all targets were scanned at an extremely high resolution specifically designed and programmed for the identification of targets. Once the target scans were completed, they were viewed via the control screen and checked for quality. If they had been captured clearly, with no noise and with no obvious obstructions, they were stored, and the TLS was moved and located at its next scan position.

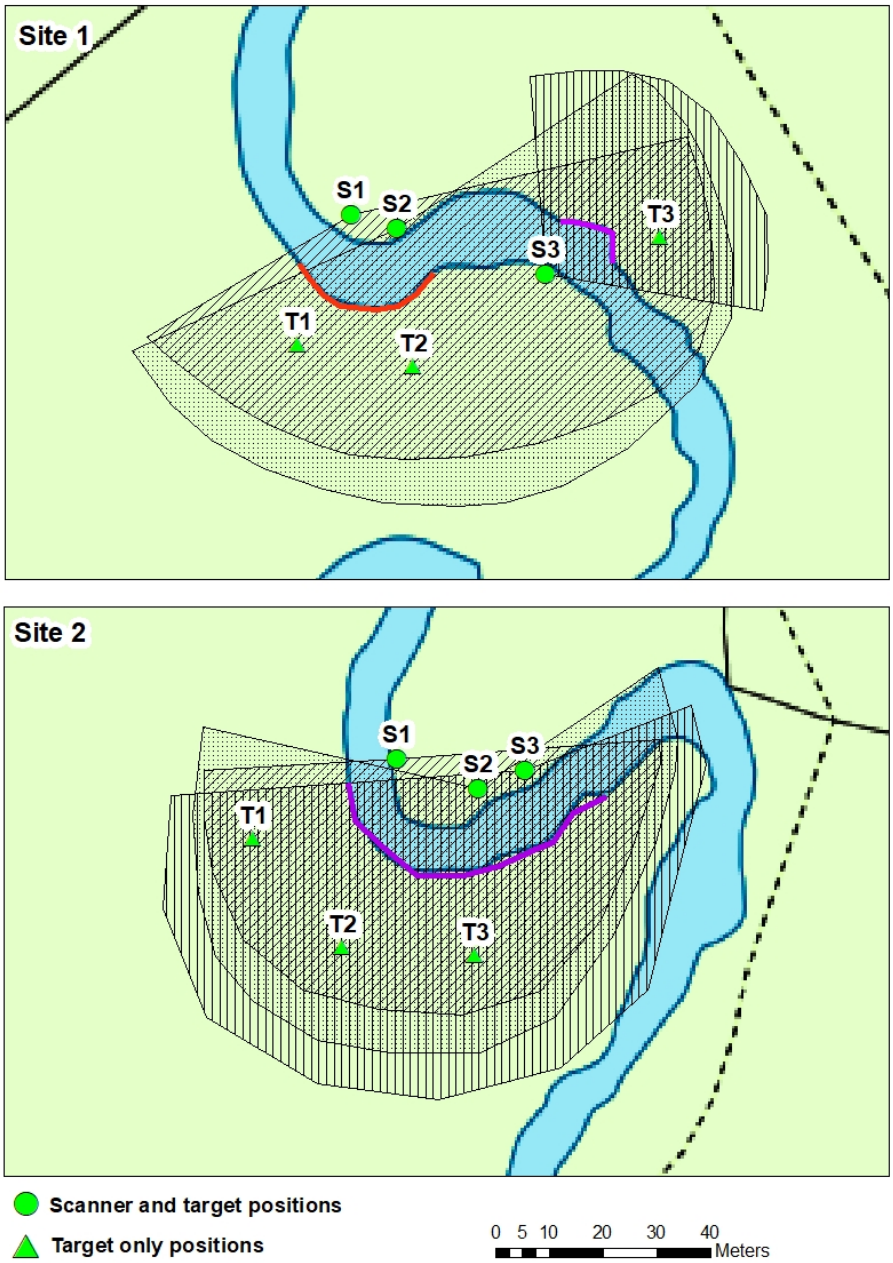

Figure 2.9: Site set-up to allow maximum coverage of study banks. Hatched areas represent the field of vision for each of the scan setups

The targets had to be named consistently across all scans to allow for accurate registering.

Following the initial set up of the sites a number of test scans were run to ensure that the protocol was appropriate and that there was user competence in the set-up of the equipment. Adjustments were made to the user defined parameters, however the site set-up was deemed to be appropriate for the data being collected and was not adjusted. When confident that the scanning protocol was as close to optimal as possible, the first full set of scans was completed on 6th and 7th May 2017.

Following the collection of baseline scans in May 2017, repeated scans were conducted at intervals between 28 and 217 days depending on site conditions, accessibility and variation in meteorological conditions experienced at the site (table 2.4).

Table 2.4: Scan data collection dates

Site 1 - Banks 1 & 2		Site 2 - Bank 3	
Scan Date	Days Elapsed	Scan Date	Days Elapsed
06/05/2017	Baseline	07/05/2017	Baseline
15/07/2017	70	16/07/2017	70
04/10/2017	81	04/10/2017	80
15/02/2018	134		
09/05/2018	83	09/05/2018	217
19/08/2018	102	19/08/2018	102
16/02/2019	181	12/02/2019	177
		16/05/2019	93

To ensure repeatability and comparability of data collection, permanent survey markers were left on the site, and targets positioned on top of those, using the edges of the markers to line up the magnetic bases. The TLS was set up over the top of the appropriate markers, although the positioning of this was done by eye as it would not be used to align the scans later in

the process.

Once the scanner and targets were in place the TLS was set up to perform the scan using the same set of user defined parameters as identified through the initial site set up phases.

2.3.4 Target based scan registration and cloud generation

Following site surveying, the data were extracted from the scanner and imported into the Leica proprietary software, Cyclone version 9.3.0 (Leica Geosystems, 2012a), for registration. Registration is the process by which a series of scans of the same location, containing some areas of overlap/-commonality, can be stitched together to create one coherent, dense and detailed point cloud of the site.

Registration can be performed using two different techniques; manual cloud-to-cloud registration or target-based registration. Manual cloud-to-cloud registration relies on clearly identifiable, stationary features that can be picked out of overlapping point clouds. These points are manually picked out of any point clouds where that feature is visible, and the manually selected points are overlapped to stitch the clouds together. This works well for scans of the built environment, where features such as signs, brick lines or corners are clear and easy to pick out of point clouds (Leica Geosystems, 2012b). Target-based registration is recommended for environments that lack regular and clearly identifiable structures, by providing specific and recognisable shapes that can be overlapped to stitch the clouds together automatically (Heritage and Hetherington, 2007)

Because of the complexity of 'natural' sites, particularly those that are actively eroding and lack any permanent and regular structures, the tech-

nique used in this study was 'target-based registration'. This allows the use of the scanner targets to align the different scans into one 'model' of the study site.

The individual scans are added into the registration file, along with the target scans and the GPS control file. The software then identifies targets that appear across multiple scan locations. The scans were then initially registered using the target positions, with an accuracy of between 0.005m and 0.009m.

Initial target-based registration was also supplemented by an automatic cloud-to-cloud registration to minimise registration error. The final average mean squared error value for each registered model varied between 0.001m and 0.005m (table 2.5), however it is important to note that those error values apply to the complete field dataset, and will include the error for the outer edges of the sites where point densities are lower than in the areas of interest.

Table 2.5: Mean absolute error values for registered point clouds

Site 1 - Banks 1 & 2		Site 2 - Bank 3	
Scan Date	Error (m)	Scan Date	Error (m)
06/05/2017	0.003	07/05/2017	0.004
15/07/2017	0.003	16/07/2017	0.005
04/10/2017	0.004	04/10/2017	0.004
15/02/2018	0.003		
09/05/2018	0.002	09/05/2018	0.004
19/08/2018	0.004	19/08/2018	0.004
16/02/2019	0.003	12/02/2019	0.003
		16/05/2019	0.005

Although data for site 2 was collected in February 2018, an issue with the target based registration resulted in a mean squared registration error of more than 0.012m, considerably higher than any other survey within this

study. As a result the decision was made not to include that data due to it's lack of spatial accuracy relative to the other surveys in the study.

Upon completion of registration, each registered point cloud is opened within its own modelspace for viewing. The modelled surveys are then cropped to the same extents to remove data that falls outside of the study area. Each point cloud is then saved to a new individual modelspace before being exported in 'xyz' format for comparison and change detection.

The mean error values are important for the success of later change detection methods as they represent the minimum level at which any change detection can be conducted. Any change detected that has values below that of the mean error cannot be attributed to changes to the surface being monitored, but rather is likely to be due to error/inaccuracies in the spatial positioning of points spread on a surface (Wheaton et al., 2010). The mean error will be smaller depending on the amount of overlap that exists between scans, the point density and the roughness of the surface of interest, as all of these things influence the positioning on points on a surface (Wheaton et al., 2010).

2.4 Point Cloud Classification

In order to separate change to the bank from changes associated with vegetation, it is important to be able to classify the point cloud into areas of bank and areas of vegetation. This can be done in CloudCompare using the CANUPO plugin (Brodu and Lague 2012). The CANUPO technique uses a process of semi-supervised machine learning to classify the point cloud with limited user input beyond initial training of the classifier. This is carried out through binary based segmentation of an existing point cloud to identify two potential classes the data can be separated into. Depending on the number of classes identified overall, the binary

process can be repeated numerous times to create a classifier capable of identifying multiple classes of point type.

The first step in creating a working classifier is creating training clouds that are representative of the different classes needing to be identified. In the case of this research, the classes required were simply bare bank and vegetation. To do this, segments were cut out of the original cloud and combined together to create a new cloud of just bare bank points, a second new cloud of vegetation and the existing cloud containing the remaining points not chosen in the segmentation (figure 2.10).

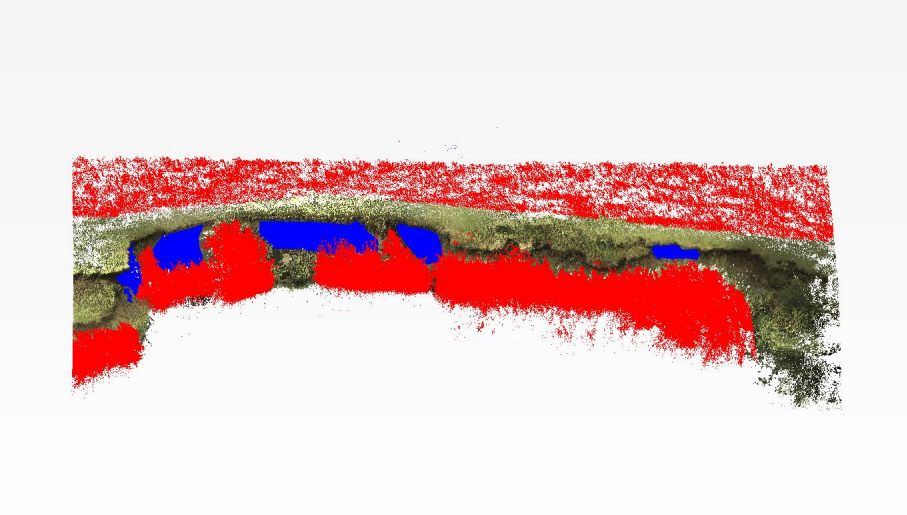

Figure 2.10: Point cloud showing segmented areas for classification training (red – vegetation, blue – bare bank, RGB points – unsegmented cloud)

Once this process is complete, the two segmented clouds are used to train the classifier. This takes the training point clouds and identifies patterns at multiple scales. The tool authors call this 'local dimensionality'. 'Local dimensionality' is the concept that, at different scales, particular features can appear to be 1-dimensional, 2-dimensional or 3-dimensional, and that the dimension they exhibit is actually scale dependent. For example, at the fine scale, a boulder would appear to have a planar 2-dimensional surface, gravels would appear to have a 3-dimensional textured struc-

ture, while a vegetation stem would appear as a 1-dimensional line. However, when zooming out to a coarser scale, the vegetation would become a 3-dimensional point mass, the gravels would become a 2-dimensional plane and the boulder would initially retain its 2-dimensional plane until the scale becomes coarser than the boulder, at which point it becomes a 3-dimensional point mass. The combination of scales and dimensions provide a signature for each different class of material, allowing the scene to be classified automatically with minimal manual interaction beyond the initial training of the classifier tool.

Once the segmented clouds have been created, they are loaded into the classifier and are used to compare the local dimensionality at a variety of different scales, 10 scales being the default. This then produces an output scatter plot to visualise the difference between the two selected surface types and shows the line along which division between the two types is calculated. The division line can be manually re-positioned and statistics run again to 'fine tune' the classification. Table 2.6 shows the results of four tests of the classifier training, comparing dimensionality at 10 scales, 20 scales, 50 scales, and 100 scales. Classification was most effective at 50 scales, with more than 98% of the 10,000 core points tested being classified accurately. Classification was least effective at 10 scales, with 96% of points correctly classified.

Table 2.6: Classification Data

	10 Scale Classifier	20 Scale Classifier	50 Scale Classifier	100 Scale Classifier
Minimum Scale (m)	0.1	0.05	0.02	0.01
Maximum Scale (m)	1.0	1.0	1.0	1.0
Step (m)	0.1	0.05	0.02	0.01
Core points compared	10,000	10,000	10,000	10,000
Bare Bank True	9792	9860	9788	9864
Bare Bank False	208	140	212	136
Vegetation True	9467	9474	9840	9707
Vegetation False	533	526	160	293
Balanced Accuracy	0.963	0.967	0.981	0.979

The different classifiers were tested on one of the survey datasets, specifically chosen due to its complexity and the amount of vegetation present (figure 2.11). The results of each classification were visually checked, with particular attention to areas where there were vegetation stems obscuring bare bank behind. It was particularly important that these areas would be correctly classified to ensure that usable bank data was maximised without including vegetation. Although the results were very similar for the different classifier tools, the 50 scale correctly classified top of bank and thin stem vegetation most consistently compared to the other scale options, whilst also maintaining the ability to correctly identify bank surfaces even behind vegetation areas. As a result of this combined visual and statistical analysis, it was decided that classification would be carried out using the 50 scale classifier. The chosen classification technique was applied to all subsequent scans and only points with a greater than 95% confidence of correct classification were used to represent bank data. The use of the 95% confidence reduced the number of incorrectly classified points even further, with only 0.8% incorrectly classified. Although there is the possibility of some points being incorrectly classified, the impact of those points should be limited due to their low occurrence.

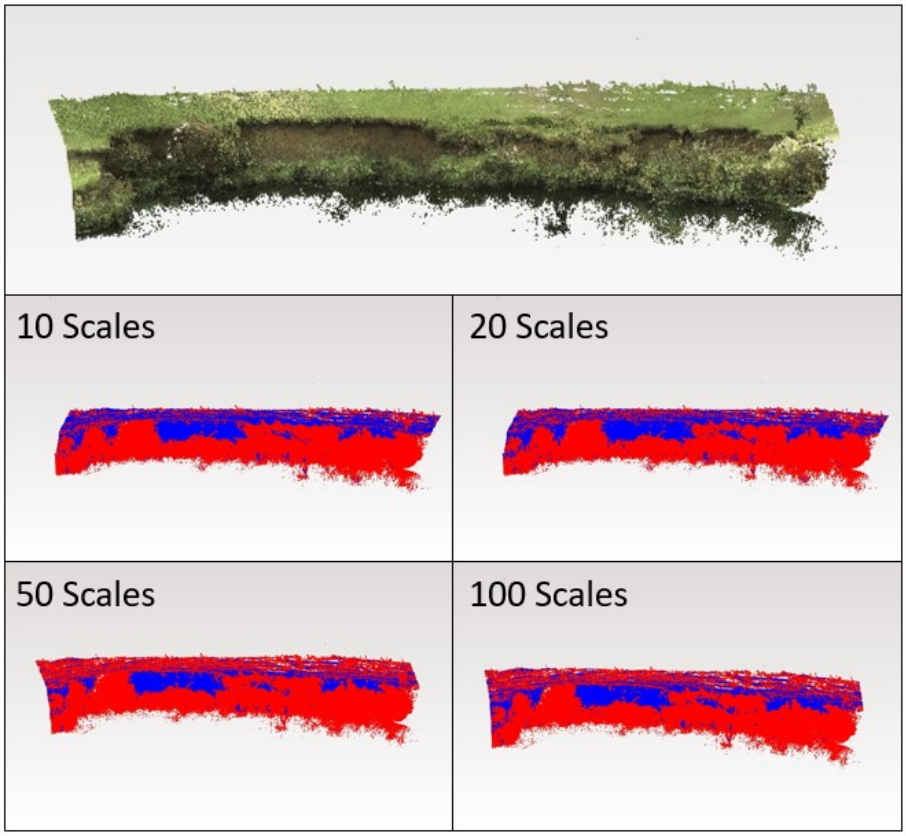

Figure 2.11: Classifier results for training dataset (blue points – bare bank, red points – vegetation)

2.5 Change Detection

Factors such as the point density, the slope of the surface of interest and the surface material will influence the effectiveness of change detection techniques on the registered data. In order to select the most appropriate change detection technique for the collected data, a pilot study (appendix A) was conceived to produce a point cloud with similar characteristics to that expected from the main research site. It was important to establish the change detection technique that would be most appropriate given the need for detection of very small scale changes in the surface of interest and that could effectively manage the very high density of data acquired. The pilot study tested three possible techniques for change detection and resulted in the decision to use CloudCompare and the Multiscale-Model-

to-Model Cloud Comparison (M3C2) (Lague et al., 2013) technique to conduct the change detection. Three main parameters were required to process the M3C2 distance. These were the normal scale, projection radius and projection max depth.

The normal scale defines the radius of a sphere used to calculate an average plane from all the points that fall within the sphere, or the 'local neighbours'. This normal surface is then used to orientate a cylinder within which other clouds/points will be searched for (figure 2.12). For the data collected at site 1, covering banks 1 and 2, the existing cloud normals were used for this calculation. However, some of the data from site 2 (bank 3) was missing cloud normals due to a download error early in the processing stage. In order to ensure continuity between scans, cloud normals were instead computed at a radius of 0.5m for all site 2 scans, even where cloud normals already existed.

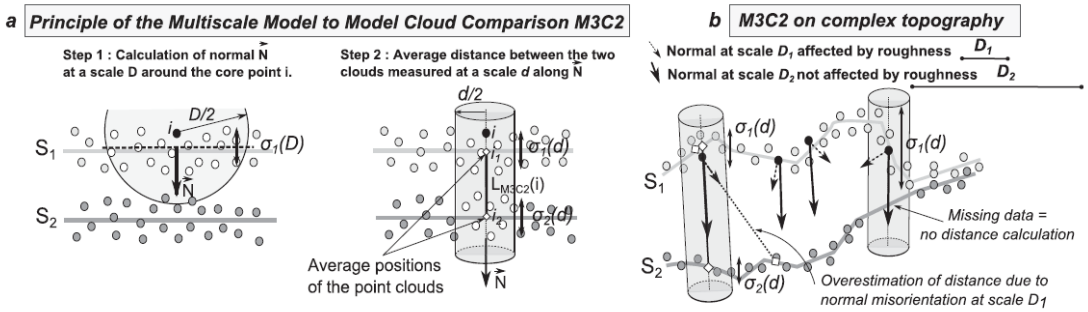

Figure 2.12: Principals of the M3C2 technique, a) step 1 - represents the calculation of the cloud normals, or the orientation of the cloud surface at the local rather than the point scale while step 2 – represents the measurement of the average distance between two clouds by averaging the points that fall within defined projection radius; b) represents the application of the tool on a complex surface (Lague et al., 2013)

The next parameter defined was that of projection radius. This defines the radius of a circle centred on each point that is orientated to the normal surface defined with the normal scale discussed previously. From that circle, a cylinder of the same radius extends to find points in the compar-

ison cloud. Points that fall within that cylinder are averaged to provide a planar surface, and the distance between those two surfaces is the detected change. The projection radius was defined as 0.03m for banks 1 and 2 and at 0.05m for bank 3. These measurements were chosen to match those used to calculate the cloud normals, where the Site 1 banks had an average normal radius of 0.03m and Bank 3 had the normal scale defined manually at 0.05m.

Finally, the maximum depth is defined. This represents the maximum length, in either direction, that the cylinder will extend to detect points in the second cloud. This was defined as 1.2m for site 1, as this encompassed the maximum amount of change, including vegetation growth. For site 2 this value was defined as 2.0m, again because this represented the maximum amount of observed change, including vegetation.

Using these variables change detection was carried between each cloud and it's subsequent cloud, showing only change between each survey time and not cumulative change from the first scan.

Following analysis using the M3C2 technique, the clouds were exported as .las files and imported into R to conduct volumetric analysis. First the data was aggregated into 0.01m by 0.01m voxels using the LidR gridmetrics3d algorithm. Voxels are 3-dimensional grids covering the area of the scan and allow the 3D surface to be aggregated without losing dimensionality. All of the points that fall within a voxel are averaged together to give a single M3C2 derived change value for that voxel (Figure 2.13).

Finally, to calculate volume change, the average change value for each remaining voxel was simply multiplied by the length and width of the voxel,

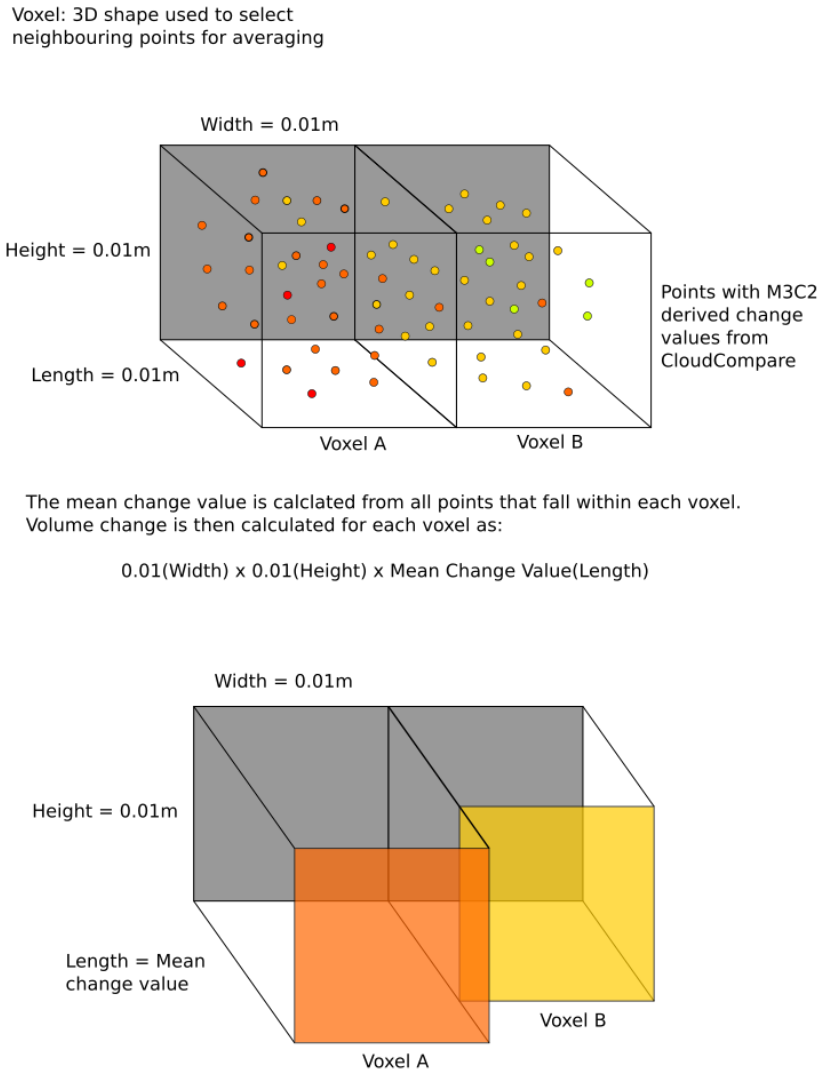

Figure 2.13: Calculation of change volume using voxels

as represented by the equation below.

$$dV = VoxelH * VoxelW * AverageChangeValue$$

The gross erosion for the site can then be calculated by summing all voxels with a negative change volume and the gross deposition can be calculated by summing voxels with a positive change volume. To account for any potential error in the GPS location or the registering of data, only those voxels with values of greater than 5mm of change (whether positive or negative) were used to calculate the erosion and deposition values.

The total area of erosion and deposition can also be calculated by counting the number of voxels with either negative (erosion) or positive (deposition) change values and dividing by 10,000. This gives the area of change in m^2.

2.6 Chapter Summary

The previous sections detail the chosen methods taken forward for the data preparation and early analysis stages of the research. Data collection will be conducted using a modified version of the recommendations provided by Heritage and Hetherington (2007) ensuring maximum comparability between scans and processed point clouds. Point cloud classification will be undertaken in CloudCompare using the CANUPO plugin Brodu and Lague (2012). This will be achieved using a self-created classifier set at 50 scales. Change detection will also be undertaken in CloudCompare using the M3C2 plugin Lague et al. (2013). Data has been tested for spatial autocorrelation and the decision has been made to use the full dataset, rather than a decimated dataset that would remove the benefit of using a spatially dense data collection technique such as TLS.

Additional analytical methods, including statistical tests, will be detailed further in chapters 3-5, where they are unique to the specific results being discussed in those chapters. The methods contained in this chapter represent those that are used throughout all subsequent investigations.

Chapter 3

Relative contributions of subaerial erosion, fluvial erosion and mass wasting processes on river bank change

This chapter addresses the first objective of the research, as presented in Chapter 1 - to identify the volume of recorded change and to identify the proportions of erosion that can be attributed to different erosion processes. First a review of the literature surrounding bank erosion is provided. This is followed by a recap of the research question and associated objectives before detailing the specific methods used for this chapter and the results obtained. It then goes on to provide a discussion of said results and a summary of the key findings that will be taken forward into the next stage of the analysis, detailed in Chapter 4.

3.1 Introduction

As described in Chapter 1, excessive erosion poses a threat to riparian infrastructure (Li et al., 2021), can destroy or severely degrade in channel habitats as a result of sedimentation (Mathers et al., 2017; Milner et al., 2021; Mathers et al., 2022), and increases downstream flood risk where there is significant deposition (Thorne et al., 2010; Nones, 2019; Liu et al., 2022).

3.1.1 Bank erosion in a Changing World

Climate change predictions in the UK see winter rainfall increasing by as much as 35% and summer rainfall decreasing by as much as 42% by 2070. Current predictions suggest that there will be a shift towards warmer and wetter winters and hotter and drier summers, with temperatures predicted to increase by up to 4.2°C in winter and 5.4°C in summer (Lowe et al., 2018). Globally, the situation is just as dire, with numerous studies predicting an increase in flooding and associated erosion hazards related to water over the coming decades (Nearing et al., 2004; Correa et al., 2016; Borrelli et al., 2020). However, much of this research is focused on the impact of soil erosion from the landscape via runoff rather than how a changing climate may impact specifically on bank erosion. Li et al. (2021) concluded that with a warming climate will come increased flood risk, which in turn will increase the hazard associated with erosion and deposition of sediment during flood events. They determined that this risk would result in increased economic loss due to flooding, with potential costs of £102-£130 million to repair damage to bridges, £9-£82 million for the impacts of sediment deposition in the urban landscape and £16-£26 million for loss of sediment from farmland, in addition to other losses related to damage to roads, property and other infrastructure in

the Cockermouth (UK) area alone.

In Bangladesh it is predicted that bank erosion will increase by 13% by 2050 and by 18% by 2100 (Aktar, 2013), putting hectares of land at risk of loss along the three largest rivers of the country alone. Venter et al. (2016) estimate that as much as 75% of the global land surface can be considered to be under considerable human pressures, and these pressures are resulting in changed water and sediment dynamics across almost all terrestrial environments (Owens, 2020). Work by Li et al. (2020) evaluated the sediments fluxes to the sea for 309 of the world largest rivers and determined that there has been a 20% decrease in the volume of sediment delivered to the sea over the last 40+ years. They determined that this was largely due to the influence of reservoirs and dams preventing sediment from reaching the lower catchments and estuary zones. Should a changing climate produce even greater sediment erosion from our landscapes, the risk of sedimentation dramatically reducing the capacity of reservoirs poses a threat to water security across the globe (Podger et al., 2021).

Abbas et al. (2023) identified that, on average, up to 25% of sediment lost from the landscape comes from river banks, but that this can be much higher depending on the catchment conditions. They also found that as catchment size increases, so does the proportion of suspended sediment sourced from river banks, as shown in figure 3.1.

The increasing climatological and anthropogenic pressures on our rivers are causing significant changes in how sediment moves through the fluvial environment. To begin to tackle some of those challenges we need to improve our understanding of fluvial erosion processes and mechanisms to help make predictions about what the future may hold under different climate scenarios and to inform our long term management of fluvial and

riparian environments.

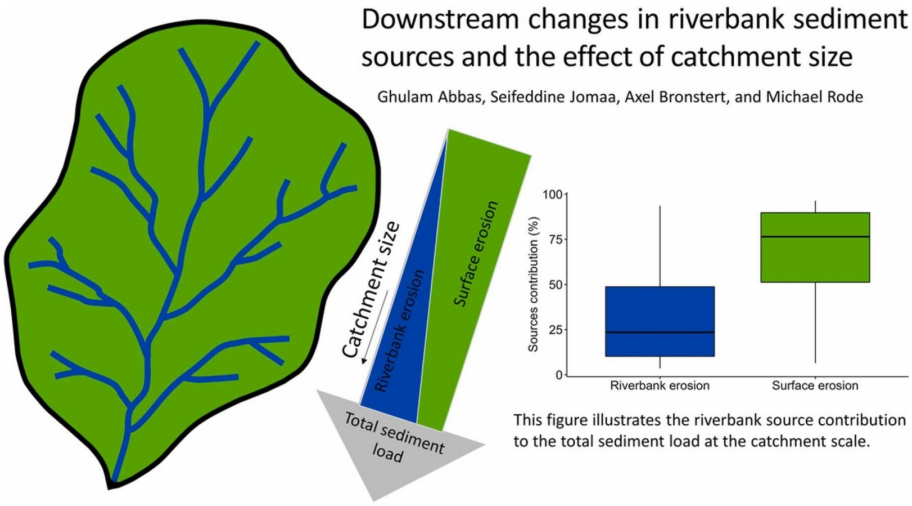

Figure 3.1: Downstream changes in sediment sources and the effect of sediment size (Abbas et al., 2023)

3.1.2 Bank Erosion - Processes and interactions

River bank erosion can be divided into three main processes - subaerial erosion working above the wetted perimeter of the river banks, fluvial erosion working below the wetted perimeter, and mass wasting which can occur both above and below the water level. These processes are complex and both spatially and temporally variable. The theory of 'Process Dominance' put forward by Lawler (1992) suggests that the dominant erosion process of a stretch of river is largely determined by stream power. Subaerial processes are considered as preparatory mechanisms, driven by micro-climatic conditions that are largely unconnected to the hydraulic and geomorphic conditions of the stream. If the conditions generating subaerial erosion remain constant as you move downstream, but the stream power increases as a result of the increased upstream catchment, then, Lawler argues, it can be reasonably assumed that the contribution of subaerial erosion will decrease the further downstream you go (Lawler et al., 1999). As subaerial processes become less influential moving down-

stream, stream power increases until a maximum is reached somewhere in the mid reaches of the channel. As stream power increases the erosive ability of the flow increases, thus resulting in fluvial erosion dominating in the mid reaches of a river. In the lower reaches of a river the problem of bank erosion is thought to be one of bank stability. Bank stability models state that there is a maximum height at which a material at a particular angle can remain stable (Osman and Thorne, 1988; Midgley et al., 2012; Konsoer et al., 2016; Duong Thi and Do Minh, 2019). Once this height is exceeded the bank becomes unstable and mass movement can occur. The greater depths associated with lower river reaches and the reduced stream power due to low channel gradients result in a switch from fluvial erosion to mass wasting as the dominant erosion process.

It is impossible to understand bank erosion without being able to recognise the importance of the interactions between the different types of erosion (Wolman, 1959; Lawler et al., 1999; Couper, 2003; Darby et al., 2007; Rinaldi and Darby, 2007; O'Neal and Pizzuto, 2011; Nardi et al., 2013; Longoni et al., 2016; Duró et al., 2020b). However, historically it has been very difficult to directly quantify the influences of different erosion processes on riverbank erosion as the widely available measurement techniques have lacked the required spatial and temporal resolution (Couper et al., 2002).

Work by Pizzuto (1994) that monitored the Powder River, Montana, USA over a 16 year period focused on the influence of discharge in generating erosive or deposition conditions. They found that discharges with a recurrence of less than 1.1 years generated approximately similar rates of erosion and deposition resulting in a very small net change in the channel form. Discharges with recurrences between 1.1 years and 2.7 years saw deposition dominate the channel, resulting in narrowing of the channel

and the creation of benches and channel bars. Discharges that exceeded 2.7 year recurrence generated net erosion conditions and greater transport of sediments.

However, discharge and process dominance alone do not account for smaller scale variations in river bank erosion. At the catchment scale, coarser less consolidated material tends to dominate in upland reaches, while lowland reaches tend to be dominated by finer sediments that are more cohesive. However, at the reach scale, where sediments tend to be more similar, there is still significant spatial variation in bank erosion (Henshaw et al., 2013).

Fluvial erosion and mass wasting have been considered to be the dominant processes determining bank erosion and lateral channel change, with subaerial processes largely being treated as preparatory, weakening the bank material for mass wasting or fluvial erosion to generate erosion (Lawler, 1992; Couper and Maddock, 2001; Jugie et al., 2018). However, an increasing body of research (e.g. Prosser et al. (2000), Couper and Maddock (2001), Couper (2003), Fox et al. (2007), Zhang et al. (2007), Defersha et al. (2011), and Zaimes et al. (2019)), is highlighting the importance of subaerial processes as an erosive agent in their own right. Understanding the dominant erosion processes working on a stretch of river is important to inform management and mitigation strategies, both at the site of erosion and in the downstream receptors of the sediment being eroded (Lane et al., 2007).

3.1.3 Bank erosion rates

The reality of river bank erosion is complex across multiple temporal and spatial dimensions. The scale of monitoring has a significant impact over what process is observed to be dominant. Jugie et al. (2018) monitored

erosion at six reaches along 13km of the Merantaise River in northern France. Over a monitoring period of 15-18 months, they found that erosion rates were most closely correlated with two hydrological parameters, the maximum discharge and the mean discharge recorded during flood events. Their study saw the most significant erosion within the mid reaches of the channel and noted that this was due mostly to a number of scour-failure cycles whereby fluvial erosion scoured the bottom of bank, resulting in failure of the upper sections of bank and the deposition of new material at the bottom of bank. This material was then eroded by flow and the cycle continued. The lower reaches of the channel exhibited very little erosion, appearing largely stable during the study period.

Foerst and Rüther (2018) observed erosion on a single meander bend of the lowland Breivikela river in Norway. A TLS was used to create point clouds covering three time periods, May - July 2011, June - October 2012 and June - July 2013 for three patches, one upstream of the meander apex and two downstream of the apex. They recorded erosion rates between $0.01m^3$ per m^2 and $0.42m^3$ per m^2, with the majority of this erosion being attributed to long term exposure to low water levels. High flow events at this site did not contribute significantly to the erosion rate.

Henshaw et al. (2013) observed erosion over 24 actively eroding banks of two upland streams of the Pontbren experimental catchment, UK. The two catchments were both first order streams. The majority of erosion at this site was attributed to fluvial processes, with less than 11% of the erosion attributed to subaerial erosion processes. However, Yumoto et al. (2006) found that subaerial erosion dominated at one site along the River Yakawa, Japan, with a contribution of 56.4% and with the remaining 43.6% coming from fluvial entrainment. However at the second site, which was less than 200m downstream, the contribution of subaerial processes

was only 20.7%, with the dominant process being mass wasting at 45.5% and the remaining 33.8% coming from fluvial entrainment.

Grove et al. (2013) identified that 41% of the measured erosion volume of the Lockyear Creek was caused by mass wasting events, despite them only contributing to 8% of the erosion area. Fluvial erosion contributed the remaining 59% of the erosion volume from 88% of the erosion area.

There is a great deal of variability in river bank erosion rates recorded within bank erosion literature, a sample of which is provided in table 3.1. Developing greater understanding of the rate of erosion on different riverbanks is vital to help manage and maintain our riparian landscapes and habitats.

3.2 Aims and Objectives

The aim of this chapter is to identify, for each of the study banks, the volume of change that has occurred and the proportions of erosion that can be attributed to fluvial erosion, sub-aerial erosion and mass wasting.

In order to achieve this aim the following objectives were undertaken:

1. To collect repeated, very high-resolution topographic data of riverbank surfaces using a Terrestrial Laser Scanner.

2. To perform change detection showing the areas of the bank that are subject to most significant change.

3. To identify the dominant erosion process - subaerial, mass wasting or fluvial erosion - by which that change has occurred and calculate their relative contributions to the overall bank erosion.

Table 3.1: A sample of studies of bank erosion

Author (Year)	Study site	Erosion value	Dominant erosion process	Additional Info
Couper and Maddock (2001)	River Arrow, UK	181mm a^{-1}	Subaerial	At end of study period a high flow event resulted in an estimated additional erosion of 500mm of material
Foerst and Rüther (2018)	Breivikela River, Norway	0.01m^3 per m^2	Low flow fluvial erosion*	*Author states most erosion occurred during low flow events while bank exposed so could attribute the erosion to subaerial processes.
Grove et al. (2013)	Lockyer Creek, Australia	2.1m to 9.7m m^{-2}	Mass failure and fluvial erosion	Mass failures covered 8% of the total bank area with approximately 1/3rd of the total volume of erosion. The remaining 2/3rds of the erosion volume came from fluvial entrainement, covering 33% of the total bank area and 81% of the total eroded bank area.
Henshaw et al. (2013)	Pontbran, Wales	7 $\pm$ 4mm y^{-1} and 299 $\pm$ 321mm y^{-1}	Fluvial erosion	Correlation values of 0.934 and 0.898 between morphological activity rates and max discharge and mean discharge respectively. Subaerial erosion only deemeed to contribute 11% of erosion.
Jugie et al. (2018)	Merantaise River, France	10mm yr^{-1} to 1170mm yr^{-1}	Fluvial erosion	Erosion deemed to be domainated by flow induced scour failures. Spatial variations in flow deemed to be a result of local variation in bank angle, protection of bank toe due to the presence of a berm, additional supply of water via pipes or local deflection of flow towards bank vie presence of debris.
Veihe et al. (2011)	Harrested Stream, Zealand, Denmark	25mm y^{-1} - 670mm y^{-1}	Subaerial, Mass Wasting and Fluvial erosion all observed	Author notes that subaerial erosion was of a low magnitude but high frequency, resulting in "frequent and accelerated erosion" over the bank face.
Yumoto et al. (2006)	River Yakawa, Japan	28 mm y^{-1} to 880mm y^{-1}	up to 56.% of erosion identified as being due to subaerial processes	Needle ice and freeze-thaw processes identified as most significant erosion mechanisms

3.3 Methods

Each site was surveyed repeatedly during the study period, which extended from May 2017 to May 2019. The dates of data collection can be seen in Chapter Two table 2.4 but have been summarised below for reference (Table 3.2)

Table 3.2: Data collection dates

	Month	Bank 1	Bank 2	Bank 3
1	May 2017	Y	Y	Y
2	July 2017	Y	Y	Y
3	October 2017	Y	Y	Y
4	February 2018	Y	Y	**N**
5	May 2018	Y	Y	Y
6	August 2018	Y	Y	Y
7	February 2019	Y	Y	Y
8	May 2019	**N**	**N**	Y

All data collection was carried out using the Leica ScanStation C10, and registered using a target based registration technique. The clouds were then imported into CloudCompare where they were manually clipped to remove any stray atmospheric returns, to remove all points obtained below the water level and to cut all clouds to the same upstream and downstream extents. The clouds were then classified into bare bank and vegetation categories using the CANUPO classification technique, with vegetation points being removed from the scans. Change detection was carried out on the bare bank points using the multiscale model-to-model cloud comparison technique (M3C2). Where the water level of the preceeding scan was higher than that of the more recent scan, only points that fall within the projection radius as defined in Chapter 2 were used to calculate change. This meant that the lower points in the more recent scan could have detected change as high as 0.03m at Banks 1 and 2 and 0.05m at Bank 3. Although the subsequent voxelisation process averaged out those potentially erroneous values, the decision not to cut off all scans at the

highest water level was made to allow for data analysis to be carried out between the different scanning dates where knowledge of the future water level was not possible. It also allowed for collection of some data at the lowest portions of the bank where fluvial processes are at their most dominant and thus ensured the maximum possible number of points for analysis. The potential consequences of this decision will be handled in the final discussion chapter.

The data was then imported into R for analysis of volumetric change via voxelisation. Details for all of the above techniques can be found in Chapter 3, with an overview of the workflow presented in figure 3.2.

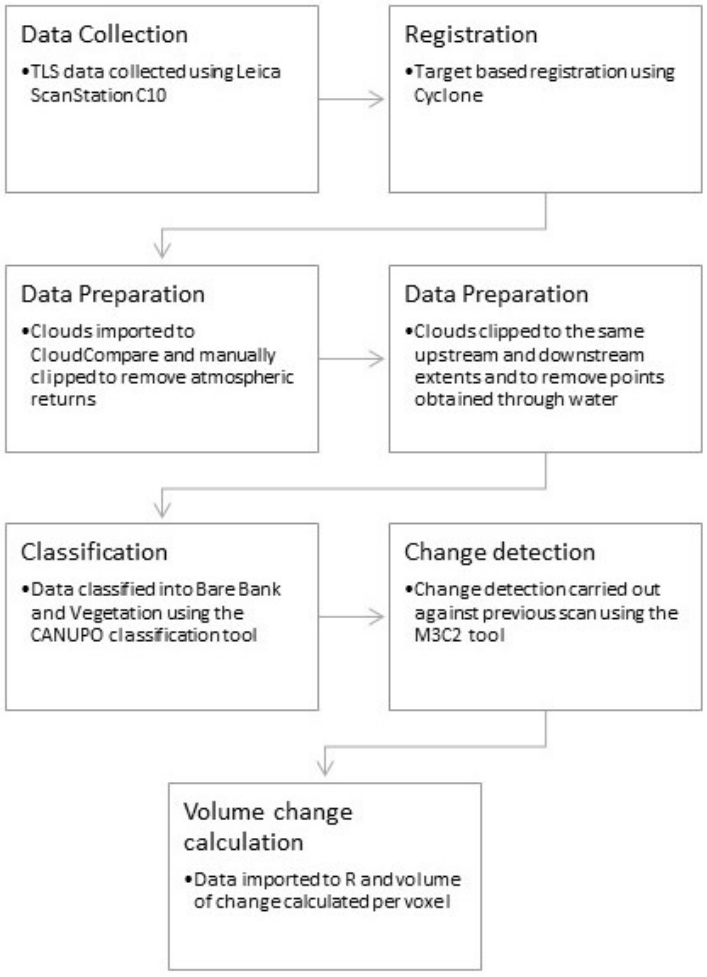

Figure 3.2: Workflow of data collection and processing for analysis

In order to establish the contributions of different erosion techniques, each compared cloud was first visually examined. Where there was a clear concentration of erosion of a similar distance it was assumed that mass wasting processes had taken place. Those areas were manually segmented from the original cloud to create a subset of points deemed to represent the contribution of mass wasting (Figure 3.3).

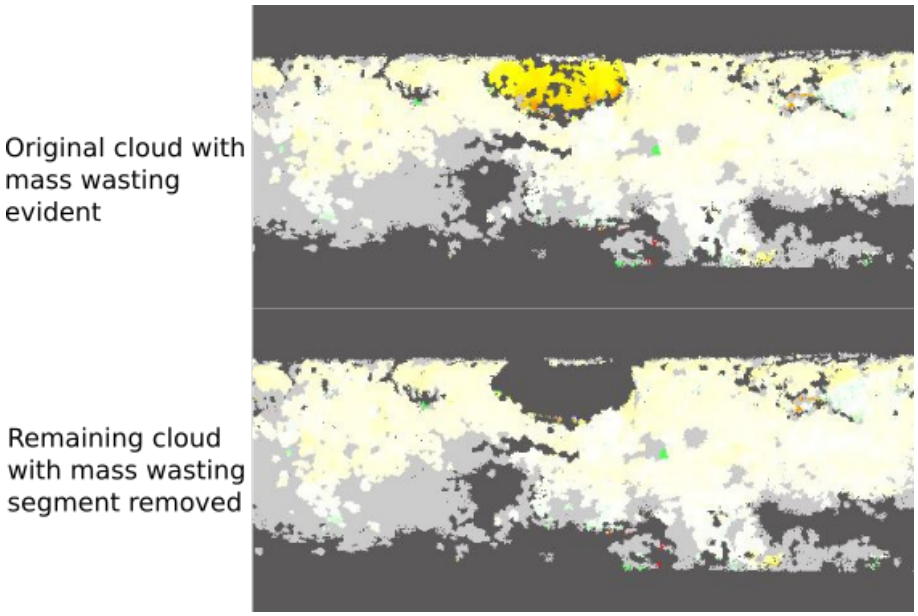

Figure 3.3: Example of manual mass wasting segmentation

A water level logger was left at the site, however it was never able to be retrieved and so, as an alternative, river level data from the Environment Agency's gauge at Studley was compared with the water heights on the bank for each scan date and linear regression was performed to convert water level at the gauging station to water height on the bank (figure 3.4).

Flow duration curves were then created using the calculated bank height data (figures 3.5), and the bank height representing the median flow (Q50), and the high flow (Q10) were calculated. The water height values for median and high flows for each bank can be seen in table 3.3. Daily discharge data was also acquired from the Studley gauge.

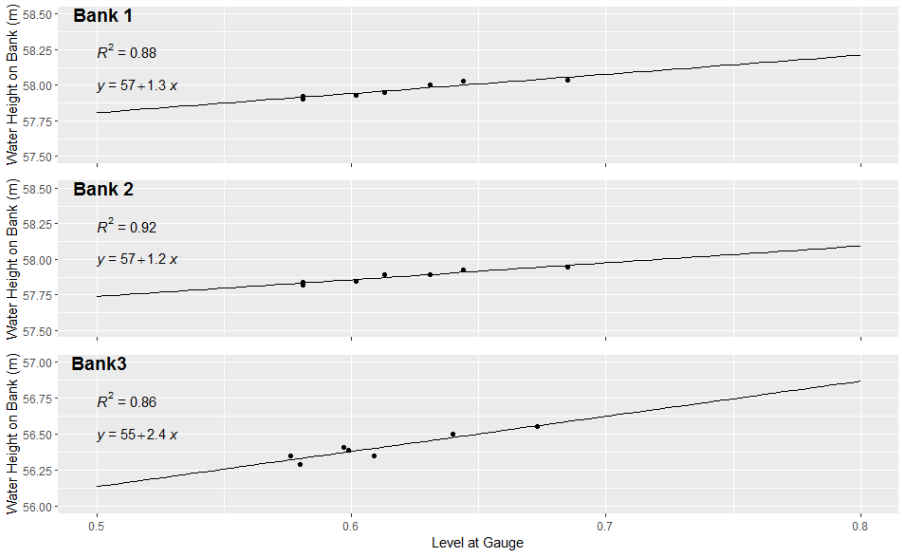

Figure 3.4: Linear regression for river level at Studley gauge vs water height on bank at time of each TLS scan

Fluvial erosion was originally calculated for two categories, the Q10 contribution and the Q50 contribution. The Q10 contribution was made up of all 1cm x 1cm voxels with a Z value below the identified Q10 bank height, while the Q50 contribution was made up of all voxels with a z value below the identified Q50 bank height. However, there were a number of occasions when the water level on the scan date was above the Q50 level, meaning no erosion below that point could be measured. As such, the decision was taken to use erosion below the Q10 level to represent the fluvial component and erosion above the Q10 level to represent the subaerial component. The choice of the Q10 value as the cut off was based largely on the existing use of the Q10 level to represent high flows and thus only in 'extreme' conditions would the water level exceed Q10 and thus an assumption could be made that the dominant process above that level would be subaerial. This decision is discussed further in later sections and chapters.

The erosion values were calculated for the whole bank surface and for each of the chosen categories (mass wasting, fluvial below Q10 and sub-

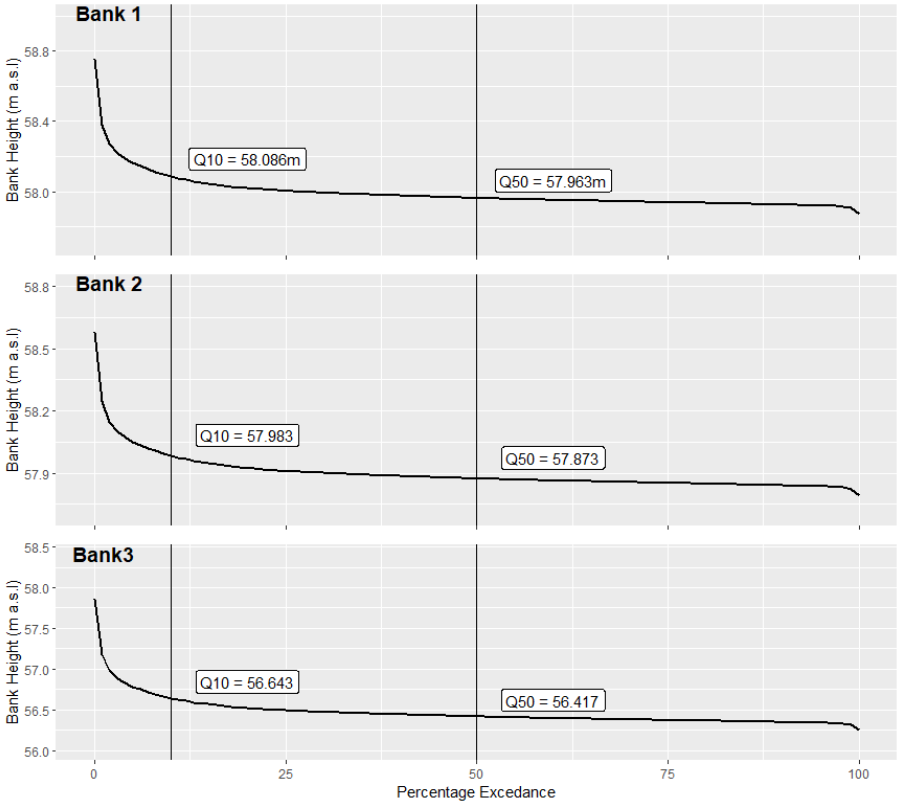

Figure 3.5: Bank height duration curves for each study bank, May 2017 - May 2019 based on the bank height data calculated in figure 3.5

Table 3.3: Bank heights at Q10 and Q50 Flows from calculate bank height data

Bank	Q10 Height (m a.s.l)	Q50 Height (m a.s.l)
Bank 1	58.086	57.963
Bank 2	57.983	57.873
Bank 3	56.643	56.417

aerial above Q10), and from those values the percentage erosion for each identified process were established.

Bank 3 was too large and had too much curvature to effectively display and analyse as a complete section, so it was cut into three sections of similar sizes, keeping areas of similar curvature together and these are identified as upstream, midstream and downstream reaches. The point cloud data for later volumetric change was also cut in the same locations, and data analysis has been conducted for each section, with some analysis also

covering the full bank.

3.4 Results

3.4.1 Data Summary

The study period ran from May 2017 to May 2019. During that period the maximum river level was recorded at 1.590m, which represents a long term exceedance percentage of 0.08% against level data collected since 2000. This means that, since 2000, the river has only peaked above that height 0.08% of the time. The lowest level recorded during the study period was 0.526m, and was the lowest level recorded at this gauge since 2000.

A summary of the raw change data collected from each bank is given in Tables 3.4, 3.5 and 3.6. Histograms of the point clouds were produced to show the spread of data between the -0.5m and 0.5m values, where over 99.5% of the data fell for each bank and each sampled time period (figures 3.6, 3.7, 3.8).

The 'total number of points on bank' represents all points that remained once points below water level and points classified as vegetation were removed, and therefore represents the total number of points on which analysis was carried out. 'No. of erosion points' represents those points with a negative change value greater than the registration error value of -0.005m, while 'No. of deposition points' represents those with a positive change value greater than 0.005m. The percentage erosion and deposition points are simply the percentage of the total points that fall into each category. The percentage of points with no measurable change was made up of all points with a change value between -0.005m and 0.005m, representing those points that sit within the potential error values and so cannot be

Table 3.4: Bank 1 Cloud Summaries

	E1 May 2017 - July 2017	**E2** July 2017 - Oct 2017	**E3** Oct 2017 - Feb 2018	**E4** Feb 2018 - May 2018	**E5** May 2018 - Aug 2018	**E6** Aug 2018 - Feb 2019
Total No. of Points on Bank	1,616,233	295,763	286,306	215,214	493,527	225,900
No. of Erosion Points	1,377,084	244,097	116,141	131,119	253,196	165,545
No. of Deposition Points	130,935	32,079	130,262	58,399	110,882	35,716
Max Erosion (m)	-2.287	-1.222	-1.123	-1.903	-1.340	-1.199
Max Deposition (m)	2.303	1.018	1.274	1.072	1.300	1.085
Mean Change (m)	-0.057	-0.029	-0.018	-0.031	-0.010	-0.032
Percentage of Erosion Points	85.2	82.5	40.6	60.9	51.3	73.3
Percentage of Deposition Points	8.1	10.8	45.5	27.1	22.5	15.8
Percentage with no measurable change	6.7	6.6	13.9	11.9	26.2	10.9

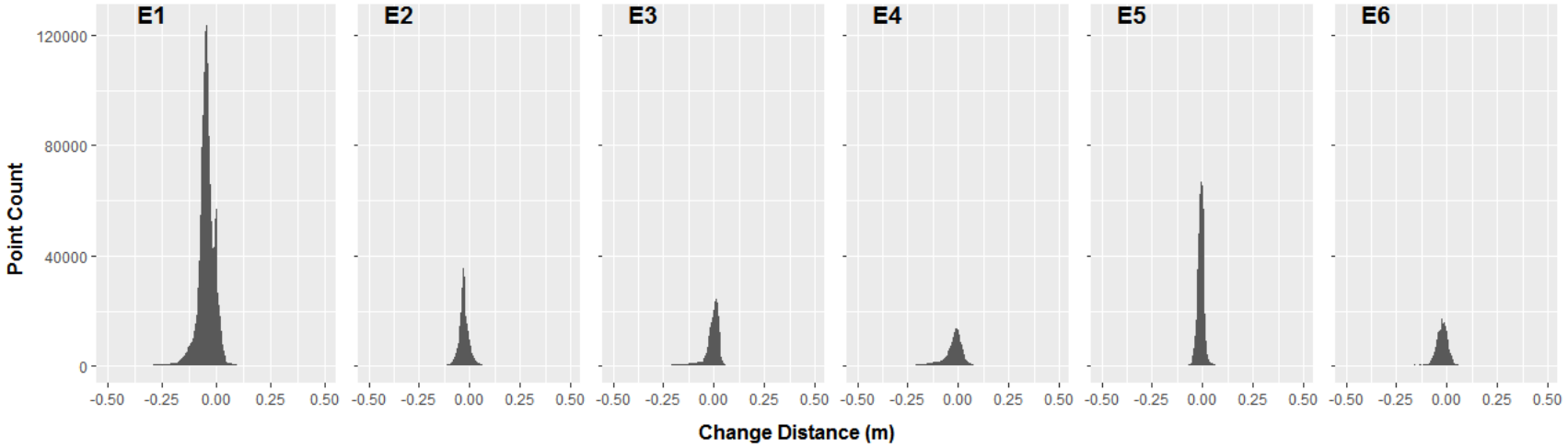

Figure 3.6: Histograms of the spread of change data recorded on bank 1

Table 3.5: Bank 2 cloud summaries

	E1 May 2017 - July 2017	E2 July 2017 - Oct 2017	E3 Oct 2017 - Feb 2018	E4 Feb 2018 - May 2018	E5 May 2018 - Aug 2018	E6 Aug 2018 - Feb 2019
Total No. of Points on Bank	309347	292320	58071	265464	208897	207780
No. of Erosion Points	229377	206113	8768	193161	186496	153414
No. of Deposition Points	63668	74089	41752	40542	21582	50987
Max Erosion (m)	-1.202	-1.066	-0.359	-0.772	-0.823	-1.046
Max Deposition (m)	1.150	1.217	1.165	1.186	1.148	1.194
Mean Change (m)	-0.030	-0.037	0.015	-0.020	-0.077	-0.058
Percentage of Erosion Points	74.1	70.5	15.1	72.8	89.3	73.8
Percentage of Deposition Points	20.6	25.3	71.9	15.3	10.3	24.5
Percentage with no measurable change	5.3	4.1	13.0	12.0	0.4	1.6

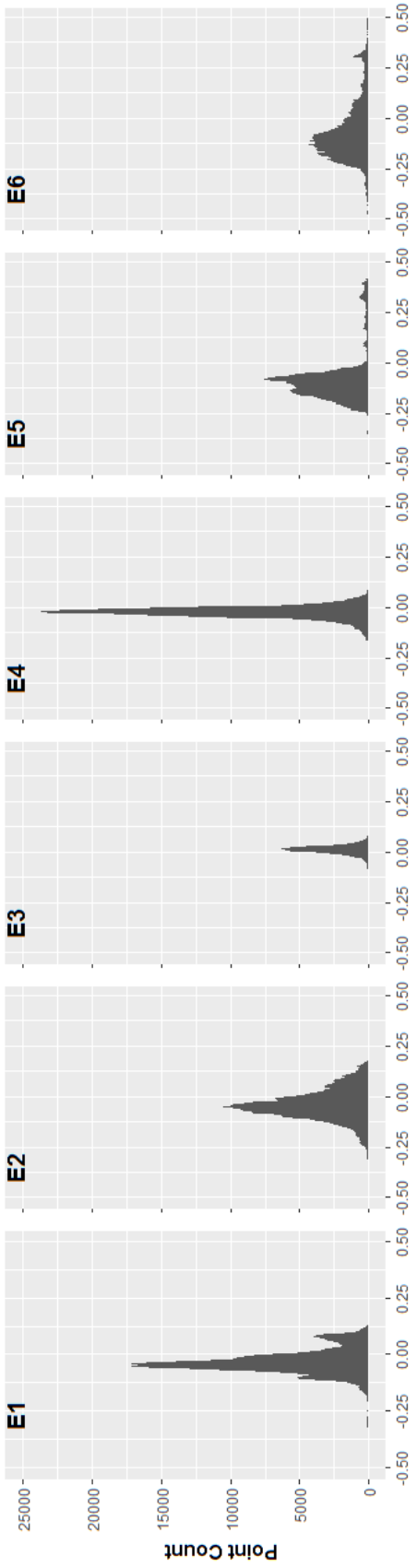

Figure 3.7: Histograms of the spread of change data recorded on bank 2

Table 3.6: Bank 3 complete cloud summaries

	E1 May 2017 - July 2017	**E2** July 2017 - Oct 2017	**E3** Oct 2017 - Feb 2018	**E4** Feb 2018 - May 2018	**E5** May 2018 - Aug 2018	**E6** Aug 2018 - Feb 2019
Total No. of Points on Bank	2486308	2375012	2665542	2640381	2678869	2509166
No. of Erosion Points	1520474	1567893	1155917	1943485	1210510	1472762
No. of Deposition Points	832407	546605	1415819	539666	1046677	733541
Max Erosion (m)	-1.999	-1.999	-2.022	-1.971	-1.993	-2.016
Max Deposition (m)	1.894	1.988	1.738	1.599	2.012	1.769
Mean Change (m)	-0.026	-0.024	0.003	-0.067	-0.011	-0.020
Percentage of Erosion Points	61.2	66.0	43.4	73.6	45.2	58.7
Percentage of Deposition Points	33.5	23.0	53.1	20.4	39.1	29.2
Percentage with no measurable change	5.4	11.0	3.5	6.0	15.7	12.1

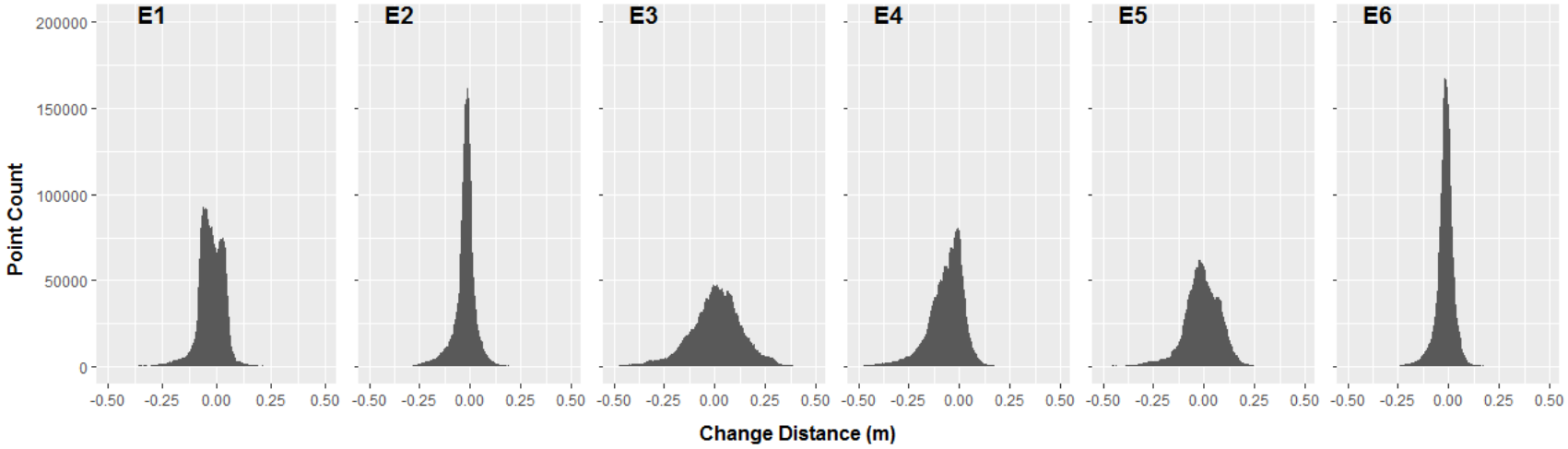

Figure 3.8: Histograms of the spread of change data recorded on bank 3

Table 3.7: Bank 3 Upstream cloud summaries

	E1 May 2017 - July 2017	E2 July 2017 - Oct 2017	E3 Oct 2017 - Feb 2018	E4 Feb 2018 - May 2018	E5 May 2018 - Aug 2018	E6 Aug 2018 - Feb 2019
Total No. of Points on Bank	1362853	1405164	1494801	1563164	1509102	1296631
No. of Erosion Points	565745	902831	650055	952995	805117	734649
No. of Deposition Points	717347	382802	792930	470208	626764	407279
Max Erosion (m)	-1.999	-1.969	-1.950	-1.292	-1.973	-1.982
Max Deposition (m)	1.505	1.634	1.034	1.599	1.452	1.530
Mean Change (m)	-0.007	-0.027	-0.000	-0.023	-0.003	-0.013
Percentage of Erosion Points	41.5	64.3	43.5	61.0	53.4	56.7
Percentage of Deposition Points	52.6	27.2	53.0	30.1	41.5	31.4
Percentage with no measurable change	5.9	8.5	3.5	9.0	5.1	12.0

Figure 3.9: Histograms of the spread of change data recorded on the upstream reach of bank 3

Table 3.8: Bank 3 Midstream cloud summaries

	E1 May 2017 - July 2017	**E2** July 2017 - Oct 2017	**E3** Oct 2017 - Feb 2018	**E4** Feb 2018 - May 2018	**E5** May 2018 - Aug 2018	**E6** Aug 2018 - Feb 2019
Total No. of Points on Bank	441834	337519	479153	761192	459865	675944
No. of Erosion Points	324761	292630	180059	549102	159197	437557
No. of Deposition Points	81072	24106	288783	27086	280289	157636
Max Erosion (m)	-1.981	-1.995	-2.022	-1.971	-1.951	-2.006
Max Deposition (m)	1.240	1.047	1.738	1.393	1.403	1.038
Mean Change (m)	-0.030	-0.031	0.049	-0.161	-0.007	-0.021
Percentage of Erosion Points	73.5	86.7	37.6	94.6	34.6	64.7
Percentage of Deposition Points	18.3	7.1	60.3	4.7	61.0	23.3
Percentage with no measurable change	8.1	6.2	2.2	4.4	4.4	11.9

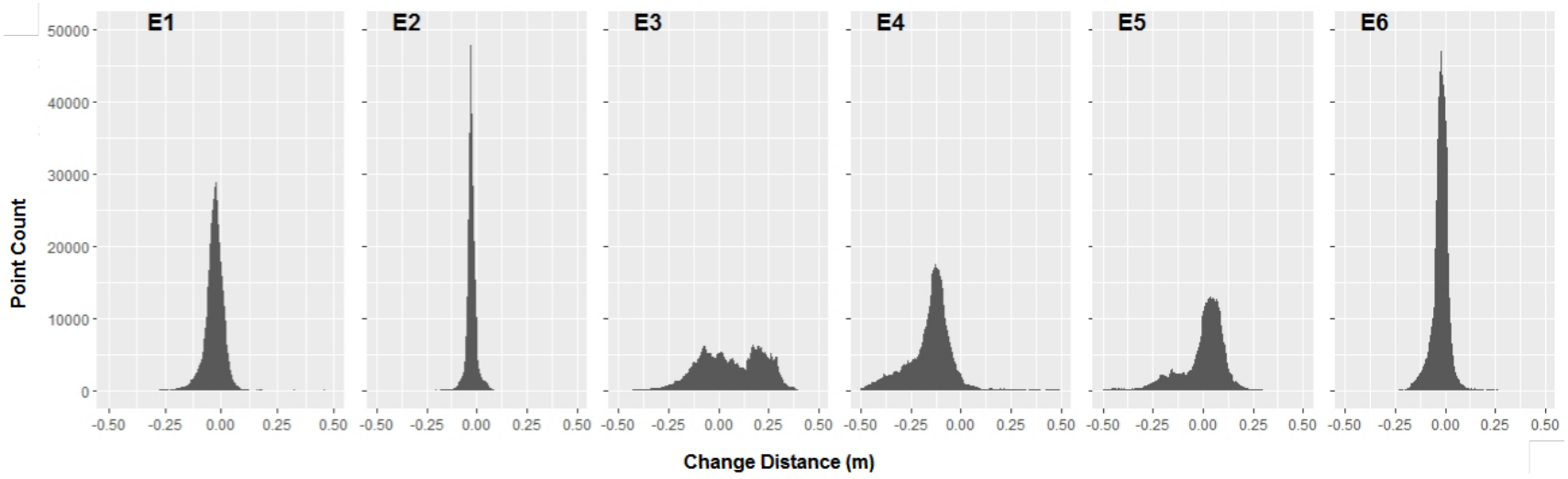

Figure 3.10: Histograms of the spread of change data recorded on the midstream reach of bank 3

Table 3.9: Bank 3 Downstream cloud summaries

	E1 May 2017 - July 2017	**E2** July 2017 - Oct 2017	**E3** Oct 2017 - Feb 2018	**E4** Feb 2018 - May 2018	**E5** May 2018 - Aug 2018	**E6** Aug 2018 - Feb 2019
Total No. of Points on Bank	681621	632329	691588	496543	404085	536591
No. of Erosion Points	629968	372432	325803	441388	246196	300556
No. of Deposition Points	33988	139697	334106	42372	139624	168626
Max Erosion (m)	-1.990	-1.999	-2.004	-1.751	-1.993	-2.016
Max Deposition (m)	1.894	1.988	1.291	1.334	2.012	1.769
Mean Change (m)	-0.061	-0.015	-0.022	-0.096	-0.043	-0.034
Percentage of Erosion Points	92.4	58.9	47.1	88.9	60.9	56.0
Percentage of Deposition Points	5.0	22.1	48.3	8.5	34.6	31.4
Percentage with no measurable change	2.6	19.0	4.6	2.6	4.5	12.6

Figure 3.11: Histograms of the spread of change data recorded on the downstream reach of bank 3

confidently defined as erosion or deposition.

As can been seen in the histograms for each bank, the spread of change values was small and usually skewed slightly to the left of 0, representing a dominance of low value erosion points. Time period E3 represented the only occasion when the results were dominated by deposition points across all three study banks.

Banks 1 and 2 both became heavily vegetated during the study period, resulting in large areas of occlusion limiting the collection of data covering the full bank face for many of the surveys. This is represented by blank areas in the change detection results, as vegetation points were identified and removed from the data (described in Chapter 3 Section 3.3) and is also reflected by the decrease in the number of recorded points on the banks from time period E1.

3.4.2 Change Detection Results

The results of change detection have been summarised in table 3.10. There was significant variation in the change values across the different banks and over the different time periods. This has been visualised in figure 3.12, which shows a comparison of the rate of change per m^2 per year, as a volume, between the different banks and the different time periods.

As noted earlier, the study banks were dominated by low level erosion across all time periods except for E3, where significant low level deposition values resulted in net deposition across bank 2 and both the upstream and midstream sections of bank 3.

Bank 1

For the majority of the time periods, Bank 1 saw widespread low magnitude erosion (figure 3.13). The highest mean change value recorded during

Table 3.10: Summary of calculated erosion values for all banks

Bank	Time Period	Total Erosion (m^3)	Erosion Area (m^2)	Total Deposition (m^3)	Deposition Area (m^2)	Net Total Change (m^3)	Change Area (m^2)	Net Volume Change per m^2 (m^3)	Volume of Change per m^2 per Year (m^3)
Bank 1	E1	-0.966	14.378	0.068	1.581	-0.899	15.958	-0.056	-0.294
	E2	-0.444	10.951	0.049	1.528	-0.395	12.479	-0.032	-0.143
	E3	-0.412	5.202	0.157	5.547	-0.255	10.749	-0.024	-0.065
	E4	-0.565	8.767	0.108	3.778	-0.458	12.545	-0.036	-0.160
	E5	-0.258	8.909	0.080	4.130	-0.179	13.039	-0.014	-0.049
	E6	-0.525	10.968	0.059	2.518	-0.465	13.486	-0.034	-0.070
Bank 2	E1	-0.709	12.876	0.241	4.186	-0.467	17.062	-0.027	-0.143
	E2	-0.887	11.572	0.226	3.567	-0.661	15.139	-0.044	-0.197
	E3	-0.021	0.826	0.104	3.909	0.083	4.736	0.018	0.048
	E4	-0.317	9.433	0.043	1.611	-0.274	11.044	-0.025	-0.109
	E5	-1.194	10.449	0.361	1.416	-0.833	11.865	-0.070	-0.251
	E6	-1.137	8.269	0.356	2.242	-0.780	10.511	-0.074	-0.150
Bank 3 All	E1	-3.649	60.168	1.093	27.363	-2.556	87.531	-0.029	-0.152
	E2	-2.884	58.582	0.549	16.541	-2.335	75.122	-0.031	-0.142
	E3	-5.019	39.489	5.381	48.871	0.362	88.360	0.004	0.007
	E4	-8.078	71.627	0.794	16.857	-7.284	88.484	-0.082	-0.295
	E5	-3.863	42.094	2.323	35.136	-1.540	77.230	-0.020	-0.041
	E6	-2.770	58.315	0.783	26.231	-1.987	84.546	-0.023	-0.092
Bank 3 Upstream	E1	-1.057	17.828	0.911	22.351	-0.147	40.178	-0.004	-0.019
	E2	-1.753	28.228	0.369	9.763	-1.384	37.991	-0.036	-0.166
	E3	-1.555	15.425	2.422	23.103	0.867	38.529	0.023	0.038
	E4	-1.625	28.979	0.519	13.606	-1.106	42.585	-0.026	-0.093
	E5	-1.383	23.010	1.172	17.421	-0.211	40.431	-0.005	-0.011
	E6	-0.958	24.472	0.366	12.107	-0.592	36.579	-0.016	-0.064
Bank 3 Midstream	E1	-0.683	14.708	0.135	3.824	-0.549	18.532	-0.030	-0.154
	E2	-0.579	15.082	0.038	1.244	-0.541	16.326	-0.033	-0.151
	E3	-1.192	8.800	2.089	12.716	0.897	21.516	0.042	0.070
	E4	-3.943	23.694	0.166	1.089	-3.777	24.783	-0.152	-0.545
	E5	-0.824	7.078	0.895	13.047	0.071	20.125	0.004	0.007
	E6	-0.910	20.678	0.188	6.793	-0.722	27.470	-0.026	-0.103
Bank 3 Downstream	E1	-2.301	35.187	0.051	1.306	-2.250	36.493	-0.062	-0.321
	E2	-0.493	18.077	0.197	7.655	-0.296	25.732	-0.012	-0.053
	E3	-1.534	14.732	1.109	16.579	-0.425	31.312	-0.014	-0.023
	E4	-2.550	23.070	0.117	2.366	-2.434	25.437	-0.096	-0.342
	E5	-1.455	12.819	0.400	6.981	-1.055	19.800	-0.053	-0.110
	E6	-0.994	16.316	0.301	9.702	-0.693	26.018	-0.027	-0.105

the study period was time period E1 (May 2017 - June 2017) of -0.057m which resulted in a net change volume of -0.899m^3 across the measurement area of 15.9m^2. Due to increased levels of vegetation, E1 represents the largest bare bank area able to be recorded during the study period, with the measured area dropping as low as 10.7m^2 during E3 when vegetation was at it's largest extent. The net change per m^2 was at it's highest during E1 at -0.056m^3 and it's lowest recorded value was during E5 when it fell to -0.014m^3.

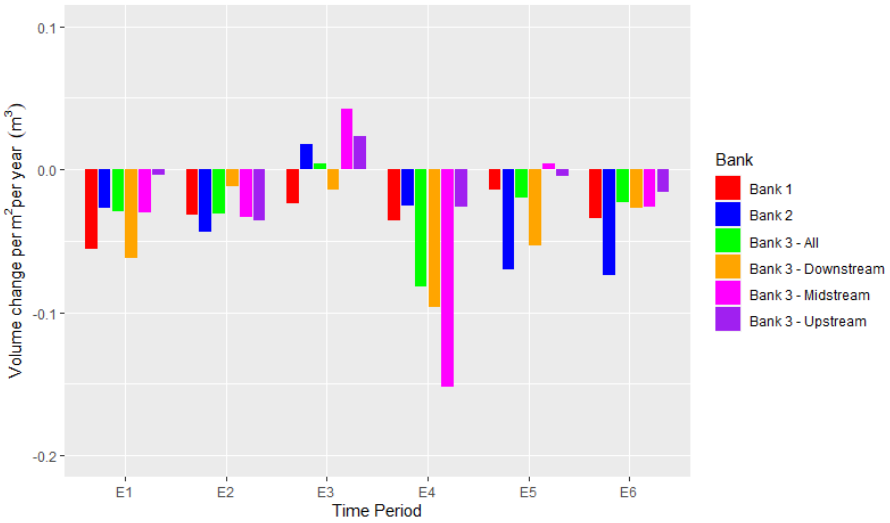

Figure 3.12: Comparison of the rate of change per metre squared per year across all of the the study banks

The largest deposition extent was recorded during E3 when the deposition area was calculated at 5.5m^2. Although there was still a net erosion during this time period, this increased area of deposition does align with the results of banks 2 and 3 which saw larger areas of deposition and a net deposition across the bank as a whole.

The most consistent areas of erosion were concentrated not at the bank toe, where it would be most regularly exposed to fluvial action, but in the mid bank regions. Top of bank was dominated by small areas defined as mass failures, but otherwise was also prone to widespread, low magnitude

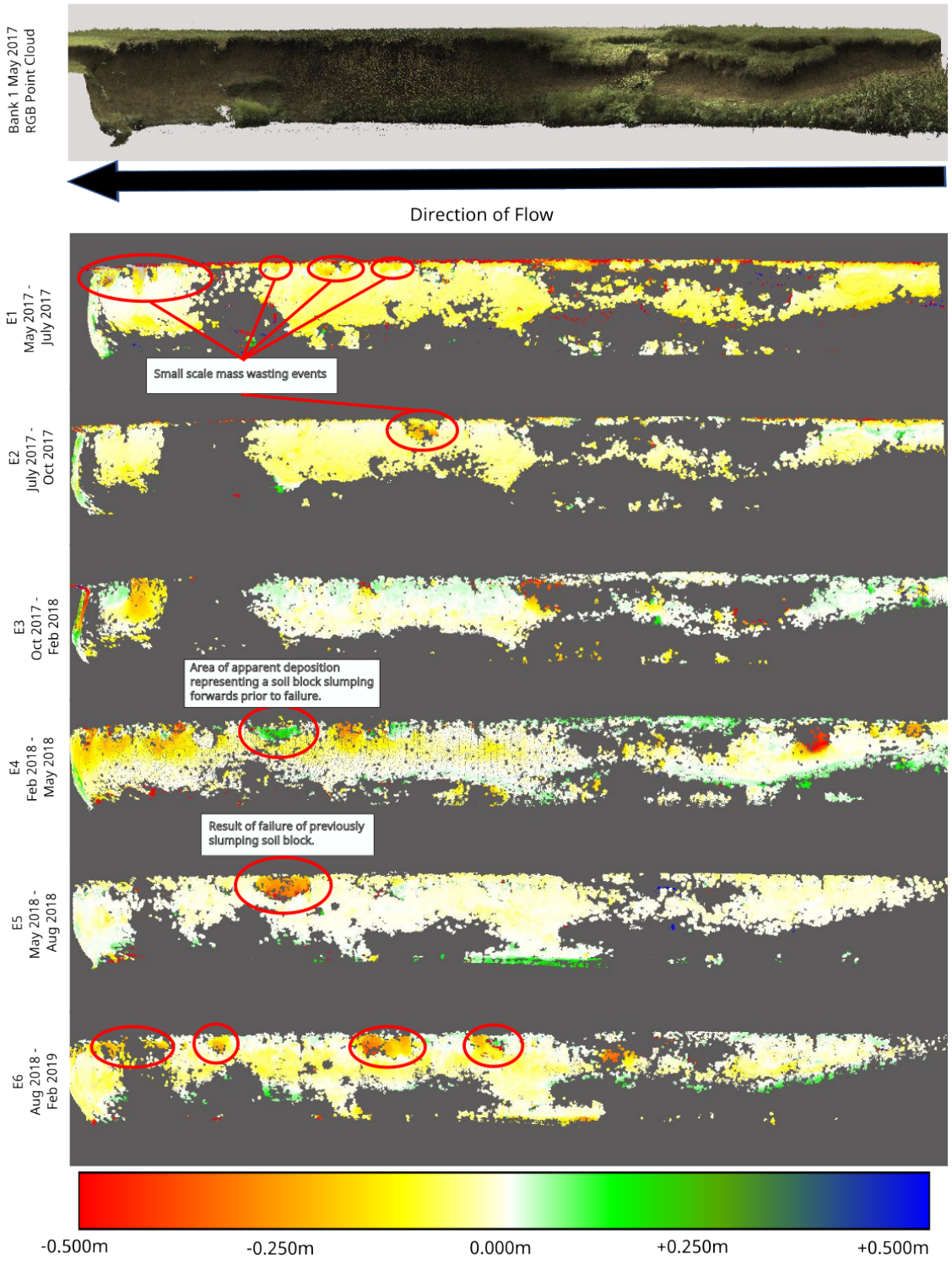

Figure 3.13: Bank 1 - Results of M3C2 change

change.

Time period E4 (February 2018 - May 2018) exhibited a small area of apparent deposition at the top of bank, while the same area in E5 shows significant localised erosion.

Bank 2

Bank 2 (figure 3.14) is located approximately 25m downstream of Bank 1, and positioned on the opposite side of the channel. Despite their proximity and the similarity in their structure and materials, Bank 2 saw very different patterns and rates of erosion compared to Bank 1.

Bank 2 was the most significantly affected by the growth of vegetation, with much of the bank area becoming occluded during the study period. This is demonstrated by the detectable change area falling as low as only 4.7m^2 during time period E3 (October 2017 - February 2018), when vegetation was at its peak. During this time very little erosion was detected, and instead widespread areas of very low deposition were recorded. This resulted in a mean change value of 0.015m across the bank and a net change volume of 0.083m^3. E4 saw widespread areas of low erosion values, however E5 and E6 saw significant areas of erosion across the site, with some small concentrations of erosion values above -0.25m and a resultant change of -0.83m^3 in E5 and -0.78m^3 in E6. However, there were also significant areas of deposition recorded in those time periods, concentrated around the extreme upstream and downstream ends of the study bank. In E5 the areas of deposition existed immediately downstream of a large area that had become heavily vegetated, and in E6 a similar area of heavy vegetation existed just outside of the study area on the upstream side. Unlike all of the other banks, no mass failures were detected on bank 2 throughout the entire study period, leaving all change the results

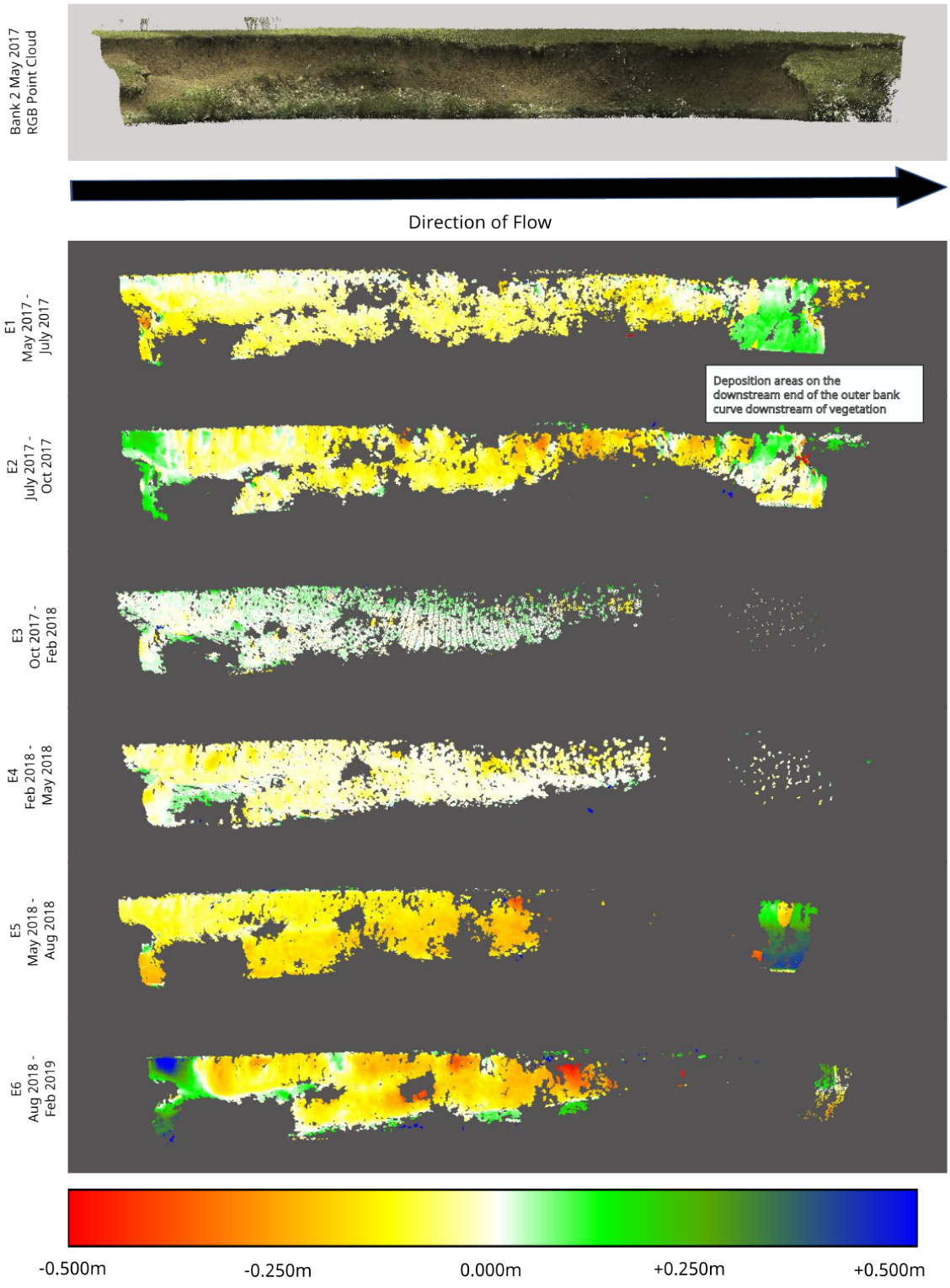

Figure 3.14: Bank 2 - Results of M3C2 change

of fluvial and subaerial processes.

Bank 3 - Upstream

The upstream reach of Bank 3 (figure 3.15) saw significant variation in change values across the bank. E1 saw erosion concentrated at the bank toe and lower bank reaches, with only small areas of more significant erosion at the top of bank resulting in a net change of -0.147m^3. The highest net change, -1.384m^3, was recorded during time period E2 across a detectable change area of 38m^2.

The upstream section of Bank 3 was the largest of the bank sections observed, with a maximum detectable change area of 40.4m^2. It was also the bank least impacted by vegetation growth with a minimum detectable change area of 36.6m^2, a loss of only 10%.

Like banks 1 and 2, time period E3 represented the largest area of detected deposition, 23.1m^2, which resulted in a net change value of 0.867m^3.

The mid bank was dominated by low deposition values. E2 saw much more widespread erosion across the whole bank face, with small areas of deposition concentrated at the bank toe. E3 again saw considerable variation across the bank, with large concentrations of both erosion and deposition values. Like bank 2, E3 was the only time period to exhibit a net deposition across the bank, total deposition volume of 0.867m^3 over a deposition area of 23.103m. E4, E5 and E6 began show more consistent and widespread erosion across the site, with only small, localised areas of deposition, frequently near the bank toe.

Bank3 - Midstream

Like the upstream reach, the midstream reach of Bank 3 (figure 3.16) also saw variation in patterns of erosion and deposition across the bank face.

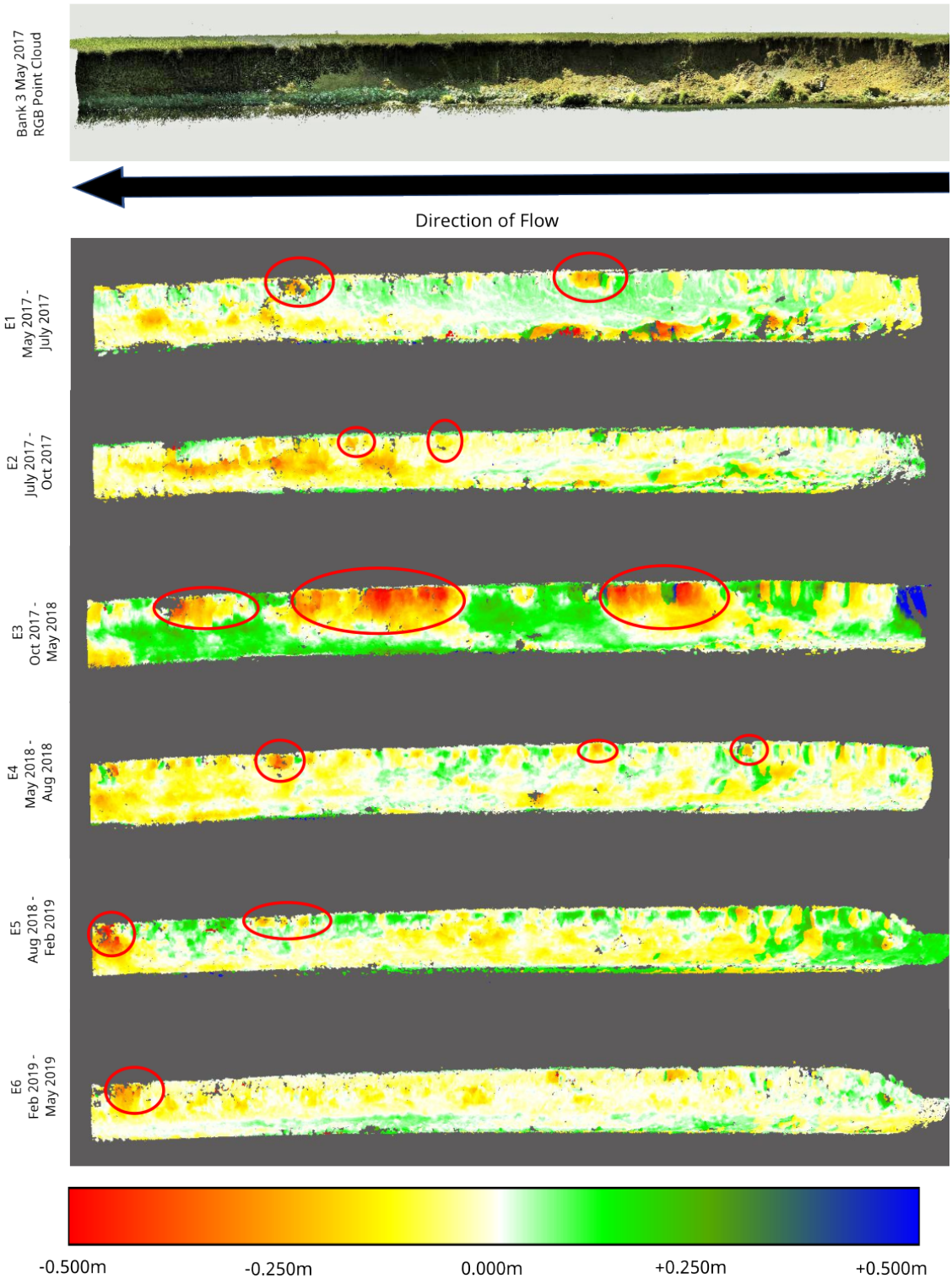

Figure 3.15: Bank 3 Upstream - Results of M3C2 change

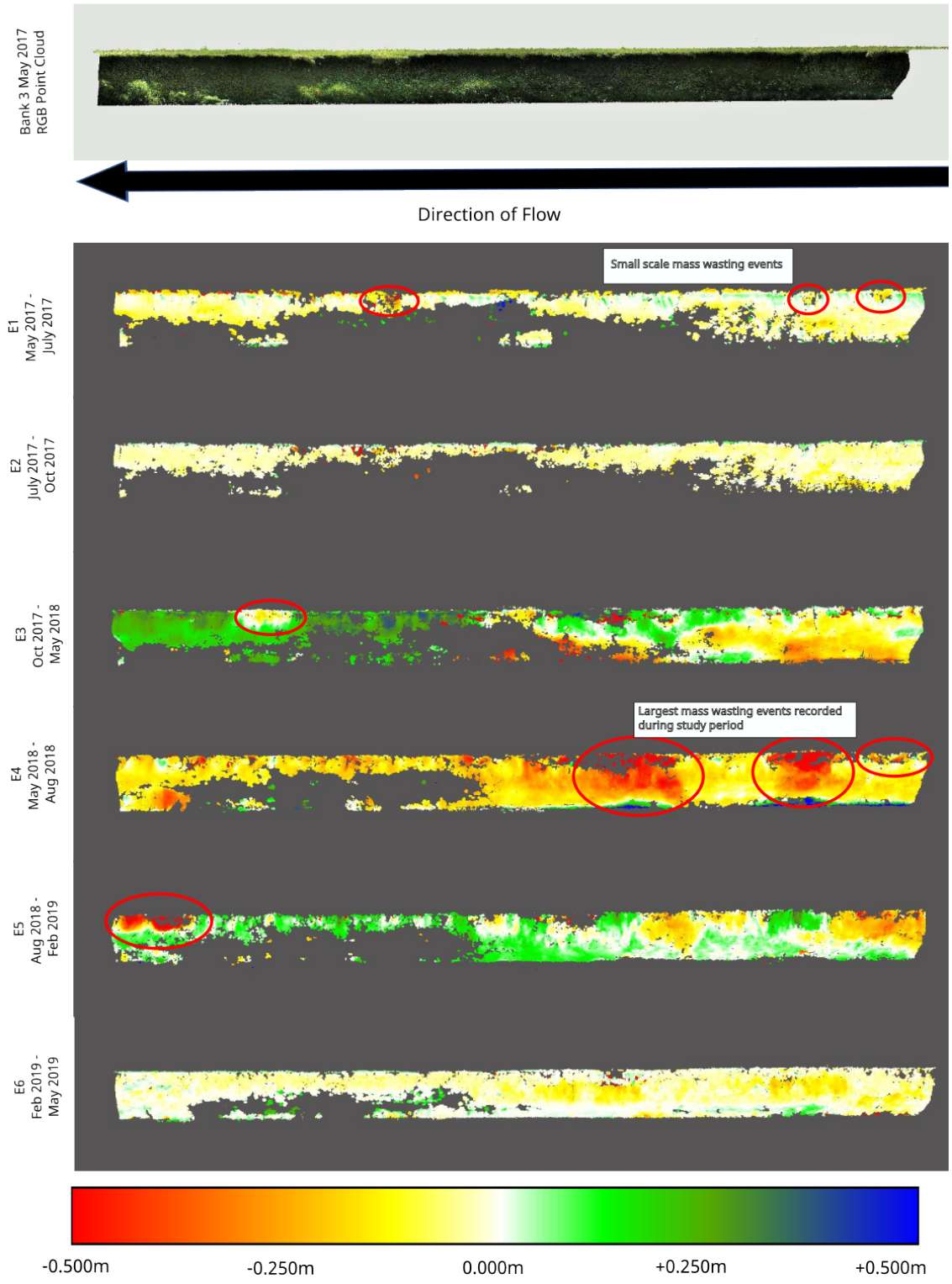

Figure 3.16: Bank 3 Midstream - Results of M3C2 change

It was also the most heavily vegetated area of Bank 3 during the study period, with the detectable change area varying by as much as 11.144m^2, from 27.470m^2 in time period E6 to 16.326m^2 in time period E2. E1 and E2 saw widespread, low erosion values across the majority of the bank face, resulting in net change values of -0.549m^3 and -0.541m^3 respectively. E3 saw widespread areas of deposition over the full bank height for much of the bank. Like bank 2 and the upstream reach of bank 3, this resulted in a net deposition of 0.897m^3. E4 saw a significant increase in erosion processes, with widespread areas of erosion along the whole length and height of the bank resulting in as much as 0.5m of erosion from some areas and a net change value of -3.777m^3, the highest recorded net change value for any bank section across the entire study period. E5 saw a return to deposition dominating the bank (net change value of 0.071m^3), while E6 returned to a dominance of low level erosion values and a net change value of -0.722m^3.

Bank 3 - Downstream

The downstream reach of bank 3 (figure 3.17) experienced very similar variation in erosion and deposition as the other bank sections, with low magnitude erosion covering much of the bank face for most of the time periods. E1 and E2 both saw widespread areas of low erosion values, with net change values of -2.250m^3 and -0.296m^3 respectively. Like all other bank sections, E3 saw the largest deposition contribution of 16.579m^2, however like bank 1 this was not enough to result in a net deposition volume across the bank face, with a net change value of -0.425m^3. Like the midstream reach of bank 3, E4 saw an almost complete dominance of erosion, with some areas showing erosion of up to 0.5m and resulting in a net change volume of -2.434m^3. Time period E5 was dominated by erosion, with a net change value of -1.055m^3, while E6 saw much lower

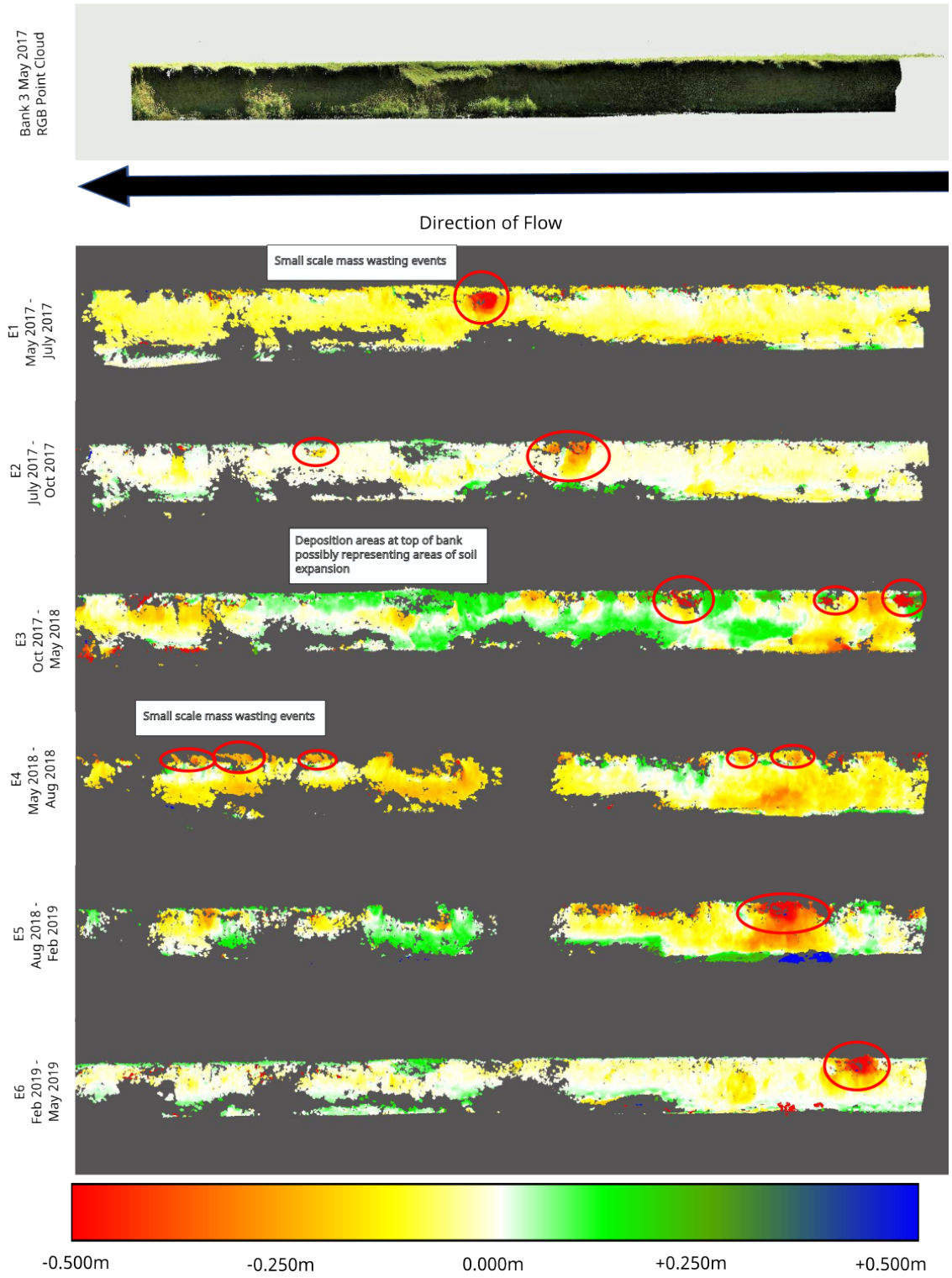

Figure 3.17: Bank 3 Downstream - Results of M3C2 change

erosion values and a net change value of -0.693m^3.

3.4.3 Relative Contributions of Erosion Processes

An initial step in the analysis was to establish whether there is any difference between erosion above and below the Q10 level, which was chosen to represent the cut off between subaerial and fluvial erosion. The Q10 level was chosen as the cut off due to its existing usage for defining the high flow of a river. However, this choice was an arbitrary one and the potential impacts of the use of Q10 as the boundary between the two processes will be discussed later in the chapter. As can be seen in table 3.11, there was no consistent pattern of higher erosion values being found in either the above or below Q10 area of bank.

Table 3.11: Mean erosion values for the above Q10 and below Q10 portions of each bank. Values in **bold** represent the larger erosion value of the two sections of bank.

Bank Section	Mean Erosion Above Q10 (m)	Points Above Q10	Mean Erosion Below Q10 (m)	Points Below Q10	Erosion Difference
Bank 1	**-0.054**	582899	-0.046	8814	0.008
Bank 2	-0.080	524000	**-0.086**	13321	0.007
Bank 3 - Upstream	**-0.061**	1250575	-0.059	128851	0.002
Bank 3 - Midstream	-0.089	827618	**-0.100**	72780	0.011
Bank 3 - Downstream	-0.076	1084041	**-0.096**	117981	0.020

Full tables of the erosion values calculated for each bank and for each erosion process can be seen in Appendix B, tables B.1 to B.17.

A summary of the percentage erosion contributions from the different erosion processes is presented in table 3.12. The contributions of mass wasting, fluvial erosion below the Q10 level and subaerial erosion above the Q10 level were then added to a ternary plot (figure 3.18) to visualise the relative impact of the different erosion processes.

All time periods were dominated by subaerial erosion, with the smallest portion of total erosion coming from fluvial erosion, however there was significant variation in the percentage contribution values across the dif-

Table 3.12: Summary of erosion contributions for each bank and each time period

Time Period	Subaerial Above Q10 Stage (%)	Fluvial Below Q10 Stage (%)	Mass Wasting (%)
	Bank 1		
E1	89.3	1.2	9.5
E2	93.0	0.8	6.1
E3	99.4	0.6	0.0
E4	99.3	0.7	0.0
E5	59.4	2.6	38.0
E6	68.8	2.3	28.8
	Bank 2		
E1	97.7	2.3	0.0
E2	98.5	1.5	0.0
E3	99.6	0.4	0.0
E4	98.9	1.1	0.0
E5	95.3	4.7	0.0
E6	100.0	0.0	0.0
	Bank 3 - Upstream		
E1	64.7	26.9	8.4
E2	87.1	11.4	1.5
E3	33.1	2.2	64.7
E4	84.0	9.8	6.2
E5	91.4	4.1	4.5
E6	90.5	2.3	7.2
	Bank 3 - Midstream		
E1	87.3	8.0	4.7
E2	94.4	5.6	0.0
E3	86.4	11.6	2.0
E4	70.6	11.8	17.6
E5	63.3	0.6	36.1
E6	96.0	4.0	0.0
	Bank 3 - Downstream		
E1	72.9	17.9	9.2
E2	50.1	9.7	40.2
E3	83.2	4.8	12.0
E4	77.8	15.8	6.5
E5	78.5	4.6	16.9
E6	64.3	12.9	22.8

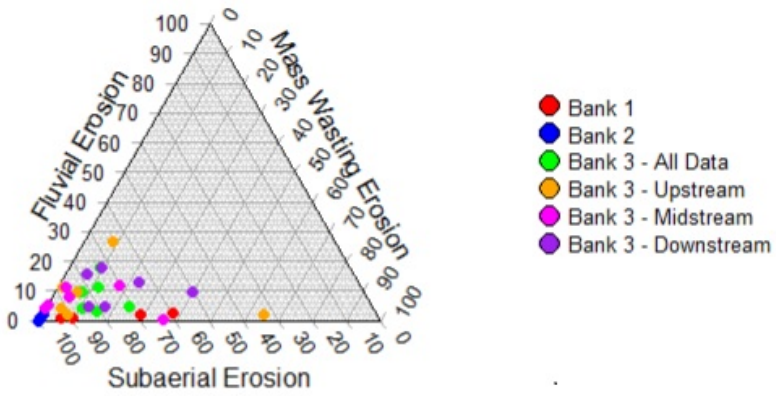

Figure 3.18: All banks - Relative contributions of erosion processes

ferent banks. Bank 1 saw between 59.4% and 99.4% of erosion volumes coming from subaerial sources in all time periods, with very little contribution from fluvial sources (0.6% to 2.6%), as shown in figure 3.19 (a). Mass wasting contributed between 0% and 38.0% of the total erosion volume.

Bank 2 saw an even more significant contribution from subaerial erosion sources, as there were no identified mass wasting events at the site during the study period. At bank 2, the minimum subaerial contribution was calculated as 95.3% (figure 3.19 (b)), with a maximum of 4.7% of erosion from fluvial sources.

Bank 3, the furthest downstream, exhibited larger variations in the relative contributions, however the site was still dominated by subaerial erosion processes (figure 3.19 (c)). Bank 3 as a whole saw upward of 71.3% of erosion coming from subaerial processes, with between 7.8% and 24.2% coming from mass wasting, while between 3.0% and 18.0% came from fluvial sources.

However, there was significantly more variation in the contribution of the

different processes between the three different sections of bank 3. The upstream section of bank 3 saw between 2.2% and 29.9% contribution from fluvial erosion, with between 1.5% and as much as 64.7% coming from mass wasting, the highest recorded proportions to come from mass wasting across all of the sites. The remaining 33.0% to 91.4% of erosion was attributed to subaerial processes (figure 3.19 (d)).

The midstream region of bank 3 saw between 0.6% and 11.8% of erosion attributed to fluvial processes, with between 0% and 36.1% due to mass wasting processes and 63.3% to 96.0% attributed to subaerial erosion processes (figure 3.19 (e)). Finally, the downstream reach of bank 3 saw between 4.6% and 17.9% of erosion from fluvial processes, 6.4% to 40.2% from mass wasting and 50.1% to 83.2% from subaerial processes (figure 3.19(f)).

3.5 Discussion

3.5.1 Patterns of erosion and deposition

As shown in figures 3.13 - 3.17, and in the tables of erosion values in Appendix B, tables B.1 to B.17, there is significant variation in erosion and deposition across the different banks during the study period.

Erosion dominates for much of the bank and for most of the study period, however there is significant deposition recorded frequently across all banks. Between a small number of scans, most notably between E4 and E5 at Bank 1, localised areas of deposition appeared in one scan and then localised erosion appeared in the subsequent scans. Upon closer inspection it was determined that this represented an area of the bank preparing to fail, with the area of apparent deposition showing where the material is beginning to separate from the bank and slump forward. This gives the

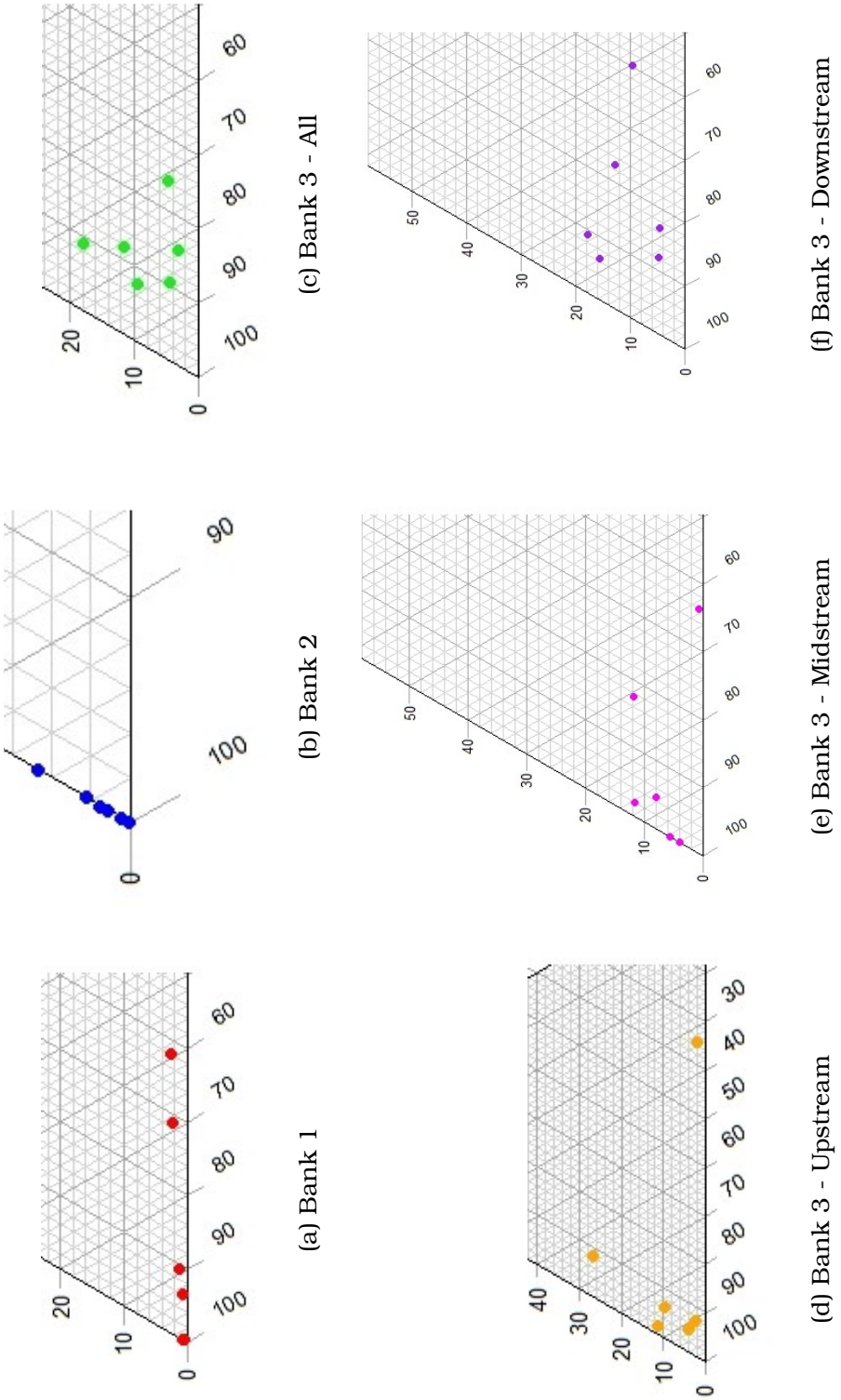

Figure 3.19: Zoomed Ternary plots showing the data for each bank

appearance of deposition, as the face of the failing block appears closer to the viewer than in previous scans, however does not actually represent an increase in the volume of material on the bank. This phenomenon has also been observed by Foerst and Rüther (2018), who saw similar results near the bank top of the outer edges of meander bends. They also attributed the apparent deposition to imminent bank failure, in most cases attributing that failure to rotating blocks of material preparing to fail.

As well as these localised features there was also much more widespread deposition across the mid-bank. The scale of the deposition was unexpected, with as much as 0.5m of deposition recorded in some places. Deposition was also recorded right up to the top of bank, and given the almost vertical bank face this too was unexpected.

Registering of the scans was checked repeatedly to ensure that there was no error in the positioning of individual scans relative to one another, and it was determined that the registration was accurate, with registration errors for each scan being less than 5mm and the target positions the same for all surveys. To confirm the registration and scan alignment accuracy, the centre points of each target were extracted for each scan. There was less than 5mm of variation in the centre point coordinates for each scan, again demonstrating the alignment accuracy of the scans. Visual examination of the scans also showed consistently accurate overlap between permanent objects within the wider field of view, including tree trunks and fence posts, again confirming the scan alignment was not responsible for incorrectly generating these apparent deposition values.

The same time periods, E3 and E5, generated similar deposition values and patterns across bank 2 and all sub sections of bank 3, again suggesting that the deposition values were generated by the site conditions

and not by scan alignment errors, as banks 2 and 3 were scanned and registered separately, but both exhibited similar patterns of deposition.

Research conducted by other authors (Leyland et al., 2015; Longoni et al., 2016; Foerst and Rüther, 2018) has also shown similar patterns of deposition within their study areas as shown in figures 3.20, 3.21 and 3.22. In each case, very little explanation was made to account for these relatively large deposition values (up to 0.4m for Longoni et al. (2016) and up to 0.5m for Foerst and Rüther (2018)).

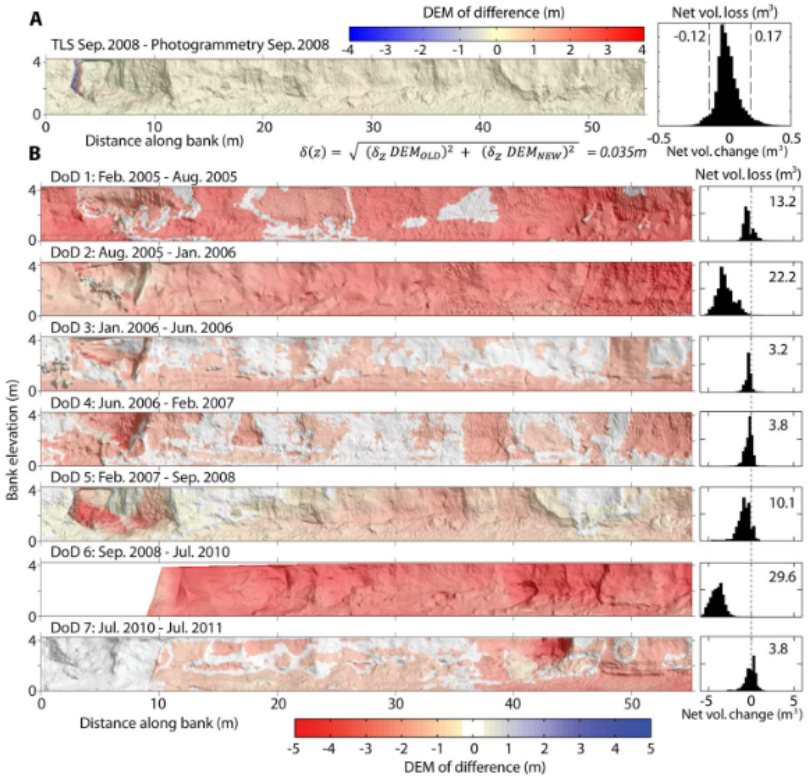

Figure 3.20: Figure from Leyland et al. (2015) showing erosion and deposition areas along the studied bank with histograms of the spread of erosion and deposition points.

Henshaw et al. (2013) also found deposition values at 21% to 40% of pins in a study of the Pontbran Catchment, Wales. The authors of this study attributed the values to deposition processes resulting from erosion in the upper bank dropping material onto the lower bank and to soil expansion

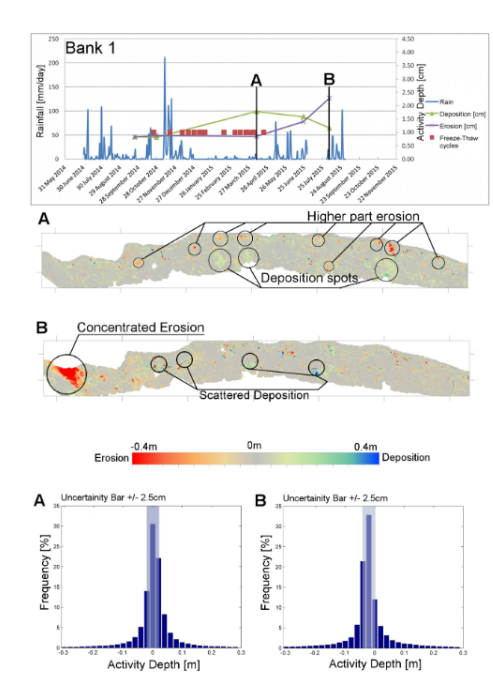

(a) Bank 1

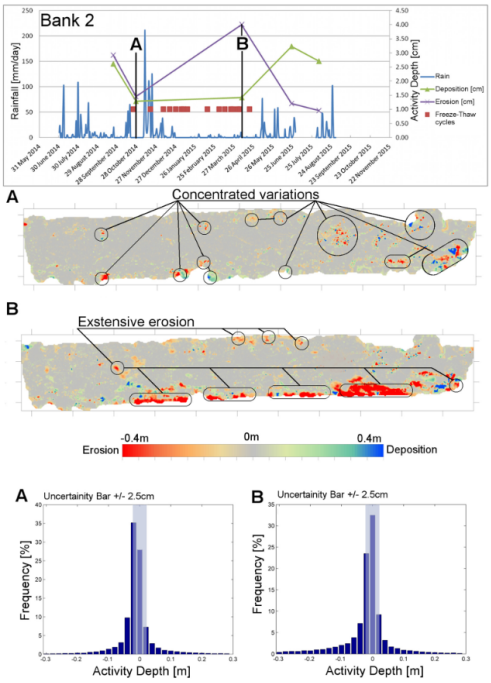

(b) Bank 2

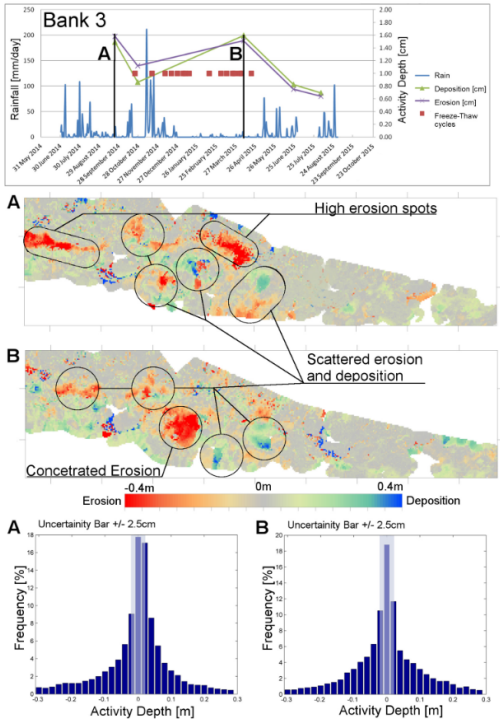

(c) Bank 3

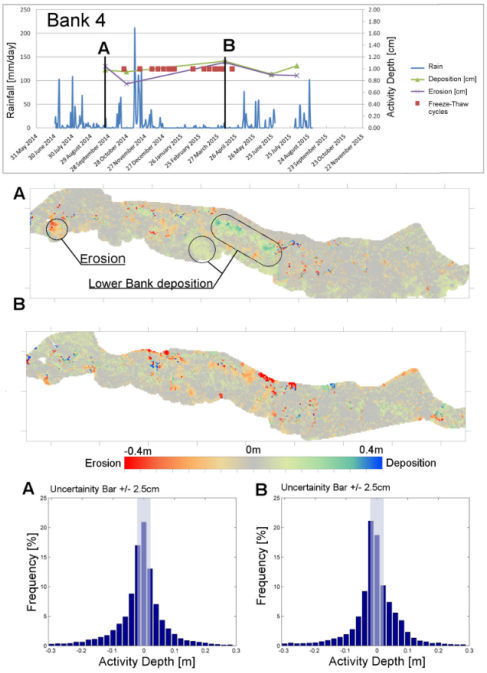

(d) Bank 4

Figure 3.21: Figures from Longoni et al. (2016) showing areas of erosion and deposition up to 0.4m along the studies banks with histograms of the spread of erosion and deposition points.

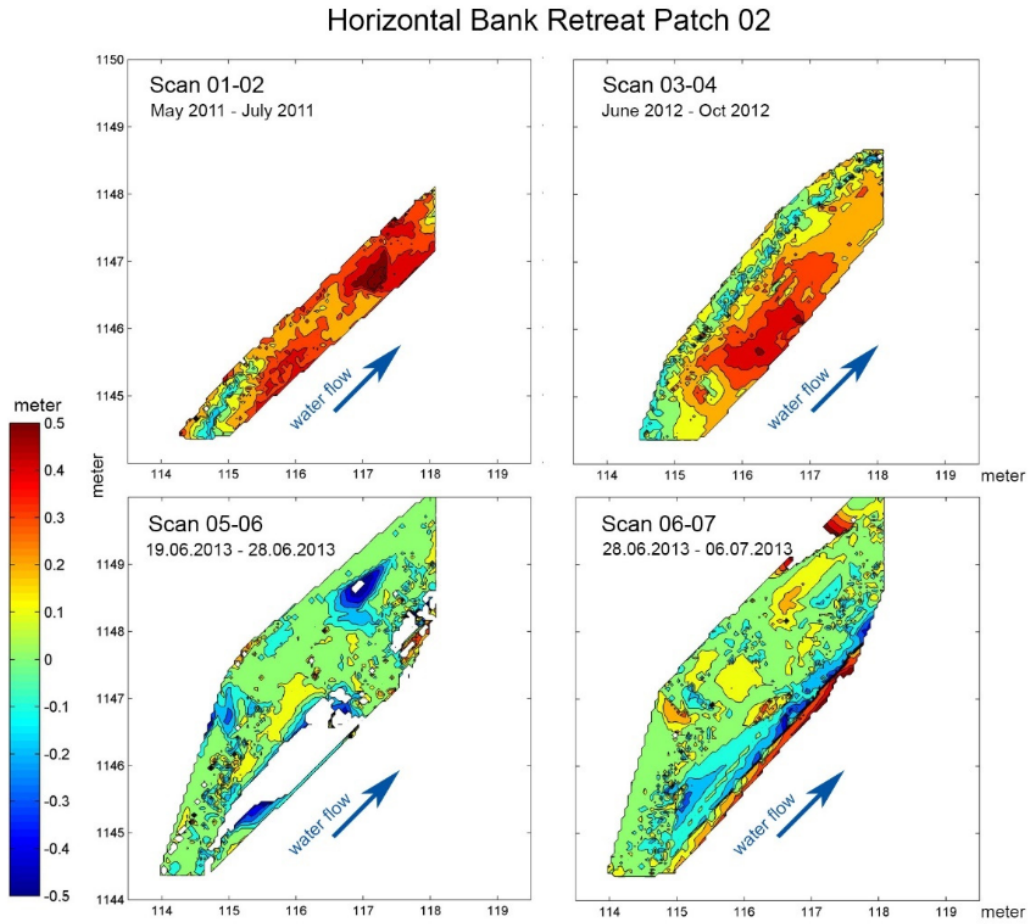

Figure 3.22: Figure from Foerst and Rüther (2018) showing erosion and deposition areas along one of the studied banks.

processes.

Both the E3 and E5 time periods encompassed the winter months, from October 2017 to May 2018 and August 2018 to February 2019 respectively. These time periods are typified by the expansion and contraction of soil as a result of freeze-thaw processes, wetting and drying processes and the potential for sediment sloughing from upper areas of the bank to settle on the lower face of the bank. Couper (2003) investigated the effect of wetting-drying and freeze-thaw cycles on the dimensions of soils blocks with different clay contents and observed dimension changes of up to 15% for wetting-drying processes and expansion of up to 5mm for a block ex-

posed to freeze-thaw cycles. Few erosion pin studies have identified such large deposition volumes, however this could be explained by pins moving with the expanding soil block and so not detecting soil expansion to this degree. In the following chapter, work was undertaken to identify whether there was a relationship between deposition and the flow and meteorological conditions experienced at the study sites, however the presence and spatial distribution of such large deposition values represents an under-investigated topic and as such should be considered as an area for further research.

3.5.2 Relative Contributions of Erosion Processes

Defining the cutoff between subaerial and fluvial processes

As introduced in section 3.6.3, the Q10 and Q50 levels were considered as division lines for areas of the bank deemed to have been subject to subaerial/fluvial processes. These values were originally chosen as they represent the high flow (Q10) and median flow (Q50) of a river and are established and meaningful values in river science. As field collection was undertaken, it became clear that the Q50 level would not be an appropriate cutoff value in this work, due to flow conditions on data collections days sometimes exceeding the Q50 level and resulting in no data being able to be collected for the bank below that point. Thus the Q10 level was chosen and the main cutoff between subaerial and fluvial processes.

However, the use of these values in this work is still largely arbitrary. The decision to use the Q10 level for ternary plotting and to take forward for further analysis in later chapters was made based on the results obtained from the work using both Q10 and Q50. The Q50 fluvial erosion contribution calculated from those scans where Q50 data was available was frequently below 0.5% with a very small range of contribution values be-

tween 0% and 5.7% whereas the Q10 fluvial erosion contribution demonstrated a range of between 0% and 26.9% with at least some erosion being attributed to this category in 29 out of 30 measurements. However, it is very important to recognise that the use of Q10 may be creating an underestimation of the amount of erosion attributed to subaerial processes, as the amount of time fluvial action is working on the below Q10 portion of the bank will vary with height. As such we may actually be attributing subaerial erosion to fluvial processes. Further investigation into the affect of different levels for defining the cutoff between subaerial and fluvial erosion in the future may help to understand the extent of this potential underestimation.

The percentage of erosion being attributed to the different processes is a function of the measurable area over which each of the different processes can be recorded. Much of the work of fluvial processes is occurring below the permanent water surface, an area that is still extremely difficult to measure with conventional techniques. A combination of measurement techniques that work both above and below the water surface is required to more accurately define the contribution of fluvial processes working below the permanent water level. However, such techniques were outside of the scope of this PhD.

Developing Erosion Dominance Model

Across all sites, erosion was dominated by subaerial process, with mass wasting contributing significant erosion volumes during discrete 'events' when failures occurred. However the contribution of fluvial erosion was much lower than expected. These findings add further weight to the importance of subaerial processes in their own right, rather than as only preparatory processes. Subaerial processes work over far more significant

time scales than fluvial processes, which are intermittent in their coverage of a bank. The low magnitude but high frequency erosion dominates at this site, despite there being periods of time when the channel was fully inundated. The presence of high flows during the study period suggests that, even when high flows do occur, they do not necessarily result in erosion events of a high enough magnitude to overcome the dominance of the constantly working sub-aerial processes.

This dominance of subaerial erosion processes at this site is broadly consistent with other studies observing subaerial erosion, and erosion at this site in particular (e.g. Prosser et al. (2000), Couper and Maddock (2001), and Wynn et al. (2008)). However there remains a significant proportion of literature that places fluvial erosion as the dominant process driving bank change (Henshaw et al., 2013; Grove et al., 2013; Foerst and Rüther, 2018; Jugie et al., 2018).

From the erosion proportions observed in this study, a model of erosion contributions was developed. The model, named the Erosion Dominance Model (EDM), was based on the concepts of the ARISE model of alpine flow contributions by Brown et al. (2009), which broke the percentage contributions of three different alpine water sources (glacial, groundwater and quickflow) into nine categories of dominance. The erosion dominance model shown in figure 3.23 follows the same principals, creating nine categories of erosion dominance which are detailed in table 3.13.

As can be seen in figure 3.24, the majority of the points (29 of 36) in this study fell into the Subaerial Dominant category, with five points falling into the Subaerial - Mass Wasting category and one point falling into each of the Subaerial - Fluvial and Mass Wasting - Subaerial categories.

In the next chapter, the influence of flow variables and meteorological

variables on the rates and volumes of erosion attributed to the different erosion processes will be examined and analysed to determine whether erosion via these different processes can be predicted.

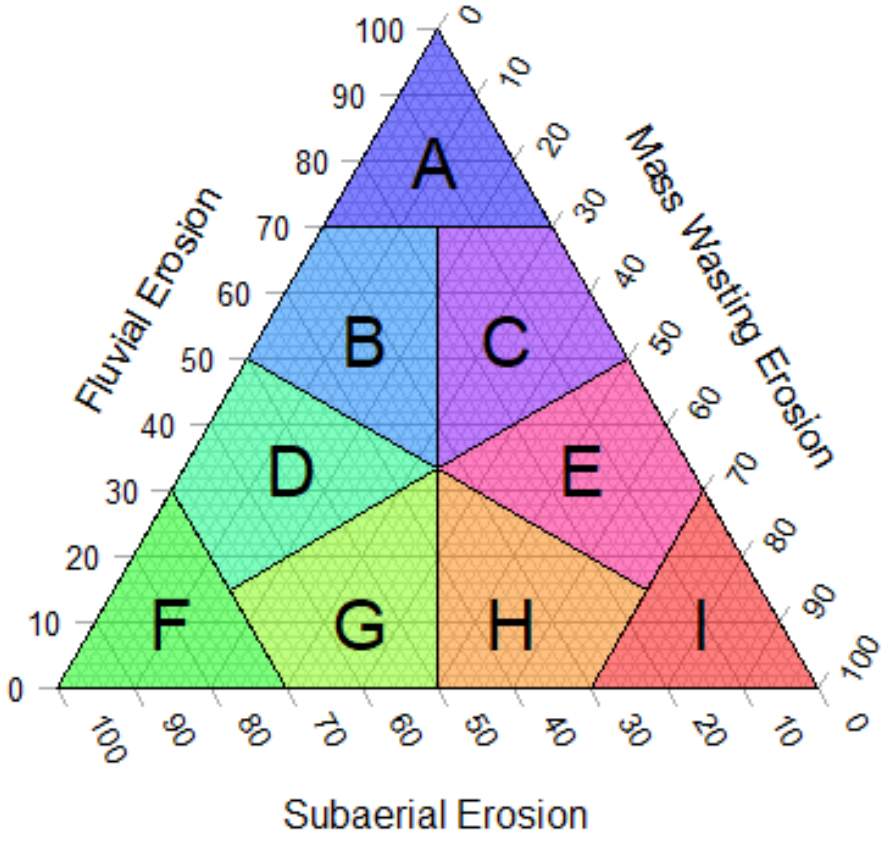

Figure 3.23: Model of erosion dominance

Table 3.13: Descriptions of the different sections of the proposed erosion dominance model shown in figure 3.23

Reference	Model Category	Category description
A	Fluvial Dominant	Fluvial Erosion contribution above 70% - Combined contribution of Subaerial and Mass Wasting processes <30%
B	Fluvial - Subaerial	Fluvial processes dominant (between 35-70%) - Contribution of Subaerial processes exceeds that of Mass Wasting
C	Fluvial - Mass Wasting	Fluvial processes dominant (between 35-70%) - Contribution of Mass Wasting exceeds that of Subaerial processes
D	Subaerial - Fluvial	Subaerial processes dominant (between 35-70%) - Contribution of Fluvial processes exceeds that of Mass Wasting
E	Mass Wasting - Fluvial	Mass Wasting dominant (between 35-70%) - Contribution of Fluvial processes exceeds that of Subaerial processes
F	Subaerial Dominant	Subaerial Erosion contribution above 70% - Combined contribution of Fluvial and Mass Wasting processes <30%
G	Subaerial - Mass Wasting	Subaerial processes dominant (between 35-70%) - Contribution of Mass Wasting exceeds that of Fluvial processes
H	Mass Wasting - Subaerial	Mass Wasting dominant (between 35-70%) - Contribution of Subaerial processes exceeds that of Fluvial processes
I	Mass Wasting Dominant	Mass Wasting contribution above 70% - Combined contribution of Fluvial and Subaerial processes <30%

3.5.3 Limitations

Extreme erosion point values

The maximum erosion and maximum deposition values were significantly above 1m across all sites and surveys, indicating that, despite the effort taken to ensure that erroneous points (e.g. vegetation, atmospheric moisture or dust reflections) were removed from the data, a small number of

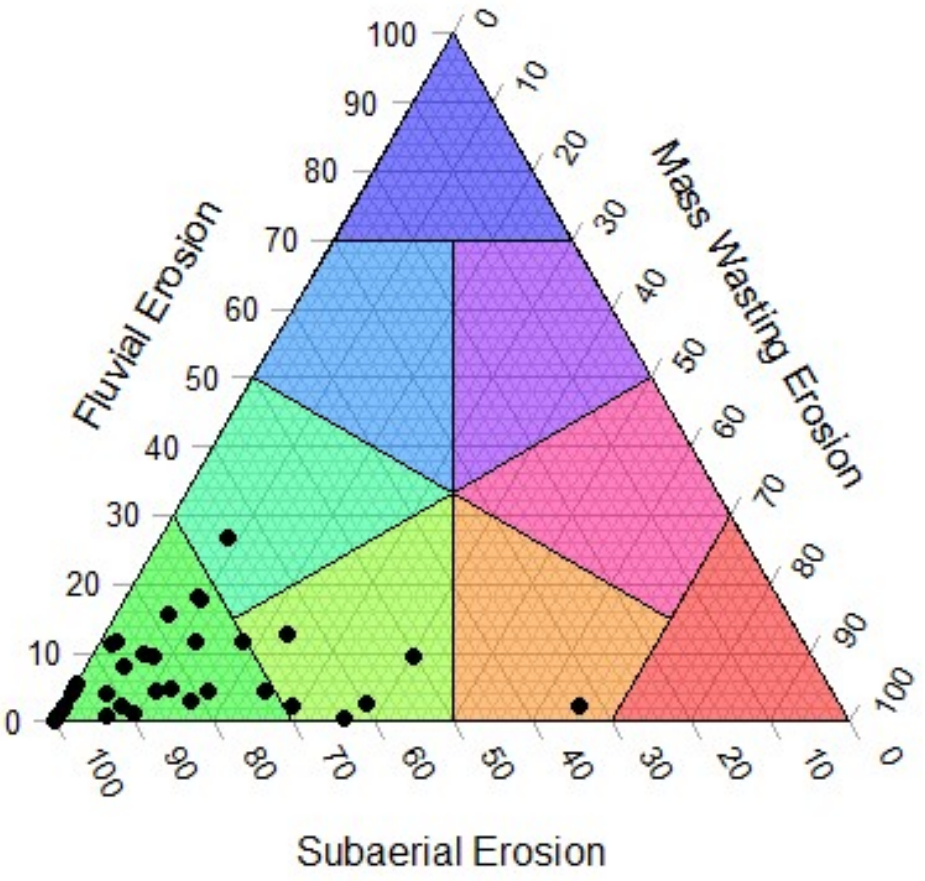

Figure 3.24: Model of erosion dominance with River Arrow erosion points

points that did not represent true change to the bank remained in the final dataset. Closer examination of the data showed that there did not appear to be a clear cut off point within the data that could be used to remove these points.

An attempt was made to remove them by excluding all points with change values more than 3 standard deviations away from the mean, however due to the spread of the data for some surveys, that process saw the removal of a significant number of points that appeared to represent true erosion, and so this approach was not taken.

Instead, the decision was made to include this small number of high change value points in the final analysis as there was no way to remove them automatically, and using an equivalent technique, from each of the different surveys without the loss of a considerable proportion of the data. However, the process of voxelisation used to calculate erosion volumes within $1cm^3$ voxels was largely effective at reducing the impact of these large erosion points by averaging out the values of all points within voxels. Because of the isolated nature of these high value points when the voxels were produced they would contain only one point with a high change value and thus the influence of that high value point would be reduced. Work is ongoing to determine a method to remove outliers from each voxel, as opposed to the whole dataset, to ensure that only values that are extreme relative to their neighbours be removed.

Scan intervals

When discussing the concept of process dominance Lawler (1992) highlighted the problem of identifying the dominant erosion processes from discontinuous erosion data, as the control variables are often able to be recorded at a much higher temporal resolution. This is a problem that

has yet to be overcome. Scan intervals for this research were chosen to be long enough that erosion above the detection threshold of the TLS and subsequent analysis would occur. This inevitably resulted in the need to generalise hydrological and meteorological conditions over the period of the scan intervals, thus reducing the temporal resolution of that data to match that of the erosion data. This potentially masks the impact of individual flow/meteorological events.

However, it can be seen from the range of the change values that were able to be detected that the equipment and analysis technique are sensitive enough to detect much smaller changes than were originally supposed, and thus a more regular scanning regime would be a viable option to detect small scale but continuous changes, as long as they are above the minimum level of detection, which can be as low as 0.005m.

Future research in this area should focus on gathering data at more regular and smaller time scales, to allow for a closer examination of the relationship between flow and erosion. The limited penetration of the laser through turbid water means that it would not be possible to collect data immediately after a flow peak, as the water levels are likely to still be high, limiting the amount of bank that can be recorded. However, timing surveys for once the river has returned to a Q10 level or below could allow for more event focused analysis of erosion and a greater understanding of the proportions of bank being impacted by the different processes at different timescales.

3.6 Chapter Summary

The aim of this chapter was 'to identify, for each of the study banks, the volume of change that has occurred and the proportions of erosion that can be attributed to fluvial erosion, sub-aerial erosion and mass wasting'.

Through the collection and subsequent analysis of TLS data it was established that low level erosion occurred across all banks during almost all time periods, except during E3 and E5 where widespread large deposition values were recorded. The patterns of erosion and deposition were unexpected, with areas of deposition covering the full height of the almost vertical bank face. Some effort has been made to understand these patterns of erosion and deposition, however further work is needed to explain such widespread deposition.

This chapter also identified the relative contributions of Fluvial Erosion, Subaerial Erosion and and Mass Wasting processes on the volume and rate of river bank erosion. It was found that subaerial erosion was the dominant process across all banks and all time periods, with fluvial erosion being consistently the lowest contributing process throughout. From this data, a model of erosion dominance was derived based on the proportions of erosion from different processes. The potential applications of this model will be discussed in Chapter 6 - discussion later in this thesis.

Chapter 4 - Meteorological and flow controls of bank erosion - will take the results of this first stage of analysis and attempt to identify the flow conditions that explain the most fluvial erosion and the meteorological conditions that explain the most sub-aerial erosion.

Chapter 4

The influence of flow and meteorological conditions on erosion processes

This chapter addresses the second objective of the research, as presented in chapter 1, which is 'to identify what conditions are responsible for the most significant amounts of bank change'. First is a brief recap of the relevant results of chapter 3 which were used to direct this next stage of the analysis. A review of the literature surrounding controls on erosion rates is then presented, before stating the specific research question and associated objectives for this chapter. The methods used to collect and calculate the required data for this chapter's analysis are explained before the results of the chosen analyses are presented and their meaning is discussed.

4.1 Introduction

With the predictions for our changing climate in mind, understanding how different conditions may impact on the frequency and intensity of erosion

becomes ever more vital to allow us to effectively mitigate the impacts of erosion and manage our river banks and riparian habitats.

It has been established in chapter 3 that subaerial erosion above the Q10 level is the dominant process affecting the banks during the study period, with between 33.1% and 100% of erosion volumes being attributed to subaerial processes. Fluvial erosion was consistently the lowest contributor to erosion volumes. Between 0% and 26.9% of erosion was attributed to fluvial erosion below the Q10 level. Mass wasting contributions varied between 0% at Bank 2, where no mass wasting events were evident, and 38.0% at Bank 1.

4.1.1 Controls on Bank Erosion

The next step of this research is to establish what meteorological or in stream flow conditions are responsible for most significant erosion. As established in earlier chapters the different erosion processes - subaerial, fluvial and mass wasting - are controlled by a combination of meteorological and flow conditions such as river discharge, freeze-thaw cycles and wetting and drying cycles. However, there is little consensus regarding the relative importance of these different conditions in generating erosion.

4.1.2 Fluvial Erosion

The relationship between flow and erosion has been investigated widely (e.g. Wolman (1959), Partheniades (1965), Rouse (1965), Hooke (1979), Thorne and Tovey (1981), Meade (1982), Lawler (1992), Lawler (1993), Lawler et al. (1999), Rinaldi and Casagli (1999), Rinaldi and Darby (2007), Henshaw et al. (2013), Jugie et al. (2018), and Arora et al. (2023)). Early work on the relationship between flow and meteorological conditions and erosion was carried out by Wolman (1959) on the Watts Branch, Mary-

land, USA. In this work the most significant rates of bank erosion were found where high flows had followed prolonged rainfall conditions that had thoroughly wetted the bank material. Theses saturated soils generate a positive pore water pressure, thus resulting in an increase in the susceptibility of surface soil particles to detachment as a result of the flow (Rinaldi and Casagli, 1999). High flows of a similar height in the summer months, against banks that were not at or near saturation, did not generate the same amount of erosion due to the negative pore water pressure of unsaturated soils. They also found that low flow conditions during the summer months generated very little erosion.

Henshaw et al. (2013) found a strong positive correlation between morphological activity and maximum discharge (0.934) and morphological activity and mean discharge (0.898) on the Pontbran catchment in Wales, where erosion pins were used on 6 pin clusters across a series of seasonal measuring periods from summer 2006 to spring 2008. The correlations above were based on the data from all pins in the six pin clusters, however the correlations at each individual site ranged from 0.524 to 0.956 for maximum discharge and 0.452 and 0.905 for mean discharge, demonstrating the variation in the strength of the relationship even across a relatively small catchment area and similar substrate.

Contrary to the findings of Wolman (1959) and Henshaw et al. (2013), Foerst and Rüther (2018) found that high water events did not result in an increase in erosion, but rather that greater erosion occurred during the low flow summer months. Their study, which used TLS techniques on three patches of the Breivikelva River in northern Norway, found that high magnitude, low frequency events were not as effective at generating erosion as medium magnitude, medium frequency events. The highest peak water level of their study period occurred between scan 6 (June 2013) and

scan 7 (July 2013) but this period also exhibited the lowest net erosion of the whole study at patch 1 (2.97m^3), and the the second lowest at patches 2 and 3 (0.55m^3 and 0.81m^3 respectively). The authors noted that lower water levels over longer time periods were responsible for the greatest erosion volumes (0.17m^3/m^2 and 0.19m^3/m^2 at patch 1 over two summers), compared to short lived high flow events (0.11m^3/m^2 during a 5-day long high flow event). This was concluded to be due to the dampening effect of the outer secondary cell, a portion of circulating flow near the outer bank that is a feature of curved banks, which reduced the shear stress exerted on the bank material, resulting in lower erosion during these short events. During low flow there is no outer secondary cell formation and thus the shear effect of the flow is greater and results in greater erosion despite the lower water level.

4.1.3 Subaerial Erosion

Recorded rates of bank erosion attributed to subaerial erosion are highly variable within the existing literature. Of the three erosion types, subaerial erosion is the most vulnerable to local meteorological conditions as the spatial distribution of rainfall and air temperature variation can have a pronounced effect on the rate of erosion at a specific site (Prosser et al., 2000; Couper and Maddock, 2001; Defersha et al., 2011).

Couper and Maddock (2001) used erosion pins on the River Arrow, Warwickshire and recorded subaerial erosion rates of up to 181mm a^{-1} during a period of prolonged low flows. The erosion rate increased to 356mm a^{-1} following a high flow event that generated an estimated 500mm erosion. Although this high flow event was deemed responsible for a large amount of erosion, it is important to note that in the 72 weeks prior to this single event, all erosion had been attributed to subaerial processes, which are

acting on the bank continuously. Couper and Maddock (2001) found no strong correlation between any of the meteorological characteristics they investigated, including freeze-thaw cycles, number of frost days, temperature range, minimum temperature, average daily minimum temperature and total rainfall, and the amount of bank erosion recorded fortnightly between December 1996 and March 1998. The strongest correlation, of -0.59, was found between mean daily minimum temperature and the percentage of erosion pins where change was recorded, however there were similar results for the number of frost days and the total rainfall per fortnight so a clear relationship could not be identified.

Research conducted by Yumoto et al. (2006) focused on assessing the importance of seasonal freeze-thaw cycles versus the diurnal freeze-thaw cycles that were exhibited along the River Yukawa, Japan. They found that a combination of seasonal thawing and diurnal freeze-thaw action resulted in significant subaerial erosion, amounting to 7.3cm per annum, or 56.4% of the overall retreat at this study site. The soils had a high water content as a result of the thawing of seasonally frozen soil and snow melt, and the high water content reduced the soils hardness, and therefore its resistance to erosion. However this does not agree with the work of Wolman (1959) who found that the winter of 1955-56 saw the greatest number of freeze-thaw cycles during their study period but was also the lowest eroding winter period of their study.

Desiccation can also cause individual soil particles to be eroded, as observed by Prosser et al. (2000) who describe layers of soil as becoming "puffed up" and loosened from the main bank material following periods of prolonged dry weather. They observed this material being redistributed lower down the bank profile but did not factor it in to rates of erosion as the material had not been transported away from the bank section of interest.

In a study on the effect of moisture content on rill erosion Defersha et al. (2011) found that air dried soil supplied 50% more soil particles to the water than soil that had been pre-wetted, while Bjorneberg et al. (2002) found that erosion rates differed across dry areas and those that had been pre-wetted via an intense surface drip irrigation versus pre-wetting with a light surface spray. The soil that was drip irrigated had a soil surface water content of 33% after wetting and saw a total soil loss of 16mg ha^{-1}. The soil that was spray irrigated had a soil surface water content of 15% and saw a total soil loss of 30mg ha^{-1}. Dry soil with a water content of 4% saw a total soil loss of 56mg ha^{-1}. Although this work was based on erosion from rills rather than on river banks, it does help to highlight the influence of soil moisture on its erodibility.

Similar processes were observed by Veihe et al. (2011), who found that subaerial processes were responsible for widespread erosion throughout winter, where conditions were wet and cold and freeze-thaw processes were working to weaken the bank material. Although they did not partition out the contribution of these processes specifically, the percentage of erosion pins that recorded more than 5cm a^{-1} of erosion at different heights on the bank was recorded. The percentages were higher at the 0-25cm heights across 4 of the 5 plots, ranging from 21% to 42%, however the 100-125cm heights also saw between 4% and 17% of the pins record change greater than 5cm despite having been subject to very limited amounts of fluvial erosion at those heights. The magnitude of subaerial erosion was small in comparison to a mass wasting or flood event, but the continuous nature of subaerial erosion meant that the overall contribution of subaerial processes was significant.

Henshaw et al. (2013) investigated a series of meteorological conditions against erosion values and found that the number of consecutive dry days

was strongly negatively correlated with erosion (-0.747), meaning that as the number of consecutive dry days increased, the rate of erosion was reduced. They also investigated the relationship between proportion of dry days (-0.707), maximum soil temperature (-0.635), maximum air temperature (-0.647), proportion of frost days (0.258), total proportion of frost time in hours (0.417), minimum soil temperature (-0.337) and minimum air temperature (-0.440), however these correlations were not significant at the 0.05 level. Despite the lack of significance, the direction of these relationships is very interesting, with most of the examined meteorological variables being negatively correlated with erosion and only frost days and total frost time being positively correlated with erosion.

4.1.4 Mass Wasting Erosion

Local meteorological conditions not only influence the rate of subaerial erosion but also the occurrence of mass failures. Increasing the water content of bank material increases the soil bulk unit weight which results in increased loading of lower portions of the bank and can result in bank collapse (Simon et al., 2000). As well as affecting the specific weight of the soil, changes in rainfall and flow characteristics also influence pore water pressure. Negative pore water pressure occurs where there is water in the channel, but very little water in the soil. This creates matric suction, whereby water is drawn from the high pressure channel into the low pressure soil pores (Pollen-Bankhead and Simon, 2010). This process results in a local increase in bank stability and soil cohesion, making the bank less susceptible to collapse. However, this is usually only a temporary state of affairs.

Positive pore water pressure occurs where the soil is heavily saturated. While flows are high, the confining pressure of the water in the channel

acts to maintain an equilibrium between the pore water and the channel water, with very little movement between them. However as water levels fall on the descending limb of the hydrograph, the confining pressure of the water is removed, and the high pressure pore water begins to move towards the lower pressure channel. This results in a reduction in the cohesion between individual particles, as well as between saturated and unsaturated areas of the bank, and so can generate small and large scale mass wasting. This was seen by Grove et al. (2013), who found that sapping and piping failures along the Lockyer Creek, Australia, were generated by the increased soil water pressure that resulted from one of the wettest periods on record. The receding floodwaters generated flow into the channel from the saturated banks, thus allowing large amounts of sediment to be removed via the exfiltrating water and the bank to subsequently collapse. These failures were often large in scale, and acted to undermine upper areas of the bank as the ground water level fell.

The soil structure is also a contributing factor in mass wasting erosion. Samadi et al. (2011) saw that greater soil density resulted in greater cohesion between the soil particles, and so a greater lateral undermining distance was required to trigger a cantilever failure. They also observed that cohesive soils failed over a longer time frame, with a longer development of tension cracks and more bank deformation prior to failure. With less cohesive soils, the failure was much more rapid, with very little prior deformation of the bank before the failure event.

Layering in soil structures can also be a contributing factor to erosion, where soil layers with different structures can exacerbate seeping and piping by creating a perched water table, acting to concentrate the exfiltration routes of groundwater and thus generate greater erosion above these more impermeable soil layers (Faulkner, 2004). Wilson et al. (2007)

found that water seeping from a Loamy Sand over an impermeable layer generated a maximum sediment concentration of 659.4 g $l^{-}1$, while a Silty Loam over an impermeable layer generated a maximum sediment concentration of 388.1 g $l^{-}1$. Fox et al. (2007) noted a similar phenomenon and noted that even relatively small differences in hydraulic conductivity between sediment layers can be adequate to generate lateral flow and thus generate localised instability and potential failure planes.

4.1.5 Summary

Overall, there is very little consensus regarding the conditions that generate most significant erosion within the literature. The influence of pore water pressure in increasing the erosive effectiveness of high flows or descending high flows has been highlighted as a key factor in a number of studies of fluvial erosion and mass wasting (e.g. Wolman (1959), Grove et al. (2013), and Fox et al. (2007). However, the effect of high flows themselves is not clear, with some studies showing high correlation between high flow and erosion (Henshaw et al., 2013) while others found that more frequent but lower flows were more effective erosive conditions (Foerst and Rüther, 2018). Wetting and drying processes, freeze-thaw cycles and desiccation due to drying have all been identified as meteorological drivers of erosion, however there is again no consensus as to the strength of these relationships nor whether they can be considered as erosive forces in their own right or merely as preparatory processes to fluvial erosion or mass wasting. The lack of clear relationships between different factors and subsequent erosion requires significantly more research to help us understand erosion processes in more detail. The work presented in this chapter hopes to provide a further body of evidence regarding the processes that drive river bank erosion.

4.2 Aims and Objectives

The aim of this chapter is to identify what flow conditions are responsible for the most significant amounts of bank change due to fluvial erosion below the Q10 portion of the bank and what meteorological conditions are responsible for the most significant amounts of change due to subaerial erosion above Q10 portions of the bank.

In order to achieve this aim the following objectives were undertaken:

1. To use the results generated from chapter 3 to identify the areas subject to fluvial and subaerial erosion.

2. To collect continuous river level, rainfall and air temperature data to cover the study site

3. To determine whether there is a relationship between erosion and flow characteristics at each site.

4. To determine whether there is a relationship between subaerial erosion and meteorological conditions at each site.

4.3 Methods

Erosion values calculated in chapter 3 are compared with supplementary data on river flow, air temperature and rainfall to attempt to establish a relationship between the flow and meteorological conditions and the obtained erosion values. As described in chapter 3, the values for fluvial and subaerial erosion have been calculated based on erosion occurring above and below the Q10 river level. The complete set of calculated erosion data can be found in Appendix B, tables B.1 to B.17.

4.3.1 Flow Data and fluvial erosion

River level and discharge data were provided by the Environment Agency from the gauge at Studley (NRFA station ID 54107, Grid Reference SP076639) located approximately 850m upstream from Site 1. River level and discharge data are recorded every 15 minutes and there were no periods of gauge outage during the study period. A time series of discharge as recorded at the Studley gauge can be seen in figure 4.2.

From a combination of discharge and river level data the max discharge, mean discharge, max height on bank, mean height on bank, number of hours water was above Q10 bank height, number of hours water was above Q50 bank height, number of times the stage peaked above the Q10 bank height and the number of times the stage peaked above Q50 bank height for each of the study periods for each study bank were calculated.

4.3.2 Meteorological data and subaerial erosion

Rainfall Data

Due to cost and logistical issues, it was not possible to install a rain gauge at the site for this study. Instead, rainfall data was acquired for four different rainfall gauges that are located around the site; Alvechurch to the north-west, Henley-in-Arden in the north-east, Sheriffs Lench in the south-west and Milcote in the south-east (figure 4.1). The average of these four rain gauges was used to represent the assumed rainfall over the study site in place of a gauge at the location.

For each time period, the mean daily rainfall and total rainfall was calculated. Additional analysis was also undertaken to provide data for wet days (the number of days when any rain fell), rain hours (total number of hours rain fell) and wetting and drying cycles (the number of times rain

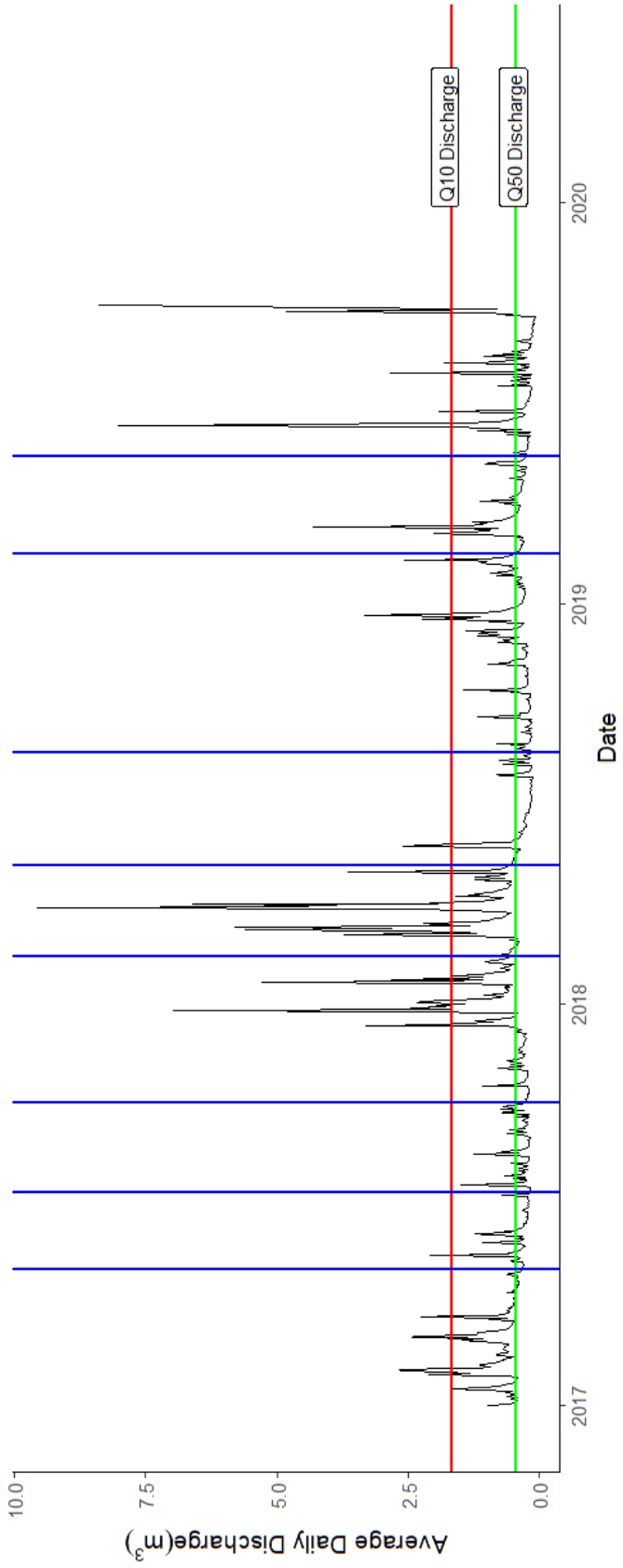

Figure 4.2: Discharge of the River Arrow as recorded at the Studley Gauge. The blue vertical lines represent the approximate dates of surveys of all banks and the horizontal lines represent the long term flow quantiles of Q10 (Red) and Q50(Green)

fell for at least an hour, followed by no rain for at least an hour).

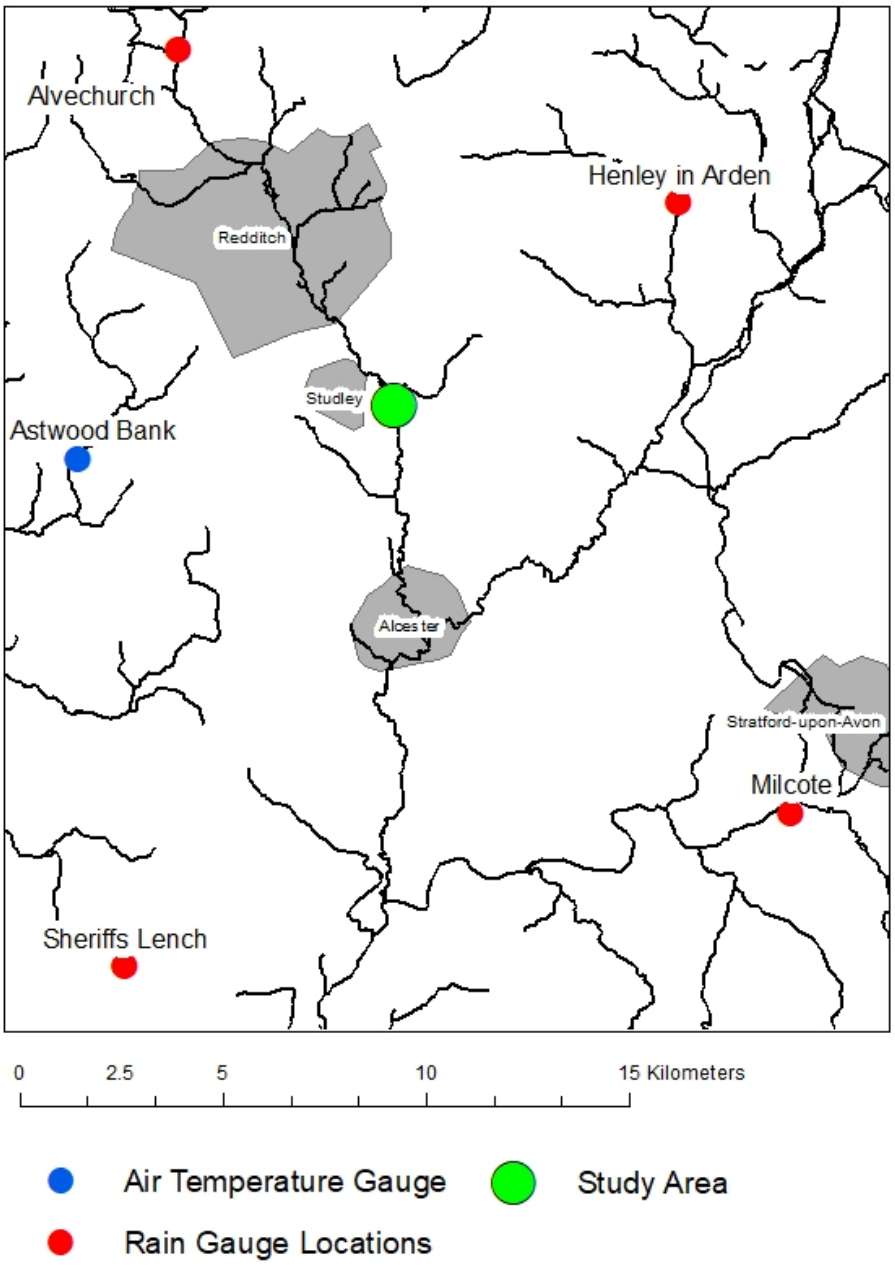

Figure 4.1: Meteorological Gauge locations

Air Temperature Data

Air temperature data was collected at the River Arrow site using a Tiny Tag air temperature logger, between the dates of 15th July 2017 and 15th February 2018. Unfortunately, data collected before and after this date

was not available due to loggers going missing from the site. Instead hourly air temperature data was provided by the Met Office taken from their meteorological station at Astwood Bank, located approximately 8km west of the River Arrow site (figure 4.1). Linear regression was performed between the temperature recorded at the River Arrow and at Astwood Bank to provide a correction equation (Figure 4.3) which was used to correct the Astwood Bank temperature data and provide an hourly data set for the length of the study.

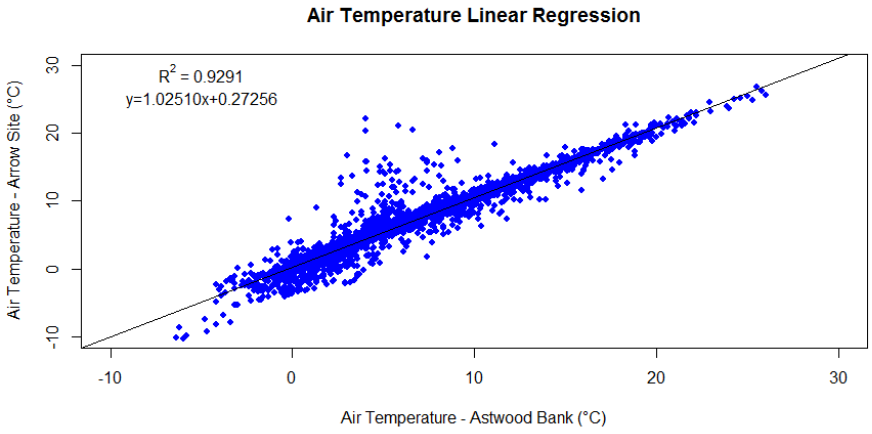

Figure 4.3: Linear regression results for air temperature

Descriptive statistics were calculated for each time period, as well as additional values for number of frost days (any day that the temperature falls to -1°C or lower), cold hours (total hours temperature is below < 0°C), Freeze-Thaw cycles (how many times the temperature drops below 0°C for at least an hour and then goes back above 0°C for at least an hour) and total hot hours (number of hours the temperature reaches the Met Offices Heat Wave temperature threshold for the County of Warwickshire set at 27°C).

4.3.3 Data Analysis

All calculated flow variables and meteorological variables were checked for normality using the Shapiro-Wilk test and all variables had p-values <0.01 and W values above 0.6 so normality was assumed. Simple Pearson correlations were carried out between the flow data/meteorological data and each of the calculated erosion values from chapter 3. These were - total erosion volume, net erosion volume, net erosion volume per m^2, volume of change per m^2 per year and volume of erosion above/below the Q10 level.

A series of multiple linear regression models were then generated, to establish the effect of a combination of the flow/meteorological variables on erosion values. A backwards step-wise regression process was undertaken, using the VIF score to identify variables for removal. The VIF score is an indicator of multicollinearity between variables, with a value of 5 or higher often being used to represent high multicollinearity and a value above 10 representing severe multicollinearity (James et al., 2013). The individual variable with the highest VIF score in each iteration of the model was removed until all scores were below 5. Once all values were below the VIF cutoff the models were checked for overall significance and insignificant variables were removed if necessary.

Finally, a Principal Components Regression (PCR) was also carried out in an effort to provide a better account of the dimensionality of the data.

4.4 Results

4.4.1 Influence of Flow Variables on Erosion

A summary of the flow characteristics experienced at each bank and for each time period can be seen in table 4.1.

Table 4.1: Summary of Flow characteristics at each bank for the study period

Time Period	Max Discharge (m^3/s)	Mean Discharge (m^3/s)	Max Stage (m AOD)	Mean Stage (m AOD)	Hours above Q10 stage	Peaks above Q10 stage	Hours above Q50 stage	Peaks above Q50 stage
				Bank 1 Variables				
E1	2.086	0.389	58.393	57.966	44	7	547	29
E2	1.500	0.359	58.464	57.958	56	14	518	65
E3	6.984	0.829	59.138	58.021	589	16	2039	46
E4	9.558	1.382	59.252	58.088	612	24	1978	9
E5	2.590	0.356	58.647	57.956	69	10	767	50
E6	3.320	0.477	58.548	57.976	312	29	1751	41
				Bank 2 Variables				
Time Period	Max Discharge (m^3/s)	Mean Discharge (m^3/s)	Max Stage (m AOD)	Mean Stage (m AOD)	Hours above Q10 stage	Peaks above Q10 stage	Hours above Q50 stage	Peaks above Q50 stage
E1	2.086	0.389	58.256	57.876	44	7	567	33
E2	1.500	0.359	58.319	57.869	56	14	535	69
E3	6.984	0.829	58.918	57.925	589	16	2061	47
E4	9.558	1.382	59.019	57.984	612	24	1980	9
E5	2.590	0.356	58.481	57.867	69	10	788	49
E6	3.320	0.477	58.393	57.885	312	29	1785	46
				Bank 3 Variables				
Time Period	Max Discharge (m^3/s)	Mean Discharge (m^3/s)	Max Stage (m AOD)	Mean Stage (m AOD)	Hours above Q10 stage	Peaks above Q10 stage	Hours above Q50 stage	Peaks above Q50 stage
E1	2.086	0.389	57.204	56.422	44	7	547	33
E2	1.500	0.359	57.332	56.408	56	14	518	69
E3	9.558	1.042	58.774	56.569	1196	40	4016	47
E4	2.590	0.356	57.667	56.404	69	10	767	9
E5	3.320	0.477	57.486	56.441	311	29	1751	49
E6	4.320	0.571	57.488	56.475	185	16	1321	46

Time series graphs of erosion and flow can be seen in Appendix C figures C.1 to C.6 and illustrate the erosion volumes between scan dates for total erosion, net total erosion, erosion per m^2, and rate of change per m^2 per year against the maximum stage, mean stage, interquartile range and the daily mean stage. These graphs show very little relationship between the different erosion quantities and the river levels experienced at

the sites between scans.

Pearsons R correlations were carried out to establish whether a statistical relationship exists between different erosion quantities and the flow variables. The results of these correlations can be seen in table 4.2.

There is no consistent correlation between the flow variables and the total erosion volume across all banks. Only Bank 2 shows significant correlations between total erosion and maximum discharge, mean stage, maximum stage and hours above Q10 level (-0.760, -0.730, -0.771 and -0.760 respectively). However, what is interesting is that each of these correlations are negative, indicating that as the flow increases the rate of erosion decreases. Only peaks above Q50 at the upstream reach of Bank 3 shows a significant positive correlation with the total erosion volume. There were significantly larger correlation values between flow variables and the net change, concentrated at the upstream reach of Bank 3 and across the data as a whole, however, like Bank 2 earlier, the majority of these correlations were negative. This pattern of correlations continues throughout the data, with negative correlations dominating the results across all of the calculated erosion values.

Looking at the combined All Data column, which brings together the results for all of the banks, it is clear that there are consistent weak correlations between mean discharge, max discharge, mean stage, max stage, peaks above the Q10 level, hours above the Q10 level and hours above the Q50 level and the erosion variables of net change volume, net change volume per m^2 and volume of change per year.

The direction of the correlations suggests that as flow variables increased the erosion decreased. This contradicts the existing literature, so to explore whether this was a symptom of the data containing extreme out-

Table 4.2: Results of Pearson's R correlation between flow variables and erosion variables for individual banks and all data. The values in **bold** represent those values that are are above the critical value (0.729 for Banks 1 - 3 where n = 7 and 0.296 for All data where n = 35) at the 0.1 significance level. Those with a * are also above the critical value (0.811 for banks 1 - 3 and 0.349 for all data) at the 0.05 significance level

			Total Erosion (m^3)			
Bank	1	2	3-Up	3-Mid	3-Down	All
Mean Discharge	-0.007	-0.715	0.027	-0.175	-0.123	-0.236
Max Discharge	-0.101	**-0.760**	0.038	-0.059	-0.035	-0.153
Mean Stage	0.022	**-0.730**	-0.078	-0.234	-0.158	-0.253
Max Stage	-0.299	**-0.771**	0.323	0.155	0.048	-0.115
Q10 Peaks	-0.189	-0.043	0.235	-0.231	-0.252	-0.056
Q50 Peaks	-0.499	0.419	**0.968***	0.147	-0.330	0.126
Hours above Q10	-0.160	**-0.760**	0.196	-0.118	-0.068	-0.081
Hours above Q50	-0.208	-0.571	0.131	-0.112	-0.073	-0.040
			Net Change (m^3)			
Mean Discharge	-0.105	-0.640	**-0.842***	-0.604	-0.506	-0.434
Max Discharge	-0.216	-0.711	**-0.833***	-0.511	-0.429	-0.451
Mean Stage	-0.079	-0.658	**-0.847***	-0.636	-0.525	**-0.448***
Max Stage	-0.419	**-0.735**	-0.709	-0.333	-0.350	**-0.378***
Q10 Peaks	-0.191	-0.010	**-0.738**	-0.662	-0.602	**-0.495***
Q50 Peaks	-0.432	0.364	0.231	0.009	-0.387	-0.008
Hours above Q10	-0.279	**-0.741**	**-0.840***	-0.587	-0.468	**-0.526***
Hours above Q50	-0.310	-0.576	**-0.848***	-0.584	-0.472	**-0.512***
			Net Change per m^2 (m^3)			
Mean Discharge	0.009	-0.492	**-0.842***	-0.665	-0.528	-0.401
Max Discharge	-0.111	-0.552	**-0.839***	-0.581	-0.429	-0.437
Mean Stage	0.037	-0.509	**-0.842***	-0.698	-0.554	**-0.421***
Max Stage	-0.320	-0.593	-0.728	-0.398	-0.317	**-0.361***
Q10 Peaks	-0.090	0.185	**-0.742**	-0.718	-0.491	**-0.435***
Q50 Peaks	-0.456	0.230	0.214	0.034	-0.289	-0.010
Hours above Q10	-0.157	-0.572	**-0.847***	-0.644	-0.462	**-0.515***
Hours above Q50	-0.208	-0.379	**-0.855***	-0.649	-0.434	**-0.498***
			Rate of Change per m^2 per year (m^3)			
Mean Discharge	-0.011	-0.523	-0.693	-0.621	-0.585	-0.385
Max Discharge	-0.148	-0.632	-0.709	-0.538	-0.515	-0.440
Mean Stage	0.005	-0.550	-0.707	-0.661	-0.598	**-0.407***
Max Stage	-0.310	-0.647	-0.575	-0.342	-0.438	**-0.369***
Q10 Peaks	-0.404	-0.211	-0.636	-0.710	-0.717	**-0.548***
Q50 Peaks	-0.415	0.238	0.413	0.072	-0.386	-0.035
Hours above Q10	-0.297	**-0.772**	-0.697	-0.596	-0.567	**-0.532***
Hours above Q50	-0.432	-0.707	**-0.733**	-0.615	-0.578	**-0.552***
			Erosion below Q10 Level (m^3)			
Mean Discharge	-0.499	-0.465	-0.637	-0.104	-0.443	-0.282
Max Discharge	-0.526	-0.449	-0.664	0.005	-0.379	-0.239
Mean Stage	-0.482	-0.497	-0.669	-0.173	-0.457	**-0.297**
Max Stage	-0.679	-0.326	-0.563	0.234	-0.311	-0.188
Q10 Peaks	0.072	-0.602	**-0.73**1	-0.219	-0.679	**-0.316**
Q50 Peaks	-0.130	0.226	0.068	0.212	-0.389	0.026
Hours above Q10	-0.486	-0.614	-0.584	-0.044	-0.445	-0.231
Hours above Q50	-0.282	-0.609	-0.681	-0.063	-0.475	-0.234

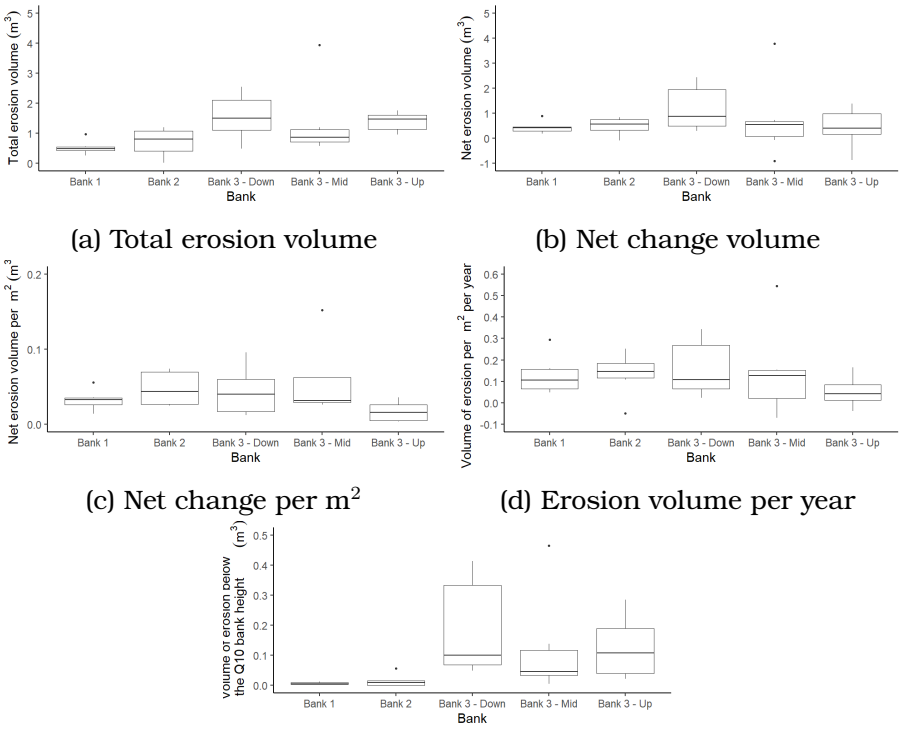

(a) Total erosion volume

(b) Net change volume

(c) Net change per m^2

(d) Erosion volume per year

(e) Erosion below Q10 level

Figure 4.4: boxplots of the different erosion variables per bank

lier values which may skew the direction of the correlations, box and whisker plots were created for each of the erosion variables. As can be seen in figures 4.4 there were a small number of outliers in the erosion values recorded at some banks. However there were not consistent outliers across all banks to explain the persistence of the negative correlations. As such, it was not deemed appropriate to remove these values from the analysis because they do not explain any significant differences in trends between banks and instead are considered to represent the variation that is inherent in data collected from the natural environment. The potential impacts of this decision will be discussed in later sections.

As no single flow variable exhibited a consistent, strong, statistically significant relationship with any of the erosion variables, the next step was to carry out multivariate regression to identify whether a combination of flow variables had a stronger relationship with erosion.

A correlation matrix of the different flow variables was created to indicate the extent of cross-correlation between the flow variables. It was clear from the correlation values that there was significant cross correlation between many of the different flow variables (figure 4.5).

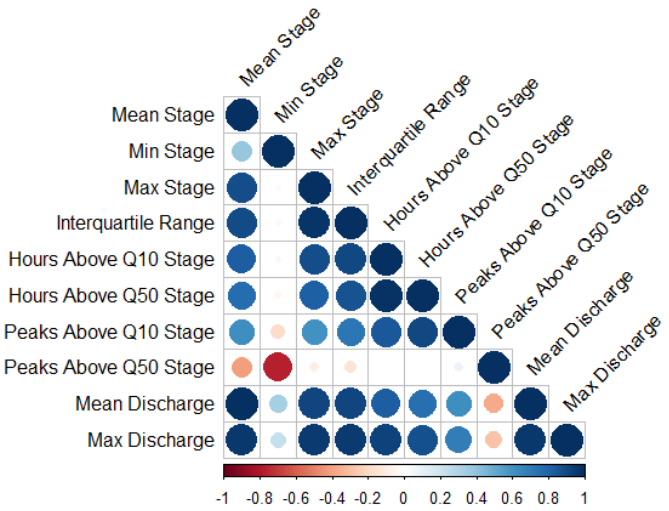

Figure 4.5: Correlation plot of flow variables for multivariate regression using all bank data

Due to this widespread autocorrelation it was not possible to identify specific variables to begin building a model from, so a backwards, step-wise regression approach was taken to identify a combination of variables that were contributing to erosion. Following analysis of each model output and the Variance Inflation Factor (VIF) values, problematic variables were removed in an iterative process until a final model was produced.

The first model included all of the flow variables except Q50 peaks, which didn't show significant correlation with any of the erosion variables. This model returned an r^2 value of 0.182 with a p-value of 0.150. However, examination of the VIF values indicated significant cross-correlation be-

tween the variables. The variable with the highest VIF value, maximum discharge, was removed to create model 2. This process was continued until VIF scores for all variables were below 5, indicating little colinearity between the remaining variables.

This process generated model 7, which used Min Stage, Peaks above Q10 and mean discharge to give an R^2 value of 0.193 and to create the first model that had a statistically significant p-value of 0.035.

The same variables were then used as explanatory variables in regressions against net volume of change per metre, volume of change per metre per year and erosion volume below the Q10 level (4.4 with r^2 values of 0.143, 0.233 and 0.020 respectively. This indicates that approximately 23% of the rate of change per meter squared per year can be attributed to flow variables and only 2% of change below the Q10 stage. This last value was surprising as it indicates that erosion below the Q10 level had a weaker relationship with flow than erosion across the whole bank face. It is also worth noting that only the volume of change per year was statistically significant.

Table 4.3: Results of backwards step-wise regression of flow variables against Net Change. Statistically significant p-values are in **bold**

Model Number	Independent Variables	variable coefficient	variable p-values	VIF Scores	adjusted r^2 value	model p-value
1	Intercept	-595.100	0.659	NA	0.182	0.150
	Mean Stage	-6858.000	0.577	5587363		
	Min Stage	7519.000	0.588	3852144		
	Max Stage	517.500	0.600	2272063		
	Interquartile Range	11600.000	0.586	9281765		
	Hours Above Q10	0.459	0.580	3705435		
	Hours above Q50	-0.014	0.490	18625		
	Peaks above Q10	2.457	0.550	77133		
	Mean Discharge	413.400	0.597	2465470		
	Max Discharge	-169.500	0.599	35398609		
2	Intercept	114.023	0.164	NA	0.210	0.103
	Mean Stage	-395.350	0.200	3529		
	Min Stage	219.784	0.474	1934		
	Max Stage	-1.510	0.771	65		
	Interquartile Range	401.143	0.496	7316		
	Hours Above Q10	0.0236	0.600	11310		
	Hours above Q50	-0.010	0.583	16237		
	Peaks above Q10	0.320	0.559	1417		
	Mean Discharge	3.100	0.914	3499		
3	Intercept	119.000	0.138	NA	0.235	0.067
	Mean Stage	-253.400	0.116	974		
	Min Stage	52.680	0.099	21		
	Max Stage	-0.323	0.944	54		
	Interquartile Range	80.040	0.213	88		
	Hours Above Q10	-0.001	0.547	20		
	Peaks above Q10	0.021	0.637	9.5		
	Mean Discharge	17.320	0.179	694		
4	Intercept	-6.554	0.515	NA	0.179	0.099
	Min Stage	9.434	0.563	5.3		
	Max Stage	2.770	0.528	45		
	Interquartile Range	21.898	0.685	59		
	Hours Above Q10	-0.002	0.170	16		
	Peaks above Q10	0.009	0.847	9.2		
	Mean Discharge	-2.677	0.336	31		
5	Intercept	-5.538	0.562	NA	0.207	0.057
	Min Stage	5.929	0.662	3.8		
	Max Stage	3.972	0.217	24		
	Hours Above Q10	-0.003	0.138	16		
	Peaks above Q10	0.016	0.691	7.7		
	Mean Discharge	-2.043	0.365	21		
6	Intercept	4.715	0.345	NA	0.188	0.055
	Min Stage	-6.489	0.489	1.8		
	Hours Above Q10	-0.001	0.374	8.6		
	Peaks above Q10	-0.020	0.499	3.9		
	Mean Discharge	0.360	0.757	5.6		
7	Intercept	3.547	0.458	NA	0.193	**0.035**
	Min Stage	-3.587	0.681	1.6		
	Peaks above Q10	-0.036	0.102	2.2		
	Mean Discharge	-0.427	0.576	2.4		

Table 4.4: Results of regression of flow variables against erosion variables. Statistically significant p-values are in **bold**

Model Number	Dependent Variable	Independent Variables	variable coefficient	variable p-values	adjusted r^2 value	model p-value
8	Net change volume per m^2	Intercept	0.199	0.323	0.143	0.07
		Min Stage	-0.245	0.504		
		Peaks above Q10	-0.001	0.135		
		Mean Discharge	-0.013	0.684		
9	Volume of change per year	Intercept	0.621	0.355	0.233	**0.019**
		Min Stage	-0.669	0.584		
		Peaks above Q10	-0.007	**0.027**		
		Mean Discharge	0.001	0.994		
10	Erosion below Q10 level	Intercept	0.576	0.454	0.020	0.330
		Min Stage	-0.729	0.604		
		Peaks above Q10	-0.004	0.275		
		Mean Discharge	-0.023	0.851		

4.4.2 Influence of meteorological variables on erosion

The time series graphs of the air temperature and rainfall data have been plotted in figures 4.6 and 4.7. The calculated values for the temperature and rainfall variables can be seen in tables 4.6 to 4.7.

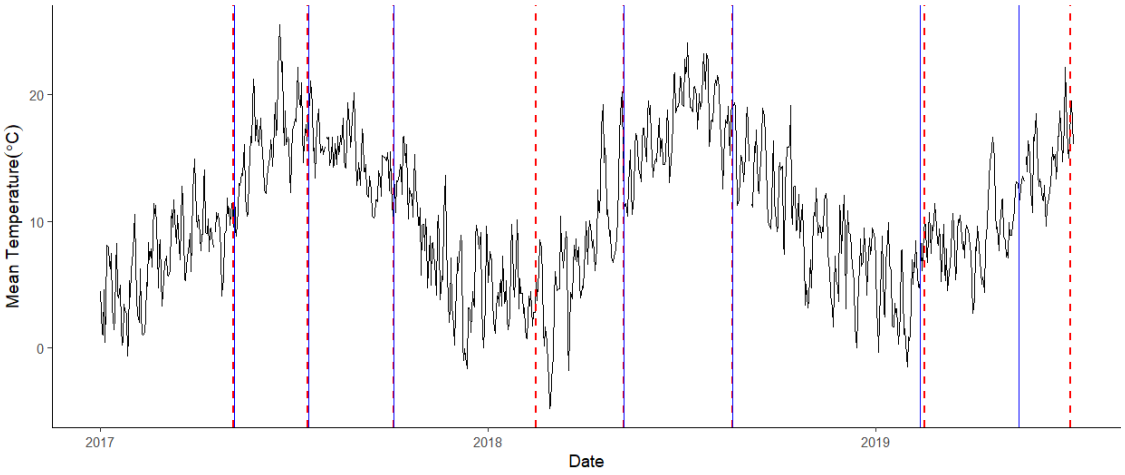

Figure 4.6: Daily air temperature data for the study period. The blue vertical lines represent the scan dates for banks 1 and 2, while the red-dashed vertical line represents the scan dates for bank 3.

Cold hours, frost days, freeze thaw cycles and hot hours all had minimum values of zero, with maximum values of 396, 30, 45 and 105 respectively. The mean temperature ranged from 7.1°C to 17.5°C with a minimum temperature ranging from -7.3°C to 5.7°C and a maximum temperature range

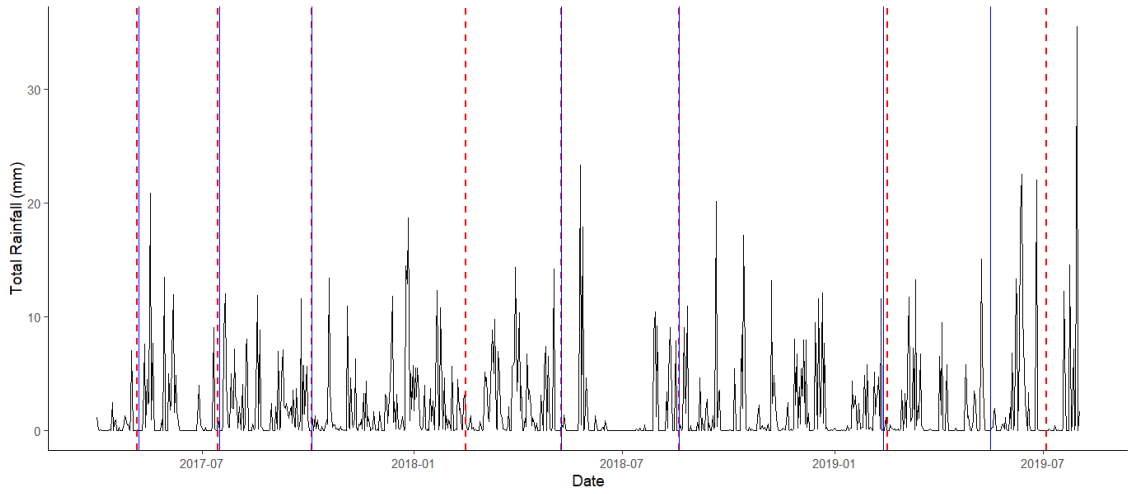

Figure 4.7: Daily rainfall data for the study period. The blue vertical lines represent the scan dates for banks 1 and 2, while the red-dashed vertical line represents the scan dates for bank 3.

from 19.7°C to 31.6°C.

Table 4.5: Summary of the calculated temperature variables for Banks 1 and 2

Time Period	Cold Hours	Frost Days	Freeze Thaw Cycles	Hot Hours	Mean Temp (°C)	Minimum Temp (°C)	Maximum Temp (°C)
E1	0	0	0	45	16.1	3.5	31.6
E2	0	0	0	0	15.2	5.7	26.9
E3	179	16	32	0	6.7	-6.3	19.7
E4	212	13	12	1	7.1	-7.3	27.0
E5	0	0	0	105	17.5	4.3	31.2
E6	165	13	24	0	8.9	-5.4	24.8

Total rainfall had a range of 117.8mm to 448.8mm across all banks and average daily rainfall was between 1.2mm and 2.3mm. There were a minimum of 112 wetting and drying cycles and a maximum of 796, while rain days had a minimum of 31 and maximum of 173. Rain hours saw the largest range with a minimum value of 169 and a maximum of 1120.

Simple Pearson correlation coefficients were calculated between the different individual meteorological variables and erosion variables calculated in chapter 3 (tables 4.9 to 4.11).

For the total erosion volume the highest correlation value was with the

Table 4.6: Summary of the calculated temperature variables for Bank 3

Time Period	Cold Hours	Frost Days	Freeze Thaw Cycles	Hot Hours	Mean Temp (°C)	Minimum Temp (°C)	Maximum Temp (°C)
E1	0	0	0	45	16.1	3.5	31.6
E2	0	0	0	0	15.2	5.7	26.9
E3	396	30	45	1	6.8	-7.3	27.0
E4	0	0	0	105	17.5	4.3	31.2
E5	165	13	25	0	9.0	-5.4	24.8
E6	19	3	7	0	8.8	-2.0	23.1

Table 4.7: Summary of the calculated rainfall variables for Banks 1 and 2

Time Period	Total Rainfall (mm)	Average Daily Rainfall (mm)	Wetting and Drying Cycles	Rain Days	Rain Hours
E1	118.4	1.7	152	33	242
E2	178.2	2.2	285	62	402
E3	258.0	1.9	500	111	683
E4	187.6	2.3	288	61	426
E5	117.8	1.2	112	31	169
E6	298.6	1.7	480	119	683

Table 4.8: Summary of the calculated rainfall variables for Bank 3

Time Period	Total Rainfall (mm)	Average Daily Rainfall (mm)	Wetting and Drying Cycles	Rain Days	Rain Hours
E1	118.4	1.7	153	33	242
E2	177.2	2.2	283	61	399
E3	448.8	2.1	796	173	1120
E4	117.8	1.2	113	31	169
E5	297.4	1.7	480	117	679
E6	134.3	1.4	230	52	320

Table 4.9: Results of Pearson's R correlation between meteorological variables and erosion variables for the full bank erosion variables. The values in **bold** represent those values that are are above the critical value (0.729 for Banks 1 - 3 where n = 6 and 0.296 for All data where n = 35) at the 0.1 significance level. Those with a * are also above the critical value (0.811 for banks 1 - 3 and 0.349 for all data) at the 0.05 significance level.

	Total Erosion Volume (m^3)					
Bank	1	2	3-Up	3-Mid	3-Down	All
Cold Hours	-0.111	-0.574	0.222	-0.156	-0.057	-0.089
Frost Days	-0.154	-0.591	0.189	-0.170	-0.077	-0.095
Freeze Thaw Cycles	-0.201	-0.512	0.147	-0.200	-0.102	-0.106
Hot Hours	-0.168	0.503	0.147	**0.873***	**0.829***	**0.471***
Mean Temperature	0.083	0.664	0.222	0.441	0.417	**0.318**
Min Temperature	0.050	0.575	0.185	0.263	0.121	0.214
Max Temperature	0.331	0.594	0.205	0.492	**0.768**	**0.404***
Total Rainfall	-0.219	-0.215	0.322	-0.238	-0.188	-0.064
Mean Rainfall	0.202	-0.601	0.390	-0.683	-0.637	**-0.415***
Wetting and Drying Cycles	-0.192	-0.400	0.268	-0.314	-0.268	-0.132
Rain Days	-0.227	-0.275	0.272	-0.285	-0.247	-0.111
Rain Hours	-0.154	-0.392	0.264	-0.315	-0.250	-0.127
	Net erosion volume (m^3)					
Cold Hours	-0.203	-0.558	**-0.851***	-0.628	-0.451	**-0.528***
Frost Days	-0.255	-0.604	**-0.855***	-0.638	-0.470	**-0.537***
Freeze Thaw Cycles	-0.298	-0.571	**-0.845***	-0.656	-0.482	**-0.527***
Hot Hours	-0.130	0.466	0.332	**0.890***	**0.886***	**0.542***
Mean Temperature	0.183	0.655	0.688	0.728	0.677	**0.531***
Min Temperature	0.149	0.573	**0.811***	0.636	0.441	**0.472***
Max Temperature	0.419	0.630	0.096	0.507	**0.785**	**0.384***
Total Rainfall	-0.254	-0.251	**-0.769**	-0.680	-0.550	**-0.532***
Mean Rainfall	0.166	-0.509	-0.233	**-0.742**	-0.716	**-0.461***
Wetting and Drying Cycles	-0.251	-0.440	**-0.774**	**-0.736**	-0.623	**-0.571***
Rain Days	-0.273	-0.323	**-0.762**	-0.712	-0.598	**-0.544***
Rain Hours	-0.212	-0.428	**-0.785**	**-0.739**	-0.606	**-0.573***
	Net erosion volume per m^2 (m^3)					
Cold Hours	-0.087	-0.360	**-0.860***	-0.683	-0.401	**-0.488***
Frost Days	-0.144	-0.422	**-0.862***	-0.696	-0.424	**-0.507***
Freeze Thaw Cycles	-0.210	-0.428	**-0.851**	-0.716	-0.412	**-0.507***
Hot Hours	-0.301	0.411	0.289	**0.882***	**0.889***	**0.516***
Mean Temperature	0.049	0.485	0.671	**0.789**	0.595	**0.502***
Min Temperature	0.048	0.375	**0.808**	0.709	0.344	**0.425***
Max Temperature	0.290	0.546	0.066	0.539	0.631	**0.380***
Total Rainfall	-0.149	-0.115	**-0.774**	**-0.724**	-0.484	**-0.494***
Mean Rainfall	0.337	-0.508	-0.206	-0.695	**-0.810**	**-0.425***
Wetting and Drying Cycles	-0.130	-0.330	**-0.773**	**-0.778**	-0.571	**-0.547***
Rain Days	-0.170	-0.204	**-0.764**	**-0.758**	-0.521	**-0.510***
Rain Hours	-0.090	-0.312	**-0.785**	**-0.780**	-0.560	**-0.546***
	Volume change per m^2 per year (m^3)					
Cold Hours	-0.323	-0.671	**-0.740**	-0.648	-0.571	**-0.547***
Frost Days	-0.403	**-0.765**	**-0.746**	-0.664	-0.588	**-0.576***
Freeze Thaw Cycles	-0.494	**-0.806**	**-0.759**	-0.696	-0.606	**-0.606***
Hot Hours	-0.057	0.581	0.172	**0.909***	**0.891***	**0.550***
Mean Temperature	0.290	**0.776**	0.619	**0.812***	**0.755**	**0.604***
Min Temperature	0.293	0.699	**0.802**	0.724	0.560	**0.543***
Max Temperature	0.505	**0.811***	0.043	0.607	**0.787**	**0.514***
Total Rainfall	-0.506	-0.548	-0.641	-0.696	-0.666	**-0.582***
Mean Rainfall	0.299	-0.416	0.025	-0.656	-0.710	**-0.343**
Wetting and Drying Cycles	-0.450	-0.701	-0.628	**-0.752**	**-0.729**	**-0.624***
Rain Days	-0.512	-0.618	-0.638	**-0.739**	-0.712	**-0.612***
Rain Hours	-0.422	-0.692	-0.641	**-0.753**	-0.714	**-0.619***

Table 4.10: Results of Pearson's R correlation between meteorological variables and erosion variables above the Q10 level. The values in **bold** represent those values that are are above the critical value (0.729 for Banks 1 - 3 where n=6 and 0.296 for All data where n = 35) at the 0.1 significance level. Those with a * are also above the critical value (0.811 for banks 1 - 3 and 0.349 for all data) at the 0.05 significance level.

	Subaerial erosion volume above Q10 level (m^3)					
Bank	1	2	3-Up	3-Mid	3-Down	All
Cold Hours	-0.033	-0.556	-0.530	-0.149	0.064	-0.163
Frost Days	-0.086	-0.573	-0.541	-0.160	0.043	-0.170
Freeze Thaw Cycles	-0.169	-0.494	-0.506	-0.199	0.018	-0.176
Hot Hours	-0.274	0.472	0.206	**0.858***	**0.794**	**0.470***
Mean Temperature	-0.019	0.644	0.487	0.422	0.331	**0.348**
Min Temperature	-0.011	0.558	0.534	0.266	0.021	0.252
Max Temperature	0.223	0.577	-0.023	0.480	0.731	**0.392***
Total Rainfall	-0.237	-0.186	-0.393	-0.242	-0.065	-0.135
Mean Rainfall	0.399	-0.582	-0.078	-0.670	-0.599	**-0.423***
Wetting and Drying Cycles	-0.159	-0.374	-0.430	-0.308	-0.150	-0.201
Rain Days	-0.233	-0.248	-0.388	-0.289	-0.125	-0.175
Rain Hours	-0.128	-0.364	-0.442	-0.311	-0.132	-0.197
	Subaerial erosion volume per m^2 above Q10 level (m^3)					
Cold Hours	0.504	-0.286	-0.098	0.510	0.538	0.257
Frost Days	0.528	-0.266	-0.133	0.494	0.529	0.256
Freeze Thaw Cycles	0.479	-0.156	-0.124	0.465	0.542	0.258
Hot Hours	-0.553	0.336	0.009	0.513	0.408	0.221
Mean Temperature	-0.604	0.375	0.393	-0.073	-0.212	-0.020
Min Temperature	-0.534	0.282	0.340	-0.309	-0.510	-0.147
Max Temperature	-0.490	0.289	0.234	0.311	0.233	0.136
Total Rainfall	0.221	0.138	0.063	0.434	0.458	0.282
Mean Rainfall	0.573	-0.614	0.439	-0.316	-0.415	-0.221
Wetting and Drying Cycles	0.391	-0.063	0.007	0.355	0.374	0.216
Rain Days	0.276	0.079	0.032	0.384	0.426	0.250
Rain Hours	0.396	-0.054	0.011	0.358	0.382	0.222
	Percentage contribution of subaerial erosion above Q10 level					
Cold Hours	-0.348	**-0.855***	**0.749**	0.158	-0.604	0.100
Frost Days	-0.324	**-0.904***	**0.731**	0.146	-0.599	0.104
Freeze Thaw Cycles	-0.215	**-0.899**	0.653	0.205	-0.606	0.102
Hot Hours	0.681	0.725	-0.086	0.389	-0.303	0.130
Mean Temperature	0.474	**0.888***	-0.320	0.045	0.314	0.090
Min Temperature	0.313	**0.879***	-0.418	-0.229	0.603	0.049
Max Temperature	0.424	**0.752**	0.280	0.175	-0.234	0.194
Total Rainfall	-0.103	**-0.882***	0.663	0.174	-0.492	0.175
Mean Rainfall	**-0.876***	-0.321	0.401	-0.418	0.363	-0.151
Wetting and Drying Cycles	-0.284	**-0.883***	0.661	0.076	-0.427	0.133
Rain Days	-0.140	**-0.875***	0.611	0.160	-0.463	0.141
Rain Hours	-0.284	**-0.903***	0.674	0.082	-0.440	0.138

Table 4.11: Results of Pearson's R correlation between meteorological variables and mass wasting erosion. The values in **bold** represent those values that are are above the critical value (0.729 for Banks 1 - 3 where n=6 and 0.296 for All data where n=35) at the 0.1 significance level. Those with a * are also above the critical value (0.811 for banks 1 - 3 and 0.349 for all data) at the 0.05 significance level.

	Mass wasting erosion volume (m^3)					
Cold Hours	-0.290	NA	**0.909***	-0.191	-0.044	0.281
Frost Days	-0.257	NA	**0.902***	-0.205	-0.014	0.284
Freeze Thaw Cycles	-0.127	NA	**0.845***	-0.191	0.089	0.269
Hot Hours	0.390	NA	-0.224	**0.800**	-0.634	0.122
Mean Temperature	0.379	NA	-0.570	0.424	-0.457	-0.058
Min Temperature	0.227	NA	-0.637	0.200	-0.381	-0.124
Max Temperature	0.400	NA	-0.024	0.410	-0.632	0.120
Total Rainfall	0.057	NA	**0.843***	-0.222	0.021	**0.305**
Mean Rainfall	-0.715	NA	0.390	-0.696	0.067	-0.131
Wetting and Drying Cycles	-0.127	NA	**0.845***	-0.318	0.063	0.264
Rain Days	0.012	NA	**0.811***	-0.256	0.099	0.269
Rain Hours	-0.105	NA	**0.849***	-0.317	0.061	0.267

number of hot hours, with correlations of 0.873, 0.829 and 0.417 for the midstream section of bank 3, the downstream section of bank 3 and the all bank data respectively. Max temperature also exhibited significant correlations with total erosion at the downstream reach of bank 3 (0.768) and for the all bank data (0.404). The only other significant correlations were for mean temperature (0.318) and mean rainfall (-0.415) with the all bank data. Most of the significant correlations between total erosion and meteorological variables were positive, meaning that as the meteorological variable increased the rate of erosion also increased, with the exception of mean rainfall, which exhibited a negative correlation, indicating that, for the all bank data, an increase in the mean rainfall value resulted in a decrease in the rate of erosion.

Net erosion volume exhibited a significant correlation with all of the different meteorological variables at at least one bank, and the combined all bank data saw significant correlations at the both the 0.1 and 0.05 significance level with all of the meteorological variables. The same pattern of correlations was seen with net erosion volume per m^2 and with the volume

of change per m^2 per year, with only mean rainfall not significant at the 0.05 significance level.

Hot hours, mean temperature, max temperature and mean rainfall were the only significantly correlated variables with the volume of subaerial erosion above the Q10 level at the mid and downstream reaches of bank 3 and in the all bank data. There were no significant correlation values for the volume of subaerial erosion per m^2 above the Q10 level however there were multiple high correlation values between the percentage contribution of subaerial erosion above the Q10 level and the meteorological variables. The only variable that did not show any significant correlations with that erosion variable was hot hours, which had dominated the significant correlation for the whole bank and above Q10 erosion values.

The low Pearson correlation coefficients suggest that no single variable consistently explains the rate of erosion within our study sites. It is important to note here that the individually low correlation coefficients are a reflection of the fact that we cannot separate out the influence of each different meteorological variable and that we are instead seeing the combined effect of multiple processes. As such, the next step was to carry out a multiple regression analysis to establish how much of the erosion values can be explained by a combination of meteorological variables.

To select the variables for the first iteration of the model a correlation matrix was calculated (figure 4.8) to show which variables were most significantly correlated with each other. As shown, there is widespread collinearity between the meteorological variables.

Using only variables with low correlation values limits the collinearity in the model, thus increasing it's validity. As such, only variables that had correlation values between 0.3 and -0.3 were chosen for the first model.

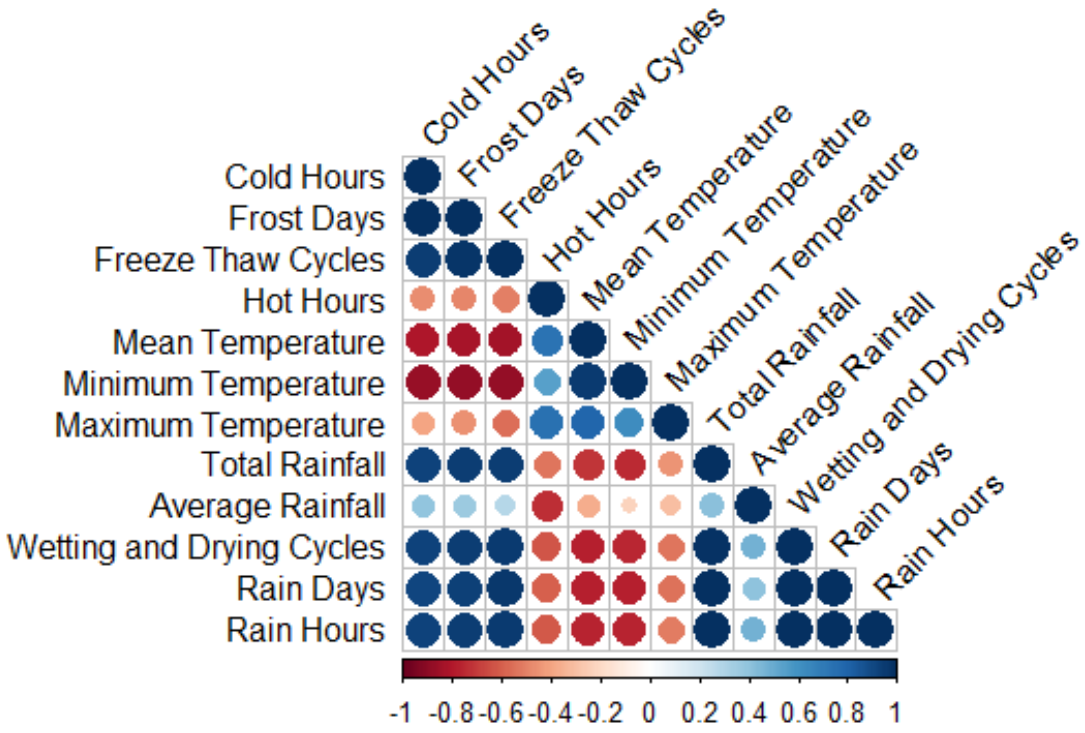

Figure 4.8: Correlation plot of meteorological variables for multivariate regression using all bank data

This identified Freeze Thaw Cycles, Minimum Temperature and Average Rainfall as the chosen variables. An initial model using these variables to predict the volume of erosion above the Q10 bank height gave an adjusted r^2 value of 0.14 and a p-value of 0.027 (table 4.12). Of each of the included variables only average rainfall had a statistically significant p-value of 0.028, while freeze thaw had a value of 0.350 and minimum temperature had a p value of 0.206. The model is insignificant at the 0.05 significance level and so are most of the included variables.

In an attempt to generate a model that explained more of the variance in the erosion data, and that was statistically significant, a backwards stepwise regression approach was taken, starting with all of the variables that had at least 3 significant correlation results, across the different banks and different erosion variables, in the earlier Pearson correlation tests (ta-

Table 4.12: Results of regression of non-correlate variables against Subaerial erosion above the Q10 level using all bank data (n=35). Statistically significant p-values are in **bold**

Model Number	Dependent Variable	Independent Variables	variable coefficient	variable p-values	VIF Scores	r^2 value	model p-value
1	Subaerial erosion above the Q10 level	Intercept	-1.899	**0.001**	NA	0.1434	0.072
		Freeze Thaw Cycles	-0.013	0.350	4.3		
		Minimum Temperature	-0.051	0.206	4.2		
		Average Rainfall	0.650	**0.028**	1.1		

ble 4.13). This gave an initial model, model 2, comprising cold hours, frost days, hot hours, mean temperature, maximum temperature, total rainfall, mean rainfall, wetting and drying cycles, rain days and rain hours. This produced a model that explained 25% of the variance in erosion, but was not statistically significant, with a p-value of 0.097. The VIF values were very high, suggesting extreme amounts of collinearity between variables. The highest VIF value was for rain hours at 859831.2.

Model 3 saw the removal of rain hours from the variables included in model 2 and this produced an even poorer model, explaining only 3% of the variation in the erosion value. The same process was carried out multiple times, removing the variable with the highest VIF value to create the next iteration of the model. Model 8 generated a model largely free of collinearity, however this model was still not statistically significant. The decision was made to omit the variable with the highest VIF value, mean temperature with a VIF value of 4.9 despite it being below the threshold for problematic variables, which led to model 9, which was statistically significant and with an R^2 value that explains 19.7% of the variation in the subaerial erosion above the Q10 level.

The final set of variables identified in model 9 - maximum temperature, total rainfall and average rainfall - were then tested against the other calculated erosion variables to identify whether they could predict a similar

Table 4.13: Results of backwards step-wise regression of meteorological variables against erosion variables using all bank data (n=35). Statistically significant p-values are in **bold**

Model Number	Dependent Variable	Independent Variables	variable coefficient	variable p-values	VIF Scores	r^2 value	model p-value
2	Subaerial erosion above the Q10 level	Intercept	195.009	**0.036**	NA	0.2513	0.097
		Cold Hours	0.146	0.401	54698.5		
		Frost Days	2.013	0.515	98646.7		
		Hot Hours	-0.358	0.337	23516.4		
		Mean Temperature	9.355	0.146	80404.7		
		Maximum Temperature	-9.682	**0.037**	26600.3		
		Total Rainfall	0.491	0.085	90636.1		
		Average Rainfall	-30.582	0.134	6135.9		
		Wetting and Drying Cycles	-1.066	**0.018**	828471.8		
		Rain Days	-1.863	**0.028**	147305.9		
		Rain Hours	0.802	**0.017**	859831.2		
3	Subaerial erosion above the Q10 level	Intercept	2.688	0.959	NA	0.031	0.404
		Cold Hours	-0.007	0.971	48291.0		
		Frost Days	0.530	0.877	95224.0		
		Hot Hours	-0.044	0.911	20970.0		
		Mean Temperature	0.614	0.918	57040.0		
		Maximum Temperature	-0.252	0.927	8154.5		
		Total Rainfall	0.000	0.999	4720.7		
		Average Rainfall	-0.607	0.974	4039.9		
		Wetting and Drying Cycles	-0.020	0.874	56899.0		
		Rain Days	0.015	0.967	24892.7		
4	Subaerial erosion above the Q10 level	Intercept	-3.009	0.935	NA	0.076	0.297
		Cold Hours	0.002	0.922	44045.6		
		Hot Hours	0.001	0.998	9641.8		
		Mean Temperature	-0.028	0.995	29556.5		
		Maximum Temperature	0.078	0.963	3244.3		
		Total Rainfall	-0.031	0.746	8961.0		
		Average Rainfall	0.910	0.952	2870.0		
		Wetting and Drying Cycles	-0.001	0.971	3221.7		
		Rain Days	0.071	0.403	1343.7		
5	Subaerial erosion above the Q10 level	Intercept	-3.360	0.295	NA	0.118	0.202
		Hot Hours	0.003	0.683	9.0		
		Mean Temperature	-0.069	0.300	7.4		
		Maximum Temperature	0.094	0.476	20.4		
		Total Rainfall	-0.030	0.262	717.5		
		Average Rainfall	1.053	0.175	7.7		
		Wetting and Drying Cycles	-0.001	0.907	173.6		
		Rain Days	0.071	0.326	1005.7		
6	Subaerial erosion above the Q10 level	Intercept	-0.483	0.708	NA	0.118	0.180
		Hot Hours	<-0.001	0.971	7.2		
		Mean Temperature	-0.034	0.538	5.4		
		Maximum Temperature	-0.016	0.818	5.8		
		Total Rainfall	-0.006	0.568	111.5		
		Average Rainfall	0.519	0.339	3.9		
		Wetting and Drying Cycles	0.002	0.681	133.3		
7	Subaerial erosion above the Q10 level	Intercept	-0.288	0.807	NA	0.148	0.114
		Hot Hours	<0.001	0.979	7.2		
		Mean Temperature	-0.036	0.503	5.3		
		Maximum Temperature	-0.031	0.595	4.2		
		Total Rainfall	-0.002	0.261	2.4		
		Average Rainfall	0.598	0.232	3.4		
8	Subaerial erosion above the Q10 level	Intercept	-0.283	0.803	NA	0.182	0.059
		Mean Temperature	-0.037	0.473	4.9		
		Maximum Temperature	-0.032	0.508	3.0		
		Total Rainfall	-0.002	0.249	2.4		
		Average Rainfall	0.609	**0.046**	1.2		
9	Subaerial erosion above the Q10 level	Intercept	-0.156	0.888	NA	0.197	**0.034**
		Maximum Temperature	-0.058	0.070	1.3		
		Total Rainfall	-0.001	0.357	1.4		
		Average Rainfall	0.609	**0.044**	1.2		

amount of variation in those variables (table 4.14. These variables were able to explain 23.7% of the total erosion volumes and 19.0% of the volume of erosion above the Q10 level per m^2. However the remaining models were not statistically significant.

Table 4.14: Results of multiple regression model of meteorological variables against erosion variables using all bank data (n=35). Statistically significant p-values are in **bold**

Model Number	Dependent Variable	Independent Variables	variable coefficient	variable p-values	VIF Scores	r^2 value	model p-value
10	Total erosion volume	Intercept	0.270	0.853	NA	0.237	**0.018**
		Maximum Temperature	-0.090	**0.035**	1.3		
		Total Rainfall	-0.002	0.149	1.4		
		Average Rainfall	0.855	**0.032**	1.2		
11	Subaerial erosion above the Q10 level per m^2	Intercept	-0.016	0.813	NA	0.190	**0.037**
		Maximum Temperature	-0.003	0.167	1.3		
		Total Rainfall	<-0.001	**0.009**	1.4		
		Average Rainfall	0.003	0.058	1.2		
12	Percentage contribution of subaerial erosion above the Q10 level	Intercept	117.0	**0.002**	NA	0.067	0.193
		Maximum Temperature	-1.431	0.146	1.3		
		Total Rainfall	-0.064	0.068	1.4		
		Average Rainfall	10.098	0.266	1.2		
13	Mass wasting erosion	Intercept	0.280	0.513	NA	0.144	0.071
		Maximum Temperature	-0.017	0.166	1.3		
		Total Rainfall	-0.001	**0.013**	1.4		
		Average Rainfall	0.156	0.168	1.2		

The last step of this analysis was to conduct Principal Components Analysis (PCA). All 12 of the meteorological variables were used for the PCA, and the components that explained a significant proportion of the variance in the data were determined by identifying the percentage contribution if all components contributed equally to the model (8.3%), and then using only the components that contributed above that value (figure 4.9). This identified components 1 (76.27%) and 2 (11.58%) as contributing significantly to the variance in the data and together explaining 87.85% of the variance in the meteorological data.

The next step was to establish which independent variables contributed most significantly to the two chosen components. First, the cutoff con-

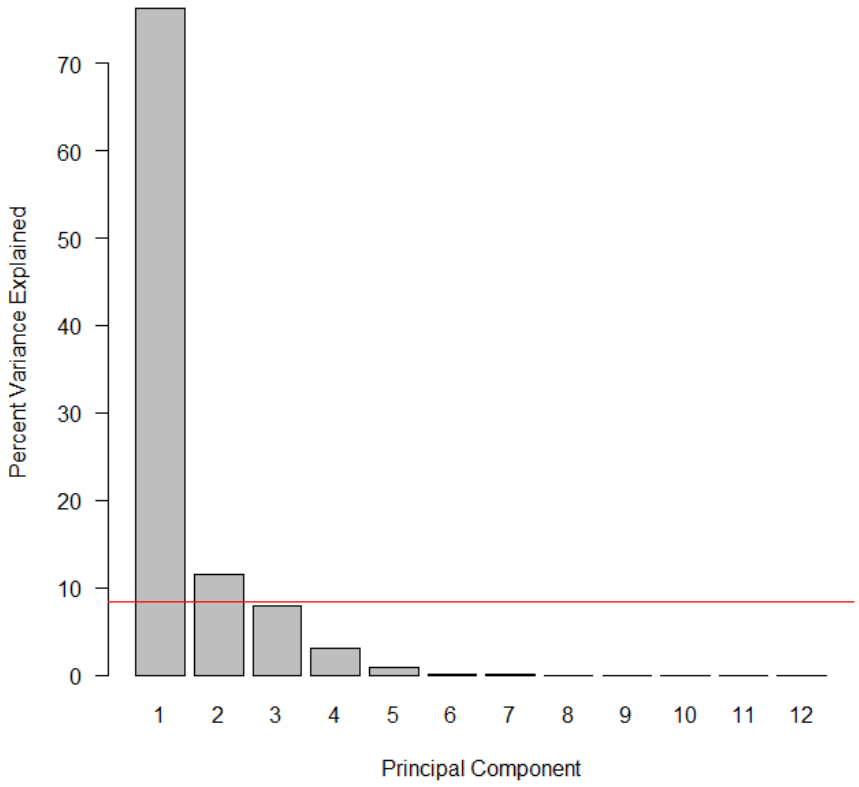

Figure 4.9: Plot of the percentage variance explained by each principal component

tribution was calculated. It should be established that, in PCA, the sum of the square of each loading should equal 1. Therefore, to calculate the level at which a variable has a large loading (i.e. contributes more than one variable's expected loading), we can calculate the cut off value using the equation $\sqrt{1/number\,of\,variables}$. In this case that value is +/- 0.289. The contributing variables are detailed in table 4.15.

Table 4.15: List of independent meteorological variables contributing to the Principal Components Analysis. Significantly contributing variables are highlighted in **bold**

Meteorological Variable	PC1	PC2
Cold Hours	**0.311**	0.215
Frost Days	**0.317**	0.210
Freeze Thaw Cycles	**0.319**	0.193
Mean Temperature	**-0.296**	0.162
Minimum Temperature	**-0.290**	-0.052
Total Rainfall	**0.313**	0.172
Wetting and Drying Cycles	**0.321**	0.081
Wet Days	**0.320**	0.112
Rain Hours	**0.321**	0.092
Maximum Temperature	-0.212	**0.438**
Average Rainfall	0.160	**-0.505**
Hot Hours	-0.229	**0.582**

PC1 shows strong positive loadings for cold hours, frost days, freeze thaw cycles, total rainfall, wetting and drying cycles, wet days and rain hours. PC1 shows strong negative loadings for mean and minimum temperature. PC2 shows strong positive loadings for maximum temperature and hot hours with a strong negative loading for average rainfall.

The first two principal components explain 87.85% of the variation in the meteorological data, and these two components combined explain 26.84% of the variation in the volume of subaerial erosion above the Q10 level. This method explains an additional 7% of the variation in the erosion data compared to simple multivariate regression techniques. However, 73.16% of the variation in subaerial erosion is still unaccounted for in the PCA model.

4.4.3 Combination of Flow and Subaerial variables to predict erosion

It is important to remember that neither fluvial nor subaerial processes work in isolation, so an understanding of the combined affect of both sets of conditions and how they work together is needed to gain a clearer picture of the dynamics of bank erosion.

An additional series of backwards step-wise regression models were created to explain the net erosion volume using the flow and meteorological variables identified in earlier model creation, as that process has already accounted for collinearity. This gave a final model that used maximum temperature, average rainfall, minimum stage, peaks above Q10 and mean discharge and gave an R^2 value of 0.230 with a statistically significant p-value of 0.043 (table 4.16. This combined model explained 4% more of the variation in net erosion volume than the flow or meteorological variables alone.

Table 4.16: Results of multiple regression model of meteorological variables against erosion variables using all bank data (n=35). Statistically significant p-values are in **bold**

Model Number	Independent Variables	variable coefficient	variable p-values	VIF Scores	r^2 value	model p-value
1	Intercept	-9.048	0.166	NA	0.267	**0.036**
	Maximum Temperature	-0.019	0.693	1.4		
	Total Rainfall	0.008	0.151	14.8		
	Average Rainfall	0.512	0.278	1.5		
	Min Stage	12.873	0.223	2.4		
	Peaks above Q10	-0.034	0.494	12.5		
	Mean discharge	-0.120	0.879	2.8		
2	Intercept	-4.001	0.471	NA	0.230	**0.043**
	Maximum Temperature	-0.031	0.531	1.4		
	Average Rainfall	0.702	0.136	1.4		
	Min Stage	4.326	0.625	1.7		
	Peaks above Q10	0.031	0.191	2.6		
	Mean discharge	-0.003	0.997	2.8		

4.4.4 Influence of meteorological variables on deposition

The previous chapter described significant areas of apparent deposition across the study banks during some of the time periods. In addition to the above models focused on erosion, correlations were calculated to establish whether there was a significant relationship between the deposition values and the meteorological conditions experienced at the site (table 4.17). The highest correlation was between deposition volume and total rainfall at 0.734, but other variables with correlations above 0.6 included freeze thaw cycles, wetting and drying cycles and frost days.

Table 4.17: Results of Pearson's R correlation between meteorological variables and deposition variables using all bank data (n=35). The values in **bold** represent those values that are are above the critical value (0.296) at the 0.1 significance level. Those with a * are also above the critical value (0.349) at the 0.05 significance level.

	Total Deposition Volume (m^3)	Total Deposition Area (m^2)
Cold Hours	**0.694***	**0.430***
Frost Days	**0.700***	**0.449***
Freeze Thaw Cycles	**0.670***	**0.452***
Hot Hours	-0.199	-0.209
Mean Temperature	**-0.390***	**-0.314**
Min Temperature	**-0.438***	**-0.317**
Max Temperature	-0.046	-0.110
Total Rainfall	**0.734***	**0.470***
Mean Rainfall	0.150	0.056
Wetting and Drying Cycles	**0.704***	**0.467***
Rain Days	**0.690***	**0.455***
Rain Hours	**0.712***	**0.470***

Another round of backwards, step-wise regression was undertaken, focused on the variables with correlation values above the significance value, highlighted bold in table 4.17. The results of these models are shown in table 4.18. The final model was comprised of mean temperature and total rainfall and resulted in an R^2 value of 0.546, indicating that 55% of the deposition recorded at the site can be attributed to the effects of temper-

ature and rainfall. These variables were then also used in a regression against deposition area and gave an R^2 value of 0.164 and a p-value of 0.034.

Table 4.18: Results of backwards step-wise regression of meteorological variables against total deposition using all bank data (n=35). Statistically significant p-values are in **bold**

Model Number	Independent Variables	variable coefficient	variable p-values	VIF Scores	r^2 value	model p-value
1	Intercept	-15.527	0.583	NA	0.709	<**0.01**
	Cold Hours	-0.089	0.450	65138		
	Frost Days	0.971	0.594	89365		
	Freeze Thaw Cycles	-0.293	0.728	49282		
	Mean Temperature	0.910	0.664	23347		
	Minimum Temperature	-1.294	0.574	41573		
	Total Rainfall	0.099	0.005	3275		
	Wetting and Drying Cycles	0.133	0.512	500542		
	Rain Days	-0.356	0.058	19522		
	Rain Hours	-0.061	0.512	197344		
2	Intercept	2.959	0.298	NA	0.717	<**0.01**
	Cold Hours	-0.0132	0.544	2324		
	Frost Days	-0.182	0.706	6462		
	Freeze Thaw Cycles	0.250	0.179	2358		
	Mean Temperature	-0.460	0.077	344		
	Minimum Temperature	0.214	0.280	309		
	Total Rainfall	0.104	0.003	3153		
	Rain Days	-0.251	0.005	3971		
	Rain Hours	0.000	0.993	304		
3	Intercept	2.031	0.139	NA	0.728	<**0.01**
	Cold Hours	-0.021	0.002	185		
	Freeze Thaw Cycles	0.183	<0.001	146		
	Mean Temperature	-0.379	0.007	93		
	Minimum Temperature	0.149	0.123	74		
	Total Rainfall	0.095	<0.001	1657		
	Rain Days	-0.228	<0.001	1822		
	Rain Hours	0.000	0.927	285		
4	Intercept	-0.092	0.956	NA	0.514	<**0.01**
	Cold Hours	0.003	0.195	19		
	Freeze Thaw Cycles	0.020	0.526	40		
	Mean Temperature	-0.014	0.914	52		
	Minimum Temperature	0.086	0.492	73		
	Total Rainfall	0.005	0.621	162		
	Rain Hours	-0.002	0.711	279		
5	Intercept	-0.598	0.522	NA	0.531	<**0.01**
	Cold Hours	0.003	0.201	16		
	Freeze Thaw Cycles	0.013	0.598	25		
	Mean Temperature	0.028	0.654	12		
	Minimum Temperature	0.048	0.495	24		
	Total Rainfall	0.001	0.671	20		
6	Intercept	-0.759	0.385	NA	0.545	<**0.01**
	Cold Hours	0.003	0.197	16		
	Mean Temperature	0.031	0.604	12		
	Minimum Temperature	0.031	0.616	18		
	Total Rainfall	0.003	0.217	9		
7	Intercept	-1.123	0.023	NA	0.558	<**0.01**
	Cold Hours	0.002	0.203	10		
	Mean Temperature	0.058	0.051	2.9		
	Total Rainfall	0.003	0.104	7.4		
8	Intercept	-1.099	0.027	NA	0.546	<**0.01**
	Mean Temperature	0.038	0.125	2.1		
	Total Rainfall	0.005	<0.001	2.1		

4.5 Discussion

4.5.1 Flow and Meteorological controls on Erosion

Fluvial erosion was frequently the lowest contributing erosion process, despite there being periods of high flows experienced during the study period. Although some statistically significant correlations were found between flow variables and the volume and rate of erosion, many of these correlations were not strong and their strength and significance varied between the different banks, despite their close proximity and their almost identical flow regimes. The strongest recorded correlation, 0.968, was between peaks above Q50 and the total erosion volume recorded at the upstream reach of bank 3, however peaks above Q50 did not have any other significant correlations at any other bank or with any of the other calculated erosion values. The flow variables most consistently correlated with erosion variables were peaks above the Q10 level and hours above the Q10 level, both with nine significant negative correlations within the data set, mean stage, with eight significant negative correlations, and hours above Q50, with seven significant negative correlations.

These results indicate high variability in the influence of flow on erosion. This pattern is very similar to that shown by Henshaw et al. (2013) on the Pontbran Catchment in Wales, who also saw significant differences between the correlations at different patches of erosion pin measurements. However their results saw a much stronger relationship between flow and erosion, with a 0.934 correlation between maximum discharge and erosion and a 0.898 correlation between mean discharge and erosion compared this study which saw correlation values between -0.008 and -0.526 between net erosion volume and discharge.

As noted in chapter 3, the lowest rates of erosion for banks 1 and 2 were recorded between October 2017 and February 2018. This time period encompasses the winter months which are traditionally believed to be the periods of time where most erosion would occur due to the associated seasonal rainfall and the corresponding high flows.

The most compelling result from the analysis carried out was the prevalence of negative correlations between the flow and erosion variables, with an increase in flow apparently resulting in a decrease in the erosion. This could be attributed to the potential redistribution of bank sediment by a combination of subaerial erosion and mass wasting processes in the upper bank causing a net deposition at the bank toe. If this additional sediment is then removed by flow, it means that the erosive energy of the flow is not being used to erode the lower bank and thus it may appear that higher flows result in less erosion because they are simply re-mobilising already eroded material.

Alternatively, high flows could be protecting the mid sections of the bank from the continued and more widespread action of subaerial processes. There is limited evidence of this phenomenon in the wider literature, however it has been suggested by Couper (2003) that higher flows could be insufficient to generate significant erosion through fluvial entrainment. Instead, higher flows protected the mid sections of the bank from the action of subaerial processes, and may also have temporarily decreased the susceptibility of the surface soils to erosion through increasing particle cohesion during wetting. The evidence of this work seems to support this theory, further evidencing the importance of subaerial processes as dominant erosive forces along this stretch of the River Arrow.

This site has been studied by other authors (Lawler, 1994; Couper and

Maddock, 2001) and differences in the effects of flow on erosion were identified by both. For example, Lawler (1994) found that a moderate flow event in October 1990 generated 11mm of erosion, however a much larger magnitude event in February 1990 generated 4mm of deposition. Lawler (1994) attributed the differences in the erosion rates to the presence of looser, unconsolidated material at the base of the bank during the October event which was easier to erode, while the February event had no such material at the bank toe and flow was instead working to erode the more consolidated and cohesive bank face. It is possible that the same process was occurring during this study, but that this cycle was not visible due to the coarse temporal resolution. This will be discussed further in the limitations.

Couper and Maddock (2001) studied the River Arrow at Studley and recorded average erosion values of between 10 mm a^{-1} and 40.1 mm a^{-1} prior to a flood and between 16.7 mm a^{-1} and 86.0 mm a^{-1} including the flood event. These values fall within the range of erosion rates per year recorded in this study which fell between 6 mm a^{-1} and 576 mm a^{-1}. The comparison between the results of the Couper and Maddock (2001) study and this study can be seen in figure 4.10. This study frequently records higher mean and maximum erosion values than those presented in Couper and Maddock (2001), which could be explained by the significantly increased number of points collected using the TLS approach over the erosion pin approach as it allows for observation of a much higher proportion of the bank. This allows more of the potential spatial variation in the erosion to be recorded. The TLS approach is also a remote sensing approach, meaning that no interference of the bank is necessary to record the data. In Couper et al. (2002) discussion of the influence of the presence of erosion pins on recorded deposition highlights the potential impacts that erosion

pins can have in generating deposition features and in possibly providing some mechanical stabilisation to the bank during their installation/use.

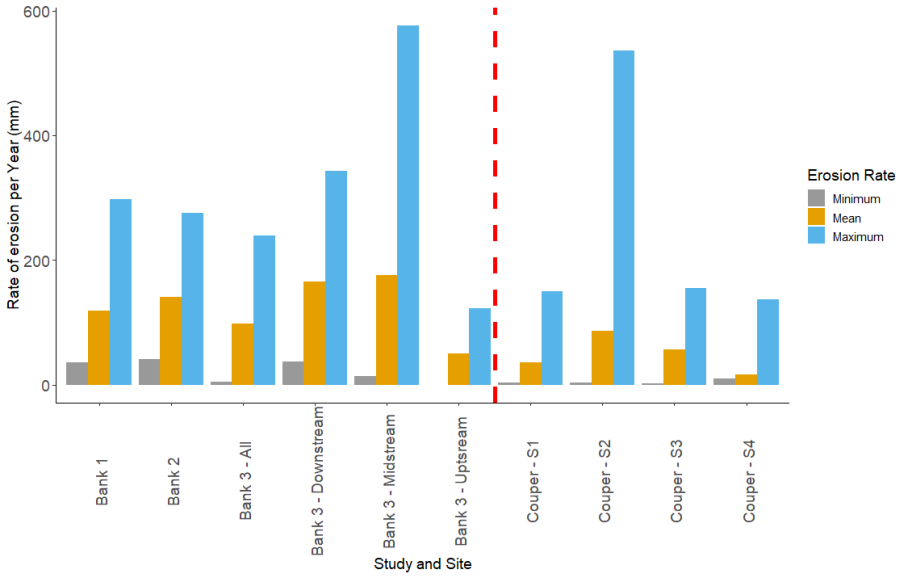

Figure 4.10: Comparison of the erosion rates between this study and that of Couper and Maddock (2001)

Similarly to the flow variables, there was only limited evidence of a relationship between erosion and meteorological variables. For example, freeze thaw cycles exhibited a maximum correlation value of -0.845 at the upstream reach of bank 3 and a correlation value of -0.527 across all bank data against the net erosion volume. Wetting and drying cycles exhibited a maximum correlation value of -0.774 at the upstream reach of bank 3 and a correlation value of -0.571 across all bank data against the net erosion volume. Hot hours had the most consistently, strong positive relationship with erosion (11 significant correlations within the data set), followed by maximum temperature and mean rainfall which had seven positive correlations and six negative correlations respectively.

Couper and Maddock (2001) found similar variability in their correlations between erosion and meteorological values, but there was more consistency in the strength of the relationships across the different banks. They

found moderate positive correlations between morphological activity and total rainfall, freeze-thaw cycles and frost days, as well as moderate negative correlations between minimum temperature and mean daily minimum temperature.

Again, it is interesting to note the direction of the relationships as found by Couper and Maddock (2001) when compared to the results of this study. The temporal scales of the two pieces of work were very different, with the Couper et al. paper monitoring every two weeks versus the much longer intervals within this study. This once again highlights the issue of scale in research of channel geomorphology, with short temporal scales exhibiting markedly different relationships than those of longer intervals.

This study undertook several different linear models, seeking to understand the relationship between erosion and combinations of flow and meteorological variables. However, for the purposes of comparison between different rivers the most useful of the dependent variables used is the rate of erosion per m^2 per year. It accounts for differences in size of river bank and length of observational duration to make estimates of erosion comparable across a multitude of different studies.

4.5.2 Meteorological Conditions and deposition

The presence of widespread and large deposition values has been discussed in chapter 2. Work was undertaken to ensure that these values were indeed a reflection of changes to the soil surface and not indicative of an error in data collection. Similar patterns have also been recorded in other papers using similar laser scanning approaches as well as in multiple erosion pin studies, pre-dating the increased use of remotely sensed change detection.

Couper et al. (2002) identified a number of studies using erosion pins

that recorded negative values, and highlighted that the handling of such negative values could have significant effects on the reporting and interpretation of mean erosion values for an area. In this study, net erosion has considered both erosion and deposition values. However, the frequency of large areas of deposition raised the question of whether there were particular conditions that generated these values.

Following a series of backwards, step-wise regression it was found that as much as 55% of the deposition can be explained by the mean temperature and total rainfall experienced at a site. This value was significantly higher than any predictions of the erosion. Both coefficients were positive, indicating an increase in mean temperature and an increase in total rainfall will result in an increase in total deposition volume by 0.038m^3 and 0.005m^3 respectively.

The presence of these two particular variables in the final multiple regression model fits with existing literature on soil expansion. Couper (2003) performed laboratory tests of reconstructed soil blocks with varying silt-clay contents. They found that with increasing silt-clay content there was evidence of expansion of the base of soil blocks after a cycle of 30 freeze-thaw cycles. For the block with 75% silt-clay this expansion was as much as 5mm. The same work also identified that with increasing freeze-thaw cycles there was also an increase in soil volume, however the extent of this change in volume was highly varied despite the cycles being uniform in length and temperature conditions (10hrs at -6°C followed by 14 hours at +6°C). The results of this change in volume can be seen in figure 4.11.

In addition, work by Ferreira et al. (2020) attempted to establish the expansion and cracking of soils under different amounts of stress. They found that a soil extracted from Paulista, Brazil, with a silt content of 250

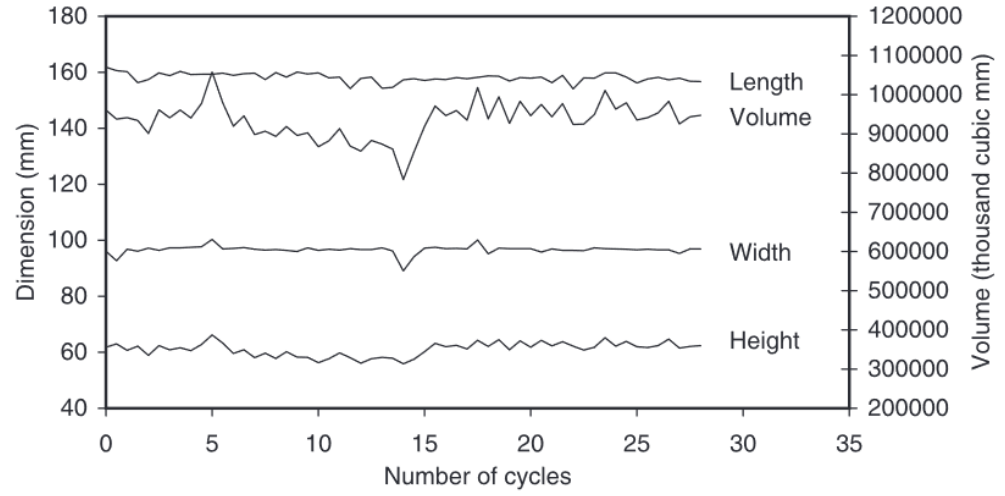

(a)

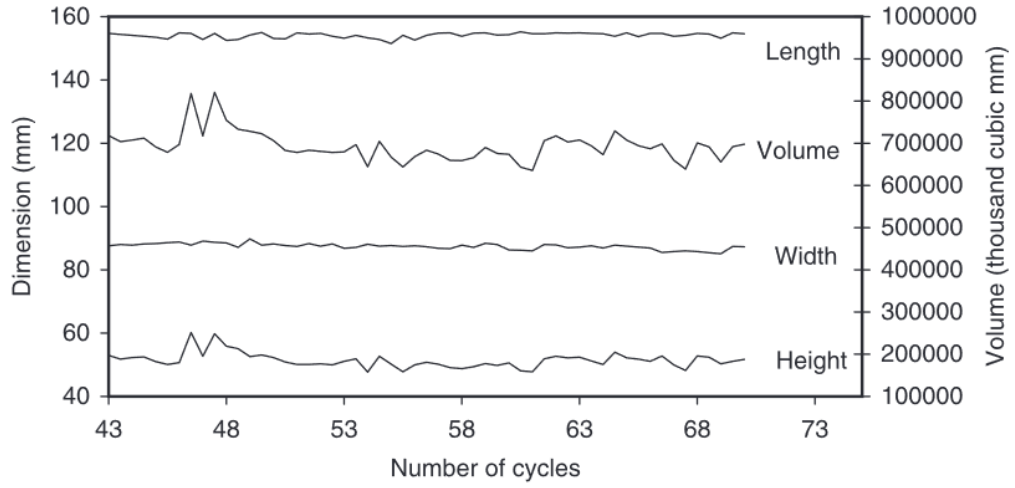

(b)

Figure 4.11: Results of soil volume changes following a) freeze-thaw cycles and b) wetting and drying cycles (Couper et al., 2002)

g $kg^{-}1$, clay content of 470 g $kg^{-}1$ and sand content of 28 g $kg^{-}1$ and held under 1kPa of pressure expanded by 8% following 70 hours of flooding. The same soil held under 10 kPa of pressure expanded by 3.49%. This suggests that soil at or near its saturation point following high flows or high rainfall has the potential to exhibit change that would be detectable by high-resolution change detection techniques such as those used in this study.

4.5.3 Limitations

Gauge data to bank height

One of the limitations of the research posed above was the lack of in situ stage measurements on the chosen banks. At the beginning of the research period a pressure sonde was installed between banks 1 and 2 to provide in situ river level measurements. However, this equipment was lost from the site and procurement issues meant it could not be replaced within the time frame of the research. This left a large gap in the required data for the project, and so a decision was made to perform a linear regression analysis based on the river height at the time of scanning and the gauged level recorded at that time. The limited range of recorded levels has meant that a considerable amount of extrapolation was needed to calculate the gauge level that may result in water reaching bank top. Those limitations meant that the decision was taken not to extrapolate out to top of bank level, but instead only to calculate a height on the bank associated with Q10 and Q50 flows. For all banks, the values for Q10 and Q50 fell within the bank height values that were obtained from surveying and so the linear regression technique was deemed adequate. For future iterations of this work, in situ measurements of stage should be seen as an integral feature of the research, or scanned data should be collected at

a significantly greater range of flows so that a more accurate regression can be carried out.

Additionally, for the purposes of this research the values of Q10 and Q50 were calculated based on the long term flow regime of the river. For future work, consideration should be given to deriving the Q10 and Q50 values relating to each individual time period, thus representing a more accurate representation of where water reached during the scan interval and how long different forces were acting on different areas of the bank. It is possible that, with a more representative exploration of the water height on the bank, the proportions of different erosion processes may be altered and the dominance of subaerial processes may become less pronounced.

Calculation of wetting and drying and freeze thaw cycles

Wetting and drying cycles were calculated based on one hour of rain followed by one hour of dry weather, however the wetting drying cycle being defined based on a time period of rainfall/no rainfall does not allow for the potential differences in saturation level that may occur between one hour of light rainfall and one hour of intense rainfall. It also does not account for the difference in potential evaporation based on the temperature conditions, wind conditions or cloud conditions on each day. As such, these values are unlikely to truly reflect wetting and drying cycles in the deeper soils and may only be accurate for soils at or very near the bank surface.

Because the research was focused on an exposed vertical bank face and erosion mechanisms are working predominantly on the exposed surface soils, this was not deemed to be a significant issue, however for future work, where the question of the impact of processes such as seepage may be relevant, a more robust method for determining wetting and drying cycles and freeze thaw cycles should be considered. This could include

the use of soils temperature and moisture loggers permanently installed at the site to gain a better understanding of the soil conditions.

Temporal Scale

The large scan intervals have already been discussed as a limitation in the previous chapter, with reference to the difficulty of attributing erosion to different processes. However, it is important to once again discuss the scan intervals and the potential impact that they may have on understanding the flow and meteorological characteristics that generate significant quantities of erosion.

This study has generated a large number of correlation coefficients between flow and meteorological conditions and resulting erosion. However, in many cases these coefficients have exhibited relationships that are in opposition to established literature. However, the problem of scale is a significant one in the research of fluvial geomorphology (Kondolf and Piégay, 2016) where the processes generating the characteristics we are observing are operating at temporal and spatial scales beyond what we frequently use to monitor and manage them. The large time periods between scans means that we are unable to pick out the effects of single events, but instead the cumulative effects of multiple events. To truly understand the effect of high flows, these events must be isolated so that their direct effects can be quantified and a better understanding of the processes can be achieved. To do this, data must be collected before and after a single high flow event in order to directly attribute the effects of a single event. Doing that in the natural environment is challenging because even if a single high flow event can be isolated, it will still be impossible to separate the effect of the flow event from the effect of the rainfall that generated the flow event.

These problems of scale also lead to a further question of statistical power, whereby small sample sizes reduce the likelihood of being able to detect a true relationship between variables. Many of the models generated from this small observation dataset were not statistically significant, and low numbers of observations also raise the question of whether statistical significance can be relied upon as reflection of a true relationship if the data were to be scaled up. Overcoming this problem of scale, then, becomes even more important not only to understand the effect of short-duration, high-magnitude events versus long-duration, low-magnitude events but also to increase confidence in the statistical significance of the results of those analyses.

At the beginning of this study, it was decided that longer time intervals between scans would be required in order to ensure that any change occurring was above the minimum level of detection of the equipment and scanning protocol being used. Refinements made to the techniques throughout the study, as well as technological improvements in new laser scanning equipment, means that the minimum level of detection is now small enough that it would be possible to detect changes attributed to single events if they can be identified, however the challenge remains to identify the direct effect of flow independent of the effect of rainfall.

This problem of scale is one of the most significant limitations of this study, and so further discussion and a series of recommendations for future study will be provided in chapter 6 - Discussion.

4.6 Chapter Summary

This chapter aimed to use a combination of flow and meteorological variables to explain the rates and volumes of erosion occurring via fluvial and subaerial erosion processes. It is evident from the low Pearson correlation

values and low R^2 values that no single variable can be used to explain significant amounts of fluvial or subaerial erosion. Multiple regression was used to identify groups of variables that, in combination, explained significantly more of the recorded erosion, but the use of Principal Component Analysis identified combinations of variables that explained a larger proportion of the recorded change than any other technique.

Of particular interest in this study was the direction of the relationships between flow variables and erosion variables, with increasing discharge and increasing water level both exhibiting a negative relationship with erosion. A number of possible reasons for this were discussed, and although no clear reason for the direction of the relationship could be confidently claimed, this author believes that it adds further evidence to the importance of subaerial processes in streams with highly cohesive bank material.

In the next, and final, results chapter, the fluvial erosion component will be further analysed to identify whether the roughness of a point can be used to explain its erosion and whether or not the roughness of upstream points contributes to the erosion of downstream points.

Chapter 5

The influence of form roughness on riverbank erosion processes

This chapter addresses the third and final objective of this research which is to identify to what extent roughness influences the rate of bank erosion below the Q10 level. This chapter provides a brief recap of relevant results from previous chapters before reviewing the literature surrounding roughness and erosion. It then states the research questions and objectives for this chapter and provides details of the specific methods used and the results obtained, before finishing with a discussion of the results and the limitations of the work conducted.

5.1 Introduction

In the two previous chapters the relative contributions of subaerial, mass wasting and fluvial erosion processes have been calculated. Flow variables and meteorological variables have been tested to try to explain the recorded erosion values for the different processes, using the total or average erosion values and a series of calculated meteorological variables for each time period.

Subaerial erosion has been identified as the dominant erosion process at this site, and a combination of maximum temperature, total rainfall and average rainfall have been identified as explaining up to 19% of the subaerial erosion above the Q10 level and 20% of the subaerial erosion above the Q50 level. Minimum stage, peaks above Q10 level and mean discharge were found to have explained 23% of the net erosion per year across the whole bank.

However, despite the apparent low contribution of fluvial erosion processes on the overall bank change, it is still important to try to understand some of the factors that impact on the rate of fluvial erosion. This chapter focuses on the fluvial erosion component of the data and will attempt to identify whether the roughness of a bank surface influences its erosion.

Roughness has been considered as a factor influencing the flow of water since Isaac Newton developed the first mathematical model of flow in the late 17th century, however it is the work of Robert Manning (1816-1897), with the development of Manning's n, and Ludwig Prandtl (1875-1953) with the definition of the boundary layer concept, who have had most significant impact on how we understand the influence of roughness today (Smith et al., 2007). The Manning's n flow resistance equation (5.1) calculates the velocity of flow (V) using the hydraulic radius and slope of the channel and an n value representing the coefficient of roughness. Values for n are most often calculated from sediment size and taken from tables of existing coefficients. Despite Manning's n being very well established, there has been a question of its appropriateness for different channel types (Okhravi, 2022) and under changing flow conditions (Ye et al., 2018) where a more dynamic representation of roughness is of greater value than a single defined numerical constant. Deeper knowledge of the influence of roughness on erosion and channel form is required to further

improve our understanding of the evolution of our fluvial environments.

$$V = \frac{1}{n} R^{2/2} S^{1/2} \tag{5.1}$$

5.1.1 Roughness and Total Shear Stress

Form roughness is the name given to the undulations that cover most natural river channel sides and beds (figure 5.1). It is believed to have a significant influence on the rate at which fluvial erosion will occur due to the friction it exerts on the flow. The total shear stress (τ_T) of a channel boundary can be partitioned into "skin friction", $\tau_S F$, and "drag stress", τ_D (equation 5.2).

Figure 5.1: River bank roughness at the River Arrow, Studley

$$\tau_T = \tau_S F + \tau_D \tag{5.2}$$

The skin friction component is the result of frictional forces between the fluid and the bank surface. The drag stress is the result of differential pressure forces generated by the protruding surface features. This pressure differential, known as 'form drag', is generated first through the deflection of flow away from the downstream surface. This creates areas of lower pressures and slower flows at the downstream end of the protrusion compared to the conditions further into the main flow. Drag stress is the form drag divided by the area over which the form drag is applied, which is dependent upon the spacing between protrusions or 'roughness elements'. The effect of these areas of lower pressure and slower flow can influence the river's ability to entrain particles from the river bank, and so affect the rate of erosion of the bank material.

The drag stress is frequently the dominant contributor to the shear stress and thus should be carefully considered in any models that try to establish the near boundary flow conditions (Smith and McLean, 1977). The drag force (F) exerted on an individual roughness element can be calculated using the equation 5.3

$$F = \frac{1}{2}\rho C_D H B u_{ref}^2 \tag{5.3}$$

Where ρ is the density of water, C_D is the drag coefficient of the roughness element, H is the height of the roughness element, B is the width of the roughness element perpendicular to the flow direction and u_{ref} is an appropriately determined reference velocity for the channel edge. Given the H, B and C_D of a roughness element, Kean and Smith (2006a) determined that it would be possible to establish the drag force on individual roughness elements within a channel.

An example of the effect of roughness can be seen in figure 5.2. The

roughness element acts as an obstruction to the flow of water, forcing it to divert away from the river bank. This area becomes the 'outer boundary layer' region, where flow conditions are most like those of near bank flows unaffected by roughness. This layer has been slowed through the friction between the water and the surface of the roughness element, but there is no continued reduction of flow once it is no longer in contact with the surface.

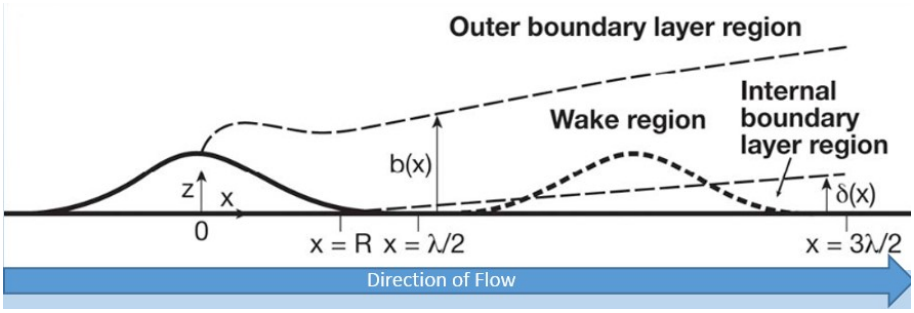

Figure 5.2: Plan view of the effect of Gaussian-shaped roughness elements on in channel flow (adapted from Darby et al. (2010)

The 'wake region' exists directly behind the roughness element, and consists of an area of lower pressure and lower flow rate than in the outer boundary layer. This layer is still in contact with the surface and so is still subject to frictional drag. The 'internal boundary layer' is the area of most significant difference in conditions in comparison to the outer boundary layer, where flow can reduce to zero, and sometimes even reverse in small localised areas.

The extent to which form roughness will influence the rate of erosion is dependent upon the height of the roughness elements, their length (in a streamwise direction) and how they are spaced along the channel length, as the combination of factors will influence the size, shape and magnitude of the differences between in channel pressures and near bank pressures.

Hopson (1999, cited in Kean and Smith (2006a) and Kean and Smith

(2006b)) used a series of flume experiments to establish the drag coefficients of a variety of unequally spaced, varying sized Gaussian shaped elements constructed against the flume wall. This was then supplemented with additional experiments to establish the same coefficients if there were a series of identical, regularly spaced elements along the flume wall. These Gaussian shaped elements were all 3cm in height but had different streamwise lengths, and so the degree of curvature from flume side to peak of the element was different. The drag force exerted on a roughness element was measured using an aluminium rod connected to the peak at one end and to a rigid frame above the flume at the other end. These experiments determined that the drag coefficient of a roughness element could be empirically determined using equation 5.4, where H is the height of the roughness element and σ is its streamwise span, equivalent to the standard deviation of the Gaussian probability distribution. Previous studies have examined the influence of roughness across a range of spatial scales from the um (Das et al., 2019) to 0.4m (Francalanci et al., 2020) as described below.

$$C_D = 1.79exp(-0.77\frac{\sigma}{H}) \tag{5.4}$$

Kean and Smith (2006a) and Kean and Smith (2006b) continued to develop the work of Hopson (1999) by applying the results of flume based calculations of drag coefficients to observations of in channel flow separation and the creation of outer boundary, inner boundary and wake regions on topographic roughness elements in Lost Creek (Montana, USA), Rock Creek (Kansas, USA) and Whitewater River (Kansas, USA). Unlike the laboratory experiments, the roughness elements observed in the field varied in height from 3cm to 58cm. The highly irregular bank profile was mod-

elled as a series of regular Gaussian curves, to provide flow properties that were deemed to be equivalent to the spatial average of the natural bank surface. They found that the comparison of measured drag forces and modelled drag forces using the regular Gaussian shapes provided an agreement of within 20% for all of the measured elements. Their approach allows for the determination of near bank flow and boundary shear stress taking into account the natural variation in the boundary surfaces of natural riverbanks, and provides a mathematical basis on which to partition the effects of skin drag and form drag within flow models.

The application of the Kean and Smith (2006a) and Kean and Smith (2006b) model to bank erosion was investigated by Darby et al. (2010) along the Lower Mekong River, Laos. Using the proposed model, they simulated both cumulative bank toe erosion and annual average erosion rates across four different sites on the Lower Mekong River, using the results of average boundary flow conditions across a number of different discharge values, recorded using an Acoustic Doppler Current Profiler (ADCP), and jet testing to establish the bank material susceptibility to erosion. The relationship between ADCP measurements of boundary flow rates and discharge was used to create a simulated bank boundary shear stress curve as a function of discharge.

This curve was then used to simulate the expected erosion conditions across the four sites based on historic discharge data. These values of simulated erosion were then compared with map and remotely sensed data of the four sites to establish actual bank retreat. They found the model highly sensitive to changes in input parameters. In particular, this work suggested that the smoother the bank, the greater the effect of increasing roughness when compared with banks that are rougher to begin with.

Work conducted by Das et al. (2019) sought to understand the influence of roughness at the very fine scale (um) by establishing the effect of sand/clay fractions on the formation of micro-eddies at the fluid-sediment boundary. This work found that the higher the roughness the higher the number of micro-eddies were generated. These micro-eddies were also larger and had more erosive power, meaning that higher roughness generated higher erosion volumes (figure 5.3).

Further work by Das et al. (2023) has again focused on the influence of very small scale roughness, but this time concentrated on the formation of undercuts in sediments with different sand-clay contents. This work identified that sediments with greater quantities of clay, or very small particle sizes with high cohesion, took longer to form erosion pits and the erosion depth was less by the end of the experiment (180h). They also found that flow velocity in the near bank region decreased with undercut depth, and that the deeper undercuts generated by the sediment with the lowest clay fraction resulted in the greatest reduction in velocity.

The effect of roughness is not limited to only the banks. Changes in bed roughness can also influence the boundary shear stress. Buffington and Montgomery (1999) found that as boundary shear stress increased the bed sediment size decreased indicating that the carrying capacity of the channel was reduced. Although this piece of work measured the carrying capacity of the river, reductions in carrying capacity can also demonstrate a reduction in the erosive power of the river as well.

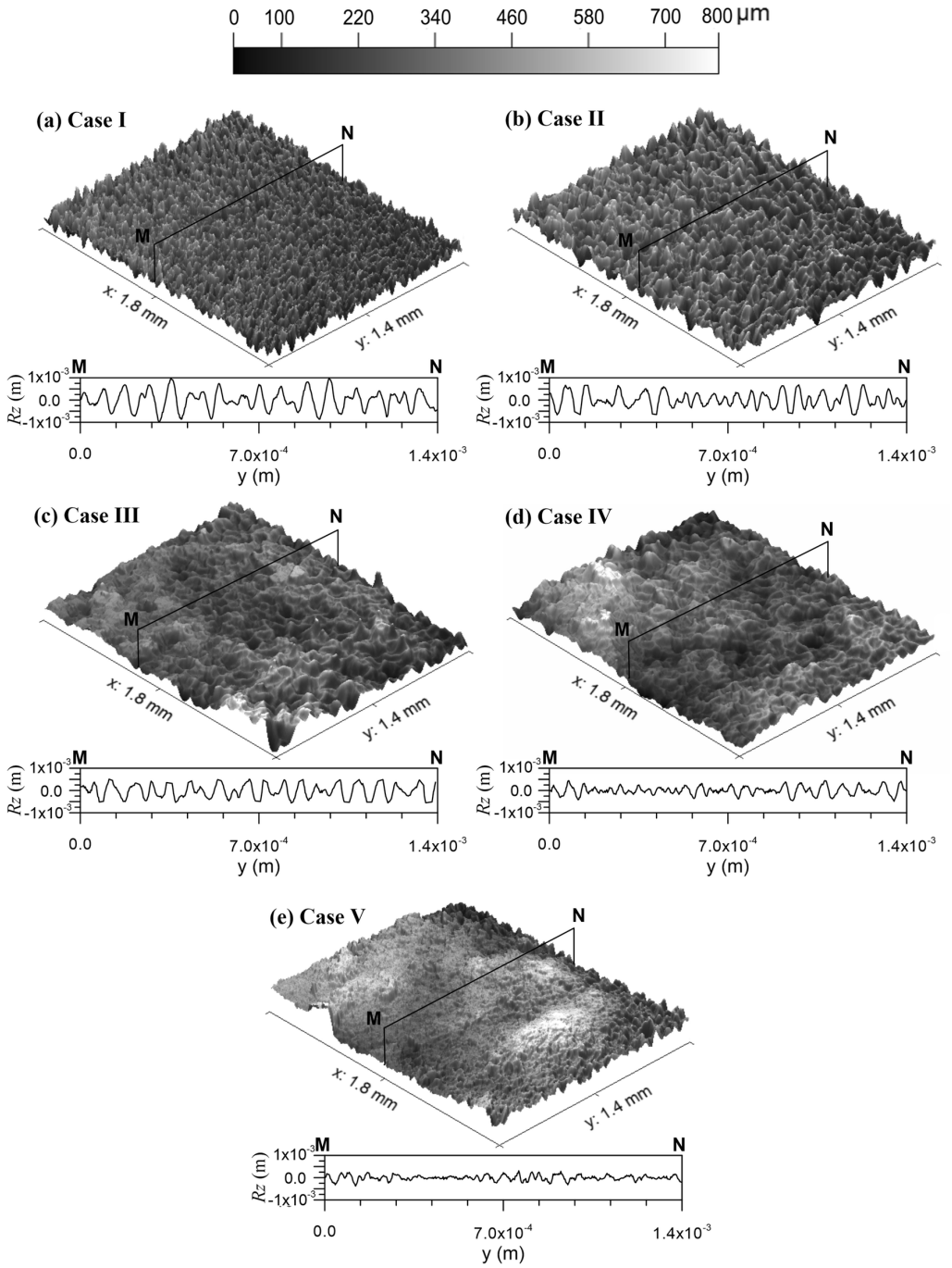

Figure 5.3: Surface roughness of five different sediments with differing sand-clay content where a) Case I = 10% clay, b) Case II = 15% clay, c) Case III = 20% clay, d) Case IV = 25% clay and e) Case V = 30% clay (Das et al., 2019)

5.1.2 Self-limiting Bank Erosion?

Much of the previous work on the effect of roughness on erosion has been carried out in flume based studies, however Leyland et al. (2015) used high

resolution topographic data (combination of photogrammetry and Terrestrial Laser Scanning techniques) to establish a simple conceptual model of self-limiting bank erosion (figure 5.4). They focused their research on the effects of fluvial erosion, proposing a cycle whereby failure of upper banks generate topographically complex lower bank regions which provide a measure of protection against subsequent erosion via a relative increase in form drag compared to skin friction. This effect is gradually reduced as low flows trim the protrusions, reducing roughness and resulting in a decrease in form drag relative to skin friction. The erosion rate begins to increase until bank instability results in a further failure, thus restarting the cycle.

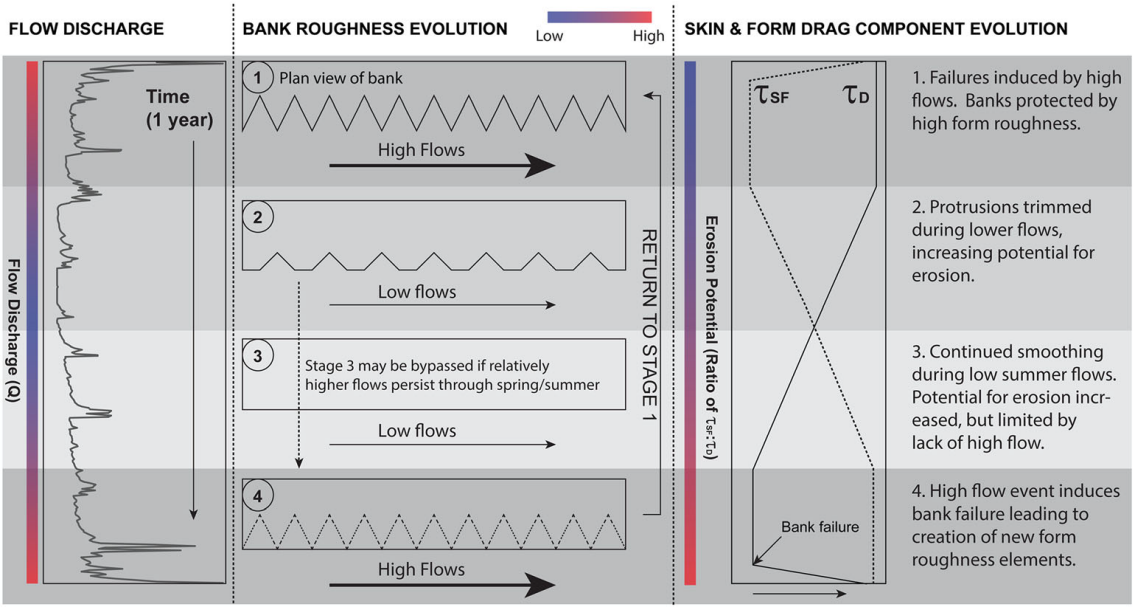

Figure 5.4: Leyland et al. (2015) conceptual model of the self-limiting bank erosion mechanism. Stage 1 immediately follows a bank failure event, when roughness is at its highest. As low flows trim the roughness elements and reduce the form drag on the elements it also increases the skin drag (stages 2 and 3). At stage 4, high flows induce bank failure, resulting in the development of new roughness elements and a return to stage 1 of the model.

Since the publication of the Leyland et al. (2015) model there have been a number of papers that have reffered to this model to discuss the potential impacts of roughness on erosion. Harvey et al. (2019) suggested that

burrowing species in river banks may also affect the form drag on a bank face. They hypothesise that single burrows could result in the creation of eddies and increased turbulence, causing entrainment of particles where eddies are strongest. However where there are many burrows together the effect could serve to increase the form drag of the boundary flow and thus reduce erosion. The roughness here would come not from protrusions of material from the bank face but instead from the inverse - the formation of depressions in the bank.

However, much of the subsequent research into bank erosion has continued to highlight the challenges of modelling highly irregular and complex natural river banks. The uniqueness of interactions between soil properties, hydraulic conditions, climate conditions and human interference mean that such a model is not yet adequately robust to aid in the quantification of erosion beyond small, reach-scale, studies (Duró et al., 2020a; Hoitink et al., 2020). Francalanci et al. (2020) highlighted the influence of changes in bump geometry as a result of high flows, where very rough surfaces generate a thicker near-bank boundary layer, reducing the skin friction of the flow and reducing the erosion effect to trimming of the roughness rather than the removal of large quantities of bank material. This negative feedback, where greater roughness results in less erosion, leads to smoothing of the surface roughness, a reduction in the near-bank boundary layer of flow and thus greater skin friction resulting in greater erosion. They suggested that the cyclical nature of this process, as presented in the Leyland et al. (2015) model, generates an average roughness overtime that is relatively constant.

Modelling roughness element heights of between 0.08m and 0.4m (which was chosen due to previous work by Leyland et al. (2015) and Nardi and Rinaldi (2010) observing roughness elements between these heights) the

work of Francalanci et al. (2020) found that roughness height had little correlation with bankfull width (R^2 = 0.24 for sand-bed rivers and R^2 = 0.19 for gravel-bed rivers) but did have a stronger correlation with bankfull discharge (R^2 = 0.74 for sand-bed rivers and R^2 = 0.46 for gravel-bed rivers). This supports the Leyland et al. (2015) model assumption that flow works to trim bank roughness, but that the time averaged roughness cannot be used to predict erosion rates in the form of bank width.

5.1.3 Gaps in our knowledge

The fact that roughness influences the skin and form drag components of boundary shear stress is clearly evidenced, however as yet, there has been little work conducted to link that to the other factors acting to influence bank erosion. The previous work conducted on form roughness often reduces bank roughness elements to longitudinal, 2-dimensional sections, without factoring in the effect of these roughness elements sitting within a 3-dimensional fabric of material. The work of Leyland et al. (2015) made good use of high resolution topographic data to develop a more 3-dimensional view of the effect of form roughness, however this generated a simple schematic model of the effect of roughness without quantifying and considering the relationship between roughness and erosion directly. The results of this study have also been contradicted at the very fine scale by the work done by Das et al. (2019) who found the opposite effect, where higher roughness resulted in higher erosion.

The problem of scale is a challenging one, and there remain holes in our knowledge to bridge the gap between the work of Das et al. (2019) at the very fine scale and Leyland et al. (2015) at the reach scale. By collecting very high resolution data on bank roughness at a variety of scales and its effect on erosion this chapter will attempt to identify whether rough-

ness conditions at different scales directly influence the erosion at that location.

5.2 Aims and Research Question

The aim of this chapter is to identify to what extent bank roughness influences the rate of bank erosion.

In order to achieve this aim the following objectives will need to be undertaken:

1. To use the results from chapter 3 to identify areas of the bank subject to fluvial erosion processes below the Q10 level
2. To quantify the roughness of the river bank surface below the Q10 level
3. To identify whether bank roughness has an influence on the rate of subsequent fluvial erosion

5.3 Methods

Scan data acquisition, classification and change detection methods have all been described in earlier chapters. In addition to those previously discussed techniques, the point clouds are also analysed for roughness. The roughness of a point is calculated using the Roughness tool in CloudCompare (figure 5.5). This tool has only one input value for 'kernel size' which represents the radius of a sphere centered on each point. All other points that fall within that sphere are averaged to create a best fitting plane using the least squares technique (Girardeau-Montaut, 2016). The roughness value generated represents the distance between the point of interest and the calculated average plane.

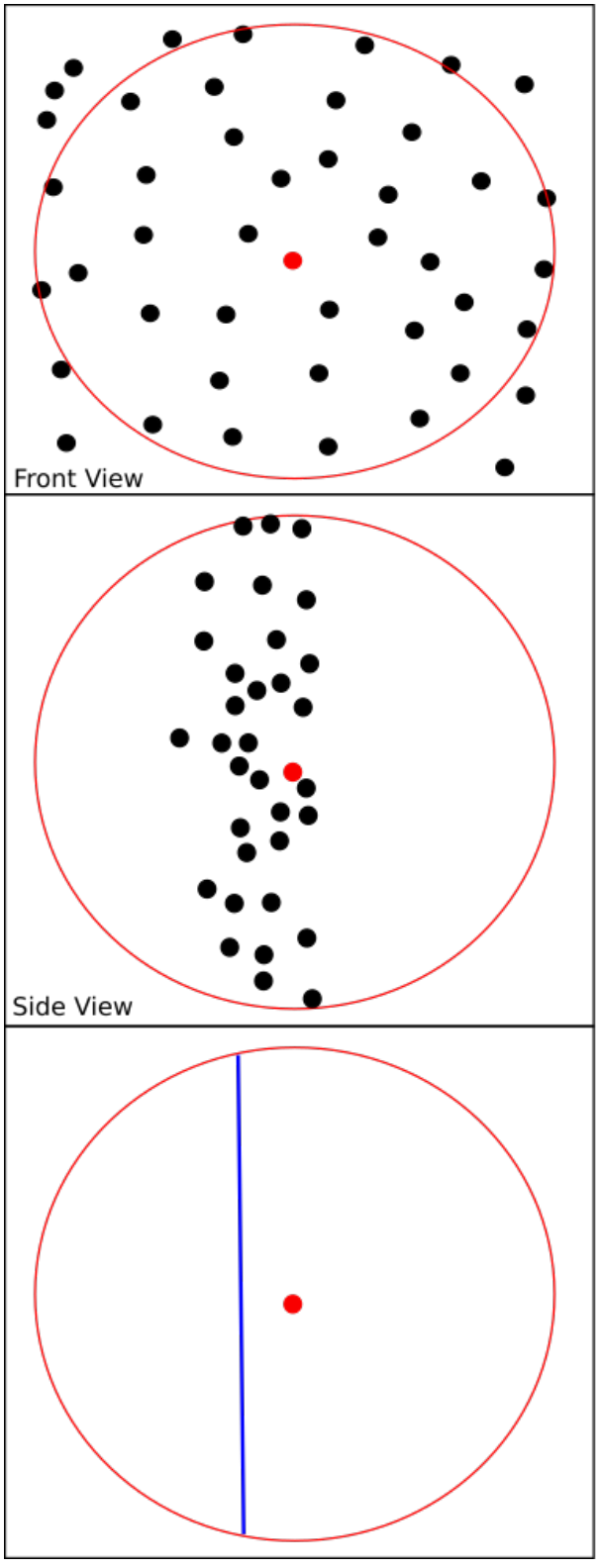

Sphere centered over each individual point. Size of sphere is based on a user provided 'Kernel Size' which represents the radius of a sphere centered on each point.

Average linear surface is calculated based on least squares regression of all points in sphere

Distance between point and linear surface is calculated. This is the roughness value.

Figure 5.5: Diagram of roughness calculation technique

The roughness calculation was performed at three different kernel sizes of 0.03m, 0.25m and 0.5m to represent small scale roughness, medium scale roughness and large scale roughness. The small scale value of 0.03m was chosen to balance the impact of the gravel sized sediments in the lower bank with the much finer sediments at the top of bank as well as to match that of the Kean and Smith (2006a) and Kean and Smith (2006b) papers, while the medium and large scale values were chosen to be large enough to represent visible differences in the bank surface, but small enough to not be affected by the larger curvature of the bank. These values were also chosen to align with observed roughness element heights from the work of Leyland et al. (2015) and Nardi and Rinaldi (2010) who modelled roughness elements between 0.08m and 0.4m. The actual values chosen were largely arbitrary, however the approach followed that of Kean and Smith (2006a) and Kean and Smith (2006b) who deemed the effect of long-wavelength oscillations, or large scale bank curvature, that was greater than 5 - 10 roughness elements in length to have a negligible contribution to localised flow resistance and were more indicative of large scale flow separation generation, which was not of interest in this study. The calculated roughness values for each point were then averaged within each 1cm^3 voxel, alongside the results of the M3C2 change detection for further analysis.

5.3.1 Statistical analysis and the problem of spatial autocorrelation

Spatial autocorrelation is the concept that observations close together will be more similar than observations taken further apart (Chappell, 2010). As most statistical analysis is predicated on observations being independent from one another, when working with spatial data we must consider

the impact of spatial autocorrelation and use methods that will factor in the impact of near observations being more similar.

To check for spatial autocorrelation within the full point cloud the data were analysed using the variogram approach. The variogram calculates the difference between observation values at two points and the distance between the points. The data is then divided into a series of 'bins' representing the 'lag' size, or the distance between the pairs of points in that bin. The semivariance value is then calculated as half of the variance in the observation value, for each lag bin (Olea, 2006).

These data are then plotted and a best fit line is created using one of many possible best fit lines including gaussian, spherical or exponent models. The model then generates three numerical values - the nugget, sill and range. The nugget is the value at which the model crosses the y-axis. Theoretically, if the distance between points is zero then the difference between their values should also be zero. However, at very small distances between points, or distances below the measuring interval, the difference in values may be greater than 0. The range represents the distance at which the line begins to flatten out, or the point at which there is no longer a relationship between the values of different points. After the range is reached, any further increase in distance between points does not generate a corresponding increase in the difference between the values of the points. The sill is the y-axis semivariance value where the range has been reached.

To compute the variograms the TLS surveys for each bank were loaded into R and the voxelisation technique described earlier was applied to the data. The data was then filtered to include only the values below the Q10 level, thus representing only the fluvial erosion contribution that has been used

throughout the previous chapters. The variogram for the filtered data was then computed utilising the gstat function in R, using 15 bins, with lags dependent on the values in the dataset being analysed. A variogram model was then applied to the data and the range, the distance above which data is no longer spatially autocorrelated, was calculated. The variograms generated can be seen in appendix E

The variograms generated surprisingly large values for the range, with some as large as 2.8m. Following the creation of the variograms, the range data was used to create a subset of the TLS data where no points were closer than the range in proximity.

This decimation process significantly reduced the amount of data and created a data set so sparse that the benefit of the extremely high resolution TLS data was lost (table 5.1). Although the variogram is considered to be the most robust method for analysing spatial autocorrelation, the amount of data loss was deeply undesirable and so an alternative approach needed to be considered. Where the variogram approach identifies spatial autocorrelation in the dependant variable, it is important to note that it is the autocorrelation of regression residuals that is actually a more significant issue in regression analysis (Beale et al., 2010). If the spatial patterns exhibited by the dependant, y, value are also present in the independent, x, values, then the assumptions of regression have not been violated. As such it was decide to conduct initial OLS regression on the full point data and then test the regression residuals for autocorrelation using the Moran's I test (as suggested by Zhang et al. (2005) and Beale et al. (2010)).

In order to do this weightings are calculated for each point compared to every other point within a set distance. The range distance from the semi-

Table 5.1: Summary of the variogram data for each bank and each time period

Bank	Time Period	Variogram Model	Nuggett	Sill	Range	Total Points	Reduced Points	Data Loss (%)
Bank 1	E1	Spherical	0.004	0.015	1.803	3125	13	99.58
	E2	Spherical	0.001	0.002	1.967	1250	9	99.28
	E3	Exponent	0.001	0.005	0.417	315	138	56.19
	E4	Spherical	0.000	0.007	0.942	951	43	95.48
	E5	Exponent	0.000	0.004	0.597	685	82	88.03
	E6	Exponent	0.000	0.004	0.424	2488	141	94.33
Bank 2	E1	Exponent	0.001	0.003	1.182	2590	26	99.00
	E2	Spherical	0.000	0.005	1.046	3032	28	99.08
	E3	Spherical	0.000	0.001	1.152	34	22	35.29
	E4	Exponent	0.000	0.001	0.796	1082	43	96.03
	E5	Gaussian	0.000	0.005	0.254	3461	254	92.66
	E6	Exponent	0.000	0.023	1.325	46	16	65.22
Bank 3 Upstream	E1	Gaussian	0.002	0.003	1.337	38571	39	99.90
	E2	Spherical	0.002	0.003	1.092	40817	49	99.88
	E3	Exponent	0.001	0.018	1.046	5605	49	99.13
	E4	Gaussian	0.001	0.326	1.397	24257	33	99.86
	E5	Exponent	0.003	0.003	0.639	14187	127	99.10
	E6	Spherical	0.001	0.001	1.397	5414	34	99.37
Bank 3 Midstream	E1	Exponent	0.001	0.009	0.461	14610	139	99.90
	E2	Gaussian	0.005	70.824	2.865	5812	11	99.88
	E3	Exponent	0.015	0.024	2.026	7697	11	99.13
	E4	Exponent	0.000	0.020	0.690	34906	76	99.86
	E5	Exponent	0.000	0.013	0.827	1164	49	99.10
	E6	Exponent	0.001	0.005	0.374	8591	246	99.37
Bank 3 Downstream	E1	Spherical	0.001	0.008	1.190	56808	39	99.93
	E2	Spherical	0.001	0.001	1.324	12249	28	99.77
	E3	Exponent	0.005	0.198	0.462	7166	183	97.45
	E4	Exponent	0.000	0.009	0.950	31399	45	99.86
	E5	Spherical	0.000	0.016	1.900	5720	12	99.79
	E6	Spherical	0.001	0.021	2.899	4639	9	99.81

variogram analysis was chosen as the maximum distance, as we had already identified that no autocorrelation is present beyond that distance.

The weightings were then used to calculate the Moran's I statistic, using the moran.test function from the spdep package in R. This function returns the Moran's I Statistic - where +1 represents perfect clustering of similar values, -1 represents perfect dispersion of similar values and zero represents perfect randomness - and the p-value. The null hypothesis of the Moran's I test is that there is no spatial autocorrelation between the data points. It was clear from the results of the Moran's I tests, which had a maximum value of 0.705, that spatial autocorrelation remained in some of the data sets and so a standard OLS model of only the variables of interest would not be a suitable technique for the analysis of this data.

To try and reduce the spatial autocorrelation of the model residuals, a series of lagged variables were created to represent the average local erosion value surrounding each point and the average roughness value surrounding each point. By including these lagged variables in an OLS regression the effect of neighbouring values on both the dependent and independent variables could be accounted for. This approach was chosen to account for the fact that erosion tends to occur in patches rather than at random points across the bank, and also to account for the non-linear nature of near bank flow, which can be deflected in any direction by local protrusions.

The inclusion of these lagged variables mimics the Spatial Lag model approach (Saputro et al., 2019) and the Spatial Lag of X approach (Halleck Vega and Elhorst, 2015), which use a lag of the dependent variable and independent variable respectively. The use of lagged dependent and independent variables is also a characteristic of the Spatial Durbin Model

approach (Mur and Angulo, 2006), which also allows for the calculation of direct and indirect effects of the lagged variables. The decision to use simple spatially lagged versions of the dependent and independent variables was made in an effort to generate the simplest model to explain the observed erosion, however the consequences of this decision and suggestions for alternative future analysis techniques will be addressed in the discussion.

5.3.2 Data analysis methods

In order to establish the relationship between roughness and erosion, OLS modelling was performed between the roughness value of each point and the detected change, with the lagged roughness and erosion values included to control for spatial autocorrelation. As well as establishing the effect of roughness at each chosen roughness scale on erosion, interaction models were also tested to establish whether the interaction between the roughness values at different scales affected the relationship between roughness and erosion. Further interaction models were also undertaken to establish whether there was an interaction between the roughness value at each point and the lagged roughness value.

5.4 Results

5.4.1 Patterns of bank roughness

A summary of the results of the bank roughness analysis can be seen in table 5.2 while figures 5.6-5.20 show the roughness at each of the three roughness scales and at each bank.

The mean measured roughness values - i.e. the value of roughness at a given point when compared to a plane derived from neighbouring points -

at the 0.5m scale were between 0.031m and 0.048m, at the 0.25m scale were 0.015m - 0.023m and at the 0.03m scale were 0.003m - 0.006m. All three banks exhibited very similar mean and maximum roughness results at all time periods and within each scale.

The highest roughness values at the 0.5m scale were often found at the top of banks associated with the bank top vegetation. At bank 1 the highest roughness values tended to be concentrated at the upstream end of the bank (right side of images) where slumping of the top of bank surface resulted in a complex bank geometry that was also affected by vegetation growth. Bank 2 exhibited similar patterns of highest roughness at bank top, however these were less pronounced than at bank 1. There were also some areas of the bank that exhibited higher roughness downstream of sections where vegetation had been removed from the scans.

The pattern of higher roughness values at the top of bank was even more apparent in the upstream reach of bank three where no lower bank vegetation obscured any part of the bank during the study period. The areas of blue and green, representing higher roughness values, are all concentrated along the top of bank, and frequently align with areas that have experienced mass wasting events during the length of the study. This pattern of highest roughness around the top of bank area is even more obvious at the 0.25m scale, however the impact of areas of vegetation seems to be lower at this scale, with less obvious areas of high roughness downstream of vegetation. The 0.03m scale saw a much less noticeable pattern of erosion over the whole bank face, but still exhibited areas of higher roughness around the top of bank.

Time periods E4 and E5 of the upstream reach of bank 3 at the small scale exhibited some areas of an apparent sudden change in roughness

values along vertical and horizontal lines (figure 5.14). These unusual roughness patterns will be discussed in more detail in later sections.

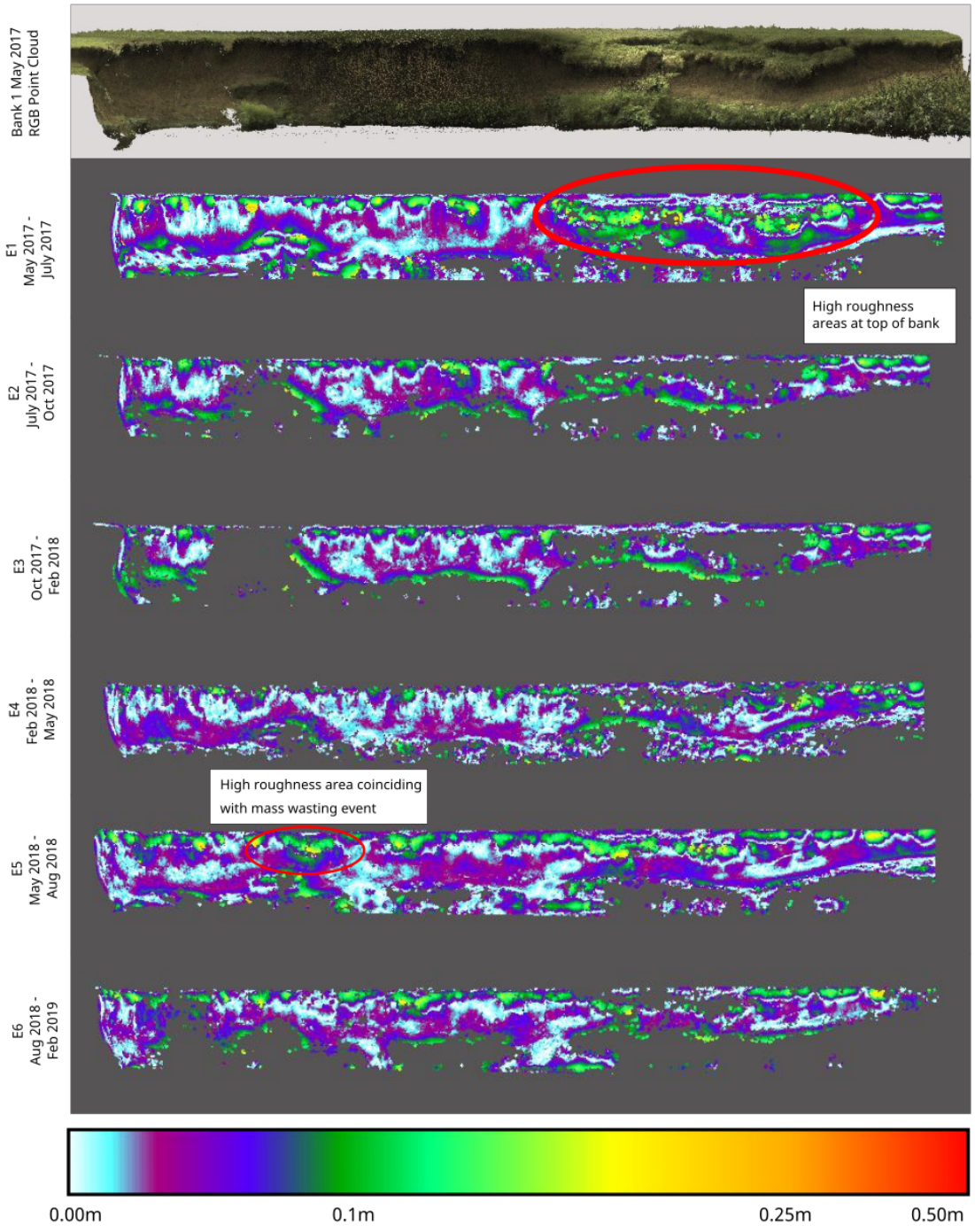

Figure 5.6: Bank 1 roughness at the large 0.5m scale

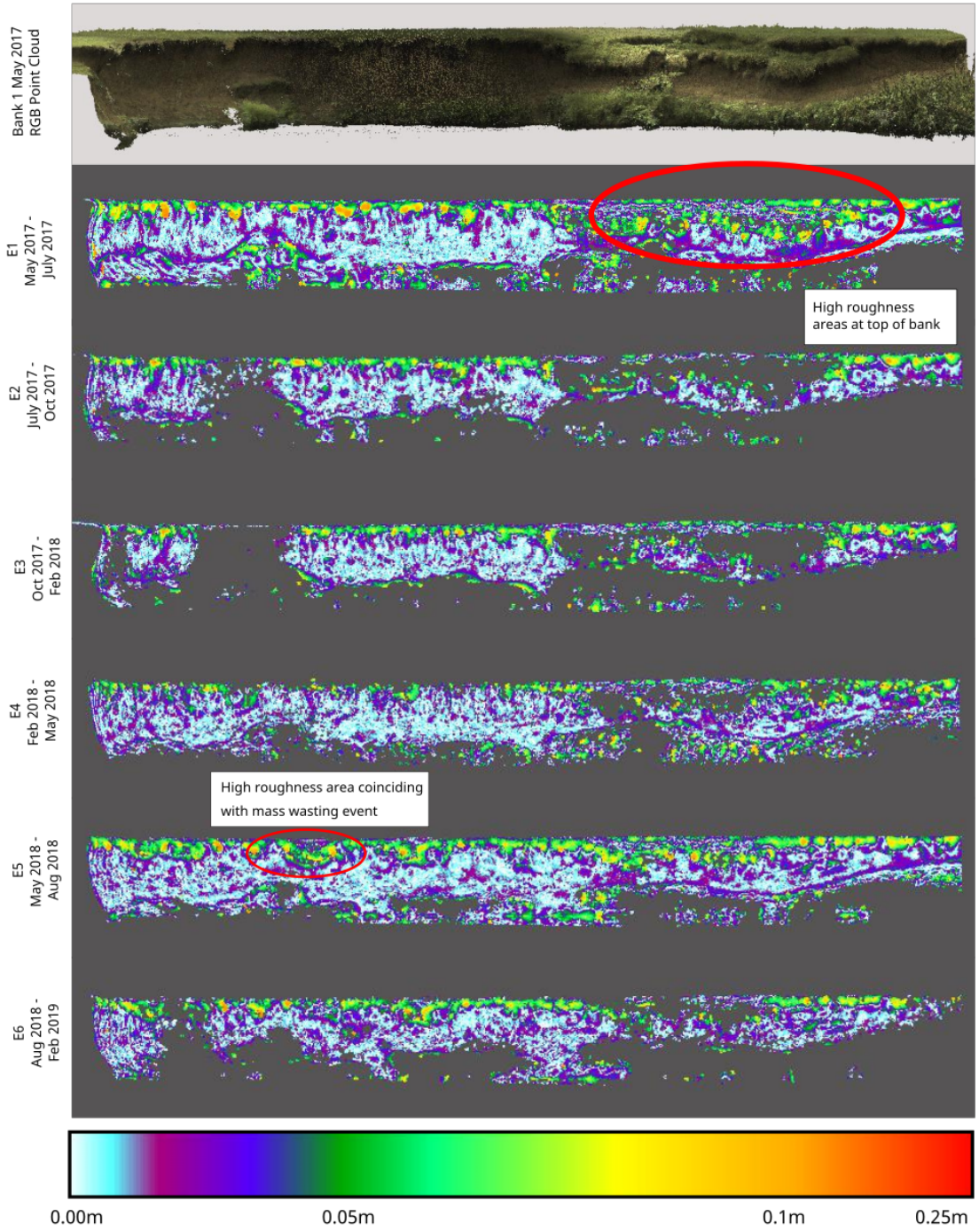

Figure 5.7: Bank 1 roughness at the medium 0.25m scale

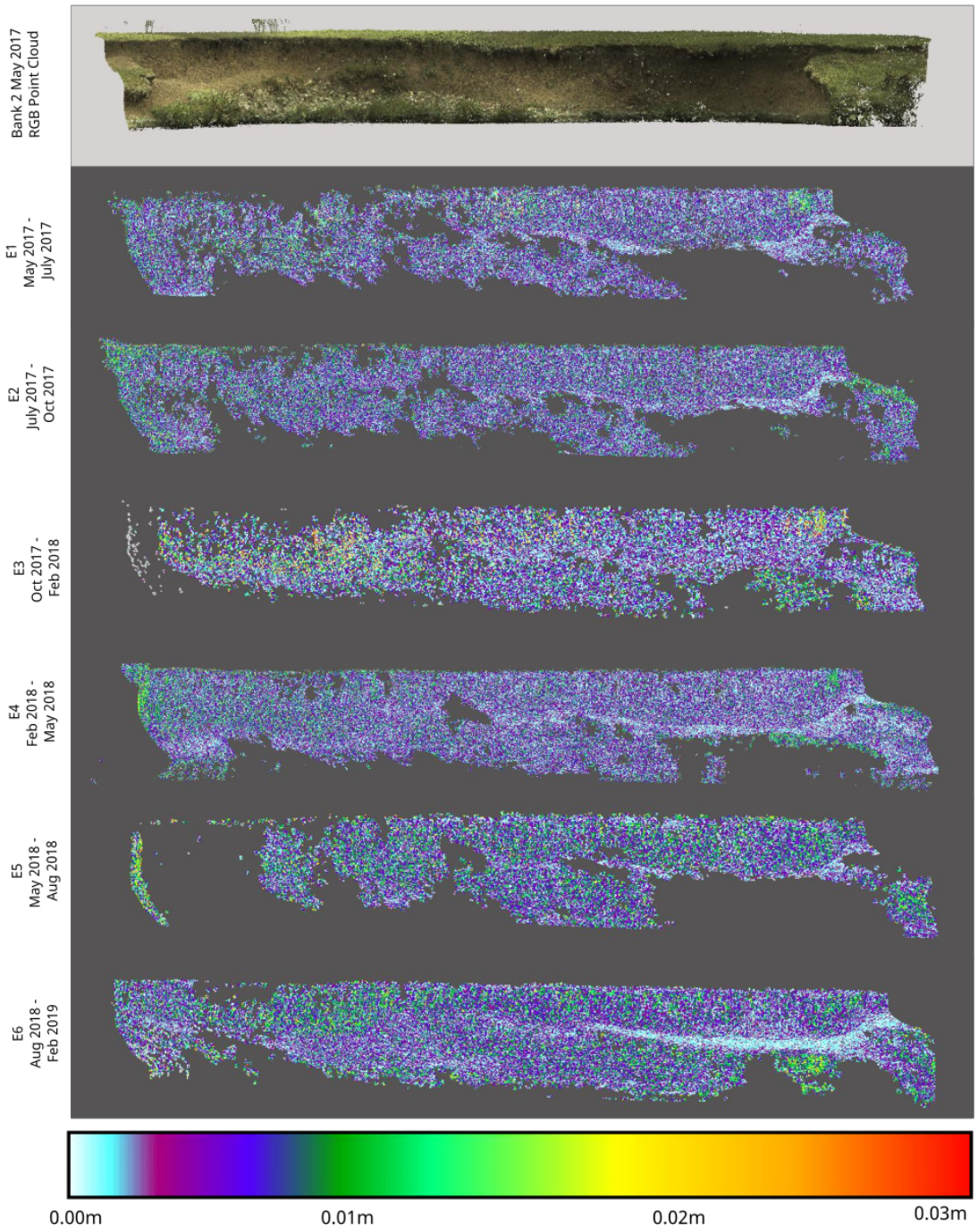

Figure 5.8: Bank 1 roughness at the small 0.03m scale

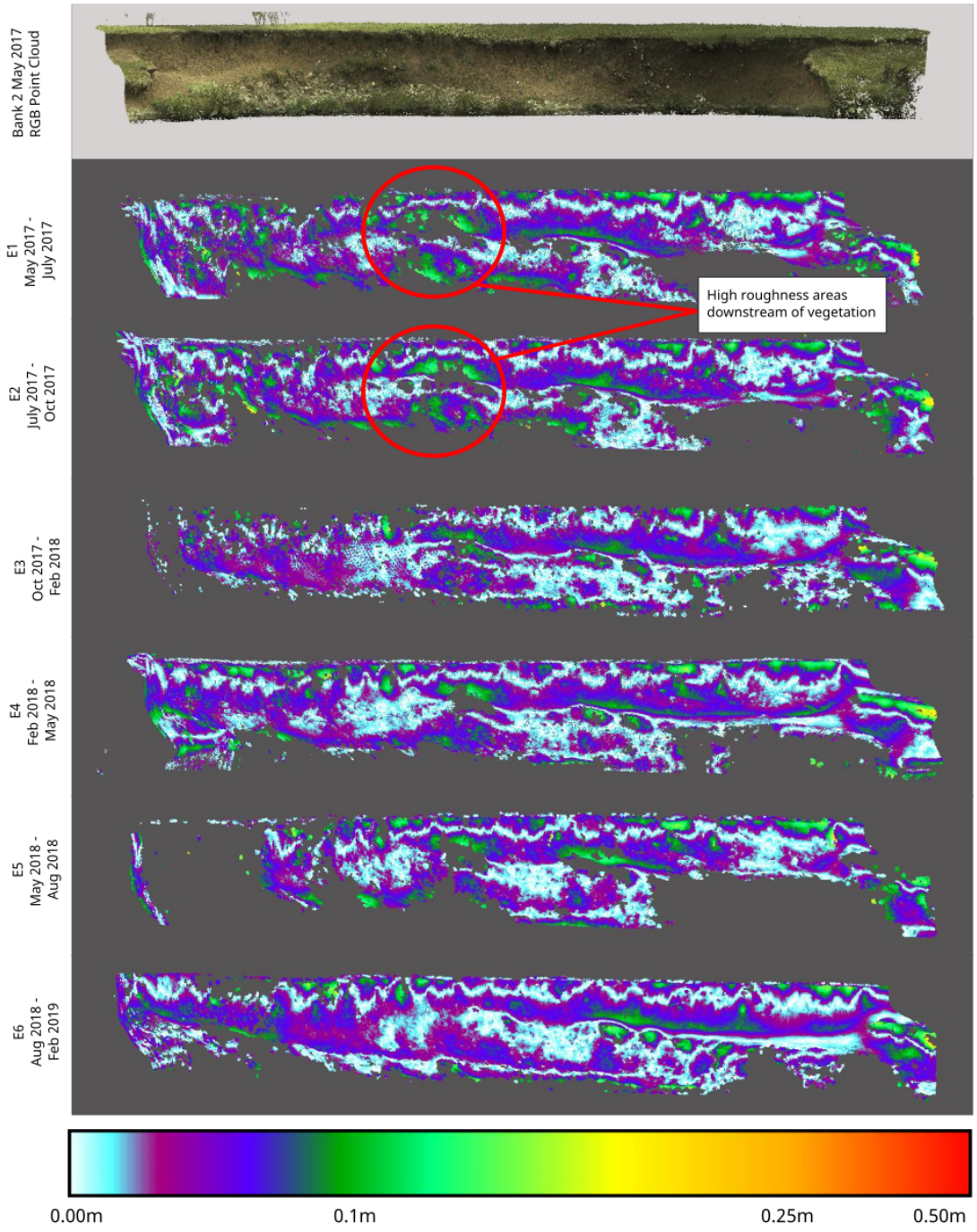

Figure 5.9: Bank 2 roughness at the large 0.5m scale

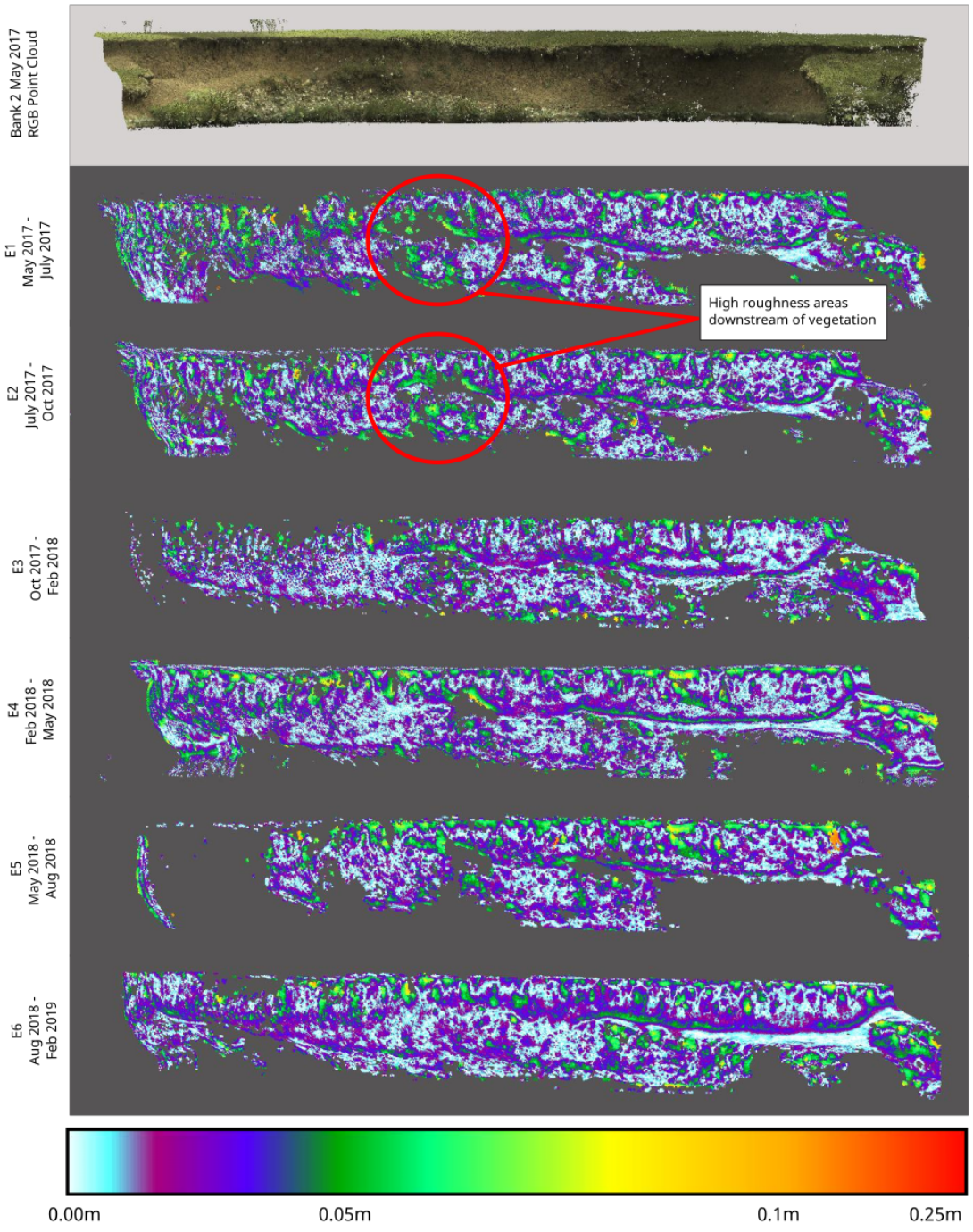

Figure 5.10: Bank 2 roughness at the medium 0.25m scale

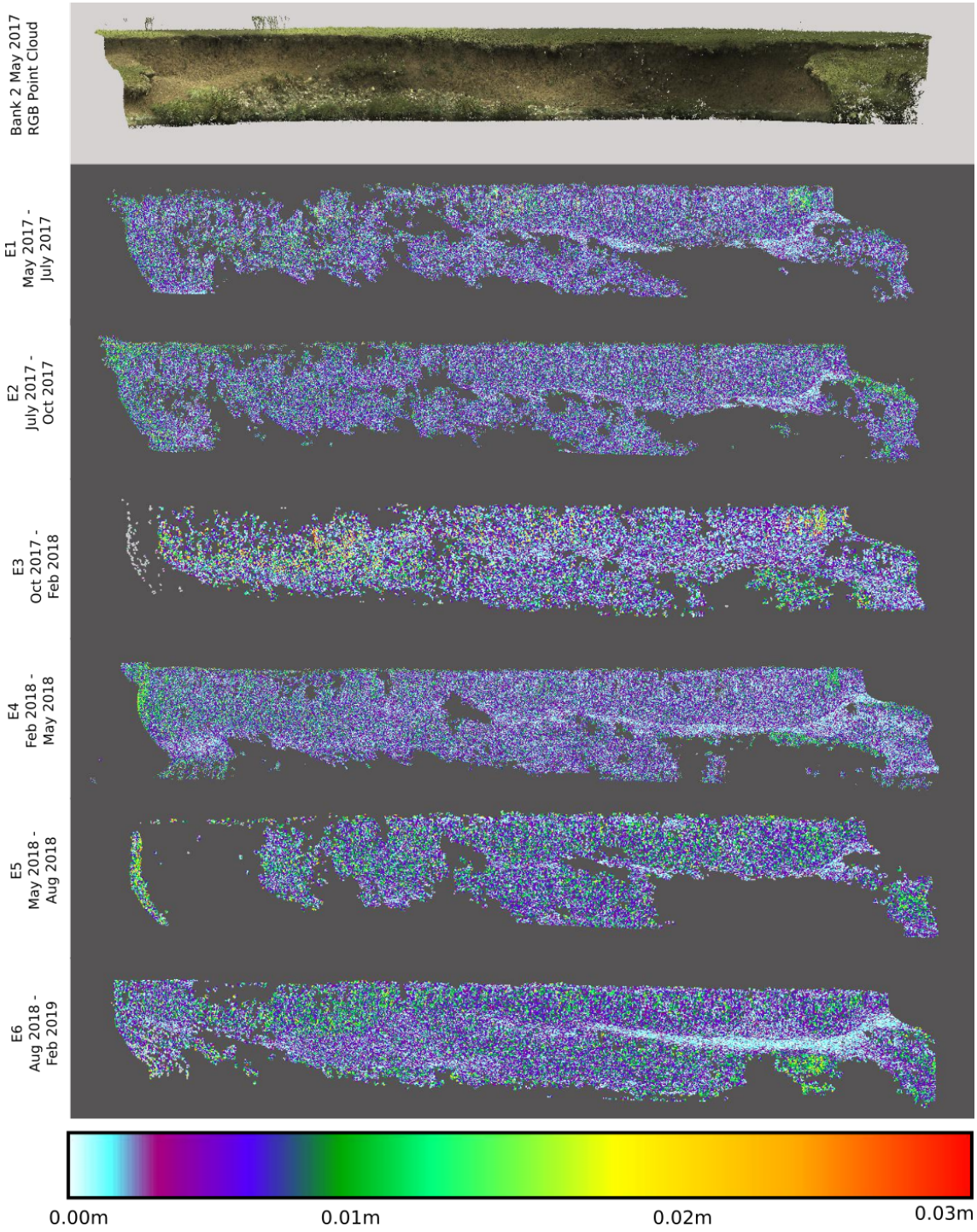

Figure 5.11: Bank 2 roughness at the small 0.03m scale

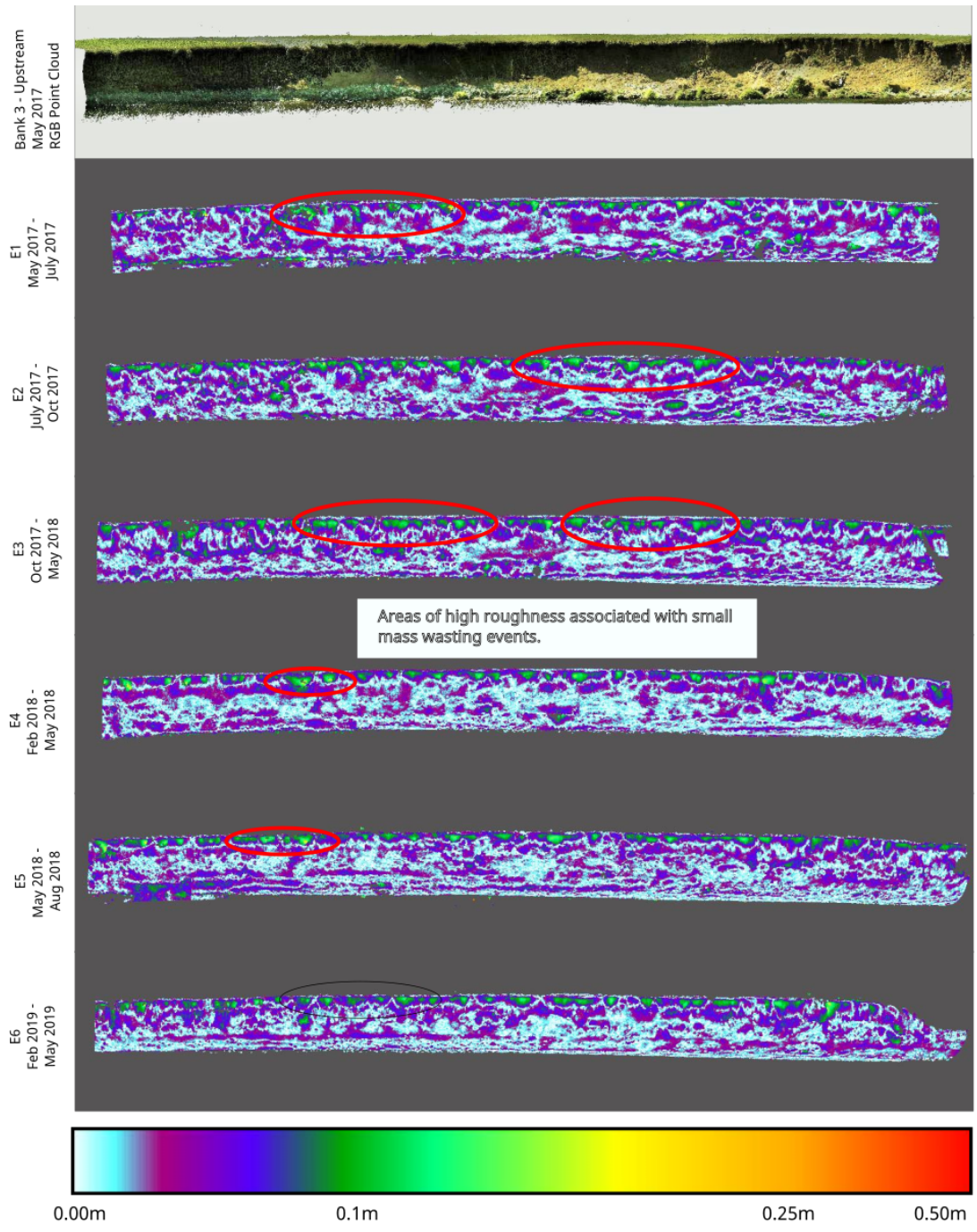

Figure 5.12: Bank 3 - Upstream roughness at the large 0.5m scale

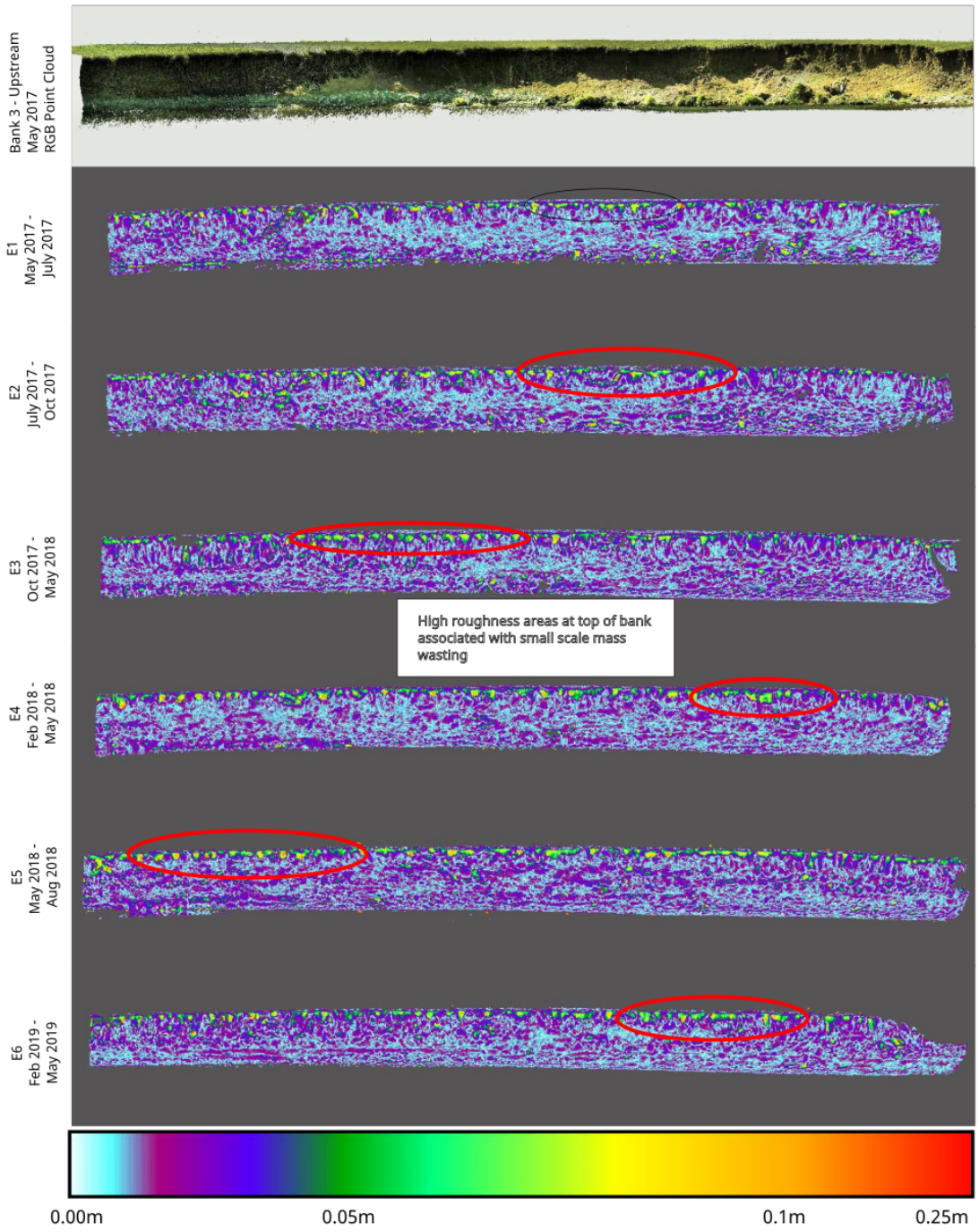

Figure 5.13: Bank 3 - Upstream roughness at the medium 0.25m scale

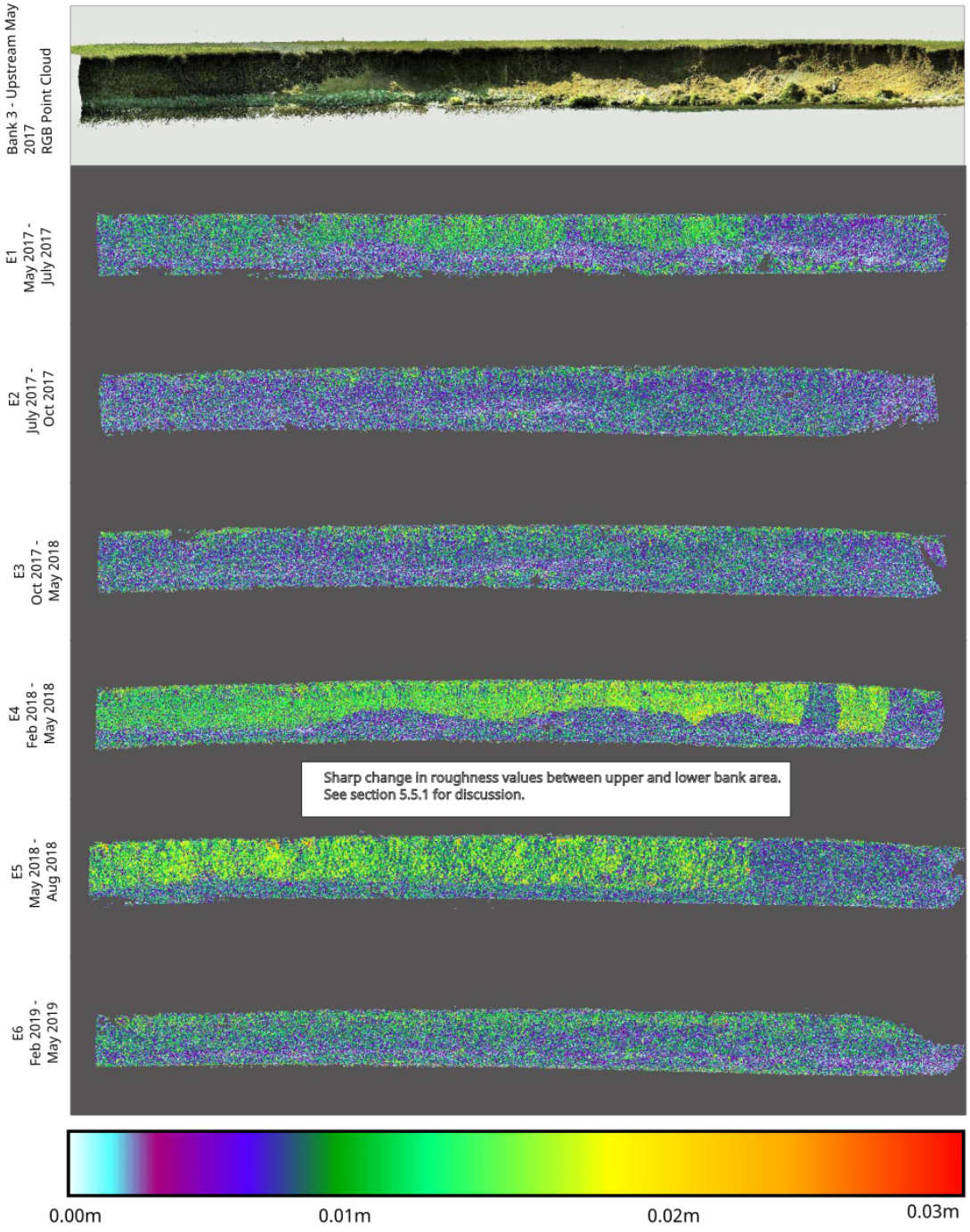

Figure 5.14: Bank 3 - Upstream roughness at the small 0.03m scale

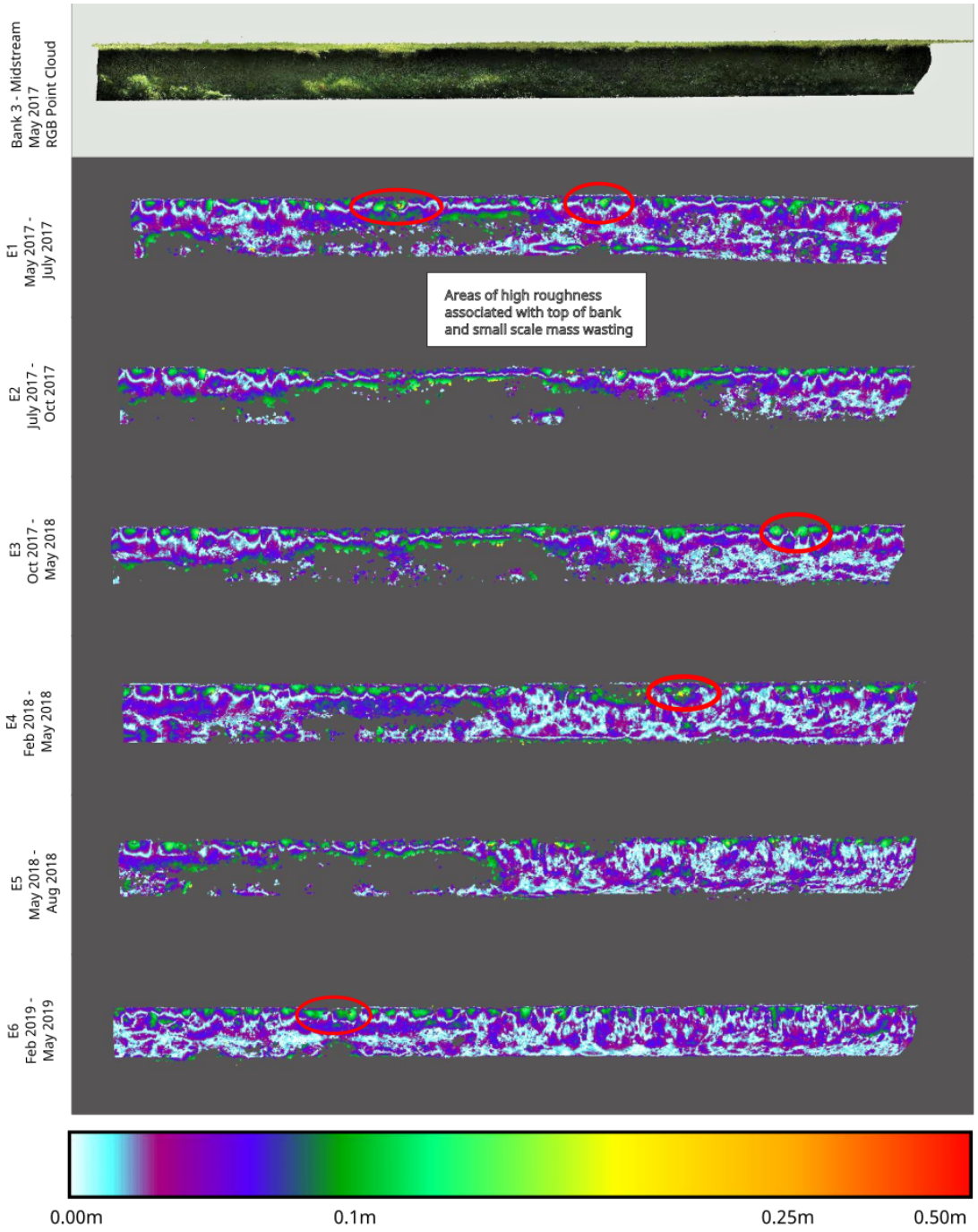

Figure 5.15: Bank 3 - Midstream roughness at the large 0.5m scale

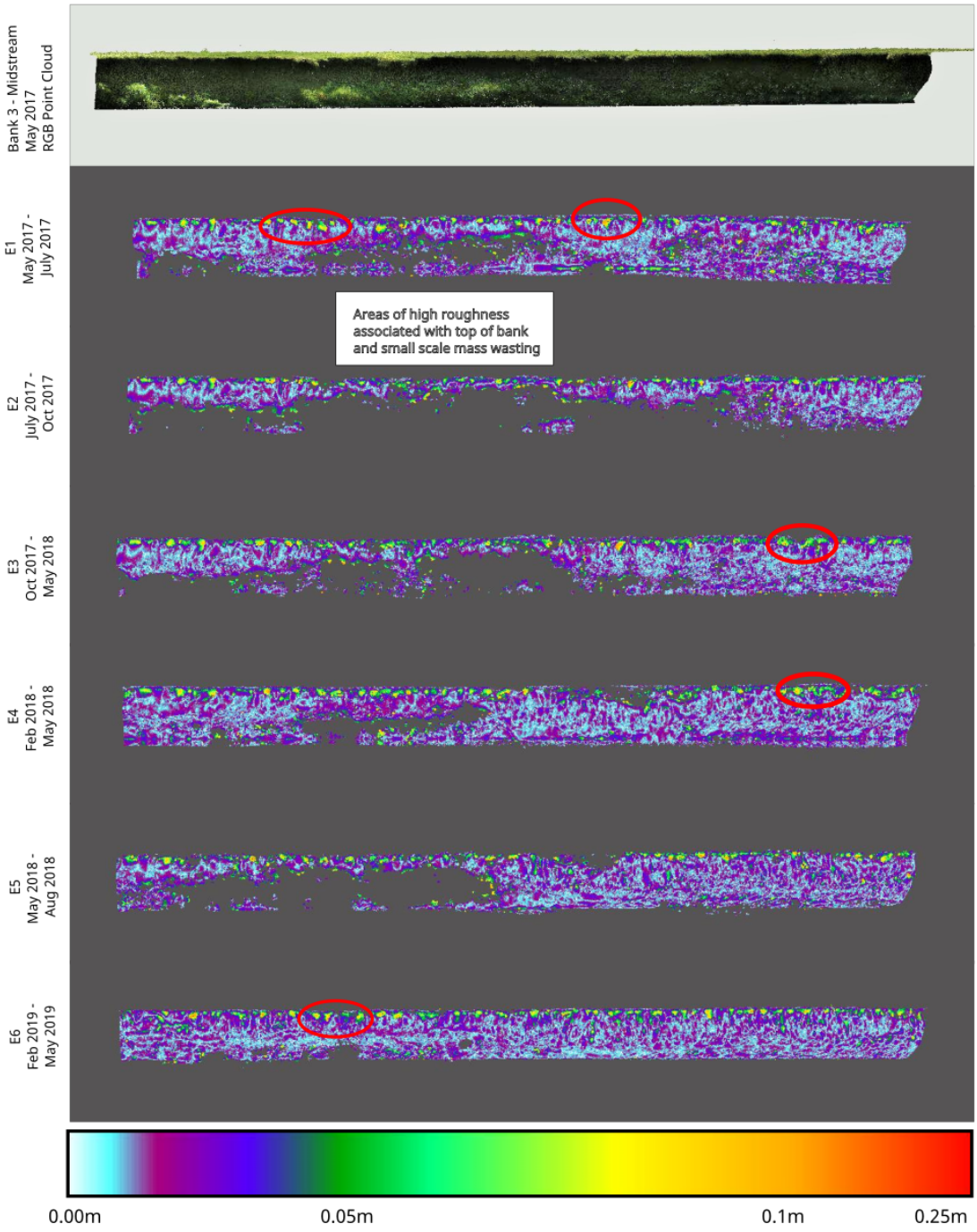

Figure 5.16: Bank 3 - Midstream roughness at the medium 0.25m scale

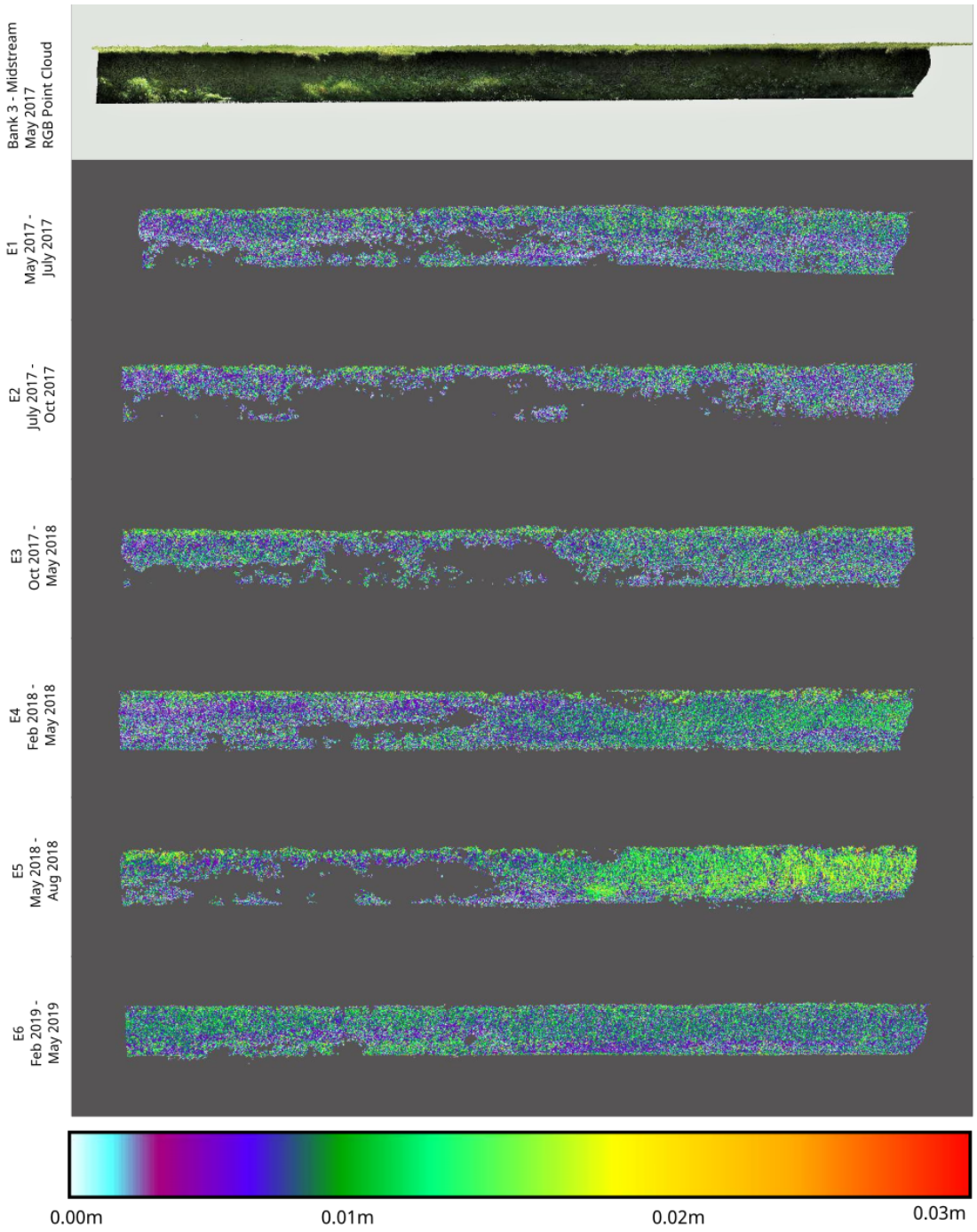

Figure 5.17: Bank 3 - Midstream roughness at the small 0.03m scale

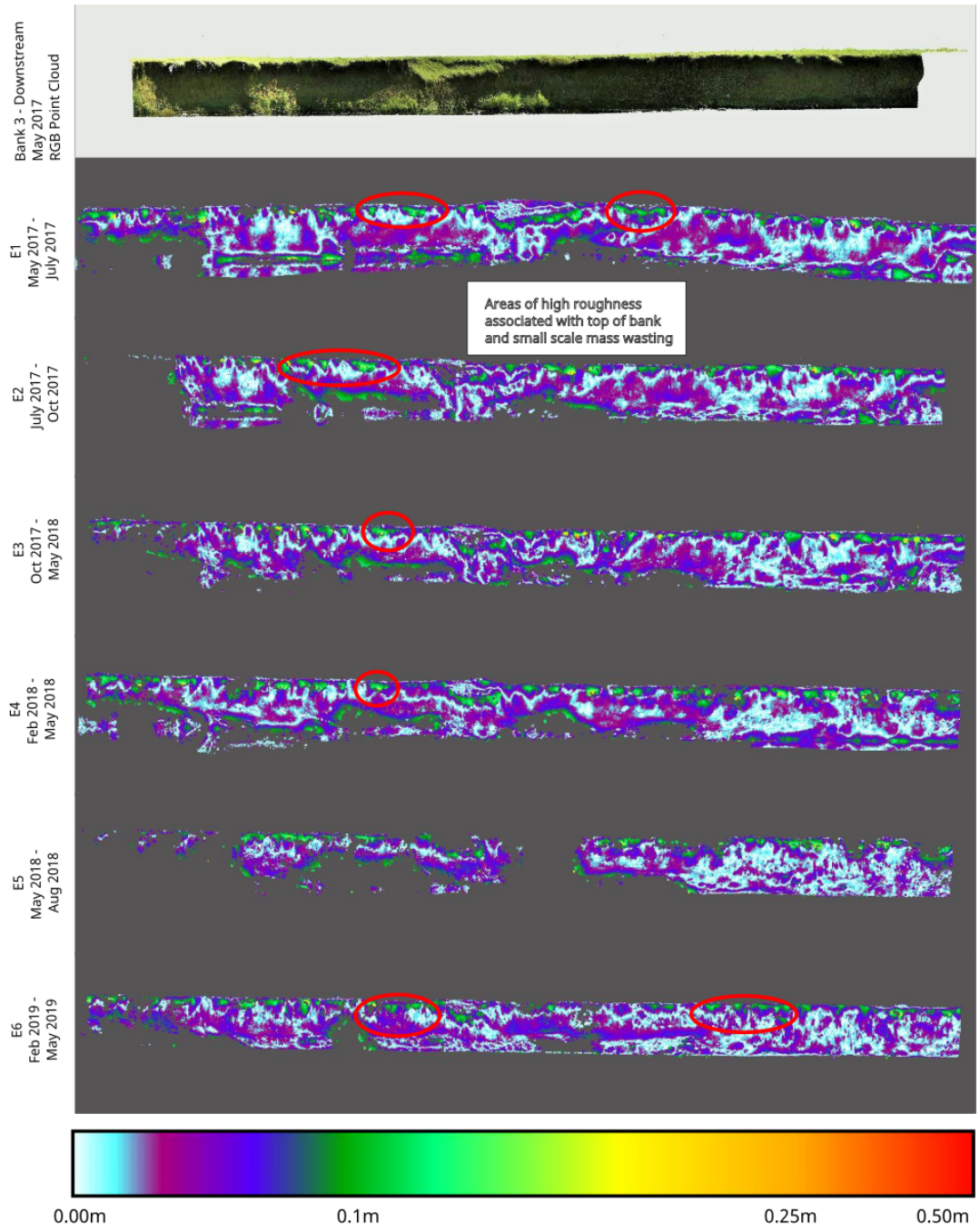

Figure 5.18: Bank 3 - Downstream roughness at the large 0.5m scale

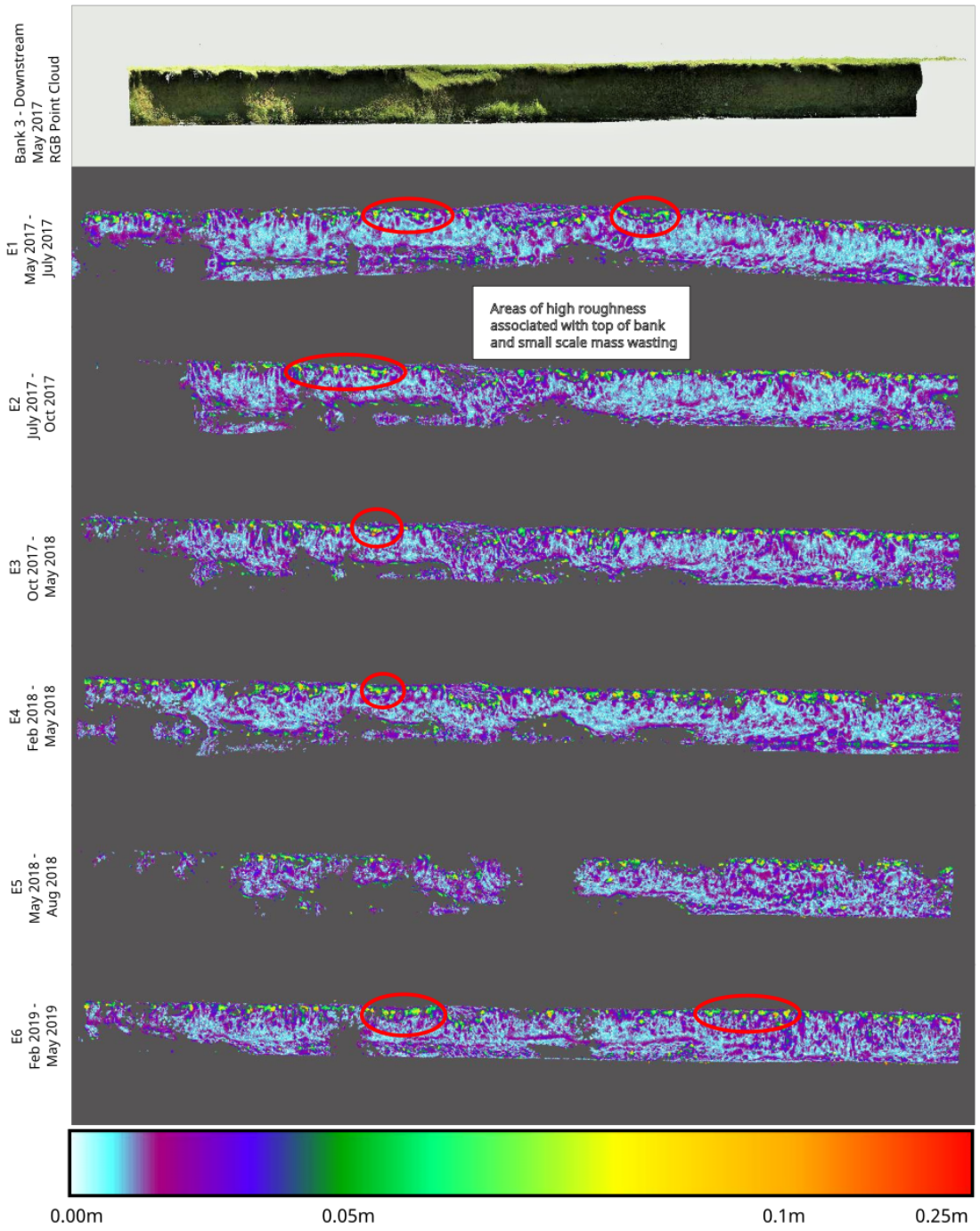

Figure 5.19: Bank 3 - Downstream roughness at the medium 0.25m scale

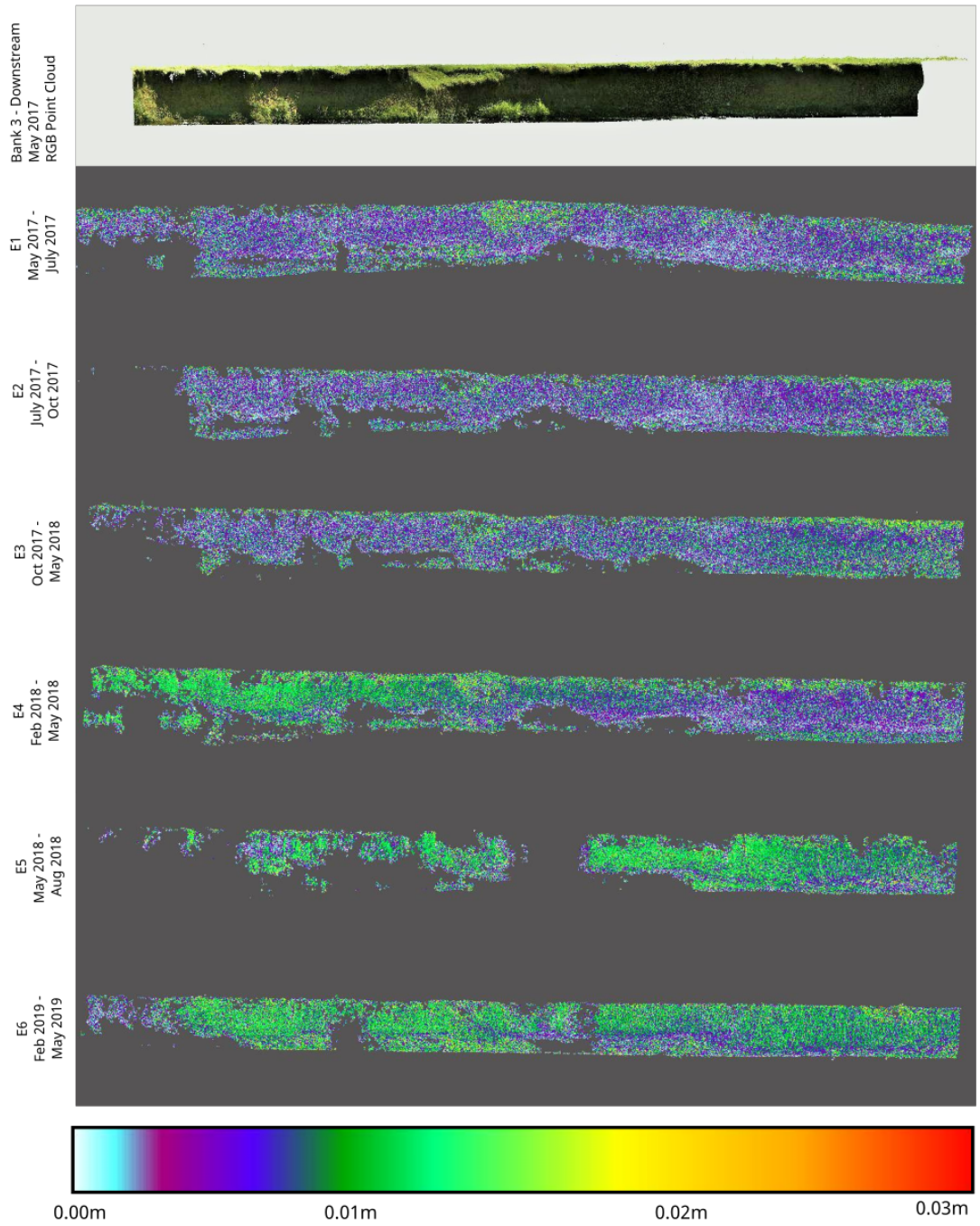

Figure 5.20: Bank 3 - Downstream roughness at the small 0.03m scale

Table 5.2: Mean and maximum roughness values per bank per time period

	Time Period	Mean roughness at the 0.5m scale (m)	Max roughness at the 0.5m scale (m)	Mean roughness at the 0.25m scale (m)	Max roughness at the 0.25m scale (m)	Mean roughness at the 0.03m scale (m)	Max roughness at the 0.03m scale (m)
Bank 1	E1	0.045	0.311	0.020	0.194	0.004	0.026
	E2	0.047	0.186	0.020	0.132	0.005	0.028
	E3	0.047	0.293	0.019	0.183	0.004	0.026
	E4	0.041	0.194	0.019	0.106	0.006	0.024
	E5	0.043	0.199	0.018	0.178	0.003	0.027
	E6	0.043	0.255	0.018	0.122	0.003	0.026
Bank 2	E1	0.041	0.205	0.018	0.163	0.004	0.028
	E2	0.040	0.203	0.018	0.122	0.004	0.026
	E3	0.036	0.201	0.015	0.109	0.003	0.026
	E4	0.039	0.196	0.017	0.110	0.004	0.026
	E5	0.039	0.185	0.017	0.138	0.003	0.026
	E6	0.038	0.205	0.016	0.107	0.003	0.027
Bank 3 - Upstream	E1	0.034	0.234	0.017	0.149	0.004	0.027
	E2	0.034	0.260	0.018	0.169	0.004	0.028
	E3	0.034	0.242	0.017	0.185	0.004	0.027
	E4	0.031	0.196	0.016	0.133	0.004	0.026
	E5	0.036	0.213	0.020	0.208	0.006	0.028
	E6	0.034	0.189	0.018	0.162	0.004	0.026
Bank 3 - Midstream	E1	0.042	0.204	0.020	0.109	0.004	0.027
	E2	0.048	0.231	0.022	0.122	0.004	0.026
	E3	0.044	0.239	0.020	0.146	0.004	0.027
	E4	0.039	0.254	0.018	0.162	0.004	0.027
	E5	0.045	0.213	0.023	0.134	0.005	0.026
	E6	0.037	0.206	0.019	0.147	0.005	0.028
Bank 3 - Downstream	E1	0.037	0.242	0.016	0.131	0.003	0.027
	E2	0.038	0.224	0.017	0.169	0.003	0.028
	E3	0.040	0.276	0.018	0.141	0.004	0.026
	E4	0.040	0.273	0.017	0.142	0.005	0.028
	E5	0.043	0.224	0.020	0.110	0.005	0.027
	E6	0.038	0.198	0.018	0.166	0.005	0.026

5.4.2 Influence of roughness on erosion values

Following the roughness evaluation of the whole bank, the results of OLS regression between roughness and erosion were calculated for all points that sit below the Q10 bank height, deemed to represent the fluvial erosion component, for each of the time periods (E1 - E6), for each bank, and for each of the three roughness scales (detailed in tables 5.3 to 5.5 and summarised in table 5.6). Within each of these models, the lagged roughness and lagged erosion were included to control for spatial autocorrelation. The plots for each individual model can be seen in appendix F figures F.1 to F.15.

At the 0.5m roughness scale (table 5.3) the R^2 values ranged from 0.061 to 0.886, indicating that between 6.1% and 88.6% of erosion can be accounted for by roughness at the 0.5m scale when the local erosion and local roughness have been accounted for. The mean R^2 value was 0.468, indicating that, on average, roughness at the 0.5m scale explained 46.8% of the erosion. The model intercepts were almost all very close to zero, indicating that the models predict that a perfectly linear surface would exhibit very limited/no erosion. All of the models were statistically significant, with p-values below 0.05.

Out of 30 OLS models, the roughness coefficient was positive in 24 models, indicating that an increase in roughness results in an increase in the erosion while a decrease in roughness results in a decrease in erosion. The coefficient values varied from the largest negative value of -0.307, indicating that a 1 unit reduction in the roughness would result in a 0.307 unit increase in the erosion value, to the smallest negative value of -0.001. Positive coefficients ranged from the smallest value of 0.018 to the largest of 1.737. The average coefficient for the 0.5m roughness scale was 0.374,

Table 5.3: Results of OLS regression between erosion and roughness at the 0.5m scale. Statistically significant p-values are in **bold**

Bank	Epoch	Model Intercept	Intercept p-value	0.5m Roughness Coefficient	Roughness p-value	Lag erosion Coefficient	Lag erosion p-value	Lag Roughness Coefficient	Lag Roughness p-value	R^2 Value	Model p-value
1	E1	-0.028	<**0.001**	-0.028	0.357	0.591	**0.002**	1.054	<**0.001**	0.061	<**0.001**
1	E2	0.089	<**0.001**	0.154	<**0.001**	0.295	0.095	-2.034	<**0.001**	0.086	<**0.001**
1	E3	-0.004	0.303	-0.219	**0.011**	1.049	<**0.001**	0.267	**0.019**	0.820	<**0.001**
1	E4	-0.002	0.763	0.688	<**0.001**	0.971	<**0.001**	-0.594	**0.006**	0.445	<**0.001**
1	E5	-0.005	0.568	1.737	<**0.001**	1.164	<**0.001**	-1.821	<**0.001**	0.537	<**0.001**
1	E6	0.006	0.109	0.964	<**0.001**	0.978	<**0.001**	-1.127	<**0.001**	0.431	<**0.001**
2	E1	-0.001	0.375	0.146	<**0.001**	1.011	<**0.001**	-0.140	**0.031**	0.477	<**0.001**
2	E2	-0.019	<**0.001**	0.318	<**0.001**	1.264	<**0.001**	0.195	0.083	0.544	<**0.001**
2	E3	-0.029	<**0.001**	0.848	<**0.001**	-5.693	<**0.001**	3.783	<**0.001**	0.886	<**0.001**
2	E4	-0.001	0.851	-0.307	<**0.001**	1.013	<**0.001**	0.313	<**0.001**	0.481	<**0.001**
2	E5	-0.001	0.769	0.125	<**0.001**	1.003	<**0.001**	-0.132	<**0.001**	0.783	<**0.001**
2	E6	0.067	**0.026**	1.389	<**0.001**	1.794	0.467	-2.983	**0.031**	0.260	<**0.001**
3 - Up	E1	-0.016	<**0.001**	0.345	<**0.001**	1.138	<**0.001**	-0.157	0.078	0.505	<**0.001**
3 - Up	E2	-0.004	<**0.001**	0.018	**0.021**	1.027	<**0.001**	0.082	**0.013**	0.177	<**0.001**
3 - Up	E3	0.010	<**0.001**	0.229	<**0.001**	1.044	<**0.001**	-0.696	<**0.001**	0.610	<**0.001**
3 - Up	E4	<-0.001	0.905	0.235	<**0.001**	1.027	<**0.001**	-0.317	<**0.001**	0.328	<**0.001**
3 - Up	E5	-0.005	<**0.001**	-0.162	<**0.001**	1.120	<**0.001**	0.174	<**0.001**	0.445	<**0.001**
3 - Up	E6	-0.004	**0.032**	0.283	<**0.001**	1.397	<**0.001**	-0.728	<**0.001**	0.384	<**0.001**
3 - Mid	E1	0.001	0.094	0.391	<**0.001**	1.025	<**0.001**	-0.442	<**0.001**	0.668	<**0.001**
3 - Mid	E2	-0.016	<**0.001**	-0.001	0.967	1.174	<**0.001**	0.188	<**0.001**	0.202	<**0.001**
3 - Mid	E3	-0.029	<**0.001**	0.796	<**0.001**	1.167	<**0.001**	-0.876	<**0.001**	0.535	<**0.001**
3 - Mid	E4	-0.005	<**0.001**	1.154	<**0.001**	1.092	<**0.001**	-1.437	<**0.001**	0.700	<**0.001**
3 - Mid	E5	0.001	0.538	0.238	<**0.001**	1.044	<**0.001**	-0.284	<**0.001**	0.514	<**0.001**
3 - Mid	E6	-0.013	<**0.001**	-0.133	<**0.001**	1.296	<**0.001**	0.266	<**0.001**	0.339	<**0.001**
3 - Down	E1	-0.019	<**0.001**	0.237	<**0.001**	1.270	<**0.001**	-0.238	<**0.001**	0.216	<**0.001**
3 - Down	E2	-0.004	**0.002**	0.270	<**0.001**	1.053	<**0.001**	-0.232	<**0.001**	0.381	<**0.001**
3 - Down	E3	<0.001	0.722	0.572	<**0.001**	1.137	<**0.001**	-0.939	<**0.001**	0.834	<**0.001**
3 - Down	E4	-0.018	<**0.001**	0.217	<**0.001**	1.068	<**0.001**	0.027	0.352	0.629	<**0.001**
3 - Down	E5	-0.087	<**0.001**	0.021	0.527	1.314	<**0.001**	1.600	<**0.001**	0.635	<**0.001**
3 - Down	E6	-0.638	<**0.001**	0.683	**0.024**	1.099	<**0.001**	17.755	<**0.001**	0.119	<**0.001**

indicating that an increase in roughness of 1cm would result in an increase in erosion of 0.374cm.

The coefficients of the lagged roughness value, representing roughness in the surrounding points calculated using the range value from earlier semivariogram calculation, saw more variation in their spread, with 12 positive and 18 negative coefficients ranging from -2.983 to 17.755, with a mean coefficient of 0.351 and a median coefficient of -0.194. The slight prevalence of negative coefficients indicates that the higher the local roughness the lower the erosion at the measured point.

The models were all statistically significant, with p-values below the 0.05 significance level, and only 3 models exhibited insignificant p-values for the influence of the roughness variable.

At the 0.25m roughness scale (table 5.4) the R^2 values ranged from 0.048 to 0.846, indicating that between 4.8% and 84.6% of the erosion could be attributed to roughness at the 0.25m scale when local erosion and 0.25m roughness have been controlled for. The average R^2 value was 0.454, which is very similar to the average of the 0.5m roughness scale. There were also only six negative coefficients at the 0.25m scale, following the pattern seen at the 0.5m scale.

The coefficients ranged from -0.759 to 3.366, with a mean coefficient value of 0.541, higher than that of roughness at the 0.5m scale. This suggests that smaller scale variations in roughness exhibit a larger effect on the rate of erosion than larger scale roughness. This could be influenced by the effect of the larger 3.336 coefficient in the 0.25m scale data, so the median coefficients were also compared and this again demonstrated that the coefficient for the 0.25m scale, 0.392, was larger than that of the 0.5m roughness at 0.238.

Table 5.4: Results of OLS regression between erosion and roughness at the 0.25m scale. Statistically significant p-values are in **bold**

Bank	Epoch	Model Intercept	Intercept p-value	0.25m Roughness Coefficient	Roughness p-value	Lag erosion Coefficient	Lag erosion p-value	Lag Roughness Coefficient	Lag Roughness p-value	R^2 Value	Model p-value
1	E1	-0.076	<**0.001**	0.099	0.111	0.972	<**0.001**	3.302	<**0.001**	0.092	<**0.001**
1	E2	0.005	0.227	0.285	<**0.001**	0.931	<**0.001**	-0.430	<**0.001**	0.048	<**0.001**
1	E3	-0.005	0.535	-0.759	<**0.001**	1.051	<**0.001**	0.904	**0.011**	0.846	<**0.001**
1	E4	0.004	0.611	0.721	<**0.001**	0.965	<**0.001**	-0.854	**0.023**	0.431	<**0.001**
1	E5	-0.047	**0.008**	1.264	<**0.001**	1.204	<**0.001**	-0.063	0.921	0.511	<**0.001**
1	E6	0.002	0.503	0.965	<**0.001**	0.982	<**0.001**	-1.054	<**0.001**	0.413	<**0.001**
2	E1	-0.002	0.460	-0.061	0.143	1.013	<**0.001**	0.082	0.440	0.471	<**0.001**
2	E2	-0.018	<**0.001**	0.805	<**0.001**	1.347	<**0.001**	-0.496	**0.008**	0.576	<**0.001**
2	E3	0.013	**0.047**	1.867	<**0.001**	-1.433	0.053	0.463	0.566	0.681	<**0.001**
2	E4	-0.009	**0.044**	-0.519	<**0.001**	1.131	<**0.001**	0.801	<**0.001**	0.504	<**0.001**
2	E5	-0.001	0.679	0.343	<**0.001**	1.006	<**0.001**	-0.407	<**0.001**	0.785	<**0.001**
2	E6	0.035	0.119	2.302	**0.002**	0.137	0.955	-4.181	0.191	0.162	**0.002**
3 - Up	E1	-0.010	<**0.001**	0.510	<**0.001**	1.147	<**0.001**	-0.552	<**0.001**	0.503	<**0.001**
3 - Up	E2	-0.003	<**0.001**	0.217	<**0.001**	1.072	<**0.001**	-0.256	<**0.001**	0.182	<**0.001**
3 - Up	E3	-0.001	0.591	0.493	<**0.001**	1.026	<**0.001**	-0.519	<**0.001**	0.616	<**0.001**
3 - Up	E4	0.013	<**0.001**	0.507	<**0.001**	1.052	<**0.001**	-1.633	<**0.001**	0.337	<**0.001**
3 - Up	E5	-0.006	<**0.001**	-0.108	<**0.001**	1.116	<**0.001**	0.208	<**0.001**	0.438	<**0.001**
3 - Up	E6	-0.004	0.055	0.263	<**0.001**	1.442	<**0.001**	-1.257	<**0.001**	0.381	<**0.001**
3 - Mid	E1	0.002	<**0.001**	0.068	0.432	<**0.001**	1.026	<**0.001**	-0.565	0.641	<**0.001**
3 - Mid	E2	-0.018	<**0.001**	0.222	<**0.001**	1.173	<**0.001**	0.187	0.126	0.206	<**0.001**
3 - Mid	E3	-0.029	<**0.001**	-0.014	0.842	1.179	<**0.001**	-0.276	0.163	0.519	<**0.001**
3 - Mid	E4	-0.007	<**0.001**	0.726	<**0.001**	1.075	<**0.001**	-0.999	<**0.001**	0.640	<**0.001**
3 - Mid	E5	<0.001	0.886	0.173	**0.003**	1.042	<**0.001**	-0.223	**0.047**	0.502	<**0.001**
3 - Mid	E6	-0.010	<**0.001**	0.038	0.416	1.288	<**0.001**	-0.062	0.618	0.338	<**0.001**
3 - Down	E1	-0.021	<**0.001**	0.616	<**0.001**	1.273	<**0.001**	-0.468	<**0.001**	0.219	<**0.001**
3 - Down	E2	-0.016	<**0.001**	0.524	<**0.001**	1.129	<**0.001**	0.177	**0.038**	0.396	<**0.001**
3 - Down	E3	0.003	**0.010**	0.661	<**0.001**	1.143	<**0.001**	-1.510	<**0.001**	0.817	<**0.001**
3 - Down	E4	-0.022	<**0.001**	0.351	<**0.001**	1.065	<**0.001**	0.539	<**0.001**	0.627	<**0.001**
3 - Down	E5	-0.124	<**0.001**	-0.056	0.271	1.246	<**0.001**	5.282	<**0.001**	0.636	<**0.001**
3 - Down	E6	-0.392	<**0.001**	3.366	<**0.001**	1.635	<**0.001**	12.685	<**0.001**	0.110	<**0.001**

Table 5.5: Results of OLS regression between erosion and roughness at the 0.03m scale. Statistically significant p-values are in **bold**

Bank	Epoch	Model Intercept	Intercept p-value	0.03m Roughness Coefficient	Roughness p-value	Lag erosion Coefficient	Lag erosion p-value	Lag Roughness Coefficient	Lag Roughness p-value	R^2 Value	Model p-value
1	E1	-0.048	<**0.001**	-0.743	**0.025**	1.743	<**0.001**	6.701	<**0.001**	0.060	<**0.001**
1	E2	0.044	**0.016**	0.031	0.904	0.366	0.175	-5.709	**0.021**	0.032	<**0.001**
1	E3	<0.001	0.952	-0.337	0.392	1.037	<**0.001**	-0.057	0.961	0.817	<**0.001**
1	E4	0.018	0.544	-0.782	0.198	0.963	<**0.001**	-2.211	0.679	0.418	<**0.001**
1	E5	-0.050	**0.021**	1.126	0.420	1.208	<**0.001**	9.578	0.090	0.500	<**0.001**
1	E6	0.001	0.891	0.884	0.208	0.983	<**0.001**	-0.872	0.781	0.408	<**0.001**
2	E1	-0.007	0.348	-0.589	<**0.001**	1.017	<**0.001**	2.123	0.280	0.475	<**0.001**
2	E2	-0.108	<**0.001**	-0.678	<**0.001**	1.402	<**0.001**	26.455	<**0.001**	0.532	<**0.001**
2	E3	-0.024	0.285	5.993	<**0.001**	-1.157	0.318	16.088	0.220	0.240	**0.002**
2	E4	0.002	0.477	-0.333	0.073	1.074	<**0.001**	-0.951	0.389	0.430	<**0.001**
2	E5	0.012	**0.003**	-0.161	0.140	1.010	<**0.001**	-4.059	**0.001**	0.781	<**0.001**
2	E6	-0.136	0.180	0.446	0.803	-3.984	**0.024**	57.921	0.059	0.044	0.120
3 - Up	E1	-0.046	<**0.001**	1.076	<**0.001**	1.110	<**0.001**	9.022	<**0.001**	0.498	<**0.001**
3 - Up	E2	0.010	<**0.001**	0.019	0.744	1.069	<**0.001**	-3.599	<**0.001**	0.177	<**0.001**
3 - Up	E3	-0.031	<**0.001**	0.128	0.344	1.067	<**0.001**	6.567	<**0.001**	0.599	<**0.001**
3 - Up	E4	-0.010	**0.006**	-0.142	0.062	1.035	<**0.001**	1.815	**0.019**	0.322	<**0.001**
3 - Up	E5	-0.016	<**0.001**	0.193	<**0.001**	1.203	<**0.001**	1.322	<**0.001**	0.439	<**0.001**
3 - Up	E6	0.015	<**0.001**	0.771	<**0.001**	1.522	<**0.001**	-8.142	<**0.001**	0.393	<**0.001**
3 - Mid	E1	<0.001	0.719	-0.381	<**0.001**	1.020	<**0.001**	0.112	0.713	0.618	<**0.001**
3 - Mid	E2	0.036	<**0.001**	0.377	<**0.001**	1.181	<**0.001**	-12.815	<**0.001**	0.214	<**0.001**
3 - Mid	E3	-0.111	<**0.001**	0.604	**0.022**	1.100	<**0.001**	18.030	<**0.001**	0.521	<**0.001**
3 - Mid	E4	-0.056	<**0.001**	0.143	0.149	1.091	<**0.001**	11.940	<**0.001**	0.632	<**0.001**
3 - Mid	E5	-0.002	0.774	-0.293	0.173	1.036	<**0.001**	0.708	0.730	0.499	<**0.001**
3 - Mid	E6	-0.044	<**0.001**	0.056	0.715	1.312	<**0.001**	6.421	<**0.001**	0.339	<**0.001**
3 - Down	E1	-0.033	<**0.001**	0.640	<**0.001**	1.277	<**0.001**	3.727	<**0.001**	0.209	<**0.001**
3 - Down	E2	-0.041	<**0.001**	0.032	0.724	1.208	<**0.001**	9.595	<**0.001**	0.365	<**0.001**
3 - Down	E3	0.023	<**0.001**	0.785	<**0.001**	1.136	<**0.001**	-9.418	<**0.001**	0.800	<**0.001**
3 - Down	E4	-0.011	<**0.001**	0.291	**0.005**	1.077	<**0.001**	0.231	0.695	0.622	<**0.001**
3 - Down	E5	-0.481	<**0.001**	-0.186	0.339	1.262	<**0.001**	91.296	<**0.001**	0.668	<**0.001**
3 - Down	E6	-2.172	<**0.001**	-1.611	0.447	1.841	<**0.001**	399.571	<**0.001**	0.147	<**0.001**

At the 0.03m roughness scale (table 5.5) the R^2 values ranged from 0.032 to 0.817, meaning that between 3.2% and 81.7% of the erosion could be attributed to the roughness at 0.03m scale, when local erosion and local roughness at the 0.03m scale have been controlled for. The average R^2 value was 0.433, meaning that, on average, roughness at the 0.03m scale explained 43.3% of the erosion. Again, this is very similar to the values for the 0.5m and 0.25m scales.

As with the 0.5m and 0.25m scales of roughness, the 0.03m roughness models had model intercepts very close to zero in the majority of cases. This smallest roughness scale saw the largest number of negative coefficients, 12 out of the 30, however positive coefficients still dominated, indicating an increase in roughness results in an increase in erosion. The coefficient values themselves ranged from -1.611 to 5.993 with an average of 0.246. This is the smallest coefficient of the three scales, indicating that very small scale roughness and large scale roughness have a smaller impact on the erosion than the roughness at the medium 0.25m scale. The median coefficient was even smaller at 0.049, still the lowest of any of the roughness scales.

Significance of the influence of the roughness value on the regression varied throughout the models, with only 13 of 30 having p-values below the 0.05 significance level at this smallest roughness scale, compared with 27 at the 0.5m scale and 25 at the 0.25m scale. However, despite this, the majority of models were significant overall, with only one that was not significant in the 30 models carried out. A summary of the model coefficients can be seen in table 5.6 and is displayed as a boxplot in figure 5.21.

Along with the influence of the point roughness, the effect of the lag roughness was also considered. The coefficient values for the lag of roughness

Table 5.6: Summary of the coefficients of the 30 OLS models.

Roughness Scale	Maximum Coefficient	Minimum Coefficient	Mean Coefficient	Median Coefficient	Positive Coefficients	Negative Coefficients
			Roughness			
R0.50	1.737	-0.309	0.374	0.238	24	6
R0.25	3.366	-0.759	0.541	0.392	24	6
R0.03	5.993	-1.611	0.246	0.049	18	12
			Lag of Roughness			
Roughness Scale	Maximum Coefficient	Minimum Coefficient	Mean Coefficient	Median Coefficient	Positive Coefficients	Negative Coefficients
R0.50	17.755	-2.983	0.351	-0.194	12	18
R0.25	12.685	-4.181	0.294	-0.266	11	19
R0.03	399.572	-12.815	21.046	1.969	20	10
			Lag of Erosion			
Roughness Scale	Maximum Coefficient	Minimum Coefficient	Mean Coefficient	Median Coefficient	Positive Coefficients	Negative Coefficients
R0.50	1.794	-5.693	0.864	1.060	29	1
R0.25	1.635	-1.433	1.014	1.073	29	1
R0.03	1.841	-3.984	0.910	1.084	28	2

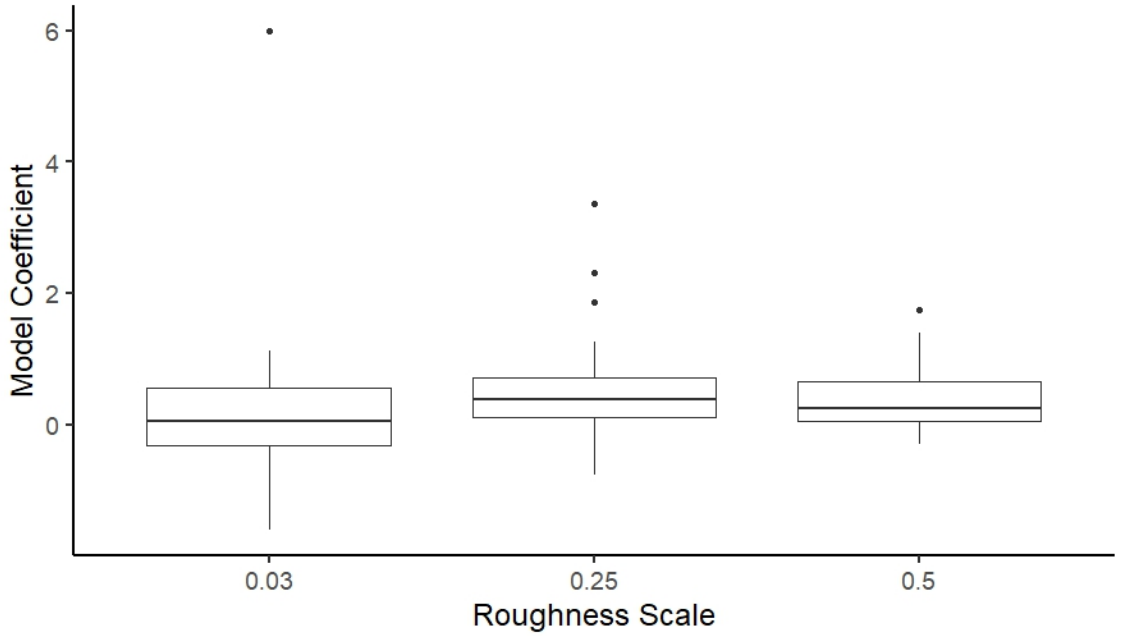

Figure 5.21: Comparison of coefficient values for the effect of roughness at the different roughness scales

had greater variation than those of roughness and there was no clearly dominant direction for the coefficients, although both the 0.5m and the 0.25m roughness scales had a slight dominance of negative coefficients, while the 0.03m scale was dominated by positive coefficients. The 0.03m scale is also the only one with a positive median while the 0.25m and the 0.5m roughness scales both had negative coefficients, indicating that at the larger roughness scales an increase in local roughness results in a decrease in erosion while at the smaller roughness scale an increase in local roughness results in an increase in erosion.

A further set of analysis was carried out that combined the data for all six time periods to create models for each bank based on all measurements taken during the study period. These results are presented in table 5.7 and figures 5.23 to 5.27

Only two of the all bank models we not significant at the 0.05 significance level and both of these were models of the smallest 0.03m scale roughness. The scatter plots are extremely dense due to the number of observations represented, however many of them show positive correlation between the model fitted values and increased erosion.

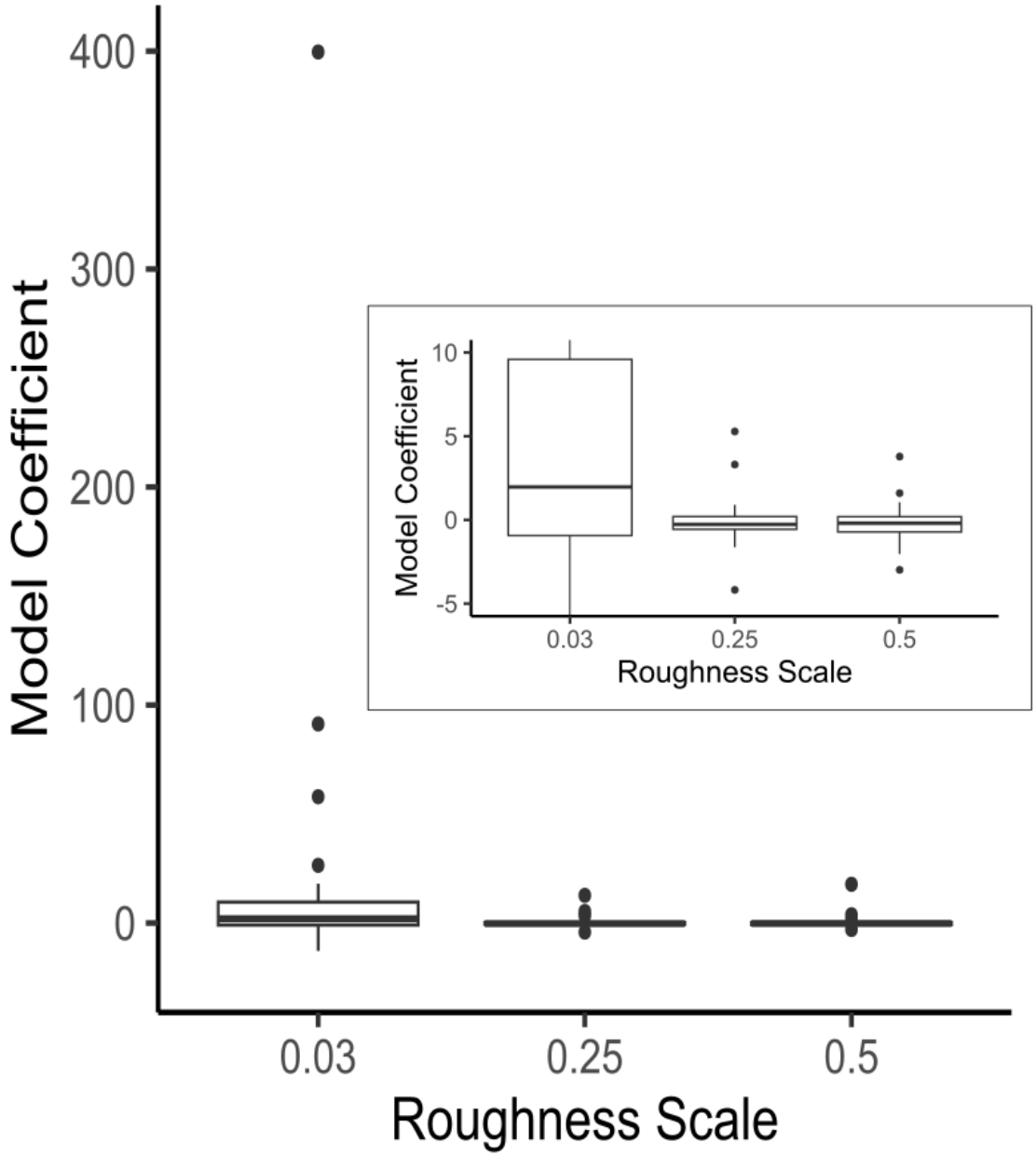

Figure 5.22: Comparison of coefficient values for the effect of the lag roughness at different roughness scales with zoomed image inset

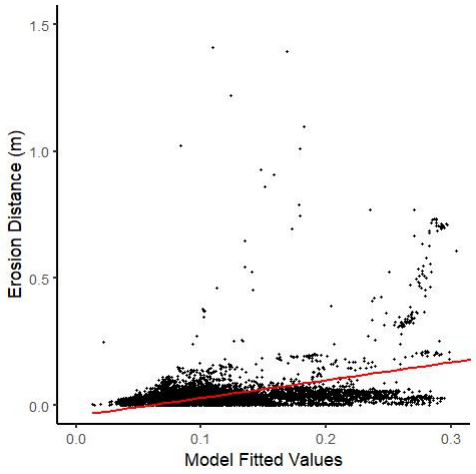

(a) 0.5m Roughness scale - R^2 = 0.399
p-value = <**0.01**

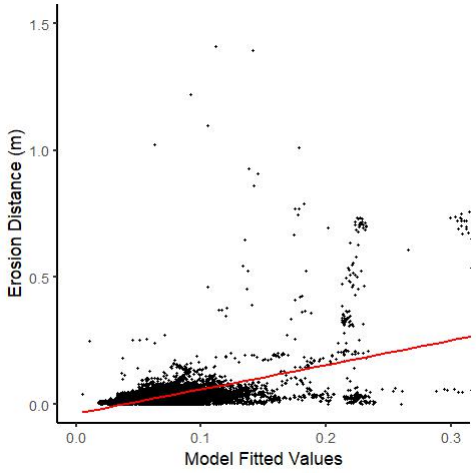

(b) 0.25m Roughness scale - R^2 = 0.396
p-value = <**0.01**

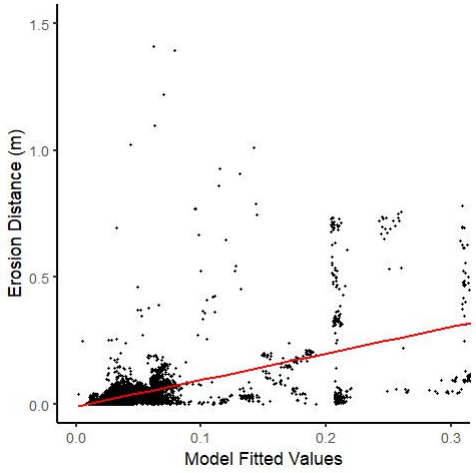

(c) 0.03m Roughness scale - R^2 = 0.393
p-value = <**0.01**

Figure 5.23: Roughness at the a) 0.5m scale, b) 0.25m scale and c) 0.03m scale against erosion for all time periods at Bank 1

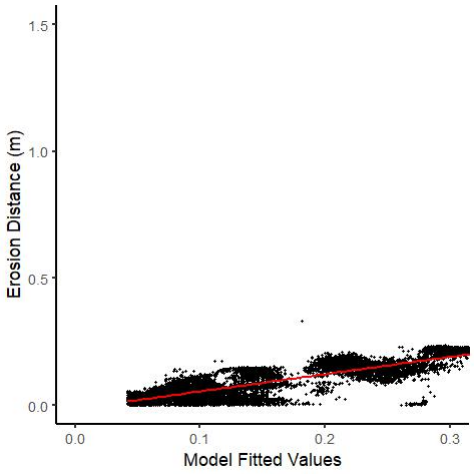

(a) 0.5m Roughness scale - R^2 = 0.893
p-value = <**0.01**

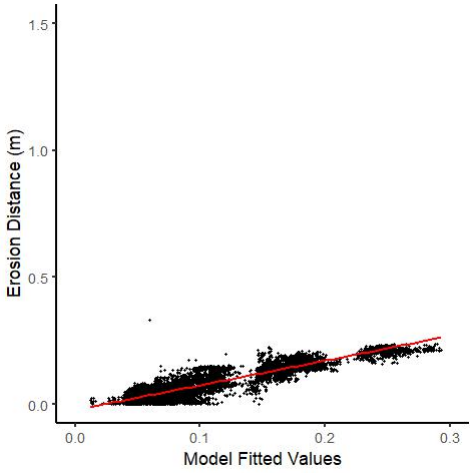

(b) 0.25m Roughness scale - R^2 = 0.893
p-value = <**0.01**

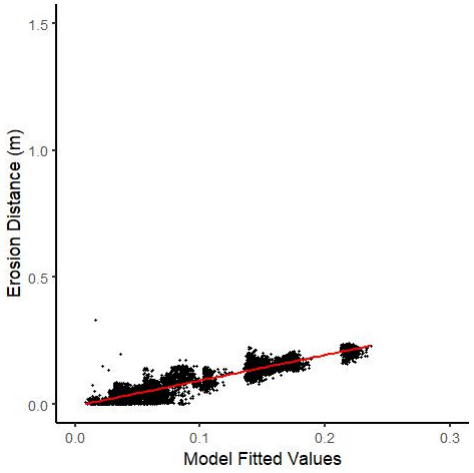

(c) 0.03m Roughness scale - R^2 = 0.892
p-value = <**0.01**

Figure 5.24: Roughness at the a) 0.5m scale, b) 0.25m scale and c) 0.03m scale against erosion for all time periods at Bank 2

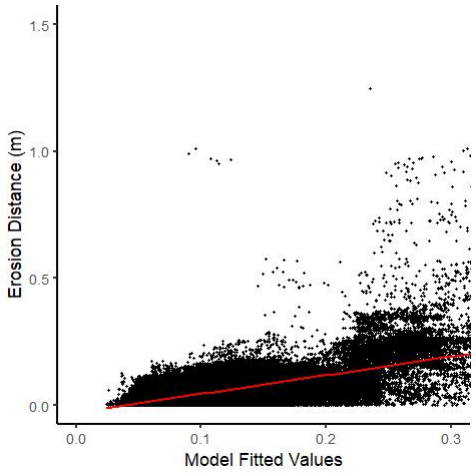

(a) 0.5m Roughness scale - R^2 = 0.469
p-value = <**0.01**

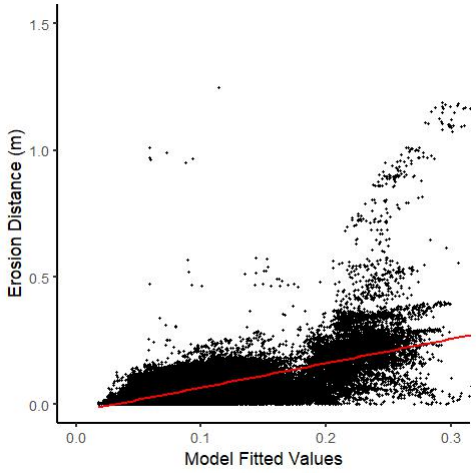

(b) 0.25m Roughness scale - R^2 = 0.470
p-value = <**0.01**

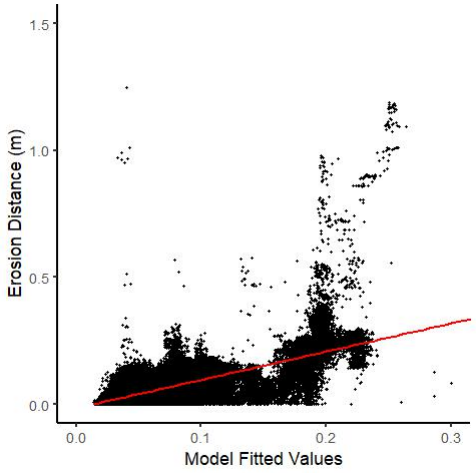

(c) 0.03m Roughness scale - R^2 = 0.465
p-value = <**0.01**

Figure 5.25: Roughness at the a) 0.5m scale, b) 0.25m scale and c) 0.03m scale against erosion for all time periods at the upstream reach of Bank 3

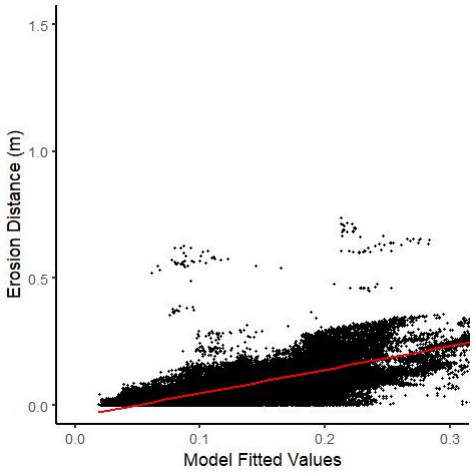

(a) 0.5m Roughness scale - R^2 = 0.732
p-value = <**0.01**

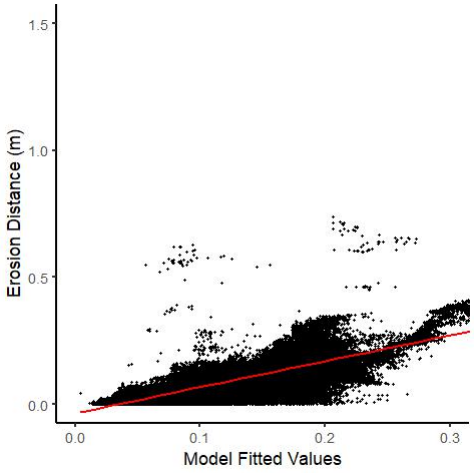

(b) 0.25m Roughness scale - R^2 = 0.715
p-value = <**0.01**

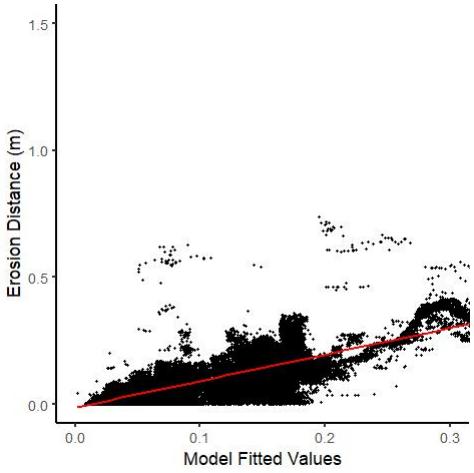

(c) 0.03m Roughness scale - R^2 = 0.712
p-value = <**0.01**

Figure 5.26: Roughness at the a) 0.5m scale, b) 0.25m scale and c) 0.03m scale against erosion for all time periods at the midstream reach of Bank 3

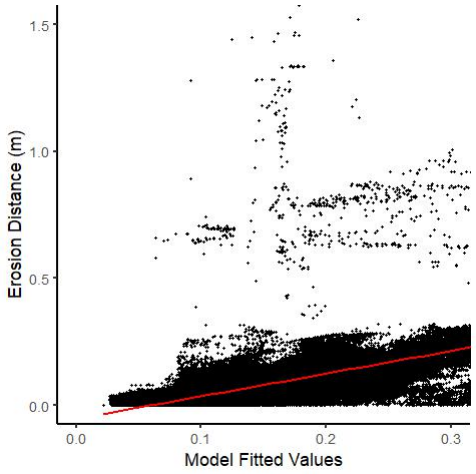

(a) 0.5m Roughness scale - R^2 = 0.256
p-value = <**0.01**

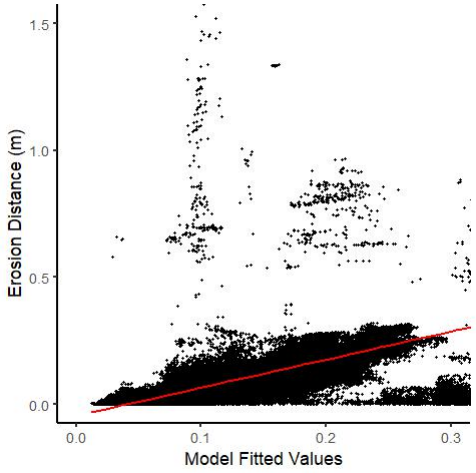

(b) 0.25m Roughness scale - R^2 = 0.257
p-value = <**0.01**

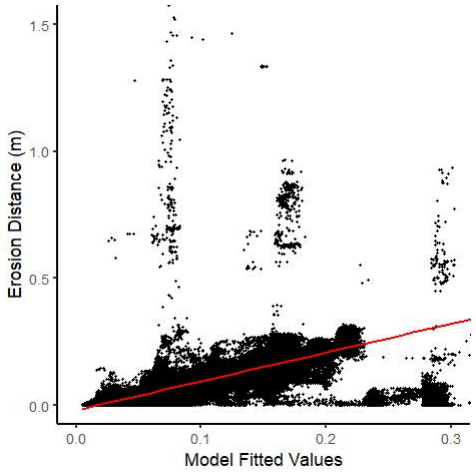

(c) 0.03m Roughness scale - R^2 = 0.254
p-value = <**0.01**

Figure 5.27: Roughness at the a) 0.5m scale, b) 0.25m scale and c) 0.03m scale against erosion for all time periods at the downstream reach of Bank 3

Table 5.7: Results of OLS regression between erosion and roughness compiled across each bank at all scales. Statistically significant p-values are in **bold**

Bank	Model Intercept	Intercept p-value	0.25m Roughness Coefficient	Roughness p-value	Lag erosion Coefficient	Lag erosion p-value	Lag Roughness Coefficient	Lag Roughness p-value	R^2 Value	Model p-value	
1	0.5m	-0.004	**0.040**	0.280	<**0.001**	1.045	<**0.001**	-0.197	<**0.001**	0.399	<**0.001**
1	0.25m	-0.008	<**0.001**	0.361	<**0.001**	1.049	<**0.001**	-0.001	0.991	0.396	<**0.001**
1	0.03m	-0.003	0.229	-0.160	0.512	1.047	<**0.001**	0.804	0.239	0.393	<**0.001**
2	0.5m	<-0.001	0.164	0.162	<**0.001**	1.007	<**0.001**	-0.163	<**0.001**	0.893	<**0.001**
2	0.25m	<-0.001	0.190	0.291	<**0.001**	1.007	<**0.001**	-0.266	<**0.001**	0.893	<**0.001**
2	0.03m	0.002	0.351	-0.452	<**0.001**	1.006	<**0.001**	-0.368	0.596	0.892	<**0.001**
3 - Up	0.5m	-0.006	<**0.001**	0.204	<**0.001**	1.116	<**0.001**	-0.219	<**0.001**	0.469	<**0.001**
3 - Up	0.25m	-0.006	<**0.001**	0.361	<**0.001**	1.117	<**0.001**	-0.415	<**0.001**	0.470	<**0.001**
3 - Up	0.03m	-0.013	<**0.001**	0.364	<**0.001**	1.118	<**0.001**	1.145	<**0.001**	0.465	<**0.001**
3 - Mid	0.5m	-0.003	<**0.001**	0.700	<**0.001**	1.044	<**0.001**	-0.780	<**0.001**	0.732	<**0.001**
3 - Mid	0.25m	-0.005	<**0.001**	0.437	<**0.001**	1.042	<**0.001**	-0.411	<**0.001**	0.715	<**0.001**
3 - Mid	0.03m	-0.013	<**0.001**	0.094	0.117	1.046	<**0.001**	2.062	<**0.001**	0.712	<**0.001**
3 - Down	0.5m	-0.015	<**0.001**	0.256	<**0.001**	1.145	<**0.001**	-0.187	<**0.001**	0.256	<**0.001**
3 - Down	0.25m	-0.013	<**0.001**	0.634	<**0.001**	1.146	<**0.001**	-0.590	<**0.001**	0.257	<**0.001**
3 - Down	0.03m	-0.017	<**0.001**	0.436	**0.001**	1.141	<**0.001**	0.901	0.097	0.254	<**0.001**

5.4.3 Roughness interactions

The previous models have assessed the influence of roughness at the three different scales individually. However, identifying any interactions between roughness at different scales is also important to understand how a combination of roughness variables might influence erosion. Interaction models were carried out for each different bank and time period, and lagged erosion and the lagged roughness at all three scales were again used to control for spatial autocorrelation.

To generate the three-way interactions, roughness at the large 0.5m scale and the medium 0.25m scale were divided into three categories: low roughness represents the effect of roughness at a value of one standard deviation below the mean, average roughness represents the effect of roughness at the mean value, and high roughness represents the effect of a roughness value that is one standard deviation above the mean.

The data for all banks and all time periods is shown in figures 5.28 to 5.31, excluding the midstream reach of Bank 3 which did not generate a significant interaction model. These results are also illustrated in table 5.8. Figure 5.28 shows that at Bank 1, low roughness at the 0.5m scale, coupled with high roughness at the 0.25m scale causes the rate of erosion to increase with increasing roughness at the 0.03m scale. When roughness at the 0.5m scale is at its average and roughness at the 0.25m scale is high, the rate of erosion also increases with an increase in roughness at the 0.03m scale. In contrast low roughness at the 0.5m scale and low roughness at the 0.25m scale causes a decrease in the rate of erosion as the roughness at the 0.03m scale increases.

The results at Bank 2 demonstrated a very different relationship, with all slopes for low roughness at the 0.25m scale being statistically insignificant

and all other interaction combinations generating negative coefficients indicating that all significant interactions between the different roughness scales generate a decrease in erosion with an increase in roughness at the 0.03m scale.

At the upstream reach of Bank 3 the relationship was directly opposite to that shown at Bank 1, with a combination of Low roughness at both the 0.5m and 0.25m scales resulting in an increase in the erosion with an increase in the 0.03m roughness scale. Low roughness at the 0.5m roughness scale and high roughness at the 0.25m scale resulted in a decrease in erosion with an increase in the roughness at the 0.03m scale.

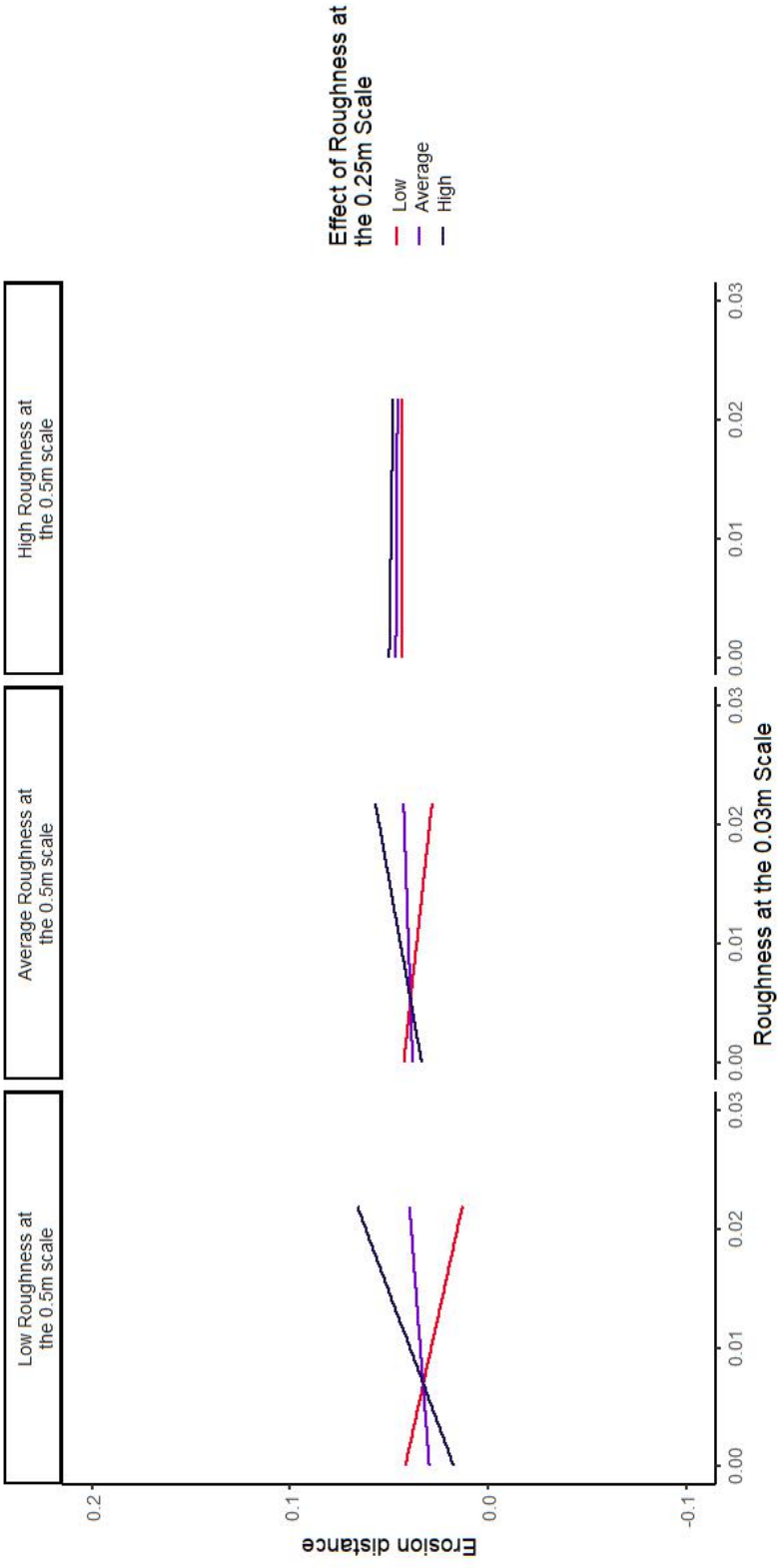

Figure 5.28: Interaction plot of the effect of roughness at each scale on erosion for the all Bank 1 data

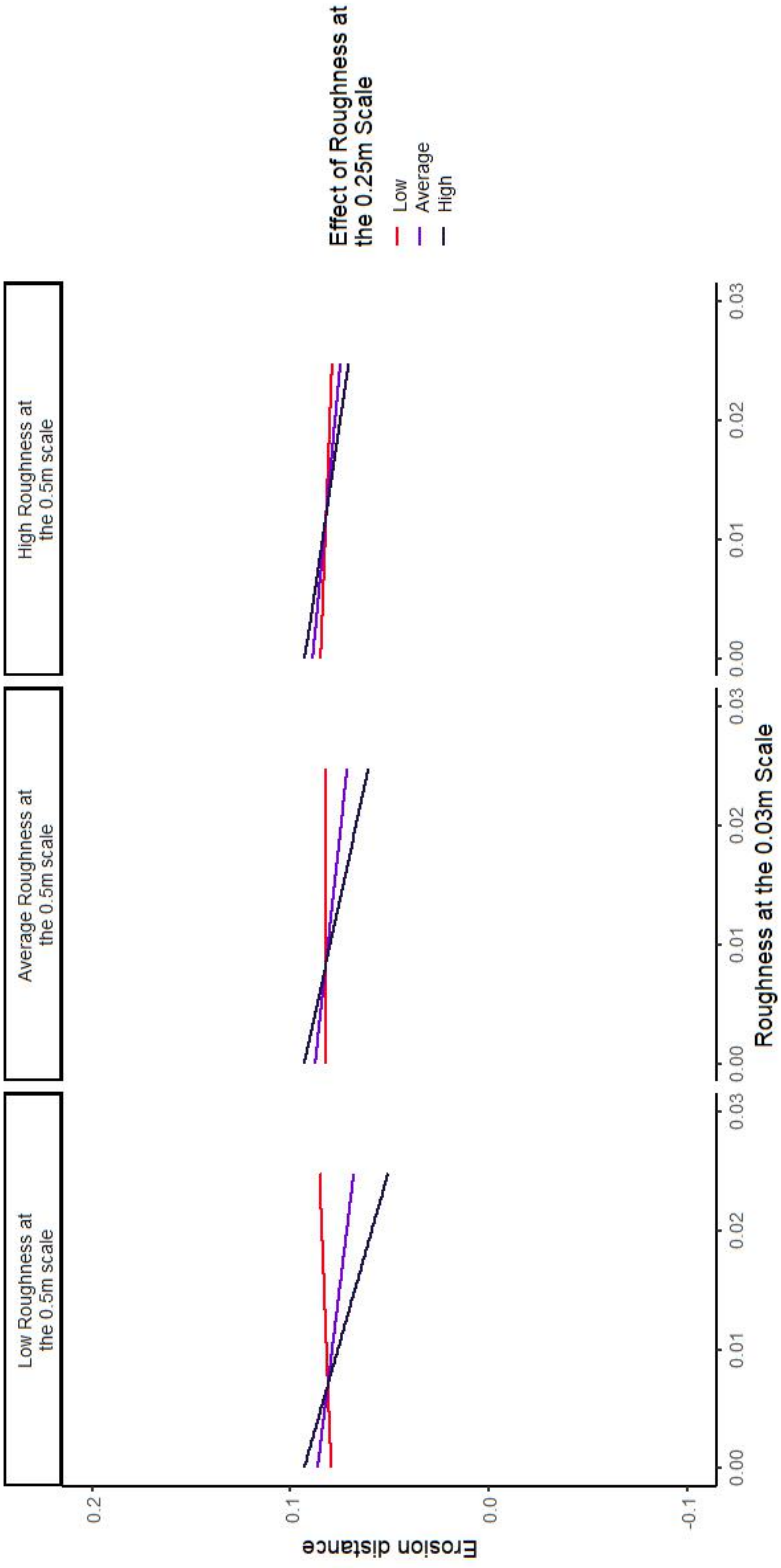

Figure 5.29: Interaction plot of the effect of roughness at each scale on erosion for the all Bank 2 data

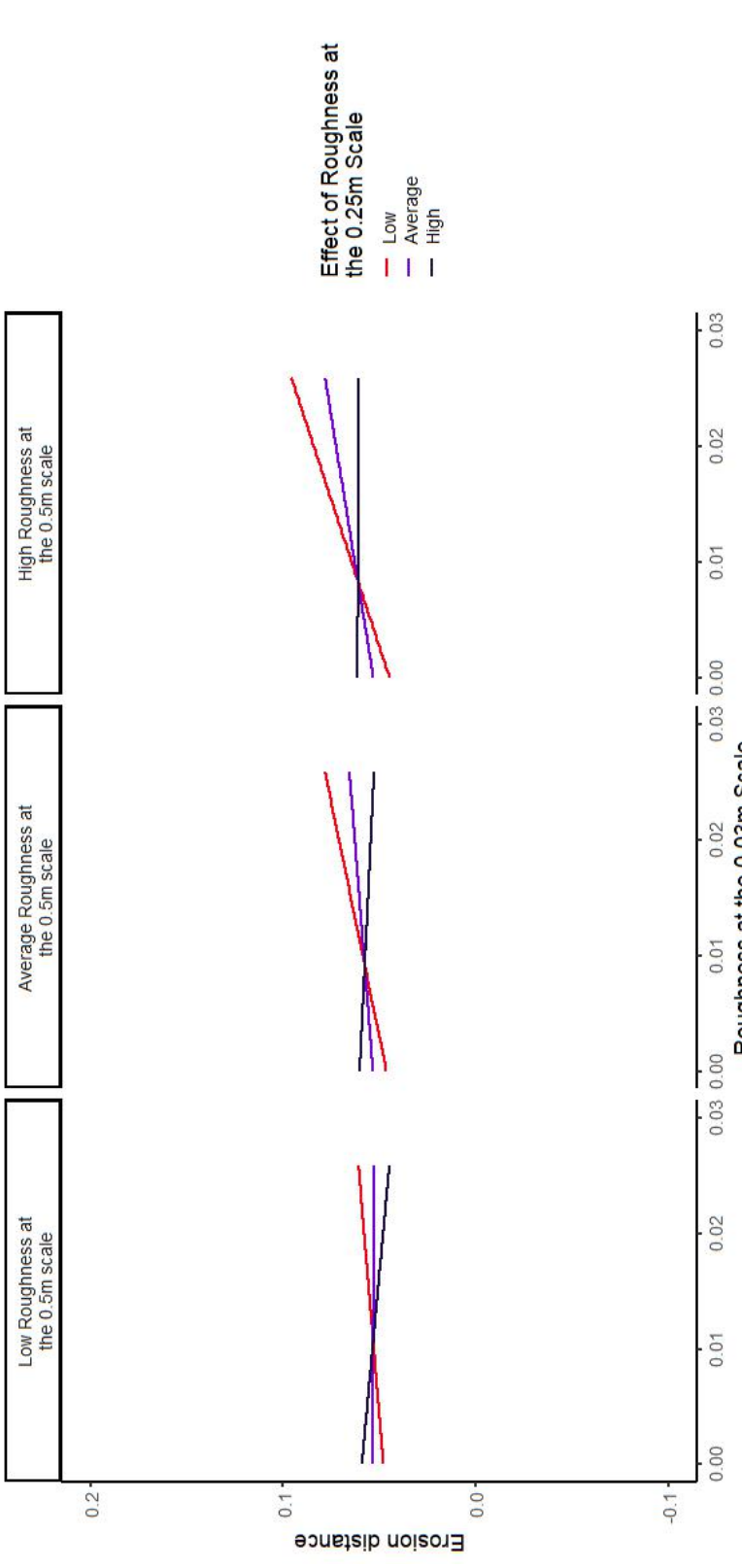

Figure 5.30: Interaction plot of the effect of roughness at each scale on erosion for the upstream reach of Bank 3.

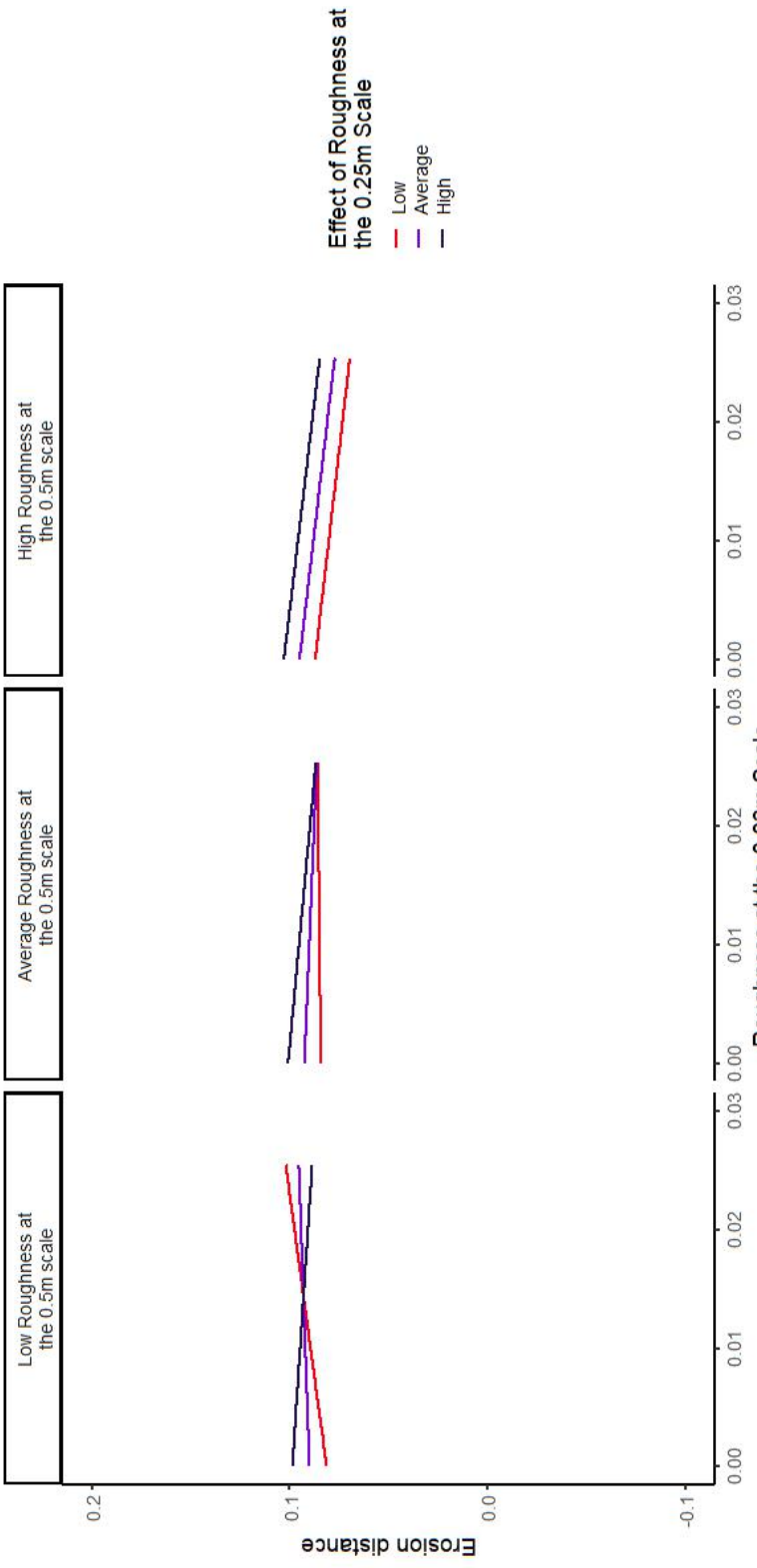

Figure 5.31: Interaction plot of the effect of roughness at each scale on erosion for the downstream reach of Bank 3.

Table 5.8: Slope coefficients for the effect of roughness at the 0.03m roughness scale against bank erosion for each combination of 0.5m scale and 0.25m scale interactions. P-values for the coefficients are provided in brackets and those that are statistically significant at the 0.05 significance level are highlighted in **bold**. For quick visual comparison, cells with a positive coefficient have been coloured green and those with a negative coefficient have been coloured orange

	Low roughness at the 0.5m scale	Average roughness at the 0.5m scale	High roughness at the 0.5m scale	Model R^2	Model P-value
			Bank 1		
Low roughness at the 0.25m scale	**-1.33 (0.01)**	-0.66 (0.12)	0.01 (0.99)		
Average roughness at the 0.25m scale	0.46 (0.20)	0.21 (0.45)	-0.04 (0.94)	0.403	<0.001
High roughness at the 0.25m scale	**2.24 (<0.01)**	**1.08 (0.01)**	-0.09 (0.81)		
			Bank 2		
Low roughness at the 0.25m scale	0.24 (0.09)	0.0 (0.99)	-0.23 (0.18)		
Average roughness at the 0.25m scale	**-0.74 (<0.01)**	**-0.65 (<0.01)**	**-0.57 (<0.01)**	0.895	<0.001
High roughness at the 0.25m scale	**-1.71 (<0.01)**	**-1.30 (<0.01)**	**-0.90 (<0.01)**		
			Bank 3 - Upstream		
Low roughness at the 0.25m scale	**0.50 (<0.01)**	**1.24 (<0.01)**	**1.97 (<0.01)**		
Average roughness at the 0.25m scale	-0.03 (0.27)	**0.47 (<0.01)**	**0.97 (<0.01)**	0.473	<0.001
High roughness at the 0.25m scale	**-0.55 (<0.01)**	**-0.29 (<0.01)**	-0.03 (0.68)		
			Bank 3 - Downstream		
Low roughness at the 0.25m scale	**0.82 (<0.01)**	0.06 (0.78)	-0.69 (0.07)		
Average roughness at the 0.25m scale	0.21 (0.33)	-0.25 (0.10)	**-0.70 (0.01)**	0.258	<0.001
High roughness at the 0.25m scale	-0.40 (0.23)	**-0.55 (0.01)**	**-0.71 (<0.01)**		

The interaction plots for each bank and time period that exhibited a statistically significant three-way interaction can be seen in appendix F, tables F.1 and F.2 and figures F.16 to F.30. As with the all bank data, there is considerable variation in the strength and direction of the slope coefficients in different roughness combinations across the different banks and different time periods. This variation in the direction of the coefficients from the interaction models highlights once again the inherent variability in the natural environment and in the processes that serve to influence and generate erosion.

In addition to the interactions between roughness scales, further interaction models were run to establish the potential impacts of local roughness on the relationship between point roughness and erosion (figures 5.32 to 5.36). The relationship between point roughness and local roughness is markedly less notable than that of interactions between the different scales of roughness. In most cases, the effect of increasing point roughness is the same regardless of the degree of local roughness, with most of the coefficients being very similar, and sometimes the same, for each of the different levels of local roughness (high, medium and low).

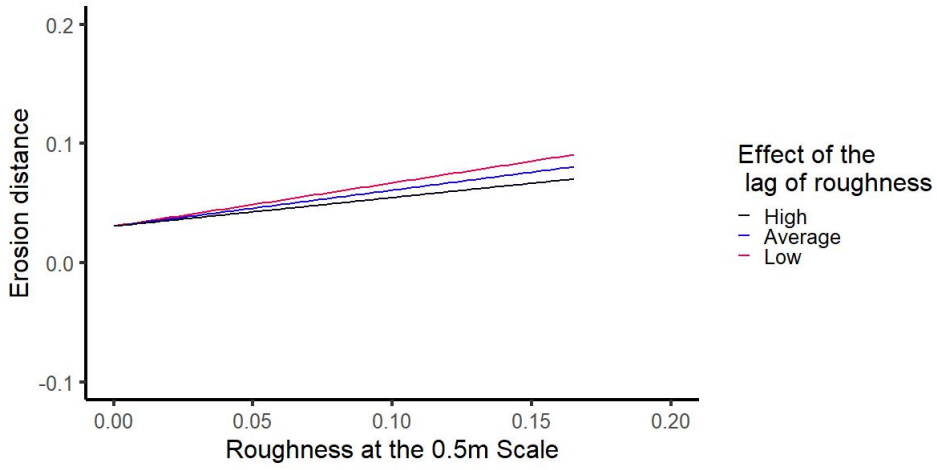

(a)

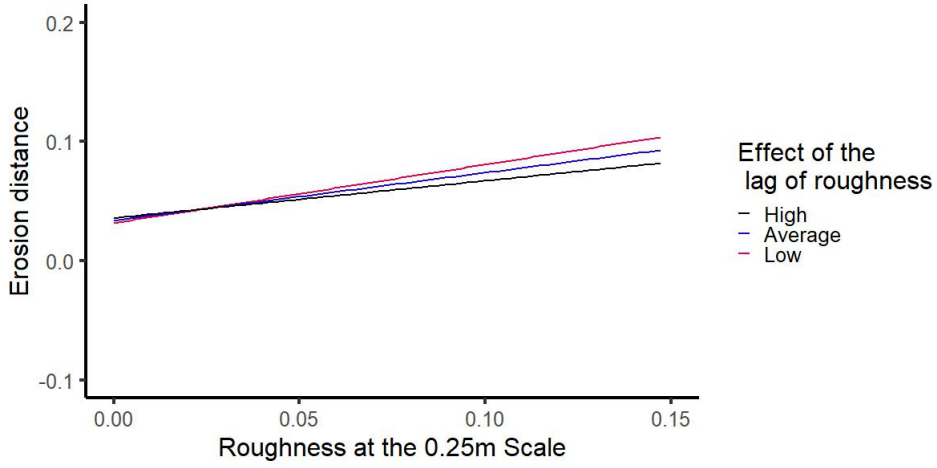

(b)

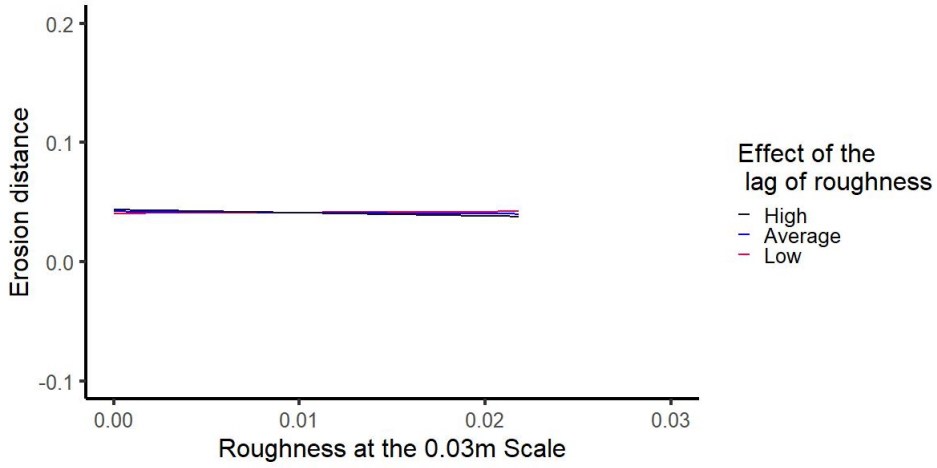

(c)

Figure 5.32: Roughness at the a) 0.5m scale, b) 0.25m scale and c) 0.03m scale against erosion for all time periods at Bank 1

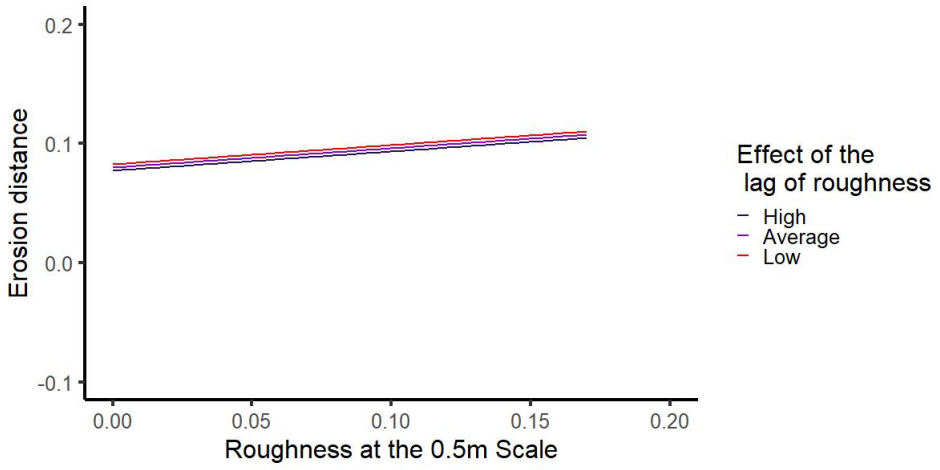

(a)

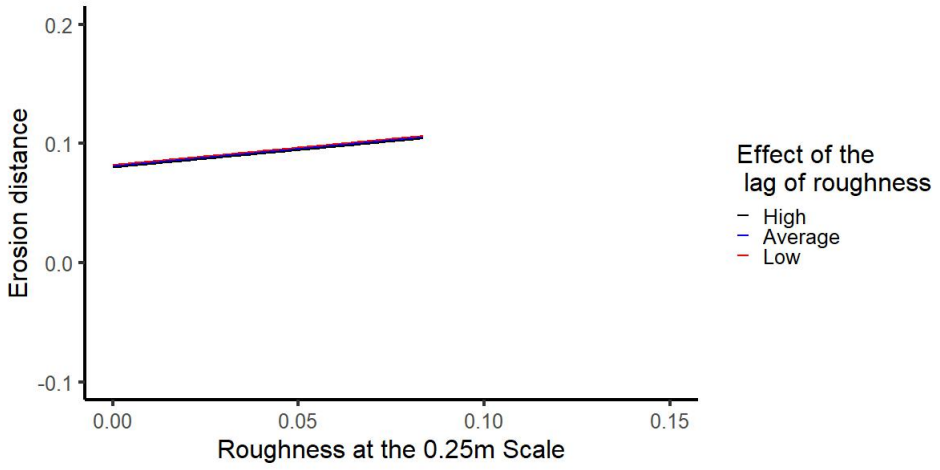

(b)

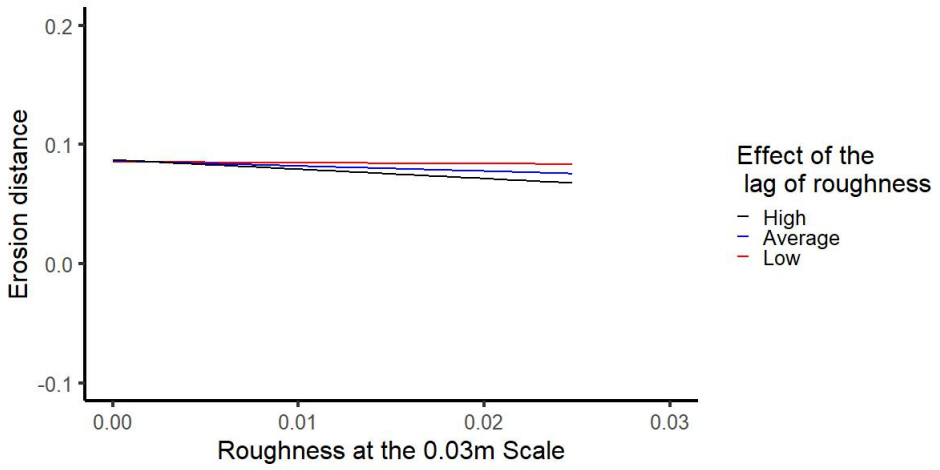

(c)

Figure 5.33: Roughness at the a) 0.5m scale, b) 0.25m scale and c) 0.03m scale against erosion for all time periods at Bank 2

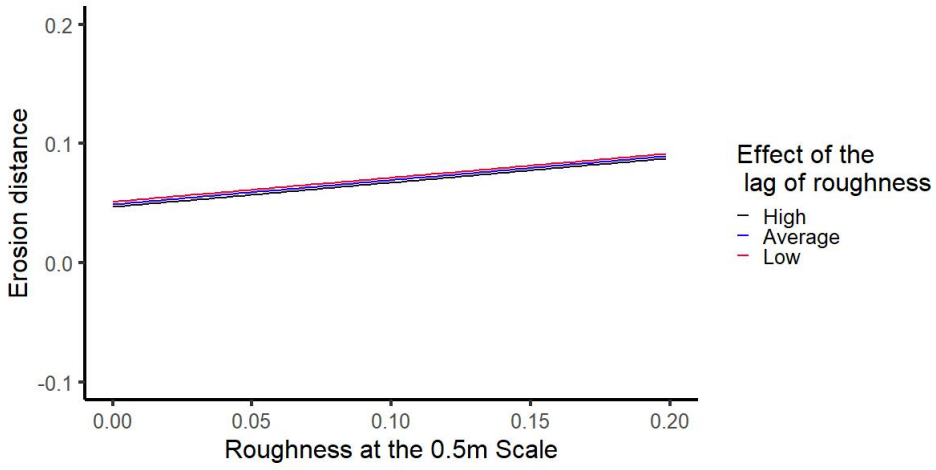

(a)

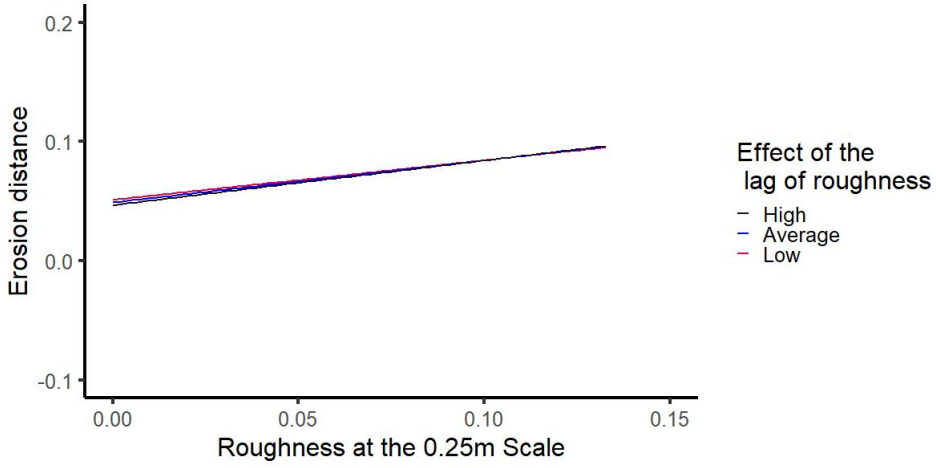

(b)

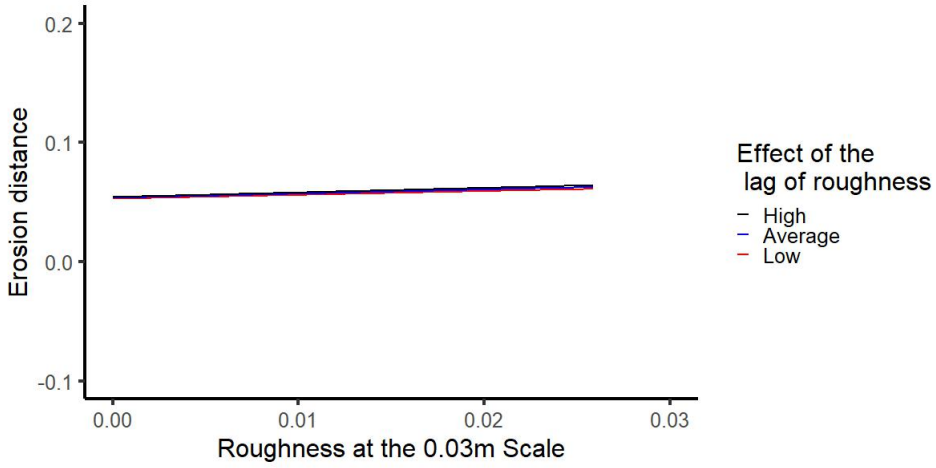

(c)

Figure 5.34: Roughness at the a) 0.5m scale, b) 0.25m scale and c) 0.03m scale against erosion for all time periods at the upstream reach of Bank 3

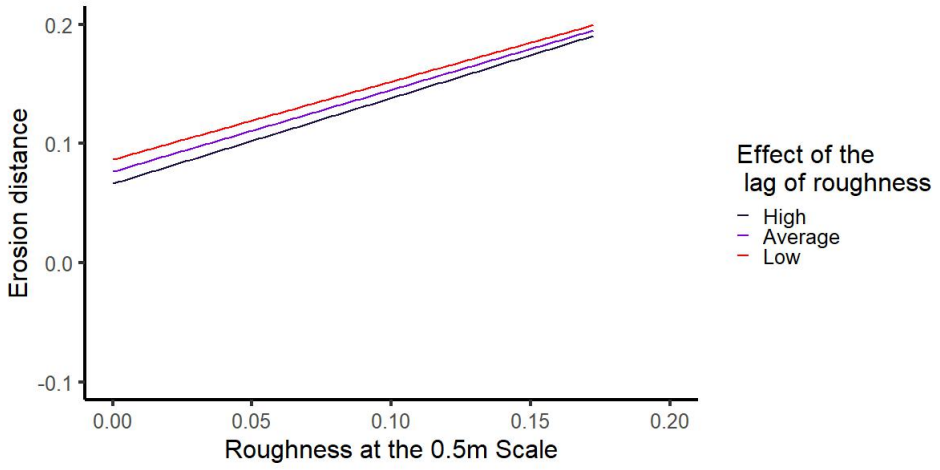

(a)

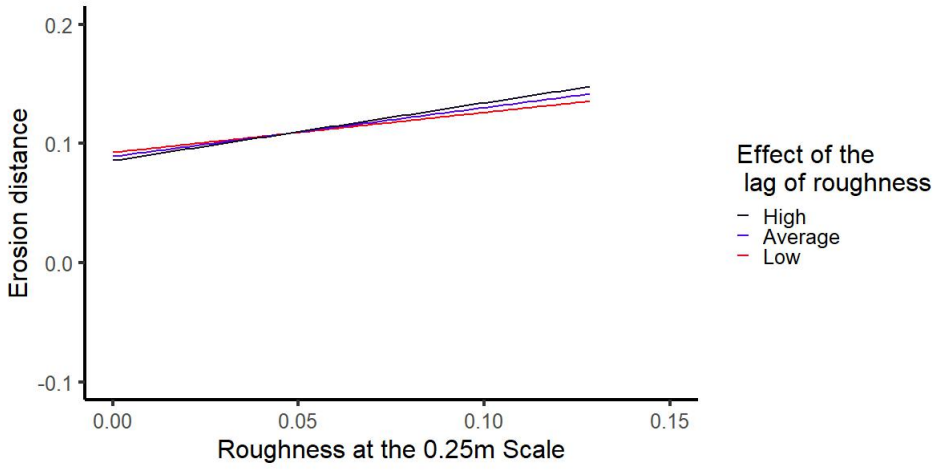

(b)

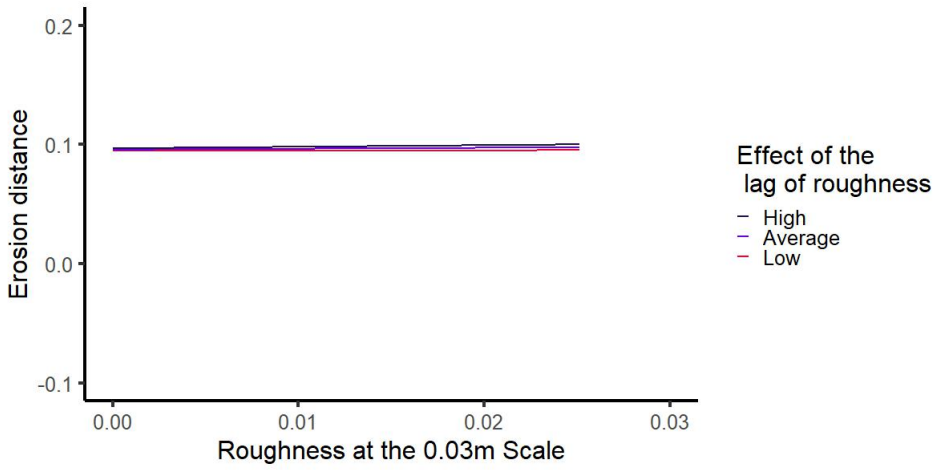

(c)

Figure 5.35: Roughness at the a) 0.5m scale, b) 0.25m scale and c) 0.03m scale against erosion for all time periods at the midstream reach of Bank 3

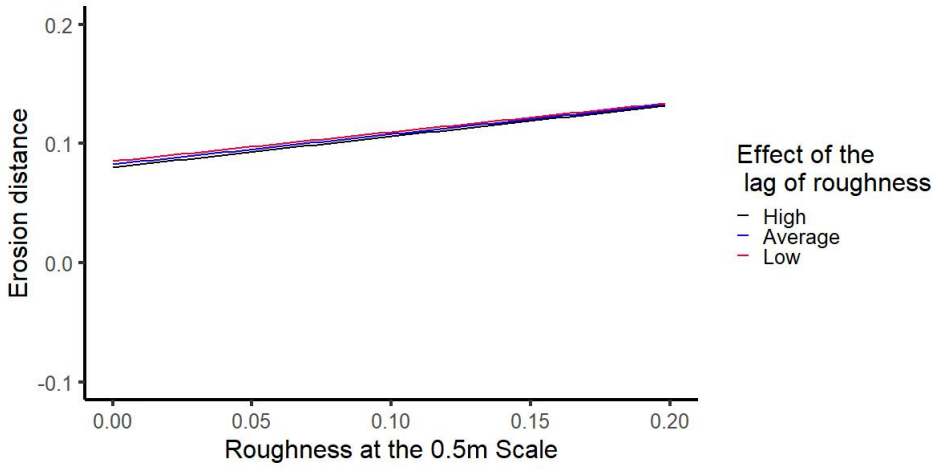

(a)

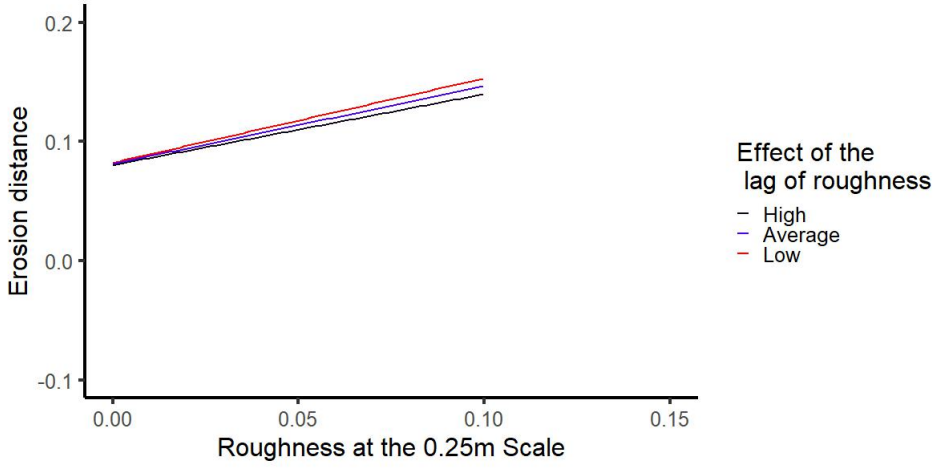

(b)

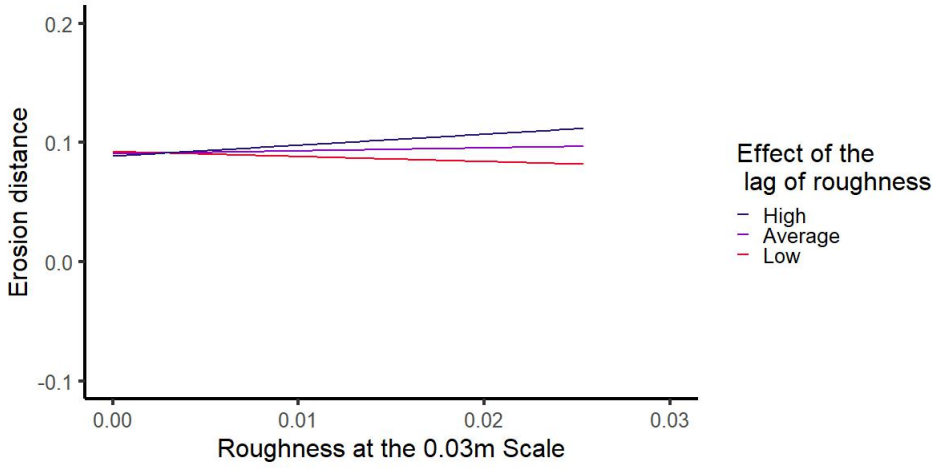

(c)

Figure 5.36: Roughness at the a) 0.5m scale, b) 0.25m scale and c) 0.03m scale against erosion for all time periods at the downstream reach of Bank 3

Table 5.9: Slope coefficients for the effect of local roughness on the relationship between point roughness and erosion. P-values for the coefficients are provided in brackets and those that are statistically significant at the 0.05 significance level are highlighted in **bold**. For quick visual comparison, cells with a positive coefficient have been coloured green and those with a negative coefficient have been coloured orange

	Low Local Roughness	Average Local Roughness	High Local Roughness	Model R^2	Model P-value
			0.5m Roughness Scale		
Bank 1	**0.36 (<0.001)**	**0.30 (<0.001)**	**0.24 (<0.001)**	0.400	**<0.001**
Bank 2	**0.16 (<0.001)**	**0.16 (<0.001)**	**0.16 (<0.001)**	0.893	**<0.001**
Bank 3 - Upstream	**0.20 (<0.001)**	**0.20 (<0.001)**	**0.20 (<0.001)**	0.469	**<0.001**
Bank 3 - Midstream	**0.65 (<0.001)**	**0.69 (<0.001)**	**0.72 (<0.001)**	0.732	**<0.001**
Bank 3 - Downstream	**0.25 (<0.001)**	**0.25 (<0.001)**	**0.26 (<0.001)**	0.256	**<0.001**
			0.25m Roughness Scale		
Bank 1	**0.49 (<0.001)**	**0.40 (<0.001)**	**0.31 (<0.001)**	0.397	**<0.001**
Bank 2	**0.29 (<0.001)**	**0.29 (<0.001)**	**0.29 (<0.001)**	0.893	**<0.001**
Bank 3 - Upstream	**0.35 (<0.001)**	**0.35 (<0.001)**	**0.37 (<0.001)**	0.470	**<0.001**
Bank 3 - Midstream	**0.34 (<0.001)**	**0.41 (<0.001)**	**0.48 (<0.001)**	0.715	**<0.001**
Bank 3 - Downstream	**0.71 (<0.001)**	**0.65 (<0.001)**	**0.60 (<0.001)**	0.257	**<0.001**
			0.03m Roughness Scale		
Bank 1	0.07 (0.87)	-0.10 (0.17)	-0.26 (0.37)	0.393	**<0.001**
Bank 2	-0.07 (0.51)	**-0.43 (<0.001)**	**-0.78 (<0.001)**	0.892	<0.001
Bank 3 - Upstream	**0.32 (<0.001)**	**0.35 (<0.001)**	**0.38 (<0.001)**	0.465	<0.001
Bank 3 - Midstream	0.03 (0.77)	0.08 (0.20)	0.13 (0.06)	0.712	<0.001
Bank 3 - Downstream	**-0.42 (0.04)**	0.25 (0.07)	**0.92 (<0.001)**	0.254	<0.001

5.5 Discussion

5.5.1 Patterns of bank roughness

The spatial patterns of bank roughness were largely consistent across all banks, with the roughest surfaces being associated with areas at the top of bank that are rarely inundated by flow and where vegetation roots, animal activity and subaerial processes are likely to be working to increase the roughness of the surface. The highest value of point roughness at the 0.5m roughness scale was 0.311m with an average roughness of between 0.031m and 0.048m. These values are similar to those of Leyland et al. (2015) who had bank averaged values of between 0.20m and 0.11m on the Cecina River, Italy. Their roughness values were calculated for the whole bank by dividing the recorded bank into five sections between the bottom and top of bank representing different sediment layers and averaging the roughness of each of those sections to give a final roughness value for the bank for each time period of their study, however no detail of the vertical distribution of roughness was reported.

The novel nature of the work undertaken has meant that there are limited studies available for comparison. To this authors knowledge, there have been no other studies to date that have mapped roughness across a vertical bank surface to the same level of detail as this work. Most other studies into the effect of roughness on bank erosion either create averaged surfaces or establish horizontal cross-sections and apply gaussian curves to these sections. As such, many of the arguments relating to the 3-dimensional structure of roughness are based on the evidence of this work only and require further studies to provide additional evidence to support or refute the assumptions of this work.

The most obvious spatial patterning of the roughness data was visible at the 0.5m scale, where the highest values were distributed along the top of bank and around areas that had become vegetated during the study period. The pattern was less obvious at the 0.25m scale, with greater variation across the bank face but still some top of bank areas of higher roughness. At the 0.03m scale the roughness exhibits an almost random distribution, with little pattern identifiable.

At the upstream reach of Bank 3 and at the 0.03m scale over time periods E4 and E5 there were some very sharp and significant changes in the roughness values across the lower bank face. These can be seen in more detail in figure 5.37. The very sudden change in roughness was initially thought to be as a result of a shadowing effect of vegetation on the opposite bank occluding the lower bank surface, this occlusion was thought to have caused a localised reduction in point density thus resulting in fewer points falling within the radius of the roughness calculation. However, that theory would explain a localised area of higher roughness in the affected area. In this case, the area thought to have been occluded exhibited roughness consistent with roughness measurements of the bank face in previous scans. It is in fact the upper bank that appears to be showing an unexplained increase in the roughness of the surface, closer to 0.02m than the previous scans which were dominated by 0.005m - 0.01m roughness.

A further review of the data did not identify a significant change in point density between the lower bank and upper bank areas nor any other data anomaly that would explain the change. Time period E4 included the spring months of 2018, from Feb 2018 to May 2018. During these months there were no significantly high flow events compared to other time periods that might have explained a change in the roughness of the upper

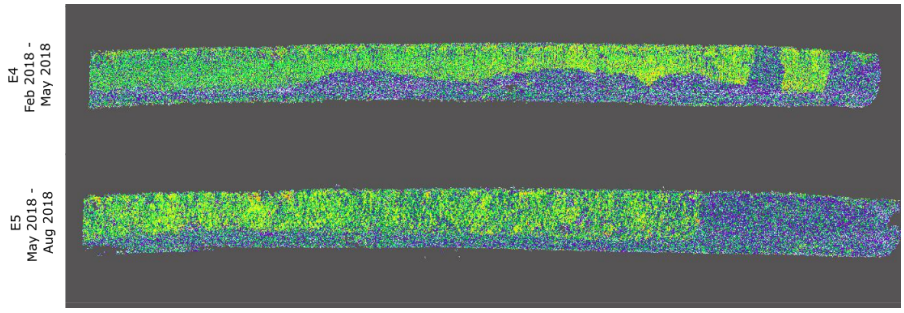

Figure 5.37: Zoomed figure of the roughness values at the 0.03m roughness scale for the upstream reach of Bank 3 during time periods E4 and E5

bank areas, nor were there any anomalies in terms of the meteorological conditions experienced at that bank during that time period. The point density was inline with previous scans and the registration errors were also consistent with other time periods. The time period exhibiting these apparent changes in bank roughness also cannot be attributed to the time periods exhibiting high deposition, as these were most significantly seen in time periods E3 and E5 at Bank 2 and all subsections of Bank 3, however these roughness alterations occurred at the Upstream reach of Bank 3 during time period E4.

The only remaining consideration was that the bank material itself could be a limiting factor in the maximum roughness that could be achieved at this scale. The lower areas of the upstream reach of Bank 3 were the most heavily dominated by pebbles and small cobbles (figure 5.38). These lower areas of the bank were also often typified by breaks of slopes and small 'bulges' in the bank surface that aligned closely to those areas of lower roughness (figure 5.39). A similar pattern of results was seen at the upstream reach of the Cecina River, Italy during work by Nardi and Rinaldi (2010) where they found the cohesive upper area of the bank exhibiting a roughness height of 0.1621m while the gravel area of the bank, which had a mean D_50 of 6.7mm, had a lower roughness height of 0.0745m. However, at the downstream region where the average D_50 was higher at

10.9mm the roughness height was also higher at 0.75m. Further research is required to fully understand these patterns of roughness at different scales, however it is possible that the smooth surfaces of gravel and cobble sized sediments resulted in lower roughness values where their sizes were larger than the 0.03m radius used for the smallest scale of roughness calculation.

Figure 5.38: Structure of the upstream reach of Bank 3 taken during initial site investigation on 23rd May 2016

As the later stages of the analysis were focused on the lower bank fluvial erosion zones, it was not deemed necessary to exclude these scans from the final data analysis, however a clear reason for the change in roughness has not yet been identified and provides an interesting opportunity for future research to establish what may cause changes in the roughness across a vertical bank surface, and how this change influences the potential susceptibility of the bank to erosion.

5.5.2 Bank roughness and erosion

Following a series of linear regression analyses, there is a significant, moderate to strong relationship between roughness and erosion, when local erosion and local roughness have been controlled for. By comparing the

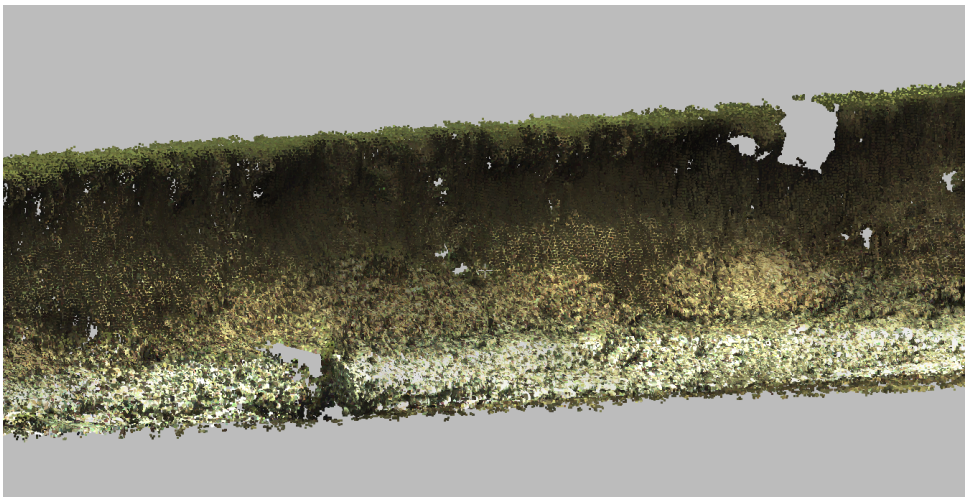

(a)

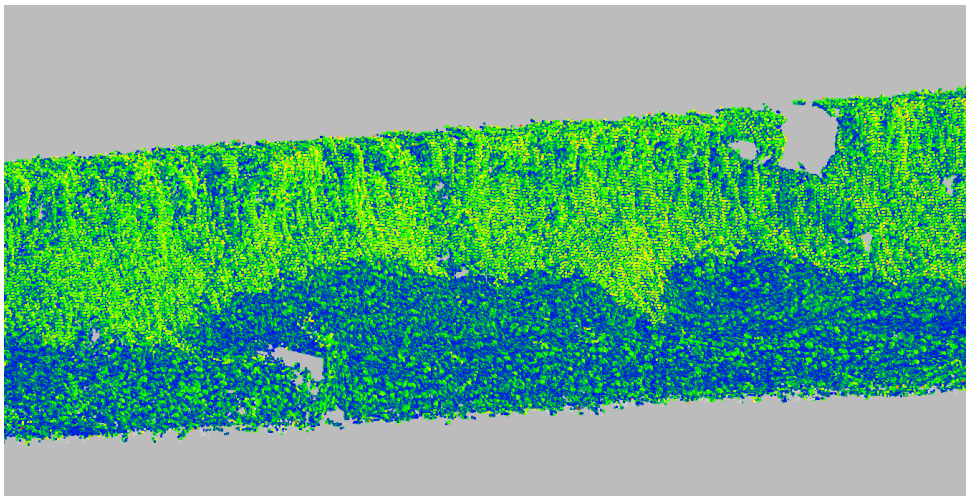

(b)

Figure 5.39: Zoomed view of a section of the Upstream reach of Bank 3 in a) true colour RGB values and b) roughness at the 0.03m scale values to demonstrate the contiguity between areas of lower roughness and areas of larger sediment and less steep bank.

R^2 values for each scale we can see that the 0.5m roughness scale explained a higher percentage of the erosion in 18 of the models, while the 0.25m roughness scale explained a higher percentage of erosion in 10 of the models, with the 0.03m roughness scale explaining a higher percentage of the erosion in the remaining two models. However, the R^2 values were very similar across the different scales within the different banks and time period combinations.

Table 5.10: Comparison of the regression results between each of the roughness scales. The direction of the relationship is also shown by the cell colour, with green representing a positive coefficient and orange representing a negative coefficient. The model with the highest R^2 value for each bank and time period is highlighted in **bold**

Bank	Epoch	0.5m roughness R^2 value	0.25m roughness R^2 value	0.03m roughness R^2 value
1	E1	0.061	**0.092**	0.060
1	E2	**0.086**	0.048	0.032
1	E3	0.820	**0.846**	0.817
1	E4	**0.445**	0.431	0.418
1	E5	**0.537**	0.511	0.500
1	E6	**0.431**	0.413	0.408
2	E1	**0.477**	0.471	0.475
2	E2	0.544	**0.576**	0.532
2	E3	**0.886**	0.681	0.240
2	E4	0.481	**0.504**	0.430
2	E5	**0.786**	0.785	0.781
2	E6	**0.260**	0.162	0.044
3 - Up	E1	**0.505**	0.503	0.498
3 - Up	E2	0.177	**0.182**	0.177
3 - Up	E3	0.610	**0.616**	0.599
3 - Up	E4	0.238	**0.337**	0.322
3 - Up	E5	**0.445**	0.438	0.439
3 - Up	E6	**0.384**	0.381	0.393
3 - Mid	E1	**0.668**	0.641	0.618
3 - Mid	E2	0.202	**0.206**	0.214
3 - Mid	E3	**0.535**	0.519	0.521
3 - Mid	E4	**0.700**	0.640	0.632
3 - Mid	E5	**0.514**	0.502	0.499
3 - Mid	E6	**0.339**	0.338	0.339
3 - Down	E1	0.216	**0.219**	0.209
3 - Down	E2	0.381	**0.396**	0.365
3 - Down	E3	**0.834**	0.817	0.800
3 - Down	E4	**0.629**	0.627	0.622
3 - Down	E5	0.635	0.636	**0.668**
3 - Down	E6	0.119	0.110	**0.147**

The relatively higher influence of large scale roughness on erosion, and the dominance of positive coefficients in the models, indicates that an

increase in bank roughness at the 0.5m scale results in an increase in erosion, and that this effect is stronger than the effect of changes in the 0.25m roughness scale and the 0.03m roughness scale. This seems to contradict the work of Leyland et al. (2015). In the Leyland model, increased roughness at the toe of the bank increases local form drag, thus slowing flows and reducing the erosion of the rough toe material, whereas in this study greater roughness is generating more erosion.

This seems to be in agreement with that of Das et al. (2019), who found that higher roughness at a very small scale resulted in greater eddy generation and thus greater erosion of rougher surfaces. Their work was conducted at the extremely fine sub-centimeter scale, but the results across the larger scales used in this study appear to support their findings, with even the smallest roughness scales still dominated by positive coefficients.

The results of interaction models to determine the effect of local roughness on the relationship between point roughness and erosion largely indicate that local roughness does not have an effect on the direction or strength of the relationship between point roughness and erosion but that point roughness will have the same effect on erosion whether or not the local roughness is greater 'high', 'average' or 'low' (where high roughness is +1SD above the mean, average roughness is within 1 SD of the mean and low roughness is -1SD below the mean).

However, there is an opportunity for further research to establish how smaller and larger definitions of 'local' erosion and 'local' roughness affect the strength of the observed relationship. The local neighbourhood in this work was defined based on the range of a semi-variogram, but future work should consider a series of arbitrary neighbourhoods to establish how strong the local erosion effect is.

The similarity between the R^2 values across all scales of roughness indicates that the control variable of local erosion has a strong and significant effect on the relationship between point roughness and erosion, and that this effect is likely stronger than the effect of roughness - both point and local - alone. This is to be expected, as soil properties and macro flow characteristics are likely to be very similar in similar locations thus resulting in similar erosion values close together. However, as with the effect of local roughness, the size of the neighbourhood used to determine what is 'local' erosion was decided based on a single value of semi-variogram range and further work should seek to identify the extent of neighbourhood size on on the definition of 'local' erosion.

Nested hierarchy of roughness scales

Following on from the individual models, interaction models were used to try and understand how the combination of roughness at different scales influenced the erosion. The results of these models were inconsistent, with some models showing that low roughness at the 0.5m and 0.25m roughness scales would result in a negative relationship between roughness at the 0.03m scale and erosion, but other models showing the reverse relationship.

Although the interaction models did result in a very slight (0.5%) increase in the predictive power of many of the models, the relatively low number of statistically significant interactions, makes it difficult to identify a pattern. The most commonly significant results show that the combination of low roughness at the 0.5m scale and high roughness at the 0.25m scale results in a positive relationship between roughness at the 0.03m scale and erosion. And that when the 0.5m roughness increases to around it's average, the slope coefficient of the relationship between roughness at the

0.03m scale and erosion falls. This indicates that as the 0.5m roughness values increases, while roughness remains high at the 0.25m scale, the strength of the relationship between roughness at the 0.03m scale and erosion falls. This was visible in the Bank 1 - E2, Bank 1 - E3, Bank 1 - E5, Bank 1 - E6, midstream Bank 3 - E4 and the All Bank 1 data. Where a negative relationship was shown, between the same combination of variables, there was still a decrease in the strength of the relationship from high 0.5m scale roughness to average 0.5m scale roughness, while 0.25m roughness remained high. This was visible in Bank 1 - E1, upstream Bank 3 - E2, All Bank 2 and Bank 3 - Upstream.

While the direction of the relationship may vary, the influence of increasing roughness at the 0.5m scale is consistent across the majority of models - a decrease in the strength of the relationship between roughness at the 0.03m scale and erosion. This again supports the results discussed in the previous section, that as 0.5m scale roughness increases erosion decreases but that this increased larger scale roughness also reduces the effect of smaller scale roughness on erosion.

Further work on these interactions is required to provide a greater understanding of the relationship between different scales of roughness and their influence on erosion. However, the results of this work appear to suggest that high roughness at the 0.5m scale represents a steeper slope to that large scale roughness element, which results in the creation of a steeper separation between the outer boundary layer region and the wake region. This weakens the effect of roughness at the 0.03m scale as separation has begun to occur prior to the peak of the smaller scale roughness element. This means that the wake region generated by the small scale roughness element sits inside the already created wake region formed by the larger element, where flow may have already been reduced below that

required for erosion (figure 5.40).

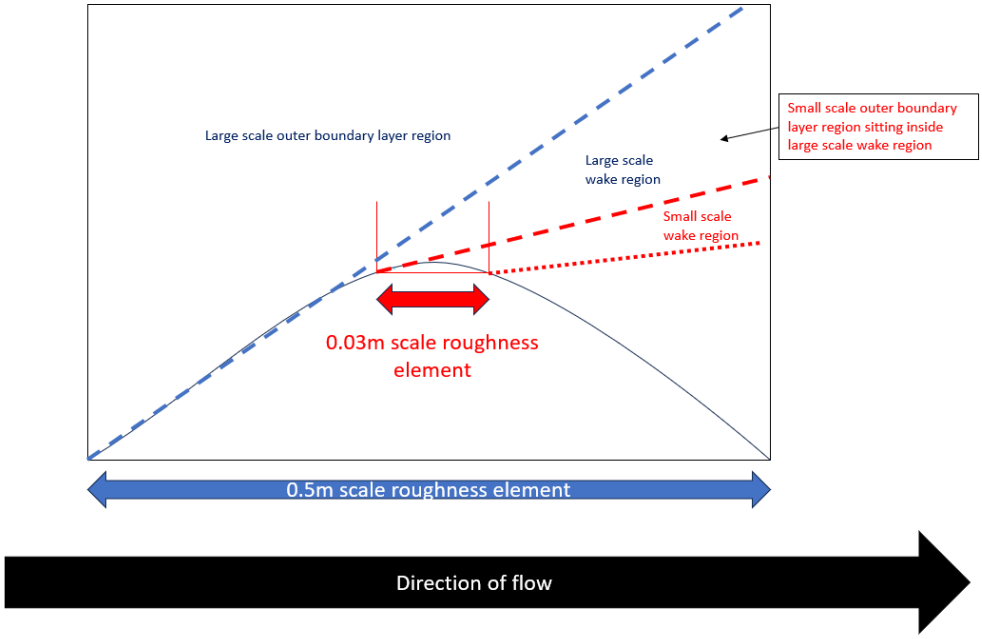

Figure 5.40: Conceptual diagram of the effect of high large scale roughness on flow separation and impact on effect of small scale roughness

However, where there is low roughness at the 0.5m scale, the formation of the outer boundary layer region is impacted less by the larger scale roughness element and the effect of the small scale roughness contributes to the formation of the wake region, resulting in a stronger relationship between the smaller scale roughness and erosion (figure 5.41).

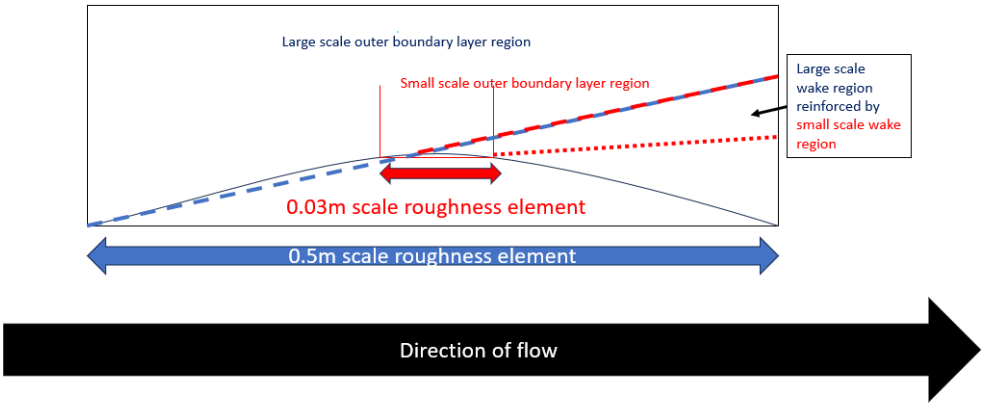

Figure 5.41: Conceptual diagram of the effect of low large scale roughness on flow separation and impact on effect of small scale roughness

5.5.3 Limitations

Defining variables

The three roughness scales chosen for this research - 0.5m, 0.25m and 0.03m - were chosen to represent large, medium and small scale roughness features on the bank. The large scale roughness value was selected to demonstrate the effect of bank roughness and not of the larger curved bank structure, which generates its own, much larger, flow deflection. Although the value of 0.5m was guided by the work of Kean and Smith (2006a) and Kean and Smith (2006b), who found that large scale curvature more than 5-10 roughness elements in length would have a minimal impact on localised flow resistance, the actual value was chosen arbitrarily to be viable across all banks, despite their differing amounts of curvature. The 0.25m roughness scale was chosen for very similar reasons and with the same overall goals of being viable across multiple banks with different levels of curvature. The 0.03m roughness scale was chosen to more directly mimic the work of Hopson (1999) (cited in Kean and Smith (2006a) and Kean and Smith (2006b)) who constructed roughness elements in a flume that were 3cm in height. Although these scales have provided an interesting new understanding of the impact of roughness on erosion, future work in this area should consider selecting roughness scales for study that are driven by the specific conditions of the banks being surveyed. Alternatively, a wider variety of scales could be analysed to better understand the influence of multiple roughness scales on erosion.

In order to establish the influence of roughness on fluvial erosion it was required to define what would represent the fluvial erosion zone. As has been discussed in previous chapters, the use of the Q10 level as the cut off point between fluvial and subaerial processes was largely arbitrary and

based on the balancing a need to identify an area of the bank that would be regularly exposed to the action of flow and the requirement for the bank to be exposed at the time of scanning. The Q10 value chosen was based on the long term flow regime, however to be more reflective of the specific conditions experienced by the bank between each scan period, the level chosen as the Q10 cut off should be based on the flow values experienced during that time period, and not on a long term flow pattern. This would allow a more accurate delineation of what areas of the bank have been exposed to fluvial action during the study time period, it would also allow for consistency if this study was to be extended to different sites and different environments.

5.5.4 Model definition and handling of spatial data

The decision to use a simple OLS regression model containing lagged dependent and independent variables was made in an effort to both account for the spatial autocorrelation of the data, but also to make use of the simplest technique to explain the relationship between erosion and roughness. The use of these lagged variables mimics the approach of the spatial Durbin model. Although the spatial Durbin model makes use of the lagged dependent and independent variables and also provides a mechanism to calculate direct and indirect effects of these variables on neighbouring cells, it is also a much more complex model to both generate and interpret while not providing significant benefit above alternatives such as the SLX model approach (Rüttenauer, 2022).

The SLX model was one of the options initially tested to account for the spatial autocorrelation within the data, however, there remained spatial autocorrelation within the residuals of the SLX model due to the unaccounted for autocorrelation associated with the dependent variable -

erosion -that is not included in the SLX model definition. As increasing numbers of studies utilise high to ultra-high resolution point data it is clear that methods for analysis that account for spatial autocorrelation but without data decimation must be more widely established. Up to now, the approaches used have been largely determined by researcher preference (Beale et al., 2010), however work by Kim (2021) indicates that the reduction in spatial autocorrelation in the residuals of different model types is a function of the degree and complexity of autocorrelation in the dependent and independent variables. With the inclusion two spatially lagged variables to the OLS model, the resulting Moran's I of residuals was very low, and therefore this approach is considered to have been a successful one.

5.6 Chapter Summary

This chapter has answered the final aim of this thesis, identifying to what extent bank roughness influences the rate of erosion. It is clear that there is a moderate to strong relationship between roughness and erosion at all scales, but that the relationship is marginally stronger at the 0.5m roughness scale than at the 0.25m and 0.03m scales. Although the relationship is stronger at the 0.5m scale, the results also indicate that the effect of roughness at the 0.25m scale is greater (larger slope coefficient) but that the strength of the relationship is not as high (lower R^2 values). There also appears to be an effect on the strength of the relationship between the 0.03m roughness scale and erosion when the 0.5m roughness scale increases from a low value to its average value. It has also shown that the effect of local roughness does not seem to change the relationship between point roughness and erosion. The final chapter will bring together and synthesise the results of both previous results chapters to discuss

the key outcomes from this research, as well as provide some suggestions for future work.

Chapter 6

Discussion and Conclusions

This chapter provides an overview of the aims and objectives for this research as introduced in Chapter 1 and gives a summary of the key findings of the preceding results chapters in relation to those aims and objectives. This is followed by a discussion of the overall success of this research. This section ends with an evaluation of the effectiveness of the chosen techniques and their limitations. Important areas for development will be highlighted, as well as additional potential areas for application of such techniques before a final conclusion brings this thesis to its close.

6.1 Aims and Objectives of this research

6.1.1 Research Aim and Objectives

As stated in Chapter 1, the overall aim of this research was; To use very-high-resolution remote sensing and change detection analysis to increase our understanding of the evolution of riverbank erosion processes and what role roughness plays in those processes. To achieve this overarching aim, the work was broken down into three main research objectives which became the aims for each individual results chapter;

1. To assess the relative importance of the three main erosion processes (sub-aerial, fluvial and mass-wasting) on the evolution of river bank surfaces.

2. To identify what conditions are responsible for the most significant amounts of bank change related to each of the three erosion processes.

3. To identify to what extent bank roughness influences the rate of fluvial erosion.

6.2 Summary of Key findings

6.2.1 Dominance of erosion processes

Bank erosion on the River Arrow during the study period was dominated by subaerial erosion processes, despite flows that reached the 0.08% exceedence level. Across all banks, the subaerial erosion contribution above the Q10 level was never less than 33% and was frequently identified as being responsible for more than 90% of the overall erosion. The fluvial erosion contribution was the lowest across all banks and all time periods, contributing a maximum of 26.9%, but frequently significantly less, while mass wasting exhibited a much more varied contribution across the different banks of interest, with no mass wasting events identified at Bank 2 during the whole study, and as much as 64% on Bank 3 during one of the time periods.

From these results, a model of erosion dominance was constructed, with the majority of points falling into the subaerial erosion dominant category (figure 6.1 and table 6.1).

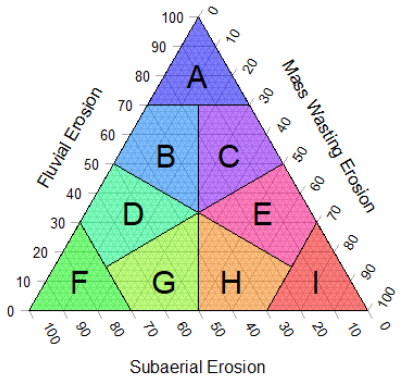

(a) Erosion dominance model

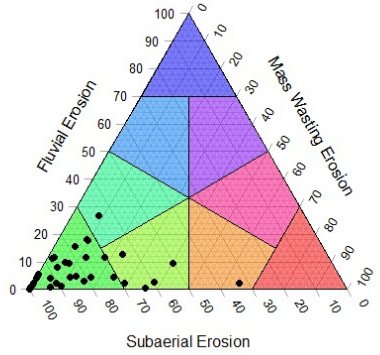

(b) Erosion dominance model with points representing the River Arrow data

Figure 6.1: Erosion dominance model (a) and model with points representing River Arrow data (b)

Table 6.1: Descriptions of the different sections of the proposed erosion dominance model shown in figure 6.1

Reference	Model Category	Category description
A	Fluvial Dominant	Fluvial Erosion contribution above 70% - Combined contribution of Subaerial and Mass Wasting processes <30%
B	Fluvial - Subaerial	Fluvial processes dominant (between 35-70%) - Contribution of Subaerial processes exceeds that of Mass Wasting
C	Fluvial - Mass Wasting	Fluvial processes dominant (between 35-70%) - Contribution of Mass Wasting exceeds that of Subaerial processes
D	Subaerial - Fluvial	Subaerial processes dominant (between 35-70%) - Contribution of Fluvial processes exceeds that of Mass Wasting
E	Mass Wasting - Fluvial	Mass Wasting dominant (between 35-70%) - Contribution of Fluvial processes exceeds that of Subaerial processes
F	Subaerial Dominant	Subaerial Erosion contribution above 70% - Combined contribution of Fluvial and Mass Wasting processes <30%
G	Subaerial - Mass Wasting	Subaerial processes dominant (between 35-70%) - Contribution of Mass Wasting exceeds that of Fluvial processes
H	Mass Wasting - Subaerial	Mass Wasting dominant (between 35-70%) - Contribution of Subaerial processes exceeds that of Fluvial processes
I	Mass Wasting Dominant	Mass Wasting contribution above 70% - Combined contribution of Fluvial and Subaerial processes <30%

6.2.2 Conditions generating most significant erosion

Although statistically significant relationships were identified between flow variables and erosion, the correlation values were highly inconsistent between different banks and bank sections, further evidencing the complexity of riverbank erosion processes and the challenges associated with identifying causal relationships between specific conditions and erosion. Backwards step-wise multiple regression generated a model containing minimum stage, peaks above Q10 level and mean discharge that explained 19.3% of net change and 23.3% of volume of change per year, but was not significant when used to model net change volume per m^2, or erosion below the Q10 level.

Similar to the flow variables, meteorological variables also exhibited a number of statistically significant correlations, however these were also not consistent across different banks or time periods. Hot hours seemed to generate the most consistent set of statistically significant regression values across the different sections of Bank 3, but the same strength of correlation was not evident at Banks 1 and 2. Another series of backwards, step-wise multiple regression was carried out on the meteorological variables and a model containing maximum temperature, total rainfall and average rainfall was derived that explained 19.7% of the subaerial erosion above the Q10 level. The same model also explained 23.7% of the total erosion volume and 19% of the subaerial erosion per m^2 but was not significant when used to model percentage contribution of subaerial erosion or mass wasting.

Given the extremely high collinearity between the different meteorological variables, a principal components analysis (PCA) was used to attempt to account for that. The PCA identified two components (shown in table 6.2

that explained 87.85% of the variance in the different meteorological conditions and these two components then explained 26.8% of subaerial erosion above the Q10 level. This was an improvement over standard multivariate linear regression of more than 7%, however it does still leave over 70% of the variation in subaerial erosion unaccounted for. This serves once again to illustrate the complexity of modelling and predicting erosion.

Table 6.2: Summary of independent meteorological variables contributing significantly to the Principal Components Analysis. Direction of the contribution is given in brackets.

PC1	PC2
Cold Hours (+)	Maximum Temperature (-)
Frost Days (+)	Average Rainfall (+)
Freeze Thaw Cycles (+)	Hot Hours (-)
Mean Temperature (-)	
Minimum Temperature (-)	
Total Rainfall (+)	
Wetting and Drying Cycles (+)	
Wet Days (+)	
Rain Hours (+)	

Finally, a model was constructed using the variables identified in the previous backwards step-wise regression approaches to create a combined flow and meteorological model to explain erosion and further model refinement was undertaken to give a final model containing maximum temperature, average rainfall, minimum stage, peaks above Q10 and mean discharge that explained 23.0% of the net erosion volume for the whole bank. This was an improvement on the individual flow and meteorological models.

This variation in the correlation values between erosion and flow and erosion and subaerial characteristics is similar to those reported by Couper and Maddock (2001) and Hamshaw et al. (2017), and they demonstrate the complex system of processes that are working continuously on banks to drive erosion. One area of study that was not undertaken as part of

this work was a quantification of the sediment types and sizes at the site, however in future work of this kind it would be advisable to consider establishing the types of sediment that exist across the different banks, as these have been proven to have significant impact on the spatial spread of erosion across even small areas of the bank (Veihe et al., 2011; Abidin et al., 2017).

In addition to assessments of erosion, the results of change detection identified large areas of deposition across the study banks during different time periods. A further set of regression models were run to try and establish the conditions that resulted in greatest deposition. A model containing mean temperature and total rainfall was able to explain 54.6% of the variation in deposition across the banks. Soil expansion as a result of freeze-thaw and wetting-drying processes was considered to be the most likely explanation of these deposition values (Couper, 2003; Ferreira et al., 2020) while the deposition of sediment from erosion further up the bank was also considered as a possible mechanism for deposition across the mid heights of the bank.

6.2.3 Impact of roughness on fluvial erosion

It was possible to determine roughness of the bank in the very small scale, and TLS techniques were deemed a successful data collection method, despite the loss of one Bank 3 data set due to an error that caused extremely high, and unsolvable, registration values. The relationship between roughness and erosion was statistically significant, with R-squared values ranging from 0.032 to 0.893. The model coefficients were dominated by positive values, with the 0.5m and 0.25 scales having 24 positive coefficients out of 30, and the 0.03m scale having fewer at 18 out of 30, however they still dominated. These positive coefficients indicate that as

roughness increases the erosion also increases.

The effect of local roughness on erosion was also measured through the use of lagged erosion variables calculated using the range values from semivariogram analysis. This demonstrated that the effect of local roughness was more varied than that of point roughness. The 0.5m scale local roughness had 18 negative coefficients, while the 0.25m and 0.03m local roughness had 19 negative and 10 negative coefficients respectively. This indicates that increasing local roughness at the 0.5m and 0.25m scale decreases erosion, while increasing local roughness at the 0.03m scale increases erosion.

Interaction models that consider the effect of the three different roughness scales in combination, did not identify a consistent pattern across all banks, but did show that the effects of interactions between roughness scales is significant in 16 out of 30 models. The most notable pattern in the interaction models seemed to show that increasing roughness at the 0.5m scale reduced the effect of roughness at the 0.03m scale and that this was most obvious when the 0.25m scale of roughness was also high.

Interactions that consider the effect of local roughness on the relationship between point roughness and erosion largely showed that local roughness does not have a strong effect, and that the relationship between point roughness remains broadly the same no matter whether local roughness is high, average or low.

These results seem broadly to support the work of Das et al. (2019) who found that increasing roughness at the very small scale generated micro-eddies that had greater erosive power and thus erosion increased. The same pattern can be identified here, where increasing point roughness increases the rate of erosion. However, the effect of local roughness, which

had more negative coefficients, is more supportive of the work of Kean and Smith (2006b), Nardi and Rinaldi (2010), Darby et al. (2010), and Leyland et al. (2015) who found that increasing roughness served to increase skin drag and thus reduce the erosive capability of the boundary layer and reduce erosion.

What is clear from this research is that the influence of roughness in 3-dimensions is highly variable and difficult to model and that further research is needed at these very high-resolution scales to help in developing our understanding of the effect of roughness at multiple scales on erosion. The novel nature of the work undertaken has resulted in some arguments being made with limited support from other research, and set an early basis from which further work in this area can progress, shedding yet more light on the influence of roughness on erosion at multiple scales across the complex bank surface.

6.2.4 Summary of study outcomes

This research has added to our understanding of the geomorphology of rivers in the following ways:

1. Development of scanning, processing and post processing methodology that allows for the generation of extremely high-resolution data on erosion and roughness of the bank surface.

2. Increased understanding of how each of the different erosion process contributes to overall bank erosion through the creation of an Erosion Dominance Model.

3. Increased understanding of the role of roughness in bank erosion.

4. The suggestion of a nested hierarchy of roughness scales through

which to further develop our understanding of the influence of roughness on erosion.

6.3 Effectiveness of TLS data collection and analysis

6.3.1 TLS data collection and preparation

Terrestrial Laser Scanning has been successfully used in river bank erosion studies for many years (e.g. Heritage and Hetherington (2007), Brodu and Lague (2012), Leyland et al. (2015), and Henshaw et al. (2013)) and this study made use of a number of existing data processing tools to generate the required information for analysis.

The first step was registration, which was carried out using the proprietary Leica Cyclone software (see Chapter 2, section 2.3.4 for detail of the registration process). The registration process was largely successful, however data collected at site 2 in February 2018 could not be used due to registration errors of over 18m. Visual inspection of the data found that there were no errors in the target naming protocol to explain such large registration errors. A number of methods were attempted to register the data, including manual point picking and automatic cloud-to-cloud registration in both Cyclone and CloudCompare. However, the lowest registration error that could be achieved was 0.012m and so the data was not deemed to be suitable for further analysis as this was a considerably larger error than much of the expected change values for the sites and was significantly larger than the registration errors of the remaining data sets.

However, at all sites and across all other time periods, the scanning pro-

tocol adapted from the work of Heritage and Hetherington, 2007 served to generate extremely dense point clouds with high spatial accuracy. Initially, the two sites were scanned over two days, however as user experience increased the field data could be collected in one day (approx. 10 hours). With increasing development of scanning equipment, particularly related to weight and ease of movement over rough terrain, this time could be decreased further, making the TLS a viable technique for bank erosion monitoring at shorter timescales.

6.3.2 Data analysis

Following data collection and registration the points were exported from Cyclone to CloudCompare for classification and change detection. Classification and change detection were both carried out using existing algorithms, CANUPO (Brodu and Lague, 2012) and M3C2 (Lague et al., 2013) (for a more detailed description of these techniques see Chapter 2). Both processes required multiple attempts utilising different parameters before an appropriate balance could be found between the processing time and the scale at which the data was being analysed. Given the spatial density of the data the final analysis time for the CANUPO classification at the chosen 50 scale classifier was over three hours per point cloud, however this was not deemed prohibitive as the difference between the processing times at the different scales was small ($<$15 minutes) and accuracy was prioritised over reduction of processing time in this case.

The processing time varied more significantly for the M3C2 technique, with some parameter combinations being abandoned after upwards of 36 hours of processing. The final combination of parameters resulted in a processing time of 7 hours per point cloud, but again this was not deemed to be prohibitive for this research.

Following the classification and change detection processes, the data was exported for statistical analysis in R. The voxelisation technique was successful in calculating the volume of erosion from individual point data and the run time for this process was under 15 minutes per point cloud. This voxelisation process generated over 350,00 voxels of data across the five bank segments, creating a statistically robust set of data for further analysis.

After the voxelisation process the first analysis of erosion was calculated. The first value acquired at this time was in excess of $5m^3$ at Bank 1 and $15m^3$ at Bank 3, an unrealistic value given the lack of any major areas of bank collapse or significant visual change. After further interrogation of the data, it was determined that there remained a small number of points representing vegetation or atmospheric returns in voxelised data. This had resulted in parts of the bank being more than 1 voxel 'thick', where the voxel at the 'back' of the data represented the bank and any voxels in front of that represented ones created from only one isolated point that had very high erosion values because of their distance from the bank. A simple additional step was added to the analysis to generate a representation of the bank that made use of the furthest voxel from the scanning origin and removed any others, creating a dataset that included only voxels that represent the very 'back' of the bank.

From there, the data analysis was typified by commonly used and robust statistical techniques that were easily transferable across multiple banks and repeatable across multiple time periods. The data generated by the TLS and voxelisation approaches meant that the roughness analysis could be carried out on a very large number of observations, however the need to summarise erosion, flow and meteorological values for each time period to compare erosion to the conditions experienced between scans meant that

those analyses were conducted on a very small number of observations, the potential limitations of which will be discussed in the next section.

Overall, the scanning methodology and data analysis techniques chosen were transferable and repeatable and generated data that was dense and suitable for a multitude of different statistical techniques. It is also evident that the techniques are sensitive enough to record sub-centimetre erosion values which could significantly decrease the time periods between scans and allow for much shorter times between scans. Future work in this field should build on the methods of Heritage and Hetherington (2007) and others (e.g. Brasington et al. (2012), Lague et al. (2013), Leyland et al. (2015), and Lague (2020)) to maximise the collection of highly dense, spatially accurate data that can be analysed at multiple scales to further expand our knowledge of erosion across whole bank faces.

6.4 Limitations of research

6.4.1 Continuous and discontinuous data and the problems of temporal scales

The ability to collect continuous, real-time hydrological and meteorological data has been a reality for some time. However, collecting continuous erosion data at high spatial resolutions is still a challenge. The PEEP system (Lawler, 1991) allows for the real-time measurement of erosion by inserting a photo-voltaic cell enclosed in glass into the bank in a similar way to the insertion of an erosion pin. Some of the limitations associated with this method have been discussed in the introduction, but by far the most significant is the need for the pin to be connected to a data logger to record the amount of electricity being generated by the cell as it is exposed to greater amounts of sunlight as more of the cell is exposed. This fact

makes PEEP systems more challenging to utilise - particularly in more challenging environments. The advantages of a remote sensing technique mean data can be recorded at a far higher spatial resolution, but there is no need to interact with the bank, which can itself cause more erosion to occur.

This study utilised very high spatial resolution data, however the time period between scans was often several months, and so nuances in the rate and spatial distribution of change were not observed. Increasing sensor accuracy means that the minimum level of detection for change is getting smaller and thus opening up new opportunities for evaluating change over smaller time periods (Hohenthal et al., 2011; Lague, 2020). More research is needed to understand the continuous processes that are working to change our river banks. Bank surveys carried out at much smaller time intervals would have the opportunity to establish the impact of the lower magnitude processes that are working constantly, and thus may open up new opportunities to limit undesirable bank erosion by reducing or mitigating these continuous processes .

In addition, the spatial distribution of apparent deposition across the different banks was not anticipated during this research and, although some attempt has been made to try to explain what may have caused such apparent deposition values to occur, it has not been satisfactorily explained. Similar results were found by Veihe et al. (2011) (figure 6.2) who stated that the mid-bank deposition readings at their site were often caused by failure of the upper bank. However they did also suggest that soil expansion as a result of changing water content and soil temperature could also be generating the appearance of deposition where not actual bank advance is occurring. Further research focused on the process of deposition of sediment, particularly on vertical or near-vertical banks. The ability to

observe these occurrences at a much shorter timescale may allow us to better identify the factors resulting in deposition, either by observing as bank expansion due to subaerial processes occurs or by observing the smaller bank failures depositing material on the lower bank face.

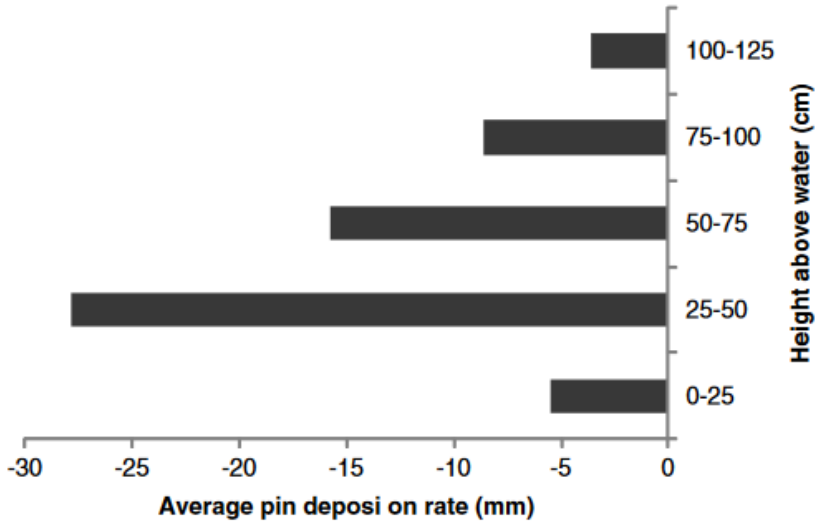

Figure 6.2: Deposition values at the Harrested Stream, Denmark from Veihe et al. (2011)

6.4.2 Spatial autocorrelation and dense spatial data

As has been discussed in Chapter 5, the problem of spatial autocorrelation is a tricky one. The assumptions of most statistical analyses is for variables to be independent (Miller, 2004). However, spatial data violates these assumptions, as described by Tobler's 'First Law of Geography' which states that "Everything is related to everything else; but near things are more related than distant things" (Tobler, 1970). The denser the spatial data we can achieve through improvements in LiDAR and TLS techniques, the greater the importance of utilising data analysis methods that suitably account for spatial autocorrelation. The use of the semivariogram is a common technique for removing autocorrelated data and leaving you with only points that are spatially independent of one another, however,

as seen in this study, that can result in needing to remove so much data that the benefits of high-resolution data collection are lost. Methods that maintain the full complexity of the data but that include lagged variables that represent the effect of spatial autocorrelation and limit spatial correlation in model residuals are becoming increasingly popular in spatial econometrics and should be further explored to determine how outcomes and predictions change dependent on the model used (Zhang et al., 2005; Mur and Angulo, 2006; Halleck Vega and Elhorst, 2015).

For future work, it would be highly valuable to run a series of different models on this data (e.g. Spatial Error, Spatial Lag of X and Spatial Durbin Models)) to determine how the approach taken here, the creation of lagged x and y variables based on the range from the semivariograms, compares to more 'sophisticated' model structures and how significant the benefit of using more complex modelling approaches actually is when considering increased complexity of model interpretation and the often higher model run-times. It would also be of interest to see how different methods for determining the 'neighbourhood' value would impact on the model outcomes and the model residuals.

6.5 Opportunities for future research

This research set out to understand the influence of different erosion processes on bank change, and how meteorological, hydrological and roughness conditions influenced the rate of erosion. In particular, the question of roughness and its influence on erosion has been a challenge to fully answer within this thesis, due to both time and word limit constraints. This discussion chapter has so far focused on the limitations associated with the work undertaken for this thesis. However, these limitations open up numerous opportunities for further study to fill the gaps in the knowledge

that this work has provided. Below represent this author's suggestions for further study to allow a fuller answer to the question posed in this work to be established.

1. Resolve the problem of temporal scale in erosion monitoring.

Improvements in scanning technology over the last 5+ years since the start of data collection for this thesis means that scanners are now becoming smaller, lighter and quicker to deploy, meaning that not only can they now be put to work in more difficult to access locations, they can also be used to undertake frequent modelling of lowland sites such as the River Arrow to begin to close the gap between low resolution erosion data and continuous data of meteorological and flow variables. Work should be undertaken to carry out a regular survey campaign of a number of river reaches at much shorter temporal scales. Weekly scanning of sites is now plausible and should be a high priority for improving understanding of the relationship between meteorological and hydrological processes and erosion.

Alternatively, scanning before and after storm events should also be considered as a priority to establish the role of high flows in removing material from the bank, however this should also be coupled with low flow scanning events to ensure that the effect of subaerial processes are properly accounted for.

2. Expand erosion dominance model to larger range of channel types.

The erosion dominance model proposed by this study has placed the lowland River Arrow consistently within the Subaerial Dominated category, with only a very small number of points (6 of 30) falling into other categories (Subaerial-Fluvial - 1 point, Subaerial-Mass Wasting - 4 points and Mass Wasting-Subaerial - 1 point). This holds with the work of Couper

and Maddock (2001) and Couper et al. (2002) who identified the site as being dominated by subaerial erosion process between 1999-2000. However, a wider range of stream types should be assessed to see whether this model could be used to extend our understanding of erosion dominance in different environments.

The concept of 'Process Dominance' was coined by Lawler (1992) and suggested that subaerial processes dominated in the upper reaches of rivers where rivers are small and discharges are low, fluvial processes dominate in the mid-reaches were discharge is higher but the bank heights are not high enough to trigger large scale collapse and that mass wasting processes dominate in the lower reaches where channel depth is such that bank stability becomes an issue. However, this research does not agree with the Lawler observations. To create a more robust model of erosion dominance, it must be further tested across a wider variety of sites and locations to establish whether an observable spatial pattern can be identified or whether the erosion process that dominates is based on more complex characteristics such as bank sediment, relative stream power or some other factor.

3. Increase understanding of the role of point vs local roughness on erosion. The influence of roughness on erosion has often been reduced to a series of Gaussian curves for modelling, however this work sought to establish the effect of roughness on erosion of the surface of interest. The inclusion of the effect of local roughness as a way to limit the spatial autocorrelation in the data also allowed for some indication of whether the effect of local roughness is more influential than that of the point roughness. It was broadly shown in this work that point roughness has a positive relationship with erosion - as point roughness increases so does erosion - while local erosion had a negative relationship with erosion - as

local roughness increased erosion decreases. However, there was significant variation throughout the data so this broad conclusion should be further tested to provide stronger evidence for the conclusions drawn. It is also important to note that this work was carried out on banks with similar soil structures and so future work in this area should consider banks of different structures and with different sediment types to establish whether the conclusions drawn here hold across different types of bank material.

There should also be further work to establish how we determine what is 'local'. In this study we used the range value from the semivariaogram, the distance value at which it is deemed that points no longer exert any influence on each other. That seems a logical choice for definition of the neighbourhood, however further study should be carried out to determine the effect of variation in the definition of the local neighbourhood.

4. Further investigation into the effect of roughness scales on erosion.

The final priority for future research should centre on the establishment of the influence of spatial scale on the relationship between roughness and erosion. This work used a series of three scale values - 0.03m, 0.25m and 0.5m, based upon the minimum and maximum scales used in other research - however these values were largely arbitrary. The influence of these different scales on erosion varied, with the 0.5m roughness scale having higher R^2 values than the 0.25m and 0.03m scales in the majority of cases. However the 0.25m scale had the highest mean model coefficient - indicating that as the 0.25m scale of roughness increased there was a larger corresponding increase in erosion that would be seen at the 0.5m and 0.03m scales. However the relationship was not as strong as the R^2

values for the 0.25m scale models were not as high.

The choice of scales used should be tested further to establish whether there is an 'optimum' scale that explains more of the erosion than others or a scale at which the effect of roughness is negligible. The arbitrary nature of the scales used may be masking an effect related to the wavelength of overall sinuosity of the bank or some other structural feature that has not been considered and so a deeper understanding of the importance of spatial scale in the establishment of roughness on a bank also needs further work. As with the previous opportunity, the conclusions drawn from this research are limited in support thanks to the novel nature of the work done and the analysis undertaken, so it is important that further work be done to establish whether the relationships observed on the River Arrow hold across different banks.

6.6 Final conclusions

Riverbanks are complex structures that experience pressures from a wide range of sources, including the meteorological, hydrological and anthropogenic. No one particular variable controls erosion and deposition within a river or it's margins due to the number and variety of the interactions between these different sources. However, this study has provided further evidence for the importance of sub-aerial processes as erosion agents in their own right, rather than as simply preparatory processes that cause banks to become more vulnerable to fluvially induced erosion. The proposed erosion dominance model of this paper builds on previous work by Lawler (1992), who proposed the concept of process dominance in bank erosion, however this model moves beyond the initial concept of process dominance being a function of stream power, but instead allows for a more complex combination of processes to be presented for different reaches.

This study focused only on the mid-reaches of a small lowland river, but with the addition of more sites to the model there is opportunity to refine and develop the model to more appropriately represent the character of the erosion dominance across multiple types of rivers and streams.

This work has also highlighted the importance of reconciling the problem of temporal scale of bank erosion studies if a deeper understanding of the influence of changing meteorological and hydrological processes is to be gained (Hoitink et al., 2020). The methods via which we record and measure bank erosion have evolved in recent years, with the proliferation of remote sensing techniques allowing for the collection of much greater volumes of data. This study has made use of an increasingly available technique, Terrestrial Laser Scanning, to detect sub-centimetre changes in the bank surface. The techniques used in this thesis have been based heavily on work conducted by Heritage and Hetherington (2007), and this remained a robust methodological approach to the collection of laser scanning data at the time of conducting the associated fieldwork. However, with the ever evolving nature of remote sensing technologies, the need for targets and manual tie points for registration is becoming less important as newer products come equipped with RTK-GPS and cloud recognition algorithms that allow for sub-centimeter accuracy automatic registration. With these advances come greater opportunities to scan areas of interest more frequently, as the burden of registration time is reduced and data processing can be done more rapidly. Thus, these technologies could be perfectly placed to help in resolving the problem of temporal scale that plagues research into bank erosion.

Finally, the influence of roughness has been an area of study for a number of years, with some of the most significant work having been undertaken by Kean and Smith (2006a) and Kean and Smith (2006b). However, much

of the work in this area has been undertaken in flume studies (e.g. Kean and Smith (2006a), Kean and Smith (2006b), Das et al. (2019), and Das et al. (2023), with only a limited number being undertaken in field studies (e.g. Darby et al. (2007), Darby et al. (2010), and Leyland et al. (2015)). However, those field studies have frequently focused on the effect of roughness elements that are reduced to a 2-dimensional form for the purposes of erosion modelling and have not considered the effect of the complex fabric of roughness that is exhibited by a natural river bank. This study has striven to explore the effect of roughness across multiple scales directly on the recorded erosion on the river bank and to generate a simple regression model to help explain how roughness is influencing erosion of the vertical bank face.

Ultimately, this work has added to the existing body of erosion research and provides a novel model with which to categorise the erosion processes that dominate across different banks. It provides yet more evidence for the utility and potential of TLS data for deepening our understanding of river-bank erosion, and seeks to use that data to open a new avenue of research on the importance of quantifying roughness as a complex, 3-dimensional structure exerting drag effects on boundary flow and thus providing a potential self-limiting effect on future erosion. It is hoped that this work will provide the impetus for further work in two main areas; 1) the refinement of the erosion dominance model to categorise the dominant erosion processes working on different types of river across different environments, and 2) further exploration of the real world effects of roughness on erosion of river banks.

Chapter 7

References

Abbas, G., Jomaa, S., Bronstert, A., and Rode, M. (2023). Downstream changes in riverbank sediment sources and the effect of catchment size. *Journal of Hydrology: Regional Studies* 46, p. 101340.

Abidin, R. Z., Sulaiman, M. S., and Yusoff, N. (2017). Erosion risk assessment: A case study of the Langat River bank in Malaysia. *International Soil and Water Conservation Research* 5(1), pp. 26–35.

Aktar, N. (2013). Impact of climate change on riverbank erosion. *International Journal of Sciences: Basic and Applied Research (IJSBAR)* 7(1), pp. 36–42.

Alexiou, S., Deligiannakis, G., Pallikarakis, A., Papanikolaou, I., Psomiadis, E., and Reicherter, K. (2021). Comparing high accuracy t-LiDAR and UAV-SfM derived point clouds for geomorphological change detection. *ISPRS International Journal of Geo-Information* 10(6), p. 367.

Allen, C. (1895). Protection of river banks at Ottumwa, Iowa. *Iowa Civil Engineers and Surveyors Society, Proc. 7th Annual*.

Allen, D. C., Datry, T., Boersma, K. S., Bogan, M. T., Boulton, A. J., Bruno, D., Busch, M. H., Costigan, K. H., Dodds, W. K., Fritz, K. M.,

et al. (2020). River ecosystem conceptual models and non-perennial rivers: a critical review. *Wiley Interdisciplinary Reviews: Water* 7(5), e1473.

Arnez Ferrel, K. R., Patsinghasanee, S., Kimura, I., and Shimizu, Y. (2018). Coupled model of bank erosion and meander evolution for cohesive riverbanks. *Geosciences* 8(10), p. 359.

Arora, S., Patel, H. K., Lade, A. D., and Kumar, B. (2023). Turbulence structure and bank erosion process in a dredged channel. *River Research and Applications* 39(4), pp. 613–628.

Avery, T. E. (1962). *Interpretation of aerial photographs*. Tech. rep.

Bangen, S. G., Wheaton, J. M., Bouwes, N., Bouwes, B., and Jordan, C. (2014). A methodological intercomparison of topographic survey techniques for characterizing wadeable streams and rivers. *Geomorphology* 206, pp. 343–361.

Beale, C. M., Lennon, J. J., Yearsley, J. M., Brewer, M. J., and Elston, D. A. (2010). Regression analysis of spatial data. *Ecology letters* 13(2), pp. 246–264.

Bjorneberg, D., Sojka, R., and Aase, J. (2002). PRE–WETTING EFFECT ON FURROW IRRIGATION EROSION: A FIELD STUDY. *Transactions of the ASAE* 45(3), p. 717.

Boon, P. (1998). River restoration in five dimensions. *Aquatic Conservation* 8(1), p. 257.

Boon, P., Calow, P., and Petts, G. (1992). Essential elements in the case for river conservation. In: *Unknown Host Publication Title*. John Wiley & Sons Ltd, Chichester, UK.

Borrelli, P., Robinson, D. A., Panagos, P., Lugato, E., Yang, J. E., Alewell, C., Wuepper, D., Montanarella, L., and Ballabio, C. (2020). Land use and climate change impacts on global soil erosion by water

(2015-2070). *Proceedings of the National Academy of Sciences* 117(36), pp. 21994–22001.

Brandt, S. A. (2000). Classification of geomorphological effects downstream of dams. *Catena* 40(4), pp. 375–401.

Brasington, J., Vericat, D., and Rychkov, I. (2012). Modeling river bed morphology, roughness, and surface sedimentology using high resolution terrestrial laser scanning. *Water Resources Research* 48(11).

Brils, J. (2008). Sediment monitoring and the European water framework directive. *Annali dell"Istituto Superiore di Sanita* 44(3).

Brodu, N. and Lague, D. (2012). 3D terrestrial lidar data classification of complex natural scenes using a multi-scale dimensionality criterion: Applications in geomorphology. *ISPRS Journal of Photogrammetry and Remote Sensing* 68, pp. 121–134.

Brown, L. E., Hannah, D. M., and Milner, A. M. (2009). ARISE: a classification tool for Alpine RIver and Stream Ecosystems. *Freshwater Biology* 54(6), pp. 1357–1369.

Buffington, J. M. and Montgomery, D. R. (1999). Effects of hydraulic roughness on surface textures of gravel-bed rivers. *Water Resources Research* 35(11), pp. 3507–3521.

Campbell, J. B. and Wynne, R. H. (2011). *Introduction to remote sensing*. Guilford Press.

Carling, P. (1988). Channel change and sediment transport in regulated UK rivers. *Regulated Rivers: Research & Management* 2(3), pp. 369–387.

Cashman, M. J., Gellis, A., Sanisaca, L. G., Noe, G. B., Cogliandro, V., and Baker, A. (2018). Bank-derived material dominates fluvial sediment in a suburban Chesapeake Bay watershed. *River Research and Applications* 34(8), pp. 1032–1044.

Cavalli, M. and Tarolli, P. (2011). Application of LiDAR technology for rivers analysis. *Italian Journal of Engineering Geology and Environment*, pp. 33–44.

Chandler, J., Ashmore, P., Paola, C., Gooch, M., and Varkaris, F. (2002). Monitoring river-channel change using terrestrial oblique digital imagery and automated digital photogrammetry. *Annals of the Association of American Geographers* 92(4), pp. 631–644.

Chappell, A. (2010). An Introduction to Geostatistics 24. *Key Methods in Geography*, p. 386.

Collins, A. L., Nadeb, P. S., Sear, D. A., Jones, J. I., Foster, I. D. L., and Morrow, K. J. H. P. (2011). Sediment targets for informing river catchment management: international experience and prospects. *Hydrological Processes* 25(13), pp. 2112–2129.

Congalton, R. G. and Green, K. (2019). *Assessing the accuracy of remotely sensed data: principles and practices*. CRC press.

Cook, K. L. (2017). An evaluation of the effectiveness of low-cost UAVs and structure from motion for geomorphic change detection. *Geomorphology* 278, pp. 195–208.

Correa, S. W., Mello, C. R., Chou, S. C., Curi, N., and Norton, L. D. (2016). Soil erosion risk associated with climate change at Mantaro River basin, Peruvian Andes. *CATENA* 147, pp. 110–124. ISSN: 0341-8162. DOI: https://doi.org/10.1016/j.catena.2016.07.003. URL: https://www.sciencedirect.com/science/article/pii/S0341816216302624.

Couper, P. (2003). Effects of silt–clay content on the susceptibility of river banks to subaerial erosion. *Geomorphology* 56(1-2), pp. 95–108.

Couper, P., Stott, T., and Maddock, I. (2002). Insights into river bank erosion processes derived from analysis of negative erosion-pin

recordings: observations from three recent UK studies. *Earth Surface Processes and Landforms* 27 (1), pp. 59–79.

Couper, P. R. and Maddock, I. P. (2001). Subaerial river bank erosion processes and their interaction with other bank erosion mechanisms on the River Arrow, Warwickshire, UK. *Earth Surface Processes and Landforms* 26 (6), pp. 631–646.

Darby, S. E., Rinaldi, M., and Dapporto, S. (2007). Coupled simulations of fluvial erosion and mass wasting for cohesive river banks. *Journal of Geophysical Research: Earth Surface* 112 (F3).

Darby, S. E., Trieu, H. Q., Carling, P. A., Sarkkula, J., Koponen, J., Kummu, M., Conlan, I., and Leyland, J. (2010). A physically based model to predict hydraulic erosion of fine-grained riverbanks: The role of form roughness in limiting erosion. *Journal of Geophysical Research: Earth Surface* 115 (F4).

Das, V. K., Debnath, K., and Sivakumar, B. (2023). On the evolution of turbulent characteristics of an eroding cohesive riverbank. *Stochastic Environmental Research and Risk Assessment* 37 (4), pp. 1371–1393.

Das, V. K., Roy, S., Barman, K., Chaudhuri, S., and Debnath, K. (2019). Study of clay–sand network structures and its effect on river bank erosion: an experimental approach. *Environmental Earth Sciences* 78, pp. 1–18.

De Rose, R. C. and Basher, L. R. (2011). Measurement of river bank and cliff erosion from sequential LIDAR and historical aerial photography. *Geomorphology* 126 (1-2), pp. 132–147.

Defersha, M., Quraishi, S., and Melesse, A. M. (2011). The effect of slope steepness and antecedent moisture content on interrill erosion, runoff and sediment size distribution in the highlands of Ethiopia. *Hydrology and Earth System Sciences*, pp. 2367–2375.

Devrani, R., Srivastava, P., Kumar, R., and Kasana, P. (2022). Characterization and assessment of flood inundated areas of lower Brahmaputra River Basin using multitemporal Synthetic Aperture Radar data: A case study from NE India. *Geological Journal* 57 (2), pp. 622–646.

Duong Thi, T. and Do Minh, D. (2019). Riverbank stability assessment under river water level changes and hydraulic erosion. *Water* 11 (12), p. 2598.

Duró, G., Crosato, A., Kleinhans, M., Roelvink, D., and Uijttewaal, W. (2020a). Bank erosion processes in regulated navigable rivers. *Journal of Geophysical Research: Earth Surface* 125 (7), e2019JF005441.

Duró, G., Crosato, A., Kleinhans, M. G., Winkels, T. G., Woolderink, H. A., and Uijttewaal, W. S. (2020b). Distinct patterns of bank erosion in a navigable regulated river. *Earth Surface Processes and Landforms* 45 (2), pp. 361–374.

Eitel, J. U., Williams, C. J., Vierling, L. A., Al-Hamdan, O. Z., and Pierson, F. B. (2011). Suitability of terrestrial laser scanning for studying surface roughness effects on concentrated flow erosion processes in rangelands. *Catena* 87 (3), pp. 398–407.

Environment Agency (2011). Sediment matters: A practical guide to sediment and its impacts in UK rivers. *Environment Agency, Research Project No: SC070024*.

European Union (2000). Directive 2000/60/EC (2000) of the European Parliament and of the Council of 23 October 2000 establishing a framework for Community action in the field of water policy (Water Framework Directive). *Official Journal of the European Communities C* L 327.

Faulkner, H. (2004). Piping hazard on collapsible and dispersive soils in Europe. In: *Soil erosion in Europe*. Ed. by J. Boardman and J. Poesen. John Wiley and Sons, Chichester, UK.

Ferreira, S. R. d. M., Araújo, A. G. D. d., Barbosa, F. A. S., Silva, T. C. R., and Bezerra, I. M. d. L. (2020). Analysis of changes in volume and propagation of cracks in expansive soil due to changes in water content. *Revista Brasileira de Ciência do Solo* 44.

Florsheim, J. L., Mount, J. F., and Chin, A. (2008). Bank erosion as a desirable attribute of rivers. *BioScience* 58(6), pp. 519–529.

Foerst, M. and Rüther, N. (2018). Bank Retreat and Streambank Morphology of a Meandering River during Summer and Single Flood Events in Northern Norway. *Hydrology* 5(4), p. 68.

Fox, G. A., Wilson, G. V., Simon, A., Langendoen, E. J., Akay, O., and Fuchs, J. W. (2007). Measuring streambank erosion due to ground water seepage: correlation to bank pore water pressure, precipitation and stream stage. *Earth Surface Processes and Landforms: The Journal of the British Geomorphological Research Group* 32(10), pp. 1558–1573.

Fox, G. A. and Wilson, G. (2010). The role of subsurface flow in hillslope and stream bank erosion: a review. *Soil Science Society of America Journal* 74(3), pp. 717–733.

Francalanci, S., Lanzoni, S., Solari, L., and Papanicolaou, A. (2020). Equilibrium cross section of river channels with cohesive erodible banks. *Journal of Geophysical Research: Earth Surface* 125(1), e2019JF005286.

Frankl, A., Stal, C., Abraha, A., Nyssen, J., Rieke-Zapp, D., De Wulf, A., and Poesen, J. (2015). Detailed recording of gully morphology in 3D through image-based modelling. *Catena* 127, pp. 92–101.

Girardeau-Montaut, D. (2016). *CloudCompareWiki*. URL: https://www.cloudcompare.org/doc/wiki/index.php/Main_Page. (accessed: 04/04/2016).

Grant, G. E., Schmidt, J. C., and Lewis, S. L. (2003). A geological framework for interpreting downstream effects of dams on rivers. *Water Science and Application* 7, pp. 209–225.

Gregory, K. J. and Lewin, J. (2014). *The basics of geomorphology: Key concepts*. Sage.

Grove, J., Croke, J., and Thompson, C. (2013). Quantifying different riverbank erosion processes during an extreme flood event. *Earth Surface Processes and Landforms* 38 (12), pp. 1393–1406.

Gutierrez, R., Gibeaut, J., Smyth, R., Hepner, T., Andrews, J., Weed, C., Gutelius, W., and Mastin, M. (2001). Precise airborne lidar surveying for coastal research and geo-hazards applications. *International Archives of Photogrammetry Remote Sensing and Spatial Information Sciences* 34 (3/W4), pp. 185–194.

Halleck Vega, S. and Elhorst, J. P. (2015). The SLX model. *Journal of Regional Science* 55 (3), pp. 339–363.

Hamshaw, S. D., Bryce, T., Rizzo, D. M., O'Neil-Dunne, J., Frolik, J., and Dewoolkar, M. M. (2017). Quantifying streambank movement and topography using unmanned aircraft system photogrammetry with comparison to terrestrial laser scanning. *River research and applications* 33 (8), pp. 1354–1367.

Harvey, G. L., Henshaw, A. J., Brasington, J., and England, J. (2019). Burrowing invasive species: An unquantified erosion risk at the aquatic-terrestrial interface. *Reviews of Geophysics* 57 (3), pp. 1018–1036.

Hassan, M. A. and Zimmermann, A. E. (2012). Channel response and recovery to changes in sediment supply. *Gravel-Bed Rivers: Processes, Tools, Environments*, pp. 464–473.

Henshaw, A. J., Thorne, C. R., and Clifford, N. J. (2013). Identifying causes and controls of river bank erosion in a British upland catchment. *Catena* 100, pp. 107–119.

Heritage, G. and Hetherington, D. (2007). Towards a protocol for laser scanning in fluvial geomorphology. *Earth Surface Processes and Landforms: The Journal of the British Geomorphological Research Group* 32 (1), pp. 66–74.

Heritage, G. L. and Milan, D. J. (2009). Terrestrial laser scanning of grain roughness in a gravel-bed river. *Geomorphology* 113 (1-2), pp. 4–11.

Hodge, R., Brasington, J., and Richards, K. (2009). In situ characterization of grain-scale fluvial morphology using Terrestrial Laser Scanning. *Earth Surface Processes and Landforms* 34 (7), pp. 954–968.

Hohenthal, J., Alho, P., Hyyppä, J., and Hyyppä, H. (2011). Laser scanning applications in fluvial studies. *Progress in Physical Geography* 35 (6), pp. 782–809.

Hoitink, A. J., Nittrouer, J. A., Passalacqua, P., Shaw, J. B., Langendoen, E. J., Huismans, Y., and Maren, D. S. van (2020). Resilience of river deltas in the Anthropocene. *Journal of Geophysical Research: Earth Surface* 125 (3), e2019JF005201.

Hooke, J. M. (1979). An analysis of the processes of river bank erosion. *Journal of hydrology* 42 (1-2), pp. 39–62.

Huff, T. P., Feagin, R. A., and Delgado, A. (2019). Understanding Lateral Marsh Edge Erosion with Terrestrial Laser Scanning (TLS). *Remote Sensing* 11 (19), p. 2208.

Hupp, C. R., Schenk, E. R., Richter, J. M., Peet, R. K., and Townsend, P. A. (2009). Bank erosion along the dam-regulated lower Roanoke River, North Carolina. *Management and restoration of fluvial systems with broad historical changes and human impacts* 451, pp. 97–108.

Immerzeel, W. W., Droogers, P., De Jong, S., and Bierkens, M. (2009). Large-scale monitoring of snow cover and runoff simulation in Himalayan river basins using remote sensing. *Remote sensing of Environment* 113(1), pp. 40–49.

Ireland, H. A., Sharpe, C. F. S., and Eargle, D. H. (1939). *Principles of gully erosion in the Piedmont of South Carolina*. 633. US Department of Agriculture.

James, G., Witten, D., Hastie, T., Tibshirani, R., et al. (2013). *An introduction to statistical learning*. Vol. 112. Springer.

Jones, J. I., Murphy, J., Collins, A., Sear, D., Naden, P., and Armitage, P. (2012). The impact of fine sediment on macro-invertebrates. *River research and applications* 28(8), pp. 1055–1071.

Joyce, K. E., Samsonov, S., Levick, S. R., Engelbrecht, J., and Belliss, S. (2014). Mapping and monitoring geological hazards using optical, LiDAR, and synthetic aperture RADAR image data. *Natural hazards* 73, pp. 137–163.

Jugie, M., Gob, F., Virmoux, C., Brunstein, D., Tamisier, V., Le Coeur, C., and Grancher, D. (2018). Characterizing and quantifying the discontinuous bank erosion of a small low energy river using Structure-from-Motion Photogrammetry and erosion pins. *Journal of hydrology* 563, pp. 418–434.

Julian, J. P. and Torres, R. (2006). Hydraulic erosion of cohesive riverbanks. *Geomorphology* 76(1-2), pp. 193–206.

Junk, W. J., Bayley, P. B., Sparks, R. E., et al. (1989). The flood pulse concept in river-floodplain systems. *Canadian special publication of fisheries and aquatic sciences* 106 (1), pp. 110–127.

Kean, J. W. and Smith, J. D. (2006a). Form drag in rivers due to small-scale natural topographic features: 1. Regular sequences. *Journal of Geophysical Research: Earth Surface* 111 (F4).

Kean, J. W. and Smith, J. D. (2006b). Form drag in rivers due to small-scale natural topographic features: 2. Irregular sequences. *Journal of Geophysical Research: Earth Surface* 111 (F4).

Kessler, A., Gupta, S., Dolliver, H., and Thoma, D. (2012). Lidar quantification of bank erosion in Blue Earth County, Minnesota. *Journal of Environmental Quality* 41 (1), pp. 197–207.

Kessler, A. C., Gupta, S. C., and Brown, M. K. (2013). Assessment of river bank erosion in Southern Minnesota rivers post European settlement. *Geomorphology* 201, pp. 312–322.

Kim, D. (2021). Predicting the magnitude of residual spatial autocorrelation in geographical ecology. *Ecography* 44 (7), pp. 1121–1130.

Kinnell, P. (2005). Raindrop-impact-induced erosion processes and prediction: a review. *Hydrological Processes: An International Journal* 19 (14), pp. 2815–2844.

Kiosses, C., Tamparopoulos, A., Tufekcioglu, M., and Zaimes, G. N. (2020). Using a 7-year timeseries of erosion pin data to evaluate the important factors for stream bank erosion and deposition. In: *Environmental Toxicants in Freshwater and Marine Ecosystems in the Black Sea Basin*, pp. 87–88.

Koehl, M., Piasny, G., Thomine, V., Garambois, P.-A., Finaud-Guyot, P., Guillemin, S., and Schmitt, L. (2020). 4D GIS FOR MONITORING

RIVER BANK EROSION AT MEANDER BEND SCALE: CASE OF MOSELLE RIVER. *International Archives of the Photogrammetry, Remote Sensing & Spatial Information Sciences*.

Kondolf, G. M. and Piégay, H. (2016). Tools in fluvial geomorphology: problem statement and recent practice. *Tools in fluvial geomorphology*, pp. 1–12.

Konsoer, K. M., Rhoads, B. L., Langendoen, E. J., Best, J. L., Ursic, M. E., Abad, J. D., and Garcia, M. H. (2016). Spatial variability in bank resistance to erosion on a large meandering, mixed bedrock-alluvial river. *Geomorphology* 252, pp. 80–97.

Kuznetsova, Y., Golosov, V., Tsyplenkov, A., and Ivanova, N. (2019). Quantifying channel bank erosion of a small mountain river in Russian wet subtropics using erosion pins. *Proceedings of the International Association of Hydrological Sciences* 381, pp. 79–86.

Lague, D. (2020). Terrestrial laser scanner applied to fluvial geomorphology. In: *Developments in Earth Surface Processes*. Vol. 23. Elsevier, pp. 231–254.

Lague, D., Brodu, N., and Leroux, J. (2013). Accurate 3D comparison of complex topography with terrestrial laser scanner: Application to the Rangitikei canyon (NZ). *ISPRS journal of photogrammetry and remote sensing* 82, pp. 10–26.

Lane, E. W. (1955). Importance of fluvial morphology in hydraulic engineering. *Proceedings (American Society of Civil Engineers); v. 81, paper no. 745*.

Lane, S., Tayefi, V., Reid, S., Yu, D., and Hardy, R. (2007). Interactions between sediment delivery, channel change, climate change and flood risk in a temperate upland environment. *Earth Surface Processes and*

Landforms: The Journal of the British Geomorphological Research Group 32 (3), pp. 429–446.

Lane, S. N., Westaway, R. M., and Murray Hicks, D. (2003). Estimation of erosion and deposition volumes in a large, gravel-bed, braided river using synoptic remote sensing. *Earth surface processes and landforms: the journal of the British Geomorphological Research Group* 28 (3), pp. 249–271.

Langat, P. K., Kumar, L., and Koech, R. (2019). Monitoring river channel dynamics using remote sensing and GIS techniques. *Geomorphology* 325, pp. 92–102.

Lausch, A. (1970). Assessment of landscape pattern and landscape functions by application of GIS and remote sensing. *WIT Transactions on Ecology and the Environment* 46.

Lawler, D. (1991). A new technique for the automatic monitoring of erosion and deposition rates. *Water resources research* 27 (8), pp. 2125–2128.

Lawler, D. (1992). *Process dominance in bank erosion systems*, pp. 117–143.

Lawler, D. (1993). The measurement of river bank erosion and lateral channel change: a review. *Earth surface processes and landforms* 18 (9), pp. 777–821.

Lawler, D. (1994). Temporal variability in streambank response to individual flow events: the River Arrow, Warwickshire, UK. *IAHS Publications-Series of Proceedings and Reports-Intern Assoc Hydrological Sciences* 224, pp. 171–180.

Lawler, D. (2008). Advances in the continuous monitoring of erosion and deposition dynamics: Developments and applications of the new PEEP-3T system. *Geomorphology* 93 (1-2), pp. 17–39.

Lawler, D., Grove, J., Couperthwaite, J., and Leeks, G. (1999). Downstream change in river bank erosion rates in the Swale–Ouse system, northern England. *Hydrological processes* 13(7), pp. 977–992.

Lawler, D., Thorne, C., and Hooke, J. (1997). Bank Erosion and Instability. In: *Applied Fluvial Geomorphology for River Engineering and Management*. Ed. by C. Thorne, R. Hey, and M. Newson. New York: John Wiley and Sons, pp. 137–172.

Leica Geosystems (2012a). *Cyclone*. English. Version Version 9.3.0. Leica Geosystems.

Leica Geosystems (2012b). *Leica ScanStation C10/C5: User Manual*. English. Version Version 5.0. Leica Geosystems. 151 pp.

Leopold, L. B. and Wolman, M. G. (1957). *River channel patterns: braided, meandering, and straight*. US Government Printing Office.

Leyland, J., Darby, S. E., Teruggi, L., Rinaldi, M., and Ostuni, D. (2015). A self-limiting bank erosion mechanism? inferring temporal variations in bank form and skin drag from high resolution topographic data. *Earth Surface Processes and Landforms* 40(12), pp. 1600–1615.

Li, L., Ni, J., Chang, F., Yue, Y., Frolova, N., Magritsky, D., Borthwick, A. G., Ciais, P., Wang, Y., Zheng, C., et al. (2020). Global trends in water and sediment fluxes of the world's large rivers. *Science Bulletin* 65(1), pp. 62–69.

Li, X., Cooper, J. R., and Plater, A. J. (2021). Quantifying erosion hazards and economic damage to critical infrastructure in river catchments: Impact of a warming climate. *Climate Risk Management* 32, p. 100287.

Liang, S. and Wang, J. (2019). *Advanced remote sensing: terrestrial information extraction and applications*. Academic Press.

Liu, H., Du, J., and Yi, Y. (2022). Reconceptualising flood risk assessment by incorporating sediment supply. *Catena* 217, p. 106503.

Longoni, L., Papini, M., Brambilla, D., Barazzetti, L., Roncoroni, F., Scaioni, M., and Ivanov, V. I. (2016). Monitoring riverbank erosion in mountain catchments using terrestrial laser scanning. *Remote Sensing* 8 (3), p. 241.

Lowe, J. A., Bernie, D., Bett, P., Bricheno, L., Brown, S., Calvert, D., Clark, R., Eagle, K., Edwards, T., Fosser, G., et al. (2018). UKCP18 science overview report. *Met Office Hadley Centre: Exeter, UK*.

Lu, D., Mausel, P., Brondizio, E., and Moran, E. (2004). Change detection techniques. *International journal of remote sensing* 25 (12), pp. 2365–2401.

Mathers, K. L., Doretto, A., Fenoglio, S., Hill, M. J., and Wood, P. J. (2022). Temporal effects of fine sediment deposition on benthic macroinvertebrate community structure, function and biodiversity likely reflects landscape setting. *Science of the Total Environment* 829, p. 154612.

Mathers, K., Collins, A., England, J., Brierley, B., and Rice, S. (2017). *The fine sediment conundrum; quantifying, mitigating and managing the issues*.

McKenzie, M., Mathers, K. L., Wood, P. J., England, J., Foster, I., Lawler, D., and Wilkes, M. (2020). Potential physical effects of suspended fine sediment on lotic macroinvertebrates. *Hydrobiologia* 847 (3), pp. 697–711.

Meade, R. H. (1982). Sources, sinks, and storage of river sediment in the Atlantic drainage of the United States. *The Journal of Geology* 90 (3), pp. 235–252.

Midgley, T. L., Fox, G. A., and Heeren, D. M. (2012). Evaluation of the bank stability and toe erosion model (BSTEM) for predicting lateral retreat on composite streambanks. *Geomorphology* 145, pp. 107–114.

Milan, D. J., Heritage, G. L., and Hetherington, D. (2007). Application of a 3D laser scanner in the assessment of erosion and deposition volumes and channel change in a proglacial river. *Earth Surface Processes and Landforms: The Journal of the British Geomorphological Research Group* 32 (11), pp. 1657–1674.

Miller, H. J. (2004). Tobler's first law and spatial analysis. *Annals of the association of American geographers* 94 (2), pp. 284–289.

Milner, V. S., Maddock, I. P., Jones, I., and Bunting, G. C. (2021). Do legacy effects of deposited fine sediment influence the ecological response of drifting invertebrates to a fine sediment pulse? *Aquatic Sciences* 83 (4), pp. 1–14.

Morche, D., Schmidt, K.-H., Sahling, I., Herkommer, M., and Kutschera, J. (2008). Volume changes of Alpine sediment stores in a state of post-event disequilibrium and the implications for downstream hydrology and bed load transport. *Norsk Geografisk Tidsskrift-Norwegian Journal of Geography* 62 (2), pp. 89–101.

Mur, J. and Angulo, A. (2006). The spatial Durbin model and the common factor tests. *Spatial Economic Analysis* 1 (2), pp. 207–226.

Myers, D. T., Rediske, R. R., and McNair, J. N. (2019). Measuring streambank erosion: A comparison of erosion pins, total station, and terrestrial laser scanner. *Water* 11 (9), p. 1846.

Nardi, L., Campo, L., and Rinaldi, M. (2013). Quantification of riverbank erosion and application in risk analysis. *Natural hazards* 69 (1), pp. 869–887.

Nardi, L. and Rinaldi, M. (2010). Modelling riverbank retreat by combining reach-scale hydraulic models with bank-scale erosion and stability analyses. In: *River Flow*. Vol. 2014. Bundesanstalt für Wasserbau Braunschweig, pp. 1286–1291.

Nardi, L., Rinaldi, M., and Solari, L. (2012). An experimental investigation on mass failures occurring in a riverbank composed of sandy gravel. *Geomorphology* 163, pp. 56–69.

National Oceanic and Atmosperic Association (2019). *What is Remote Sensing?* URL: https://oceanservice.noaa.gov/facts/remotesensing.html#:~:text=Remote%5C%20sensing%5C%20is%5C%20the%5C%20science,by%5C%20NOAA's%5C%20National%5C%20Geodetic%5C%20Survey.. (accessed 21/09/2020).

National River Flow Archive (2023). *Catchment Statistics - 54107 - Arrow at Studley*. URL: https://nrfa.ceh.ac.uk/data/station/spatial/54107. (accessed 13/04/2023).

Nearing, M., Pruski, F., and O'neal, M. (2004). Expected climate change impacts on soil erosion rates: a review. *Journal of soil and water conservation* 59 (1), pp. 43–50.

Nilsson, C., Jansson, R., Malmqvist, B., and Naiman, R. J. (2007). Restoring riverine landscapes: the challenge of identifying priorities, reference states, and techniques. *Ecology and Society* 12 (1).

Nones, M. (2019). Dealing with sediment transport in flood risk management. *Acta Geophysica* 67 (2), pp. 677–685.

O'Neal, M. A. and Pizzuto, J. E. (2011). The rates and spatial patterns of annual riverbank erosion revealed through terrestrial laser-scanner surveys of the South River, Virginia. *Earth Surface Processes and Landforms* 36 (5), pp. 695–701.

Office for Environmental Protection (2022). Available at https://www.theoep.org.uk/office-environmental-protection. Accessed on 11th October 2022.

Okhravi, S. (2022). The use of the Manning equation is not safe for different river types. What are the alternatives. In: *Proc. 34 th Conference of Young Hydrologists Professionals in Water Sciences. International Hydrological Program of UNESCO, Slovak Hydrometeorological Institute, November*. Vol. 10.

Olea, R. A. (2006). A six-step practical approach to semivariogram modeling. *Stochastic Environmental Research and Risk Assessment* 20 (5), pp. 307–318.

Osman, A. M. and Thorne, C. R. (1988). Riverbank stability analysis. I: Theory. *Journal of Hydraulic Engineering* 114 (2), pp. 134–150.

Otepka, J., Ghuffar, S., Waldhauser, C., Hochreiter, R., and Pfeifer, N. (2013). Georeferenced point clouds: A survey of features and point cloud management. *ISPRS International Journal of Geo-Information* 2 (4), pp. 1038–1065.

Owens, P. N. (2020). Soil erosion and sediment dynamics in the Anthropocene: a review of human impacts during a period of rapid global environmental change. *Journal of Soils and Sediments* 20, pp. 4115–4143.

Owens, P., Batalla, R., Collins, A., Gomez, B., Hicks, D., Horowitz, A., Kondolf, G., Marden, M., Page, M., Peacock, D., et al. (2005). Fine-grained sediment in river systems: environmental significance and management issues. *River research and applications* 21 (7), pp. 693–717.

Painter, R., Blyth, K., Mosedale, J., and Kelly, i. (1974). The effect of afforestation on erosion processes and sediment yield. *Effects of Man on the Interface of the Hydrological Cycle with the Physical Environment* 113, pp. 150–157.

Parker, C., Simon, A., and Thorne, C. R. (2008). The effects of variability in bank material properties on riverbank stability: Goodwin Creek, Mississippi. *Geomorphology* 101 (4), pp. 533–543.

Partheniades, E. (1965). Erosion and deposition of cohesive soils. *Journal of the Hydraulics Division* 91 (1), pp. 105–139.

Patsinghasanee, S., Kimura, I., Shimizu, Y., and Nabi, M. (2017). Cantilever failure investigations for cohesive riverbanks. In: *Proceedings of the Institution of Civil Engineers-Water Management*. Vol. 170. 2. Thomas Telford Ltd, pp. 93–108.

Petts, G. E. (1979). Complex response of river channel morphology subsequent to reservoir construction. *Progress in Physical Geography* 3 (3), pp. 329–362.

Phillips, J. D. and Slattery, M. C. (2006). Sediment storage, sea level, and sediment delivery to the ocean by coastal plain rivers. *Progress in Physical Geography* 30 (4), pp. 513–530.

Picco, L., Mao, L., Cavalli, M., Buzzi, E., Rainato, R., and Lenzi, M. (2013). Evaluating short-term morphological changes in a gravel-bed braided river using terrestrial laser scanner. *Geomorphology* 201, pp. 323–334.

Piégay, H., Darby, S., Mosselman, E., and Surian, N. (2005). A review of techniques available for delimiting the erodible river corridor: a sustainable approach to managing bank erosion. *River research and applications* 21 (7), pp. 773–789.

Pinter, N. and Heine, R. A. (2005). Hydrodynamic and morphodynamic response to river engineering documented by fixed-discharge analysis, Lower Missouri River, USA. *Journal of Hydrology* 302 (1-4), pp. 70–91.

Pizzuto, J. E. (1994). Channel adjustments to changing discharges, Powder River, Montana. *Geological Society of America Bulletin* 106(11), pp. 1494–1501.

Podger, G. M., Ahmad, M.-D., Yu, Y., Stewart, J. P., Shah, S. M. M. A., and Khero, Z. I. (2021). Development of the Indus River system model to evaluate reservoir sedimentation impacts on water security in Pakistan. *Water* 13(7), p. 895.

Poff, N. L., Allan, J. D., Bain, M. B., Karr, J. R., Prestegaard, K. L., Richter, B. D., Sparks, R. E., and Stromberg, J. C. (1997). The natural flow regime. *BioScience* 47(11), pp. 769–784.

Polcyn, F. C. and Rollin, R. (1969). *Remote sensing techniques for the location and measurement of shallow-water features*. Tech. rep.

Pollen-Bankhead, N. and Simon, A. (2010). Hydrologic and hydraulic effects of riparian root networks on streambank stability: Is mechanical root-reinforcement the whole story? *Geomorphology* 116(3-4), pp. 353–362.

Pratomo, D., Putranto, B., and Khomsin (2019). Analysis of the green light penetration from Airborne LiDAR Bathymetry in Shallow Water Area. 389(1), p. 012003.

Prosser, I. P., Hughes, A. O., and Rutherfurd, I. D. (2000). Bank erosion of an incised upland channel by subaerial processes: Tasmania, Australia. *Earth Surface Processes and Landforms: The Journal of the British Geomorphological Research Group* 25(10), pp. 1085–1101.

RESTORE Partnership (2013). *Rivers by Design:Rethinking Development and River Restoration*. Tech. rep. Environment Agency.

Rhoades, E. L., O'Neal, M. A., and Pizzuto, J. E. (2009). Quantifying bank erosion on the South River from 1937 to 2005, and its importance in assessing Hg contamination. *Applied Geography* 29(1), pp. 125–134.

Rinaldi, M. and Casagli, N. (1999). Stability of streambanks formed in partially saturated soils and effects of negative pore water pressures: the Sieve River (Italy). *Geomorphology* 26(4), pp. 253–277.

Rinaldi, M. and Darby, S. E. (2007). Modelling river-bank-erosion processes and mass failure mechanisms: progress towards fully coupled simulations. *Developments in Earth Surface Processes* 11, pp. 213–239.

Rollet, A., Piégay, H., Dufour, S., Bornette, G., and Persat, H. (2014). Assessment of consequences of sediment deficit on a gravel river bed downstream of dams in restoration perspectives: application of a multicriteria, hierarchical and spatially explicit diagnosis. *River Research and Applications* 30(8), pp. 939–953.

Rouse, H. (1965). Critical analysis of open-channel resistance. *Journal of the Hydraulics Division* 91(4), pp. 1–23.

Rüttenauer, T. (2022). Spatial regression models: a systematic comparison of different model specifications using Monte Carlo experiments. *Sociological Methods & Research* 51(2), pp. 728–759.

Samadi, S., Davoudi, M., and Amiri-Tokaldany, E. (2011). Experimental study of cantilever failure in the upper part of cohesive riverbanks. *Research Journal of Environmental Sciences* 5(5), p. 444.

Saputro, D., Muhsinin, R., Widyaningsih, P., et al. (2019). Spatial autoregressive with a spatial autoregressive error term model and its parameter estimation with two-stage generalized spatial least square procedure. In: *Journal of Physics: Conference Series*. Vol. 1217. 1. IOP Publishing, p. 012104.

Saylam, K., R. Averett, A., Costard, L., D. Wolaver, B., and Robertson, S. (2020). Multi-sensor approach to improve bathymetric lidar mapping

of semi-arid groundwater-dependent streams: Devils River, Texas. *Remote Sensing* 12 (15), p. 2491.

Simon, A., Collison, A. J., and Layzell, A. (2003). Incorporating bank-toe erosion by hydraulic shear into the ARS bank-stability model: Missouri River, Eastern Montana. In: *World Water & Environmental Resources Congress 2003*, pp. 1–11.

Simon, A., Curini, A., Darby, S. E., and Langendoen, E. J. (2000). Bank and near-bank processes in an incised channel. *Geomorphology* 35 (3-4), pp. 193–217.

Smith, J. D. and McLean, S. (1977). Spatially averaged flow over a wavy surface. *Journal of Geophysical research* 82 (12), pp. 1735–1746.

Smith, M. W., Cox, N. J., and Bracken, L. J. (2007). Applying flow resistance equations to overland flows. *Progress in Physical Geography* 31 (4), pp. 363–387.

Sutarto, T., Papanicolaou, A., and Wilson, C. (2020). Low amplitude of streambank erosion: distinguishing mass and surface fluvial erosions. In: *IOP Conference Series: Earth and Environmental Science*. Vol. 451. 1. IOP Publishing, p. 012093.

Taylor, K. G. and Owens, P. N. (2009). Sediments in urban river basins: a review of sediment–contaminant dynamics in an environmental system conditioned by human activities. *Journal of Soils and Sediments* 9 (4), pp. 281–303.

The Water Environment (Water Framework Directive) (England and Wales) Regulations 2017. Available at https://www.legislation.gov.uk/uksi/2017/407/made. Accessed on 11th October 2022.

The Water Environment (Water Framework Directive) Regulations (Northern Ireland) 2017. Available at

legislation.gov.uk/nisr/2017/81/contents/made. Accessed on 11th October 2022.

Thorn, C. E. and Welford, M. R. (1994). The Equilibrium Concept in Geomorphology. *Annals of the Association of American Geographers* 84 (4). Publisher: [Association of American Geographers, Taylor & Francis, Ltd.], pp. 666–696. ISSN: 0004-5608. URL: https://www.jstor.org/stable/2564149 (visited on 08/01/2022).

Thorne, C., Wallerstein, N., Soar, P., Brookes, A., Wishart, D., Biedenharn, D., Gibson, S., Little Jr, C., Mooney, D., Watson, C. C., et al. (2010). Accounting for sediment in flood risk management. *Flood risk science and management*, pp. 87–113.

Thorne, C. R. and Tovey, N. K. (1981). Stability of composite river banks. *Earth Surface Processes and Landforms* 6 (5), pp. 469–484.

Tobler, W. R. (1970). A computer movie simulating urban growth in the Detroit region. *Economic geography* 46 (sup1), pp. 234–240.

Tomsett, C. and Leyland, J. (2019). Remote sensing of river corridors: A review of current trends and future directions. *River Research and Applications* 35 (7), pp. 779–803.

Trimble, S. W. (1975). Denudation studies: can we assume stream steady state? *Science* 188 (4194), pp. 1207–1208.

Trimble, S. W. (1983). A sediment budget for Coon Creek basin in the Driftless Area, Wisconsin, 1853-1977. *American Journal of Science* 283 (5), pp. 454–474.

Tsouchlaraki, A. and Achilleos, G. (1970). Spatial analysis of visual environmental information in urban landscapes: attempting to detect homogeneous areas through a GIS. *WIT Transactions on Ecology and the Environment* 84.

Van Rijn, L. C. et al. (1993). *Principles of sediment transport in rivers, estuaries and coastal seas*. Vol. 1006. Aqua publications Amsterdam.

Vannote, R. L., Minshall, G. W., Cummins, K. W., Sedell, J. R., and Cushing, C. E. (1980). The river continuum concept. *Canadian journal of fisheries and aquatic sciences* 37 (1), pp. 130–137.

Veihe, A., Jensen, N. H., Schiøtz, I. G., and Nielsen, S. L. (2011). Magnitude and processes of bank erosion at a small stream in Denmark. *Hydrological Processes* 25 (10), pp. 1597–1613.

Venter, O., Sanderson, E. W., Magrach, A., Allan, J. R., Beher, J., Jones, K. R., Possingham, H. P., Laurance, W. F., Wood, P., Fekete, B. M., et al. (2016). Sixteen years of change in the global terrestrial human footprint and implications for biodiversity conservation. *Nature communications* 7 (1), p. 12558.

Vietz, G. J., Lintern, A., Webb, J. A., and Straccione, D. (2018). River bank erosion and the influence of environmental flow management. *Environmental management* 61 (3), pp. 454–468.

Visser, F., Woodget, A., Skellern, A., Forsey, J., Warburton, J., and Johnson, R. (2019). An evaluation of a low-cost pole aerial photography (PAP) and structure from motion (SfM) approach for topographic surveying of small rivers. *International Journal of Remote Sensing* 40 (24), pp. 9321–9351.

Vörösmarty, C. J., Meybeck, M., Fekete, B., Sharma, K., Green, P., and Syvitski, J. P. (2003). Anthropogenic sediment retention: major global impact from registered river impoundments. *Global and planetary change* 39 (1-2), pp. 169–190.

Walling, D. E. and Collins, A. L. (2005). Suspended sediment sources in British rivers. *Sediment budgets* 1 (291), pp. 2005123–33.

Walling, D. E., Owens, P. N., and Leeks, G. J. (1999). Fingerprinting suspended sediment sources in the catchment of the River Ouse, Yorkshire, UK. *Hydrological processes* 13 (7), pp. 955–975.

Wang, Q., Liu, J., Wu, L., Xu, Z., Fan, S., and Qian, A. (2016). Analysis of gully erosion hazard using high resolution terrestrial LiDAR. In: *2016 IEEE International Geoscience and Remote Sensing Symposium (IGARSS)*. IEEE, pp. 7469–7472.

Ward, J. (1989). The four-dimensional nature of lotic ecosystems. *Journal of the North American Benthological Society* 8 (1), pp. 2–8.

Water Environment and Water Services (Scotland) Act 2003. Available at https://www.legislation.gov.uk/asp/2003/3/contents. Accessed on 11th October 2022.

Weng, Q. (2002). Land use change analysis in the Zhujiang Delta of China using satellite remote sensing, GIS and stochastic modelling. *Journal of environmental management* 64 (3), pp. 273–284.

Wheaton, J. M., Brasington, J., Darby, S. E., and Sear, D. A. (2010). Accounting for uncertainty in DEMs from repeat topographic surveys: improved sediment budgets. *Earth surface processes and landforms: the journal of the British Geomorphological Research Group* 35 (2), pp. 136–156.

Wilson, G., Periketi, R., Fox, G., Dabney, S., Shields, F., and Cullum, R. (2007). Soil properties controlling seepage erosion contributions to streambank failure. *Earth Surface Processes and Landforms: The Journal of the British Geomorphological Research Group* 32 (3), pp. 447–459.

Wolman, M. G. (1959). Factors influencing erosion of a cohesive river bank. *American Journal of Science* 257 (3), pp. 204–216.

Woodget, A., Carbonneau, P., Visser, F., Maddock, I., and Habit, E. (2014). Quantifying Fluvial Topography Using UAS Imagery and SfM-Photogrammetry.

Woodget, A. S., Visser, F., Maddock, I. P., and Carbonneau, P. (2016). The accuracy and reliability of traditional surface flow type mapping: Is it time for a new method of characterizing physical river habitat? *River Research and Applications* 32 (9), pp. 1902–1914.

Wynn, T., Henderson, M., and Vaughan, D. (2008). Changes in streambank erodibility and critical shear stress due to subaerial processes along a headwater stream, southwestern Virginia, USA. *Geomorphology* 97 (3-4), pp. 260–273.

Yarnell, S. M., Mount, J. F., and Larsen, E. W. (2006). The influence of relative sediment supply on riverine habitat heterogeneity. *Geomorphology* 80 (3-4), pp. 310–324.

Ye, A., Zhou, Z., You, J., Ma, F., and Duan, Q. (2018). Dynamic Manning's roughness coefficients for hydrological modelling in basins. *Hydrology Research* 49 (5), pp. 1379–1395.

Yoshimura, T. and Hasegawa, H. (2003). Comparing the precision and accuracy of GPS positioning in forested areas. *Journal of Forest Research* 8 (3), pp. 147–152.

Young, A. P., Olsen, M., Driscoll, N., Flick, R., Gutierrez, R., Guza, R., Johnstone, E., and Kuester, F. (2010). Comparison of airborne and terrestrial lidar estimates of seacliff erosion in southern California. *Photogrammetric Engineering & Remote Sensing* 76 (4), pp. 421–427.

Yumoto, M., Ogata, T., Matsuoka, N., and Matsumoto, E. (2006). Riverbank freeze-thaw erosion along a small mountain stream, Nikko volcanic area, central Japan. *Permafrost and Periglacial Processes* 17 (4), pp. 325–339.

Zaimes, G. N., Tufekcioglu, M., and Schultz, R. C. (2019). Riparian land-use impacts on stream bank and gully erosion in agricultural watersheds: What we have learned. *Water* 11 (7), p. 1343.

Zhang, J., Liu, S., and Yang, S. (2007). The classification and assessment of freeze-thaw erosion in Tibet. *Journal of Geographical Sciences* 17 (2), pp. 165–174.

Zhang, L., Gove, J. H., and Heath, L. S. (2005). Spatial residual analysis of six modeling techniques. *Ecological Modelling* 186 (2), pp. 154–177.

Zhang, Y., Swift, D. J., Yu, Z., and Jin, L. (1998). Modeling of coastal profile evolution on the abandoned delta of the Huanghe River. *Marine Geology* 145 (1-2), pp. 133–148.

Chapter 8

Appendices

Appendix A

Pilot study of change detection techniques

Pilot Study Method

In order to ensure that the most appropriate change detection method was utilised for this research, a pilot study was carried out to test the sensitivity of three documented change detection techniques that have been used on similar high-resolution data in previous research. These were: Geomorphic Change Detection (GCD) (Wheaton et al., 2010), Multiscale Model-to-Model Cloud Comparison (M3C2) (Lague et al., 2013) and Direct Cloud to Cloud comparison (C2C) (e.g. Lane et al. (2003)). Given the very small scale changes that this research is trying to observe and quantify, it was important to find a way to test their accuracy when dealing with not only small scale changes, but also with different types of change, i.e. areas of scour versus areas of surface roughness change.

To simulate the fine scale changes expected in the field, a mock river bank was constructed to test the accuracy of the different change

Figure A.1: Mock river bank setup used for pilot study

detection techniques mentioned above. A wooden frame was created, measuring 0.75m tall and 1.0m wide, and filled with a narrow gravel layer at the base and silt and clay materials above to mimic the material and composition of the river bank in the study reaches along the River Arrow (figure A.1)

This frame was scanned using the Leica ScanStation C10 TLS that was subsequently used for the field-based research. The scanner was positioned approximately 3m from the frame and scanned at high resolution (point spacing of 0.050m at 100m from scanner) to mimic the point density that had been achieved during test scans conducted at the field sites. Point spacing is smaller closer to the scanner, but deteriorates as distance from scanner increases due to the spreading of the laser pulse, refraction through the atmosphere and the effect of the earth's curvature (Leica Geosystems, 2012). An initial scan was collected, then the frame was divided by eye into three vertical columns (figure A.2). The first column was left unchanged to act as a control area. The centre column had three areas of scour dug out using a small trowel. A metal rod was first inserted into the material and a line marked to represent the soil height. This was measured to provide an approximate depth of

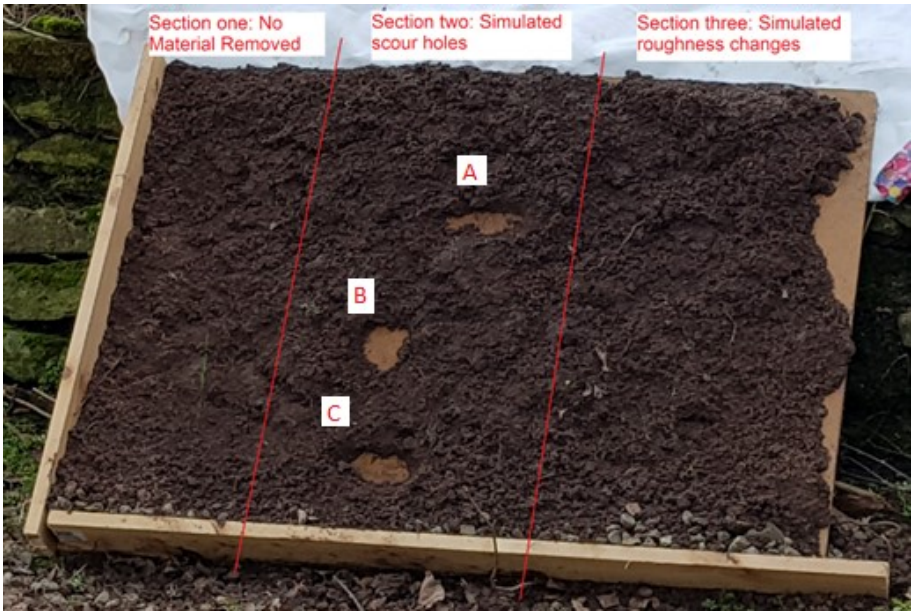

Figure A.2: Mock bank after soil removal

removed material before the scour hole was dug down to the back of the frame. A funnel was held underneath the areas being dug to catch as much of the material being removed as possible and to prevent that material being deposited onto the lower areas of the frame.

The deepest area of scour was located in section 2C, where the scour hole was 5.2cm deep at it's deepest point. Section 2B was roughly 3.4cm deep and 2A was 4.1cm deep. In section three, a layer of surface material was removed using a soft bristled brush to replicate small scale but large area change in a bank surface. The change in material depth in section three was difficult to measure as the material was removed in a much thinner layer, however estimation of the volume of change across the area was calculate using the removed material.

Because the laser scanner was not moved between scans, and used the same target area for each scan, it was not necessary to collect GPS data for georeferencing as all the data was collected within the same relative coordinate system. The scan data was then transferred to Cyclone for

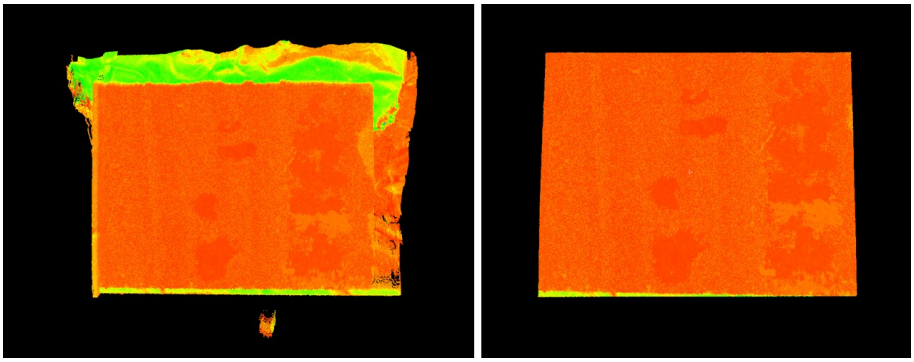

Figure A.3: Pilot study point clouds pre and post cropping

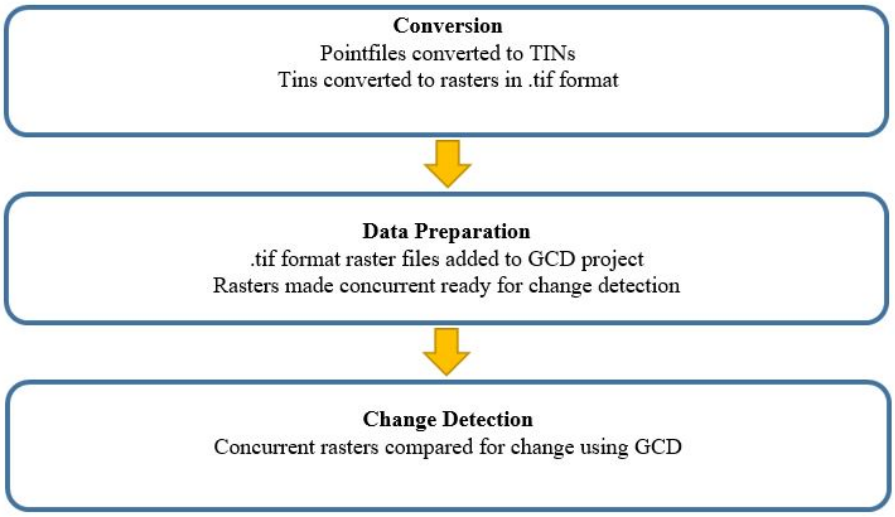

Figure A.4: Pilot study change detection workflow

initial visualisation. Once in Cyclone, all the scans were imported into one Modelspace and cropped to the same boundaries to ensure that all of the later change detection methodologies were being applied to the same surface area (figure A.3) The individual scans were then exported in text format for import into the appropriate change detection software; .txt for use in ArcGIS and .pts for use in CloudCompare.

For comparison using the GCD, the .txt files were added to a blank file in ArcMap 10.5, and processed into .tif raster files for comparison using the GCD7.4 add-in (available from http://gcd.riverscapes.xyz/). The complete data preparation workflow can be seen in figure A.4.

For the purposes of this pilot study, error values will be assumed as +/- 0.005m, which is equal to the positional accuracy of the TLS. The pilot study data was analysed twice within the GCD, once using a minimum level of detection (MLoD) of 0.01m (or 1cm), the lowest available option, and once using a minimum level of detection of 0.02 (or 2cm). In addition, a traditional DEM of Difference was produced using the raster calculator in ArcGIS 10.5 to add an additional layer of comparison. For comparison using the C2C and M3C2 techniques the ptx files were imported into CloudCompare. The scan 1 and scan 3 were then compared using the C2C technique, with Scan 3 set as the 'compared' cloud and Scan 1 set as the 'reference' cloud, as per the software guidance.

Pilot Study Results

The initial stage of analysing the two raster datasets, was to create a DEM of Difference (DoD), using the raster calculator tool (figure A.5). The 'old' raster was subtracted from the 'new' raster to give erosion as a negative number and deposition as a positive number. The DoD raster was then visualised with any values between -0.01m and 0.01m left hollow (blank) to mimic a minimum level of detection of 0.01m (i.e. only change deemed to be of greater than 0.01m is displayed). The resulting DoD can be seen in figure A.6.

This analysis detects the areas of deep scour well, picking out the outline of sections 2A and 2B clearly, while 2C is a little less well defined but still clearly visible. There was a small underestimation of the depth of scour, with the maximum depth being calculated as 0.046m. The much less well defined areas of change in section three were also well represented by change of between 0.01m and 0.03m. However, the

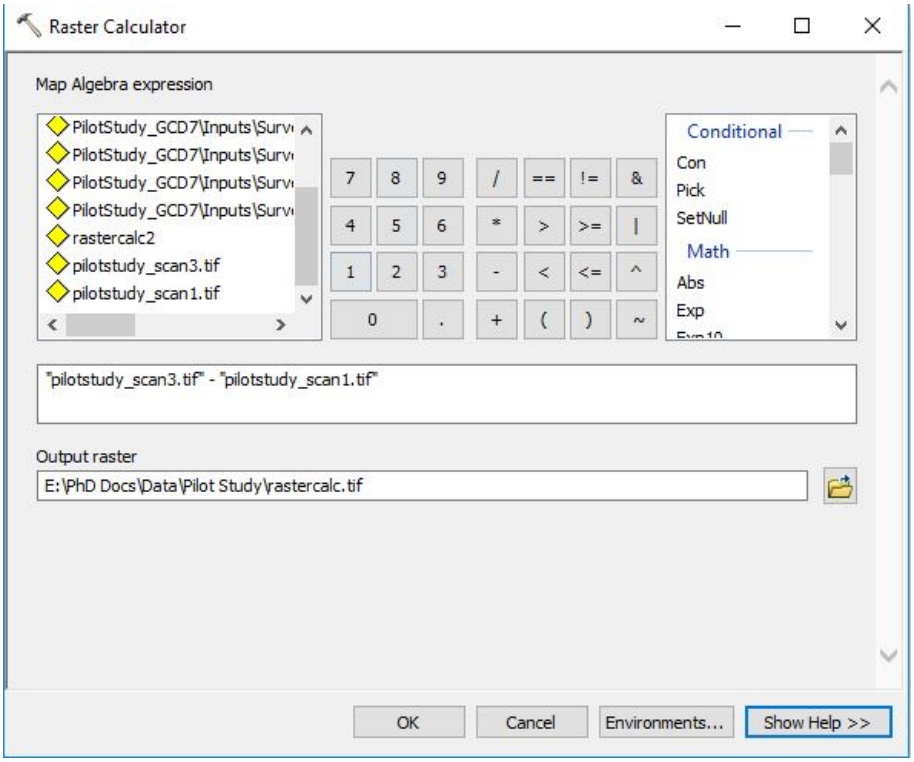

Figure A.5: Raster calculation settings

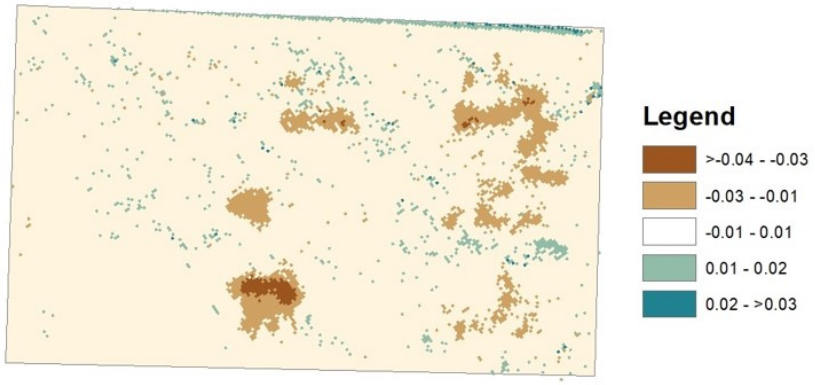

Figure A.6: Results of the raster calculation

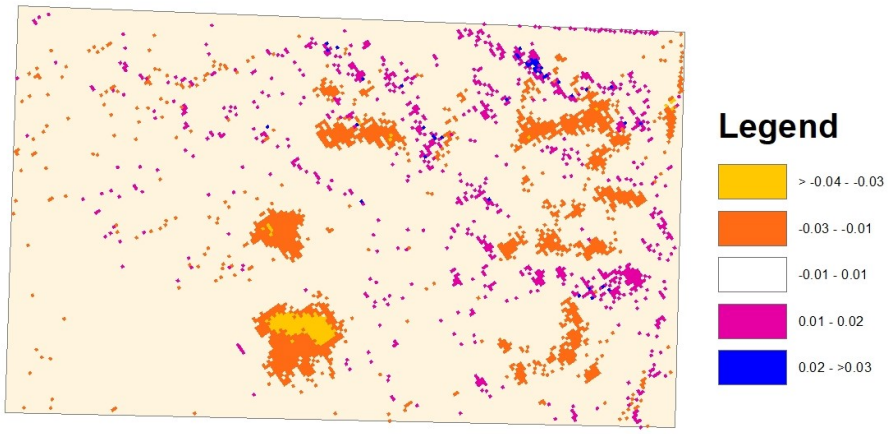

Figure A.7: Results of the GCD calculation with a minimum level of detection of 1cm

technique did pick up small areas of perceived deposition of between 1cm and 3cm. Some areas of deposition along the bottom of the frame were anticipated as they could have been as a result of material being dislodged from higher areas on the frame but not being caught by the funnel, but this did not appear to be the case. Instead, the areas of deposition were much more widespread, and varied across all three sections of the frame, including section one which had been left unaltered as a control. The change detection results for the GCD can be seen in figures A.7 and A.8 The results of MLoD 0.01m are very similar to those of the raster calculator tool, with the shapes of the scour holes being represented clearly. The depths of the scour holes were still being underestimated slightly, with a maximum scour depth of 0.048m calculated. The technique also detected the smaller scale changes of the brushed surface in section three. As with the DoD, the GCD MLoD 0.01m data also displayed significant amounts of perceived deposition, with a very similar spatial spread to that of the raster calculator.

The same cannot be said of the MLoD 0.02m change detection results. The results of that analysis showed far fewer areas of deposition, with

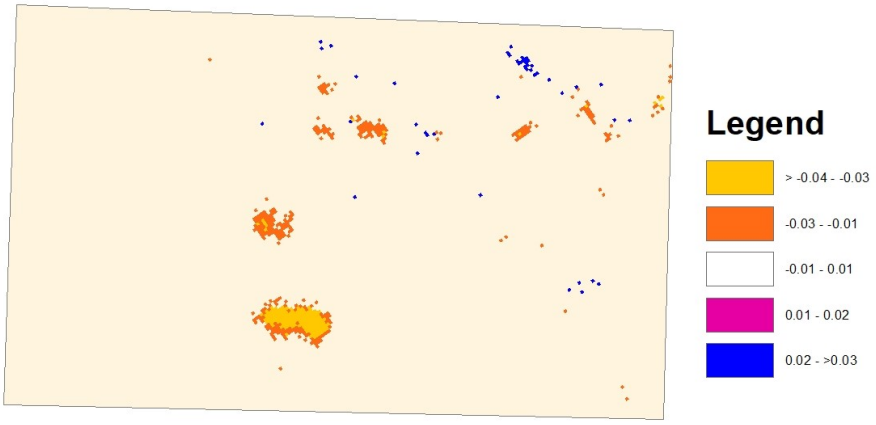

Figure A.8: Results of the GCD calculation with a minimum level of detection of 2cm

the exception of a small area in section three, while still representing the deepest areas of the scour holes to the same depth as that of the previous analysis, 0.048m. However, the area of small-scale change in section three was too shallow to be clearly identified, with little to no detected change in that area, and the overall areas of the scour holes was underestimated compared to the MLod 0.01m analysis.

The results of the Cloud to Cloud (C2C) change detection technique can be been in figure A.9. The C2C data showed a broad underestimation of change across the entire frame with a maximum depth change recorded of only 0.033m. Unlike the GCD, the C2C technique only measured change as a positive number of distance from the corresponding point cloud, rather than a positive or negative value of erosion and/or deposition. The C2C technique was able to identify small scale changes within section three, but again gave far smaller values of the depth of change than the GCD technique measured, with most of the change in that section falling between 0.003m – 0.009m. This means that some of the detected change is actually falling below the error value, and so

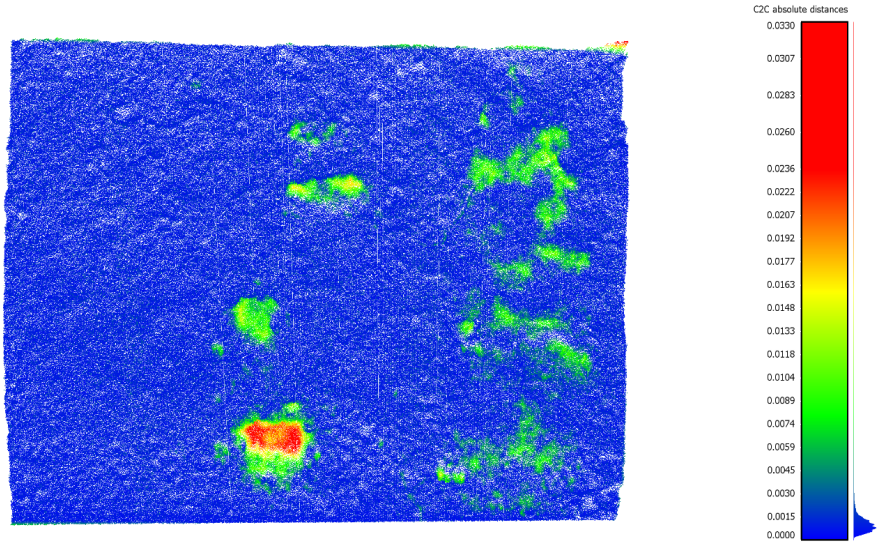

Figure A.9: Results of the Cloud-to-Cloud comparison technique

should be disregarded. The final technique was Multi-scale Model-to-Model Cloud Comparison (M3C2). This was also carried out in CloudCompare and the results can be seen in figure A.10. This technique provided deposition as a negative number and erosion as a positive number. M3C2 provided a much more realistic figure for the erosion depth in the scour holes, with some slight overestimation of 0.058m. The erosion detected in section three of the frame was also largely above the error values for data, with calculated values of between 0.014m and 0.03m.

A final comparison of the technique's values can be seen in tableA.1. For each sub-section of the frame where a known depth of material was removed, a comparison of the maximum depth of removed material and the maximum calculated depth of change was performed. The actual depth of scour was subtracted from the calculated depth to show underestimations of change as minus number and overestimations as positive numbers. The C2C technique was the most consistently

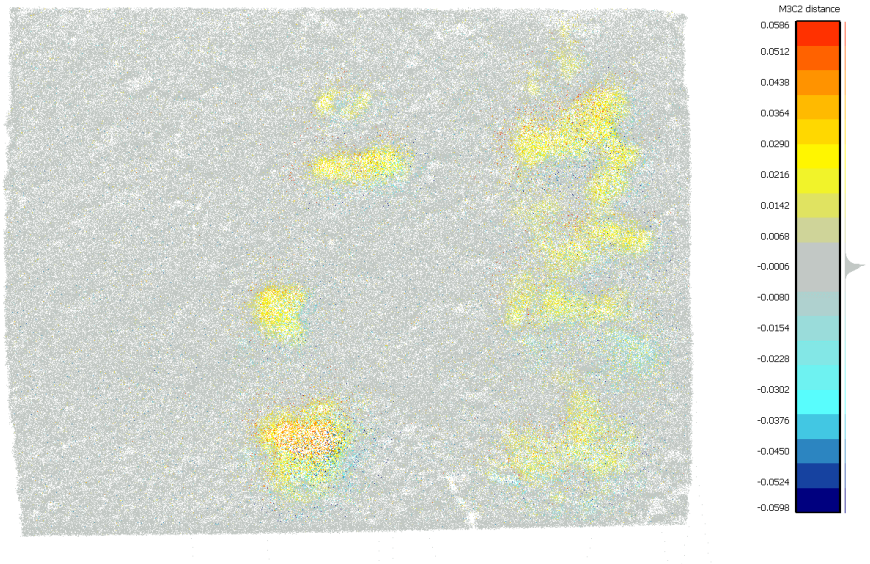

Figure A.10: Results of the Multiscale Model to Model Cloud comparison technique

different from the actual figures, with an average variance of -0.019m compared to the actual values. The DoD method came in second, with an average variance of -0.009m. Both GCD techniques had an average variance of -0.005m and the M3C2 technique had an average variance of 0.005m. Because the depth change in section three was not recorded the different techniques were compared against the average of the deepest calculated change in that section. The C2C technique was again the most different from the average, with a variance of -0.009m, and the DoD had a variance from average of 0.008m. The M3C2 technique had a variance from average of 0.006m, whereas both GCD techniques had a variance of only -0.002m.

Table A.1: Comparison of change detected by each tested change detection technique

	Actual Erosion (m)	DoD Method (m)	GCD MLoD 0.01m (m)	GCD MLoD 0.02m (m)	C2C Method (m)	M3C2 Method (m)
Section 2A	0.041	0.032	0.034	0.034	0.020	0.049
Variance		-0.009	-0.007	-0.007	-0.021	0.008
Section 2B	0.034	0.023	0.031	0.031	0.017	0.036
Variance		-0.011	-0.003	-0.003	-0.017	0.002
Section 2C	0.052	0.046	0.048	0.048	0.033	0.058
Variance		-0.006	-0.004	-0.004	-0.019	0.006
Average Variance		-0.009	-0.005	-0.005	-0.019	0.005
Section 3		-0.031	0.021	0.021	0.014	0.029
Variation from Average		0.008	-0.002	-0.002	-0.009	0.006

Pilot Study Discussion and Chosen technique

The results of this pilot study show that the GCD software produces the results with some of the smallest differences for the areas of simulated scour and material removal, however they showed a considerable amount of noise across the surface of the frame at the 0.01m MLoD . Although this was largely solved by using a MLoD of 0.02m, this also reduced the areas of change recorded by the technique, and as such could potentially result in areas of change on the study banks not being detected due to being below a MLoD required to reduce noise. Complications also arose with the use of the GCD software when attempting to georeference scans taken in the field. The banks of interest are all vertical faces, which posed an issue when trying to display them in ArcGIS. To overcome this, registration was performed in Cyclone, and then the geographic coordinate system was replaced with a virtual coordinate system which displayed the z values along the horizontal axis instead of the vertical. This allowed for the bank face to be tested for change, however also meant that any changes to the top of bank had to

be separated and re-projected in order to detect changes along both the vertical and horizontal planes. This process of cutting and re-projecting was complex and time consuming, making it difficult to maintain positional accuracy across multiple datasets that had slightly different extents. Although these problems could have been overcome with improved user confidence and experience, the ease with which the data was visualised and analysed within CloudCompare and using the M3C2 plugin made it unnecessary and so the decision was made to move forward with change detection using the M3C2 technique.

Appendix B

Volume change results

Volume change results

The following tables provide the contributions of different erosion processes, including fluvial erosion contributions (tables B.1, B.4 and B.15), mass wasting contributions (tables B.2 and B.16) and subaerial erosion contributions (tables B.3, B.5 and B.17).

The methods used to generate these data can be found in Chapter 2 - Methods (scanning protocol, post processing and and voxelisation) and in Chapter 3 - Relative contributions of subaerial, fluvial and mass wasting processes on river bank change (derivation of Q10 and Q50 bank heights).

This data was used to create figures 3.18 and 3.19 in chapter 3, and to generate the Pearson's R correlations tables for both flow conditions (table 4.2) and meteorological conditions (tables 4.9, 4.10 and 4.11) in chapter 4.

The data was generated using R (version 3.6.3). A summary of the four author created functions for the data analysis can be seen below:

```
## Required libraries ##

library(lidR)
library(dplyr)
library(data.table)

## Specialist Function creation ##

# Create Metrics function - This function voxelises the data into
# 1cm cubes and averages the different CloudCompare derived values
# per voxel before compiling the data into a data frame with rows
# representing each voxel (x y z coordinates for the rear top left
# corner of the voxel)

createmetrics<-function(cloud) {
  (M3C2<- voxel_metrics(cloud, ~mean(M3C2distance), 0.01))
  (Rough0.5<- voxel_metrics(cloud, ~mean(Roughness0.5), 0.01))
  (Rough0.25<- voxel_metrics(cloud, ~mean(Roughness0.25), 0.01))
  (Rough0.03<- voxel_metrics(cloud, ~mean(Roughness0.03), 0.01))
  (Count<- voxel_metrics(cloud, ~length(X), 0.01))
  (x<- c(M3C2$X))
  (y<- c(M3C2$Y))
  (z<- c(M3C2$Z))
  (M3C2dist <- c(M3C2$V1))
  (Vol<- c(0.01*0.01*M3C2$V1))
  (R0.5<- c(Rough0.5$V1))
  (R0.25<- c(Rough0.25$V1))
  (R0.03<- c(Rough0.03$V1))
  (count<- c(Count$V1))
  (data.frame(x, y, z, M3C2dist, Vol, R0.5, R0.25, R0.03, count))
}

# Remove Duplicates Function - This function identifies and removes
    any
```

```
34 # voxel that has either the same x,z coordinates or y,z coordinates
       as
35 # another voxel, therefore ensuring that only voxel representing
      the
36 # bank and not areas in front of the bank.
37 # Or, in other words, keeping the bank data only one voxel 'thick'
38
39 removedups<-function (grid) {
40   (y <- grid %>%
41      group_by(x, z) %>%
42      filter(y == (min(y))))
43   (x <- grid %>%
44       group_by(y, z) %>%
45       filter(x == (min(x))))
46   (E <- rbind(y,x))
47   (data.table(E[!duplicated(E[c(1,2,3)]),]))
48 }
49
50 # Erosion Calc Function - This function identifies and subsets all
      voxels
51 # that have a derived mean change value lower than -5mm. Thus
      limiting
52 # the change calculation to values above the registration error/
      survey error
53
54 Ecalc<- function(grid){
55   filter(grid, M3C2dist< -0.005)
56 }
57
58 # Deposition Calc Function - This function identifies and subsets
      all voxels
59 # that have a derived mean change value greater than 5mm. Thus
      limiting
60 # the change calculation to values above the registration error/
```

```
    survey error

Dcalc<- function(grid) {
  filter(grid, M3C2dist> 0.005)
}
```

Table B.1: Bank 1 - fluvial erosion contribution

Time period	Q10 Erosion Volume (m^3)	Q10 Area Volume (m^2)	Q10 Erosion Contribution (%)	Q10 Area Contribution (%)	Q50 Erosion Volume (m^3)	Q50 Area Volume (m^2)	Q50 Erosion Contribution (%)	Q50 Area Contribution (%)
May 2017 - July 17	-0.011	0.312	1.182	2.174	-0.004	0.116	0.444	0.808
July 2017 - October 2017	-0.004	0.125	0.818	1.141	-0.001	0.039	0.259	0.358
October 2017 - February 2018	-0.002	0.032	0.582	0.606	0.000	0.000	0.000	0.000
February 2018 - May 2018	-0.004	0.095	0.732	1.085	0.000	0.000	0.000	0.000
May 2018 - August 2018	-0.007	0.068	2.603	0.769	-0.001	0.010	0.496	0.109
August 2018 - February 2019	-0.012	0.249	2.329	2.268	0.000	0.000	0.000	0.000

Table B.2: Bank 1 - mass wasting contribution

Time Period	Mass Wasting Events	Mass Wasting Erosion (m^3)	Mass Wasting Area (m^2)	Mass Wasting Erosion Contribution (%)	Mass Wasting Area Contribution (%)
May 2017 - July 17	8	-0.092	0.774	9.487	5.384
July 2017 - October 2017	1	-0.027	0.198	6.134	1.809
October 2017 - February 2018	0	0.000	0.000	-0.000	0.000
February 2018 - May 2018	0	0.000	0.000	-0.000	0.000
May 2018 - August 2018	1	-0.098	0.368	37.962	4.135
August 2018 - February 2019	5	-0.151	0.855	28.834	7.795

Table B.3: Bank 1 - subaerial erosion contribution

Time Period	Subaerial above Q10 level Volume (m^3)	Subaerial above Q10 level area (m^2)	Subaerial above Q10 erosion contribution (%)	Subaerial above Q10 area contribution (%)	Subaerial above Q50 level Volume (m^3)	Subaerial above Q50 level area (m^2)	Subaerial above Q50 erosion contribution (%)	Subaerial above Q50 area contribution (%)
May 2017 - July 17	-0.863	13.291	89.331	92.442	-0.870	13.487	90.069	93.808
July 2017 - October 2017	-0.413	10.628	93.048	97.050	-0.415	10.714	93.607	97.833
October 2017 - February 2018	-0.410	5.170	99.418	99.394	-0.412	5.202	100.000	100.000
February 2018 - May 2018	-0.561	8.672	99.268	98.915	-0.565	8.767	100.000	100.000
May 2018 - August 2018	-0.154	8.472	59.435	95.096	-0.159	8.531	61.542	95.756
August 2018 - February 2019	-0.361	9.864	68.836	89.936	-0.373	10.113	71.166	92.205

Table B.4: Bank 2 Fluvial erosion

Time period	Q10 Erosion Volume (m^3)	Q10 Area Volume (m^2)	Q10 Erosion Contribution (%)	Q10 Area Contribution (%)	Q50 Erosion Volume (m^3)	Q50 Area Volume (m^2)	Q50 Erosion Contribution (%)	Q50 Area Contribution (%)
May 2017 - July 17	-0.016	0.259	2.270	2.012	-0.004	0.074	0.585	0.572
July 2017 - October 2017	-0.014	0.303	1.529	2.620	-0.001	0.034	0.124	0.298
October 2017 - February 2018	-0.000	0.003	0.416	0.411	0.000	0.000	-0.000	0.000
February 2018 - May 2018	-0.004	0.108	1.149	1.147	0.000	0.000	-0.000	0.000
May 2018 - August 2018	-0.056	0.346	4.706	3.312	-0.012	0.077	1.045	0.734
August 2018 - February 2019	-0.000	0.005	0.009	0.056	0.000	0.000	-0.000	0.000

Table B.5: Bank 2 - sub-aerial erosion contribution

Time Period	Subaerial above Q10 level Volume (m^3)	Subaerial above Q10 level area (m^2)	Subaerial above Q10 erosion contribution (%)	Subaerial above Q10 area contribution (%)	Subaerial above Q50 level Volume (m^3)	Subaerial above Q50 level area (m^2)	Subaerial above Q50 erosion contribution (%)	Subaerial above Q50 area contribution (%)
May 2017 - July 17	-0.693	12.617	97.730	97.988	-0.705	12.802	99.415	99.428
July 2017 - October 2017	-0.873	11.269	98.471	97.380	-0.886	11.538	99.876	99.702
October 2017 - February 2018	-0.021	0.823	99.584	99.589	-0.021	0.826	100.000	100.000
February 2018 - May 2018	-0.314	9.324	98.851	98.853	-0.317	9.433	100.000	100.000
May 2018 - August 2018	-1.138	10.103	95.294	96.688	-1.181	10.372	98.955	99.266
August 2018 - February 2019	-1.137	8.264	99.991	99.944	-1.137	8.269	100.000	100.000

Table B.6: Bank 3 - fluvial erosion contribution

Time period	Q10 Erosion Volume (m^3)	Q10 Area Volume (m^2)	Q10 Erosion Contribution (%)	Q10 Area Contribution (%)	Q50 Erosion Volume (m^3)	Q50 Area Volume (m^2)	Q50 Erosion Contribution (%)	Q50 Area Contribution (%)
May 2017 - July 2017	-0.657	9.776	18.002	16.247	-0.174	2.609	4.755	4.336
July 2017 - October 2017	-0.275	5.717	9.550	9.759	-0.017	0.373	0.600	0.637
October 2012 - May 2018	-0.230	1.909	4.581	4.833	0.000	0.000	-0.000	0.000
May 2018 - August 2018	-0.938	8.498	11.617	11.864	-0.160	1.295	1.979	1.807
August 2018 - February 2019	-0.117	2.032	3.023	4.828	0.000	0.000	-0.000	0.000
February 2019 - May 2019	-0.120	1.805	4.321	3.096	-0.003	0.022	0.103	0.038

Table B.7: Bank 3 - mass wasting contribution

Time Period	Mass Wasting Events	Mass Wasting Erosion (m^3)	Mass Wasting Area (m^2)	Mass Wasting Erosion Contribution (%)	Mass Wasting Area Contribution (%)
May 2017 - July 2017	5	-0.326	1.422	8.939	2.364
July 2017 - October 2017	5	-0.225	1.181	7.788	2.015
October 2012 - May 2018	9	-1.212	5.391	24.159	13.653
May 2018 - August 2018	11	-0.957	2.988	11.853	4.171
August 2018 - February 2019	6	-0.600	1.787	15.532	4.245
February 2019 - May 2019	2	-0.295	0.957	10.663	1.641

Table B.8: Bank 3 - subaerial erosion contribution

Time Period	Subaerial above Q10 level Volume (m^3)	Subaerial above Q10 level area (m^2)	Subaerial above Q10 erosion contribution (%)	Subaerial above Q10 area contribution (%)	Subaerial above Q50 level Volume (m^3)	Subaerial above Q50 level area (m^2)	Subaerial above Q50 erosion contribution (%)	Subaerial above Q50 area contribution (%)
May 2017 - July 2017	-2.666	48.971	73.058	81.389	-3.149	56.137	86.305	93.300
July 2017 - October 2017	-2.384	51.684	82.662	88.226	-2.642	57.028	91.612	97.348
October 2012 - May 2018	-3.576	32.189	71.260	81.514	-3.806	34.098	75.841	86.347
May 2018 - August 2018	-6.182	60.142	76.530	83.965	-6.960	67.345	86.168	94.021
August 2018 - February 2019	-3.147	38.275	81.445	90.928	-3.263	40.307	84.468	95.755
February 2019 - May 2019	-2.355	55.553	85.015	95.263	-2.471	57.336	89.234	98.321

Table B.9: Bank 3 Upstream - fluvial erosion contribution

Time period	Q10 Erosion Volume (m^3)	Q10 Area Volume (m^2)	Q10 Erosion Contribution (%)	Q10 Area Contribution (%)	Q50 Erosion Volume (m^3)	Q50 Area Volume (m^2)	Q50 Erosion Contribution (%)	Q50 Area Contribution (%)
May 2017 - July 2017	-0.285	3.857	26.936	21.635	-0.058	0.838	5.469	4.699
July 2017 - October 2017	-0.200	4.082	11.393	14.460	-0.011	0.250	0.643	0.885
October 2012 - May 2018	-0.034	0.560	2.190	3.634	0.000	0.000	-0.000	0.000
May 2018 - August 2018	-0.159	2.426	9.781	8.370	-0.014	0.166	0.865	0.574
August 2018 - February 2019	-0.057	1.419	4.117	6.166	0.000	0.000	-0.000	0.000
February 2019 - May 2019	-0.022	0.541	2.329	2.212	0.000	0.000	-0.000	0.000

Table B.10: Bank 3 Upstream - mass wasting contribution

Time Period	Mass Wasting Events	Mass Wasting Erosion (m^3)	Mass Wasting Area (m^2)	Mass Wasting Erosion Contribution (%)	Mass Wasting Area Contribution (%)
May 2017 - July 2017	2	-0.089	0.545	8.407	3.056
July 2017 - October 2017	2	-0.027	0.217	1.517	0.770
October 2012 - May 2018	5	-1.007	4.021	64.731	26.067
May 2018 - August 2018	3	-0.101	0.528	6.213	1.824
August 2018 - February 2019	3	-0.062	0.398	4.516	1.728
February 2019 - May 2019	1	-0.069	0.330	7.156	1.346

Table B.11: Bank 3 Upstream- subaerial erosion contribution

Time Period	Subaerial above Q10 level Volume (m^3)	Subaerial above Q10 level area (m^2)	Subaerial above Q10 erosion contribution (%)	Subaerial above Q10 area contribution (%)	Subaerial above Q50 level Volume (m^3)	Subaerial above Q50 level area (m^2)	Subaerial above Q50 erosion contribution (%)	Subaerial above Q50 area contribution (%)
May 2017 - July 2017	-0.683	13.426	64.657	75.309	-0.910	16.445	86.124	92.245
July 2017 - October 2017	-1.527	23.929	87.090	84.770	-1.715	27.761	97.840	98.345
October 2012 - May 2018	-0.514	10.844	33.079	70.300	-0.549	11.405	35.269	73.933
May 2018 - August 2018	-1.365	26.025	84.006	89.806	-1.510	28.284	92.922	97.602
August 2018 - February 2019	-1.264	21.194	91.368	92.107	-1.321	22.613	95.484	98.272
February 2019 - May 2019	-0.868	23.601	90.514	96.441	-0.890	24.142	92.844	98.654

Table B.12: Bank 3 Midstream - fluvial erosion contribution

Time period	Q10 Erosion Volume (m^3)	Q10 Area Volume (m^2)	Q10 Erosion Contribution (%)	Q10 Area Contribution (%)	Q50 Erosion Volume (m^3)	Q50 Area Volume (m^2)	Q50 Erosion Contribution (%)	Q50 Area Contribution (%)
May 2017 - July 2017	-0.055	1.461	7.985	9.933	-0.013	0.378	1.890	2.569
July 2017 - October 2017	-0.032	0.581	5.586	3.854	-0.001	0.034	0.244	0.223
October 2012 - May 2018	-0.138	0.770	11.601	8.747	0.000	0.000	-0.000	0.000
May 2018 - August 2018	-0.464	3.491	11.776	14.732	-0.080	0.625	2.020	2.636
August 2018 - February 2019	-0.005	0.116	0.601	1.644	0.000	0.000	-0.000	0.000
February 2019 - May 2019	-0.037	0.859	4.039	4.155	-0.000	0.000	0.001	0.002

Table B.13: Bank 3 Midstream - mass wasting contribution

Time Period	Mass Wasting Events	Mass Wasting Erosion (m^3)	Mass Wasting Area (m^2)	Mass Wasting Erosion Contribution (%)	Mass Wasting Area Contribution (%)
May 2017 - July 2017	2	-0.032	0.251	4.685	1.709
July 2017 - October 2017	0	0.000	0.000	-0.000	0.000
October 2012 - May 2018	1	-0.024	0.361	2.017	4.101
May 2018 - August 2018	4	-0.694	1.635	17.601	6.898
August 2018 - February 2019	2	-0.297	0.890	36.081	12.579
February 2019 - May 2019	0	0.000	0.000	-0.000	0.000

Table B.14: Bank 3 Midstream- subaerial erosion contribution

Time Period	Subaerial above Q10 level Volume (m^3)	Subaerial above Q10 level area (m^2)	Subaerial above Q10 erosion contribution (%)	Subaerial above Q10 area contribution (%)	Subaerial above Q50 level Volume (m^3)	Subaerial above Q50 level area (m^2)	Subaerial above Q50 erosion contribution (%)	Subaerial above Q50 area contribution (%)
May 2017 - July 2017	-0.597	12.996	87.330	88.358	-0.639	14.079	93.425	95.722
July 2017 - October 2017	-0.546	14.501	94.414	96.146	-0.577	15.048	99.756	99.777
October 2012 - May 2018	-1.030	7.669	86.383	87.152	-1.168	8.439	97.983	95.899
May 2018 - August 2018	-2.785	18.569	70.622	78.369	-3.169	21.435	80.378	90.466
August 2018 - February 2019	-0.522	6.071	63.318	85.776	-0.527	6.188	63.919	87.421
February 2019 - May 2019	-0.873	19.819	95.961	95.845	-0.910	20.677	99.999	99.998

Table B.15: Bank 3 Downstream - fluvial erosion contribution

Time period	Q10 Erosion Volume (m^3)	Q10 Area Volume (m^2)	Q10 Erosion Contribution (%)	Q10 Area Contribution (%)	Q50 Erosion Volume (m^3)	Q50 Area Volume (m^2)	Q50 Erosion Contribution (%)	Q50 Area Contribution (%)
May 2017 - July 2017	-0.413	5.681	17.934	16.145	-0.131	1.695	5.675	4.817
July 2017 - October 2017	-0.048	1.225	9.662	6.776	-0.005	0.098	0.999	0.542
October 2012 - May 2018	-0.073	0.717	4.787	4.864	0.000	0.000	-0.000	0.000
May 2018 - August 2018	-0.402	3.140	15.760	13.610	-0.078	0.584	3.050	2.530
August 2018 - February 2019	-0.067	0.572	4.588	4.462	0.000	0.000	-0.000	0.000
February 2019 - May 2019	-0.128	0.464	12.898	2.843	-0.003	0.021	0.272	0.129

Table B.16: Bank 3 Downstream - mass wasting contribution

Time Period	Mass Wasting Events	Mass Wasting Erosion (m^3)	Mass Wasting Area (m^2)	Mass Wasting Erosion Contribution (%)	Mass Wasting Area Contribution (%)
May 2017 - July 2017	1	-0.212	0.641	9.216	1.821
July 2017 - October 2017	3	-0.198	0.641	40.199	3.544
October 2012 - May 2018	3	-0.185	1.021	12.049	6.932
May 2018 - August 2018	4	-0.165	0.843	6.463	3.653
August 2018 - February 2019	1	-0.246	0.508	16.944	3.964
February 2019 - May 2019	1	-0.227	0.508	22.836	3.114

Table B.17: Bank 3 Downstream- subaerial erosion contribution

Time Period	Subaerial above Q10 level Volume (m^3)	Subaerial above Q10 level area (m^2)	Subaerial above Q10 erosion contribution (%)	Subaerial above Q10 area contribution (%)	Subaerial above Q50 level Volume (m^3)	Subaerial above Q50 level area (m^2)	Subaerial above Q50 erosion contribution (%)	Subaerial above Q50 area contribution (%)
May 2017 - July 2017	-1.676	28.866	72.850	82.035	-1.958	32.852	85.109	93.363
July 2017 - October 2017	-0.247	16.211	50.139	89.680	-0.290	17.338	58.802	95.914
October 2012 - May 2018	-1.276	12.995	83.164	88.204	-1.349	13.711	87.951	93.068
May 2018 - August 2018	-1.983	19.088	77.777	82.737	-2.308	21.644	90.487	93.817
August 2018 - February 2019	-1.142	11.739	78.468	91.574	-1.208	12.311	83.056	96.036
February 2019 - May 2019	-0.639	15.344	64.266	94.043	-0.764	15.787	76.891	96.757

Appendix C

Time Series Graphs of Erosion Values against Flow Variables

This section contains time series graphs of different calculated erosion variables against flow data for each bank and across all time periods. The time series graphs show little clear relationship between the erosion and flow variables, and the reasons why this may be the case have been discussed in the discussion section of chapters 3 and 4 and in the main discussion and conclusions chapter 6. The coarse temporal resolution means it is difficult to draw conclsions regarding relationships between the flow and erosion variables due to the need for averaging of continuous flow data into single values for each erosion monitoring period.

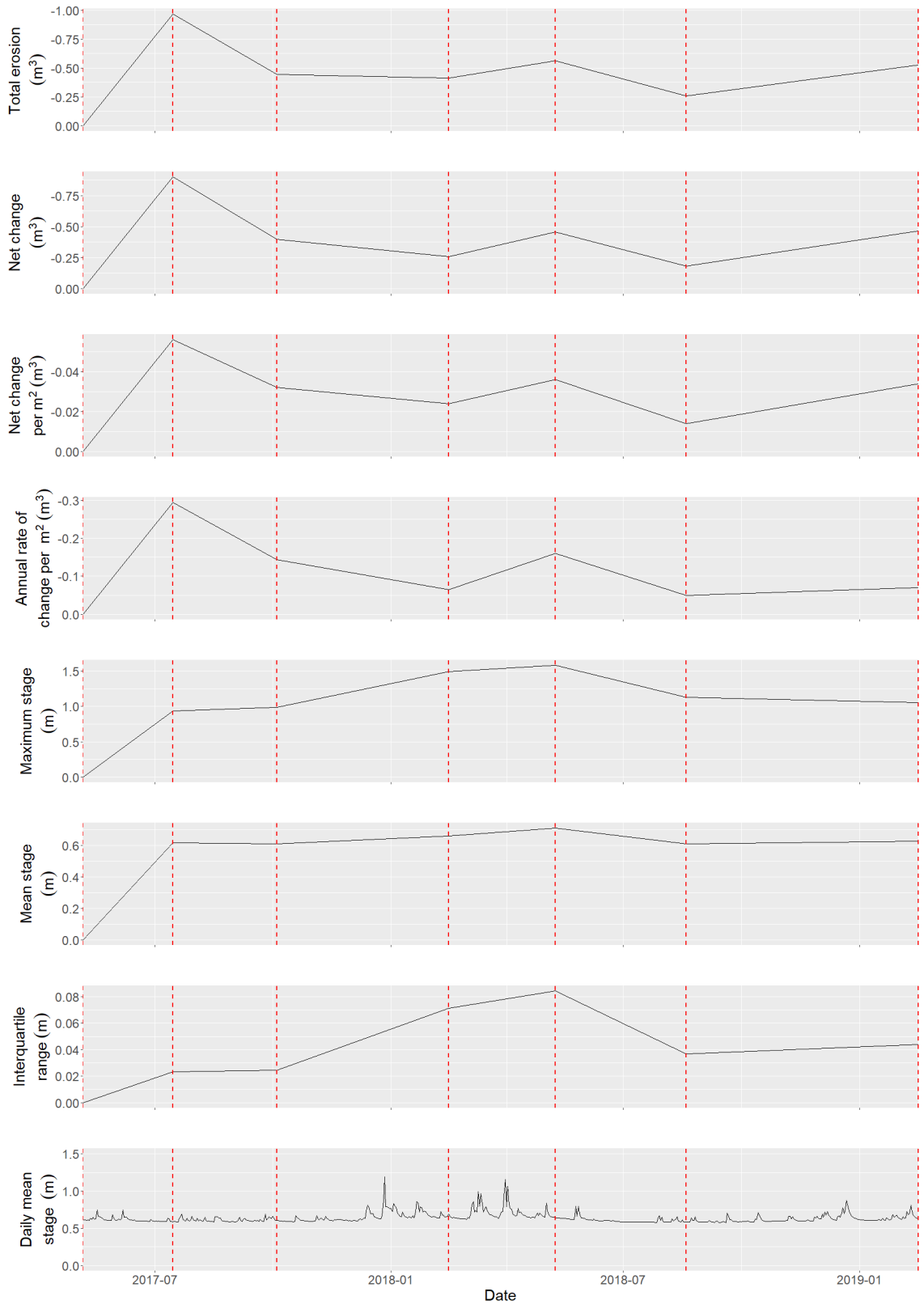

Figure C.1: Time series of Bank 1 erosion variables and river level

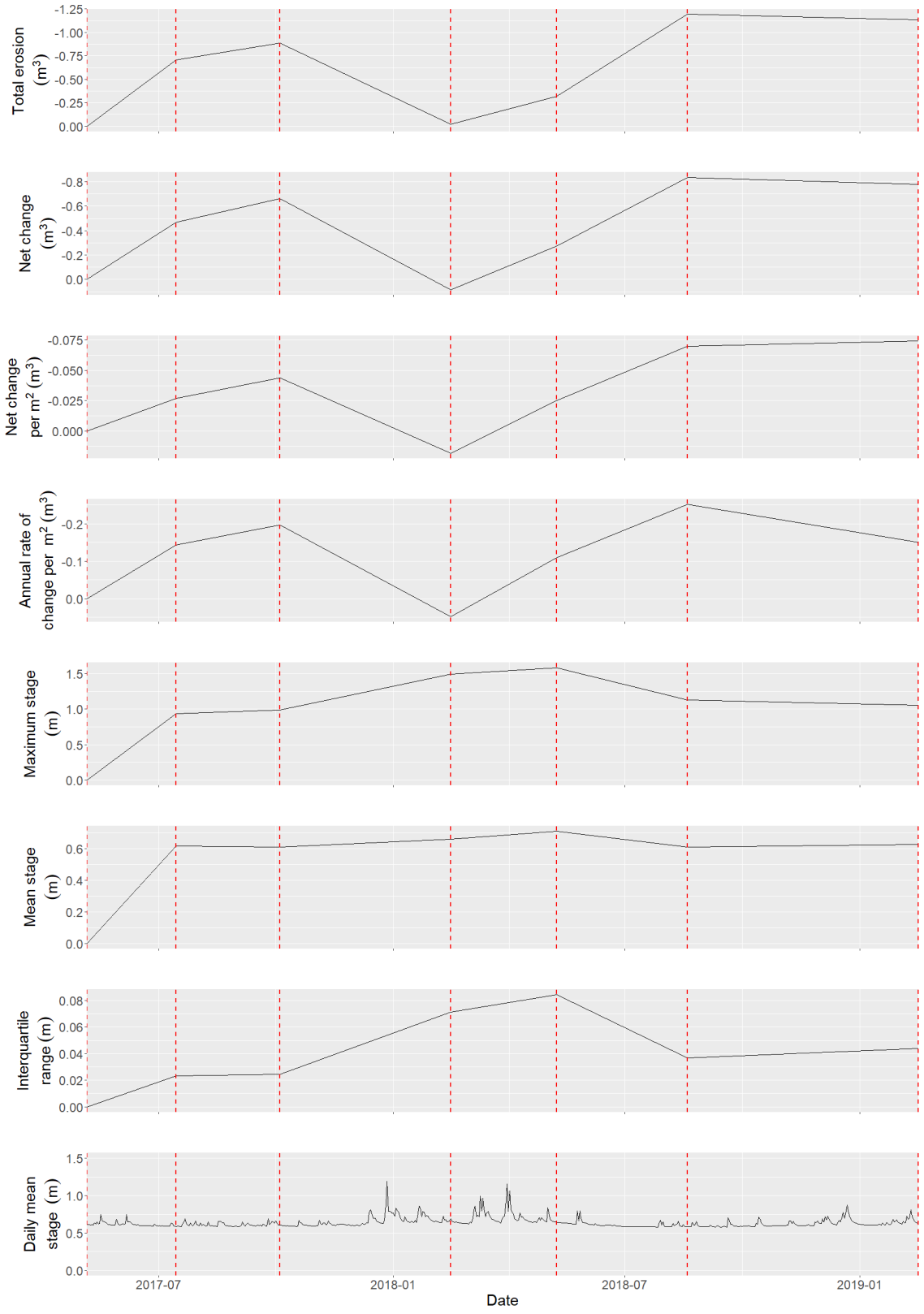

Figure C.2: Time series of Bank 2 erosion variables and river level

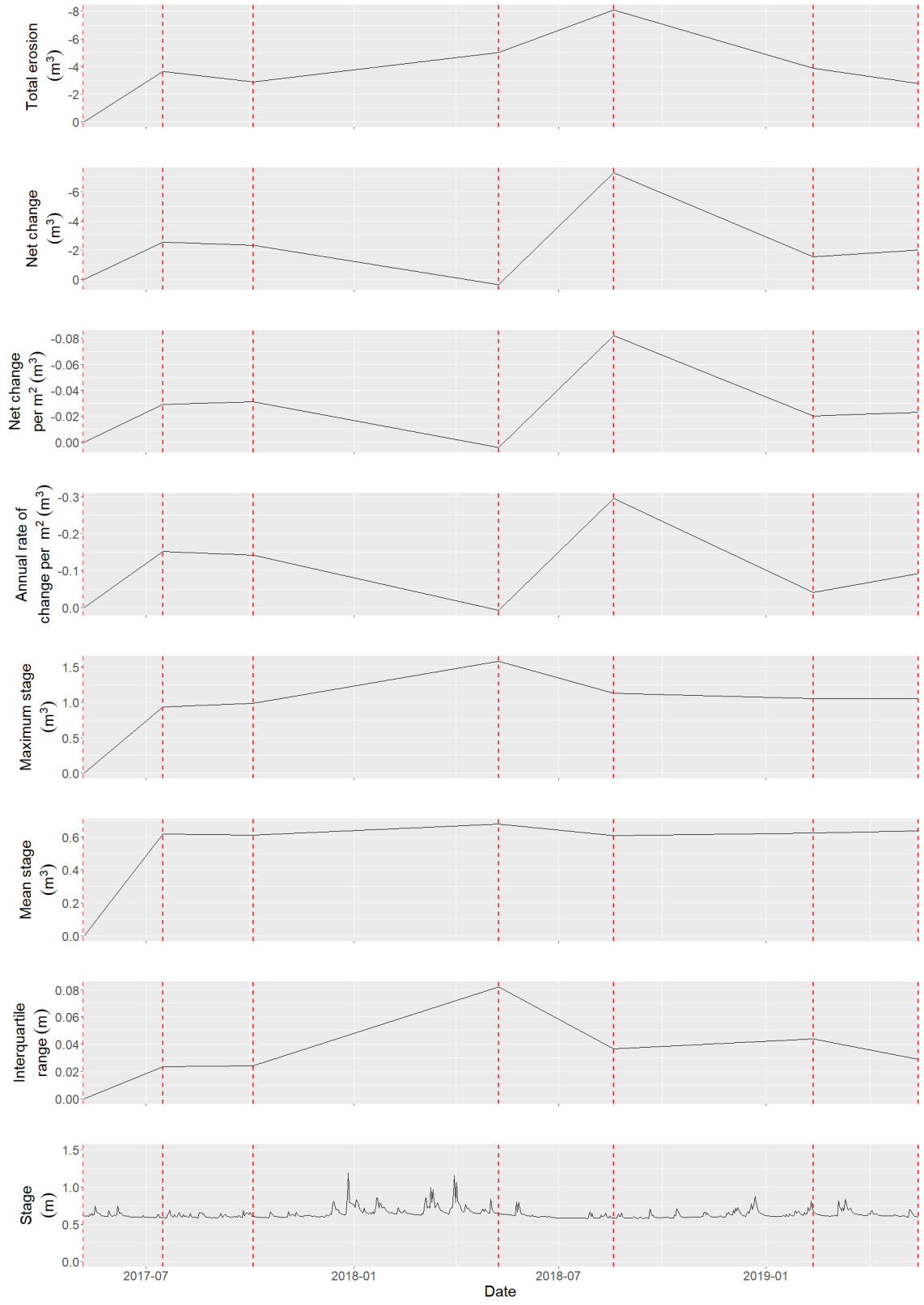

Figure C.3: Time series of total Bank 3 erosion variables and river level

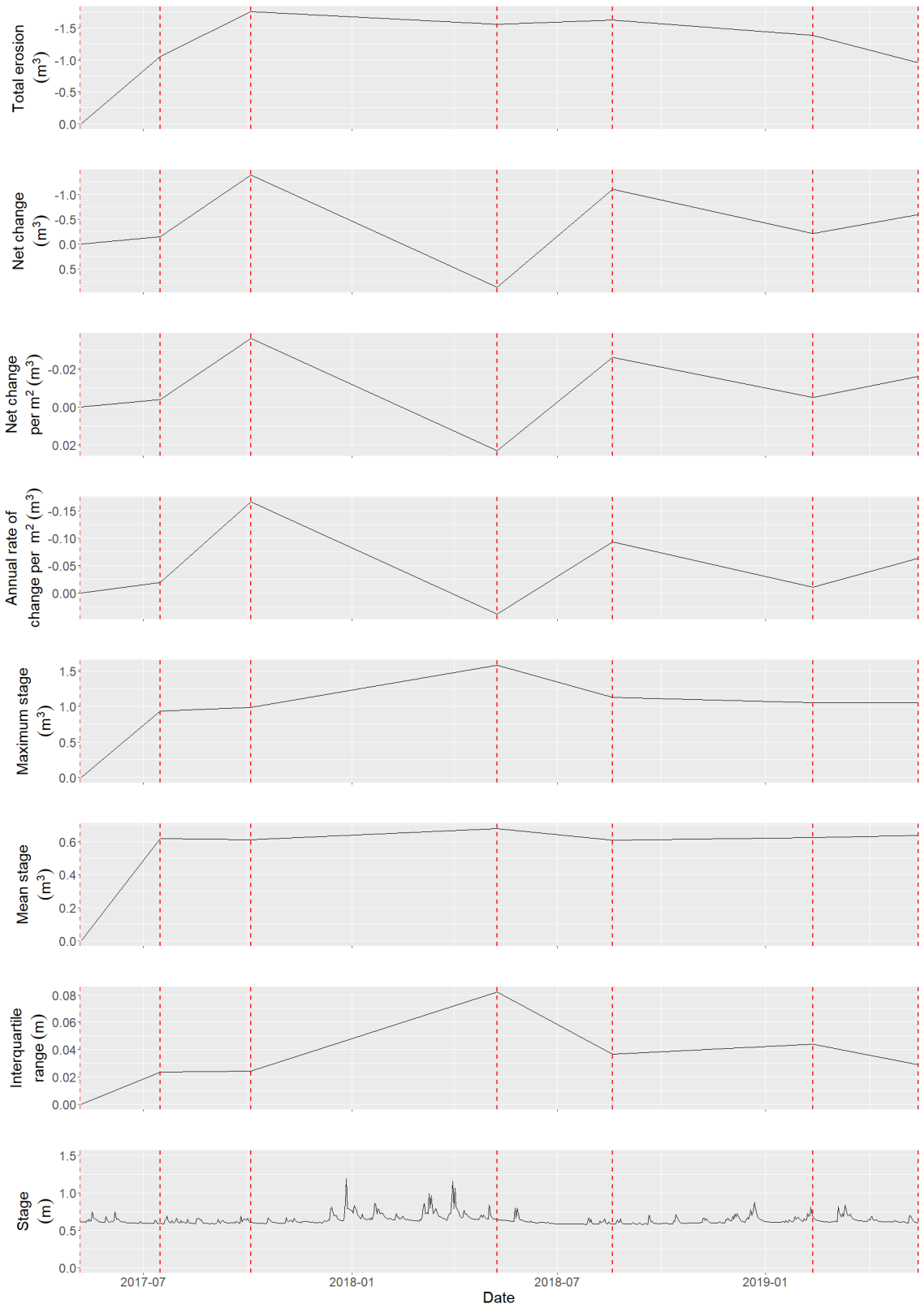

Figure C.4: Time series of Bank 3 Upstream reach erosion variables and river level

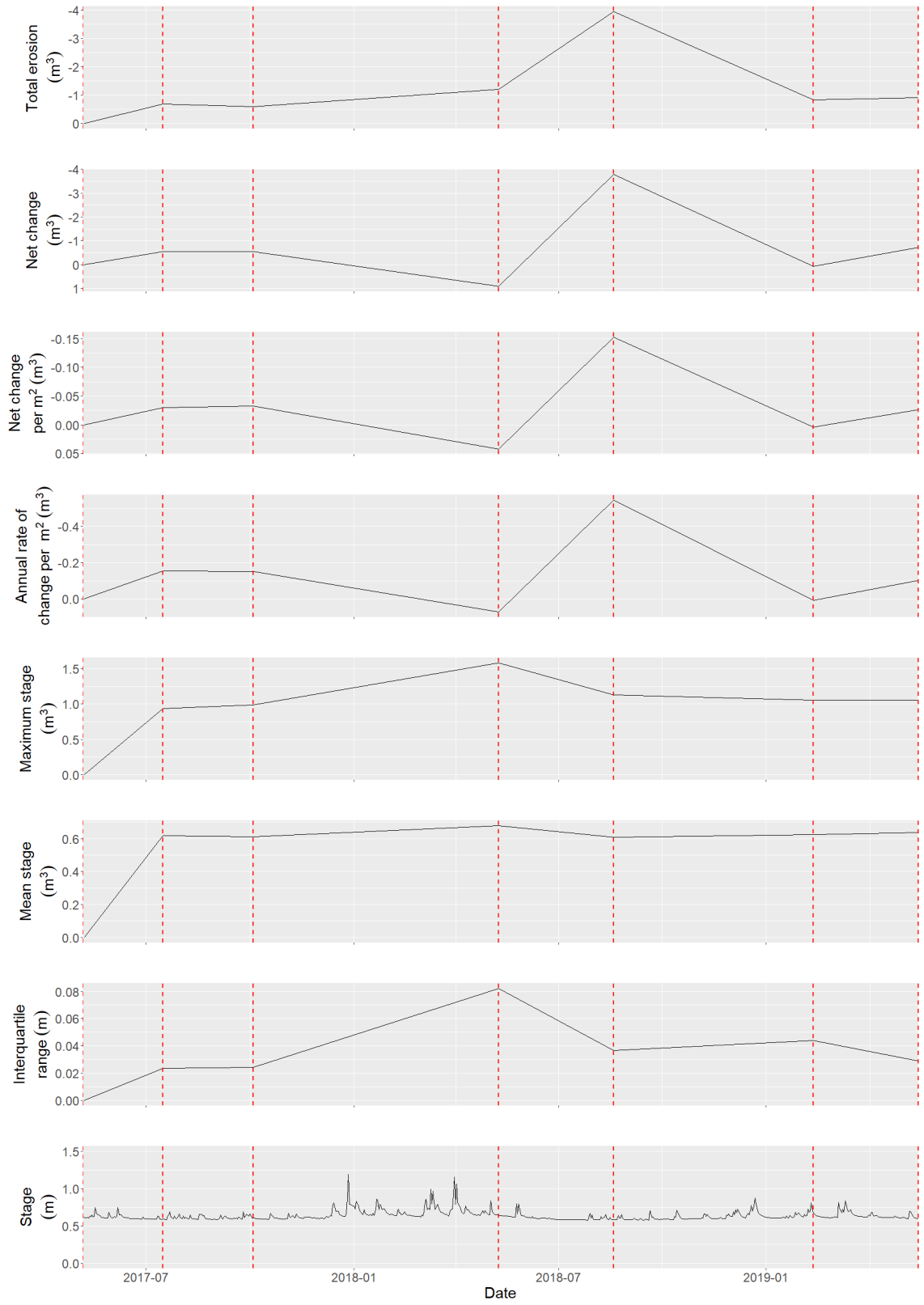

Figure C.5: Time series of Bank 3 Midstream reach erosion variables and river level

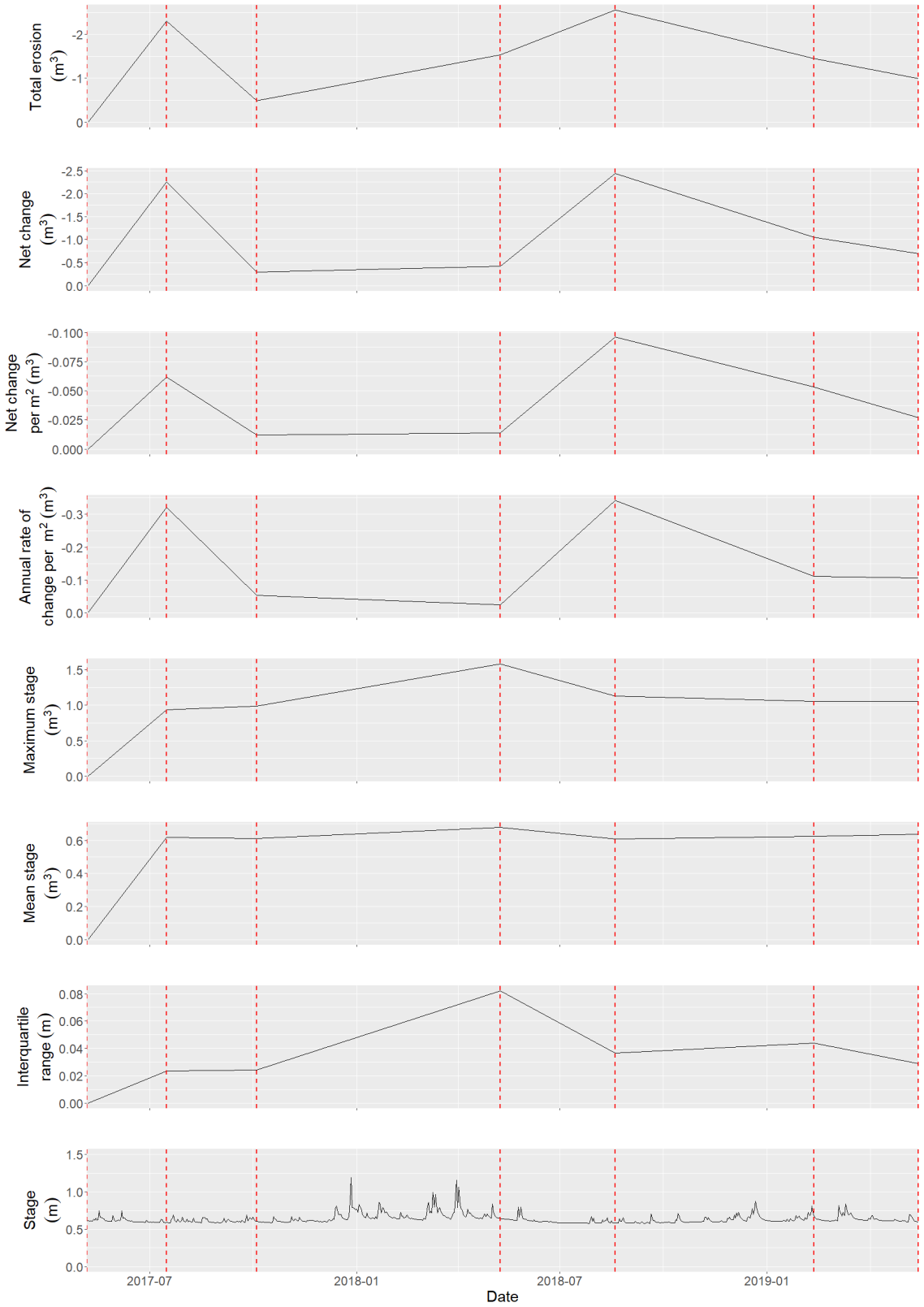

Figure C.6: Time series of Bank 3 Downstream reach erosion variables and river level

Appendix D

Results of Correlation of Meteorological Variables

Establishing independence of observations for multiple linear regression was carried out through the creation of a correlation matrix to show where different variables were cross-correlated. An alternative approach was also taken, and is detailed in chapter 4, whereby backwards, step-wise regression was carried out using VIF scores to remove variables that were highly cross-correlated.

Table D.1: Results of simple linear regression to establish Independence of Observations for Multiple Linear Regression

	Cold Hours	Frost Days	Freeze Thaw Cycles	Hot Hours	Mean Temp	Min Temp	Max Temp	Total Rainfall	Mean Rainfall	Wetting and Drying Cycles	Rain Days	Rain Hours	Mean Discharge	Max Discharge
Cold Hours	1.000	0.993	0.946	-0.466	-0.803	-0.862	-0.390	0.929	0.396	0.922	0.911	0.928	0.783	0.865
Frost Days	0.993	1.000	0.976	-0.483	-0.823	-0.872	-0.453	0.944	0.361	0.945	0.937	0.948	0.744	0.846
Freeze Thaw Cycles	0.946	0.976	1.000	-0.501	-0.832	-0.871	-0.555	0.946	0.283	0.956	0.961	0.955	0.623	0.753
Hot Hours	-0.466	-0.483	-0.501	1.000	0.735	0.548	0.747	-0.539	-0.743	-0.622	-0.596	-0.616	-0.423	-0.364
Mean Temp	-0.803	-0.823	-0.832	0.735	1.000	0.953	0.791	-0.719	-0.371	-0.774	-0.771	-0.768	-0.760	-0.793
Min Temp	-0.862	-0.872	-0.871	0.548	0.953	1.000	0.630	-0.741	-0.222	-0.760	-0.773	-0.761	-0.774	-0.822
Maximum Temp	-0.390	-0.453	-0.555	0.747	0.791	0.630	1.000	-0.441	-0.308	-0.538	-0.547	-0.513	-0.352	-0.382
Total Rainfall	0.929	0.944	0.946	-0.539	-0.719	-0.741	-0.441	1.000	0.415	0.988	0.991	0.991	0.530	0.643
Mean Rainfall	0.396	0.361	0.283	-0.743	-0.371	-0.222	-0.308	0.415	1.000	0.472	0.406	0.475	0.476	0.351
Wetting and Drying Cycles	0.922	0.945	0.956	-0.622	-0.774	-0.760	-0.538	0.988	0.472	1.000	0.994	0.999	0.562	0.671
Rain Days	0.911	0.937	0.961	-0.596	-0.771	-0.773	-0.547	0.991	0.406	0.994	1.000	0.993	0.516	0.632
Rain Hours	0.928	0.948	0.955	-0.616	-0.768	-0.761	-0.513	0.991	0.475	0.999	0.993	1.000	0.568	0.674
Mean Discharge	0.783	0.744	0.623	-0.423	-0.760	-0.774	-0.352	0.530	0.476	0.562	0.516	0.568	1.000	0.965
Maximum Discharge	0.865	0.846	0.753	-0.364	-0.793	-0.822	-0.382	0.643	0.351	0.671	0.632	0.674	0.965	1.000

Appendix E

Results of Variogram Analysis

Below are the semivariograms produced for each study bank and each time period, showing the model type and the nugget, sill and range values. These semivariograms were used to inform the data decimation process. As a result of this decimation process, over 90% of the collected point data was lost and therefore spatial autocorrelation was dealt with via a different technique, detailed in chapter 5 Section 5.3.1.

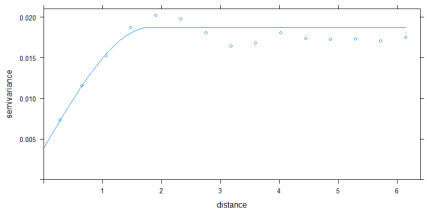

(a) E1 - Model = Spherical
Nugget = 0.004, Sill = 0.015
Range = 1.803

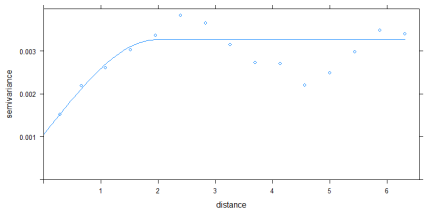

(b) E2 - Model = Spherical
Nugget = 0.001, Sill = 0.002
Range = 1.976

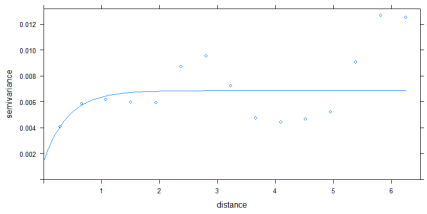

(c) E3 - Model = Exponential
Nugget = 0.001, Sill = 0.005
Range = 0.417

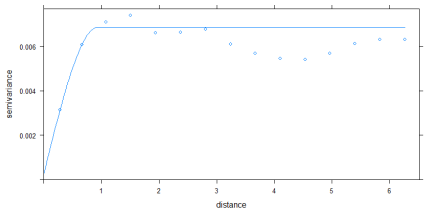

(d) E4 - Model = Spherical
Nugget = 0.000, Sill = 0.007
Range = 0.942

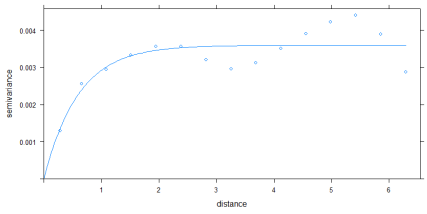

(f) E5 - Model = Exponential
Nugget = 0.000, Sill = 0.004
Range = 0.597

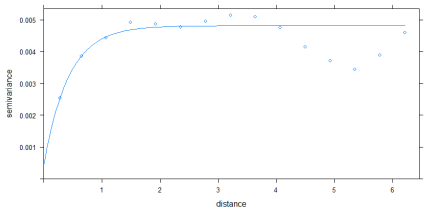

(f) E6 - Model = Exponential
Nugget = 0.000, Sill = 0.004
Range = 0.424

Figure E.1: Variogram models for each time period on Bank1

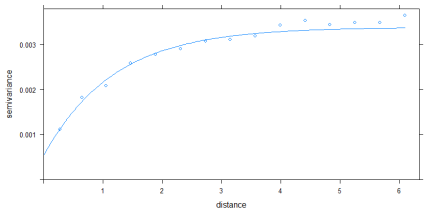

(a) E1 - Model = Exponent
Nugget = 0.001, Sill = 0.003
Range = 1.182

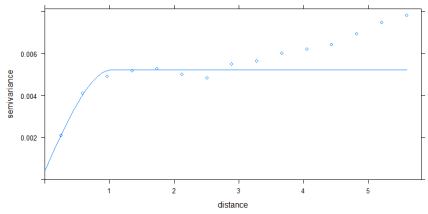

(b) E2 - Model = Spherical
Nugget = 0.000, Sill = 0.005
Range = 1.046

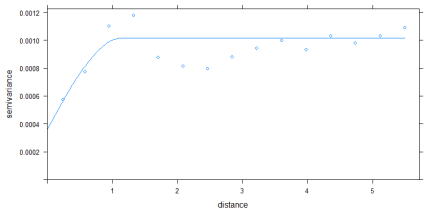

(c) E3 - Model = Spherical
Nugget = 0.000, Sill = 0.001
Range = 1.152

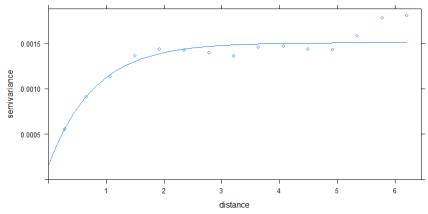

(d) E4 - Model = Exponent
Nugget = 0.000, Sill = 0.001
Range = 0.796

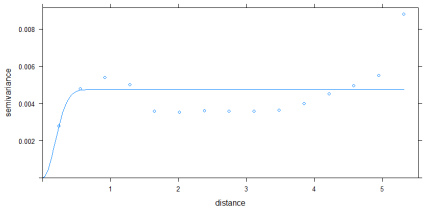

(f) E5 - Model = Gaussian
Nugget = 0.000, Sill = 0.005
Range = 0.254

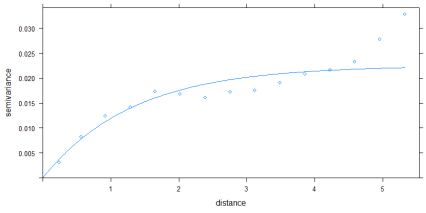

(f) E6 - Model = Exponent
Nugget = 0.000, Sill = 0.023
Range = 1.325

Figure E.2: Variogram models for each time period on Bank 2

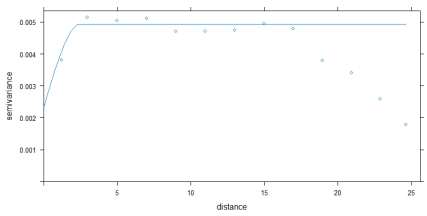

(a) E1 - Model = Gaussian
Nugget = 0.002, Sill = 0.003
Range = 1.337

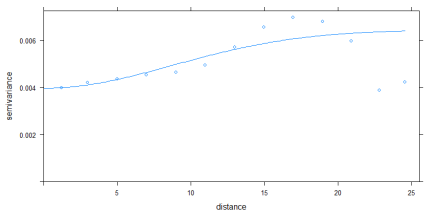

(b) E2 - Model = Spherical
Nugget = 0.002, Sill = 0.003
Range = 1.092

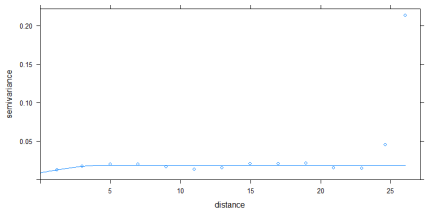

(c) E3 - Model = Exponent
Nugget = 0.001, Sill = 0.018
Range = 1.046

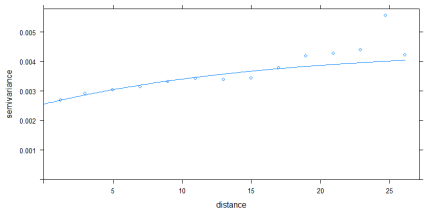

(d) E4 - Model = Gaussian
Nugget = 0.001, Sill = 0.326
Range = 1.397

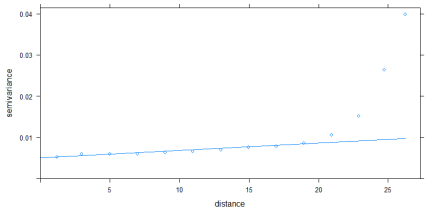

(f) E5 - Model = Exponent
Nugget = 0.003, Sill = 0.003
Range = 0.639

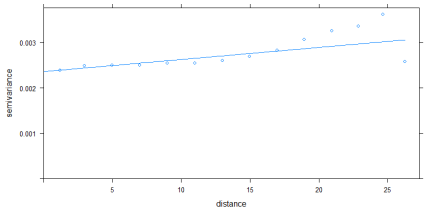

(f) E6 - Model = Spherical
Nugget = 0.001, Sill = 0.001
Range = 1.397

Figure E.3: Variogram models for each time period on the upstream reach of Bank 3

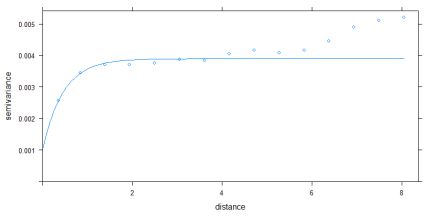

(a) E1 - Model = Exponent
Nugget = 0.001, Sill = 0.009
Range = 0.461

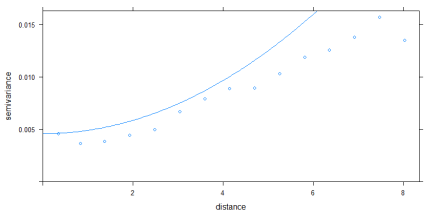

(b) E2 - Model = Gaussian
Nugget = 0.005, Sill = 70.824
Range = 2.865

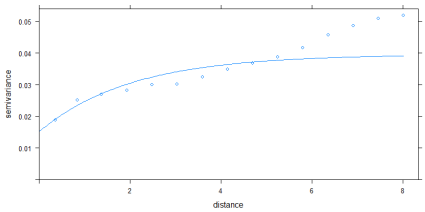

(c) E3 - Model = Exponent
Nugget = 0.015, Sill = 0.024
Range = 2.026

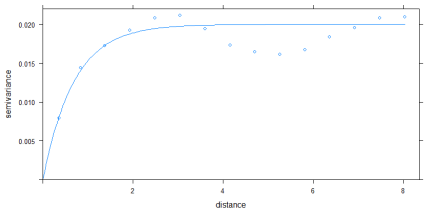

(d) E4 - Model = Exponent
Nugget = 0.000, Sill = 0.020
Range = 0.690

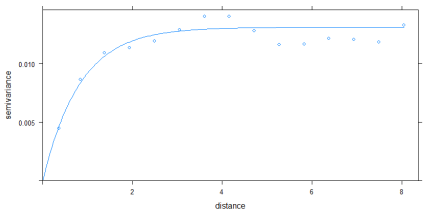

(f) E5 - Model = Exponent
Nugget = 0.000, Sill = 0.013
Range = 0.827

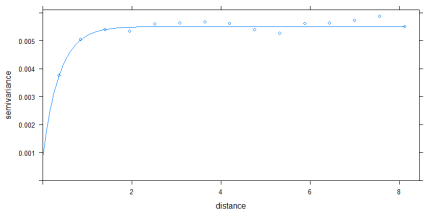

(f) E6 - Model = Exponent
Nugget = 0.001, Sill = 0.005
Range = 0.374

Figure E.4: Variogram models for each time period on the midstream reach of Bank 3

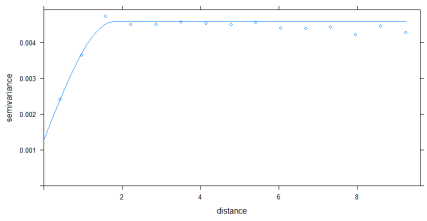

(a) E1 - Model = Spherical
Nugget = 0.001, Sill = 0.008
Range = 1.190

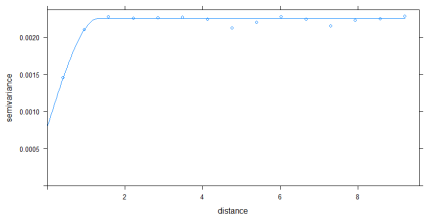

(b) E2 - Model = Spherical
Nugget = 0.001, Sill = 0.001
Range = 1.324

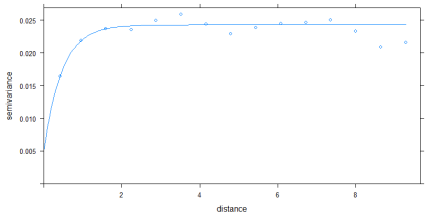

(c) E3 - Model = Exponent
Nugget = 0.005, Sill = 0.198
Range = 0.462

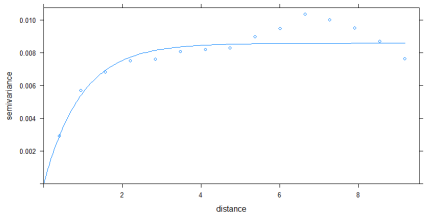

(d) E4 - Model = Exponent
Nugget = 0.000, Sill = 0.009
Range = 0.950

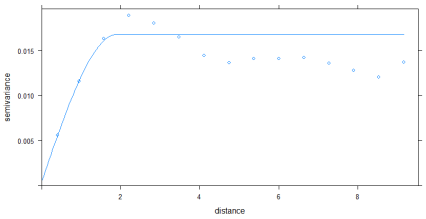

(f) E5 - Model = Spherical
Nugget = 0.000, Sill = 0.016
Range = 1.900

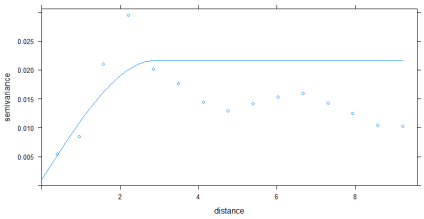

(f) E6 - Model = Spherical
Nugget = 0.001, Sill = 0.021
Range = 2.899

Figure E.5: Variogram models for each time period on the downstream reach of Bank 3

Appendix F

Linear regression of erosion against roughness and controls

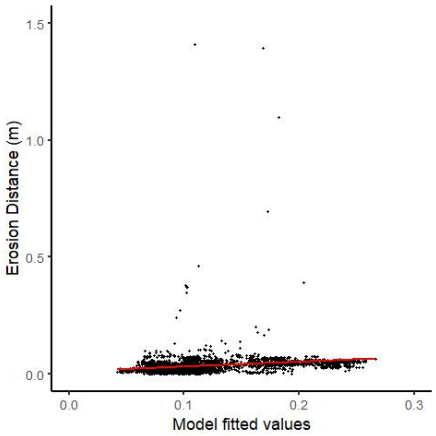

(a) E1 - R^2 = 0.061
p-value = <**0.001**

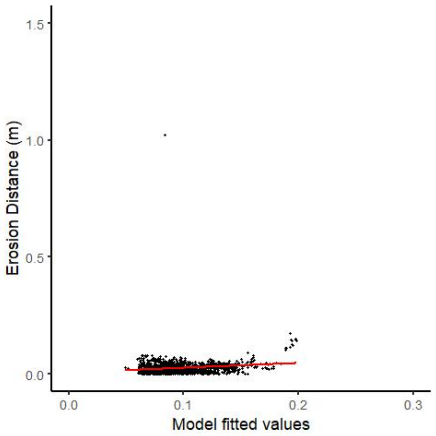

(b) E2 - R^2 = 0.086
p-value = <**0.001**

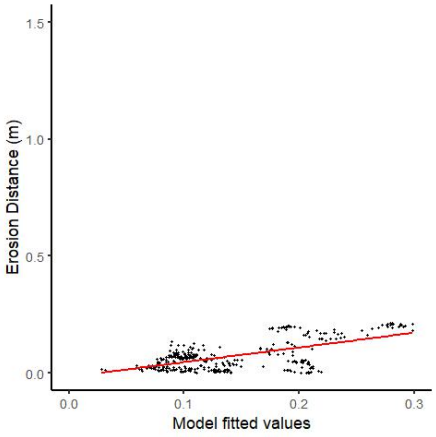

(c) E3 - R^2 = 0.0160
p-value = <**0.001**

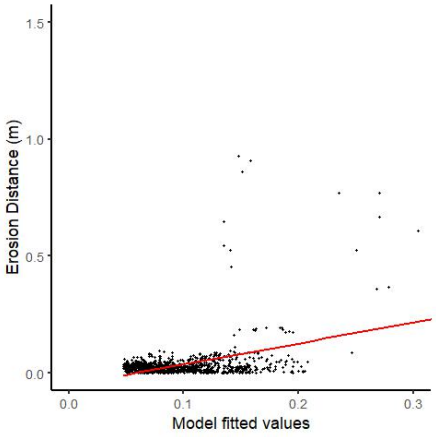

(d) E4 - R^2 = 0.0126
p-value = <**0.001**

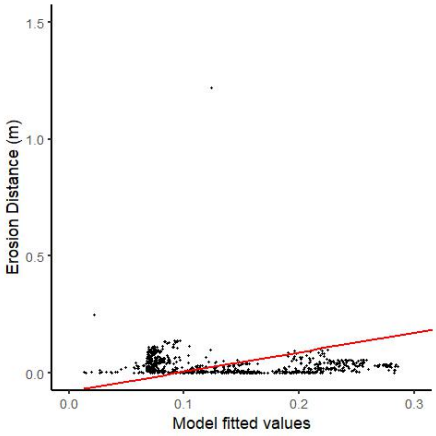

(e) E5 - R^2 = 0.0318
p-value = <**0.001**

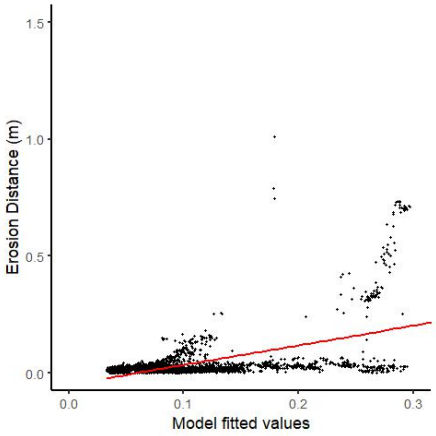

(f) E6 - R^2 = 0.0004
p-value = <**0.001**

Figure F.1: Linear regression plots of change due to fluvial erosion below the Q10 level against roughness at the 0.5m scale for each survey period on Bank 1

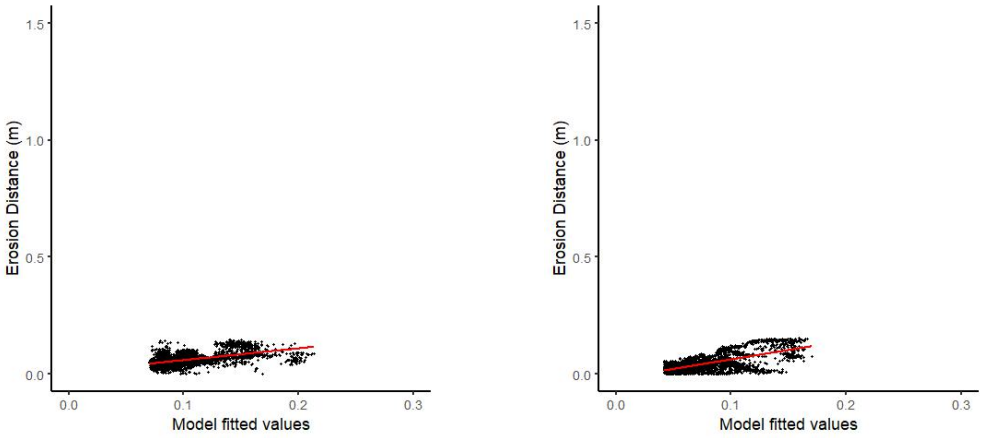

(a) E1 - R^2 = 0.477
p-value = <**0.001**

(b) E2 - R^2 = 0.544
p-value = <**0.001**

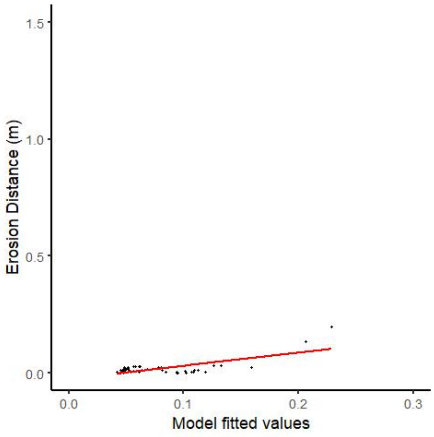

(c) E3 - R^2 = 0.886
p-value = <**0.001**

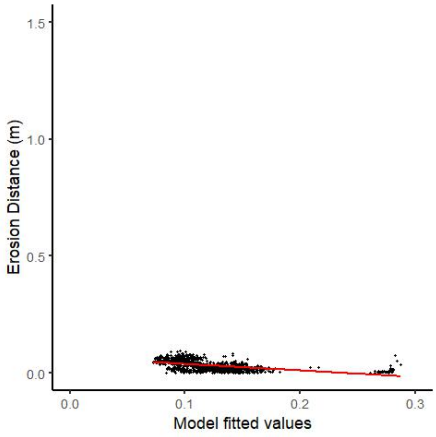

(d) E4 - R^2 = 0.481
p-value = <**0.001**

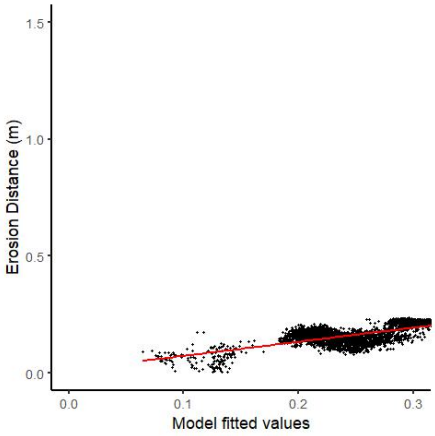

(e) E5 - R^2 = 0.783
p-value = <**0.001**

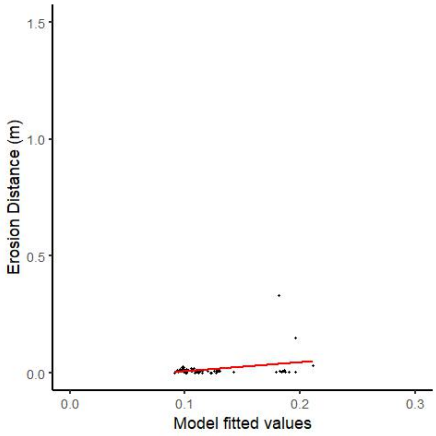

(f) E6 - R^2 = 0.260
p-value = <**0.001**

Figure F.2: Linear regression plots of change due to fluvial erosion below the Q10 level against roughness at the 0.5m scale for each survey period on Bank 2

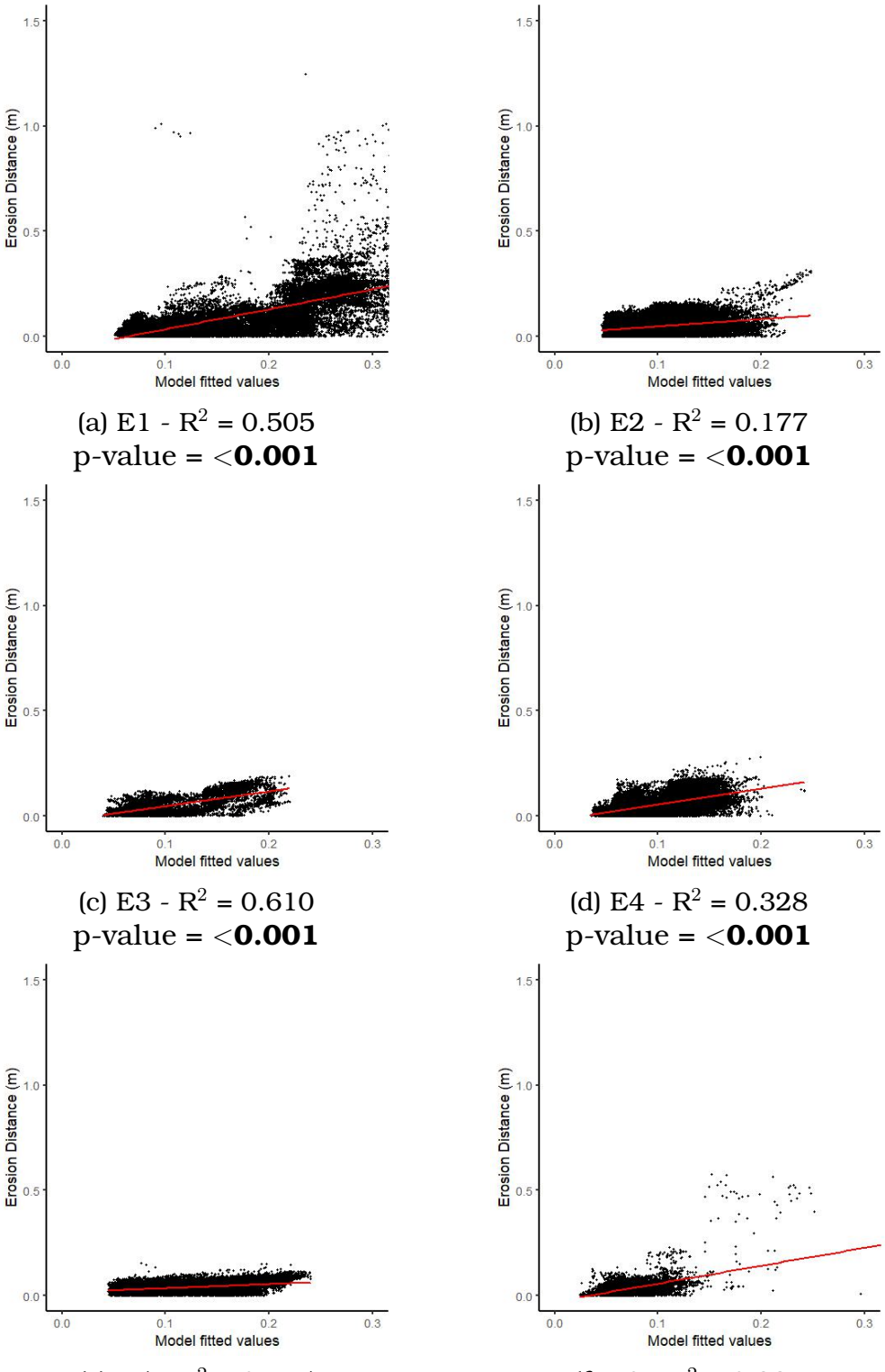

(a) E1 - R^2 = 0.505
p-value = <**0.001**

(b) E2 - R^2 = 0.177
p-value = <**0.001**

(c) E3 - R^2 = 0.610
p-value = <**0.001**

(d) E4 - R^2 = 0.328
p-value = <**0.001**

(e) E5 - R^2 = 0.445
p-value = <**0.001**

(f) E6 - R^2 = 0.384
p-value = <**0.001**

Figure F.3: Linear regression plots of change due to fluvial erosion below the Q10 level against roughness at the 0.5m scale for each survey period on the upstream reach of Bank 3

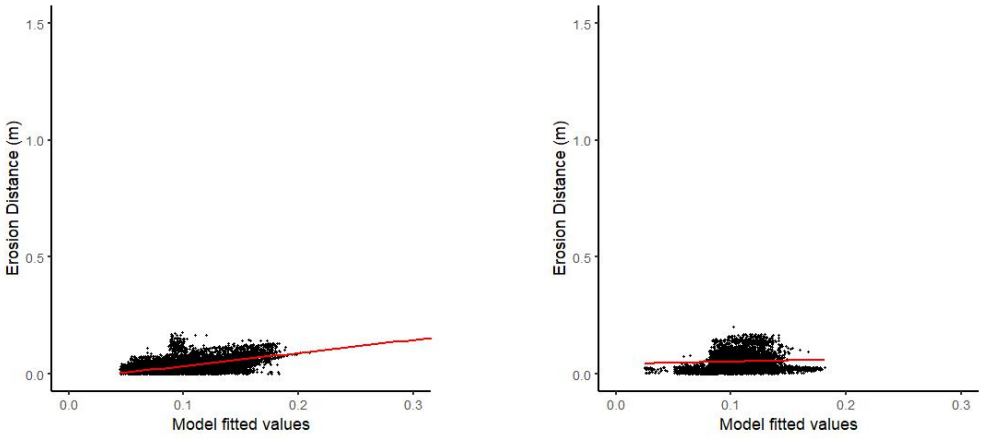

(a) E1 - R^2 = 0.668
p-value = <**0.001**

(b) E2 - R^2 = 0.202
p-value = <**0.001**

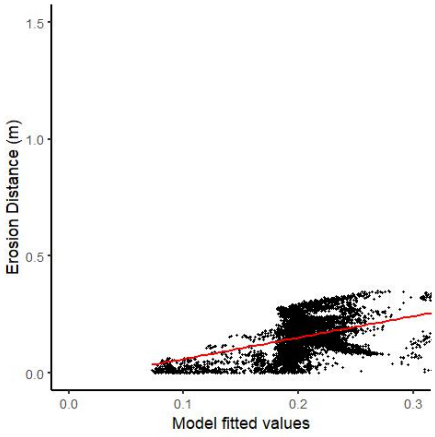

(c) E3 - R^2 = 0.535
p-value = <**0.001**

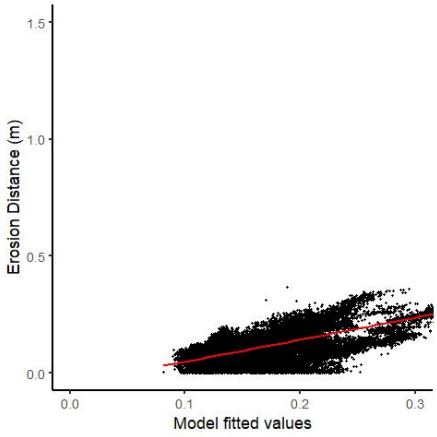

(d) E4 - R^2 = 0.700
p-value = <**0.001**

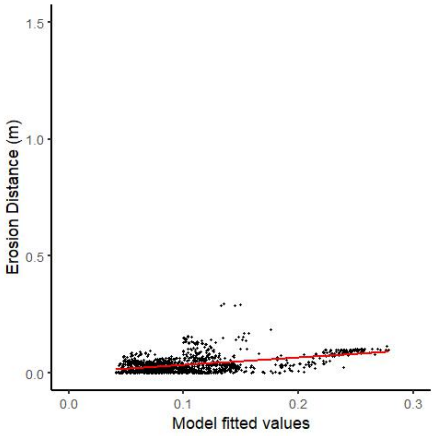

(e) E5 - R^2 = 0.514
p-value = <**0.001**

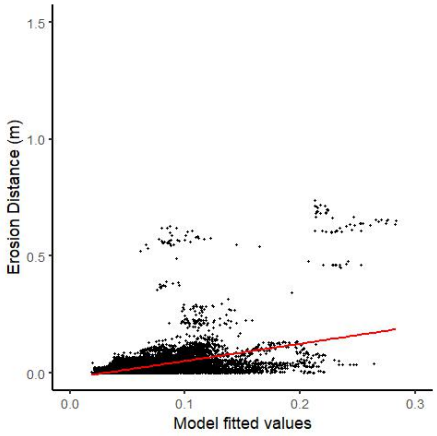

(f) E6 - R^2 = 0.339
p-value = <**0.001**

Figure F.4: Linear regression plots of change due to fluvial erosion below the Q10 level against roughness at the 0.5m scale for each survey period on the midstream reach of Bank 3

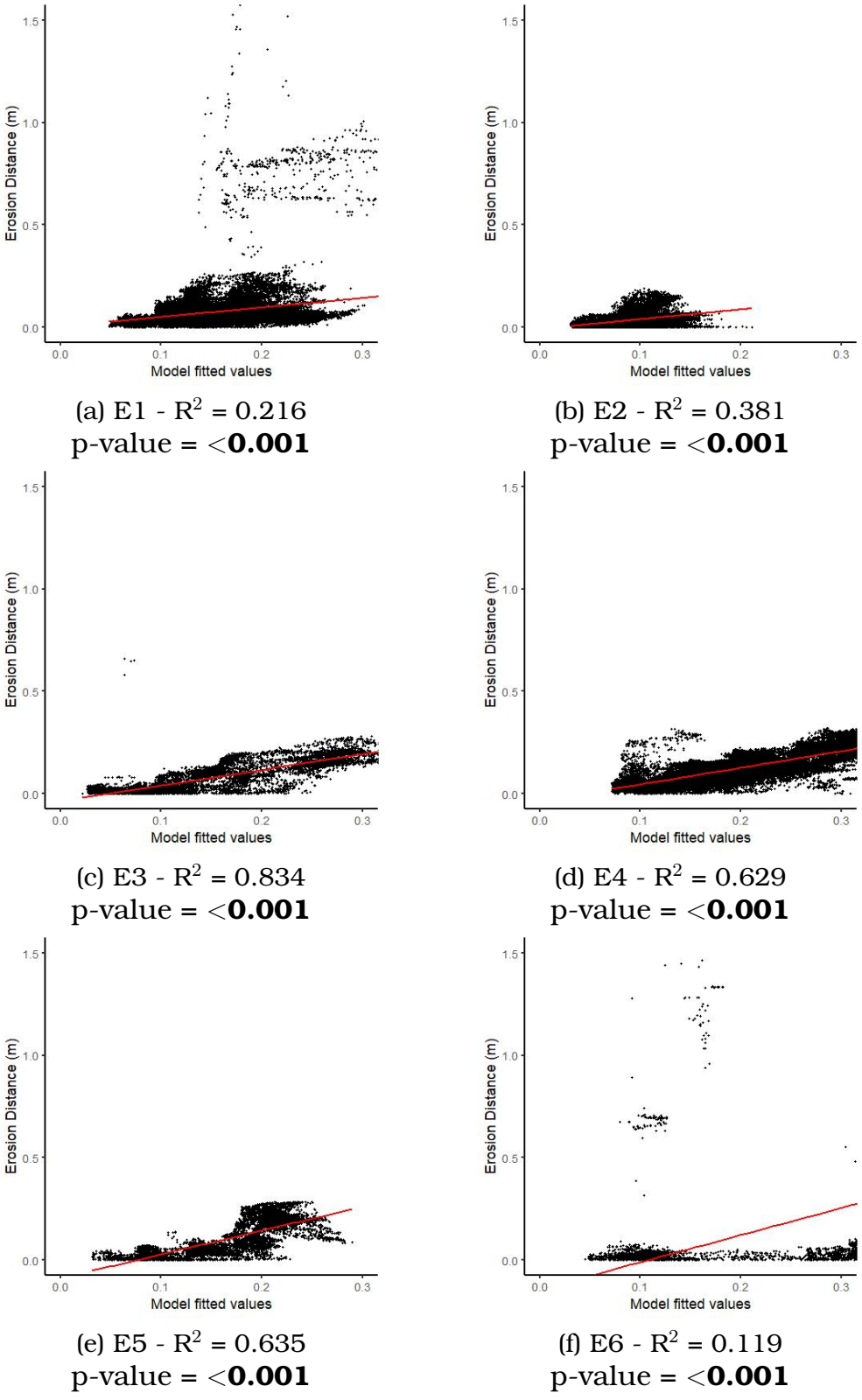

(a) E1 - R^2 = 0.216
p-value = <**0.001**

(b) E2 - R^2 = 0.381
p-value = <**0.001**

(c) E3 - R^2 = 0.834
p-value = <**0.001**

(d) E4 - R^2 = 0.629
p-value = <**0.001**

(e) E5 - R^2 = 0.635
p-value = <**0.001**

(f) E6 - R^2 = 0.119
p-value = <**0.001**

Figure F.5: Linear regression plots of change due to fluvial erosion below the Q10 level against roughness at the 0.5m scale for each survey period on the downstream reach of Bank 3

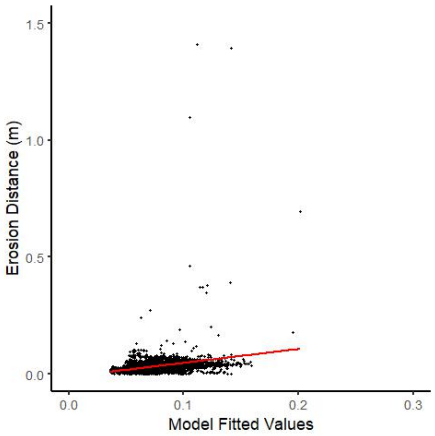

(a) E1 - R^2 = 0.092
p-value = <**0.001**

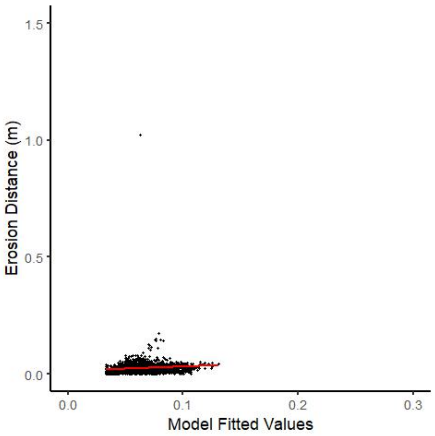

(b) E2 - R^2 = 0.048
p-value = <**0.001**

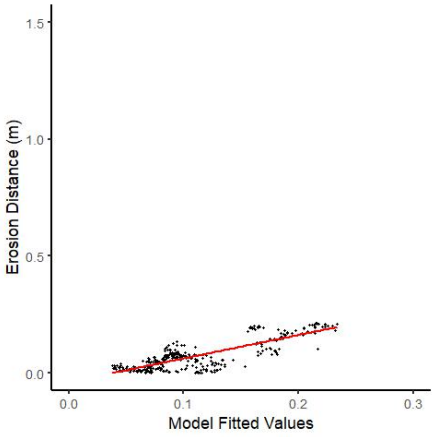

(c) E3 - R^2 = 0.846
p-value = <**0.001**

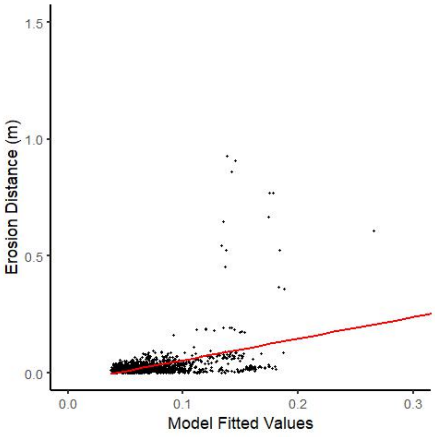

(d) E4 - R^2 = 0.431
p-value = <**0.001**

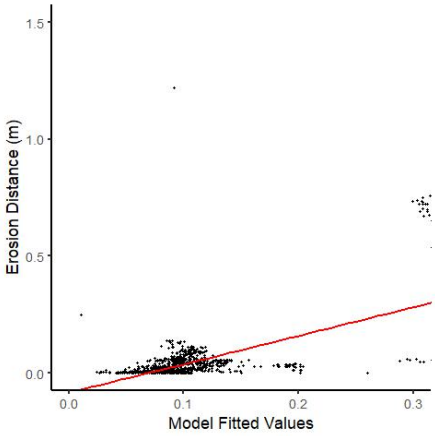

(e) E5 - R^2 = 0.511
p-value = <**0.001**

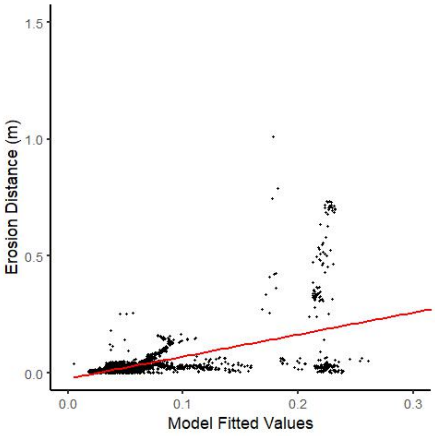

(f) E6 - R^2 = 0.413
p-value = <**0.001**

Figure F.6: Linear regression plots of change due to fluvial erosion below the Q10 level against roughness at the 0.25m scale for each survey period on Bank 1

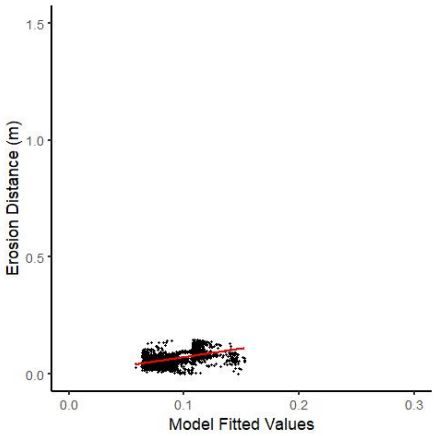

(a) E1 - R^2 = 0.471
p-value = <**0.001**

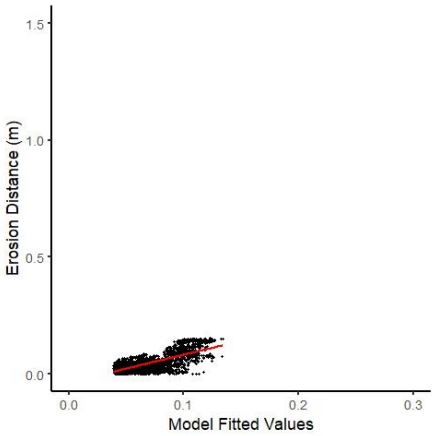

(b) E2 - R^2 = 0.576
p-value = <**0.001**

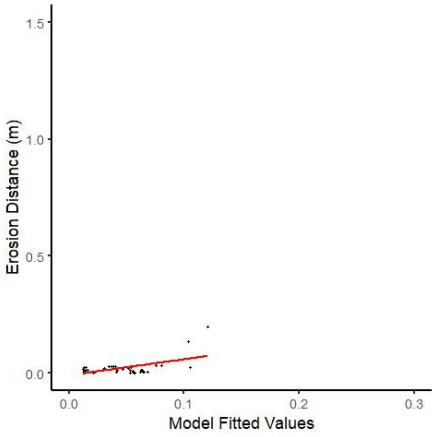

(c) E3 - R^2 = 0.681
p-value = <**0.001**

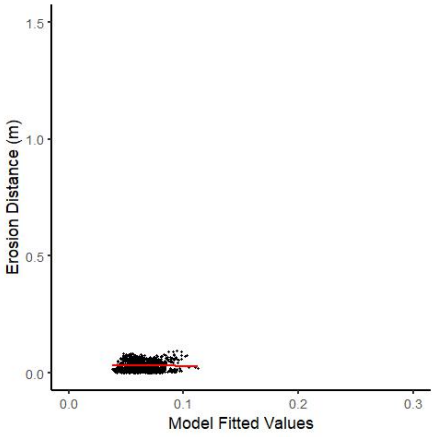

(d) E4 - R^2 = 0.504
p-value = <**0.001**

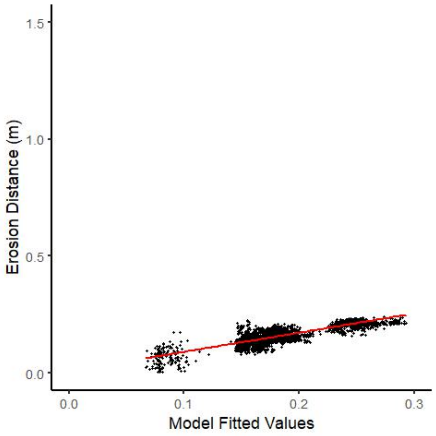

(e) E5 - R^2 = 0.785
p-value = <**0.001**

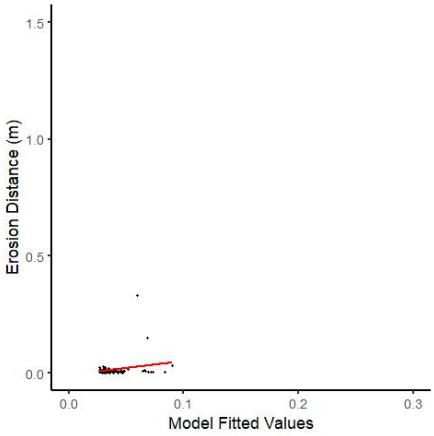

(f) E6 - R^2 = 0.162
p-value = **0.002**

Figure F.7: Linear regression plots of change due to fluvial erosion below the Q10 level against roughness at the 0.25m scale for each survey period on Bank 2

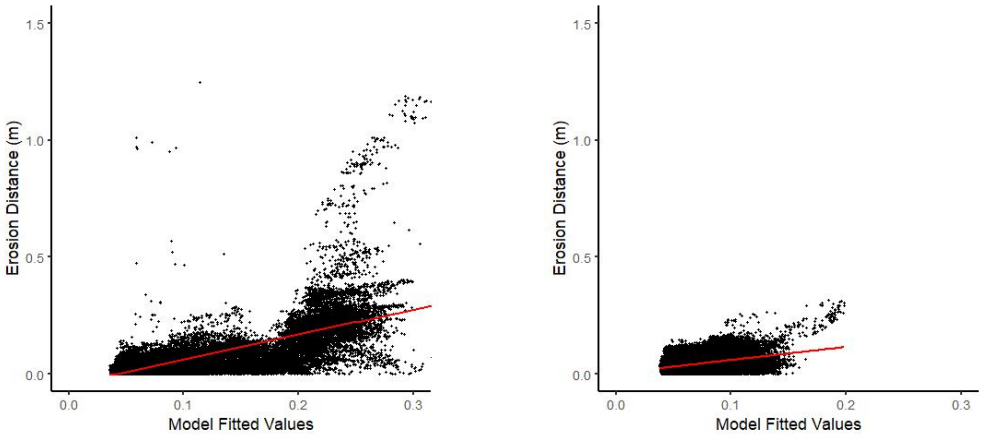

(a) E1 - R^2 = 0.503
p-value = <**0.001**

(b) E2 - R^2 = 0.182
p-value = <**0.001**

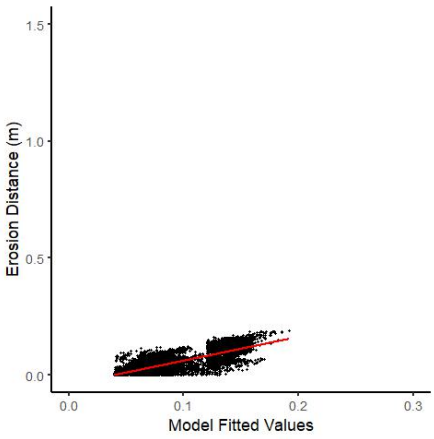

(c) E3 - R^2 = 0.616
p-value = <**0.001**

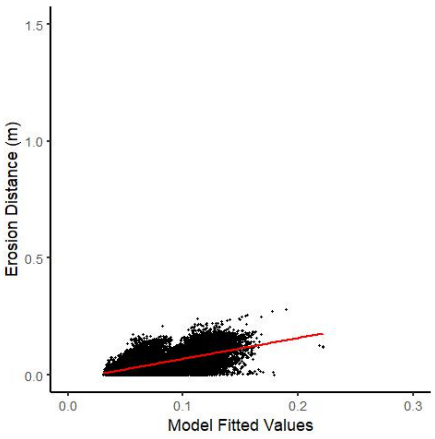

(d) E4 - R^2 = 0.337
p-value = <**0.001**

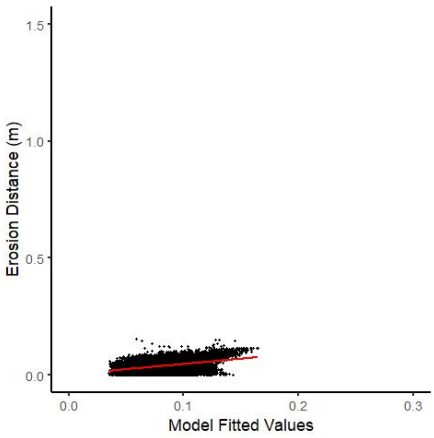

(e) E5 - R^2 = 0.438
p-value = <**0.001**

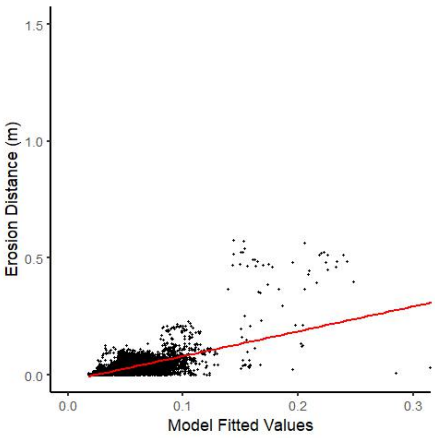

(f) E6 - R^2 = 0.381
p-value = <**0.001**

Figure F.8: Linear regression plots of change due to fluvial erosion below the Q10 level against roughness at the 0.25m scale for each survey period on the upstream reach of Bank 3

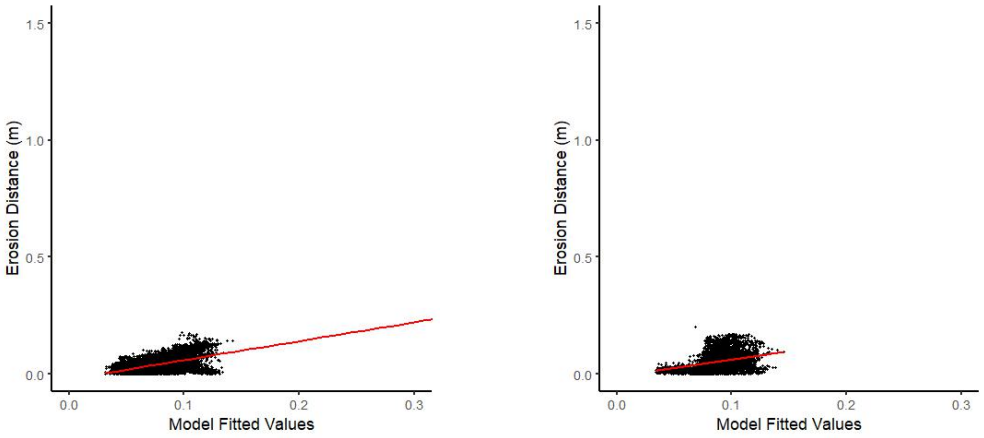

(a) E1 - R^2 = 0.641
p-value = <**0.001**

(b) E2 - R^2 = 0.206
p-value = <**0.001**

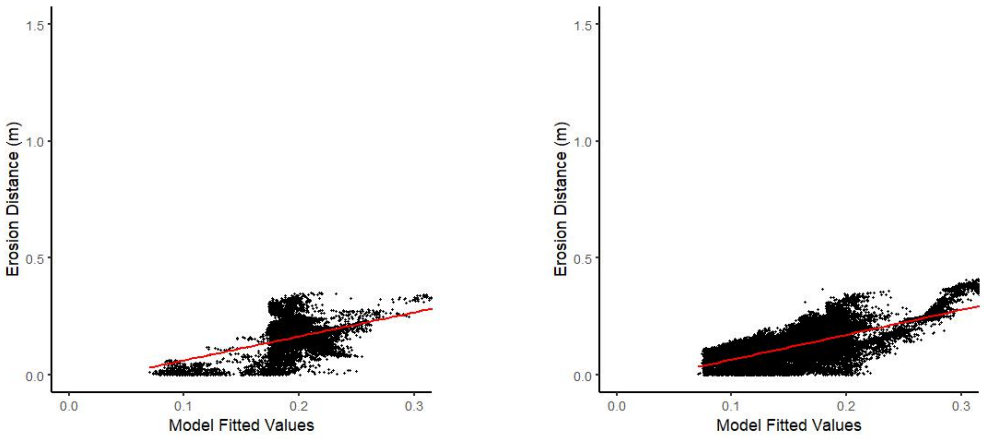

(c) E3 - R^2 = 0.519
p-value = <**0.001**

(d) E4 - R^2 = 0.640
p-value = <**0.001**

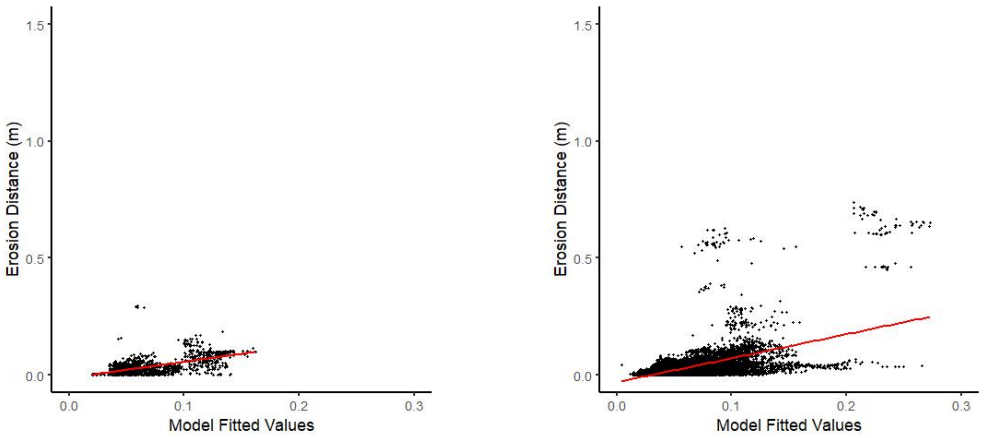

(e) E5 - R^2 = 0.502
p-value = <**0.001**

(f) E6 - R^2 = 0.338
p-value = <**0.001**

Figure F.9: Linear regression plots of change due to fluvial erosion below the Q10 level against roughness at the 0.25m scale for each survey period on the midstream reach of Bank 3

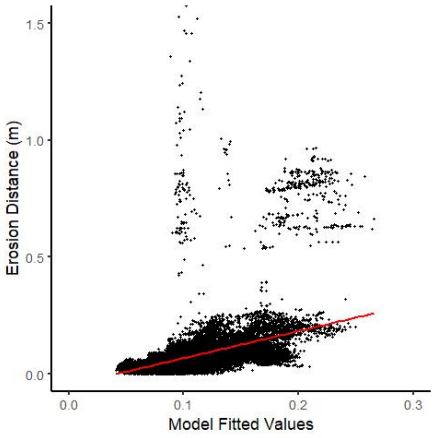

(a) E1 - R^2 = 0.219
p-value = <**0.001**

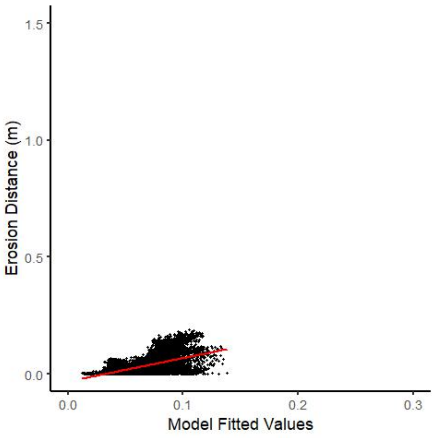

(b) E2 - R^2 = 0.396
p-value = <**0.001**

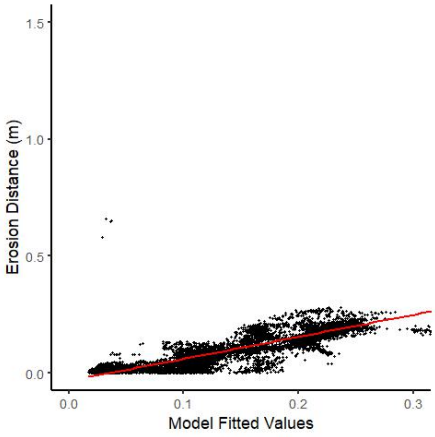

(c) E3 - R^2 = 0.817
p-value = <**0.001**

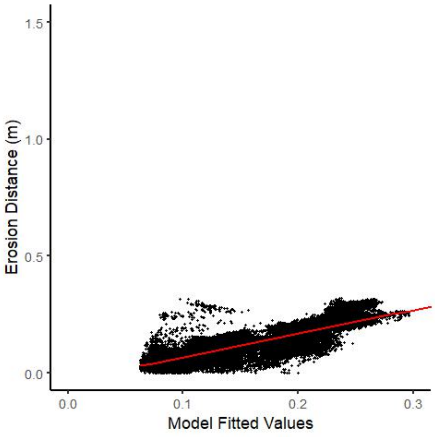

(d) E4 - R^2 = 0.627
p-value = <**0.001**

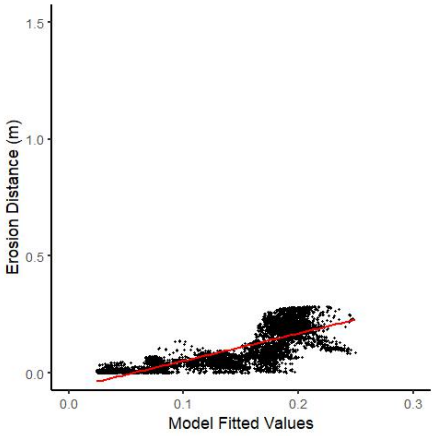

(e) E5 - R^2 = 0.636
p-value = <**0.001**

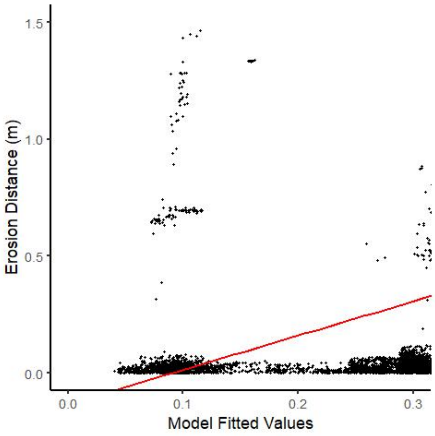

(f) E6 - R^2 = 0.110
p-value = <**0.001**

Figure F.10: Linear regression plots of change due to fluvial erosion below the Q10 level against roughness at the 0.25m scale for each survey period on the downstream reach of Bank 3

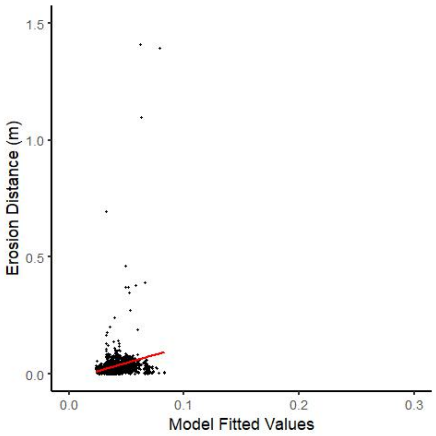

(a) E1 - R^2 = 0.060
p-value = <**0.001**

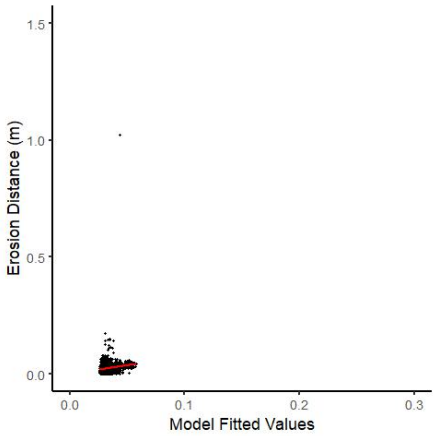

(b) E2 - R^2 = 0.032
p-value = <**0.001**

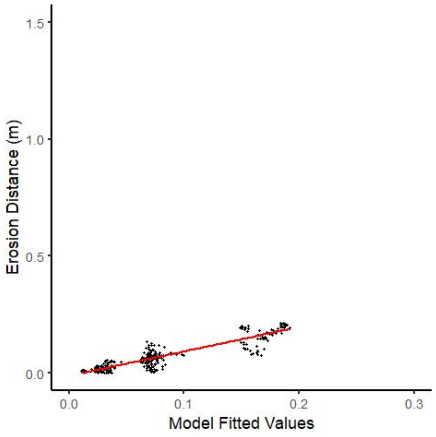

(c) E3 - R^2 = 0.817
p-value = <**0.001**

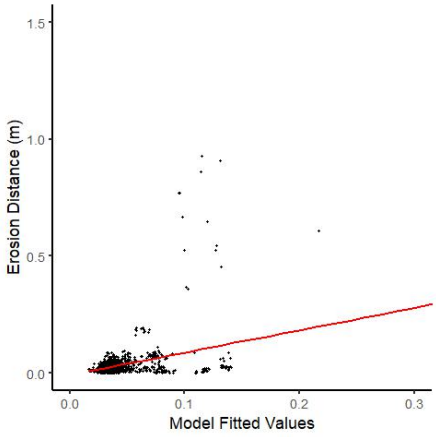

(d) E4 - R^2 = 0.418
p-value = <**0.001**

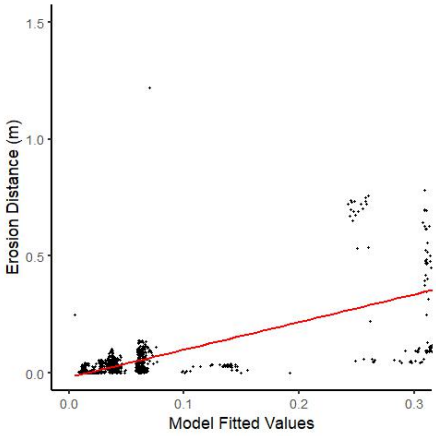

(e) E5 - R^2 = 0.500
p-value = <**0.001**

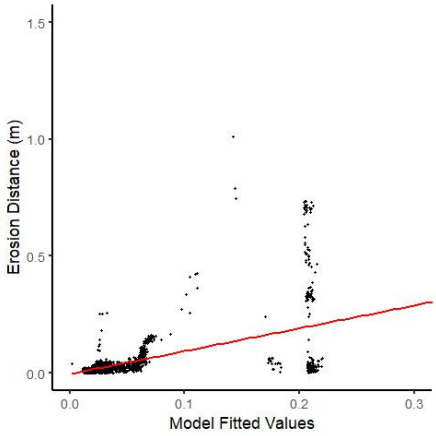

(f) E6 - R^2 = 0.408
p-value = <**0.001**

Figure F.11: Linear regression plots of change due to fluvial erosion below the Q10 level against roughness at the 0.03m scale for each survey period on Bank 1

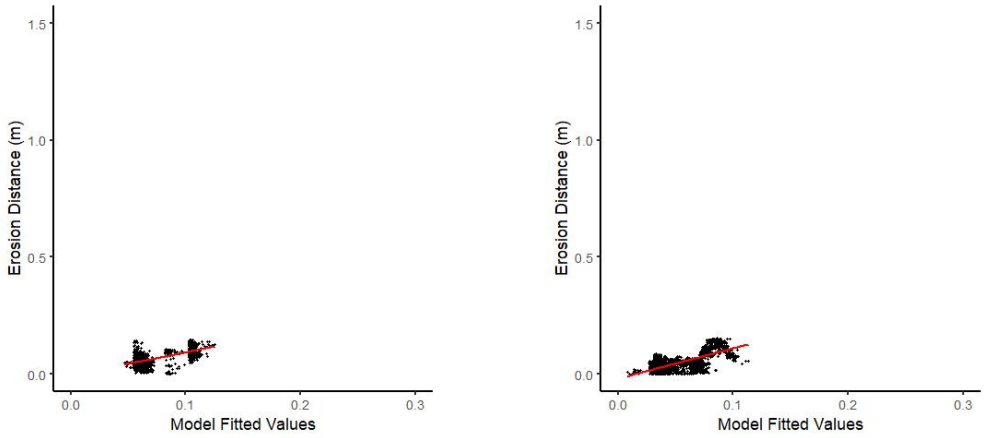

(a) E1 - R^2 = 0.475
p-value = <**0.001**

(b) E2 - R^2 = 0.532
p-value = <**0.001**

(c) E3 - R^2 = 0.240
p-value = <**0.001**

(d) E4 - R^2 = 0.430
p-value = <**0.001**

(e) E5 - R^2 = 0.781
p-value = <**0.001**

(f) E6 - R^2 = 0.044
p-value = 0.120

Figure F.12: Linear regression plots of change due to fluvial erosion below the Q10 level against roughness at the 0.03m scale for each survey period on Bank 2

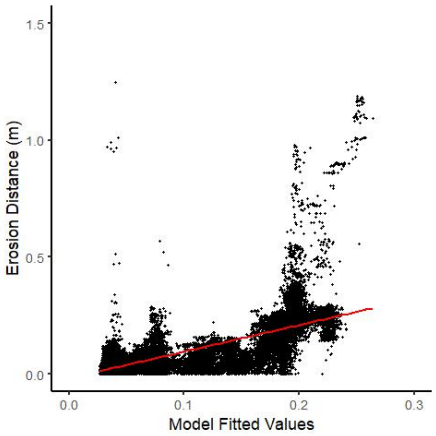

(a) E1 - R^2 = 0.498
p-value = <**0.001**

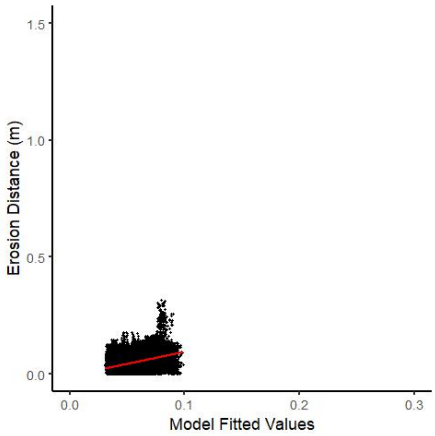

(b) E2 - R^2 = 0.177
p-value = <**0.001**

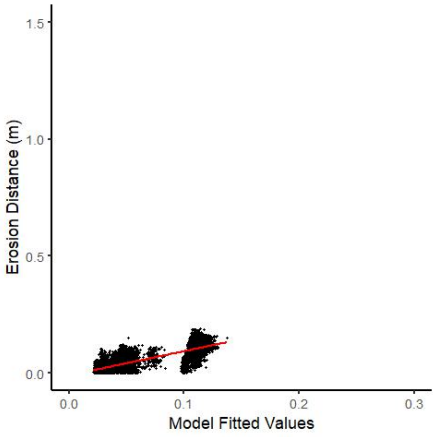

(c) E3 - R^2 = 0.599
p-value = <**0.001**

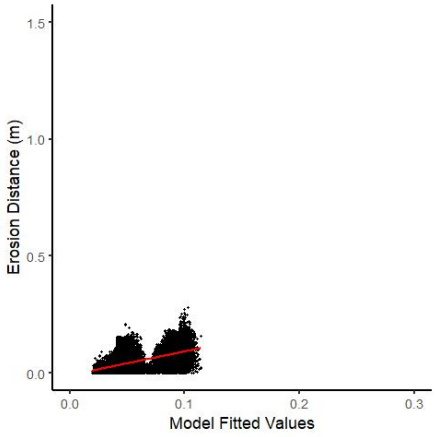

(d) E4 - R^2 = 0.322
p-value = <**0.001**

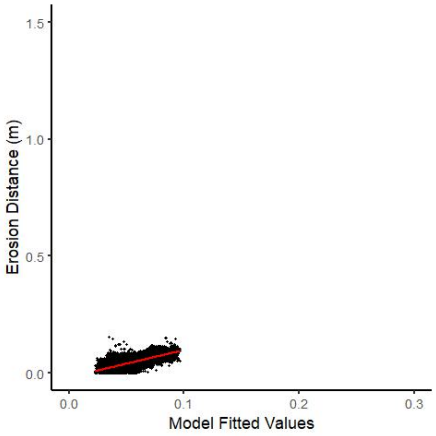

(e) E5 - R^2 = 0.439
p-value = <**0.001**

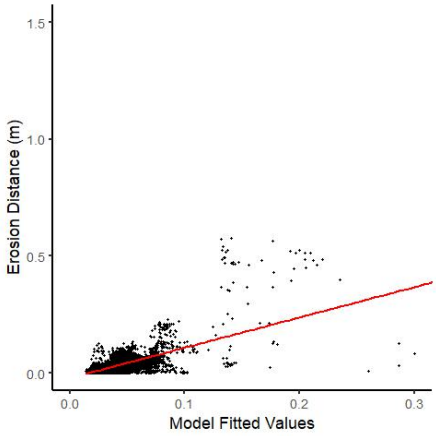

(f) E6 - R^2 = 0.393
p-value = <**0.001**

Figure F.13: Linear regression plots of change due to fluvial erosion below the Q10 level against roughness at the 0.03m scale for each survey period on the upstream reach of Bank 3

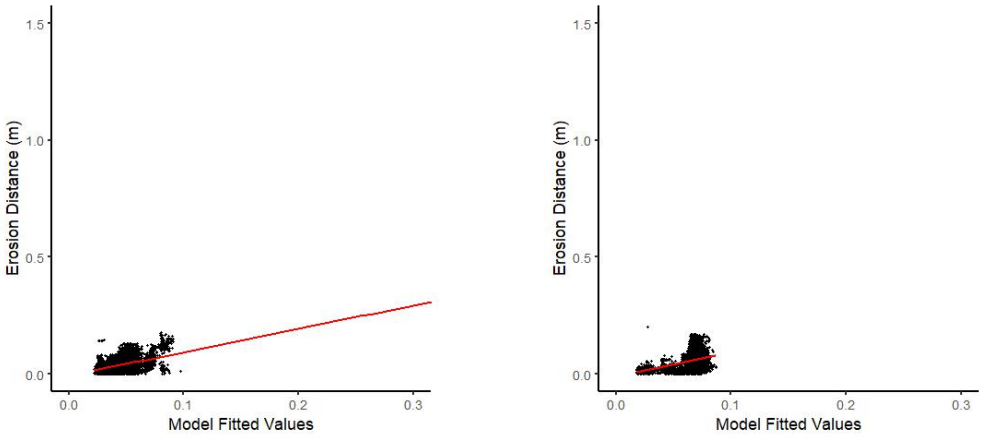

(a) E1 - R^2 = 0.618
p-value = <**0.001**

(b) E2 - R^2 = 0.214
p-value = <**0.001**

(c) E3 - R^2 = 0.521
p-value = <**0.001**

(d) E4 - R^2 = 0.632
p-value = <**0.001**

(e) E5 - R^2 = 0.499
p-value = <**0.001**

(f) E6 - R^2 = 0.339
p-value = <**0.001**

Figure F.14: Linear regression plots of change due to fluvial erosion below the Q10 level against roughness at the 0.03m scale for each survey period on the midstream reach of Bank 3

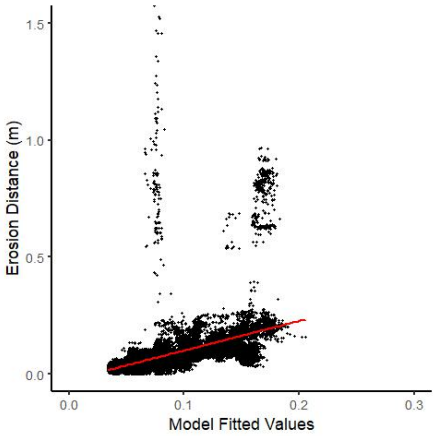

(a) E1 - R^2 = 0.209
p-value = <**0.001**

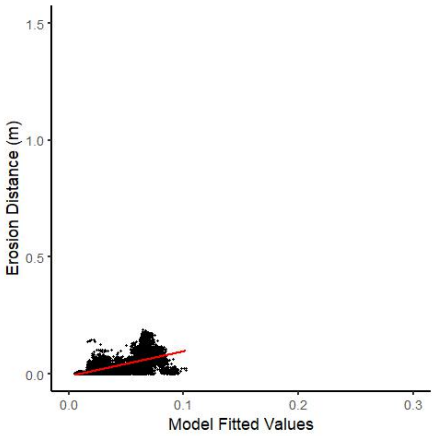

(b) E2 - R^2 = 0.365
p-value = <**0.001**

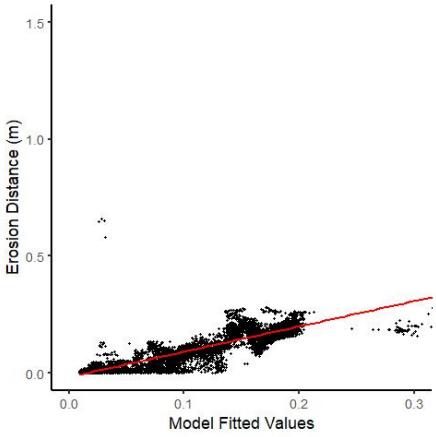

(c) E3 - R^2 = 0.800
p-value = <**0.001**

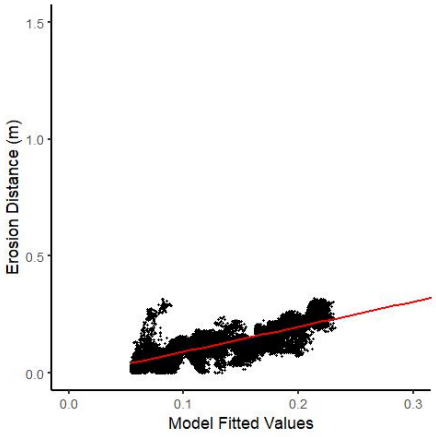

(d) E4 - R^2 = 0.622
p-value = <**0.001**

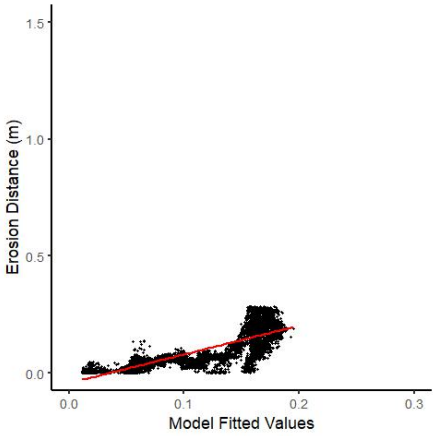

(e) E5 - R^2 = 0.668
p-value = <**0.001**

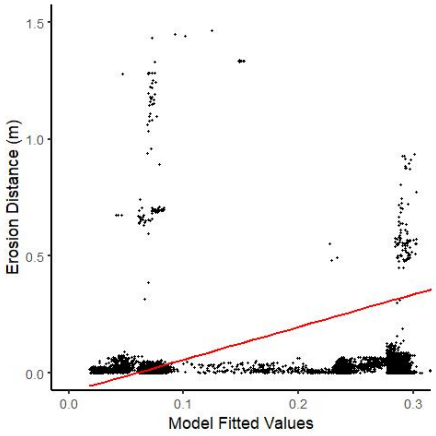

(f) E6 - R^2 = 0.147
p-value = <**0.001**

Figure F.15: Linear regression plots of change due to fluvial erosion below the Q10 level against roughness at the 0.03m scale for each survey period on the downstream reach of Bank 3

Interaction plots

This section provides the individual interaction plots for each of the banks and time periods that exhibited statistically significant 3-way interaction - all of bank 1 time periods, Bank 2 time period E5, Bank 3 Upstream time periods E1, E2 and E5, Bank 3 Midstream time periods E1, E4 and E6 and finally Bank 3 Downstream time periods E2 and E6.

Table F.1: Slope coefficients for the effect of roughness at the 0.03m roughness scale against bank erosion for each combination of 0.5m scale and 0.25m scale interactions. P-values for the coefficients are provided in brackets and those that are statistically significant at the 0.05 significance level are highlighted in **bold**. For quick visual comparison, cells with a positive coefficient have been coloured green and those with a negative coefficient have been coloured orange

	Low roughness at the 0.5m scale	Average roughness at the 0.5m scale	High roughness at the 0.5m scale	Model R-Squared	Model P-value
Bank 1 - E1					
Low roughness at the 0.25m scale	**-3.43 (<0.01)**	**-2.08 (<0.01)**	-0.73 (0.48)		
Average roughness at the 0.25m scale	-0.06 (0.90)	-0.26 (0.50)	-0.46 (0.53)	0.117	<0.01
High roughness at the 0.25m scale	**3.30 (<0.01)**	**1.55 (0.01)**	-0.19 (0.72)		
Bank 1 - E2					
Low roughness at the 0.25m scale	-0.37 (0.40)	-0.08 (0.84)	0.21 (0.76)		
Average roughness at the 0.25m scale	**-1.09 (0.01)**	-0.35 (0.22)	0.39 (0.38)	0.101	<0.01
High roughness at the 0.25m scale	**-1.80 (0.01)**	-0.62 (0.17)	0.56 (0.12)		
Bank 1 - E3					
Low roughness at the 0.25m scale	-0.28 (0.70)	-0.36 (0.37)	-0.99 (0.43)		
Average roughness at the 0.25m scale	**2.13 (<0.01)**	**0.92 (0.04)**	-0.29 (0.74)	0.865	<0.01
High roughness at the 0.25m scale	**4.53 (<0.01)**	**2.47 (<0.01)**	0.41 (0.49)		
Bank 1 - E4					
Low roughness at the 0.25m scale	-0.32 (0.78)	-0.22 (0.82)	-0.11 (0.95)		
Average roughness at the 0.25m scale	1.17 (0.18)	0.07 (0.91)	-1.03 (0.34)	0.490	<0.01
High roughness at the 0.25m scale	2.66 (0.06)	0.36 (0.71)	**-1.95 (0.03)**		
Bank 1 - E5					
Low roughness at the 0.25m scale	-4.31 (0.07)	-2.06 (0.43)	0.18 (0.97)		
Average roughness at the 0.25m scale	3.12 (0.11)	2.06 (0.20)	1.00 (0.71)	0.561	<0.01
High roughness at the 0.25m scale	**10.56 (<0.01)**	**6.19 (<0.01)**	1.82 (0.32)		
Bank 1 - E6					
Low roughness at the 0.25m scale	-3.00 (0.06)	-1.39 (0.21)	0.22 (0.90)		

Table F.2: Slope coefficients for the effect of roughness at the 0.03m roughness scale against bank erosion for each combination of 0.5m scale and 0.25m scale interactions. P-values for the coefficients are provided in brackets and those that are statistically significant at the 0.05 significance level are highlighted in **bold**. For quick visual comparison, cells with a positive coefficient have been coloured green and those with a negative coefficient have been coloured orange

	Low roughness at the 0.5m scale	Average roughness at the 0.5m scale	High roughness at the 0.5m scale	Model R-Squared	Model P-value
Bank 2 - E5					
Low roughness at the 0.25m scale	0.34 (0.10)	0.17 (0.34)	-0.01 (0.98)		
Average roughness at the 0.25m scale	**-0.40 (0.01)**	**-0.35 (<0.01)**	-0.30 (0.12)	0.788	<0.01
High roughness at the 0.25m scale	**-1.14 (<0.01)**	**-0.886 (<0.01)**	**-0.58 (<0.01)**		
Bank 3 - Upstream - E1					
Low roughness at the 0.25m scale	**1.19 (<0.01)**	**1.90 (<0.01)**	**2.61 (<0.01)**		
Average roughness at the 0.25m scale	**0.70 (<0.01)**	**1.15 (<0.01)**	**1.60 (<0.01)**	0.510	<0.01
High roughness at the 0.25m scale	0.21 (0.49)	**0.40 (0.05)**	**0.60 (<0.01)**		
Bank 3 - Upstream - E2					
Low roughness at the 0.25m scale	0.02 (0.85)	**0.95 (<0.01)**	**1.88 (<0.01)**		
Average roughness at the 0.25m scale	**-0.40 (<0.01)**	**0.21 (<0.01)**	**0.82 (<0.01)**	0.222	<0.01
High roughness at the 0.25m scale	**-0.81 (<0.01)**	**-0.52 (<0.01)**	**-0.23 (0.01)**		
Bank 3 - Upstream - E5					
Low roughness at the 0.25m scale	**0.50 (0.01)**	**1.21 (0.01)**	**1.93 (<0.01)**		
Average roughness at the 0.25m scale	0.08 (0.32)	**0.58 (0.01)**	**1.07 (<0.01)**	0.466	<0.01
High roughness at the 0.25m scale	**-0.34 (0.02)**	-0.06 (0.44)	**0.22 (<0.01)**		

Table F.3: Slope coefficients for the effect of roughness at the 0.03m roughness scale against bank erosion for each combination of 0.5m scale and 0.25m scale interactions. P-values for the coefficients are provided in brackets and those that are statistically significant at the 0.05 significance level are highlighted in **bold**. For quick visual comparison, cells with a positive coefficient have been coloured green and those with a negative coefficient have been coloured orange

		Bank 3 - Midstream - E1			
Low roughness at the 0.25m scale	**-0.32 (<0.01)**	0.14 (0.14)	**-0.60 (<0.01)**		
Average roughness at the 0.25m scale	**-0.21 (<0.01)**	-0.08 (0.24)	0.05 (0.63)	0.686	<0.01
High roughness at the 0.25m scale	-0.10 (0.50)	**-0.29 (<0.01)**	**-0.49 (<0.01)**		
		Bank 3 - Midstream - E4			
Low roughness at the 0.25m scale	**0.79 (<0.01)**	**1.04 (<0.01)**	**1.30 (<0.01)**		
Average roughness at the 0.25m scale	**0.68 (<0.01)**	**0.85 (<0.01)**	**1.02 (<0.01)**	0.717	<0.01
High roughness at the 0.25m scale	**0.58 (0.01)**	**0.66 (<0.01)**	**0.74 (<0.01)**		
		Bank 3 - Midstream - E5			
Low roughness at the 0.25m scale	-0.87 (0.06)	0.35 (0.31)	**1.56 (<0.01)**		
Average roughness at the 0.25m scale	**-0.95 (0.01)**	-0.01 (0.96)	**0.93 (0.02)**	0.519	<0.01
High roughness at the 0.25m scale	-1.04 (0.07)	-0.37 (0.34)	0.29 (0.39)		
		Bank 3 - Downstream - E1			
Low roughness at the 0.25m scale	0.12 (0.57)	0.35 (0.07)	0.57 (0.07)		
Average roughness at the 0.25m scale	-0.21 (0.26)	0.08 (0.51)	0.37 (0.09)	0.221	<0.01
High roughness at the 0.25m scale	-0.54 (0.07)	-0.19 (0.31)	0.16 (0.33)		
		Bank 3 - Downstream - E2			
Low roughness at the 0.25m scale	**0.71 (<0.01)**	0.08 (0.61)	**-0.55 (0.04)**		
Average roughness at the 0.25m scale	-0.13 (0.38)	**-0.46 (<0.01)**	**-0.79 (<0.01)**	0.408	<0.01
High roughness at the 0.25m scale	**-0.96 (<0.01)**	**-1.00 (<0.01)**	**-1.04 (<0.01)**		
		Bank 3 - Downstream - E6			
Low roughness at the 0.25m scale	**12.52 (<0.01)**	0.37 (0.91)	**-11.77 (0.02)**		
Average roughness at the 0.25m scale	4.95 (0.10)	-3.26 (0.15)	**-11.50 (0.02)**	0.206	<0.01
High roughness at the 0.25m scale	-2.62 (0.57)	**-6.93 (0.02)**	**-11.23**		

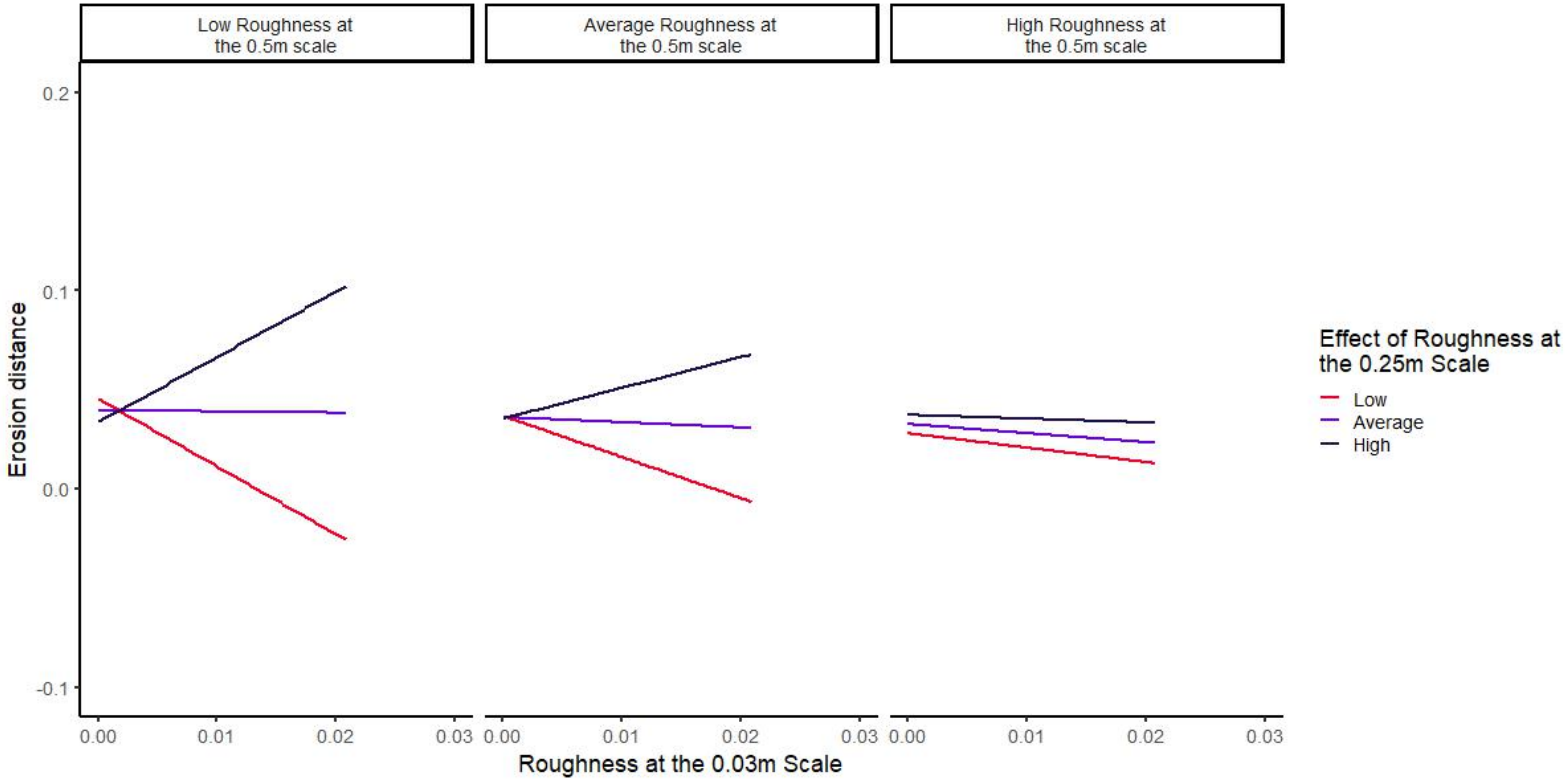

Figure F.16: Interaction plot of the effect of roughness at each scale on erosion for time period E1 on Bank 1

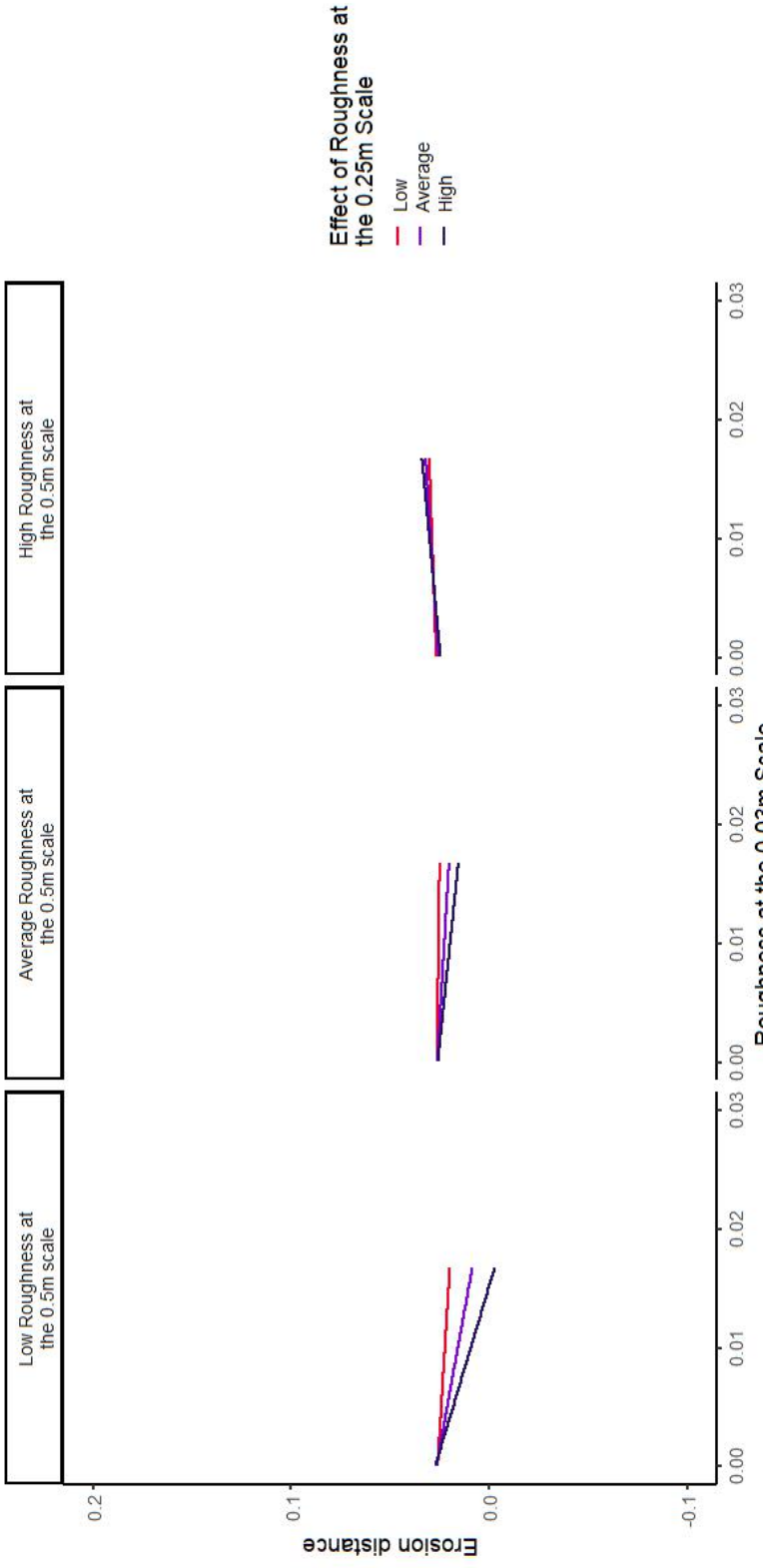

Figure F.17: Interaction plot of the effect of roughness at each scale on erosion for time period E2 on Bank 1

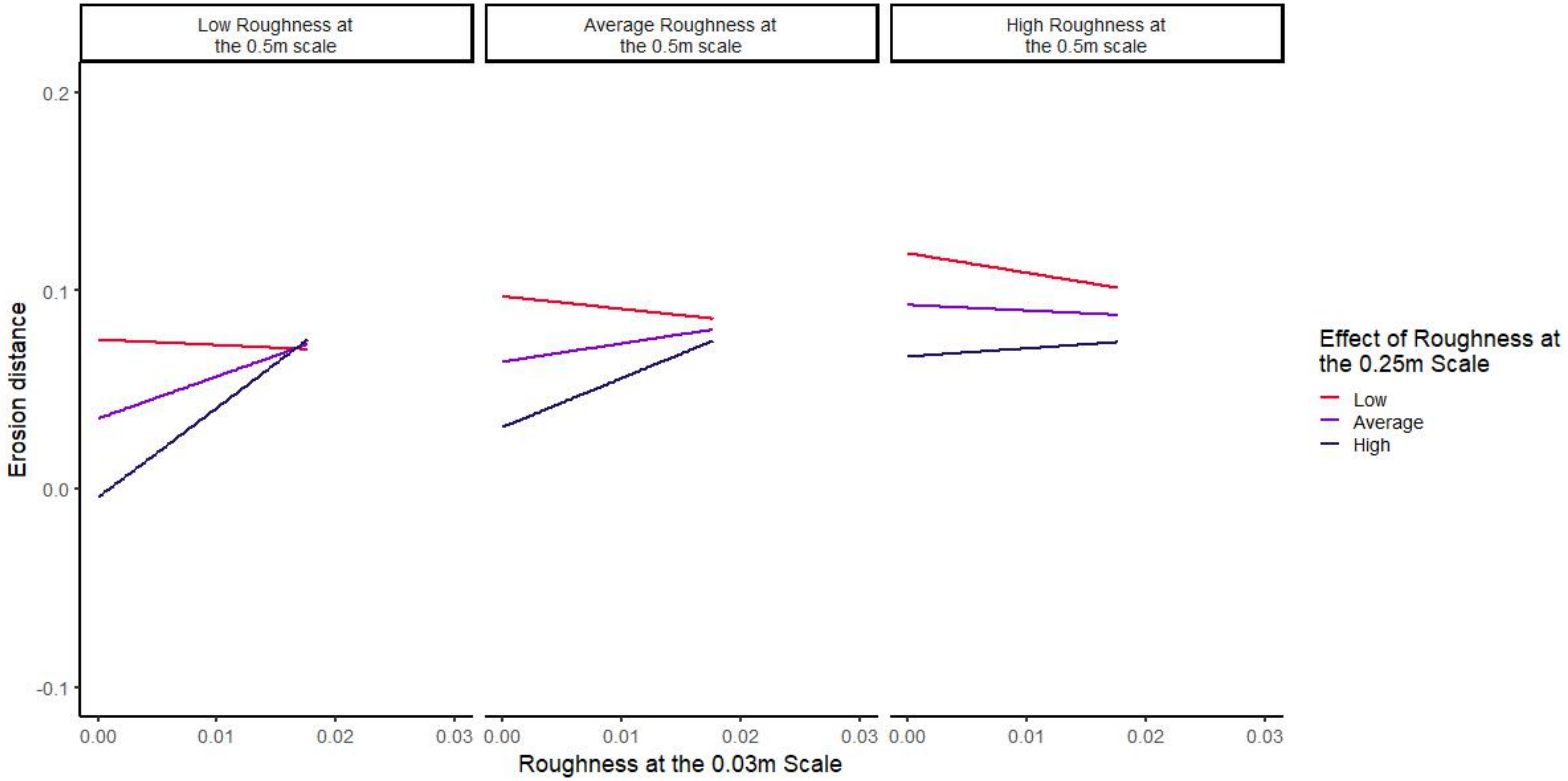

Figure F.18: Interaction plot of the effect of roughness at each scale on erosion for time period E3 on Bank 1

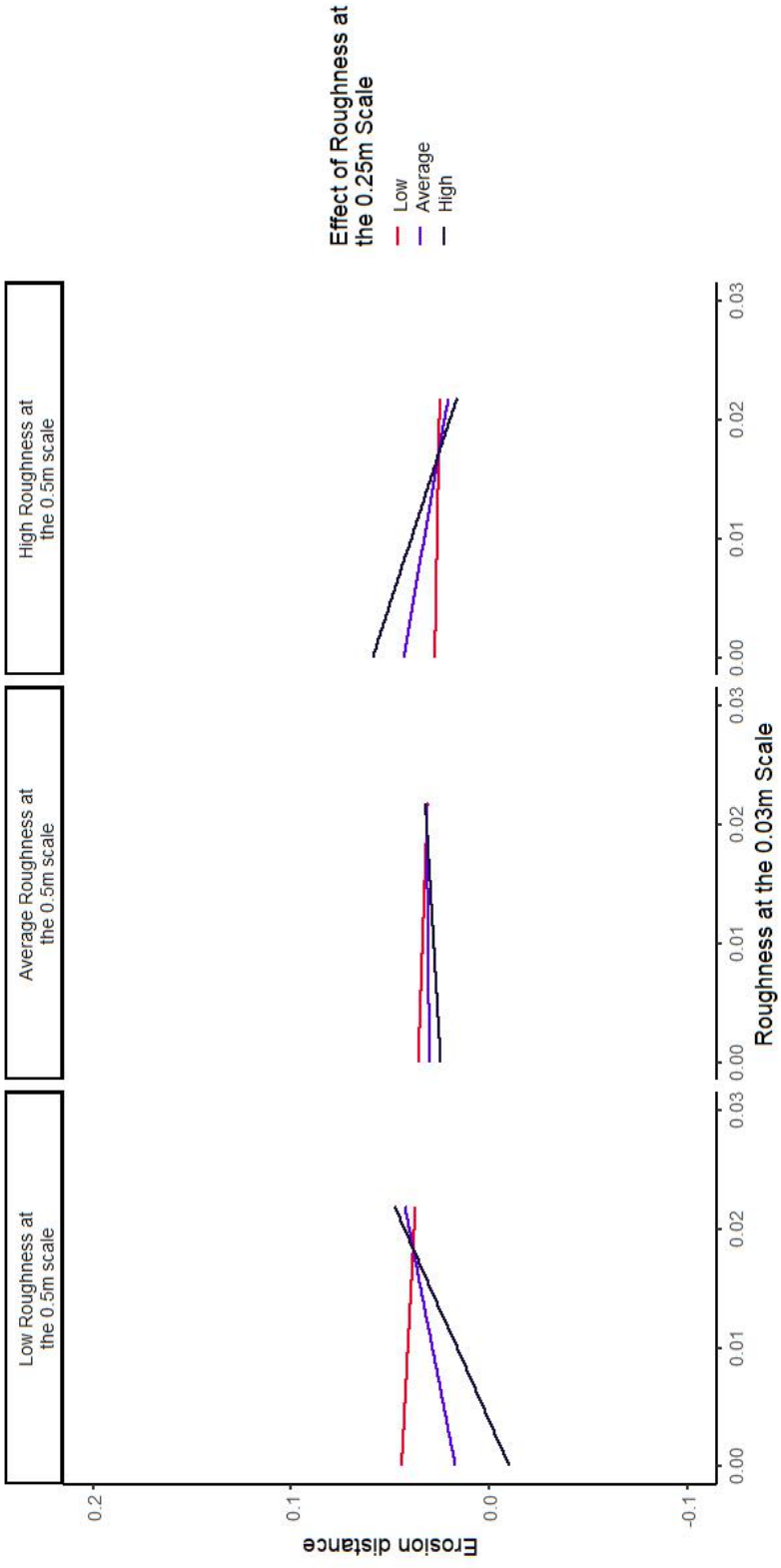

Figure F.19: Interaction plot of the effect of roughness at each scale on erosion for time period E4 on Bank 1

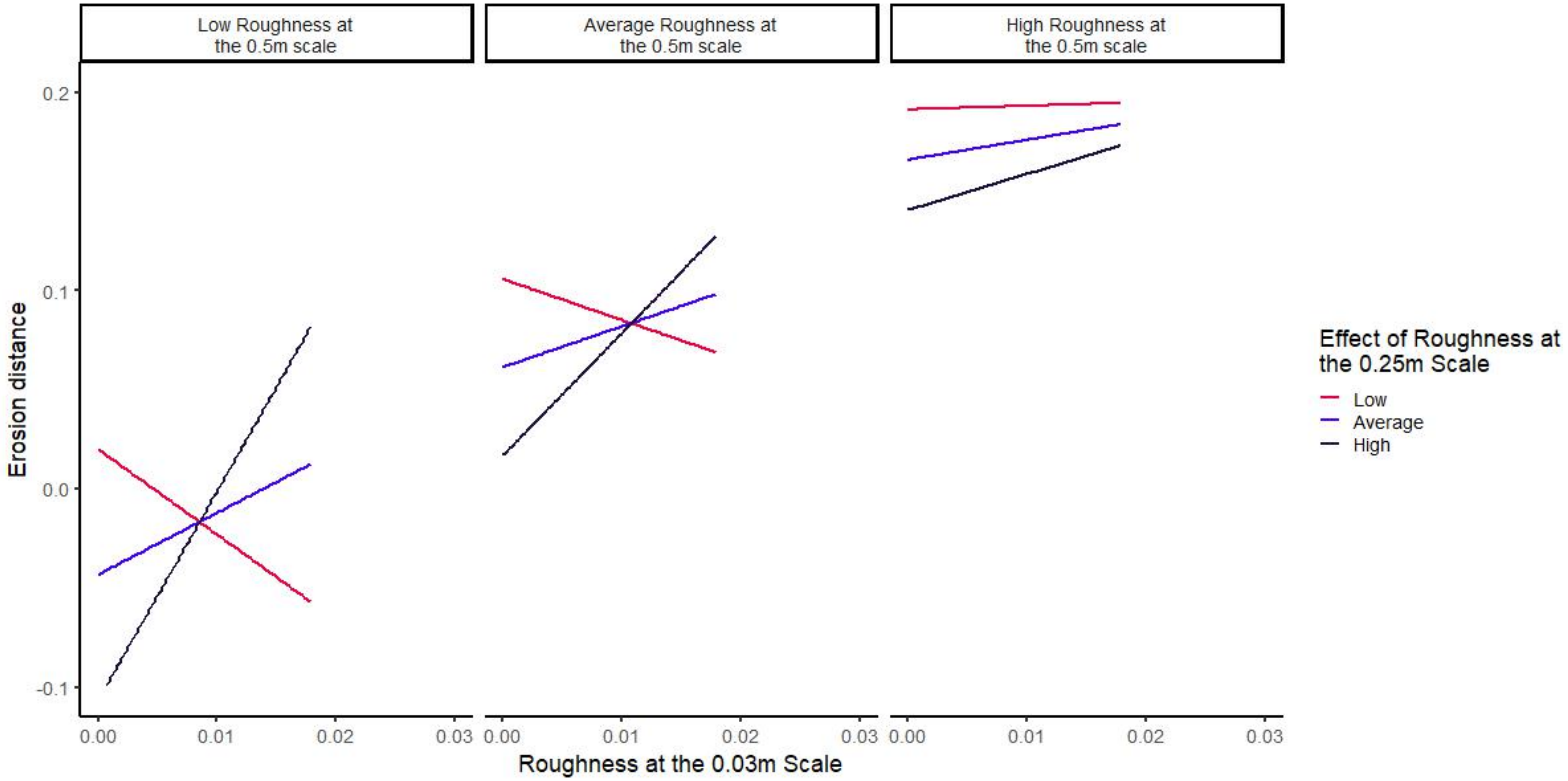

Figure F.20: Interaction plot of the effect of roughness at each scale on erosion for time period E5 on Bank 1

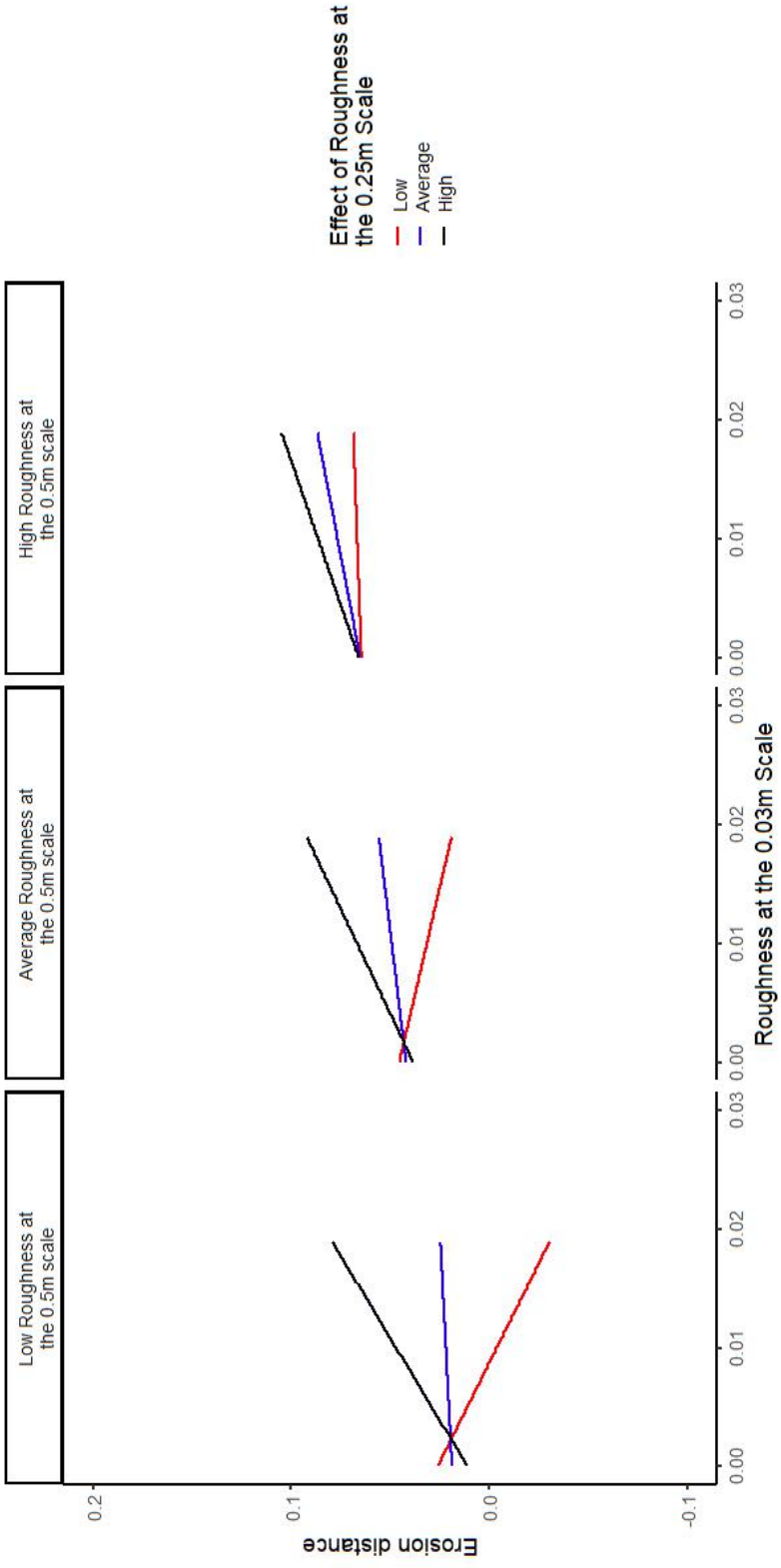

Figure F.21: Interaction plot of the effect of roughness at each scale on erosion for time period E6 on Bank 1

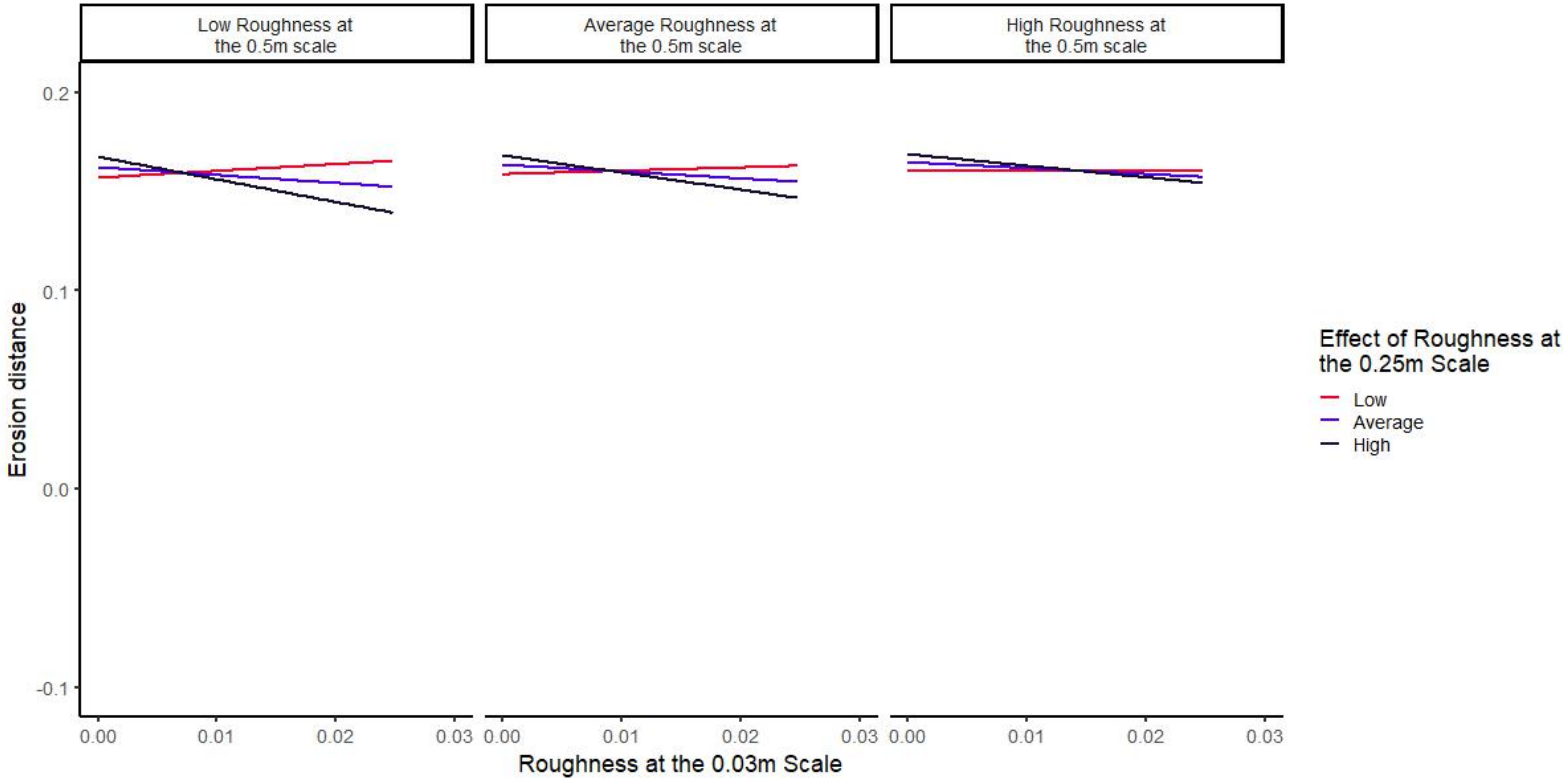

Figure F.22: Interaction plot of the effect of roughness at each scale on erosion for time period E5 on Bank 2

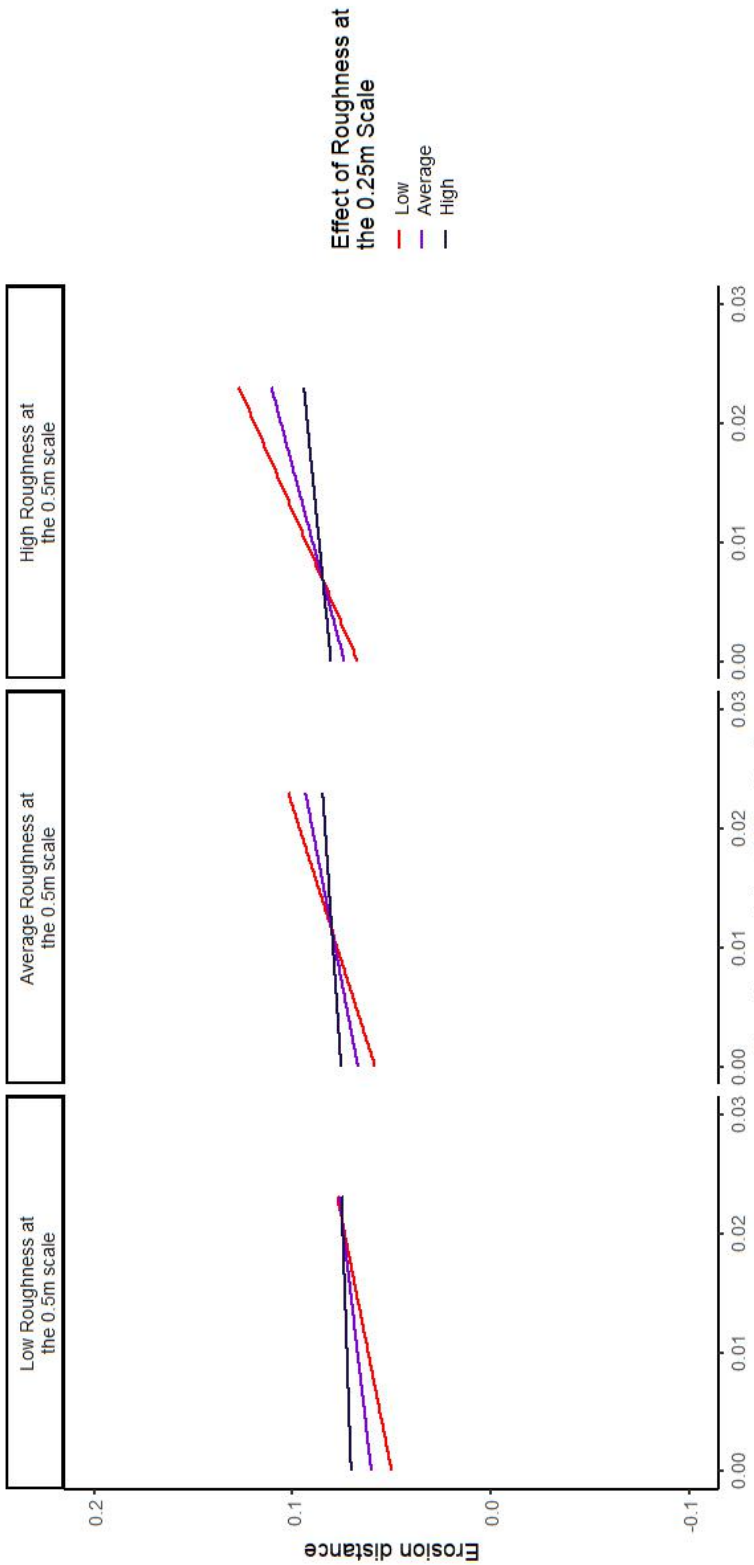

Figure F.23: Interaction plot of the effect of roughness at each scale on erosion for time period E1 on the upstream reach of Bank 3

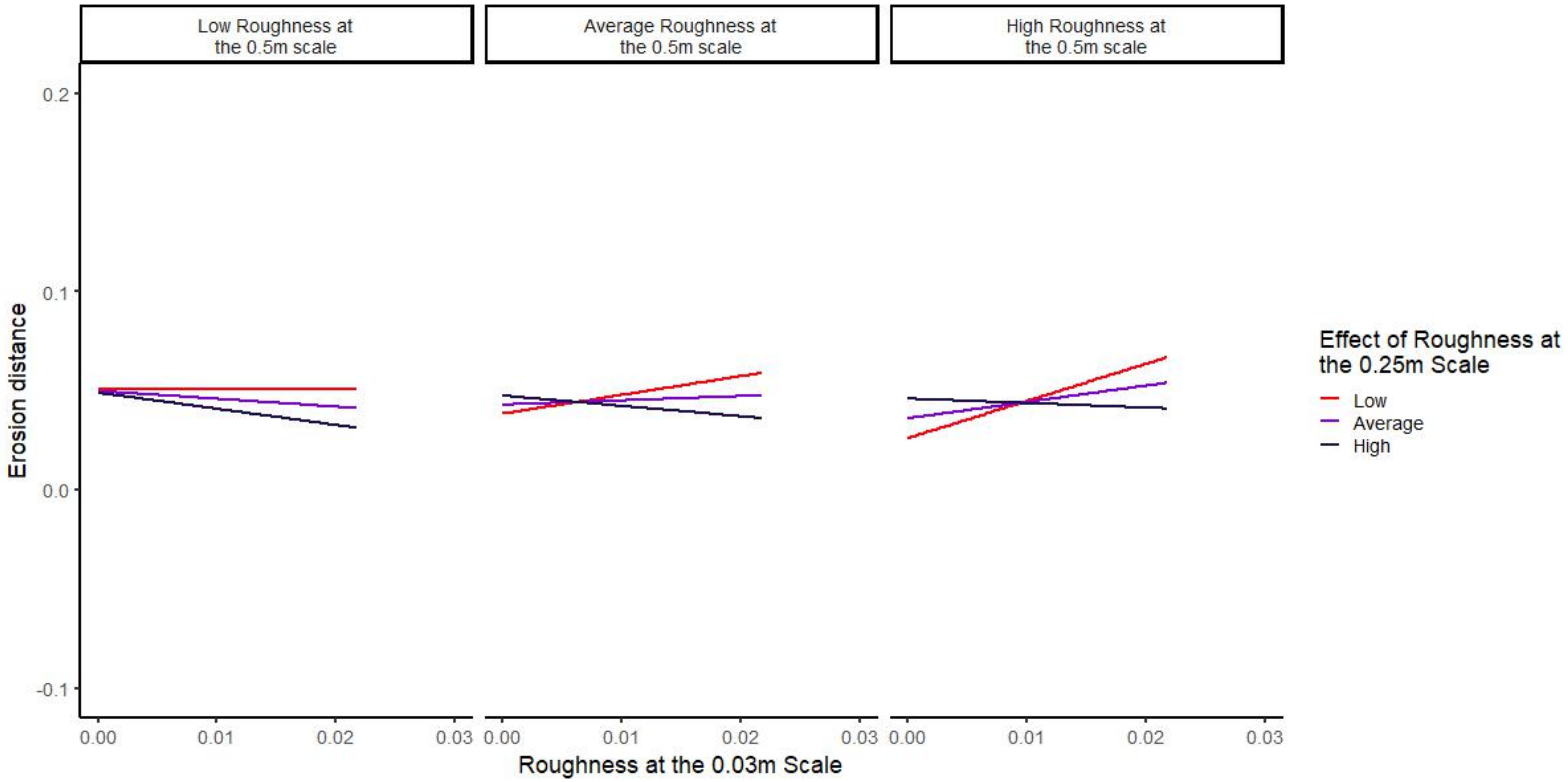

Figure F.24: Interaction plot of the effect of roughness at each scale on erosion for time period E2 on the upstream reach of Bank 3

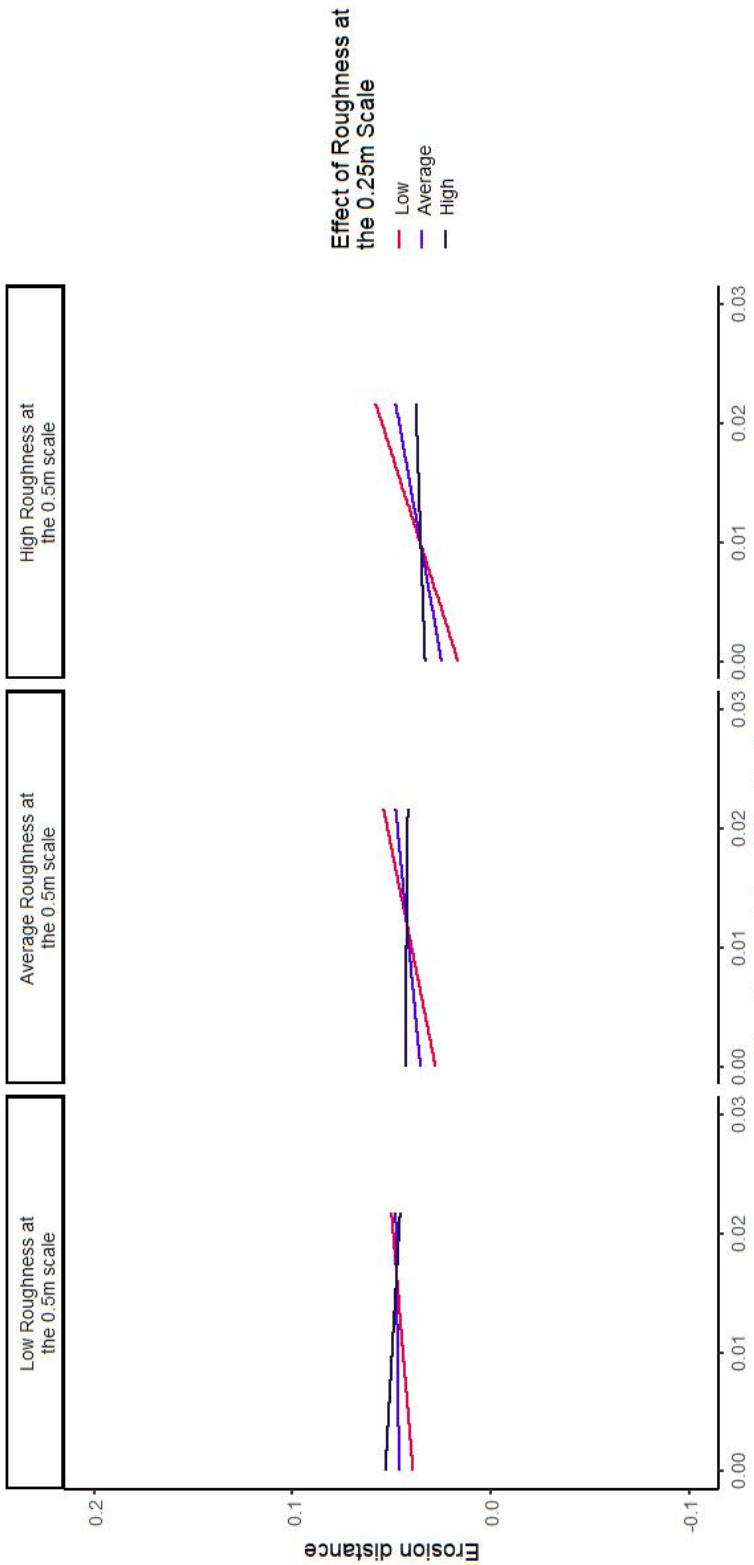

Figure F.25: Interaction plot of the effect of roughness at each scale on erosion for time period E5 on the upstream reach of Bank 3

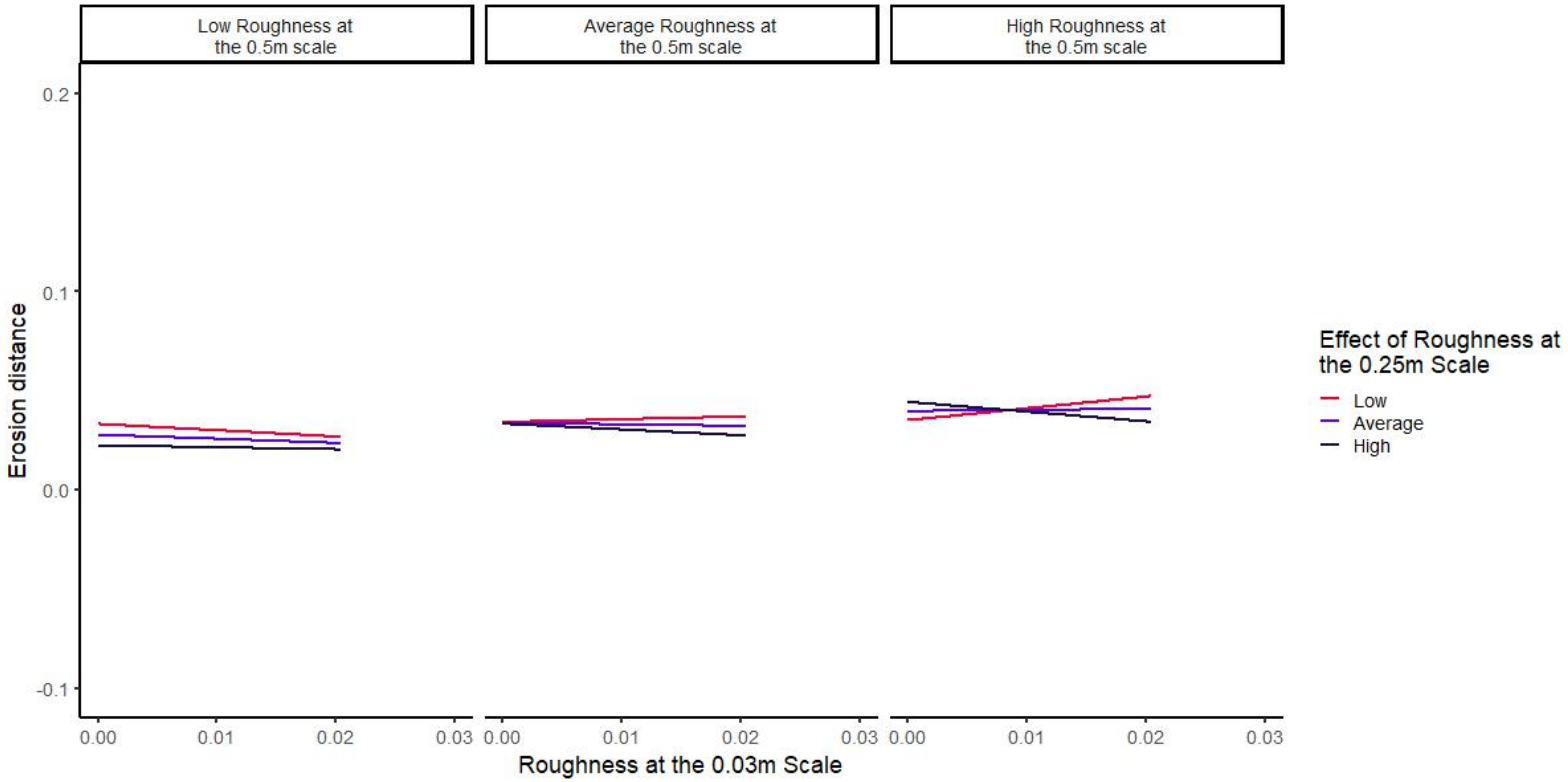

Figure F.26: Interaction plot of the effect of roughness at each scale on erosion for time period E1 on the midstream reach of Bank 3

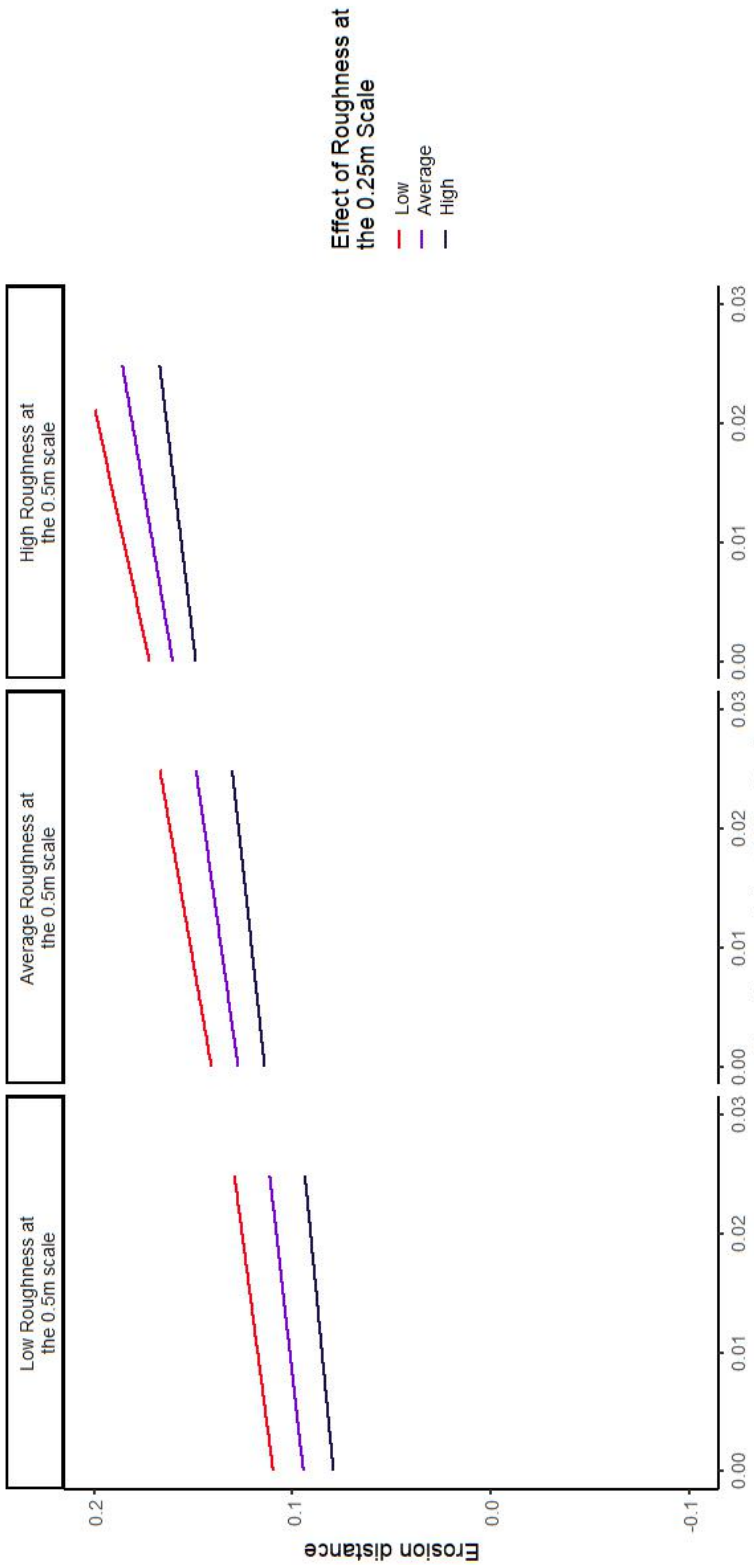

Figure F.27: Interaction plot of the effect of roughness at each scale on erosion for time period E4 on the midstream reach of Bank 3

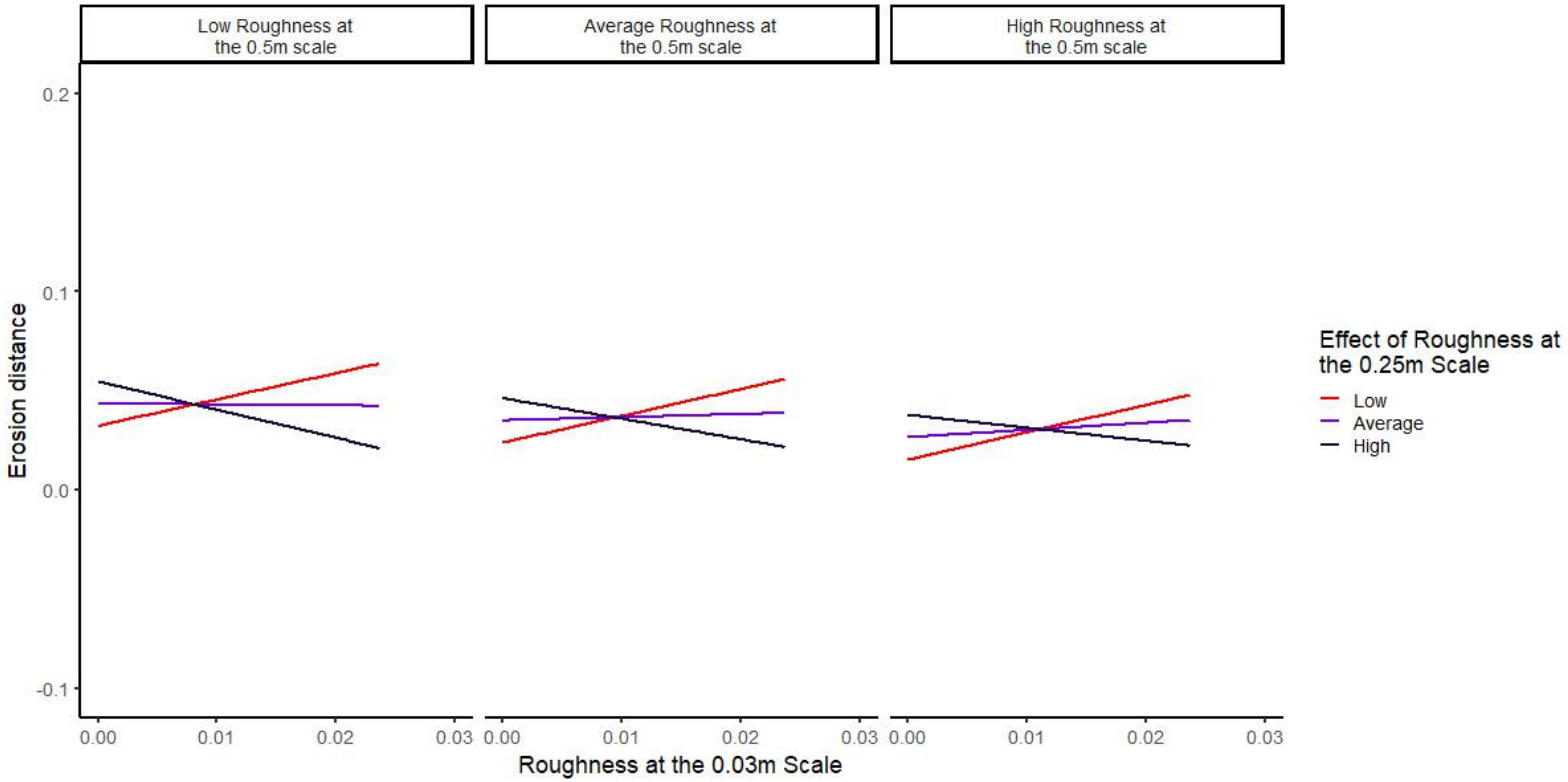

Figure F.28: Interaction plot of the effect of roughness at each scale on erosion for time period E6 on the midstream reach of Bank 3

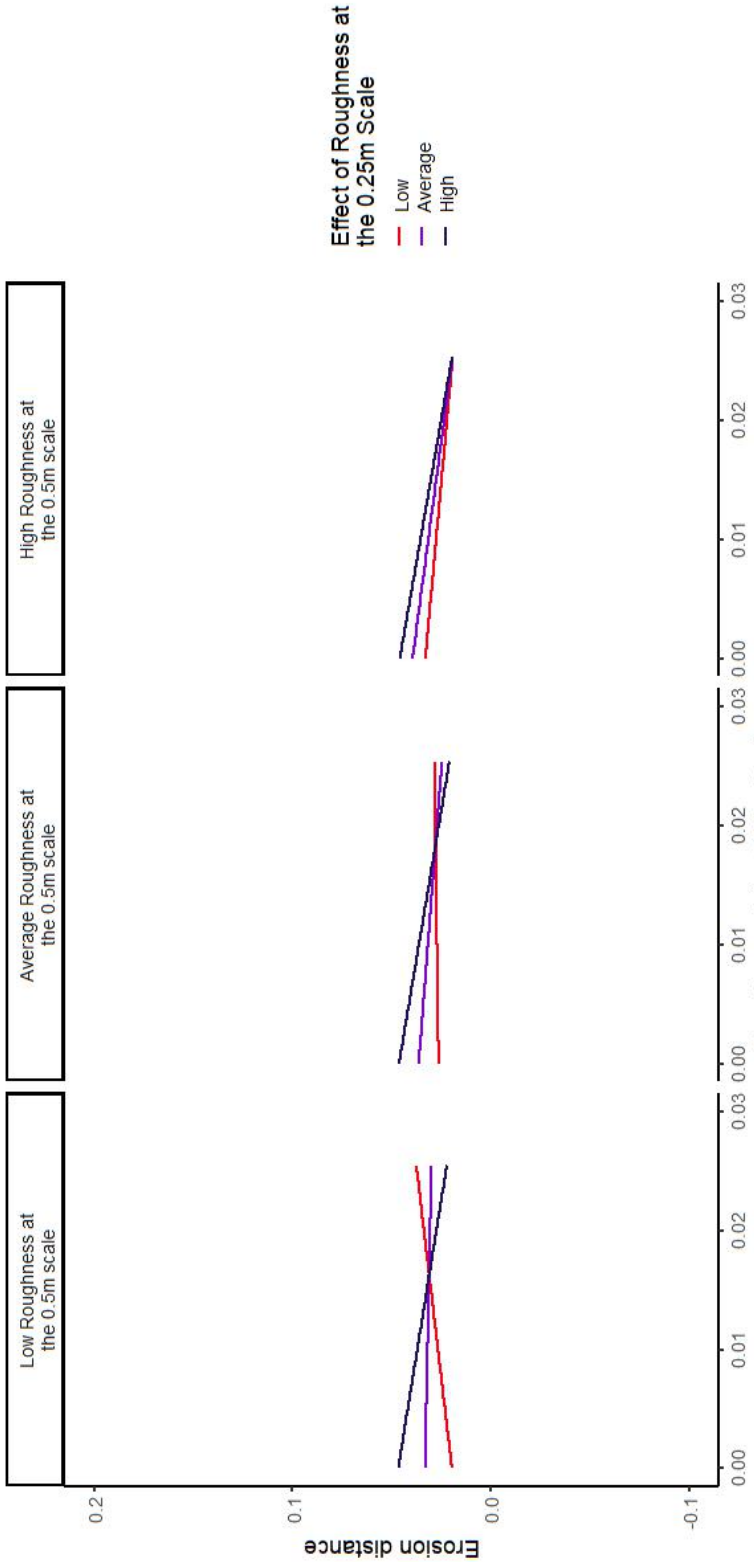

Figure F.29: Interaction plot of the effect of roughness at each scale on erosion for time period E2 on the downstream reach of Bank 3

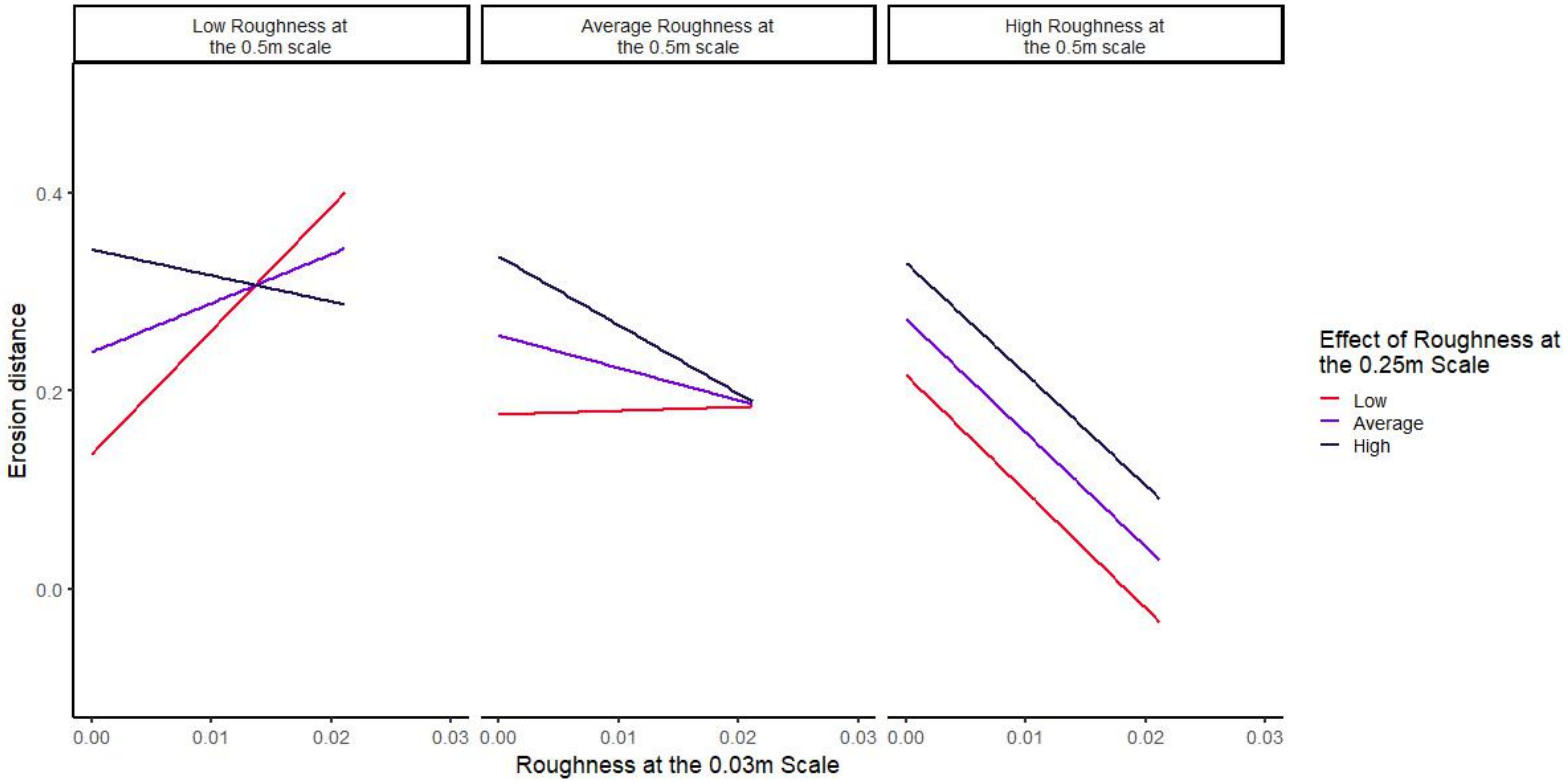

Figure F.30: Interaction plot of the effect of roughness at each scale on erosion for time period E6 on the downstream reach of Bank 3